COST 724 final report

Developing the scientific basis for monitoring, modelling and predicting Space Weather

The COST 724 members

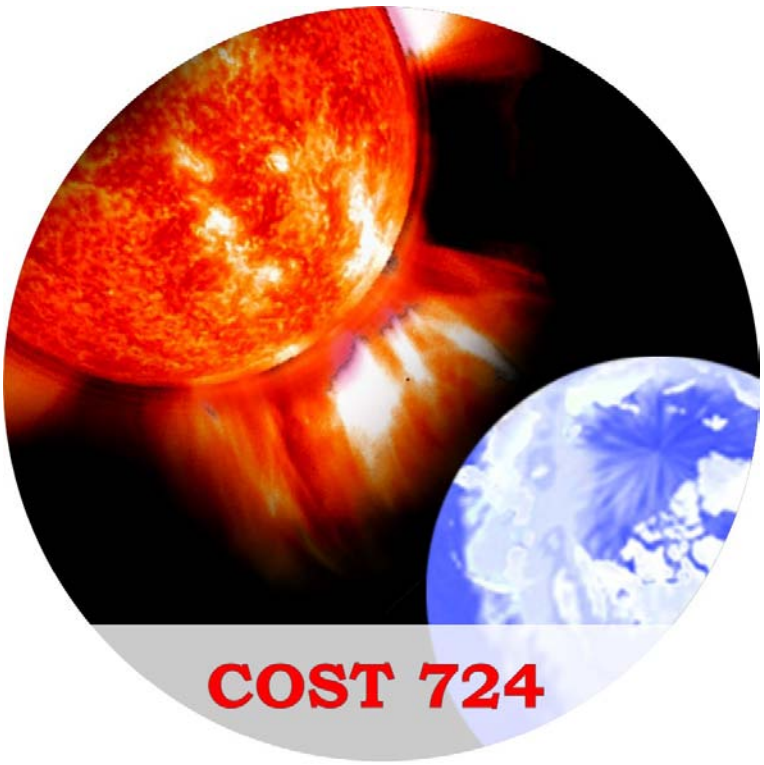

Contents

Part I

Introduction

Introduction to COST 724

Developing the scientific basis for monitoring, modelling and predicting Space Weather

J. Lilensten[1] and A. Belehaki[2]

[1] Laboratoire de Planetologie de Grenoble, OSUG-CNRS, France
jean.lilensten@obs.ujf-grenoble.fr
[2] Ionospheric Group, Institute for Space Applications and Remote Sensing, National Observatory of Athens, Metaxa and Vas. Pavlou, 15236 Palaia Penteli, Greece belehaki@space.noa.gr

1 Introduction and content of this report

Thanks to the COST 724 action, space weather has now a European definition:
Space weather is the physical and phenomenological state of natural space environments. The associated discipline aims, through observation, monitoring, analysis and modelling, at understanding and predicting the state of the Sun, the interplanetary and planetary environments, and the solar and non-solar driven perturbations that affect them, and also at forecasting and nowcasting the potential impacts on biological and technological systems. This definition (see the dedicated paper in the WG4 chapter in this book) is the result of a long and difficult effort. It did not exist prior to the start of our action. It is one of the numerous deliverables that COST 724 provided. We chose to write it as the very first item of this introduction because it attests the main success of the action: to gather a community of 28 countries and work together in spite of different cultures. These countries are (in alphabetical order) Armenia, Austria, Belgium, Bulgaria, Canada, Czech Republic, Denmark, Finland, France, Germany, Greece, Hungary, Ireland, Israel, Italy, Norway, Poland, Romania, Russia, Serbia, Slovakia, Slovenia, Spain, Sweden, Switzerland, Turkey, Ukraine and United Kingdom. Last not least, ESA and the COST action 296 were associated with us. This report is a clear result of this diversity.
It is organized in the following way:

- This introduction gives an overview of the organization of the action. It then compares briefly what had been foreseen in the Memorandum of Understanding and what has actually been delivered.
- Each of the four working groups has one chapter where it reports the achievements obtained in the course of this action. The four chapters are organized largely in the same way.
  - A synthesis section outlines the rationale of the working group and makes a more detailed comparison between the statements of the MoU and the results obtained by the working group.

– Several topical papers review the state of the art in selected areas of relevance to this action and report on specific work done by working group members in the frame of the action. Each paper has been reviewed internally and anonymously.

The rationale sections combined with material from the topical review papers will constitute a special issue of *Space Science Review* that will be published in 2009. The topical research papers will constitute a special issue of *Acta Geophysica* which is planned for December 2008. Both journals are peer review journals. That means that our action will still produce significant deliverables after its completion. This report has been prepared by the whole Management Committee (MC). In order to work efficiently on its completion, we applied to the International Space Science Institute in Bern (Switzerland) for team meeting support and were successful. A core group of 12 COST 724 members gathered one week in January 2007 and one week in September 2007.

2 Birth of the action

In 1996, the European Space Agency (ESA) organized a round table on Space Weather in order to discuss options for a European counterpart to the US National Space Weather Programme. The first Space Weather workshop was launched two years later. At that time the community was developing and the perspective for a coordinated effort in the field of Space Weather was investigated.
ESTEC maintained a key role in structuring the field in Europe, primarily by organising annual workshops from 1998 to 2003. In parallel, it funded a study on the feasibility of a European Space Weather Programme for which two broadly based international consortia were appointed. In order to coordinate their work on the feasibility studies the Space Weather Working Team (SWWT) was created. The results of the two parallel studies were published in 2001. They proposed several strategies to develop Space Weather related activities in Europe and clearly demonstrated that Europe has very strong assets which could potentially be exploited in European or International Space Weather services.
It was clearly understood that the coordination and development of Space Weather services would enhance the efficiency of these activities and provide new opportunities for the use of resources across domains that are currently separated from each other.
The SWWT continued to be active in its advisory role following the end of the two parallel studies. One of the recommendations of the SWWT was to apply for a COST action targeted at the science underpinning Space Weather. This led eventually to COST 724 which started in November 2003.

3 Organization of the action

From its beginning, the action has been organized around a bureau composed of the chairman J. Lilensten, the vice chair A. Belehaki, and the four working group leaders (WG1: M. Messerotti; WG2: R. Vainio; WG3: J. Watermann). During the first two years F. Jansen was the leader of WG4. He was subsequently replaced by the chairman of the action. When

deemed beneficial for the work, experts from the MC were invited to the bureau for certain periods (M. Candidi, D. Heynderickx). The bureau prepared the MC meetings, served as a think tank and took such decisions which did not require approval by the whole MC. Of course, the bureau did not take decisions on items which are under the authority of the whole MC. Specific tasks of the bureau concerned the management of our budget and of the numerous short term scientific missions.

4 Achievements of the action versus the Memorandum of Understanding

The MoU states in its introduction that *The main objective of the Action is to develop further within a European framework the science underpinning space weather applications, as well as exploring methods for providing a comprehensive range of space weather services to a variety of users, based on modelling and monitoring of the Sun-Earth system*. After four years of existence of COST 724 this has resulted in:

- Eleven MC meetings, most of them combined with scientific meetings. After the kick-off meeting in November 2003 in Brussels (Belgium), we organised three scientific and MC meetings in 2004, in Nice (France), Trieste (Italy) and Noordwijk (The Netherlands). In 2005, we met in Vienna (Austria), Athens (Greece) and Noordwijk again. In the following year we had a meetings in Antalya (Turkey) and Brussels. Finally, in 2007, we had a meeting in Sofia (Bulgaria) and have one in Brussels to close the action. Two proceedings collections where published on CD-ROM, and most of the scientific contributions to the Noordwijk and Brussels meetings reside on ESA/ESTEC meeting web sites.
- Fifteen short term scientific missions. They involved about 35 researchers from many of our participating countries. The outcomes of these missions are described in different chapters of this report.
- An international space weather school (2-19 May 2006). Initiated by the chairman J. Lilensten and organised under the leadership of our Italian national delegate M. Messerotti this school took place at ICTP in Trieste (Italy). COST 724 was co-organiser together with the ICTP and the US National Science Foundation. About 30 participants from our OCDE/COST countries were funded by COST and NSF, and the same number of students from developing countries were funded by ICTP - UNESCO.
- Creation of the Space Weather Web Portal. This is one of a major deliverables of our action. It is physically located in Brussels, but it is mainly a distributed facility where codes can be run from distant computers, data can be downloaded, catalogues may be consulted. A large part of this portal is dedicated to public outreach. This part was translated by our MC members into 15 European languages. The portal is described in the WG4 chapter.
- Initiation and organization of the European Space Weather Week (ESWW). COST 724 assumed the main role in this activity which will be emphasized hereafter. This also is a major outcome of our action.
- Two books. One explains space weather to a broad educated but non-specialist audience. The other constitutes the outcome of the ESWW 2. Finally, this report will be published by OPOCE ed. in 2008 in the forms of a book and an online version.

- Two special issues of Annales Geophysicae. One of them focusses on ESWW 1 and the other on ESWW 3. ESWW 4 will hopefully have its papers published jointly by the European Geosciences Union (EGU) and the American Geophysical Union (AGU) in the peer reviewed AGU journal "Space Weather". This is expected to open a collaboration between the EGU and AGU to create a common peer reviewed journal devoted to the discipline. Also this is a joint COST 724 - ESA initiative. Also foreseen is a special issue of Acta geophysica and a special issue of Space Science Reviews devoted to the outputs of our action. Publications are expected in December 2008 or early 2009.
- More than 350 scientific papers in international refereed journals. It is not possible to determine the exact number, partly because it is difficult to determine whether a paper published by one of the COST 724 members is really relevant to the action, and partly because authors often forget to inform the working group leaders about their recent publications.
- Four partially interactive working group web sites. Working groups 1, 2 and 3 created their own web sites as working and communication tools. For instance, detailed lists of space weather related publications by COST 724 members were collected by the WG leaders and published on the WG web sites. The fourth one is a tool for the whole action http://cost724.obs.ujf-grenoble.fr/ from which the three first can be reached.
- An international team funded by the International Space Science Institute (Bern, Switzerland) with the objective of compiling the COST 724 final report. Twelve experts from our action participated in this team.

Behind this quantitative approach, a lot of scientific progress has been made. The MoU states the following tasks:

- MC:
  1. Manage liaisons with external groups;
  2. Consolidate the WG output into annual reports;
  3. Organise annual workshops
- WG1
  1. Create a catalogue of existing sources of data and models;
  2. Review scientific understanding
  3. Recommend, implement and evaluate a scheme for predicting SEP onset;
  4. Recommend, implement and evaluate a scheme for predicting CME initiation;
  5. Recommend, implement and evaluate a scheme for predicting solar EUV radiation variations
- WG2
  1. Create a catalogue of existing sources of data and models and of reported space weather events when humans, satellite and avionic technology was affected
  2. Review scientific understanding
  3. Recommend, implement and evaluate a scheme for modelling SEP effects, trapped radiation and galactic cosmic radiation at the Earth;
- WG3
  1. Create a catalogue of existing sources of data and models;
  2. Review scientific understanding

3. Recommend, implement and evaluate a scheme for modelling CME propagation to, and interaction with, the Earth;
4. Recommend, implement and evaluate a scheme for modelling induced ground electric fields; Create a catalogue of reported events when ground-based technology was affected

- WG4
  1. Create and manage website with links to data sources identified by WG1-3; Incorporate outreach material.
  2. Identify where standards on data exchange need to be set, and propose solutions;
  3. Implement and maintain catalogues of reported events on the web site;
  4. Manage web links to models implemented by WGs incorporating data exchange standards;
  5. Summarise usage statistics;
  6. Manage space weather events catalogue

Management committee: We liased with ESTEC along the course of the action. ESTEC has created an advisory board called the *"Space Weather Working Team"* (SWWT). Its leaders, M. Hapgood and A. Glover from ESTEC, have been permanent members of our MC. Similarly, J. Lilensten, chair of the COST 724 action has been included in the SWWT. Following the two ESA parallel feasibility studies quoted above, ESA embarked in 2003 upon a 2-year Space Weather Applications Pilot Project which incorporated 17 ESA co-funded Service Development Activities (SDAs) and a number of additional independently funded SDAs. The pilot project as a whole is named the "Space Weather European NETwork" (SWENET). It is not surprising that many of the colleagues involved in the COST 724 action are also involved in one of the SDAs. It was therefore one of the main tasks of the MC to maintain a very close cooperation with ESTEC, SWENET and the SWWT, as natural partners.

Our action also created strong links with COST 296 devoted to ionospheric applications. This is described in the WG4 chapter. We also had permanent contacts with the board of the International Heliophysical year. Y. Tulunay, from COST 724 was officially elected as our representative to the IHY management committee. Our action is also linked to the International Electronic Year. M. Messerotti, from COST 724 is our official representative there. We are also connected to the International Polar Year (IPY). J. Watermann served as program chair of the Greenland Space Science Symposium and will be guest editor of a special issue of JASTP devoted to scientific results from that symposium and from the ICESTAR initiative. Both are elements of the IPY project #63 "ICESTAR/IHY", the only genuine STP project among the proposals officially endorsed by IPY. Through M. Candidi, National Italian representative, our action is also linked to the ICESTAR programme. The goal of the ICESTAR programme is to create an integrated, quantitative description of the upper atmosphere over Antarctica, and its coupling to the geospace environment.

Our delegates to these actions regularly reported during our Management Committee meetings and gave reports on our COST action during these program meetings. Mutual invitations have been made in order to link the different communities and with different exchanges of informations.

Finally, we established relationships with the meteorological community. This has been

a long way, and we are not yet at the end. From the first European Space Weather week, we organized a plenary session devoted to meteorology. This allows our community to meet some meteorologists and start linking together. In the other way round, one of our MC members (M. Messerotti) convenes a session at the 2007 European Meteorological Society annual meeting.

As stated above, we had much more than one annual report, and much more than one annual meeting.

WG1, WG2 and WG3: catalogues of existing sources of data and models have been compiled and are available on the Space Weather Portal through a link to the INAF-Astronomical Observatory of Trieste that maintains them. The review of the scientific understanding is particularly clear in some of the topical papers included in this report and are often achievements of short term scientific missions.

The evaluation and recommendation of predicting schemes have *not* been performed. This is due to the lack of funding. In this extend, the MoU was too ambitious. Such a task would necessitate a board of engineers to run the codes and compare the outputs *a.s.o.* However, we implemented codes in most of the domains. SEP, CME and EUV in WG1 have all been adressed. Special attention must be given to the EUV problematics. Here, because of the small number of existing codes, our group could review all of them and give recommendations. WG2 implemented codes for trapped radiation and galactic cosmic radiation at Earth. Again, special mention must be made of the cosmic radiations. Several STSM were devoted to this topic, and for the first time, the existing codes have been compared. Several papers are devoted to this in the report. Finally, in WG3, models of CME and SEP evolution and interaction with the Earth environment have been developped. Specially mentioned should be codes for computing geomagnetically induced ground electric fields where applications have been developed.

Finally, each WG created its own web server:

- http://ca724wg1.ts.astro.it/ for WG1
- http://theory.physics.helsinki.fi/~space/cost724/ for WG2
- http://www.dmi.dk/projects/COST724_WG3/home.htm for WG3

WG4 As mentioned, a web site with links to data sources identified by WG1-3 was created along with the catalogues. The catalogue of events was focussed on the reported spacecraft failures and constitutes the largest list ever assembled in this field. In the rationale paper introducing the WG4 chapter, an analysis is made of where it succeeded, where it went further than the MoU and where it failed.

WG4 was also in charge of dissemination and outreach activities. As far as outreach is concerned, COST 724 through its WG4 participated in different activities, ranging from the development of educational laboratory experiments to participation in a European space weather fair. All these are reported in this volume. On the European web portal, most of the outreach pages are translated into different languages. That was our decision, and is now underlined by many users of different countries: they like very much the fact that they get information in their own langage (Greek, French, German, Slovenian, to name just a few). Another point is that we asked primary school pupils from several COST countries to illustrate space weather. Their artwork is now on our web site and, because of friendly relationships with the International Heliophysical Year committee,

it was shared with them. This resulted in participation of COST 724 people in several school programs.

5 Conclusion

From our point of view, it was certainly of great value to our community that an action on space weather was accepted by COST. Although COST provides cement funding only this proved to be very powerful. In the concluding chapter of this report, we give some hints on what the future might be, and how our community should now evolve.
We have been working hard to make our discipline known by the decision makers. We met delegates from different commissions of the European Union, we met scientific advisors in different national ministries. We also met space, aircraft, telecommunication (...) industrials. Now, thanks to ESTEC and to our action, the term *space weather* is known in Europe. However, nothing is secured yet. We see in Europe several countries capable of creating *the* European Space Weather Centers which will sustain our discipline on our continent. But that will still take some years. In the meantime, no other instrument but a COST action is that powerful to maintain a unified European community in our field.

Acknowledgements We thank the french space agency CNES for providing our action with a secretariat during the three last years. That was an invaluable help to our success. We thank ISSI for having offered us their facility in order to finalize this final report.

Appendix All over this report, many accronyms are used. Although they are usually written out at the first use, it may be useful to have a complete glossary at hand. Our action produced one which resides at the European Space Weather Web Portal. However, it is often usefull to have more than one dictionary. This is why we suggest here links to several solar terrestrial glossaries:

- http://www.spaceweather.eu
- http://www.movingsatellites.com/glossary.html
- http://web.hao.ucar.edu/public/education/glossary.html
- http://mcdonaldobservatory.org/research/glossary/
- http://www-spof.gsfc.nasa.gov/Education/wgloss.html
- http://www.ngdc.noaa.gov/stp/GLOSSARY/glossary.html

Part II

Working Group 1:
Monitoring and predicting solar activity for Space Weather

Monitoring and Predicting Solar Activity for Space Weather

M. Messerotti[1,2], F. Zuccarello[3], and W. Schmutz[4]

[1] INAF-Astronomical Observatory of Trieste, Loc. Basovizza n. 302, 34012 Trieste, Italy, messerotti@oats.inaf.it
[2] Department of Physics, University of Trieste, Via A. Valerio n. 11, 34127 Trieste, Italy, Mauro.Messerotti@ts.infn.it
[3] Department of Physics and Astronomy, University of Catania, Via S.Sofia 78, 95123 Catania, Italy, Francesca.Zuccarello@oact.inaf.it
[4] PMOD/WRC, Dorfstrasse 33, 7260 Davos Dorf, Switzerland, werner.schmutz@pmodwrc.ch

1 Introduction

Working Group 1 (WG1), *Monitoring and Predicting Solar Activty for Space Weather* (http://ca724wg1.oats.inaf.it/), of COST Action 724 (CA724) was aimed at dealing with the most relevant aspects of solar activity as the primary driver of space weather. More than 50 specialists from institutes all over Europe participated in this joint effort by submitting specific Expression of Committments relevant to their respective research fields.

The WG1 Kickoff Meeting was held in Trieste on May 2004. The discussion during that meeting and the dynamic fine tuning occurred at a later time led to the formation of the following Work Packages (WP):

WP 10000 Coordination Activities.
WP 11000 Solar Magnetic Activity Analysis.
WP 12000 Solar Electromagnetic Radiation Analysis.
WP 13000 Solar Particle Emission Analysis (in collaboration with WG2).
WP 14000 Coronal Mass Ejection Analysis.
WP 15000 Liason with CA 296.
WP 16000 Liason with CA 724 WG4.

The final structure of WG1 is reported in Fig. 1, where the Leaders and Co-Leaders of the WPs are specified.

The activities of each WP were devoted to:

- Reviewing of available models and data.
- Developing models.
- Performing experimental research.

In the papers included in this chapter, a selection of important results achieved in WG1 during the four years of the action are presented. In addition to such specific papers describing and reviewing the actual work, highlights on the advancements in solar activity understanding

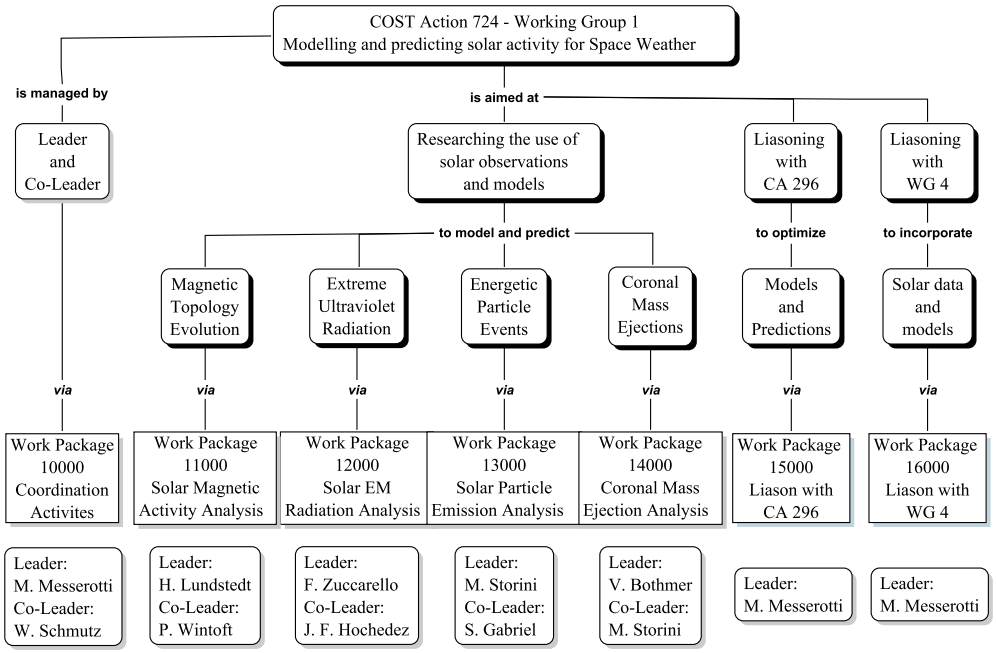

Fig. 1. Structure of COST Action 724 Working Group 1.

and predicting is given in the first paper. Due to the variety of the solar activity phenomenology, this paper gives some background information only on a selected subset of solar activity features, which can anyway serve as an introduction to the specific papers. Therefore, it not aimed at providing a comprehensive review of the physics underpinning solar activity.

The reviewed solar models and data sources are schematically presented in the following sections. The online archiving system for the data and model reviews by WG1, WG2 and WG3 (http://ca724wg1.oats.inaf.it/mod_data.php) was developed by WG1 as a contributed activity to WG4.

In addition to the physical background presented in the first paper, the specific papers of the chapter are providing additional reviews and original results on the following topics: (1) *Zuccarello et al.* describe some aspects relevant to the emergence of magnetic structures on the solar surface; (2) *Zuccarello et al.* report some results obtained from multi-wavelength observations carried out to study the mechanisms operating in flares and filament eruptions; (3) *Lundstedt* discusses the understanding of solar activity based on mathematical concepts and what should be observed for predictions; (4) *Kretschmar et al.*present recent efforts to quantify the solar extreme (EUV) and far ultraviolet (FUV) irradiance variability and discuss what should and could be measured in order to retrieve the solar EUV and FUV spectrum; (5) *Storini et al.* review available long-term and short-term forecast techniques for Solar Energetic Particle (SEP) events and a recent work on the development of a new short-term warning technique for SEP event occurrence that is based on flare location and integrated soft X-ray and low-frequency radio emission; (6) *Žigman et al.* present the research of the lower iono-

sphere, in terms of D-region electron density enhancements during Solar X- ray flares caused by the Sun eruptive activity. (7) *Messerotti and Chela-Flores* review the understanding about the role of solar activity for life emergence and evolution focusing on the interrelationships between space weather and Astrobiology.

The above papers represent just a selection of results achieved by WG1. In fact, e.g., on the monitoring side there are presently no European space experiments except those on SoHO or minor participation on non-European experiments such as e.g. RHESSI or recently, STEREO. At the start of the CA724 it was foreseen that the ESA technology mission PROBA2, with its solar experiments SWAP (Berghmans et al., 2006) and LYRA (Hochedez et al., 2006) would bring a European mission for solar monitoring with a launch that was originally set to 2006. In the course of the COST action the date of launch of PROBA2 has been delayed to 2008, which implies that at the end of the Action there is still no dedicated European space weather mission. Nevertheless, there are many missions monitoring the Sun, which are accessible to the European community and Europeans are actively involved in using the data to address space weather issues (Hochedez et al., 2005). Moreover, fundamental research work has been performed on CMEs which can be found in the literature (Bothmer and Daglis , 2007).

2 Summary of Solar Models Reviewed by WG1

The models reviewed by the members of WG1 are listed in Tables 1, 2 and 3. Each line in the tables contains data for one model. The first column gives the name of the model, the second column gives the domain of the model, the third indicates whether the model is a physical (P), empirical (E) or a semi-empirical one (S-E), the fourth column gives the most important input parameters or data to the model, the fifth column describes the output of the model, and the sixth column gives some reference information, a website about the model. Some of the models are also decribed in more detail in the specific papers of this chapter.

3 Summary of Solar Data Sources Reviewed by WG1

Table 2 reports a selection of solar and solar-terrestrial data sources that where either provided or identified by WG1. The resources are categorized according to their operational features as (see Table 2):

- Archive Portals, which provide web-based data search and retrieval on limited datasets.
- Data Grids, which provide web-based complex data search and retrieval on geographically distributed repositories.
- Catalog Search facilities, which provide web-based cross-search on data catalogs.
- Virtual Observatories, which provide web-based data search, retrieval and visualization on geographically distributed repositories.
- Space Weather facilities, which provide web-based space weather products.

The list of resources is far from being a comprehensive one, but it express the fact that most resources not explicitly listed are available through the listed ones, a typical role played by the Virtual Observatories.

Table 1. Solar activity models reviewed by WG1.

Model	Domain	Type	Objective (Purpose)	Input	Output	Ref.
ENLIL (P. MacNeice)	Fluid motions	P	A time-dependent 3D MHD model of the heliosphere	Boundary condition information from either the WSA or MAS models	Plasma mass, momentum and energy density, and magnetic field of heliosphere	ccmc.gsfc.nasa.gov/models/ENLIL.php
Exospheric Solar Wind Model (M. Kuznetsova)	Fluid motions	P	An exospheric model of the solar wind with only protons and electrons	Radial Distance of the Exobase, Electron Temperature at Exobase, Proton Temperature at Exobase, Kappa Index Value, Max Radial Distance	Total normalized potential of the protons, electrostatic potential, number density of electrons, number density of protons, flux of electrons, flux of protons, bulk velocity of the solar wind electrons, bulk velocity of the solar wind protons	ccmc.gsfc.nasa.gov/models/exo.php
FROMAGE (T. Amari)	Solar Magnetic Field	P	Calculation of vector magnetic field B, at different altitudes of the solar atmosphere	Maps obtained with magnetographs	Magnetic configuration of the extended corona (till 2.5 solar radii)	dasop.obspm.fr/fromage
Heliospheric Tomography Model (M. Kuznetsova)	Solar Energetic Particle Emission	E	Reconstruction the global structure of the solar wind from interplanetary scintillation	Remote sensing data of the solar wind (currently IPS observations form the STELab in Nagoya, Japan)	Solar wind density and velocity throughout the inner heliosphere	ips.ucsd.edu/index_br_wson_bt_wson.html
JPL (J. Feynman)	Solar Energetic Particle Emission	P	Interplanetary fluences of protons at a distance of one Astronomical Unit	The mission length at a constant heliocentric distance of 1 A.U. and the required confidence level	Proton Fluence Model	modelweb.gsfc.nasa.gov/sun/jpl.html

Table 2. Solar activity models reviewed by WG1.

Model	Domain	Type	Objective (Purpose)	Input	Output	Ref.
MAS (L. Rastaetter)	Solar Magnetic Field	P	MHD Model of Solar Corona, 1 - 30 solar radii	Coronal base plasma temperature, density, radial magnetic field Br from synoptic magnetograms	Solar coronal temperature, plasma pressure, density, velocity, magnetic fields	shadow.adnc.net/corona/coronal_modeling.html
NIRVANA (U. Ziegeler)	Fluid motions	P	NIRVANA is a numerical code for non-relativistic, compressible, time-dependent, ideal or nonideal magneto-hydrodynamics	User defined boundary and initial conditions for MHD equations	MHD dynamics and variables	nirvana-code.aip.de
PFSS (P. MacNeice)	Solar Magnetic Field	P	Solar coronal magnetic field based on observed photospheric fields	Spherical harmonic coefficients for specific date	Magnetic field of the Sun from one solar radius to the source surface radius	ccmc.gsfc.nasa.gov/models/PFSS.php
SIR (L. Bellot)	Solar Electro-magnetic Radiation	P	Synthesis and inversion of spectral lines formed in the presence of magnetic fields	Stokes profiles from magnetognams	Temperature, pressure, magnetic field, and velocity in function of the optical depth of the lines	iaa.es/hinode_europe/index.php/gb/inversion_codes/sir
Solar2000 (W. Kent Tobiska)	Solar Electro-magnetic Radiation	P	Model of daily 1 AU adjusted or observed solar irradiance products	–	Daily time step of irradiance products	spacewx.com/Products.html#s2k_rg_grade
Solar Software packages (S. L. Freeland)	Solar Magnetic Field	P	Suite of routines of solar data analysis	User provided	General means of solar data analysis are the start basis of Space Weather studies	lmsal.com/solarsoft/ssw_packages_info.html
SOLPRO)	Solar Energetic Particle Emission	P	Interplanetary solar proton fluences at 1 A.U.	Mission duration (in months), energy threshold (in MeV), and confidence level (in percent)	Solar proton fluences (10 MeV to 100 MeV)	modelweb.gsfc.nasa.gov/sun/solpro.html

Table 3. Solar activity models reviewed by WG1.

Model	**Domain**	**Type**	**Objective (Purpose)**	**Input**	**Output**	**Ref.**
SWMF/SC-IH (P. MacNeice)	Solar Magnetic Field	P	Model of the ambient corona and inner heliosphere	Magnetospheric and ionospheric plasma parameters	User selection of the carrington rotation	csem.engin.umich.edu/swmf
WSA/PF+CS-IH (P. MacNiece)	Solar Electro-magnetic Radiation	S-E	A model of the global coronal magnetic field between the solar surface and a bounding spherical surface	–	Determine the local solar wind speed	ccmc.gsfc.nasa.gov/models/WSA.php
ZEUS (M. L. Norman)	Fluid motions	P	A magnetohydrody-namics code developed for simulations	User defined boundary and initial conditions for MHD equations	MHD dynamics and variables	lca.ucsd.edu/portal/software

Table 4. Main characteristics of reviewed solar and solar-terrestrial data sources. (Acronyms in Table 2)

Data Resource	Host Institution	Contact	Category	Data Type	Download	URL
DISCO	INAF-OAC	G. Severino severino@oac.inaf.it	AP	DOPM MAGM	Y	http://disco.na.astro.it/
PSPT	INAF-OARM	T. Ermolli ermolli@mporzio.astro.it	AP	N-B FD IMG	Y	http://www.mporzio.astro.it/solare/Immagini PSPT.htm
SOLRA	INAF-OATS	M. Messerotti messerotti@oats.inaf.it	AP	m-dm MC Radio F/ CP	Y	http://radiosun.ts.astro.it/eng/solra.php
SOLAR	INAF-OATO	A. Volpicelli volpicelli@oato.inaf.it	AP	SOHO Data	Y	http://solar.to.astro.it/
SOLARNET	INAF-OATO	A. Volpicelli volpicelli@oato.inaf.it	DG	Italian SAR + SOHO	Y	http://solarnet.to.astro.it:8080/portal
EGSO	EGSO Consortium	R.D. Bentley rdb@mssl.ucl.ac.uk	DG	M-B, M-I + VISUAL	Y	http://www.egso.org/
SEC/EGSO	INAF-OATS	M. Messerotti messerotti@oats.inaf.it	CS	17 S-T Catalogs	Y	http://sec.ts.astro.it/sec_ui.php
SEC SWDP	SEC/NOAA	SEC.Webmaster@noaa.gov	SWDP	S-T Datasets	Y	http://sec.noaa.gov/Data/index.html
VSO	NSO	F. Hill fhill@nso.edu	VO	Solar Datasets	Y	http://vso.nso.edu/
VSPO	NASA-GSFC	A. Smith aaron.smith@aquilent.com	VO	S-T Datasets	Y	http://vspo.gsfc.nasa.gov/websearch/dispatcher
RWCS	SISP	H. Lundstedt henrik@lund.irf.se	SWDP	S-T Datasets	Y	http://www.lund.irf.se/rwc/
SIDC	ROB	J.-F. Hochedez hochedez@oma.be	SWDP	S-T Datasets	Y	http://sidc.oma.be/
RSPRM	OBSPM	M. Pick Monique.Pick@obspm.fr	SWDP	Radio Datasets	Y	http://secchirh.obspm.fr/

Table 5. List of Acronyms used in Table 2

AP	Archive Portal
CP	Circular Polarization
CS	Catalog Search
DG	Data Grid
dm	Decimetric Band
DISCO	Data Interface to the Sun at Capodimonte Observatory
DOPM	Dopplergram
EGSO	European Grid of Solar Observations
F	Flux
FD	Full-Disk
IMG	Images
INAF-OAC	INAF-Astronomical Observatory of Capodimonte
INAF-OARM	INAF-Rome Astronomical Observatory
INAF-OATO	INAF-Turin Astronomical Observatory
INAF-OATS	INAF-Trieste Astronomical Observatory
m	Metric Band
MAGM	Magnetogram
M-B	Multi-Band
M-I	Multi-Instrument
N-B	Narrow-Band
NSO	National Solar Observatory
OBSPM	Observatoire de Paris Meudon
PSPT	Precision Solar Photometric Telescope
RWCS	Regional Warning Center Sweden
ROB	Royal Observatory of Belgium
RSPRM	Radio Survey Project and Radio Monitoring
SAR	Solar Archive
SEC/EGSO	Solar Event Catalog/EGSO
SEC/NOAA	Space Environment Center/NOAA
SEC SWDP	Space Environment Center - Space Weather Data Products
SIDC	Solar Influences Data Analysis Center
SISP	Swedish Institute for Space Physics
SOLAR	SOho Long-Term Archive
SOLARNET	SOLar Archive NETwork
SOLRA	SOLar Radio Archive
SPWDP	Space Weather Data Products
S-T	Solar-Terrestrial
VISUAL	Visualization
VO	Virtual Observatory
VSO	Virtual Solar Observatory
VSPO	Virtual Space Physics Observatory

The SOLARNET facility was consolidated in the light of CA724 and the related data made available. In particular, the Solar Radio Archive (SOLRA) of the Trieste Solar Radio System (TSRS; http://radiosun.oats.inaf.it/) has been providing solar radio indices with a time cadence of 1 minute in the metric and decimetric bands (among which the 11cm one of relevance as proxy of solar activity and for ionospheric modelling and prediction), which have been fed on a routinary basis into the European Space Weather Network (SWENET; http://esa-spaceweather.net/swenet/index.html) with the related 1-min ahead forecast.

During the action, advanced space weather services were set up at the following collaborating institutions:

- Lund Space Weather Center in Sweden(http://www.lund.irf.se/) for solar activity forecasting.
- Solar Influences Data Analysis Center in Belgium (SIDC; http://sidc.oma.be/) for activity feature identification and tracking on solar images.
- Paris Observatory in France (http://secchirh.obspm.fr/) for radio monitoring of Coronal Mass Ejections (CME).

4 Conclusions and Outlook

In the following, we enumerate the aims of WG1 as stated in the Memorandum of Understanding (MoU) by reviewing relevant progresses achieved for each of them.

A1. *To research the use of solar observations (eg. extreme ultraviolet images, X-ray observations, radio emissions) and models (eg. magneto-hydrodynamic models of flux tubes) for predicting energetic particle events.* An extensive work has been carried out about the evolution of active regions and the pre-flaring conditions based on multi-band, high-resolution observations (e.g. Zuccarello et al., this issue; (Hochedez et al., 2005); Žigman et al., this issue). The original approach for analysing and predicting solar activity by Lundstedt (this issue) was improved and extended and a new model for SEP forecasting by Storini et al. (this issue) represent a significant step forward. An automated system for solar radio indices prediction was set up in Trieste. The effects of solar activity on living species was considered in the context of Astrobiology (Messerotti and Chela-Flores , 2007).

A2. *To research the use of solar observations and models (as above) for predicting Coronal Mass Ejections (CME).* New image segmentation techniques and algorithms for CME identification and tracking have been set up (e.g. Delouille et al. (2005), Barra et al. (2005), (de Wit , 2006)). Oservations and modelling of CMEs have been extensively carried out (Bothmer and Daglis (2007) and references therein).

A3. *To research the modelling and prediction of solar extreme ultraviolet radiation (EUV) which affects atmospheric density and hence drag on satellites at low Earth orbit altitudes.* A model for the reconstruction of the EUV/FUV spectrum from a selected subset of spectral lines was developed (see Kretschmar et al., this issue, and references therein). This technique appears quite promising and further refinements are expected when new data will be made available from space missions.

A4. *To liaise with COST Action 271 (*Effects of the Upper Atmosphere on Terrestrial and Earth-Space Communications*; http://www.cost271.rl.ac.uk/) where monitoring and modelling of solar activity is relevant to ionospheric radiopropagation. COST Action 271 ended in 2004 and its role was taken over by COST Action 296 (*Mitigation of Ionospheric Effects on Radio Systems*; (http://www.cost296.rl.ac.uk/).* In this framework, CA296 prepared a comprehensive catalog of ionospheric models.

A5. *To liaise with COST Action 724 Working Group 4 to ensure relevant data and models are incorporated in a European Space Weather Network.* An archive for data and model reviews, common to WG1-WG2-WG3 was developed and incorporated in the space weather portal. The models developed about the various aspects of solar activity described above have been still either under refinement or under testing and validation due to their innovative approach, and cannot be made available yet. WG1 actively collaborated with WG4 for spreading the information and participated in various I*Y activities with special attention to IHY (International Heliophysical Year) and eGY (electronic Geophysical Year). A detailed analysis of the terminology, the concepts and the research fields of space weather was performed via concept maps as a basis for the construction of a space weather knowledge model and ontology (M. Messerotti, this issue).

In summary, WG1 added many significant tiles to the knowledge framework of monitoring and predicting solar activity, but the full accomplishment of the above aims showed to be a quite ambitious goal on the timescale of the Action in the light of the complexity of the solar phenomenology and of the lack of a set of self-consistent models capable of successfully reproducing the observed phenomenology. As we stress in the paper on advances in solar activity understanding, the chaotic nature of the Sun as a complex plasma system requires real-time high resolution observations from the ground and from space as well as advanced mathematical techniques for analysing the observations, for modelling the physical processes and for predicting the transient, the medium- and the long-term behaviour. This is the most promising perspective for gaining a step forward in the prediction of solar weather and solar climate.

References

Barra, V., Delouille, V., Hochedez, J.-F., Chainais, P.: Segmentation of EIT Images Using Fuzzy Clustering: a Preliminary Study. In Proc. 11th European Solar Physics Meeting "The Dynamic Sun: Challenges for Theory and Observations" (ESA SP-600). 11-16 September 2005, Leuven, Belgium. Editors: D. Danesy, S. Poedts, A. De Groof and J. Andries. Published on CDROM., p.77.1

Berghmans, D., Hochedez, J.-F., and 15 Co-Authors: SWAP onboard PROBA 2, a new EUV imager for solar monitoring. Adv. Sp. Res., **38**, 1807–1811 (2006)

Bothmer, V., Daglis, I.A.: Space Weather - Physics and Effects. Springer, Berlin (2007)

Delouille, V., de Patoul, J., Hochedez, J. F., Jacques, L., Antoine, J. P.: Wavelet Spectrum Analysis Of Eit/Soho Images. Solar Phys., **228**, 1, 301–321 (2005)

de Wit, T. Dudok: Fast Segmentation of Solar Extreme Ultraviolet Images. Solar Phys., **239**, 1–2, 519–530 (2005)

Hochedez, J.-F., Zhukov, A., Robbrecht, E., van der Linden, R., Berghmans, D., Vanlommel, P., Theissen, A., Clette, F.: Solar weather monitoring. Ann. Geophys., **23**, 3149–3161 (20005)

Hochedez, J.-F., Schmutz, and 37 Co-Authors: LYRA, a solar UV radiometer on Proba2. Adv. Sp. Res, **37**, 303–312 (2006).

Messerotti, M., Chela-Flores, J.: Signatures of the Ancient Sun Constraining the Early Emergence of Life on Earth. In Space Weather: Research towards Applications in Europe, J. Lilensten (ed.), Springer, Berlin, 49–59 (2007)

Advances in Solar Activity and Solar Weather Modelling and Predicting

M. Messerotti[1,2], F. Zuccarello[3], and H. Lundstedt[4,5]

[1] INAF-Astronomical Observatory of Trieste, Loc. Basovizza n. 302, 34012 Trieste, Italy
messerotti@oats.inaf.it
[2] Deptartment of Physics, University of Trieste, Via A. Valerio n. 2, 34127 Trieste, Italy
Mauro.Messerotti@ts.infn.it
[3] Universitá di Catania, Dipartimento di Fisica e Astronomia, Sez. Astrofisica, Via S. Sofia 78, 95123, Catania, Italy fzu@oact.inaf.it
[4] Swedish Institute of Space Physics, Scheelv. 17, 223 70 Lund, Sweden, henrik@lund.irf.se
[5] International Space Environment Service (ISES)

Summary. This work aims to review some advances relevant to the comprehension, modelling and prediction of solar activity. We emphasize the chaotic nature of the plasma processes that underpin solar activity and focus on key topics and techniques considered in the light of the solar models review carried out in the framework of COST Action Working Group 1.

1 Introduction

Since a long time, the occurrence of the 11-year activity cycle of the Sun is known. This cycle affects many characteristics of Sun variables: the number of active regions, their position on the solar surface, the total solar irradiance, the EUV and radio fluxes, the number of flares and CMEs, the solar wind parameters, the heliosphere characteristics and so on. Further, as it is the primary driver of Space Weather. it is important to improve our knowledge on solar phenomena. In the last decades, it has greatly improved thanks to high resolution observations performed by means of ground-based and satellite instruments. In this period there have also been important advances in the theory, thanks to a new generation of computational tools. In this work we provide some highlights on selected key topics relevant to solar activity in the light of the models that were identified and reviewed as a goals of COST Action 724 Working Group 1.

The paper is organized as follows. In Section 2 we briefly elaborate on the physical nature of solar activity and its descriptors. Advanced analysis and prediction techniques are outlined in Section 3. A classification of solar models is discussed in Section 4. Phenomena related to the emergence of magnetic flux are presented in Section 5 and solar weather in Section 6. Mid- and long-term solar activity are considered in Section 7. The conclusions are drawn in Section 8.

2 Solar Activity: Nature

Solar weather, the physical state of the solar plasma in the outer layers, is driven by the interplay between the plasma flow and the magnetic field. We therefore need to observe these quantities with the highest temporal and spatial resolution. However, not only are regions of the solar surface connected. They are also connected with processes below the solar surface and above, in the solar corona and in the interplanetary medium.

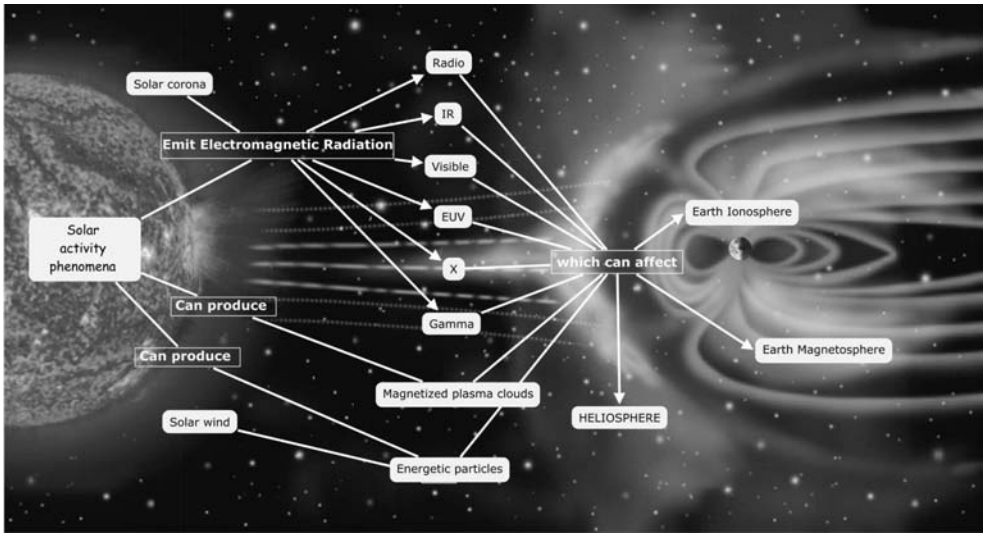

Fig. 1. Solar Weather in the solar-terrestrial environment

Particle and electromagnetic emissions that characterize Solar Weather determine the physical state of the Heliosphere and, in particular, of the Geospace (Fig. 1). The time and space evolution of such emissions are related to Solar Activity and their drivers are identified in the variety of plasma processes that occur inside the Sun and in its atmosphere. A rough scheme of these drivers and their relationships can be represented by a Concept Map such as the one reported in Fig. 2.

2.1 The Sun as a Complex Plasma System

A heuristic representation of the Sun and the key agents which determine Solar Activity can be schematized as in Fig. 3: the Sun is a complex plasma system that is subject to: (a) inner global fluid motions; (b) generation of a global magnetic field; (c) differential and to non-axisymmetric motions; (d) generation of localized magnetic fields; (e) external global fluid motions; (i) generation of a large-scale magnetic field. Hence Solar Activity is a manifestation of coupled, multi-scale, chaotic processes (Fig. 4)

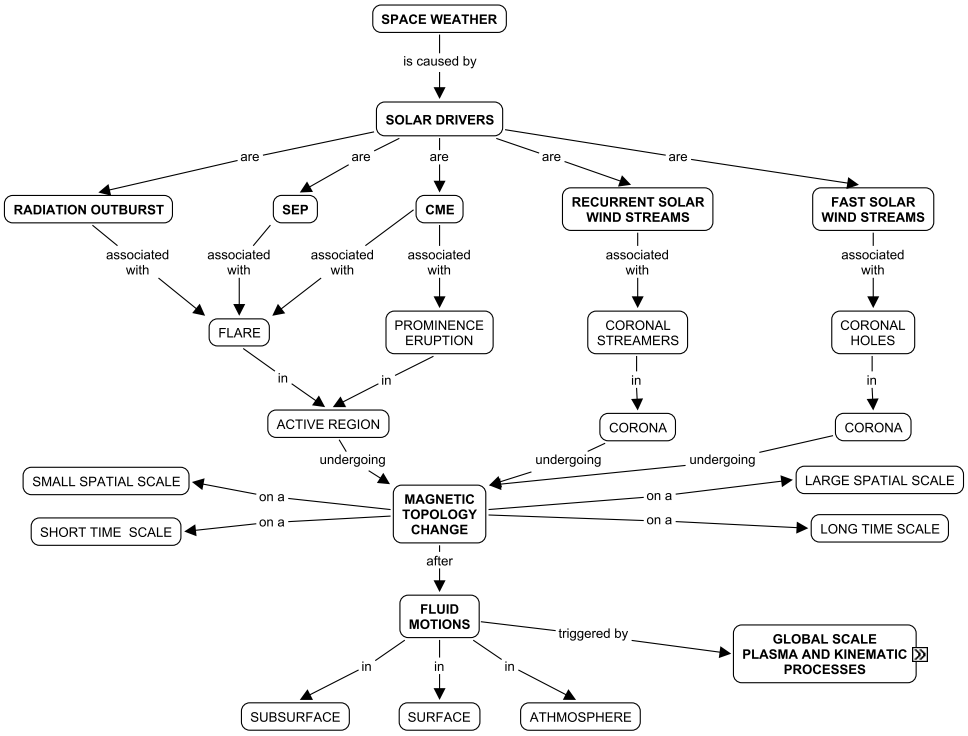

Fig. 2. Activity triggers and solar drivers of solar weather

2.2 Solar Activity as a Manifestation of Coupled, Multi-Scale, Chaotic Processes

Various aspects of the chaotic nature of the Sun have been considered in the literature e.g.: - Mandal and Raychaudhuri (2005) elaborated on a proof of the chaotic nature of the Sun through neutrino emission; - an evidence of a chaotic behaviour in the solar dynamo from the variations of the Sun's magnetic field in the last 100 years was indicated by Lockwood et al. (1999); - the evidence for a chaotic Sun from the analysis of the period and phase of the 88-year solar cycle was discussed by Feynman and Gabriel (2004); - a model of chaotic reconnection due to fast mixing of vortex-current filaments was proposed by Yatsuyanagi et al.(2000); - stochastic reconnection was considered by Lazarian et al. (2004). Hence the chaotic nature of the processes cannot be disregarded when modelling any of the manifestations of Solar Activity like Active Regions (AR) (Fig. 5) and Solar Flares (Fig. 6).

2.3 Solar Activity: Description

The common way to describe solar activity is based on a set of descriptors (e.g. Messerotti (2001), that are defined as either observable or observable-derived entities:

$$\mathbf{A} = \mathbf{A}(\mathbf{s}; t; \mathbf{E}) \tag{1}$$

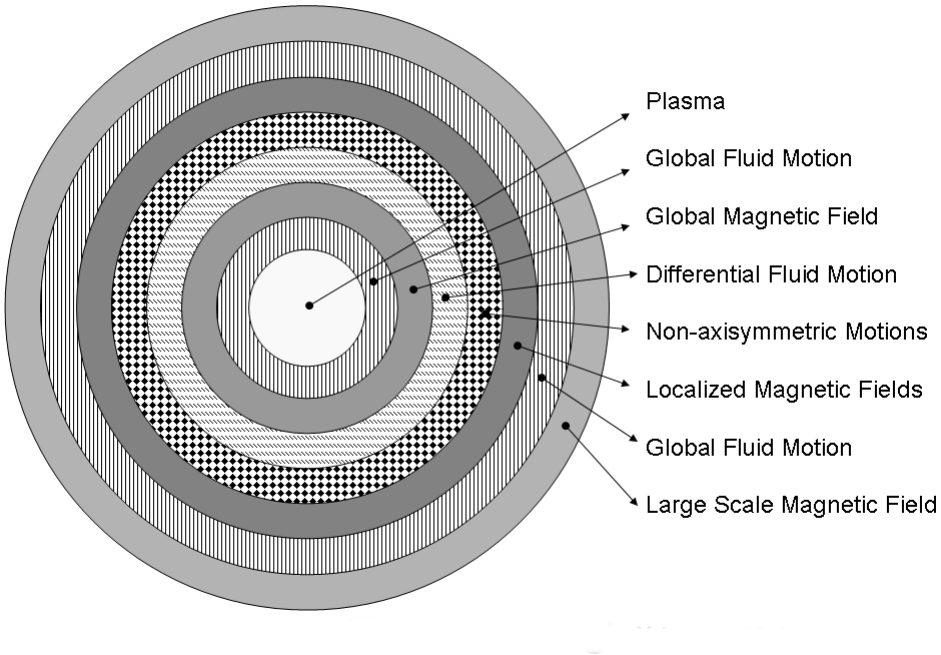

Fig. 3. The Sun as a complex plasma system

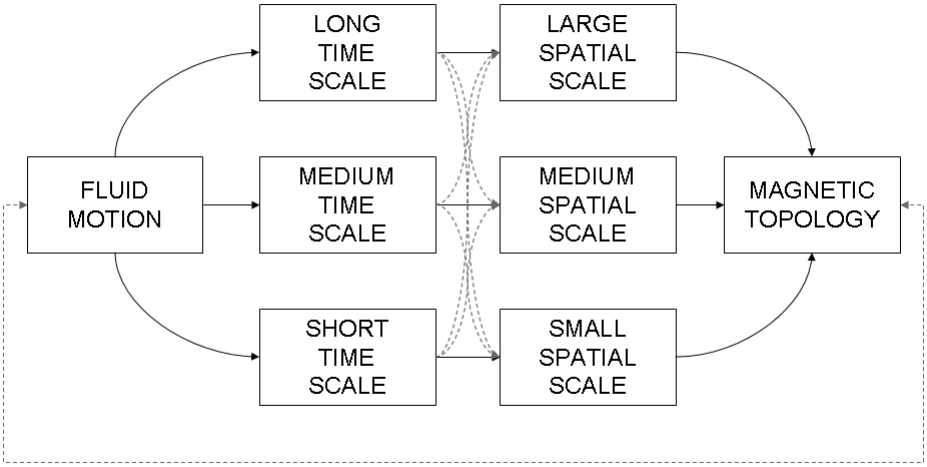

Fig. 4. The Sun as a chaotic plasma system

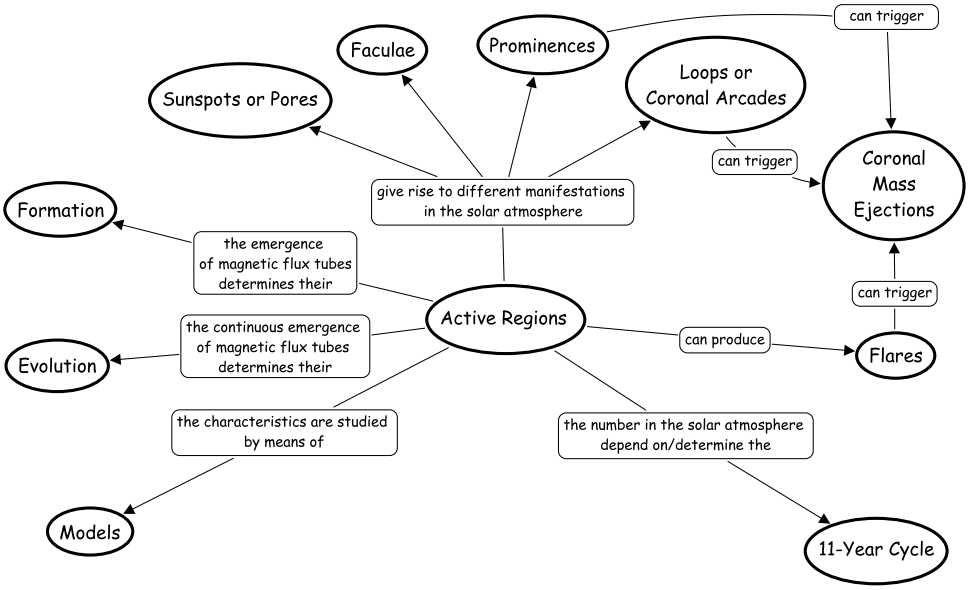

Fig. 5. Synopsis of active regions

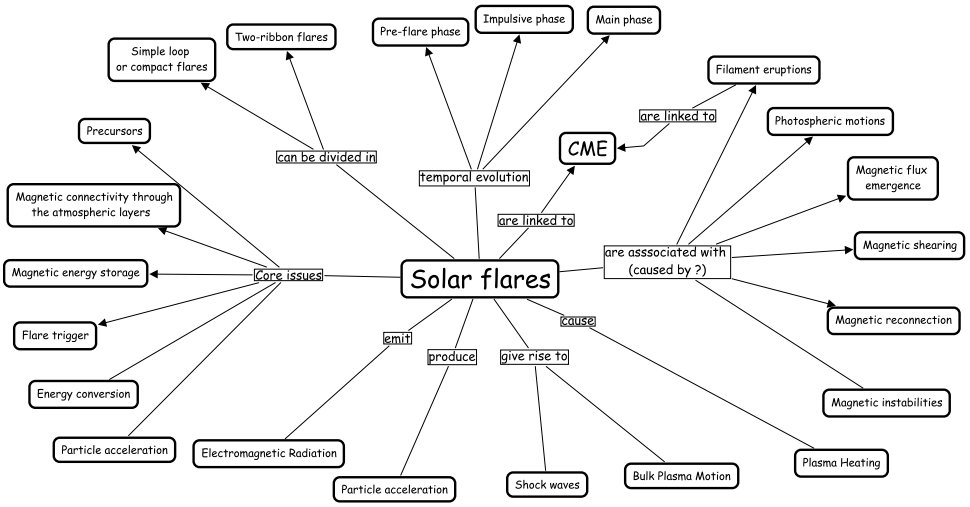

Fig. 6. Synopsis of solar flares

where $\mathbf{A}\epsilon\mathbb{R}^n$, $\mathbf{s}\epsilon\mathbb{R}^3$ is a spatial variable, $t\epsilon\mathbb{R}^1$ is a time variable, and $\mathbf{E}\epsilon\mathbb{R}^n$ is an energy variable.

In such a case, a descriptor is named ”index”, whereas it is named ”proxy” when it has no direct relationship with the considered observable but it is instead inferred from other observables which have a tight or a loose physical coupling with the considered one.

An Active Region can be characterized via a Morphology Descriptor M:

$$M = M(x, y, z) \tag{2}$$

and via a Magnetic Descriptor $\boldsymbol{M}$

$$\boldsymbol{M} = \boldsymbol{M}(x, y, z) \tag{3}$$

which lead to a classification based on a defined set of variation ranges.

The evolution of an AR is characterized by the time evolution of the above descriptors, which has to be interpreted according to a formation process model:

$$\begin{aligned} M &= M(x, y, z; t) \\ \boldsymbol{M} &= \boldsymbol{M}(x, y, z; t) \end{aligned} \tag{4}$$

Similarly, its geoeffectivity potentiality in terms of capability to generate or to trigger geoeffective events can be estimated by the time evolution of the descriptors. In particular, assuming a formation process and taking into account specific observations, a relevant precursor framework can be identified.

The inadequacy of global descriptors appears evident when considering the chaotic nature of the underpinning processes which greatly expand the complexity of the behaviour of the Sun as a complex physical system. Hence more refined analyses and mathematical descriptions of the physics are needed to improve the understanding and the prediction reliability.

3 Advanced Analysis and Prediction Techniques

The non-linearity and chaotic nature of solar magnetic activity make the use of intelligent hybrid system very powerful (Lundstedt, 2006).

Solar magnetic activity is interpreted in terms of the interplay between the solar plasma flow vector (V) and the solar magnetic field vector (B). Solar magnetic activity is then described using both mathematical and physical concepts. The two descriptions will then be integrated into a hybrid neural network. The concepts and relations are illustrated in a concept map (C-Map) (e.g. Messerotti, 2002) (Fig. 7).

Two examples of predictions based on observations of the plasma flow and the magnetic field are presented in the following sections.

3.1 Solar Flares and Subsurface Flows

A significant correlation between strong plasma downflows and high magnetic activity, indicated by strong solar flares, was found in Jensen et al. (2004) (Fig. 8). A neural network was trained to predict an event of at least one major solar flare based on maps of subsurface flows. The predictions were promising, despite the lack of a large input dataset (Jensen et al., 2004). Such large dataset and near-real time maps will become available from both Global Oscillation Network Group (GONG) and will come shortly from SDO (Solar Dynamics Observatory).

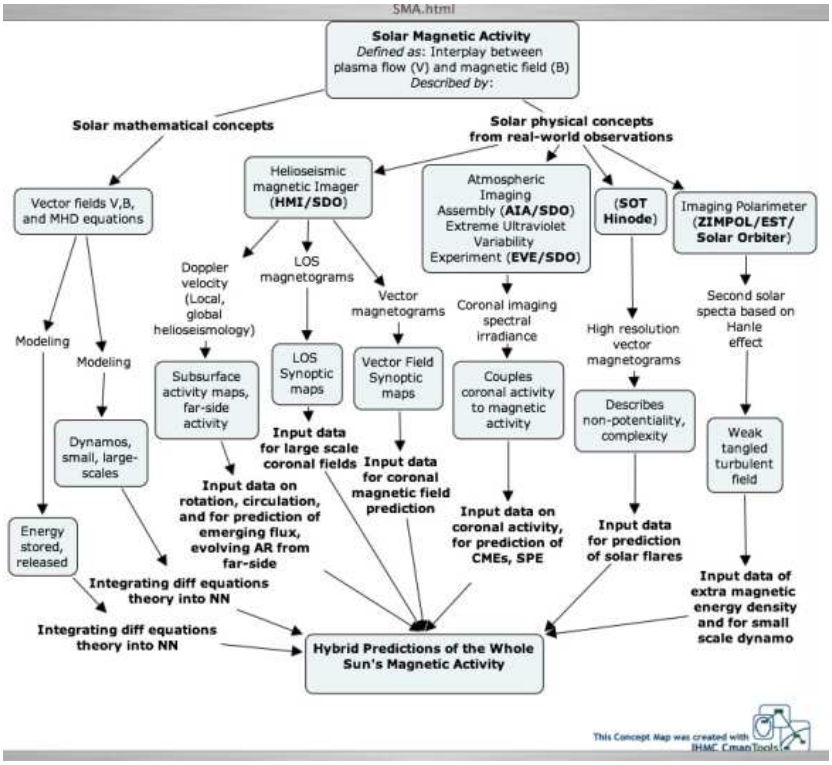

Fig. 7. C-Map of solar magnetic activity and its predictions.

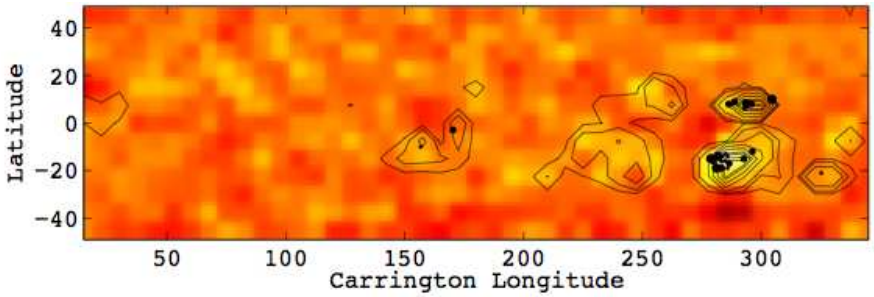

Fig. 8. The synoptic map shows the divergence of the observed flows at a depth of 4.6Mm. Bright regions represent inflow and dark outflow. The contour lines show the magnitude of magnetic field strength. The size of the dots indicate flare from small C, medium M and large X. The synoptic map shows Carrington rotation 2009, i.e. during the Halloween event 2003.

3.2 Magnetic Activity Years Ahead

Solar synoptic maps provide an important visualization of global patterns. Maps are available of sub-surface flows, photospheric and coronal magnetic fields. In Lundstedt et al. (2006) we averaged longitudinally synoptic maps from Wilcox Solar Observatory (WSO) at Stanford. The data cover three cycles from 1976 up to present. The averaged map is shown in Fig. 9. Many interesting features are visible: The variation of the Butterfly diagrams, the transport of flux to the poles, and the asymmetry for the both hemispheres.

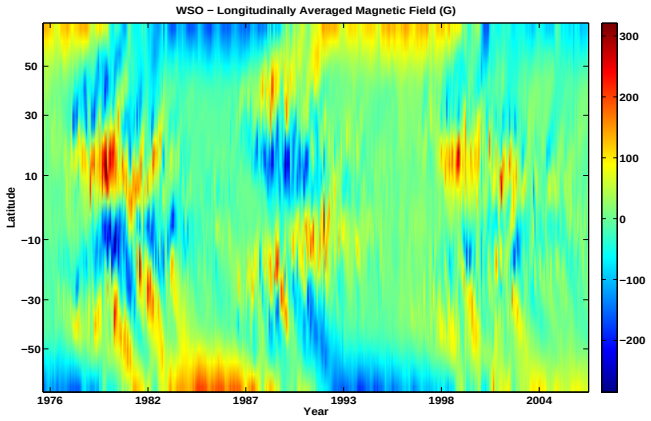

Fig. 9. Longitudinally averaged synoptic magnetic fields.

Neural networks have been trained, based on data from the longitudinally averaged synoptic map, to predict the total magnetic flux Carrington rotations ahead. A correlation coefficient of 0.82 was reached between the predicted and observed values two years ahead (Lundstedt et al., 2006). Similar studies are planned using SDO data.

4 Classification of Solar models

All our knowledge about the Sun is resumed by models, which try to describe the several phenomena which involve our star. Among the models we can distinguish various levels, or orders, depending on the scale considered and on the depth of the physical description of the phenomena analyzed (see Fig. 10).

In this scenario, the zero order model is represented by the Solar Standard Model (SSM), describing the structure of the solar interior, not directly accessible through the analysis of the electromagnetic radiation, due to the high plasma opacity (see, e.g., Christensen-Dalsgaard et al. (1996); Bahcall et al. (2001)) .

In the last years, the Solar Standard Model has been clearly confirmed by the analysis of the helioseismic data (Gough et al. (1996); Kosovichev et al. (1997)).

First order models can be considered those concerning the Solar Interior, the Quiet Atmosphere, the Interaction between the physics of Magnetic Field and the Solar Plasma.

Models concerning the Solar Interior can be divided in those concerning the nuclear reactions (EM emission, solar neutrinos (Cleveland et al. (1998); Fukuda et al. (1999); Ahmad et al. (2001), Bahcall et al. (2001); Ahmad et al. (2002); Bandyopadhyay et al. (2002); Bahcall et al. (2003), etc.), the oscillations (causality, modality, detectability) (Leightonet al. (1962); Ulrich (1970); Leibacher and Stein (1971); Deubner (1975); Ando and Osaki (1975); Antia et al. (1982); Unno et al. (1989); Christensen-Dalsgaard and Berthomieu (1991); Gough et al. (1996); Kosovichev et al. (1997)), the solar rotation (rotation as a function of the solar radius, differential rotation, meridional flows, interaction between rotation and convection)(Skumanich (1972); Gilman and Miller (1986); Glatzmaier (1987); Brummell et al. (1998); MacGregor and Charbonneau (1994); Hathaway et al. (1996); Thompson et al. (1996); Schou et al. (1998)), and the convection (mixing length, giant cells, supergranules, granules).

Models concerning the Solar Atmosphere divide in those concerning the quiet atmosphere (density, pressure and temperature stratification), the granulation, the photospheric turbulence, the chromospheric and coronal heating, and the coronal expansion into the interplanetary space to form the heliosphere.

Models concerning the Interaction between Magnetic Field and Solar Plasma divide in those concerning solar dynamo (change in the magnetic field configuration from poloidal to toroidal and reverse (see, e.g. Cowling (1933); Parker (1955); Babcock (1961); Steenbeck and Krause (1969); Yoshimura (1975); Stix (1976); Krause and Radler (1980); Stix (1991)), active region formation and evolution, loop stability and heating, eruptive phenomena (flares, CME), solar wind modulation and acceleration and so on.

More detailed models are second order models, like for instance those concerning waves formation and dissipation, magnetic field configuration (and extrapolation), flux tube emergence (e.g. Moreno-Insertis (1986); Choudhuri and Gilman (1987); Fan et al. (1993); Schussler et al. (1994); Caligari et al. (1995); Fischer et al. (2000)), magnetic reconnection, magnetic helicity, coronal loops.

Finally, the most sophisticated models, that are third order models. Among these models, we remember those concerning the configuration of magnetic field (potential, linear force-free, non-linear force-free, non force-free magnetic field), slender flux tube model (one-dimensional approximation), Ω-loop (two- or three- dimensional approach, see Fig. 11), loop models (static, stationary, MHD), magnetic reconnection modeling, magnetic helicity input, magnetic breakout and internal reconnection models, chromospheric evaporation, and so on.

Among all these models, those relevant to activity phenomena are especially important when we want to attempt to predict solar activity and its effect on Space Weather.

In this context, we will describe the principal phenomena related to solar activity, regarding them both as individual phenomena, as well as a whole when the activity cycle is concerned. This description will be performed, for each topic, by reviewing the observational main characteristics, the main open questions and the available models; moreover, when appropriate, also the information on the relevant data sets will be given.

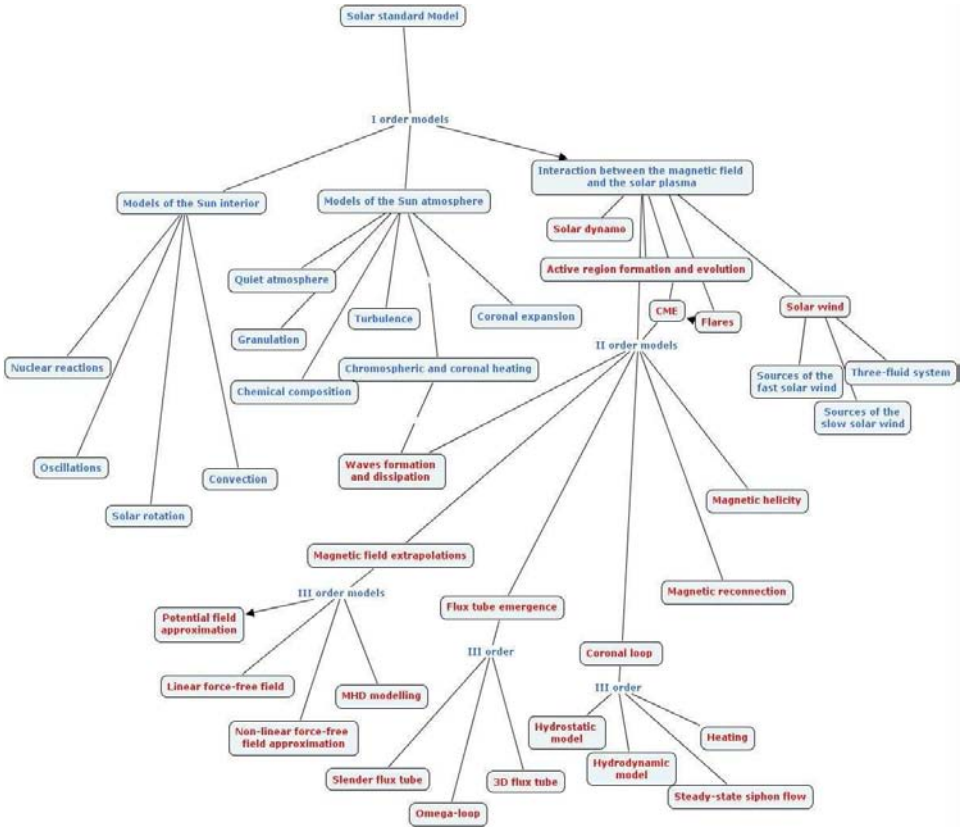

Fig. 10. Models classification.

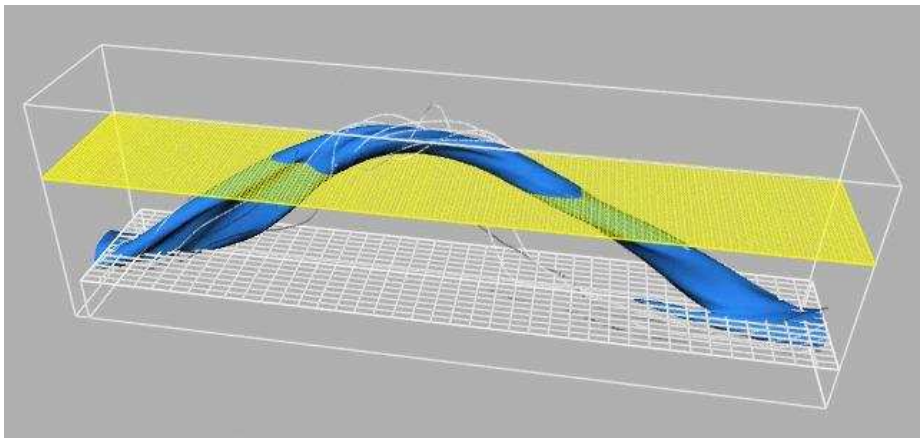

Fig. 11. Simulation of a twisted flux tube crossing the photosphere.

5 Phenomena Related to the Emergence of Magnetic Flux in the Solar Atmosphere

It is now established that the emergence of bundles of magnetic flux tubes in the solar atmosphere is at the basis of active regions (AR) formation.

During the first phases of active region formation, many physical processes are at work: magnetic coalescence, arch filament system (AFS) formation (see Fig. 12), plasma downflows along the rising flux tubes, decreasing upward velocities of the magnetic flux tubes, magnetic reconnection between the rising flux tubes and the ambient magnetic field lines.

As deeply reviewed by van Driel (2002), the scenario of the emergence of active regions is very complex. It is now established that the appearance of active regions on the Sun is due to the emergence of magnetic flux tubes from subphotospheric layers. More precisely, observations seem to indicate that active regions form due the emergence of several small (radius 200 Km), intense (500 G, 1018 Mx) flux tubes, which are separate during the first phase of their appearance, but that soon cluster to 2-4 103 G over 100 Km (Fragos et al., 2004), and references therein). The flux tubes clustering tendency takes place until new magnetic flux emerges from subphotospheric layers and vanishes as soon as their emergence ceases (Zwaan, 1985). For the first evolutionary phases of an active region the following scenario emerged:

- It is observed an increase of magnetic flux ($\sim 10^{20} - 10^{21}$ Mx) in photosphere.
- Hot (bright) EUV and X-ray loops form.
- A compact bipolar plage appears in the H_α and K CaII lines, which expands.
- Connecting the outer edges of the plage of opposite magnetic polarity, an Arch Filament System (AFS) appears in H_α, which is formed by a bundle of dark arches. The AFS arches show a rising velocity at their tops of $\sim$ 10 - 20 km s^{-1} and downflows at their endpoints of 10 -50 km s^{-1}. The individual arches have lengths of 1 - 3 $\times 10^4$ km and a lifetime of the order of $\sim$ 20 - 30 min; the AFS exists as long as magnetic flux is emerging.
- In the emergence site structure on little scale ($\sim 10^3$ km) appear, which indicate the emergence of undulatory flux tubes (sea-serpent topology) (Strous & Zwaan, 1999).
- Under the hot coronal and cool chromospheric loops (AFS) the granulation looks fuzzy in the photosphere. Between the forming flux concentrations (pores and spots) dark intergranular lanes (dark alignments) appear, along which upflow is observed, while at the ends bright facular grains are coupled with a downflow (Strous & Zwaan, 1999). The individual lane alignments appear where the tops of magnetic flux tubes are crossing the photosphere and they last for 10-30 minutes.
- Above sunspots and pores strong chromospheric and photospheric downflow is observed ($\sim$ 2 km s^{-1}), indicating that convective collapse is taking place, increasing the magnetic field strength from 500 - 600 G to 1500 G (Zwaan, 1985).
- At the beginning of the flux emergence (on the first day) there is no single magnetic inversion line, but individual flux emergence events appear all over the active region, small bipoles of $\sim$ 2000 km (Wang & Zirin, 1992; Bernasconi et al., 2002). These flux emergence sites may be recurrent and they may appear with a wave-like regularity (Strous & Zwaan, 1999).
- In general, opposite polarities become almost separated after 24 hours (Wang & Zirin, 1992).

- Magnetic flux elements move and merge (coalescence) to form pores and sunspots at the outer edges of the emerging flux region (EFR). The bipoles move apart fast at first (v = 2 km s^{-1} during the first half hour), then during the next six hours they diverge with a speed of v = 0.7 - 1.3 km s^{-1}. Pores and sunspots of the same polarity, but formed by different EFR, may merge forming a single sunspot (Zwaan, 1985).
- Facular motions, emergence locations, flux emergence events (FEE), their subsequent footpoint motions, H_α AFS, EUV and X-ray loops, all line up in the same direction (Strous & Zwaan, 1999).
- The orientation of the bipole may be arbitrary at first, but generally in 1-3 days it becomes almost parallel to the equator (Joy's law), having a latitude-dependent inclination of few degrees with the leading polarity closer to the equator.
- When a single bipole is emerging, we see a divergence of opposite polarity spots. Normally, preceding (p) spots move faster westward ($\sim$ 1 km s^{-1}) than their following (f) counterparts eastward.

Moreover, there are still several open questions: it is impossible at this moment to forecast if the emergence of flux tubes will cause the formation of a fully evolved active region or it will give rise to the formation of an active region which will disappear after a short time (hours, days). It is still unclear what causes the different complexity of active regions and why some active regions are more flare-productive than others.

Very recent observations of emerging active regions have given new insights on the knowledge of physical phenomena occurring during this phase (see, e.g. Spadaro et al. (2004), Zuccarello et al. (2005)). In this framework, it is worthwhile to report the results obtained by these authors. These researches were carried out with the aim to distinguish, since the initial phases of magnetic flux emergence, whether the new forming region would have been characterized by a short or a long lifetime.

The common features observed in both long-lived and short-lived active regions are: 1) the first signatures of these ARs emergence are initially observed in the outer atmospheric layers (transition region and corona) and later on (i.e. with a time delay of 6 - 7 h) in chromosphere; 2) the ARs appearance in the outer atmospheric layers seems to be synchronous with the sudden increase of magnetic flux in photosphere; 3) the loops of the AFS observed in chromosphere are characterized by a decreasing upward motion during the AR's lifetime; 4) the downward plasma motion in the AFS loop legs is asymmetrical. The differences observed between the long-lived and short-lived active regions are: 1) the short-lived AR appearance in photosphere is almost synchronous with that in chromosphere, while there is a time delay of $\sim$ 8 hours between the long-lived AR appearance in chromosphere and photosphere; 2) during the AR formation the magnetic flux increases by about one order of magnitude in the long-lived AR and by only a factor 2 in the short-lived AR; 3) the displacement of the center of symmetry of each polarity in the short-lived AR is mainly directed westward, while it is diverging from the neutral line in the recurrent AR; 4) in the short-lived AR the higher plasma downflow is measured in the preceding leg, while in the long-lived AR it is observed in the following leg.

5.1 Ephemeral Regions and Quiet Sun

Active regions are not the only features associated to the photospheric magnetic field. Quiet network contains small-scale, short-lived bipolar magnetic regions, referred to as ephemeral regions. These are magnetic bipolar regions with magnetic fluxes of $\sim 10^{19}$ Mx and typical size of 10 Mm, recognized and studied for many years (Harvey (1993)). These features are called "active ephemeral regions" due to their lifetime, i.e. the time they can be recognized as bipolar structures: first estimation of lifetime was of the order of the day (Harvey and Martin, 1973), from which the term "ephemeral", short-lived. Now, uninterrupted high resolution observations allow us to follow the emergence and evolution of such ephemeral regions in sufficient detail to determine the fate of the emerging flux. The Michelson Doppler Imager (MDI) on *SOHO* has revealed ephemeral regions with typical fluxes of 3×10^{18} Mx and average fields of 50 Gauss (Schrijver et al., 1997).

These bipolar regions emerge near the center of supergranules, their footpoints move fast apart and separate of ~ 7000 km in about half an hour. Recent estimations show that the average lifetime of ephemeral regions spans from 8 to 16 hours (Hagenaar et al., 2003). For what concerns the evolution and the decay of ephemeral regions, it has been noticed that after the first half an hour, the speed of separation of the footpoints drops down to ~ 0.4 km/s. Harvey and Zwaan (1993) showed that ephemeral regions decay in a complex way, and they are strongly biased by the surrounding magnetic network. Their decay appears as the result of expanding newly emerged ephemeral regions, of their absorption by existing network, of intrusion of magnetic elements of the network, and of the vanish of little flux concentrations of opposite polarity (magnetic cancelation).

Ephemeral regions are believed to have a common origin with active regions in the global dynamo (Harvey and Zwaan, 1993), but it is also thought that they are generated locally everywhere by turbulent convection near the surface (Nordlund et al., 1992). A third way involves both the global dynamo and flux processing in the convective envelope: magnetic flux merged in active region can be recycled and emerge newly in ephemeral regions, due to meridional motions (Nordlund et al., 1992). Their origin remains rather speculative: it is also possible that globally operating cyclic dynamo and small-scale dynamo are two distinct, but coupled, sources of solar bipolar regions.

Magnetic regions with flux $\approx 10^{19} - 10^{20}$ Mx vary their frequency of emergence during the solar sunspot cycle with a flux-independent factor (~ 2), while for regions with flux $< 10^{19}$ Mx frequency varies very weakly, in opposite phase with respect to sunspot cycle. Regions with magnetic flux lower than 10^{19} Mx also show a wide scatter in latitude, however avoiding latitudes of active regions, and do not appear to have a preferential orientation of bipole axis (Hagenaar et al. 2003). The value of total magnetic flux is very important to determine the original cluster of each ephemeral region, its statistical behavior (e.g. agreement with Joy's and Hale's laws, and comparison with butterfly diagram) and to investigate about the effective origin of these features.

Theoretical models approach the treatment of the ephemeral regions from two points of view. The first approach, concerning the analysis of the emergence of magnetic flux tubes, consider ephemeral regions as an efficient tool to test MHD-simulation codes, since it is obviously more simple building a simulation of a single magnetic flux tube which rises and forms a

small bipole than the emergence of a complex nested active region, and it is easier to compare the results of models with observations.

On the other hand, for what concerns the total balance of magnetic flux on solar surface and its dynamics, properties of ephemeral regions can help to better understand the mechanism of solar dynamo. This means to include local, small-scale processes on the Sun, in order to match a detailed knowledge of the phenomena involved with solar dynamo and to shed some more light on the stellar magnetism.

5.2 Active Regions: Sunspots

The most striking evidence of the solar activity is undoubtedly represented by sunspots. A very wide review about this phenomenon is given by Solanki (2003). These dark magnetic features visible in the solar photosphere possess a bipolar structure, usually with two main concentrations of magnetic flux of opposite polarity, aligned nearly in east-west direction on solar surface, in agreement with Joy's law. The problem of what causes the cooling of the sunspot umbra is a longstanding debate in the solar community.

As referred by van Driel (2002), big and complex active regions are often formed by the coalescence of several ephemeral regions which emerge separately into the photosphere, but that are spatially and temporally close within a few days (Schrijver and Zwaan, 2000). Harvey and Zwaan (1993) found an interval of $4 - 5$ days between subsequent emergences of bipolar flux, while Harvey and Zwaan (1993) found an emergence rate 22 times higher within active regions than elsewhere, confirming previous results. This trend of the regions of emerging flux to appear almost in the same locations involves the physics of tachocline, but it is also related to the origin of ephemeral regions.

5.3 Coronal loops

Coronal loops are the building blocks of the confined corona. They appear in the quiet or active areas as bright, arch-shaped structures, connecting regions with locally intensified magnetic fields of opposite polarities. They are hot (10^6 K) and have a thin transition to the chromosphere (10^4 K) near their footpoints (see Fig. 13). Each loop is dynamically and thermally insulated from the other loops and can be described as an independent region.

At present, we still do not know what are the detailed profiles of the plasma temperature, density and flow along these magnetic structures, particularly close to the loop footpoints and what is their behaviour as a function of time. It would also be important to clarify if coronal loops can be described as single monolithic structures, or as collections of hundreds or thousands of unresolved strands, each with its own independent dynamics, and to understand where and how the heating deposition occurs in the loop plasma.

Several authors state that at the basis of the heating of coronal loops there can be the so-called AC mechanism, whose associated time-scale is shorter than the typical dynamic timescale: it is due to dissipation of Alfvén waves generated either by global loop oscillations, or by impulsive phenomena. The problem is how to move the wave energy to sufficiently small scales to be efficiently dissipated, like in resonant absorption or phase mixing. It has been noticed that the presence of chaotic field lines increases the efficiency of this mechanism.

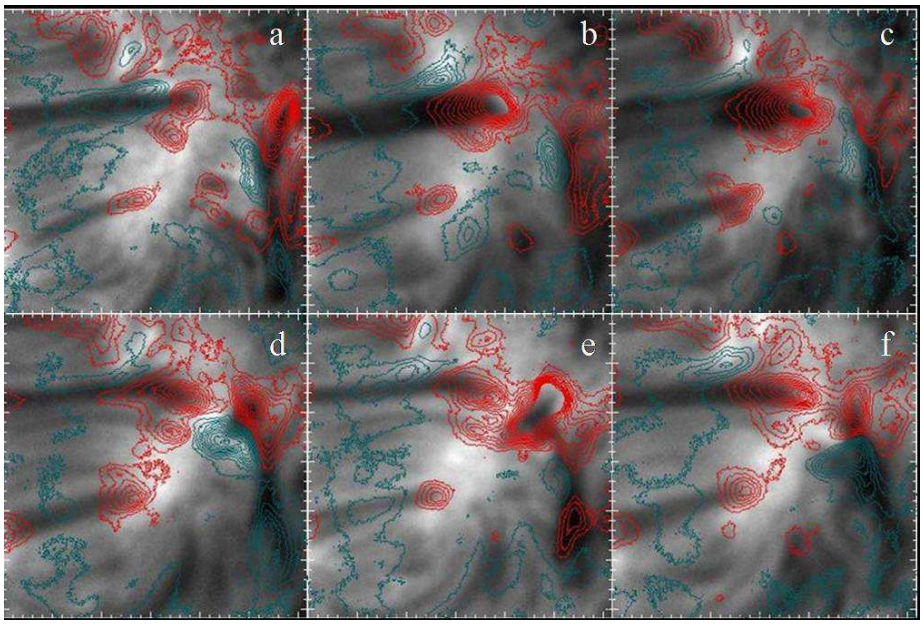

Fig. 12. Sequence of images, acquired by THEMIS telescope along the profile of Hα line, showing the emergence of an AFS. Red contours indicate downflows, blue contours upflows.

Fig. 13. Loops in the corona (image acquired by TRACE at 171 Å).

There is another proposed mechanism to explain the heating: it is the so-called DC mechanism or microflare heating. In this view, the heating is due to the motions of the photospheric footpoints of magnetic field lines which are continuously shuffled around by convective motions. These motions may lead to the formation of tangential discontinuities or current sheets in the corona where energy can be dissipated through magnetic reconnection. This process would work in two phases: a primary energy release at coronal level and a secondary one at chromospheric level, called chromospheric evaporation.

The main open questions concerning this topic are: where is actually acting the process of heating: is it localized in small parts of the loops or spread on a large part of them; is it deposited at the footpoints or higher in the coronal part of the loop ? Further, we still ignore if the heating is transient or continuous, impulsive or gradual.

6 Solar Weather Phenomena

6.1 Solar Flares

A solar flare is a sudden release of energy, from 10^{23} erg in nanoflares to 10^{32} erg in large two-ribbon flares, with a time-scale of rise of a few minutes; it is localized, with a length-scale $\ell \sim 10^6 \div 10^8$ m, during which magnetic energy is converted into radiation across the entire electromagnetic spectrum, heating, particle acceleration and mass motions.

Solar flares are the most powerful explosions in the solar system. Radiation and particle emitted during flares may strongly interact with Earth ionosphere and magnetosphere.

Despite the remarkable step forwards made in the last decades, there are still many obscure points. They represent an optimal tool to understand the several physical processes involved in magnetic reconnection.

We usually distinguish two typologies of solar flare. Compact or simple-loop flares are characterized by $\ell \sim 10^6 - 10^7$ m, electron density $n_e \sim 10^{17} - 10^{18}$ m^{-3}, and total energy $E_{tot} \sim 10^{29} - 10^{31}$ erg. They generally occur in single loops whose shape and volume do not change significantly during the flare and do not present particle emission.

Two-ribbon flares occur in arcades and show two areas of emission on both sides of the magnetic inversion line. The strands separate at $\sim 5 - 20$ km/s while the filament lying between them rises higher and higher in the corona.

A lot of questions interest people involved in flare studies. It is important to determine what is the magnetic configuration in the pre-flare phase, by recognizing observational signatures such as for instance non-potential configurations in sheared magnetic fields and sheared structures in the corona, as the sigmoids, or canceling magnetic features occurring during the filament activation phase. We still do not know the exact way in which energy is released and how the complex magnetic configuration becomes unstable and the flare is triggered.

The main imputed is magnetic reconnection, which may be caused by several phenomena, like emerging flux tubes, which causes loop interactions and filament eruption. It seems that the energy is released in corona, but the site of the energy release, i.e. the current sheet, is expected to have dimensions ($\sim 10^2 - 10^3$ m) much lower than the spatial resolution, therefore the identification is indirect, e.g. by means of the observations of cusps, in-falling dark blobs, inflows. Finally, it is unclear what happens after the energy is released. We do

not know what fraction goes into heating, particle acceleration, and mass motions, and which effects are directly related to the energy release itself and with the subsequent transport effects.

6.2 Coronal Mass Ejections

Coronal mass ejections (CME) are ejections of $\sim 10^{15} - 10^{16}$ g of mass from the Sun. They are often associated with flares and eruptive prominences and the mass is ejected with a speed between $100 - 2700$ km/s. The occurrence rate varies with the 11-year cycle: from 1 a day at minimum to 6 a day at maximum of solar activity cycle.

A CME is a three-part structure, with a circular front surrounding a dark region, called cavity, with inside a core of a bright, erupting prominence. An example is shown in Fig. 14.

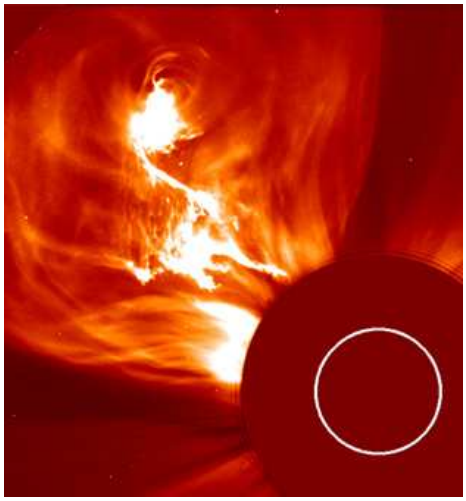

Fig. 14. An image of a CME as seen by SOHO/LASCO.

A CME can be due to the disruption of balance between the upward pressure of the strongly sheared large-scale magnetic field and the downward force due either to the magnetic tension or to the weight of an overlying mass distribution. There are a few of possible mechanisms which can explain the formation of CME. Magnetic breakout could occur when the tension is removed by reconnection of overlying and neighboring magnetic field lines. On the other hand, flux rope models suggest that magnetic reconnection could occur below the filament. It can also act the mechanism of mass loading, which is due to magnetic buoyancy which leads to the collapse of the overlying mass.

Recent works have contributed to understand some mechanisms acting during these phenomena (see, e.g. Aschwanden et al. (2007); Bothmer (2006a); Bothmer (2006b); Bothmer and Daglis (2006); Bothmer and Hady (2006); Bothmer and Tripathy (2006); Bothmer and Tripathy (2007); Cremades et al. (2005); Cremades et al. (2006); Forsyth et al. (2006); Howard et al. (2007); Huttunen et al. (2005); Mc Comas et al. (2007); Panasenco et al. (2005); Tripathy et al. (2005); Veselovsky et al. (2005); Wimmer-Schweingruber et al. (2006))

Still, at present, we do not know how CME are initiated and how they evolve. We should investigate if there are different mechanisms which accelerate fast, with uniform or decelerating speed, and gradual, with accelerating speed, CME. Further, we have to know if the coronal dimming is due to density depletion or to temperature variations, and how coronal EIT waves are related to chromospheric Moreton waves.

6.3 Solar Wind

The fast solar wind, with a speed of ~ 800 km/s, has higher temperatures and lower densities than the slow solar wind (~ 400 km/s); it presents a 27-days periodicity, which indicates the origin in a localized solar source, such as a coronal hole. The interaction of the low latitude fast streams with the Earth magnetosphere causes a recurrent magnetic disturbance.

At solar minimum the fast wind at 800 km/s fills most of the heliosphere whereas the slow wind at 400 km/s is confined toward the low latitude regions. With increasing solar activity the slow wind becomes predominant and the heliosphere is more symmetric, with a highly variable solar wind speed. Observations have also shown that the helium abundance varies through the cycle, showing a correlation with wind speed.

At the basis of the corona the solar wind is emanating from regions along boundaries of the magnetic networks. The highest acceleration of the solar wind emanating from the polar coronal holes at solar minimum occurs between 1.6 and 2 solar radii.

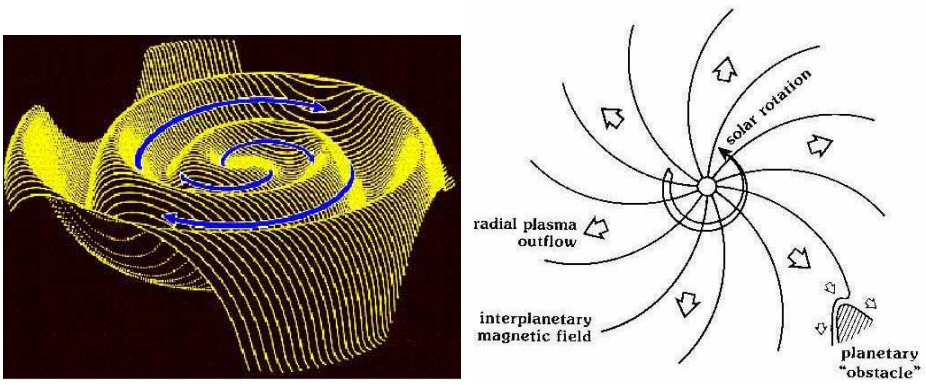

Fig. 15. On the left, an image of the neutral current sheet often called the "ballerina skirt". The Parker spiral is indicated by the arrows. Image is courtesy of J. Jokipii, University of Arizona. On the right, a representation of Parker spiral and its interactions with the interplanetary environment. Image is courtesy of J. G. Luhmann, Space Sciences Laboratory, University of California.

UVCS/SOHO has shown that the heavy ions move faster than protons and are more effectively accelerated across the magnetic field, as seen for the O VI. Elements with first potential ionization (FIP) lower than 10 eV appear to be more abundant, and it is possible that the magnetic field plays a still undiscovered role.

Observations show very small deviation from a Maxwellian distribution, indicating the presence of some dissipative mechanism favoring the isotropization: turbulence plays a central

role in re-distributing the energy from large to kinetic scales. In order to understand the heating and expansion of corona and the correlations with solar wind, the relevant processes must be traced throughout the solar atmosphere (analysis in the range from the visible to the X-ray domain).

The open question about this topic concerns the origin of the solar wind. We ignore what are the mechanisms that heat and accelerate the fast wind and where, within the coronal holes, the solar wind originates. Also, we have to understand where the slow wind is accelerated and what is the mechanism which accelerates it.

7 Mid- and Long-Term Solar Activity

The short-term solar activity, the so called solar weather, is modulated on mid- and long-terms. The mid-term modulation, or a periodicity of about 11 year, is the most well-known. However, long-term modulation of periodicities of about 90 years (Gleissberg cycle), 200 years (DeVries cycle) and about 2300 years (Hallstatt cycle) are also found.

7.1 Indicators of Mid- and Long-Term Solar Activity

The most often used indicator of mid-term solar activity is the sunspot number. The sunspot number R_z is defined as, $R_z = k(10g + s)$, where g is the number of sunspot groups, s the number of individual sunspots, and k a correction factor depending on the observer. The sunspot group number R_g is defined as, $R_g = (\frac{12.08}{n} \sum kG)$ (Hoyt and Schatten , 1998), where n is the number of observers, G the number of sunspot groups and k a correction factor. The group sunspot number is a manifestation of an east-west magnet produced by the stretching of an initial poloidal north-south field under the effect of a non uniform rotation.

During each cycle, the mean latitude of emergence of sunspots decreases as the cycle evolves. This behaviour is well represented by the butterfly diagram, which shows that at the beginning of a cycle sunspots appear at high latitudes, between 25° and 45°, while at the end of a cycle they appear at low latitudes, between 0° and 20°.

The sunspot number is also used as an indicator of long-term solar magnetic activity. At most, the sunspot number covers only 23 sunspot cycles. These cycles largely differ both in amplitude and length. During the so called Maunder Minimum (MM) 1645-1715, almost no sunspots were observed. Though the ^{14}C production showed about 11-year variations during the MM (Fig. 16) (Lundstedt et al. , 2006).

A non-linear chaotic dynamic system shows many similarities with the variation of the solar activity, indicated by the sunspot number. Tobias et al. (1997) managed to reproduce many of the features, with a low order differential system based on Lorenz equations.

7.2 Solar Dynamo

Cyclic evolution of solar magnetic fields is believed to be due to a dynamo process operating in the Sun. A dynamo is a process by which the magnetic field in an electrically conducting fluid is maintained against Ohmic dissipation. In the solar plasma there can also be various

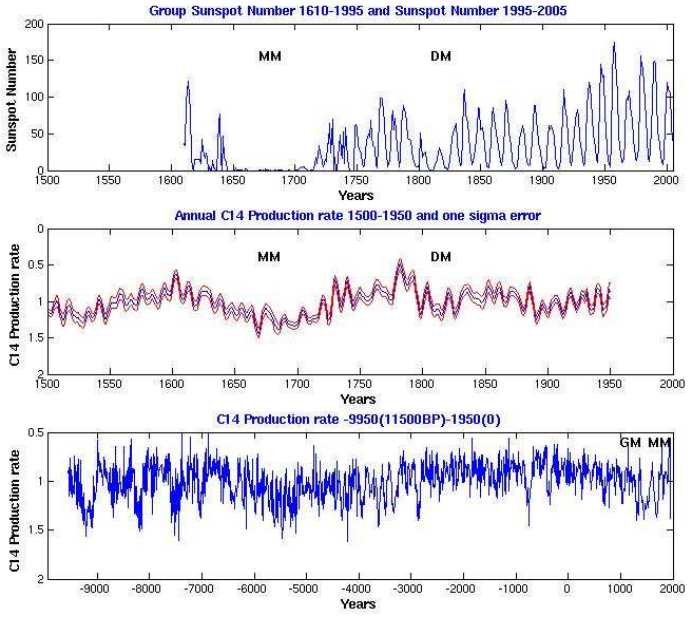

Fig. 16. The upper panel shows the group sunspot number R_G 1610-1995 and the sunspot number R_z 1995-2005. The middle panel shows the ^{14}C production rate 1500-1950. The lower panel shows the ^{14}C production rate 9950 BC to 1950AD. MM stands for Maunder Minimum, DM for Dalton Minimum and GM for Grand Maximum.

kinds of dynamo actions such as small-scale, turbulent dynamos as well as global growing, decaying or oscillatory dynamos. An extensive recent review is given by Ossendrijver (2003).

The solar dynamo continues to pose a challenge to observers and theoreticians. Recent high resolution observations of the solar surface reveal a magnetic field with a complex, hierarchical structure with widely different length-scales. In order to explain the magnetic phenomena, dynamo theory provides all the necessary ingredients including the alpha effect, magnetic field amplification by differential rotation, turbulent diffusion, magnetic pumping, flux storage, magnetic buoyancy, stochastic variations and nonlinear dynamics. By means of advances in helioseismology, observations of stellar magnetic fields and computational facilities, significant progresses have been made in our understanding of various aspects such as the role of the tachocline, convective plumes and magnetic helicity conservation.

First solar dynamo models were developed about the past half a century (Parker, 1955), and they evolved to accommodate observational constraints. The large-scale solar dynamo involves three basic processes: (i) the generation of toroidal fields by shearing the pre-existing poloidal fields by differential rotation (the Ω-effect); (ii) re-generation of poloidal fields by lifting and twisting the toroidal flux tubes (the α-effect); (iii) flux transport by meridional circulation. The third mechanism was introduced in order to explain the weak, diffuse fields outside the sunspots belts: this peculiar feature was not reproduced by any large-scale dynamo

model of pure α-Ω type. Incorporating a meridional circulation in each hemisphere, they have been constructed so-called flux-transport dynamos which success in reproducing many of features, as the full cycle period of $\sim$ 22 years, the field strength ($\sim$ 100kG) of toroidal field at the bottom of the convection zone, about a 10G polar field, the magnetic coupling between the North and South hemispheres, in agreement with Hale's polarity rule (Dikpati, 2004).

Other dynamo processes which seem to act in the Sun are described by local dynamo models. Local dynamo involves turbulence in the convection zone. In order to obtain a realistic description of the dynamo process, we have to include all physical aspects of solar convection that are judged to be necessary, such as compressibility, stratification, differential rotation, and the presence of an overshoot layer (Ossendrijver, 2003). This approach can explain the origin of small flux concentrations which are not affected by the 11-year activity cycle modulation (Hagenaar et al., 2003).

A number of question still remains unanswered: we do not understand why there are differences in the activity level in each solar cycle, what causes the different periodicities and the long minima periods, such as the Maunder Minimum, and why the IMF is slowly increasing in time. Also, they remain uncertainties about the nature of the deep-seated toroidal magnetic field and the alpha effect, and the forbidding range of length scales of the magnetic field and the flow have thus far prevented the formulation of a coherent model for the solar dynamo.

8 Conclusions

We provided some highlights about key topics in solar activity (SA) and solar weather modelling and predicting techniques with special attention to the most advanced approach, capable of partially coping with its complexity nature that is due to:

- Stochastic and chaotic character of nonlinearly-coupled plasma processes.
- Plasma processes occurrence at different temporal and spatial scales.
- Time-space-energy coupling among concurrent physical processes.

Hence a global model of SA is perhaps impossible to set up, as even localized phenomena occur as outcome of the evolution of the global complex plasma system. To date, the prediction success at all time and spatial scales is far from being satisfactory, but the forthcoming ground- and space-based high resolution observations can add fundamental tiles to the modelling framework as well as the application of advanced mathematical approaches.

One has to rely on the time series analysis of diachronic measurements of descriptors to improve the models for getting reliable forecasts, and to use advanced analysis and prediction techniques...

Acknowledgements: This work has been carried out in the framework of COST Action 724 WG1. MM acknowledges the support from the Italian Space Agency (ASI).

References

Ahmad, Q. R., Allen, R. C., Andersen, T. C., et al.: Measurement of the Rate of $\nu_e + d \rightarrow p + p + e^-$ Interactions Produced by ^8B Solar Neutrinos at the Sudbury Neutrino Observatory. Phys. Rev. Lett., **87**, 071301 (2001)

Ahmad, Q. R., Allen, R. C., Andersen, T. C., et al.: Direct Evidence for Neutrino Flavor Transformation from Neutral-Current Interactions in the Sudbury Neutrino Observatory. Phys. Rev. Lett., **89**, 271301 (2002)

Ando, H., Osaki, Y.: Nonadiabatic nonradial oscillations - an application to the five-minute oscillation of the Sun. PASJ, **27**, 581-603 (1975)

Antia, H. M., Chitre, S. M., Narasimha, D.: Overstability of acoustic modes and the solar five-minute oscillations. Solar Phys., **77**, 303-327 (1982)

Aschwanden, M., Antiochos, S.K., J.W. Cook, R.A. Howard, J.T. Karpen, J.A. Klimchuk, N.R. Sheeley, L.A. Fisk, T.I. Gombosi, N. Lugaz, W.I.V. Manchester, I.I. Roussev, T.H. Zurbuchen, L.F. Burlaga, M.L. Kaiser, C.K. Ng, D.V. Reames, M.J. Reiner, C.J. Farrugia, A. Galvin, M.A. Lee, J.A. linker, Z. Mikic, P. Riley, D. Alexander, A.W. Sandman, E. De Jong, P.C. Liewer, D. Odstrcil, V. Pizzo, J. Luhmann, B. Inhester, R.W. Schwenn, S. Solanki, V.M. Vasyliunas, T. Wiegelmann, J.-L.H. Bougeret, M. Maksimovich, J.-L. Steinberg, I.H. Cairns, P.A. Robinson, H. Kunow, R. Wimmer-Schweingruber, P.A. Lamy, A. Llebaria, P. Bochsler, V. Bothmer, K. Kecskemety, J. Kota, M. Scholer: Theoretical Modeling for the STEREO Mission, Space Sci. Rev., in press, (2007)

Babcock, H. W.: The Topology of the Sun's Magnetic Field and the 22-YEAR Cycle. Astrophys. Jour., **133**, 572-587 (1961)

Bahcall, J. N., Pinsonneault, M. P., Basu, S.: Solar Models: Current Epoch and Time Dependences, Neutrinos, and Helioseismological Properties. Astrophys. Jour., **555**, 990-1012 (2001)

Bahcall, J. N., Gonzalez-Garcia, M. C., Pena-Garay, C.: Solar Neutrinos Before and After KamLAND. J. High Ener. Phys., **02**, 009 (hep-ph/0212147) (2003)

Bandyopadhyay, A., Choubey, S., Gandhi, R., Goswami, S., Roy, D. P.: What Can SNO Neutral Current Rate Teach Us About the Solar Neutrino Anomaly. Modern Physics Letter A, **17**, 1455-1464 (2002)

Bernasconi, P. N., Rust, D. M., Georgoulis, M. K., Labonte, B. J.: Moving Dipolar Features in an Emerging Flux Region. Solar Phys. **209**, 119-139 (2002)

Bothmer, V.: The Solar Atmosphere and Space Weather. In Solar System Update, Eds. P. Bondel and J.W. Mason, Springer/Praxis, 1-53 (2006)

Bothmer, V.: The Sun as the prime source of space weather. In "Space Weather - Physics and Effects", Eds. V. Bothmer and Y. Daglis, Springer/Praxis, 31-102 (2006)

Bothmer, V., I.A. Daglis, Eds. "Space Weather - Physics and Effects", Springer/Praxis (2006)

Bothmer, V., A. Hady, Eds. "Solar Variability and its Magnetic Origin" (IAUS 233), Proceedings of the International Astronomical Union Symposia and Colloquia, Cambridge University Press (2006)

Bothmer, V., and Tripathi, D.: Photospheric field evolution in the source regions of coronal mass ejections, Proceedings of SOHO 17 "10 Years of SOHO and Beyond, ESA SP-617 (2006)

Bothmer, V., and Tripathi, D.: Evolution of the photospheric magnetic field in the source regions of coronal mass ejections, Modern Solar Facilities - Advanced Solar Science, F. Kneer, K. G. Puschmann, A. D. Wittmann (eds.), Universitätsverlag Göttingen, 257-260 (2007)

Brummell, N. H., Hurlburt, N. E., Toomre, J.: Turbulent Compressible Convection with Rotation. II. Mean Flows and Differential Rotation. Astrphys. Jour., **493**, 955-969 (1998)

Caligari, P., Moreno-Insertis, F., Schussler, M.: Emerging flux tubes in the solar convection zone. 1: Asymmetry, tilt, and emergence latitude. Astrophys. Jour., **441**, 886-902 (1995)

Choudhuri, A.R., Gilman, P. A.: The influence of the Coriolis force on flux tubes rising through the solar convection zone. Astrophys. Jour., **316**, 788-800 (1987)

Christensen-Dalsgaard, J., Berthomieu, G.: Theory of solar oscillations. In Solar interior & atmosphere, eds. A. N. Cox, W. C. Livingston and M. Matthews, Space Science Series (University of Arizona Press, Tucson) 401-478 (1991)

Christensen-Dalsgaard, J., Dappen, W., Ajukov, S. V., et al.: The Current State of Solar Modeling. Science, **272**, 1286-1292 (1996)

Cleveland, B. T., Daily, T., Davis, R., Jr., Distel, J. R., Lande, K., Lee, C. K., Wildenhain, P. S., Ullman, J.: Measurement of the Solar Electron Neutrino Flux with the Homestake Chlorine Detector. Astrophys. Jour., **496**, 505-526 (1998)

Cowling, T. G.: The magnetic field of sunspots. MNRAS, **94**, 39-48 (1933)

Cremades, H. and Bothmer, V.: Geometrical Properties of Coronal Mass Ejections. In Proc. IAU Symp. 226 on Coronal and Stellar Mass Ejections, eds. K.P. Dere, J. Wang, and Y. Yan, 48-54 (2005)

Cremades, H., V. Bothmer, D. Tripathi: Properties of Structured Coronal Mass Ejections in Solar Cycle 23, Adv. Space Res., **38**, 3, doi:10.1016/j.asr.2005.01.095, 461-465 (2006)

Démoulin, P., Priest, E. R.: How to Form a Dip in a Magnetic Field Before the Formation of a Solar Prominence. Lecture Notes in Phys., **363**, 269, Springer Berlin / Heidelberg (1990)

Deubner, F.-L.: Observations of low wavenumber nonradial eigenmodes of the Sun. Astron. Astrophys., **44**, 371-375 (1975)

Dikpati, M. 2004, in ASP Cont. Ser. 325: Solar Dynamo Models. In: The Solar-B Mission and the Forefront of Solar Physics, 37

Fan, Y., Fisher, G.H., DeLuca, E.E.: The origin of morphological asymmetries in bipolar active regions. Astrophys. Jour., **405**, 390-401 (1993)

Feynman, J., Gabriel, S.B.: Period and phase of the 88-year solar cycle and the Maunder minimum: Evidence for a chaotic sun, Solar Physics, **127**, 2, 303–403 (2004)

Fisher, G.H., Fan, Y., Longcope, D.W., Linton, M.G., Pevtsov, A.A.: The Solar Dynamo and Emerging Flux. Solar Phys., **192**, 119-139 (2000)

Forsyth, R.J., and Bothmer, V., Co-Chairs, Cid, C., Crooker, N.U., Horbury, T.S., Kecskemety, K., Klecker, B., Linker, J.A., Odstrcil, D., Reiner, M.J., Richardson, I.G., Rodriguez-Pacheco, J., Schmidt, J.M., Wimmer-Schweingruber, R.F., ICMEs in the inner heliosphere: Origin, evolution and propagation effects, Report of WG G, Space Sci. Rev., 383-416 (2006)

Fragos, T., Rantsiou, E., Vlahos, L.: On the distribution of magnetic energy storage in solar active regions. Astron. Astrophys., **420**, 719-728 (2004)

Fukuda, Y., Hayakawa, T., Ichihara, E., et al.: Constraints on Neutrino Oscillation Parameters from the Measurement of Day-Night Solar Neutrino Fluxes at Super-Kamiokande. Phys. Rev. Lett., **82**, 1810-1814 (1999)

Gilman, P. A., Miller, J.: Nonlinear convection of a compressible fluid in a rotating spherical shell. ApJS, **61**, 585-608 (1986)

Gough, D. O., Kosovichev, A. G., Toomre, J., et al.: The Seismic Structure of the Sun. Science, **272**, 1296-1300 (1996)

Glatzmaier, G. A.: A Review of What Numerical Simulations Tell Us About the Internal Rotation of the Sun. In The Internal Solar Angular Velocity, eds. B. R. Durney and S. Sofia (Reidel, Dordrecht), **137**, 263 (1987)

Hagenaar, H. J., Schrijver, C. J., Title, A. M.: The Properties of Small Magnetic Regions on the Solar Surface and the Implications for the Solar Dynamo(s). Astrophys. Jour., **584**, 1107-1119 (2003)

Harvey, K. L.: Magnetic dipoles on the Sun. PhD thesis, Astronomical Instistute, Utrecht University (1993)

Harvey, K. L., & Martin, S. F.: Ephemeral Active Regions. Solar Phys., **32**, 389-402 (1973)

Harvey, K. L., Zwaan, C.: Properties and emergence of bipolar active regions. Solar Phys., **148**, 85-118 (1993)

Hathaway, D. H., Gilman, P., Harvey, J. W., et al.: GONG Observations of Solar Surface Flows. Science, **272**, 1306-1309 (1996)

Howard, R.A., J.D. Moses, A. Vourlidas, J.S. Newmark, D.S. Socker, S.P. Plunkett, C.M. Korendyke, J. C. Cook, A. Hurley, J. M. Davila, W. T. Thompson, O.C. St Cyr, E. Mentzell, K. Mehalick, J.R. Lemen, J.P. Wuelser, D.W. Duncan, T.D. Tarbell, R. A. Harrison, N. R. Waltham, J. Lang, C.J. Davis, C.J. Eyles, J.P. Halain, J.M Defise, E. Mazy, P. Rochus, R, Mercier, M. F. Ravet, F. Delmotte, F. Auchere, J.P. Delaboudiniere, V. Bothmer, W. Deutsch, D. Wang, N. Rich, S. Cooper, V. Stephens, G. Maahs, R. Baugh, D. McMullin: Sun Earth Connection Coronal and Heliospheric Investigation (SECCHI). Space Sci. Rev., in press (2007)

Hoyt, D.V., and Schatten, K.: Group Sunspot Numbers: A New Solar Activity Reconstruction, Solar Physics, **181**, 491–512 (1998)

Huttunen, K.E.J., R. Schwenn, V. Bothmer, and H.E.J. Koskinen: Properties and geoeffectiveness of magnetic clouds in the rising, maximum and early declining phases of solar cycle 23. Annales Geophysicae, **23**, 1-17 (2005)

Jensen, J. M., Lundstedt, H., Thompson, M. J., Pijpers, F. P., Rajaguru, S. P.: Application of Local-Area Helioseismic Methods as Predictors of Space Weather, in Helio- and Asteroseismology: Towards a Golden Future, ed. D. Danesy, Proc. SOHO 14/GONG+ 2004 Meeting, ESA SP-559, 497–500 (2004)

Kippenhahn, R., Schluter, A.: Eine Theorie der solaren Filamente. Mit 7 Textabbildungen. Zeitschrift für Astrophysik, **43**, 36-72 (1957)

Kosovichev, A. G., Schou, J., Scherrer, P. H., et.al.: Structure and Rotation of the Solar Interior: Initial Results from the MDI Medium-L Program. Solar Phys., **170**, 43-61 (1997)

Krause, F., Radler, K. H.: Mean-field Magnetohydrodynamics and Dynamo Theory (Akademie-Verlag, Berlin) (1980)

Kuperus, M., Raadu, M. A.: The Support of Prominences Formed in Neutral Sheets. Astron. Astrophys., **31**, 189-193 (1974)

Lazarian, A., Vishnian, E.T., Cho, J.: Magnetic Field Structure and Stochastic Reconnection in a Partially Ionized Gas, Ap. J., **603**, 180–197 (2004)

Leibacher, J. W., Stein, R. F.: A New Description of the Solar Five-Minute Oscillation. Astrophys. Lett., **7**, 191-192

Leighton, R. B., R. W. Noyes, and G. W. Simon: Velocity Fields in the Solar Atmosphere. I. Preliminary Report. Astrophys. J., **135**, 474–499 (1962)

Lockwood, M., Stamper, R., Wild, M.N.: A Doubling of the Sun's Coronal Magnetic Field during the Last 100 Years, Nature, **399**, 437–439 (1999)

Lundstedt, H.: Solar activity modelled and forecasted: A new approach, Adv. Space Res., **38**, 862–867 (2006a)

Lundstedt, H., Liszka, L., Lundin, R., Muscheler,R.: Long-Term Solar Activity Explored with Wavelet Methods, Annal. Geophys., **24**, 1–9 (2006b)

MacGregor, K. B., and P. Charbonneau: Angular Momentum Evolution of Late-Type Stars: A Theoretical Perspective, in Cool Stars, Stellar Systems, and the Sun, ed. J.-P. Caillault, Astron. Soc. Pac. Conf. Ser., **64**, 174–186 (1994)

Mandal, A.S., Raychaudhuri, P.: A Proof of Chaotic Nature of the Sun through Neutrino Emission, Proc. 29th International Cosmic Ray Conference Pune, **9**, 123-126 (2005)

McComas, D.J., M. Velli, W.S. Lewis, L.W. Acton, M. Balat-Pichelin, V. Bothmer, R.B. Dirling, Jr., W.C. Feldman, G. Gloeckler, S.R. Habbal, D.M. Hassler, I. Mann, W.H. Matthaeus, R.L. McNutt, Jr.,R.A. Mewaldt, N. Murphy, L. Ofman, E.C. Sittler, Jr., C.W. Smith, T.H. Zurbuchen: Understanding coronal heating and solar wind acceleration: The case for near-Sun measurements. Rev. in Geophys., **45**, RG10004, 1-26 (2007)

Messerotti, M.: Solar Activity Monitoring. An Introduction to Solar Activity Features and Descriptors. In The Dynamic Sun, Proc. of the Summerschool and Workshop held at the Solar Observatory Kanzelhöhe, Kärnten, Austria, August 30 - September 10, 1999, eds. A. Hanslmeier, M. Messerotti and A. Veronig, Kluwer Academic Publishers, Dordrecht/Boston/London, Astrophysics and Space Science Library, **259**, 69 (2001)

Messerotti, M.: Embedding knowledge in scientific databases via concept maps as metadata. In Proc. "SOLSPA: The Second Solar Cycle and Space Weather Euroconference", Vico Equense, Italy, 24-29 September 2001, ESA SP-477, 607–610 (2002)

Moreno-Insertis, F.: Nonlinear time-evolution of kink-unstable magnetic flux tubes in the convective zone of the sun. Astron. Astrophys., **166**, 291–395 (1986)

Nordlund, A., A. Brandenburg, R. L. Jennings, M. Rieutord, J. Ruokolainen, R. F. Stein, and I. Tuominen: Dynamo action in stratified convection with overshoot. Astrophys. J., **392**, 647–652 (1992)

Ossendrijver, M.: The solar dynamo. Astron. Astrophys. Rev., **11**, 287–367 (2003)

Panasenco, O., I.S. Veselovsky, A.V. Dmitriev, A.N. Zhukov, O.S. Yakovchouk, I.A. Zhitnik, A.P. gnat'ev, S.V. Kuzin, A.A. Pertsov, V.A. Slemzin, S.I. Boldyrev, E.P. Romashets, A. Stepanov, O.I. Bugaenco, V. Bothmer, S. Koutchmy, A. Adjabshirizadeh, Z. Fazel, S. Sobhanian: Solar Origin of Intense Geomagnetic Storms in 2002 as seen by the CORONAS-F Satellite. Adv. Space Res., 1595-1603 (2005)

Parker, E. N.: Hydromagnetic Dynamo Models. Astrophys. J., **122**, 293–314 (1955)

Sakurai, T.: A New Approach to the Force-Free Field and Its Application to the Magnetic Field of Solar Active Regions. Publ. Astron. Soc. Japan, **31**, 209-230 (1979)

Schou, J., H. M. Antia, S. Basu, et al.: Helioseismic Studies of Differential Rotation in the Solar Envelope by the Solar Oscillations Investigation Using the Michelson Doppler Imager. Astrophys. J., **505**, 390–417 (1998)

Schrijver, C. J., A. M. Title, A. A. van Ballegooijen, and R. A. Shine, Sustaining the Quiet Photospheric Network: The Balance of Flux Emergence, Fragmentation, Merging, and Cancellation. Astrophys. J., **487**, 424–436 (1997)

Schrijver, C. J., and C. Zwaan: Solar and Stellar Magnetic Activity. (Cambridge: Cambridge University Press) (2000)

Schussler, M., P. Caligari, A. Ferriz-Mas, and F. Moreno-Insertis: F. Instability and eruption of magnetic flux tubes in the solar convection zone. Astron. Astrophys., **281**, L69–L72 (1994)

Skumanich, A.: Time Scales for CA II Emission Decay, Rotational Braking, and Lithium Depletion. Astrophys. J., **171**, 565–567 (1972)

Solanki, S. K.: Sunspots: An overview. Astron. Astrophys. Rev., **11**, 153–286 (2003)

Spadaro, D., S. Billotta, L. Contarino, P. Romano, and F. Zuccarello: AFS dynamic evolution during the emergence of an active region. Astron. Astrophys., **425**, 309–319 (2004)

Steele, C.D.C., Priest, E. R.: Thermal equilibria of coronal magnetic arcades. Solar Phys., **127**, 65-94 (1990)

Steenbeck, M., and F. Krause, F.: On the Dynamo Theory of Stellar and Planetary Magnetic Fields. I. AC Dynamos of Solar Type. Astron. Nachr., **291**, 49–84 (1969)

Stix, M.: Dynamo Theory and the Solar Cycle, in Basic Mechanisms of Solar Activity, IAU Symp. 71, eds. V. Bumba, J. Kleczek (D. Reidel, Dordrecht), 367–388 (1976)

Stix, M.: The Sun: An Introduction (Springer-Verlag, Berlin) (1991)

Strous, L.H., Zwaan, C.: Phenomena in an Emerging Active Region. II. Properties of the Dynamic Small-Scale Structure. Astrophysis. Jour., **527**, 435-444 (1999)

Thompson, M. J., J. Toomre, E. Anderson, et al.: Differential Rotation and Dynamics of the Solar Interior. Science, **272**, 1300–1305 (1996)

Tobias, S., Weiss, N.O., Kirk, V.: Chaotically modulated stellar dynamos, Mon. Not. R. Astron. Soc., **273**, 1150–1166 (1995)

Tripathi, D.K., V. Bothmer, S.K. Solanki, R. Schwenn, M. Mierla, and G. Stenborg: SoHO/EIT observation of a coronal inflow. In Proc. IAU Symposium 226 on Coronal and Stellar Mass Ejections, eds. K.P. Dere, J. Wang, and Y. Yan, 133-134 (2005)

Ulmschneider, P.: The Physics of Chromospheres and Coronae. Lectures on Solar Physics, Edited by H. M. Antia, A. Bhatnagar, P. Ulmschneider, **619**, 232-280 (2003)

Ulrich, R. K.: The Five-Minute Oscillations on the Solar Surface. Astrophys. J., **162**, 993–1002 (1970)

Unno, W., Y. Osaki, H. Ando, H. Saio, and H. Shibahashi: Nonradial Oscillations of Stars, 2nd ed. (University of Tokyo Press, Tokyo) (1989)

van Driel-Gesztelyi, L.: Emergence and loss of magnetic flux on the solar surface, in ESA SP-505: SOLMAG 2002. Proceedings of the Magnetic Coupling of the Solar Atmosphere Euroconference, 113–120 (2002)

Vernazza, J. E., Avrett, E. H., Loeser, R.: Structure of the solar chromosphere. III - Models of the EUV brightness components of the quiet-sun. Astrophys. Jour. Suppl. Ser., **45**, 635–725 (1981)

Veselovsky, I., Bothmer, V., Cargill, P., Dmitriev, A.V., Ivanov, K.G., Romashets, E., Zhukov, A.N., Yakovchouk, O.S.: Magnetic Storm Cessation During Sustained Northward IMF. Adv. Space Res., **36**, 2460-2464 (2005)

Wang, H., Zirin, H.: Flows around sunspots and pores. Solar Phys., **140**, 41-54 (1992)

Wimmer-Schweingruber, R.F., N. Crooker, A. Balogh, V. Bothmer, R.J. Forsyth, P. Gazis, J.T. Gosling, T. Horbury, A. Kilchenmann, I. Richardson, J. Richardson, P. Riley, L. Rodriguez, R. von Steiger, P. Wurz, T.H. Zurbuchen, Understanding interplanetary coronal mass ejection signatures, Space Sci. Rev., 177–21 (2006)

Yatsuyanagi, Y., Hatori, T., Kato, T.: Chaotic Reconnection Due to Fast Mixing of Vortex-Current Filaments, Progress of Theoretical Physics Suppl., **138**, 714–715 (2000)

Yoshimura, H.: Solar-cycle dynamo wave propagation. Astrophys. J., **201**, 740–748 (1975)

Zuccarello, F., V. Battiato, L. Contarino, P. Romano, D. Spadaro, and L. Vlahos: AFS dynamics in a short-lived active region. Astron. Astrophys., **442**, 661–671 (2005)

Zwaan, C.: The emergence of magnetic flux. Solar Phys., **100**, 397-414 (1985)

Emergence and evolution of active and ephemeral regions: comparison between observations and models

F. Zuccarello[1], S.L. Guglielmino[1], V. Battiato[2], L. Contarino[2], D. Spadaro[2] and P. Romano[2]

[1] Universitá di Catania, Dipartimento di Fisica e Astronomia, Sez. Astrofisica, Via S. Sofia 78, 95123, Catania, Italy fzu@oact.inaf.it
[2] INAF Osservatorio Astrofisico di Catania, Via S. Sofia 78, 95123, Catania, Italy

Summary. This work aims to describe some aspects relevant to the emergence of magnetic structures on the solar surface. Using high resolution photospheric and chromospheric data, the dynamics of rising flux tubes is studied. It is shown that, for both long-lived and short-lived magnetic regions, the flux tubes are initially characterized by a high rising velocity, which eventually decreases while the region develops. Other results concern the timeline of the active regions appearance in the atmospheric layers and the asymmetries in plasma downflows between preceding and following legs. These results are briefly discussed in the light of most recent models.

1 Introduction

It is now established that the emergence of bundles of magnetic flux tubes in the solar atmosphere is at the basis of active regions (AR) formation. During this phase many physical processes are at work: magnetic coalescence, arch filament system (AFS) formation, plasma downflows along the rising flux tubes, photospheric diverging motions of opposite polarities (see van Driel-Gesztelyi 2002 for a review).

However, there are still several open questions: it is impossible at the moment to forecast if the emergence of flux tubes will cause the formation of a fully evolved AR or it will give rise to the formation of an AR disappearing after a short time (hours, or few days). It is still unclear what causes the different complexity of ARs and why some ARs are more flare-productive than others. These questions are very important, since the appearance of new ARs strongly influences the variability of the total solar irradiance, which is related to climate changes on the Earth (Tuillier et al. 2006).

Moreover, ARs are not the only features associated to the photospheric magnetic field. The quiet Sun network cell centres contain small-scale, short-lived bipolar magnetic structures (with magnetic fluxes of $\sim 10^{18}$ Mx and typical size of 10 Mm), called *active ephemeral regions (ERs)* (Harvey & Martin 1973).

In this paper we report very recent results, on the emergence and evolution of ARs and ERs, obtained using high resolution data. We discuss these results in the framework of most recent models of magnetic flux tube emergence.

2 Observations

2.1 Recurrent active region

Spadaro et al. (2004) analyzed the first evolutionary phases of the recurrent AR NOAA 10050, using high resolution Hα (6562.808 Å), Fe I (5380.960 Å)and broad band images acquired by the THEMIS telescope during an observational campaign carried out in July 2002, coordinated with other instruments (INAF - Catania Astrophysical Observatory, TRACE, EIT/SOHO, MDI/SOHO). Their analysis indicates that the first evidence of the emerging AR is observed in the EIT bands (forming in the transition region and lower corona); later on the AR appears in Hα (chromosphere) and white light (photosphere) images, with a delay of $\sim$ 6 hours.

The magnetic flux shows a sudden increase, nearly simultaneous with the AR appearance in the transition region and lower corona. In the following 6 days a steep increase, from $\sim 2.5\times10^{22}$ Mx to approximately $\sim 1.5\times10^{23}$ Mx, is observed; subsequently the magnetic flux increase slows down, while an increasing magnetic flux difference between the two magnetic polarities is observed.

During the early phases of the NOAA 10050 development an AFS appeared: it was located between the two emerging polarities, and composed by tens of arches of length 14000 km, grouped in bundles, generally parallel to each other and perpendicular to the magnetic inversion line. This structure represents the observational evidence of an Ω-loop breaking through the photosphere, the fragmentation into nearly parallel strands indicating the difficulty encountered by the flux tube to cross the photosphere (van Driel-Gesztelyi 2002).

The Doppler analysis indicates that the arches of the AFS show an upward motion at their tops and downward motions at their extremities. The values of both downflow and upflow velocities decrease during the AR evolution (see Table 1). The AFS top upward motion is indicative of the buoyancy of the magnetic flux tubes and of their rise toward higher atmospheric levels, while the downward motion observed in the arch legs could be due to one (or a combination) of the following reasons: a) action of the Coriolis force on the rising flux tube; b) sliding motion associated with the Parker instability; c) remnant of a longitudinal flow in the original equilibrium (Moreno-Insertis 1997).

Another aspect which was evidenced by Spadaro et al. (2004) concerns the asymmetries between the preceding (p) and following (f) parts of the AR: for instance, the f-side shows a higher downflow than the p-side. This result, while confirming the validity of the model of a thin flux tube rising in the photosphere (Caligari et al. 1995), appears to be in contrast with the observations carried out by Cauzzi et al. (1996), probably because of differences in the initial magnetic field strength, or of different inclination of the two legs with respect to the vertical. It is anyway interesting that in both works the asymmetry decreases as the region evolves.

Short lived active region

In order to determine what are the characteristics shared by all emerging ARs, and whether some elements can be used to discriminate between ARs having a full evolution and others decaying after a short time, Zuccarello et al. (2005) studied a short-lived AR (NOAA 10407).

This AR, characterized by a lifetime of 7 days, was observed during a Campaign performed at THEMIS telescope (July 2003).

This analysis confirms that, within the limits set by the time cadence and the spatial resolution of the instruments used, the first evidence of the emerging AR is observed in the EIT bands. After 7 hours the AR appears almost contemporaneously in H_α and white light. The appearance of the AR in the EIT bands corresponds to a marked increase in the magnetic flux, that continues afterward: however, the magnetic flux increase in this AR is only a factor two, while in the recurrent region it was about two orders of magnitude.

Zuccarello et al. (2005) note that only one polarity appears to move away from the magnetic inversion line, while the other is directed toward it. The peculiar westward motion of the following polarity is in disagreement with models describing emerging flux tubes (van Driel-Gesztelyi & Petrovay 1990, Caligari et al. 1995, Moreno-Insertis 1997) and indicates that the flux emergence in this region occurs differently from the recurrent AR, where both polarities regularly move away from the magnetic inversion line.

The arches of the AFS observed in NOAA 10407 show an upward motion at their tops and generally downward motions at their extremities. The values of both upflow and downflow velocities measured on consecutive days confirm a decrease during the AR evolution (see Table 1). It was also noticed an asymmetry in the downflows, being the velocity at the p-leg systematically higher than that at the f-leg. This asymmetry, which might be partially determined by geometrical effects, decreases in the following days of observations. It differs from those generally reported in the literature, but it is consistent with the results of Cauzzi et al. (1996).

All these observational signatures fit quite well in a scenario where the short-lived AR is not anchored in the toroidal, subphotospheric magnetic field and is therefore more subject to turbulence than a long-lived, strongly anchored AR.

Ephemeral region

Ephemeral regions are bipolar structures characterized by typical fluxes of 3×1018 Mx and average fields of 50 Gauss (Schrijver et al. 1997). They emerge near the centre of supergranules, and their footpoints move fast apart and separate of 7000 km in about half an hour. Recent estimations show that the average lifetime of ERs spans from 8 to 16 hours (Hagenaar et al. 2003). Their decay appears, in turn, as the result of expanding newly emerged ERs, of their absorption by the existing network, of intrusion of magnetic elements from the network, and of the vanishing of little flux concentrations of opposite polarity (magnetic cancellation).

ERs are believed to originate from the global dynamo, as well as ARs (Harvey 1993), but it is also thought that they are locally generated by the turbulent convection near the surface (Nordlund et al. 1992). A further way involves both the global dynamo and flux processing in the convective envelope: magnetic flux merged in ARs can be recycled and emerge again in ERs, due to meridional motions (Nordlund et al. 1992). However, their origin still remains almost speculative: it is also possible that globally operating cyclic dynamo and small-scale dynamo are two distinct, but coupled, sources of these solar magnetic bipolar regions.

As referred by van Driel-Gesztelyi (2002), big and complex ARs are often formed by the coalescence of several ERs which emerge separately into the photosphere, but that are spatially and temporally close within a few days.

A recent analysis of an ER (Guglielmino et al. 2006), carried out using spectropolarimetric data acquired by the Advanced Stokes Polarimeter (Elmore et al. 1992), and adopting two different inversion techniques, aimed to verify the reliability of theoretical models and to improve our knowledge about the first phases of the emergence process.

This analysis points out that the ER has a classical bipolar structure; the maps of field strength and zenith angle, i.e. the angle of the magnetic field vector with the vertical, have shown that the central parts of the bipole, i.e. the emergence zone, have a horizontal zenith angle, weak field strength (lower than 600 Gauss), and filling factor higher than elsewhere in the region. The emergence zone is also characterized by upflows, and represents the emerging top of the loop. Conversely, the footpoints have a vertical zenith angle, high field strength and exhibit downflows (see Table 1). It is not possible to recognize the presence of a magnetic twist in the ER, due to the low signal-to-noise ratio in Stokes parameters Q and U.

The morphology of the ER is consistent with theoretical model predictions (Caligari et al. 1995) about the structure of the emerging flux tubes. However, a distortion in the tube is noticed: the f polarity appears to be more spatially concentrated than the p one, that exhibits a less vertical zenith angle and lower field strength, as shown by the model. Moreover, a cross-correlation analysis points out that the p polarity moves faster westward than the f one eastward.

Table 1. Mean velocities observed in emerging magnetic flux regions, expressed in km s-1. The interval between initial and final values refers to consecutive days for long-lived and short-lived ARs, while for ER it refers to a gap of three hours

	V elocity at the top		V elocity in p-leg		V elocity in f-leg	
	Initial	Final	Initial	Final	Initial	Final
Long-lived AR	+9	+3	-6	+1	-16	-3
Short-lived AR	+2	+1	-6	-3	-3	-1
ER	+0.9	+0.3	-1	-0.8	-1.3	-1.2

3 Discussion

We have described the results obtained in very recent researches carried out with the aim of distinguishing, since the initial phases of the magnetic flux emergence, whether the new forming region would have been characterized by a short or a long evolution (see, e.g. Spadaro et al. 2004, Zuccarello et al. 2005, Guglielmino et al. 2006).

One of the results obtained in these works is that the flux tubes forming the Ω-loops are initially characterized by a higher rising velocity, which eventually decreases: this may indicate the presence of some physical process which slows down the magnetic flux emergence as more and more flux tubes rise toward higher atmospheric layers. Moreover, important differences that might help to recognize whether a new forming AR will have a short or a long evolution are: different values of the AFS arch top upward velocity, different downward mo-

tions between the p and the f legs, different directions of the horizontal velocities in the p and f legs.

We would like to stress the result concerning the appearance of the ARs firstly in the outer atmospheric layers and later on in the photosphere and chromosphere. We suggest that this phenomenon might be related to magnetic reconnection events occurring between the emerging flux field lines and the coronal ambient magnetic field, as foreseen by most recent models of magnetic flux emergence (Archontis et al. 2004).

4 Acknowledgements

This work reviews some results obtained by the authors in the framework of COST Action 724 - WG1. It has been partially supported by the Agenzia Spaziale Italiana (contract ASI I/035/05/0) and by the European Commission trough the SOLAIRE Network (MTRN-CT-2006-035484).

References

Archontis, V., F. Moreno Insertis, K. Galsgaard, A. Hood, and E. O'She: Emergence of magnetic flux from the convection zone into the corona, Astron. Astrophys., **426**, 1047-1063 (2004)

Caligari, P., F. Moreno Insertis, and M. Schüssler: Emerging flux tubes in the solar convection zone. I: Asymmetry, tilt, and emergence latitude, Astrophys. Jour., **441**, 886-902, (1995)

Cauzzi, G., R. C. Canfield, and G. H. Fisher: A Search for Asymmetric Flows in Young Active Regions, Astrophys. Jour., **456**, 850-860, (1996)

Elmore, D. F., B. W. Lites, S. Tomczyk, A. Skumanich, R. B. Dunn, J. A. Schuenke, K. V. Streander, T. W. Leach, C. W. Chambellan, Hull, and L. B. Lacey: Advanced Stokes polarimeter: a new instrument for solar magnetic field research, SPIE Polarization Analysis and Measurement Proc., **1746**, 22-33 (1992)

Guglielmino, S. L., V. Martínez Pillet, B. Ruiz Cobo, F. Zuccarello, and B. W. Lites: A Detailed Analysis of an Ephemeral Region, Mem. Soc. Astron. Ital. Supplement, **9**, 103-105 (2006)

Hagenaar, H. J., C. J. Schrijver, and A. M. Title: The Properties of Small Magnetic Regions on the Solar Surface and the Implications for the Solar Dynamo(s), Astrophys. Jour., **584**, 1107-1119 (2003)

Harvey, K. L., and S. F. Martin: Ephemeral Active Regions, Solar Phys., **32**, 389-402 (1973)

Harvey, K. L., and C. Zwaan: Properties and emergence of bipolar active regions, Solar Phys., **148**, 85-118 (1993)

Moreno Insertis, F.: Emergence of magnetic flux from the solar interior, Mem. Soc. Astron. Ital., **68**, 429-447 (1997)

Nordlund, A., A. Brandenburg, R. L. Jennings, M. Rieutord, J. Ruokolainen, R. F. Stein, and I. Tuominen: Dynamo action in stratified convection with overshoot, Astrophys. Jour., **392**, 647-652 (1992)

Schrijver, C. J., A. M. Title, A. A. van Ballegooijen, and R. A. Shine: Sustaining the Quiet Photospheric Network: The Balance of Flux Emergence, Fragmentation, Merging, and Cancellation, Astrophys. Jour., **487**, 424-436 (1997)

Spadaro, D., S. Billotta, L. Contarino, P. Romano, and F. Zuccarello: AFS dynamic evolution during the emergence of an active region, Astron. Astrophys., **425**, 309-319 (2004)

Tuillier, G., S. Dewitte, W. Schmutz and The PICARD team, 2006: Simultaneous measurement of the total solar irradiance and solar diameter by the PICARD mission, Advances in Space Research, **38**, 1792-1806 (2004)

van Driel-Gesztelyi, L.: Emergence and loss of magnetic flux on the solar surface, "ESA SP-505: SOLMAG 2002", Magnetic Coupling of the Solar Atmosphere Euroconference Proc., 113-120 (2002)

van Driel-Gesztelyi, L., and K. Petrovay: Asymmetric flux loops in active regions, Solar Phys., **126**, 285-298 (1990)

Zuccarello, F., V. Battiato, L. Contarino, P. Romano, D. Spadaro, and L. Vlahos, AFS dynamics in a short-lived active region: Astron. Astrophys., **442**, 661-671 (2005)

Kagan, A.M., Linnik, Y.V., Rao, C.R.: Characterization Problems in Mathematical Statistics. Wiley, New York (1973)

Meyer, P.A.: A short presentation of stochastic calculus. In: Emery, M. (ed) Stochastic Calculus in Manifolds. Springer, Berlin Heidelberg New York (1989)

Miller, B.M., Runggaldier, W.J.: Kalman filtering for linear systems with coefficients driven by a hidden Markov jump process. Syst. Control Lett., **31**, 93–102 (1997)

Ross, D.W.: Lysosomes and storage diseases. MA Thesis, Columbia University, New York (1977)

Multi-wavelength observations of flares and eruptive filaments

F. Zuccarello[1], L. Contarino[2], P. Romano[2], V. Battiato[2] and S.L. Guglielmino[1]

[1] Universitá di Catania, Dipartimento di Fisica e Astronomia, Sez. Astrofisica, Via S. Sofia 78, 95123, Catania, Italy fzu@oact.inaf.it
[2] INAF Osservatorio Astrofisico di Catania, Via S. Sofia 78, 95123, Catania, Italy

Summary. In this paper we report some results obtained from multi-wavelength observations carried out to study the mechanisms at work in flares and filament eruptions. Most of these studies have given indication of the presence of phenomena that might be considered signatures of magnetic reconnection, while others have stressed the important role played by magnetic helicity transport in corona before the eruptive phase. Theses researches were carried out in the framework of the COST Action 724, aimed at investigating *Available models and data sets relevant to the modelling and prediction of solar activity*.

1 Introduction

The comprehension of the physical processes at the basis of activity phenomena occurring in the solar atmosphere might have a relevance not only in the context of an improvement of our knowledge of the physics of the Sun's atmosphere and magnetism, but also concerning Sun-Earth relationships.

In this scenario, it is worthwhile to stress that more energetic flares (classes M and X) and filament eruptions, if associated with Coronal Mass Ejections (CME) directed towards the Earth, can have remarkable consequences on Space Weather and can give rise to a number of phenomena that can interfere with several human activities (systems of radio communications, GPS positioning systems, electrical distribution networks, etc). As a consequence, in a society more and more based on electronic systems, it becomes extremely important to be able to forecast such events.

The possibility to forecast such events relies on on a deep comprehension of the sequence of phenomena which are responsible of their occurrence, but at present there are still several unclear points related to many aspects, both observational and theoretical. In particular, many authors concentrated their efforts to investigate two important aspects: the effects of magnetic reconnection during eruptive phenomena, by means of comparisons between observations and model previsions (see, e.g. Priest & Forbes, 2000), and the role played by magnetic helicity transport in corona during the pre-eruption phase (Moon et al., 2002; Demoulin & Berger, 2003).

In this paper we review the results we obtained on these subjects during the COST Action 724, devoted to the study of activity phenomena on the Sun.

2 Flares

Solar flares are extremely complex phenomena, characterized by a sudden and localized energy release ($10^{29} - 10^{32}$ erg), that produces emission of electromagnetic radiation, heat flow, bulk plasma motions, particle acceleration. The observations have put into evidence that the primary energy release takes place in corona and subsequently it involves the underlying layers of the solar atmosphere (Priest & Forbes, 2002). Therefore the study of flares from the observational point of view must be carried out comparing data acquired in various spectral ranges, in order to have information on the physical processes occurring in the various atmospheric layers.

The results obtained from these studies seem to confirm the hypothesis that one of the physical processes at the basis of flares is magnetic reconnection, caused by breaking and successive merging of magnetic field lines. However, further observations are still necessary to clear the role of some phenomena linked to magnetic reconnection: mechanisms of energy transport during the first phases of reconnection, chromospheric plasma evaporation in post-flare loops, role of shock waves in heating the plasma, etc (Priest & Forbes, 2000).

These subjects have lead the authors to utilize two different approaches in order to contribute to sketch a clearer scenario of eruptive phenomena: a statistical study of the characteristics that active regions must have in order to give rise to flares of classes X or M, and more specific studies on the possible physical mechanisms at the base of eruptive phenomena, carried out using high resolution multi-wavelength observations, performed both from Earth and from satellites.

The first aspect has been faced by means of a statistical analysis, based on data in the visible range (some acquired at INAF-Catania Astrophysical Observatory (IOACT), others provided by NOAA), on MDI magnetograms and on data in the X range provided by the GOES satellite. This analysis allowed us to determine what are the conditions which characterize ARs hosting M and X flares, for instance: i) Zurich class D, E, F; ii) penumbra in the largest sunspot characterized by a large asymmetry and a diameter greater than 2,5 degrees; iii)β, $\beta\gamma$, and $\beta\gamma\delta$ magnetic configuration. Moreover, the analysis of the flare productivity as a function of the group evolutionary stage indicated that the flaring probability of sunspots slightly increases with the spot age during the first passage on the solar disk, and that flaring groups are characterized by longer lifetimes than non-flaring ones (Ternullo et al., 2006).

The second approach has been tackled by carrying out the analysis of images acquired at several wavelengths (visible range: IOACT, THEMIS, BBSO; EUV: TRACE, EIT/SOHO; X: YOHKOH, RHESSI) and magnetograms acquired from ground-based observatories (BBSO, Mitaka) and from space (MDI/SOHO).

In particular, a study carried out on a sequence of flares occurred in NOAA 8421 has given the following results: i) the flares were triggered by processes of magnetic reconnection caused by the interaction between the magnetic field lines of a coronal arcade and new magnetic flux tubes emerging from the subphotospheric layers (see Heyvaerts et al. 1977, for a theoretical model of this type of events); ii) presence of reconnection in the loops of an arcade at gradually increasing heights as a filament rises towards the more external layers; iii) process of chromospheric evaporation at the basis of an increase of brightness in the moss surrounding the footpoints of an arcade (Zuccarello et al. 2003).

Another work based on the analysis of RHESSI and TRACE data relevant to an M2.5 flare that occurred on 16 April 2005 has shown that the event was characterized by a morphology in which the X-ray sources changed from an X to a Y magnetic configuration; moreover, the formation of a thin, filamentary structure, compatible with what is expected from the collapse of an X-point in a current sheet, was observed; also, the height of the top of the observed EUV loops and the separation between the footpoints showed an increase with time (see Contarino et al. 2006). These observational signatures are those expected from theory during the formation of a current sheet and consequent reconnection, and allowed us to interpret the event in the framework of the Kopp and Pneuman model (Kopp & Pneuman 1976). This fits quite well with the reconnection scenario described by Miklenic et al. (2007) for a two-ribbon flare.

In another paper (Romano et al. 2007), we studied the magnetic configuration of active region NOAA 10672, where two different mechanisms seem to contribute to its instability, to the subsequent M1.5 flare and to a Halo CME. In particular, the analysis of full disk MDI magnetograms and of WL and 171 Å TRACE images showed that both flux emergence and horizontal displacements of photospheric flux concentrations had a key role in triggering the event. Moreover, the flare evolution observed by TRACE and the two-step profile in X-ray emission observed by GOES, were interpreted in the framework of a multi-reconnection process.

2.1 Filament eruption

As far as the prominence activation and the occurrence of associated CME are concerned, many authors have put into evidence the role carried out by the helicoidal configuration of the magnetic field.

In this context, an event occurred in AR 9077 was studied by approximating the prominence to a curved cylindrical flux tube and by measuring the helicoidal twist of the magnetic field lines. The critical twist value at which the eruption took place was estimated and a decrease of the total torsion of the field in time was evidenced. The conclusion drawn from this study was that the prominence was initially destabilized by a kink-mode instability and, not succeeding in finding a new equilibrium configuration, it erupted (Romano et al. 2003a).

In another study, using magnetograms of AR 8375 acquired by MDI/SOHO, we estimated the rate of magnetic helicity transport in corona, related to the emergence of new flux tubes and to their horizontal motions at photospheric level. Such analysis allowed us to confirm the fundamental role played by helicity in prominence destabilization, and to recognize the emergence of the already twisted magnetic field as the more efficient mechanism for the attainment of an unstable configuration (Romano et al. 2003b). However, the previous conclusion should not be generalized because, in a successive study concerning another active region (AR 9502), the analysis of the relevant MDI magnetograms showed that the transport of magnetic helicity exceeding the limit for the kink instability was primarily due to photospheric motions, while the contribution from the emerging flux was negligible (Romano et al. 2005).

In the context of filament eruption, we also mention another event where two distinguished reconnection phenomena have been observed: the former in the low solar atmosphere, near a structure called CMF (cancelling magnetic feature), that caused the destabilization of a filament and the successive eruption of part of it, and the latter in corona, caused by the

passage of the filament through the overlying arcade (Contarino et al. 2003; Contarino et al. 2006). Such events were interpreted in the framework of the model of reconnection in the low solar atmosphere, proposed by Litvinenko & Somov (1994) and Litvinenko (1999).

The occurrence of a CMF was observed also in a small ($\sim$ 20 arcsec) filament that, after two consecutive surge events, disappeared. More precisely, high resolution observations performed at the THEMIS telescope, together with MDI data, showed the presence of a CMF in the same area where dark H surges occurred; the temporal behaviour of the velocity fields in the surges and the presence of bright H patches in the CMF area, suggested a scenario where the coronal arcade initially sustaining the filament might have undergone consecutive reconnection processes. As a consequence, the plasma filament was no longer confined in the arcade and this caused its destabilization and disappearance (Zuccarello et al. 2007).

3 Discussion

We have described the results obtained in the framework of studies on flares and filament eruptions. In particular, we have stressed that many of these events showed phenomena expected from the theory of magnetic reconnection. In most of the cases studied it was evidenced the presence of magnetic flux emergence in already developed active regions: this process may lead to the interaction between old and new magnetic flux tubes and, when the two different magnetic domains have the suitable relative orientation, magnetic reconnection should take place.

Moreover, a number of these studies allowed us to investigate the role played by the transport of magnetic helicity in corona before eruptive phenomena: it has been shown that in one case the magnetic helicity increase was mainly caused by new flux emergence, while in another case, the increase was due to photospheric motions. Therefore we presume that both phenomena might alternatively contribute to this increase and consequently to the filament eruption.

However, several points remain open, in both scenaria, i.e., in reconnection and magnetic helicity mechanisms: we believe that the instruments onboard HINODE will greatly contribute to solve many of these questions, especially as far as the magnetic field configuration is concerned. At the same time, an improvement in the models and in the techniques of magnetic field extrapolation are needed.

4 Acknowledgements

This work reviews some results obtained by the authors in the framework of COST Action 724 - WG1. It has been partially supported by the Agenzia Spaziale Italiana (contract ASI I/035/05/0) and by the European Commission trough the SOLAIRE Network (MTRN-CT-2006-035484).

References

Contarino, L., P. Romano, F. Zuccarello, and V. B. Yurchyshyn: THEMIS, BBSO, MDI and TRACE observation of a filament eruption, Solar Phys., **216**, 173-188 (2003)

Contarino, L., P. Romano, and F. Zuccarello: RHESSI and TRACE observations of an M2.5 flare: a direct application of the Kopp and Pneuman model (Research Note), Astron. Astrophys., **458**, 297-300 (2006)

Contarino, L., P. Romano and F. Zuccarello: Cancelling magnetic feature and filament activation, Astron. Nachr., **327**, 674-679 (2006)

Demoulin, P., and M. A. Berger: Magnetic energy and helicity fluxes at the photospheric level, Solar Phys., **215**, 203-215 (2003)

Heyvaerts, J., E. R. Priest, and D. M. Rust: An emerging flux model for the solar flare phenomenon, Astrophys. Jour., **216**, 123-137 (1977)

Kopp, R.A., and G. W. Pneuman: Magnetic reconnection in the corona and the loop prominence phenomenon, Solar Phys., **50**, 85-98 (1976)

Litvinenko, Y. E.: Photospheric Magnetic Reconnection and Canceling Magnetic Features on the Sun, Astrophys. Jour., **515**, 435-440 (1999)

Litvinenko, Y. E., and B. V. Somov: Magnetic reconnection in the temperature minimum region and prominence formation, Solar Phys., **151**, 265-270 (1994)

Miklenic, C.H., A. M. Veronig, B. Vršnak and A. Hanslmeier: Reconnection and energy release rates in a two-ribbon flare, Astron. Astrophys., **461**, 697-706 (2007)

Moon, Y.J., Chae, J., Choe, G.S. et al.: Flare Activity and Magnetic Helicity Injection by Photospheric Horizontal Motions, Astrophys. Jour., **574**, 1066-1073 (2002)

Priest, E. R., and T. G. Forbes: Magnetic Reconnection: MHD Theory and Applications, Cambridge University Press (2000)

Priest, E. R., and T. G. Forbes: The magnetic nature of solar flares, Astron. Astrophys. Rev., **10**, 313-377 (2002)

Romano, P., F. Zuccarello, and L. Contarino: Eruption of a helically twisted prominence, Solar Phys., **214**, 313-323 (2003)

Romano, P., F. Zuccarello, and L. Contarino: Magnetic helicity transport in corona and filament eruptions, Solar Phys., **218**, 137-150 (2003)

Romano, P., F. Zuccarello, and L. Contarino: Observational evidence of the primary role played by photospheric motions in magnetic helicity transport before a filament eruption, Astron. Astrophys., **433**, 683-690 (2005)

Romano, P., F. Zuccarello, and L. Contarino: An M1.5 flare triggered by a multi reconnection process, Solar Phys., **240**, 49-61 (2007)

Ternullo, M., L. Contarino, P. Romano, and F. Zuccarello: A statistical analysis of sunspot groups hosting M and X flares, Astron. Nachr., **327**, 674-679 (2006)

Zuccarello, F., L. Contarino, P. Romano, and E. R. Priest: Flare activity in AR 8421 observed by TRACE, Astron. Astrophys., **402**, 1085-1102 (2003)

Zuccarello, F., V. Battiato, L. Contarino, P. Romano, and D. Spadaro; Plasma motions in a short-lived filament related to a magnetic flux cancellation, Astron. Astrophys., **468**, 299-305 (2007)

On the Prediction of Solar Magnetic Activity

H. Lundstedt[1,2]

[1] Swedish Institute of Space Physics, Scheelv. 17, 223 70 Lund, Sweden, henrik@lund.irf.se
[2] International Space Environment Service (ISES)

Summary. We ascribe the solar magnetic activity to the interplay between the plasma flow and the magnetic field. We then discuss the understanding based on mathematical concepts and what should be observed for predictions. We present predictions using neural networks, both on short-, and on long-term such as of next sunspot cycle. Further we describe the outcome of the cycle 24 prediction panel. Finally recommendations are given for making improved predictions.

1 Introduction

Space weather is mainly driven by solar magnetic activity, which is therefore very important to be able to predict in a reliable way (Lundstedt (2005) ; Lundstedt (2006a)). However, we believe that predictions can be successful only if they are based on observations of physical quantities which are related to physical mechanisms. These predictions can become operational for space weather services of International Space Environment Service (ISES), when real-time observations will be made available from the Solar Dynamics Observatory (SDO) which will produce such real-time data.

2 Interpretation and description of solar magnetic activity

We start by interpreting solar magnetic activity in terms of the interplay between the solar plasma flow vector (V) and the solar magnetic field vector (B). We describe the solar magnetic activity using both mathematical and physical concepts. The two descriptions will then be integrated into a hybrid neural network. The concepts and relations are illustrated in a concept map (C-Map) (Messerotti, 2002) (Fig. 1).

2.1 Based on solar mathematical concepts

The plasma flow (V) and magnetic flux density (B) are described with vector fields which are purely mathematical entities. The relation between these entities are expressed in MHD equations. Energy storage and release, and dynamo mechanisms are described by with these

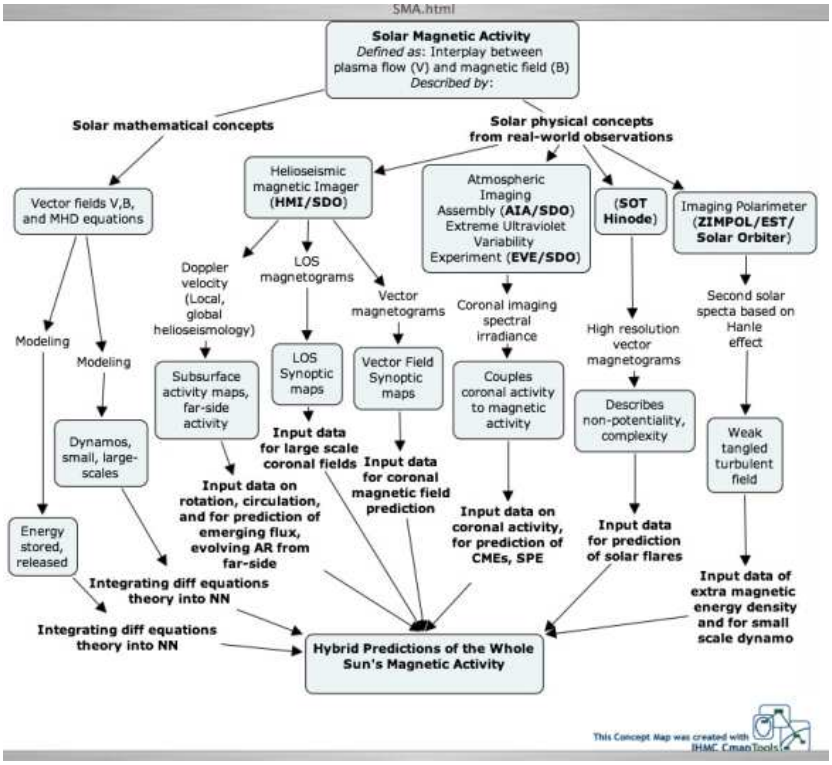

Fig. 1. C-Map of solar magnetic activity and its predictions.

equations. The relevant understanding is subsequently reached when we recognize the patterns the mathematical equations describe (Devlin, 2002).

2.2 Based on solar physical concepts

Real-world coupling is obtained through observations of physical concepts. In Fig 1. we illustrate observations using instruments onboard the Solar Dynamics Observatory, the Solar Optical Telescope (SOT) onboard Hinode and the Zurich Imaging Polarimeter (ZIMPOL) planned for Solar Orbiter.

The Helioseismic Magnetic Imager (HMI) onboard SDO will be used to obtain subsurface maps, data on far-side activity, line-of-site (LOS) synoptic maps and vector magnetogram (VF) maps. The Atmospheric Imaging Assembly (AIA) and the Extreme Ultraviolet Variability Experiment (EVE), both onboard SDO, will make the connection to coronal activity.

SOT onboard Hinode produces high resolution vector magnetograms (Fig. 2).

With ZIMPOL a second solar spectrum has been discovered (Stenflo, 2004). The different polarized structures in the second solar spectrum, are affected through the Hanle effect and by a hidden magnetic field. This hidden (to the Zeeman effect) weak and tangled turbulent field carries more magnetic-energy density than earlier thought (Stenflo, 2004).

3 Neural network prediction based on V and B

Three examples of predictions based on observations of the plasma flow and the magnetic field are presented in the following sections.

3.1 Solar flares and subsurface flows

A significant correlation between strong plasma downflows and high magnetic activity, indicated by strong solar flares, was found in Jensen et al. (2004) (Fig. 2). A neural network was trained to predict an event of at least one major solar flare based on maps of subsurface flows. The predictions were promising, despite the lack of a large input dataset Jensen et al. (2004). Such large dataset and near-real time maps will become available from both Global Oscillation Network Group (GONG) and will come shortly from SDO.

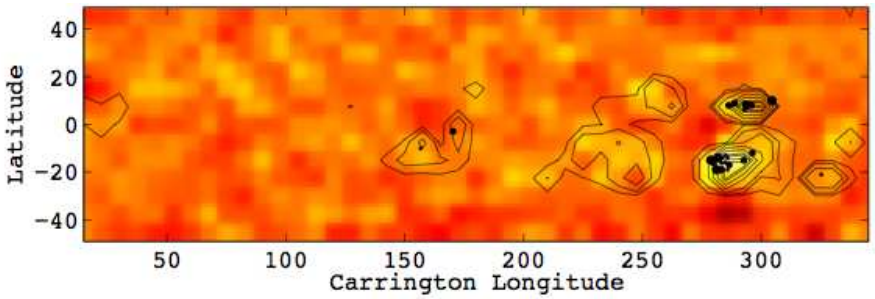

Fig. 2. The synoptic map shows the divergence of the observed flows at a depth of 4.6Mm. Bright regions represent inflow and dark outflow. The contour lines show the magnitude of magnetic field strength. The size of the dots indicate flare from small C, medium M and large X. The synoptic map shows Carrington rotation 2009, i.e. during the Halloween event 2003.

3.2 Solar flares and vector magnetic fields

It has been known for a long time that solar flare activity is related to the non-potentiality and complexity of the solar magnetic activity.

Cui et al. (2006) describe the non-potentaility and complexity by introducing three quantities: Maximum horizontal gradient, length of neutral line and the number of singular points. They found an interesting relation between the solar flare productivity and the above mentioned quantities. The relationship can be fitted with a sigmoid function and herewith modeled with a neural network. The three quantities can be derived from vector magnetograms, such as shown in Fig 3. Operational forecasts will be possible with real-time vectormagnetograms, which will be available from SDO.

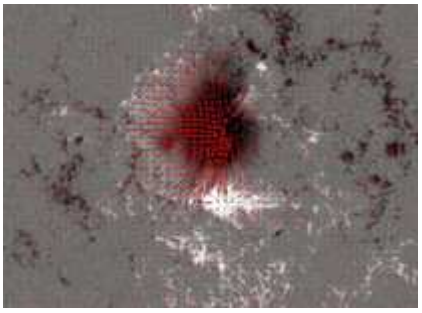

Fig. 3. Vector magnetogram observed on 13 December 2006. Courtesy Hinode.

3.3 Magnetic activity years ahead

Solar synoptic maps provide an important visualization of global patterns. Maps are available of sub-surface flows, photospheric and coronal magnetic fields. In Lundstedt et al. (2007) we averaged longitudinally synoptic maps from Wilcox Solar Observatory (WSO) at Stanford. The data cover three cycles from 1976 up to present. The averaged map is shown in Fig. 4. Many interesting features are visible: The variation of the Butterfly diagrams, the transport of flux to the poles, and the asymmetry for the both hemispheres.

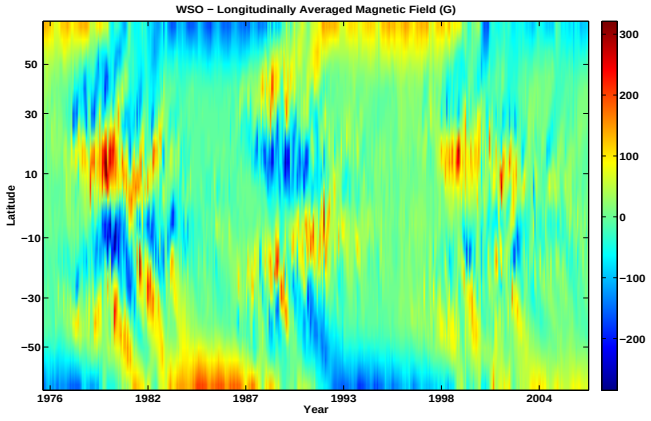

Fig. 4. Longitudinally averaged synoptic magnetic fields.

Neural networks have been trained, based on data from the longitudinally averaged synoptic map, to predict the total magnetic flux Carrington rotations ahead. A correlation coefficient of 0.82 was reached between the predicted and observed values two years ahead Lundstedt et al. (2007). Similar studies are planned using SDO data.

4 Prediction of sunspot cycles

Ever since the sunspot cycle was discovered by H. Schwabe in 1843, using only 17 years of data, scientists have described solar activity cycles by the sunspot number.

4.1 The Cycle 24 Prediction Panel

NOAA/NASA/ISES sponsored a panel, consisting of 11 participants, to try to reach a consensus on the next sunspot cycle, Cycle 24. Over 40 different predictions were examined, based on climatology methods, spectral analysis, neural networks, precursor methods and dynamo models. Predictions range from very weak to very strong: Svalgaard et al. (2005) predicted Cycle 24 to be the weakest in 100 years based on the polar field strength. Dikpati et al. (2004) predict a strong Cycle 24 based on applying a dynamo model. It is interesting that Choudhuri et al. (2007), also using a dynamo model, however conclude that Cycle 24 will be weak.

On Aril 25, 2007 the panel announced their first predictions: Solar Minimum will occur on March, 2008 ($\pm$6 months), which marks the end of Cycle 23 and start of Cycle 24. The length of Cycle 23 will then be 11.75 years, i.e. longer than the average of 11 years.

The Cycle 24 will peak at a sunspot number of 140($\pm$20) in October, 2011 or it will peak at a sunspot number of 90($\pm$10) in August, 2012. An average solar cycle peaks at 114 and therefore the next cycle will neither be extreme, nor average.

But, the panel is split down the middle on whether it will be bigger or smaller than average. The panel will re-evaluate conditions on the sun every 3 months and update this prediction annually, or as things change.

4.2 Sunspot number as an indicator of solar magnetic activity

The sunspot number is used as an indicator of long-term solar magnetic activity. At most, the sunspot number covers only 23 sunspot cycles. These cycles largely differ both in amplitude and length. During the so called Maunder Minimum (MM) 1645-1715, almost no sunspots were observed. Though the ^{14}C production showed about 11 year variations during the MM (Fig. 6) (Lundstedt, 2006b).

4.3 Extreme solar radio bursts during sunspot minimum

Also showing the sunspot number might not give us the general picture of the solar magnetic activity is the following event close to sunspot minimum.

Activity increased to high levels on 05 and 06 December 2006 as Region 930 produced three major flares: an X9/2N at 05/1035 UTC associated with Types II (estimated velocity 860 km/sec) and IV radio sweeps and a 12000 sfu Tenflare, an M6/SF at 06/0823 UTC associated with a Type IV radio sweep and 340 sfu Tenflare, and an X6/3B at 06/1847 UTC (Fig. 7).

This very unexpected activity even made Strong and Saba (2007) raise the question: Are we looking at the Solar Cycle in completely the wrong way?

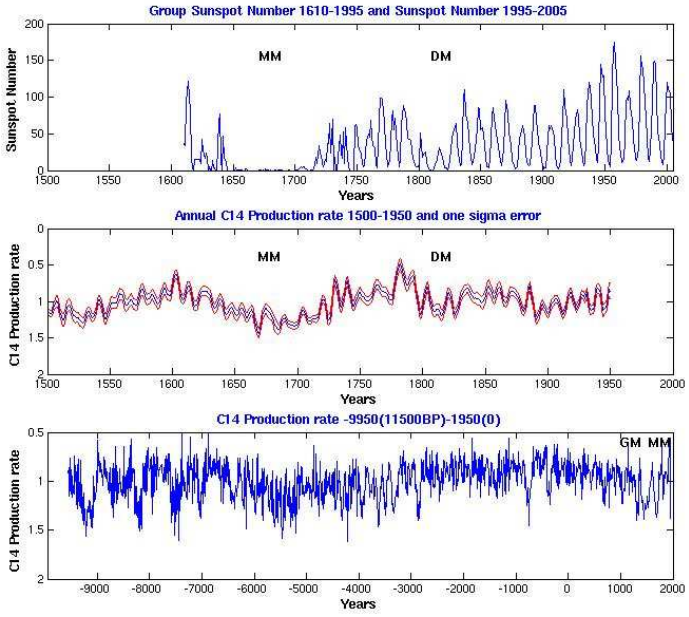

Fig. 5. The upper panel shows the group sunspot number R_G 1610-1995 and the sunspot number R_z 1995-2005. The middle panel shows the ^{14}C production rate 1500-1950. The lower panel shows the ^{14}C production rate 9950 BC to 1950. MM stands for Maunder Minimum, DM for Dalton Minimum and GM for Grand Maximum.

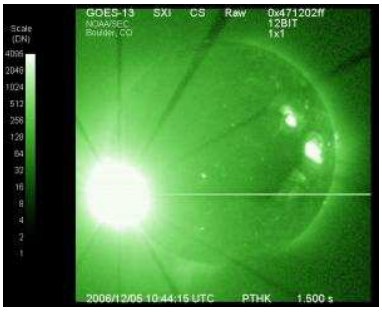

Fig. 6. The Xray flare associated with the extreme radioburst on December 5, 2006. Courtesy GOES-13.

5 Discussions and conclusions

To improve understanding and predictions of solar magnetic activity we need observations of the plasma flow (V) and magnetic field (B) below and on the surface and in the corona. Real-time synoptic maps can adequately visualize the activity.

To predict explosive events, such as solar flares, we need real-time vector magnetic field observations at all scales.

The difficulties in predicting the so called Schwabe's sunspot cycle, using both data and theory-driven models Bushby and Tobias (2007), might point out new aspects that lead to rethink about solar cycles.

Observations of V and B by Hinode, SDO, Solar Orbiter and other upcoming missions will play a very important role in improving our knowledge.

Acknowledgements: This work has been carried out in the framework of COST Action 724 WG1.

References

Bushby, P. J., Tobias, S.: On Predicting the Solar Cycle using Mean-Field Models, accepted for Ap. J. (2007).

Choudhuri, A.R., Chatterjee, P., Jiang, J.: Predicting Solar Cycle 24 With a Solar Dynamo Model, Phys. Rev. Lett., **98**, 131103 (2007).

Cui, Y., Li R., Zhang, L., He, Y., Wang, H., Correlation Between Solar Flare Productivity and Photospheric Magnetic Field Properties, Solar Phys., 237, 1 August (2006).

Devlin, K.; The Language of Mathematics - Making the Invisible Visible, A.W.H. Freeman, OWL Books, New York (2002).

Dikpati, M., de Toma, G., Gilman, P.A.: Predicting the strength of solar cycle 24 using a flux-transport dynamo-based tool, Geophys. Res. Lett., **33**, L05102, (2006).

Jensen, J. M., Lundstedt, H., Thompson, M. J., Pijpers, F. P., and Rajaguru, S. P.: Application of Local-Area Helioseismic Methods as Predicters of Space Weather, in Helio- and Asteroseismology: Towards a Golden Future, ed. D. Danesy, Proc. SOHO 14/GONG+ 2004 Meeting, ESA SP-559, 497-500, (2004).

Lundstedt, H.: Progress in space weather predictions and applications, Adv. Space Res., **36**, 2516-2523, (2005).

Lundstedt, H.: Solar activity modelled and forecasted: A new approach, Adv. Space Res., **38**, 862-867, (2006a).

Lundstedt, H., Liszka, L., Lundin, R., and Muscheler,R., Long-Term Solar Activity Explored with Wavelet Methods, Annal. Geophys., 24, 1-9, (2006b).

Lundstedt, H., Wik, M., Wintoft, P.: Multiresolution analysis of synoptic solar magnetic fields, submitted to Ann. Geophys., (2007).

Messerotti, M.: Embedding knwoledge in scientific databases via concept maps as metadata,in Proc. "SOLSPA: The Second Solar Cycle and Space Weather Euroconference", Vico Equense, Italy, 24-29 September 2001, ESA SP-477, 607-610, (2002).

Stenflo, J.O.: Hidden magnetism, Nature, **430**, 15 July (2004).

Strong, K.T., Saba, J.L.R.: Are We Looking at the Solar Cycle in Completely the Wrong Way, presented at Space Weather Workshop, April 24-27 (2007).
Svalgaard, L., Cliver, E.W., Kamide, Y.: Cycle 24: the smallest sunspot cycle in 100 years?, Geophys. Res. Lett., **32** (2005).

Solar EUV/FUV irradiance variation: analysis and observational strategy

M. Kretzschmar[1,2], T. Dudok de Wit[1], J. Lilensten[3], J.F. Hochedez[2], J. Aboudarham[4], P.-O. Amblard[5], F. Auchère[6], and S. Moussaoui[7]

[1] LPCE, CNRS and Université d'Orléans, 3A avenue de la Recherche Scientifique, 45071 Orléans cedex 2, France matthieu.kretzschmar@cnrs-orleans.fr ddwit@cnrs-orleans.fr
[2] SIDC, Royal Observatory of Belgium, ringlaan -3- av. circulaire, 1180 Brussels, Belgium hochedez@oma.be
[3] LPG, CNRS and Université Joseph Fourier, Bâtiment D de Physique, BP 53, 38041 Saint-Martin d'Hères cedex 9, France, jean.lilensten@obs.ujf-grenoble.fr
[4] LESIA, Observatoire de Paris, 5 Place Jules Janssen, 92195 Meudon, France, jean.aboudarham@obspm.fr
[5] GIPSA-lab/Dept. Images and Signals- CNRS UMR5216, Grenoble, France, bidou.amblard@lis.inpg.fr
[6] IAS, Université Paris-Sud, 91405 Orsay, France, frederic.auchere@ias.u-psud.fr
[7] IRCCYN, Bureau ECN S211, 1 rue de la No, BP 92101 - 44321 Nantes Cedex 3, France said.moussaoui@irccyn.ec-nantes.fr

Summary. The monitoring of solar extreme and far ultraviolet irradiance variations are essential for the characterization of the Earth's upper atmosphere. For a long time, they have been -quite successfully- based on empirical models, which are themselves based on proxies. However, the accurate modeling and prediction of the near Earth environment necessitate to improve the precision on the irradiance and its variations. Here, we present recent efforts -made in the context of the COST724 action- to quantify the irradiance variability. We find a high level of redundancy that allows to envisage to measure only a small portion of the spectrum without losing essential knowledge. Finally, we discuss what should and could be measured in order to retrieve the solar extreme and far ultraviolet spectrum.

1 Introduction

The solar irradiance (or solar flux) in the extreme (EUV, from 10 nm to 121 nm) and far ultraviolet (FUV, from 122 nm to 200 nm) spectral ranges is of great importance for space weather. First, it is responsible for the ionization, dissociation, and heating of the upper terrestrial atmosphere. The specification of ionospheric quantities such as the Total Electron Content (TEC) heavily relies on it. Second, this part of the spectrum is highly variable on both long and short time scales. During intense solar flares, the flux may increase by more than an order of magnitude, especially shortward of 20 nm. These variations have important consequences on the ionosphere, but also on the lower atmospheric layers. For a recent review on the importance of the EUV flux for space weather, see Lilensten et al. (2007a).

The solar EUV spectrum has been poorly observed in the past. In particular, there has been no continuous monitoring of the solar EUV irradiance between the end of measurements by Atmosphere Explorer E measurements in 1981 and the launch of the NASA Thermospher Ionosphere Mesosphere Energetics Dynamics (TIMED) spacecraft in January 2002 (see Woods et al. (2005) for details on EUV measurements history). To compensate for this lack of data, which has been termed the "EUV hole", several models have been developed. Most of these models, such as SERF1 (Hinteregger et al., 1981), EUVAC (Richards et al., 1994), and SOLAR2000 (Tobiska et al., 2000) are based on the use of proxies such as F10.7, the solar radio flux at 10.7 cm. Recently, new proxies have been introduced: E10.7, that represents the whole solar EUV flux scaled to F10.7, and E140, that is the flux integrated from 1 to 40nm (Tobiska et al., 2001). The NRLEUV model (Warren et al., 2001) uses emission measure distributions and full-disk spatially-resolved solar images. These models perform well, but space weather operations require an even more precise knowledge of the solar flux (Lathuillère et al., 2002). What is urgently needed is not just spectral and temporal coverage but also radiometric accuracy. For reviews on the comparison between models and observations, see Lean (1990), Tobiska (1993) and Woods et al. (2005).

The SEE (Solar Extreme-ultraviolet Experience) instrument onboard TIMED measures since early 2002 the solar spectrum from 26 nm to 193 nm, with a 0.4 nm resolution (Woods et al., 2005). TIMED/SEE makes up to 15 measurements per day of the solar spectrum, averaged over 3 min each. This instrument offers a unique opportunity to improve our knowledge of the spectral variability and to investigate which parameters are important for retrieving the solar flux when no direct measurements exist. In this paper, we present efforts that have been made in this direction in the framework of the COST 724 action. In Sec. 2, we present results on the quantification of the spectral variability redundancy and how it agrees with solar indices. Section 3 concentrates on the implications of these results for defining what should be measured and we explicitly propose sets of spectral lines that should be observed. Finally, we discuss our results and conclude in Sec. 4.

2 Analysis of the solar EUV spectrum

The solar irradiance EUV spectrum under quiet conditions is well understood (Lilensten et al., 2007a). The irradiance consists of continuum emission that is mainly caused by composed of free-bound transitions (electronic recombinations), and of spectral lines corresponding to atomic transitions of the ions that are present in the solar atmosphere.

Figure 1 shows three different solar spectra obtained under quiet conditions. The first one (black) is the spectrum integrated over the whole solar surface as measured by TIMED/SEE on March 16, 2007, when no sunspots were present. The second one (red) has been measured at very high spectral resolution on a quiet portion of the solar disk by the SUMER spectrometer (Curdt et al., 2001), and the third one (blue) has been modelled using atomic data and the average quiet Sun intensity of about 20 spectral lines (Kretzschmar et al., 2004). The last two intensity spectra have been converted into irradiance by multiplying by $\pi R_{\odot}^2/d_{\odot,T}^2$, where $R_{\odot}$ is the solar radius and $d_{\odot,T}$ is the Sun-Earth distance, and degraded to the spectral resolution of TIMED/SEE. As can be seen on the figure, the main features of the spectrum (i.e. the continuum and the spectral lines) agree between the different spectrums. In particular, the fact

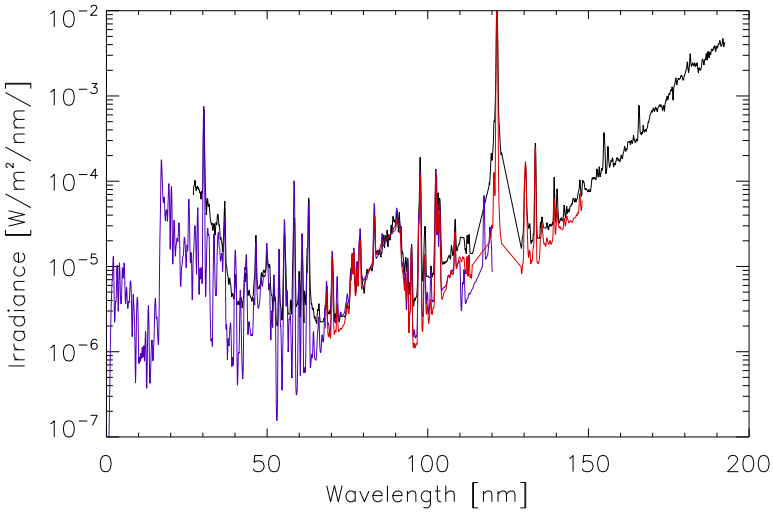

Fig. 1. Solar irradiance spectra for quiet conditions. The black curve corresponds to TIMED/SEE measurements for a quiet Sun, the red curve is from Curdt et al. (2001) and the blue one is from (Kretzschmar et al., 2004).

that the modeled spectrum can reproduce the observed ones indicate that our understanding of the underlying mechanism is not so bad. However, there are some disagreement for the absolute value of the flux, mainly fo the continuum above 90 nm and below 70 nm. This can be explained in part by the different spectral resolution of the instrument and the integration over the solar disk. A true inter-calibration study should be performed to go beyond these explanations but this is not the purpose of this paper.

For an operational space weather service, it is crucial to know the true variation of the solar EUV spectrum with solar activity. To answer this question, one would ideally require continuous observations of the Sun over at least one solar cycle and monitoring of the irradiance with a very good temporal and spectral coverage, as well as an excellent absolute calibration. This is not feasible, although the EVE instrumental suite (Woods et al., 2006) onboard the Solar Dynamics Observatory (to be launched in 2008) will significantly improve the monitoring of the EUV spectrum. TIMED/SEE, however, has now been monitoring the solar irradiance for several years with up to 15 measurements per day. Enough data have been accumulated to answer the question in a statistical sense. This is the approach developed by Dudok de Wit et al. (2005), whose first objective was to quantify the remarkable degree of redundancy observed between the time evolutions of various EUV spectral lines. To do so, the spectral irradiance matrix $I(\lambda, t)$, after proper normalisation, is decomposed into a set of separable functions of time t and wavelength λ : $I(\lambda, t) = \sum_i c(\lambda, i) f(i, t)$. This decomposition is unique and is done by Singular Value Decomposition (Golub and van Loan, 1996). The $f(i, t)$ components describe the independent (actually orthonormal) temporal variations associated with the spec-

trum, while $c(\lambda, i)$ can be seen as the projection of $I(\lambda, t)$ on the i'th temporal component. The components $c(1, \lambda)$, $c(2, \lambda)$, ... are conventionally sorted in decreasing order of variance.

The first result of Dudok de Wit et al. (2005) is that over 95% of the variance of $I(\lambda, t)$ can be described with two components only. This result indicates that the variation of the irradiance is strongly redundant between different wavelengths. It also allows us to represent the similarities and differences in the irradiance variation in a very compact way. Since the two first components describe the salient features of the spectral variability, we can plot $c(2, \lambda)$ vs $c(1, \lambda)$, see Fig. 2. In this two-dimensional map, each point corresponds to a wavelength. The distance between each pair of wavelengths reflects their degree of similarity: the closer two points are, the more similar the irradiance variations are.

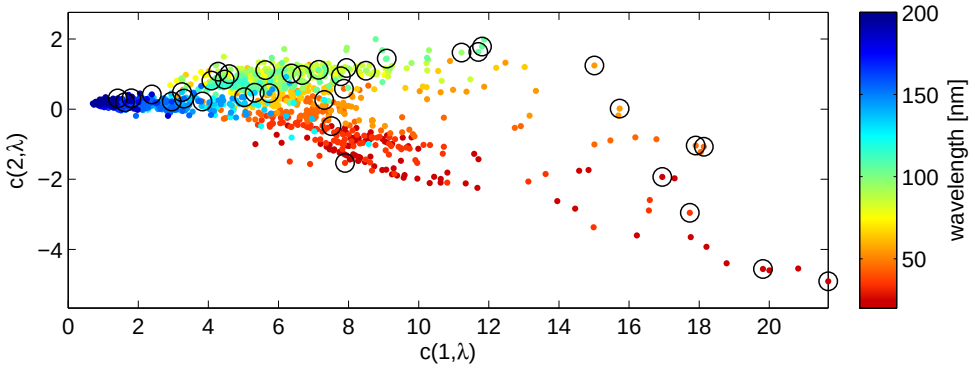

Fig. 2. 2D representation of spectral similarities in irradiance variations. Each point is colour coded by its corresponding wavelength. The 38 strongest spectral lines are circled. The meaning of the axes is discussed in (Dudok de Wit et al., 2007); what matters here is the relative distance between the points. Plot based on TIMED/SEE level 2 data between Feb 25, 2002 and May 1, 2007.

As expected, long wavelengths are tightly grouped together and short wavelengths are located far from long ones. The dispersion of very short wavelengths reflects the marked differences between emissions originating from the hot corona. Some wavelengths stand out of the cluster of points; this is notably the case for the hydrogen and helium lines, which exhibit a relative singular behavior.

More recently, Dudok de Wit et al. (2007) have used the same representation to determine how well different solar activity proxies can reproduce the spectral variability. For that purpose, they could not distinguish a particular index (excluding instrumental constraints), apart from the sunspot number, which is the least appropriate by our standards. Their results show that no single index can successfully describe both the level of variability on different time scales. The Mg II and the Ca K indices are appropriate for describing the long-term (> 27 days) evolution of the least-energetic part of the EUV spectrum but less so for modelling the short-term evolution. Conversely, the Mg II, Ca K and He I indices are found to be rather good proxies of the short-term evolution of coronal lines. Finally, no combination of indices was found to be capable of reproducing the variability of the EUV spectrum. Why not, then, try to

reconstruct the EUV irradiance from a linear combination of a few spectral lines (or spectral bands) that are monitored with a dedicated instrument ?

3 Observational strategy

The results obtained so far support the idea that from a small number of properly chosen wavelengths, one could reconstruct the whole EUV/FUV spectrum with a precision that meets the requirements of a space weather service. This idea has been investigated in two complementary approaches.

The first approach is physics-based. Kretzschmar et al. (2006) selected intense spectral lines from the SEE spectra, with the constraint that 1) these lines must cover the range of temperatures found in the solar atmosphere, and 2) they can be assumed to be optically thin. They then computed the whole Sun differential emission measure (DEM) for each observing day, which allowed in turn to compute the non-observed part of the spectrum (i.e. all optically thin spectral lines to the exception of the extracted ones) for that day. The optically thick part of the spectrum was deduced empirically (i.e. through least square fitting) from one observation. Based on this, they determined six spectral lines from which the whole spectrum could be computed for each observation. Relative temporal variations were well reproduced in this study and a good general agreement has been found between the absolute value of the computed and observed spectra, especially for spectral lines (basically within 15%). The disagreement between observed and modeled spectrum in this study can be due to the failure of one or several assumptions made to use the DEM formalism (e.g. constant abundance), errors in atomic data, non-inclusion of weak spectral lines that contribute to the continuum, and non-proportionality between the various optically thick parts of the spectrum.

Table 1. Set of 14 lines that are appropriate for reconstructing the salient features of the solar EUV/FUV spectrum. From this, a subset of typically 6 non-redundant lines must be chosen.

He II	30.38 nm	Mg X	60.98 nm	O I	130.43 nm
Fe XVI	33.54 nm	O III	70.38 nm	C II	133.51 nm
Fe XV	41.73 nm	O II	83.42 nm	C IV	154.95 nm
Ne VII	46.52 nm	C III	97.70 nm	Si II	181.69 nm
O IV	55.43 nm	H I	121.57 nm		

The second approach is statistical, based on the decomposition presented in Sec. 2. Dudok de Wit et al. (2005) built a dendrogram of the 38 most intense spectral lines measured by TIMED/SEE, see Fig. 3. In such a plot, redundant lines with very similar dynamics are linked by a short branch. Dendrograms therefore provide a simple strategy for selecting spectral lines that describe the different facets of the spectral variability. From this, the authors extracted a first set of 14 lines, from which a smaller subset of 6 lines was found to minimise the error on the reconstructed spectrum. The 14 lines are listed in Table 1. Interestingly, the best candidates for spectral reconstruction are almost the same as those selected by Kretzschmar et al. (2006).

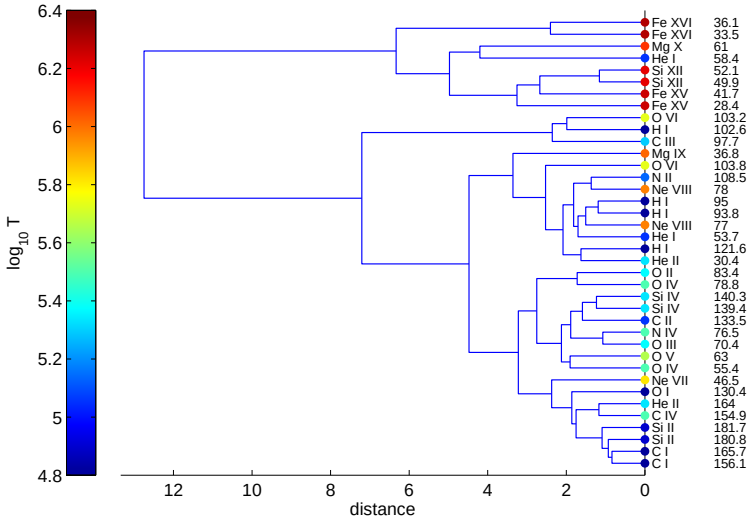

Fig. 3. Dendrogram of the strongest 38 EUV lines. The horiontal distance between each pair of lines reflects their degree of similarity. The colour code gives the characteristic emission temperature of each line. See Dudok de Wit et al. (2005) for a detailed explanation.

4 Discussion and conclusion

Ionospheric specification models require increasingly accurate measurements of the solar EUV/FUV spectrum, for which currently available proxies are of limited use. By using both a physics-based and a statistical approach, we have shown that the variability of the EUV/FUV spectrum exhibits a strong degree of redundancy, 2 dimensions being able to capture more than 95% of the variance . This leads us to advocate a different strategy, in which the EUV/FUV spectrum and its variability are reconstructed from the measurement of a few (typically 6) carefully chosen spectral lines or spectral bands. The choice of the best set of lines is application dependent. Lilensten et al. (2007b) describe a methodology for determining the lines that are most appropriate for ionospheric specification. A solar physicist may want to use a different set, to optimize for example the information on the solar atmosphere contained in the spectrum.

There is also a strong instrumental motivation for reconstructing the spectrum from a few lines only. Spectrographs are costly and like all EUV/FUV instruments, suffer from ageing. One could use instead arrays of photodiodes, for which more robust technologies are being developed. The LYRA radiometer (Hochedez et al., 2006) onboard the PROBA2 satellite (due for launch in 2008), will provide the first experimental ground to our approach as it will cover 4 bands: 1-20 nm, 17-70 nm, 115-125 nm and 200-220 nm. In Fig. 4, we give an example of how the response of diodes with different types of metallic filters compares against the various wavelengths between 26 and 193 nm, using the same representation as in Fig. 2. One can readily check that the diodes with Au, Pd, Ag and Cu filters are redundant, as are the diodes

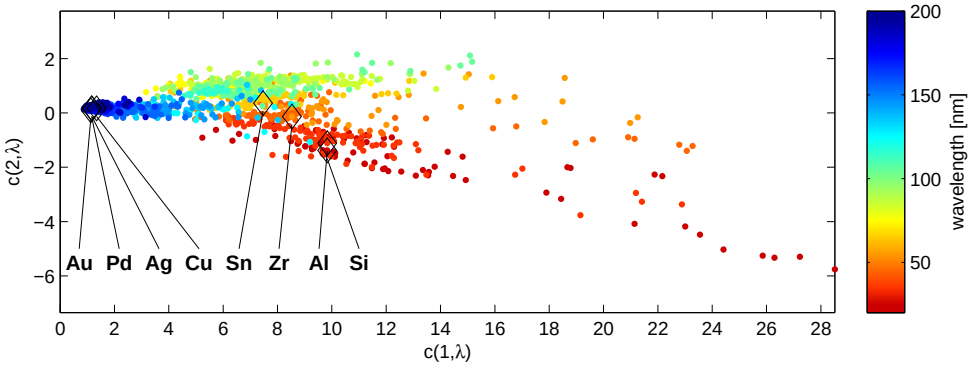

Fig. 4. Location of diodes with various spectral bands (given by their multilayer metal filter name), using the same representation as in Fig. 2.

with Al and Si filters.

Several aspects still need to be investigated for enhancing further the accuracy and the precision of the solar spectrum reconstruction. Concerning the nature of the proxies themselves, we might advantageously extend them to time-series that are not made only of spectral irradiance. For example, we may think to gross estimates of the disc proportion covered by Active regions and by Quiet Sun, which should allow higher precisions for mid-term reconstruction. This is one of the reason why the second generation of LYRA radiometers could include EUV imaging channels at relatively low spatial resolution. Multi-layers would permit a two-fold benefit on top of their being focusing mirrors. First, they can pave the EUV spectrum with overlapping passbands, or alternatively sample the most linearly independent wavelength ranges. Second, they can act as photocathodes, delivering a signal that could serve to correct for long-term drifts in the performance.

The impact of flares on the spectral reconstruction (Kretzschmar et al., 2007) must be taken into account; the method could then be implemented for several temporal scales in order to account for the difference in the physics controlling short-term brightenings (flares) and the longer terms (rotation, solar cycle). Another important point is the spectral variability below 26 nm, for which we must wait for SDO/EVE to cover that range with a good spectral resolution. The spectral variability above 193 nm is relatively easier to reconstruct. Work on this is in progress, using data from spacecraft such as UARS/SUSIM.

The authors of this paper intend to continue their efforts in this direction.

Acknowledgements: We gratefully acknowledge the TIMED/SEE team for providing the data and the COST 724 action for financial support. M. Kretzschmar acknowledges the support from the Belgian Federal Science Policy Office through the ESA-PRODEX programme.

References

Curdt, W., Brekke, P., Feldman, U., Wilhelm, K., Dwivedi, B. N., Schühle, U. and Lemaire,

P., *Astronomy & Astrophysics*, **375**: 591–613 (2001).

Dudok de Wit, T., Lilensten, J., Aboudarham, J., Amblard, P.-O. and Kretzschmar, M., Retrieving the solar EUV spectrum from a reduced set of spectral lines, *Annales Geophysicae*, **23**:3055-3069 (2005).

Dudok de Wit, T., Kretzschmar, M., Lilensten, J., Aboudarham, J., Amblard, P.-O., Auchère, F. and Moussaoui, S., Which solar EUV indices are best for reconstructing the solar EUV irradiance ? *Adv. Space Res.*, in press (2007).

Golub, G. H. and van Loan, C. F., Matrix Computations, Johns Hopkins Press, Baltimore, 3rd edition (1996).

Hinteregger, H. E., Fukui, K. and Gilson B. R., Observational, reference and model data on solar EUV, from measurements on AE-E, *Geoph. Res. Lett.*, **8**:1147-1150 (1981).

Hochedez, J.-F., Schmutz, W., Stockman, Y., et al., LYRA, a solar UV radiometer on Proba2, *Adv. Space Research*, **37**:303-312 (2006).

Kretzschmar, M., Lilensten, J. and Aboudarham, J., Variability of the EUV quiet Sun emission and reference spectrum using SUMER, *Astronomy & Astrophysics*, **419**: 345–356 (2004).

Kretzschmar, M., Lilensten, J., and Aboudarham, J., Retrieving the solar EUV spectral irradiance from the observation of 6 lines, *Adv. Space Research*, **37**:341-346 (2006).

Kretzschmar, M., Dudok de Wit, T., Lilensten, J., Aboudarham, J., Amblard, P.-O., Auchère, F. and Moussaoui, S., Retrieving he solar EUV irradiance from a few lines: the effect of flares, *Annales Geophysicae*, submitted (2007).

Lathuillère, C., Menvielle, M., Lilensten, J., Amari, T., and Radicella, S. M., From the Sun's atmosphere to the Earth's atmosphere: an overview of scientific models available for space weather developments, *Annales Geophysicae*, **20**:1081-1104 (2002).

Lean, L., A comparison of models of the sun's extreme ultraviolet irradiance variations, *J. Geophys. Res*, **95**:11933-11944 (1990).

Lilensten, J. and Bornarel, J., Space Weather, Environment and Societies, Springer Verlag, Dordrecht (2005).

Lilensten, J., Dudok de Wit, T., Kretzschmar, M., Amblard, P.-O., Moussaoui, S., Aboudarham, J. and Auchère F., Review on the solar variability spectrum for space weather purposes, *Annales Geophysicae*,Volume 25, Issue 6, pp.1299-1310 (2007a).

Lilensten, J., Dudok de Wit, T., Amblard, P.-O., Aboudarham, J., Auchère F. and Kretzschmar, M., Recommendation for a set of solar EUV lines to be monitored for aeronomy applications, *Annales Geophysicae*, Volume 25, Issue 6, pp.1299-1310 (2007b).

Richards, P. G., Fennelly, J. A., and Torr, D. G., EUVAC: A solar EUV flux model for aeronomic calculations, *J. Geophys. Res.*, **99**:8981–8992 (1994).

Tobiska, K., Recent solar extreme ultraviolet irradiance observations and modeling: A review, *J. Geophys. Res*, **98**:18879-18893 (1993).

Tobiska, W. K., Woods, T., Eparvier, F. , Viereck, R., Floyd, L., Bouwer, D., Rottman, G. and White, O.R., The SOLAR2000 empirical solar irradiance model and forecast tool, *Journal Atmos. Terr. Physics*, **60**:1233–1250 (2000).

Tobiska, W. K. Validating the solar EUV proxy, E10.7, *Journal of Geophysical Research*, **106**, Issue A12, p. 29969-29978 (2001).

Warren, H. P., Mariska, J. T. and Lean, J. A new model of solar EUV irradiance variability: 1. Model formulation, *J. Geophys. Res*, **106**:15745-15758 (2001).

Woods, T. N., Eparvier, F. G., Bailey, S. M., Chamberlin, P. C., Lean, J., Rottman, G. J., Solomon, S. C., Tobiska, W. K., and Woodraska, D. L., Solar EUV Experiment (SEE): Mission overview and first results, *J. Geophys. Research*, **110**, 1312 (2005).

Woods, T. N., Eparvier, F. G., Jones, A. et al., The EUV Variability Experiment (EVE) on the Solar Dynamics Observatory (SDO): science plan and instrument overview, in *ESA SP-617*, SOHO-17 conference: 10 Years of SOHO and Beyond (2006).

Forecasting Solar Energetic Particle Events

M. Storini[1], E. W. Cliver[2], M. Laurenza[1], and C. Grimani[3]

[1] IFSI-Roma/INAF, Via del Fosso del Cavaliere, 100 - 00133 Roma, Italy
storini@ifsi-roma.inaf.it
[2] AFRL, Space Vehicles Directorate, Hanscom AFB, MA, USA
[3] Physics Institute, Urbino University, Via S. Chiara, 27 - 61029 Urbino, Italy

Summary. We present a brief review of available long-term (years to solar cycle) and short-term (minutes to hours) forecast techniques for Solar Energetic Particle (SEP) events. We describe recent work on the development of a new short-term warning technique for SEP event occurrence that is based on flare location and integrated soft X-ray and low-frequency radio emission. For cycle 23, this method yielded a Probability of Detection of about 63 % and a False Alarm Rate of about 45 %, establishing benchmarks for automated SEP event alerts.

1 Introduction

Space exploration has focused attention on the hazards presented by both galactic cosmic ray (CR) particles and solar energetic particles (SEPs) (see, for instance, Storini, 2006; Baker et al., 2007). These hazards include damage to satellite components, single event upsets on spaceborne computers, and radiation threat to astronauts. The principal processes involved are: nuclear interactions, ionisation/excitation of atoms/molecules and the destruction of crystal structures (e.g., in memory banks or solar panels) or of molecular chains (resulting in skin penetration, free radical generation, and DNA damage). Galactic CRs represent long-lived radiation hazards because they furnish a continuous flux, while SEPs are short-lived hazards. The fluxes of these two suprathermal particle populations of the interplanetary medium differ in their energy spectra and their opposite relation to the solar activity cycle.

In this article we will focus on SEPs, treating CR particles as the background on which SEP events occur. Even though the discovery of SEPs dates back to 1942 (Forbush, 1946), there are many uncertain aspects of SEP generation/acceleration and propagation that make SEP forecasting on either long (solar cycle) or short (minutes to hours) time scales difficult. SEP data collected by ground and space based instruments over the years, and the SEP event lists constructed from these data, furnish the basis to develop SEP event forecast models. It is necessary to keep in mind that the definition of a SEP event can differ among the various available event lists. For example, the SEP event definition applied by NOAA/SEC (Boulder - U.S.A.) on GOES data series, is as follows: *Event Start* $\rightarrow$ when the proton flux J[E $>$ 10 MeV] $\geq$ 10 pfu (pfu = part. cm^{-2}s^{-1}sr^{-1}) for three consecutive 5-min intervals and *Event End* $\rightarrow$ when J falls below 10 pfu.

Here we summarize work performed under WG-1 of COST 724 Action for the SEP/Space Weather relationship. In Sect. 2 we review existing long-term models for SEP forecasts, while in Sect. 3 we present a brief account of recent work on a short-term SEP event warning technique. The conclusion is given in Sect. 4.

2 Long-term SEP Forecast Techniques

Models for long-term (mission lifetime or solar cycle) SEP predictions were started during the 1970s (King, 1974). Currently, four models are mainly in use: KING/SOLPRO, JPL, ESP (see, for instance, http://www.spenvis.oma.be/spenvis/help/models/sep.html for model descriptions) and MSU (Nymmik, 2007a, and references therein).

2.1 To distinguish between models

KING/SOLPRO model

The KING model, derived by using SEP data recorded from 1966 to 1972, was mainly used to predict mission integrated solar fluences (King, 1974). The code version of the model is called SOLPRO (Stassinopoulos, 1975) and offers outputs for energies E $>$ 10 MeV to $>$ 100 MeV.

JPL fluence model

The first version of the JPL model (JPL-85) was based on data taken during cycles 19-21 (Feynman et al., 1990). The JPL model uses a log-normal distribution to fit the solar proton events size distribution (a worst case should be imposed). Results can be obtained only for the active phase of the solar cycle. The most recent version of the model (JPL-91), based on data from 1963 to early 1991, runs after selecting a lower threshold value to start proton fluence computation at various integrated energy channels ($>$ 1 MeV to $>$ 60 MeV; Feynman et al., 1993). More details can be found in Feynman et al. (2002).

Emission of Solar Protons - ESP model

The ESP model predicts integral omnidirectional solar proton fluences at 1 AU, in the energy range $>$ 1 MeV to $>$ 300 MeV (Xapsos et al., 1999a). The model employs the maximum entropy method (Xapsos et al., 1999b, 2000). It is able to predict cumulative solar proton fluences and worst-case solar proton events as functions of mission duration and user confidence level.

MSU model

The model of the Moscow State University (MSU) was developed during the 1990s (Nymmik, 1999c) to compute the probability for the $\geq$ 10 MeV/nucleon SEP fluences and peak fluxes in near-Earth space for different solar activity levels. The most recent version of the model can be found at http://elana.sinp.msu.ru/nymmik/models/sep.php (see also Kuznetsov et al., 2005; Nymmik, 2007b).

2.2 Looking to the next solar activity cycle

During the next solar activity cycle several space missions will be carried out, including LISA (Laser Interferometer Space Antenna). Nymmik (1999a,b) reported a model to estimate the SEP fluence distribution as a function of the solar activity. In their model, the SEP fluence distribution follows a power-law function with an exponential steepening for large fluences (see also Nymmik, 2001). This model applies to solar proton fluences in the range 10^6 - 10^{11} protons/cm^2 for proton energies E $>$ 30 MeV; it was inferred from the analysis of IMP data (solar cycles: 20-22) and from the proton fluxes derived from the analysis of radionuclides in lunar rocks.

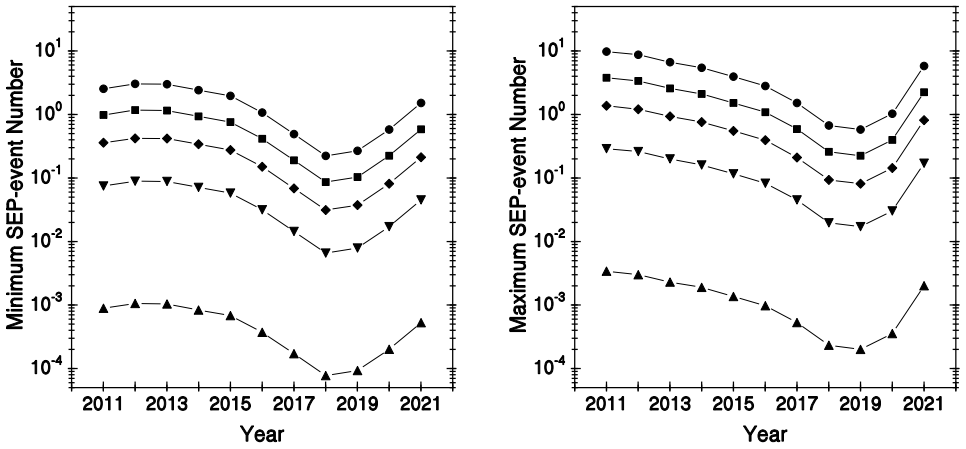

Fig. 1. Minimum (left panel) and maximum (right panel) expected SEP events with E $>$ 30 MeV for 2011-2021, derived from Nymmik (1999a,b) model. Fluence intervals: circle for 10^6 - 10^7 protons/cm^2, square for 10^7 - 10^8 protons/cm^2, diamond for 10^8 - 10^9 protons/cm^2, inverted triangle for 10^9 - 10^{10} protons/cm^2, triangle for 10^{10} - 10^{11} protons/cm^2.

Here the expected number of proton events in individual intervals of fluence during 2011 - 2021 was evaluated as follows. As a first step, the minimum and maximum yearly number N_p of expected proton events were derived by using the relation N_p = 0.0694 W (Nymmik, 1999b), where W is the minimum and maximum yearly predicted Wolf number (as reported by Wass et al., 2003), respectively. As a second step, two values of the constant C were determined for each year by integrating the function

$$dN_p = C\Phi^{-1.41} e^{-\Phi/\Phi_c} d\Phi \tag{1}$$

(where Φ is the fluence and Φ_c was assumed equal to 4x10^9; see Nymmik, 1999a, for details) and by imposing N_p to be the values computed in the first step. The integration was carried out above 10^6 protons/cm^2. Finally, after constant C determination, eq. (1) allowed to compute the minimum and maximum number of expected events per fluence interval, as reported in Fig. 1. Results suggest at most 15 (2) SEP events with fluences larger than 10^6

protons/cm^2 at solar maximum (minimum) of solar activity cycle n. 24. These estimates decrease of one order of magnitude for fluences above 10^9 protons/cm^2.

3 Short-term SEP Forecasting Techniques

Ideally, short-term forecasting techniques should be in principle of the engineering type. In other words, real-time forecast requires automated codes running on information systems without forecaster input. Attempts to develop such techniques began several years ago. Nevertheless, to our knowledge only two models/codes were accurately validated (PROTONS and PPS). They are semi-empirical models based on SEP properties derived from a large series of registered events, and some experimental/theoretical results. They do not predict a solar event and its proton output in advance but run after a solar flare occurrence, using flare parameters as input for the proton forecast.

3.1 The current validated methods

PROTONS code

The PROTONS code was first implemented in real time operation during the 1970s (Heckman, 1979; Balch & Kunches, 1986; Heckman et al., 1992). It is based on precursor information (X-ray flare location, X-ray half-power fluence and Type II/IV radio burst occurrence). Current PROTONS code (see Balch, 1999, for details) is running at NOAA/SEC (Boulder - U.S.A.). The main outputs of the code are: SEP event occurrence probability, predicted SEP rise time (time from X-ray flare maximum to SEP flux maximum), and the predicted peak flux at the Earth. PROTONS was recently validated by Balch (private communication, 2007) by using data from 1986-2004. He found that, when the optimal Heidke skill score is used with a probability threshold of 20-30 %, the False Alarm Rate (FAR) is 57 % and the Probability of SEP Detection (PoD) = 55%.

PROTON PREDICTION SYSTEM - PPS code

The PPS code, initially PPS76, was developed during the 1970s (Smart & Shea, 1979) and updated as PPS-87 (Advanced Proton Prediction System; Smart & Shea, 1989) during the 1980s. Input parameters include: flare signatures, fixed time for particle injection into the interplanetary magnetic field (0.25 h after flare onset) and a longitudinal SEP intensity gradient. Outputs include: SEP occurrence (not probability), timing, intensity, spectrum and elemental composition for different energy channels ($E_{min} > 5$ MeV). The PPS code was recently validated by Kahler et al. (2007), considering $\geq$ M5 X-ray flares during 1997-2001. Those authors found roughly equal numbers of correct and false predictions.

3.2 Potential short-term forecasting methods

Recently, several additional short-term SEP forecasts have also been proposed, although none of these have received independent validation.

Garcia (2004a) discussed the use of the empirical connection existing between SEPs and low-temperature soft X-ray flares, while Garcia (2004b) considered the SEP/hard X-ray flare relationship. The second work, based on May 2000 - December 2002 data (107 hard X-ray flares and 16 SEP-associated flares), noted that flares characterized by hard x-ray spectra hardening for at least 3 min have a high association with SEPs. In fact, 14 SEPs were correctly identified, 2 SEPs were missed, and 3 false alarms predicted.

Recently, Posner (2007) proposed an up to 1-hour forecast technique for proton events by using relativistic electron intensities in space (since electron onset precedes proton onset). The technique was tested on SOHO/COSTEP data for eleven months of 2003. A detailed description of the possible advanced forecast is furnished, including the forecasting contingency matrix and the evaluation of false and missed warnings (see their Table 3). The model is not complete because in the present version it is only able to forecast SEP onset. Nevertheless, if completed, it looks as a promising forecasting technique.

At the University of Southampton (U.K.), neural network techniques were used to give forecasts with lead times of the order of 48 hr (Gabriel & Patrick, 2003) by using the ratio of the GOES X-ray (hard and soft channels) fluxes as inputs. After trying different input combinations the best success rate was about 65 %. Nevertheless, their contingency table shows a very high number of predicted SEP events that were not actually observed (see, for more details, Gabriel, 2007).

Artificial neural networks are potentially useful tools to improve SEP forecasts; currently they are also used in near-real time for some application models (e.g., SEP event dose-time profiles, Hoff & Townsend, 2003). These application models evaluate the impact of charged-particle fluxes on materials, instruments and biological bodies (see, for cosmic ray effects on micro-electronics, Tylka et al., 1997).

3.3 A new forecasting method

A new forecasting method to provide short-term warnings for flare associated SEP events is under construction by Laurenza et al. Those authors adopted an empirical approach by using flare parameters as *yes* or *no* indicators of particle acceleration at the Sun. The parameters include: (i) flare longitude, (ii) flare size as indicated by its integrated soft X-ray intensity, and (iii) particle acceleration/escape, as indicated by the time integrated 1 MHz radio intensity. In this technique, alerts are issued 10 minutes after the maximum of $\geq$ M2 soft X-ray flares. The model set up was accomplished by creating two databases for a defined time interval:

- SEP events with their associated flares,
- $\geq$ M2 soft X-ray flares.

The databases were built-up from data retrieved at: http://spidr.ngdc.noaa.gov/spidr/index.jsp and http://lep694.gsfc.nasa.gov/waves/waves.html.

A comprehensive SEP catalogue has been prepared for SEP events occurring between January 1995 and December 2005, by selecting all proton enhancements meeting the current NOAA SEP definition (see Sect. 1). SEP events originating from distinct solar sources were separated (even if a pre-existing event was still in progress; note that this procedure is not used by NOAA/SEC). We associated each identified SEP event with a solar source (see Laurenza et al., 2007, for details), either (1) a visible disk flare, or (2) a partially observed, or inferred, behind-the-limb eruption. Generally, we identified the largest soft X-ray flare near the SEP

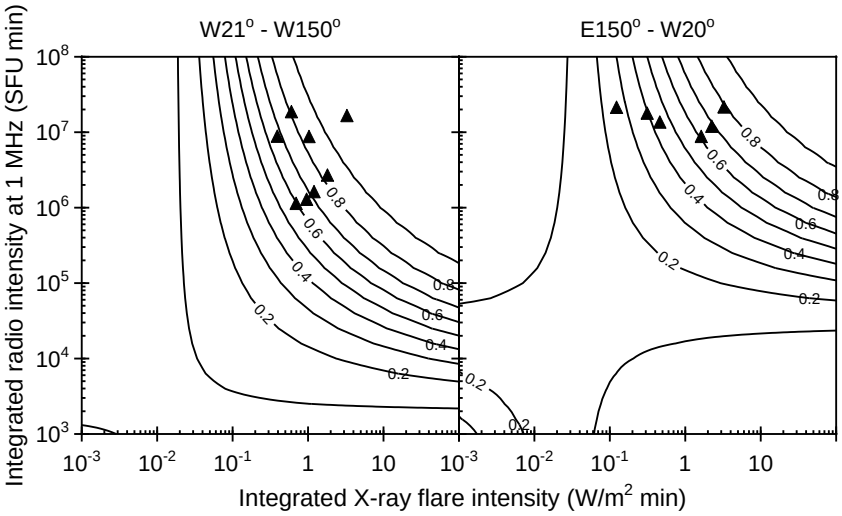

Fig. 2. Probability contours for SEP occurrence forecast for flare location W 21° - W 150° (left panel) and W 20° - E 150° (right panel), as derived with the new SEP forecasting method, together with the parameters for GLEs (triangles) occurring from January 1995 to December 2005 (GLE55 to GLE69, except for GLE61 initiated beyond the solar limb).

event start time as the SEP source, taking into account the time coincidence with type II and IV radioemission events and fast CMEs.

The second database consists of 704 X-ray flares of class $\geq$ M 2.0, for which the association of the soft X-ray bursts with H-alpha flares was checked by using the NGDC lists (as in Laurenza et al., 2007, for $\geq$ M5.0 flares). For bursts not associated to H-alpha records, we determined the flare location from the active region histories. For each flare we computed the key parameters for the analysis.

The time integrated flux of the X-ray flare was derived from the 1/3 power point before the peak to the 1/3 power point after. If the X-ray intensity drops by a factor 3 within 10 min of the peak, the integration stops, otherwise an exponential fit of the X-ray intensity curve is used to extrapolate the intensity curve to the 1/3 power point.

The integrated flux of the radio emission at 1 MHz was computed from 10 min before the time of the 1/3 power point on the rise of the soft X-ray burst until 10 min after the X-ray peak. The choice of this interval resulted from a process of trial and error.

Note that both the soft X-ray and radio integrations are terminated within 10 minutes after the flare maximum to allow a prompt warning.

The probability of the SEP event occurrence is estimated by performing the logistic regression technique (McCullagh&Nelder, 1989) over the constructed data series. Figure 2 shows the probability levels computed for two heliographic longitude intervals (W21° - W150°, left panel; E150° - W20°, right panel) as a function of the time integrated X-ray intensity and radio emission.

Every solar flare characterized by the above parameters can be located in such a diagram to evaluate the probability of a subsequent SEP event. An example is provided in Figure 2, where the flares associated with ground level enhancements (GLEs) from January 1995 to December 2005 are indicated (solid triangles). It can be seen that they lie above the 60 % (25 %) probability for the W 21° - W 150° (E 150° - W 20°) longitude range.

The method allows, after the selection of a probability threshold, a *yes/no* binary response for the occurrence of a SEP event: if flare parametes (integrated X-ray flare intensity, integrated radio intensity at 1 MHz) are located above the threshold a warning is issued, otherwise no alert is given.

A preliminary evaluation of the model under test was performed by comparing the forecast signals with SEP observations during 1995-2005 in terms of PoD and FAR . We obtained PoD = 63 % and FAR = 45 % (by using a probablity threshold level of 0.25-0.35 %), that exceed current standards for SEP event alerts (see Sect. 3.1).

A detailed description of the above SEP short-term forecast model, results and implications will be published (Laurenza et al., in preparation).

4 Conclusion

This paper offers a brief summary of acquired knowledge on SEP forecast during COST 724 Action. It is shown that the performance of the available codes is still low; further work is needed to reach Space Weather requirements.

Acknowledgement. MS and ML acknowledge support from IFSI-Roma/INAF, EWC from the EOARD Window on Europe program, and CG from INFN of Italy. COST 724 Action is acknowledged together with A. G. Ling for invaluable help during the different stages of the new model development. MS also thanks S. B. Gabriel for acting as co-leader of WG1/WP13000.

References

Baker, D. N., Braby, L. A., Curtis, S., Jokipii, J. R., Lewis, W. S., Miller, J., Schimmerling, W., Singer, H., Strachan, L., Townsend, L. W., Turner, R. E., Zurbuchen, T. H.: Space Radiation Hazards and the Vision for Space Exploration; A Report on the October 2005 Wintergreen Conference. Space Weather, **5**, S02004, doi:10.1029/2007SW000313 (2007)

Balch, C. C.: SEC proton prediction model: Verification and analysis. Rad. Meas., **30**, 231-250 (1999)

Balch, C. C., Kunches, J.: SESC Methods for Proton Event Forecasts. In: Simon, P.A., Heckman, G., Shea, M.A. (eds) Solar-Terrestrial Predictions, 353-356, Boulder, CO: National Oceanic and Atmospheric Administration (1986)

Forbush, S. E.: Three unusual cosmic-ray increases possibly due to charged particles from the Sun. Phys. Rev., **70**, 771-772 (1946)

Feynman, J., Armstrong, T. P., Dao-Gibner, L., Silverman, S.: New Interplanetary Proton Fluence Model, J. Spacecraft and Rockets, **27**, 403- 410 (1990)

Feynman, J., Spitale, G., Wang, J., Gabriel, S. B.: Interplanetary Proton Fluence Model: JPL 1991. J. Geophys. Res., **98**, 13,281-13,294 (1993)

Feynman, J., Ruzmaikin, A., Berdichevsky, V.: The JPL proton fluence model: an update. J. Atmos. Sol. Terr. Phys., **64**, 1679-1686 (2002)

Gabriel, S. B.: Prediction of solar energetic particle events, In: This volume. COST 724 Action (2007)

Gabriel, S. B., Patrick G. J.: Solar energetic particle events: Phenomenology and prediction. Space Sci. Rev., **107 (1-2)**, 55-62 (2003)

Garcia, H. A.: Forecasting methods for occurrence and magnitude of proton storms with solar soft X-rays. Space Weather, **2**, S02002, doi:10.1029/2003SW000001 (2004a)

Garcia, H. A.: Forecasting methods for occurrence and magnitude of proton storms with solar hard X-rays. Space Weather, **2**, S06003, doi:10.1029/2003SW000035 (2004b)

Heckman, G. R.: Predictions of the Space Environment Services Center. In: Donnelley, R.F. (ed) Solar-Terrestrial Predictions, vol. 1, 322-349, US Dept. of Commerce, Washington, DC (1979)

Heckman, G. R., Kunches, J. M., Allen, J. H.: Prediction and evaluation of solar particle events based on precursor information. Adv. Space. Res., **12 (2-3)**, (2)313-(2)320 (1992)

Hoff, J. L., Townsend, L.W.: Prediction of energetic solar particle event dose-time profiles using artificial neural networks. IEEE Trans. Nucl. Sci., **50 (6)**, 2296-2300 (2003)

Kahler, S.W., Cliver, E.W., Ling, A. G.: Validating the proton prediction system (PPS). J. Atmos. Sol. Terr. Phys., **69**, 43-49 (2007)

King, J. H.: Solar Proton Fluences for 1977-1983 Space Missions. J. Spacecraft Rockets, **11 (6)**, 401-408 (1974)

Kuznetsov, N. V., Nymmik, R. A., Panasyuk, M. I.: Models of solar energetic particle fluxes: The main requirements and the development prospects. Adv. Space Res., **36**, 2003-2011 (2005)

Laurenza, M., Hewitt, J., Cliver, E. W., Storini, M., Ling, A.: Solar energetic proton events and Soft X-ray flares, Contributed paper to 20^{th} ECRS, September 5-8, 2006, Lisbon (Portugal). Available on line at http://www.lip.pt/events/2006/ecrs/proc/ecrs06-s1-34.pdf (2007)

McCullagh, P., Nelder, J. A.: Generalized Linear Models, Second Edition, Chapman and Hall (1989)

Nymmik, R. A.: SEP event distribution function as inferred from spaceborne measurements and lunar rock isotopic data. In: Proc. 25^{th} ICRC, Salt Lake City, USA, vol. 6, 268-271 (1999a)

Nymmik, R. A.: Relationship among solar activity, SEP occurrence frequency, and solar energetic particle event distribution function. In Proc. 25^{th} ICRC, Salt Lake City, USA, vol. 6, 280-283 (1999b)

Nymmik, R. A.: Probabilistic model for fluences and peak fluxes of solar energetic particles. Rad. Meas., **30**, 287-296 (1999c)

Nymmik, R. A.: The main characteristics of the solar energetic particle events relevant to solar activity. In: Proc. 27^{th} ICRC, Hamburg, Germany, 3197-3200 (2001)

Nymmik, R. A.: Improvement environment radiation models. Adv. Space Res., **40**, 313-320 (2007a)

Nymmik, R. A.: Probabilistic model of solar energetic proton fluxes, In: This volume. COST 724 Action (2007b)

Posner, A.: Up to 1-hour forecasting of radiation hazards from solar energetic ion events with relativistic electrons. Space Weather, **5**, S05001, doi:10.1029/2006SW000268 (2007)

Smart, D. F., Shea, M. A.: PPS76: a computerized event mode solar proton forecasting technique. In: Donnelley, R. F. (ed) Solar-Terrestrial Predictions, vol. 1, 406-427, US Dept. of Commerce, Washington, DC (1979)

Smart, D. F., Shea M. A.: PPS-87-a new event oriented solar proton prediction model. Adv. Space Res., **9 (10)**, 281-284 (1989)

Stassinopoulos, E. G.: SOLPRO: A Computer Code to Calculate Probabilistic Energetic Solar Proton Fluences. NSSDC 75-11, Greenbelt, Maryland (1975)

Storini, M.: The relevance of cosmic rays to Space and Earth Weather. Invited talk to 20^{th} ECRS, September 5-8, 2006, Lisbon (Portugal). Available on line at http://www.fis.uniroma3.it/∼svirco/STORINI_ECRS06.pdf (2006)

Tylka, A. J., Adams, J. H. Jr., Boberg, P. R., Brownstein, B., Dietrich, W. F., Flueckiger, E. O., Petersen, E. L., Shea, M,. A., Smart, D. F., Smith, E. C.: CREME96: A revision of the Cosmic Ray Effects on Micro-Electronics code. IEEE Trans. Nucl. Sci., **44**, 2150-2160 (1997)

Wass, P., Araújo, H., Sumner, T.: LISA Int. Collaboration, internal note (2003)

Xapsos, M. A., Barth, J. L., Stassinopoulos, E. G. , Burke, E. A., Gee, G. B.: Space Environment Effects: Models for emission of solar protons (ESP) - Cumulative and Worst-Case Event Fluences. NASA/TP-1999-209763, MSFC, Alabama (1999a)

Xapsos, M. A., Summers, G. P., Barth, J. L., Stassinopoulos, E. G., Burke, E. A.: Probability Model for Worst Case Solar Proton Event Fluences. IEEE Trans. Nucl. Sci., **46**, 1481-1485 (1999b)

Xapsos, M. A., Summers, G. P., Barth, J. L., Stassinopoulos, E. G., Burke, E. A.: Probability Model for Cumulative Solar Proton Event Fluences. IEEE Trans. Nucl. Sci., **47**, 486-490 (2000)

Impact of Solar X-ray Flares on the Lower Ionosphere - Observations and Modelling

V.Žigman[1], D.Grubor[2] and D.Šulić[3]

[1] University of Nova Gorica, Nova Gorica, Slovenia vida.zigman@p-ng.si
[2] University of Belgrade, Faculty of Mining and Geology, Serbia davorkag@rgf.bg.ac.yu
[3] Institute of Physics, Belgrade, Serbia dsulic@phy.bg.ac.yu

Summary. The present study addresses the research of the lower ionosphere, in terms of D-region electron density enhancements during Solar X- ray flares caused by the Sun eruptive activity. The research relies on ground- and space-based measurements: the VLF amplitude perturbance, recorded by the Belgrade facility (AbsPAL) has been related to the X-ray irradiance measured by the GOES -12 satellite, for 120 flare induced events, registered through May-August 2004-2007. Upon the analysis of the two database sets, a new model for determining electron density time profiles has been proposed. The results arrived at are found in good agreement with measurements by different techniques and independent estimates of the Wait ionosphere model.

1 Introduction

The lower ionosphere, i.e. the D-region, is the 60-90 km altitude range of the spherical ionized shell surrounding the Earth. It is the ionospheric region closest to Earth, yet probably the most complex in terms of its species content and their interactions. The standard sounding of the ionosphere, using ionosonde networks or IRS campaigns (HF and VHF/UFH-band radio waves, respectively) is not applicable, as D-region electron densities are well below the critical one to cause signal reflection. Lower frequencies needed for continuous observations of the D-region, are provided by middle frequency radars (Holdsworth et al., 2002), and very low frequency (VLF) man-made transmitters (McRae & Thomson, 2000). These VLF signals, and the naturally generated VLF waves, associated with lightning discharges, propagate along the duct between the Earth surface and the lower reflective boundary of the D-region - the Earth-ionosphere waveguide. This makes them suitable for studying the lower ionosphere under the deeply penetrating X-ray radiation during solar flares (Thomson & Clilverd, 2001; Thomson et al., 2005; Ohya et al., 2006). Although the main source of ionization, the H-Lyman-α emission, is enhanced as well, the X-ray radiation, during the flare event, overwhelms all other ionization sources, leading to the increase of D-region electron density by 1-2 orders of magnitude.

VLF signals, continuously emitted from transmitters with well stabilized phase and amplitude, reveal regular diurnal, and seasonal variations under undisturbed ionospheric conditions. In particular, the change in propagation caused by sudden energy bursts from X-ray solar

flares is most distinctly impressed on the VLF signal, by amplitude and phase abrupt increase or decrease (see Figs. 1,2). These are understood as signatures of the prominent change of the lower ionosphere electron density profile, under the intense 0.1-0.8 nm part of the solar X-ray spectrum. Increased electron densities lower the effective reflection height and advance the phase of the wave at the receiver, resulting in the registered irregularities in both amplitude and phase. In this way, VLF radiowaves make an efficient tool in exploring the nature of the lower ionosphere, during solar X-ray flare disturbances.

Over the last two decades, programmes for simulating VLF propagation, developed by the Naval Ocean Systems Center (NOSC) have been extensively used (Thomson & Clilverd, 2001; Thomson et al., 2005). The Long Wave Propagation Capability (LWPC) and the ModeFinder programmes (Ferguson, 1995) take the input path variables and calculate the full wave solution parameters (reflection coefficients), to predict the VLF phase and amplitudes along the complete path, from transmitter to receiver. They usually operate on the 'Wait two-parameter ionosphere' model for the D-region (e.g. Wait, 1970), with two parameters, the ionospheric 'sharpness' β, and the reflection height H' by which VLF propagation characteristics can be restored along the whole Earth-D-region bottom waveguide. When solar flares are concerned, by matching the measured and simulated perturbed amplitudes and phases, β and H' are retrieved to give the electron density *height* profile $N(z)$, at the flare flux maximum (e.g. Wait & Spies, 1964; Thomson 1993).

In the present study, in the attempt to complement the above approach, we address the time-dependent behaviour of the solar X-ray flux and model the transient electron density $N(t)$ response to the flare. The time delay Δt - the time interval by which the amplitude (and phase) extremum lags behind the flare flux maximum - evolved as a key parameter. The Δt parameter allows to estimate the effective recombination coefficient α and to predict $N(t)$ in time, locally at the chosen height, throughout the duration of the flare. VLF data from three different propagation Great Circle Paths (GCP) i.e different transmitters, have been used in the analysis, with the aim to compare the VLF effects of a single flare against different waveguide properties. The results of the presently outlined model have been found to be in good agreement with the ones obtained with LWPC simulations; as well as with independent experimetal electron density estimates under flare conditions.

2 Measurements and data analysis

The VLF ground-based measurements, presented here, were performed with the AbsPAL (Absolute Phase and Amplitude Logger) facility, installed at the Institute of Physics, Belgrade (44.85 N; 20.38 E). The receiver has been in stable operation since 2004, providing continuous and well-calibrated data of VLF signals from several transmitters. From the wealth of recorded data we focus on well stabilized signals from three paths: 1) GQD/22.1 kHz emitted from Skelton (54.72 N; 02.88 W) and propagating, over the 1982 km long GCP, in nearly N-S direction over the Northern hemisphere; 2) NAA/24.0 kHz emitted from Cutler (44.65 N; 67.3 W) and propagating, over the 6548 km long GCP, in W-E direction over the Northern hemisphere and 3) NWC/19.8 kHz emitted from Harold E. Holt (21.8S; 114.2 E) and propagating, over the 11974 km long GCP in SE-NW direction, from Southern to Northern hemisphere. During the summer months from 2004 to 2007, the diurnal variations of VLF

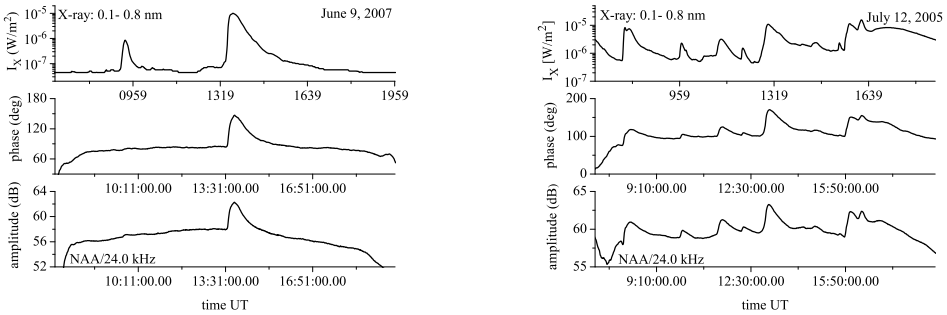

Fig. 1. *left:* The X-ray irradiance of two separate flares, B7 class at 0941 UT and M1 class at 1348 UT (upper panel) and the NAA/24.0 kHz signal phase and amplitude (middle and lower panel respectively), plotted for the daytime interval of 09June2007. (It is indicative to notice that the B class flare at 0941 UT has apparently no influence on the VLF signal characteristics.) *right:* Several separate flares between the C7.5 at 0812 UT, and the M1 at 1306 UT, and two successive afternoon flares,(upper panel) and the NAA signal phase and amplitude (middle and lower panel respectively), plotted for the daytime interval of 12July2005.

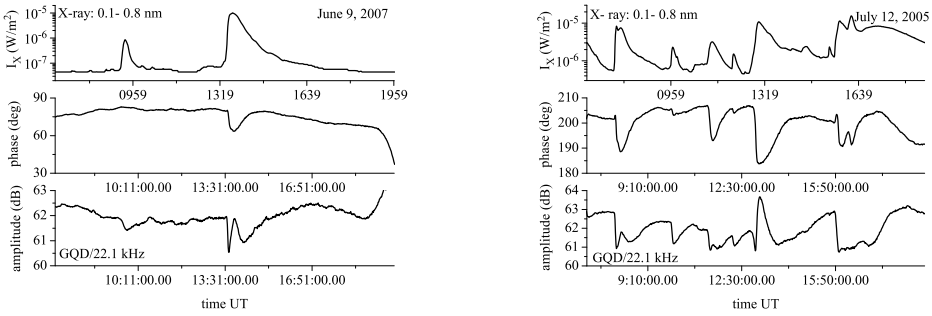

Fig. 2. *left:*The flare, reported at 1348 UT on 09June2007 (also presented in Fig1, upper panels,) and the phase and amplitude of the GQD/22.1 kHz signal (middle and lower panel respectively). *right:* The X-ray irradiance for the flare active 12July2005, (upper panel as in Fig. 1), and the phase and amplitude response on the GQD path.

amplitude and phase of the three signals, with clear solar flare signatures were examined. The analysis of 150 registered VLF perturbation events was paralleled with the inspection of the corresponding solar fluxes retrieved from the GOES-12 X-ray data lists, in the wavelength range 0.1-0.8 nm, via NOAA (www.sec.noaa.gov), both data sets taken with 1min resolution. As shown by the example in Figs.1,2 the features of enhanced X-ray irradiance are most remarkably impressed upon the amplitude/phase characteristic, either for the isolated flare of class M1 on 09June2007, or for the series of flares on the rather active 12July2005. Though, apparently different, in dependence of the path (e.g. Fig.1-NAA, Fig.2-GQD), the

disturbances show stable patterns: always phase enhancement on long NAA and NWC paths, and always phase decrease on the short GQD path. Amplitude increase is regularly reproduced on both NAA and NWC, while amplitude perturbations on the GQD path display more complexity (e.g. Fig. 2): both increase and decrease and also oscillations in dependence of the flare intensity (Grubor et al., 2005).

Regardlessly of the type of amplitude disturbance, it has been found that almost invariably, the extreme amplitude value (maximum, minimum, or the first maximum in the oscillation pattern) is delayed in time with respect to the peak of the X-ray flare flux. The time interval by which the extreme amplitude value appears distinctly separated from the irradiance maximum is denoted as *time delay* Δt. The term was introduced to describe the time-shifted response of the ionosphere in terms of electron density enhancement, to the diurnal solar irradiance at minimum solar zenith angle (Appleton, 1953). The time lag both at regular diurnal insolation (20-40 min) and at flare occurrence (1-7 min), though distinctly different in duration, characterizes the transient state of the D-region. To identify the time delay and to quantify it in connection with the flare phenomenon was of crucial importance, as it provides the basis to estimate the effective electron recombination coefficient α in flare regime.

3 Modelling the electron density during solar X-ray flares

The developed model rests on two basic assumptions:

1. The VLF amplitude responds to the flare-induced variations of electron density almost instantaneously: the time delay of the amplitude extreme value with respect to the X-ray flux maximum is as well the delay of the electron density maximum behind the flux maximum.

2. Excluding large flares (higher class M and X) that induce amplitude detain (Thomson et al., 2005), the unambiguous determination of the amplitude extremum was possible in around 120 events (out of 150 registered), with the time delay measured to range from 1min to at most 7 min. A rather short time delay as compared to the duration of the flare, lasting from 40-60 min, makes us assume that the value of the electron density at $I_{\max}$, i.e. $N(I_{\max})$ is *close* to the maximum value $N_{\max}$ induced by the flare.

Neglecting diffusion, on timescales of flare duration, and taking into account the global electroneutrality of the sunlit lower ionosphere, leads to the electron continuity equation that describes the flare-induced temporal evolution of the electron density $N(t,h)$ at the specified height h:

$$\frac{dN}{dt} = q(t) - \alpha N^2, \quad (z = h). \tag{1}$$

The key input data are the electron production rate q and the effective electron recombination coefficient α. During flares q is dominantly driven by the increased X-ray flux I, and is taken to vary proportionally, $q(t) = k\, I(t)$. According to e.g. Budden (1988), $q = (CI/eH)\cos\chi$, so that one has $k \equiv (C/eH)\cos\chi$, where e is the base of the natural logarithm. For the ionization efficiency C we extrapolate the values given by Whitten & Poppof (1965) to the 0.1-0.8 nm range, and for the scale height $H(= RT/Mg)$ we take 7 km. The local solar zenith angle χ is taken at the time $t(I_{\max})$. To determine the effective recombination coefficient α, not well known at flare conditions, the measured time delay is used. The procedure, described in detail by Žigman et al. (2007), relies on assumption (2), i.e. takes into account the

connection between $N_{\max}$ and $N(I_{\max})$ values separated by Δt, leading to the relationship $k \cdot \alpha = const$. With k known, the particular value of α is inferred.

The electron density for *preflare* conditions, was determined by running the LWPC programme. It was found that the β and H' parameters that reproduce overall well the quiet-daytime amplitudes measured at Belgrade, for the three traces, correspond to $\beta = 0.30$ 1/km and $H' = 74$ km. These (β, H') values at the altitude h, taken as the reflection height of the quiet ionosphere (H'= 74 km), yield the adopted *initial* electron density value $N(0, h = H') = 2.18 \times 10^8 \mathrm{m}^{-3}$.

4 Results and Summary

The effective recombination coefficient assigned to the state of the lower ionosphere, in flare conditions versus maximum flare flux is shown in Fig.3 *left panel*. The obtained domain of α is in accordance with the values inferred from different experimental techniques in the altitude range from 65-100 km (Collis et al., 1996; Rodger et al., 1998; Ulich et al., 2000). The decrease of the D-region effective recombination coefficient with increasing flare flux I (i.e. ionization rate q), evidenced in a number of studies, (Mitra, 1974, ch.8,9 and references therein), has been outstandingly confirmed. The electron density results for characteristic flare

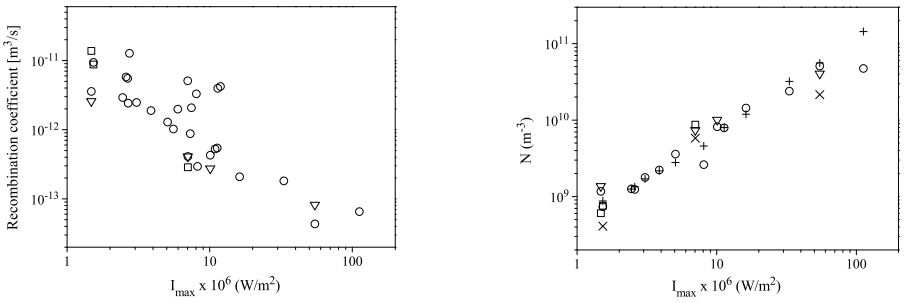

Fig. 3. *left*: Effective electron recombination coefficient α, and *right*: electron densities, during flare occurrence, versus maximum flare flux $I_{\max}$ at 74km height. Present results, $N(t)$-method: α and maximum electron density $N_{\max}$, recovered at paths, NAA - circles, NWC - squares, GQD - triangles; LWPC: electron density at maximum flare flux, $N(I_{\max})$, at GQD - $\times$. According to and McRae & Thomson (2004), $(\beta_{\mathrm{f}}, H'_{\mathrm{f}})$- data: NAA - +

events from class C to X are summarized on the *right panel* of Fig.3, representing the $N_{\max}$ values at 74 km height, in function of the maximum flare flux $I_{\max}$. The results for the NAA path in particular, are found to be in very good agreement with the Wait model, incorporated into the LWPC code, when the $(\beta_{\mathrm{f}}, H'_{\mathrm{f}})$ input parameters of McRae & Thomson (2004) are applied. The overall good agreement between the results obtained from VLF data on different traces, gives credit to the $N(t)$ model. Predictions of $N(t)_h$, for a specified height according

to the proposed model and of $N(z)_t$, at the specified time according to the LWPC (Wait model) anticipate the complementary way in which the two approaches may be merged into the unified $N(t, z)$ description of the flare-driven electron density in the D-region.

Acknowledgements: This work has been carried out in the framework of COST Action 724 WG1, the National Projects P2-0056 (V.Ž) and Pr.141033 (D.G.& D.Š.) and the bilateral Slovenian - Serbian Project BI-SCG05/06-025.

References

Appleton, E. V. , 1953. A note on sluggishness of ionosphere, Journal of Atmospheric and Terrestrial Physics, **3**, 282-284.

Budden, K. G., 1988. The propagation of radio waves. Cambridge University Press.

Collis, P. N, Hargreaves, J. K. and White, G. P., 1996. A localised co-rotating auroral absorption event observed near noon using imaging riometer and EISCAT", Ann. Geophysicae **14**, 1305-1316.

Ferguson, J. A., 1995. Ionospheric model validation at VLF and LF, Radio Science **30** (3), 775-782.

Gledhill, J. A., 1986. The effective recombination coefficient of electrons in the ionosphere between 50 and 150 km. Radio Science, **21** (3), 399-407.

Grubor, D., Šulic D., Žigman, V., 2005. Influence of solar X-ray flares on the Earth-ionosphere waveguide, Serb. Astron. J. N0 171, 29-35.

Holdsworth, D. A., Rupa Vuthaluru, Reid, Iain M., and Vincent Robert A, 2002. Differential absorption measurements of mesospheric and lower thermospheric electron densities using the Buckland Park MF radar, Journal of Atmospheric and Solar-Terrestrial Physics **64** (18), 2029-2042

McRae, W. M., Thomson, N. R., 2000. VLF phase and amplitude: daytime ionospheric parameters, Journal of Atmospheric and Solar-Terrestrial Physics **62**, 609-618.

McRae, W. M., Thomson, N. R., 2004. Solar flare induced ionospheric D-region enhancements from VLF amplitude observations, Journal of Atmospheric and Solar-Terrestrial Physics **66**, 77-87.

Mitra, A.P., 1974. Ionospheric Effects of Solar Flares, Astrophysics and space science library, Vol 46, D. Reidel Publishing Company, Boston.

Ohya, H., Nishino, M., Murayama, Y., Igarashi, K. and Saito, A., 2006. Using tweek atmospherics to measure the response of the low-middle latitude D-region ionosphere to a magnetic storm. Journal of Atmospheric and Solar-Terrestrial Physics **68** (18), 697-709.

Rodger, C. J., Molchanov, O. A., Thomson, N. R., 1998. Relaxation of transient ionization in the lower ionosphere, Journal of Geophysical Research, **103** (A4), 6969-6975.

Thomson, N.R., 1993. Experimental daytime VLF ionospheric parameters, Journal of Atmospheric and Solar-Terrestrial Physics 55 (2), 173-184.

Thomson, N. R., Clilverd, M. A., 2001. Solar flare induced ionospheric D-region enhancements from VLF amplitude observations. Journal of Atmospheric and Solar-Terrestrial Physics **63**, 1729-1737.

Thomson, N.R., Rodger, C. J., Clilverd, M. A., 2005. Large solar flares and their ionospheric D region enhancements, Journal of Geophysical Research, VOL. 110, A06306, doi:10.1029/2005JA011008

Ulich, Th., Turunen, E., Nygren, T., 2000. Effective recombination coefficient in the lower ionosphere during bursts of auroral electrons, Adv. Space Res. **25** (1), 47-50.

Wait, J.R., Spies, K.P., 1964. Characteristics of the Earth-ionosphere waveguide for VLF radio waves. NBS Technical Note 300.

Wait, J.R., 1970. Electromagnetic Waves in Stratified Media, Pergamon Press, Oxford

Whitten R.C., Poppoff I.G., 1965. Physics of the Lower Ionosphere, Prentice- Hall, Inc. Englewood Cliffs, N. J.

Žigman, V., Grubor, D. and Šulić, D., 2007. D-region electron density evaluated from VLF amplitude time delay during X-ray solar flares. Journal of Atmospheric and Solar-Terrestrial Physics **69** (7), 775-792.

Solar Activity and Life. A Review

M. Messerotti[1,2] and J. Chela-Flores[3,4]

[1] INAF-Trieste Astronomical Observatory, Loc. Basovizza n. 302, 34012 Trieste, Italy
messerotti@oats.inaf.it
[2] Department of Physics, University of Trieste, Via A. Valerio 2, 34127 Trieste, Italy
[3] The Abdus Salam ICTP, Strada Costiera 11, 34014 Trieste, Italy chelaf@ictp.it
[4] Instituto de Estudios Avanzados, IDEA, Caracas 1015A, R.B. Venezuela

Summary. Recent claims advocate a downward revision of the solar oxygen abundance Socas-Navarro (2007). This is a reflection of what may be called a 'solar crisis' whereby we mean that previous consensus in our understanding of our nearest star was unfounded. The implications for solar physics, and chemistry, are obvious and much research in the near future will give us a much clearer understanding of the Sun. We wish to review and update recent work concerning the frontier between Space Weather (SpW) and Astrobiology Messerotti (2004); Messerotti & Chela-Flores (2007a,b); Chela-Flores & Messerotti (2007); Chela-Flores et al. (2007). We argue that the present robust programs of various space agencies reinforce our hope for a better understanding of the bases of Astrobiology. Eventually with a more realistic model of the Sun, more reliable discussions of all the factors influencing the origin of life on Earth will be possible.

1 Introduction

During the early stages of the study of the origin of life **?**Ponnamperuma & Chela-Flores (1995) not enough attention was paid to the question of the correlation of chemical evolution on Earth and the all-important evolution of the still-to-be understood early Sun Messerotti (2004). Today, due to the advent of a significant fleet of space missions and the possibility of performing experiments in the International Space Station (ISS), a meaningful study begins to be possible concerning factors that led to an early onset of life on Earth.

Solar climate during the first billion years (Gyr) of the Earth was radically different. The earliest relevant factor was excessive solar-flare energetic particle emission, a phenomenon that has been recorded in meteorites Goswami (1991). These extraterrestrial samples provide information on events that took place during this early period after the collapse of the solar nebula disk. Gas-rich meteorites have yielded evidence for a more active Sun. A considerable number of young stars with remnants of accretion disks show energetic winds that emerge from the stars themselves. Similar ejections are still currently observed from our Sun. For this reason we believe that some of the early Solar System material must keep the record of such emissions. Information on the energetic emission of the Sun during this period can be inferred from data on X ray and ultraviolet (UV) emission (larger than 10 electron-volt, eV) from pre-main-sequence stars Lal & Ligenfelter (1991). We may conclude that during pre-

main-sequence period, solar climate and weather presented an insurmountable barrier for the origin of life anywhere in the Solar System. In the most remote times of the Archean eon (2.5 - 3.8 Gyr before the present, BP), and in the Hadean (earlier than 3.8 Gyr BP), conditions may still have been somewhat favorable, especially with the broad set of UV defense mechanisms that are conceivable. The high UV flux of the early Sun would, in principle, cause destruction of prebiotic organic compounds due to the presence of an anoxic atmosphere without the present-day ozone layer Canuto et al. (1983). Some possible UV defense mechanisms have been proposed in the past, such as atmospheric absorbers and prebiotic organic compounds. We expect that the early microbes must have used various means of avoidance of radiation damage, including inhabiting in deep subsurface environments Gold (1992). Some of these are attenuation by the water column of their aquatic habitats by the presence of some UVR absorbing substance. It is known that water itself does not protect life. Indeed, UVR is known to penetrate the water column up to at least 50 meters. But if the water contains iron, or nitrogenous salts, UVR is efficiently screened. In addition, related relevance of SpW on the origin of life is demonstrated with two sets of experiments have established that UV radiation plays a significant role in the synthesis of some of the precursors of the biomolecules, especially the amino acids Bernstein et al. (2002); Munoz et al. (2002).

Solar systems originate out of interstellar dust, namely dust constituted mainly out of the fundamental elements of life Ehrenfreund & Charnley (2000), such as C, N, O, P, S and a few others. We refer to this set as 'the CNOPS elements'. Just before a star explodes into its supernova stage, all the elements that have originated in its interior out of thermonuclear reactions are expelled, thus contributing to the interstellar dust. Recent work has some implications on the question of SpW. Our solar system may have been triggered over 5 Gyr BP by the shock wave of a supernova explosion. Indeed, there is some evidence for the presence of silicon carbide (carborundum, SiC) grains in the Murchison meteorite, where isotopic ratios demonstrate that they are matter from a type II supernova Hoppe et al. (1997). Around 4.6 Gyr BP on the nascent planet, the organic compounds may have arisen At the end of accretion when they would have been incorporated or delivered by small bodies, both comets and meteorites. Then, planetary processes, such as those that may have occurred close to hydrothermal vents, may have synthesized organic compounds. Comets are another source of CNOPS elements, which develop gaseous envelopes when they are in the close vicinity of the Sun. Gas leaves the comet, carrying some of the dust particles. On the other hand, the Earth's biosphere is that part of this planet where life can survive; it extends from a few kilometers into the atmosphere to the deep-sea vents of the ocean, as well as into the crust of the Earth itself. The Delsemme model is based on the assumption of the cometary origin of the biosphere Delsemme (2000). According to this viewpoint, an intense bombardment of comets has brought to the Earth most of the volatile gases present in our atmosphere and most of the carbon extant in the carbonate sediments, as well as in the organic biomolecules. With the measuring ability that was available throughout last century, molecules have been identified by their spectra in a wide range of wavelengths, and even by *in situ* mass spectrometry during spacecraft flybys of comet P/Halley. These measurements provided composition of parent volatiles and dust, properties of the nuclei and physical parameters of the coma. Besides the Halley comet already mentioned, two other comets were particularly useful objects for remote sensing measurements: comet Hale-Bopp, and comet Hyakutake Campins (2000).

These comets led to the detection of HCN, methane, ethane, carbon monoxide, water, as well as a variety of biogenic compounds.

In big bang cosmology, when the primordial high temperature had decreased sufficiently, hydrogen atoms were formed and helium atoms arose from the combination of deuterium with itself. However, fast cosmic expansion did not allow the formation of a thermonuclear steady. This generated a fraction of deuterium. It is estimated that this cosmic ratio of D/H had an upper bound of some 30 parts per million (ppm). Deuterium cannot be created *de novo*. So the variable presence of D/H is a marker for understanding various aspects of the evolution of solar systems. Since deuterium can react easily inside stars, it is not surprising that its abundance in interstellar matter be smaller than the original cosmic abundance. Yet, in Jupiter the value is higher than in interstellar matter, reflecting its abundance in the proto-planetary nebula. The Jupiter abundance is of the order of 20 ppm, closer to the expected cosmic abundance. In the Earth's seawater this ratio is about 8 times the value of the solar nebula. The D/H ratio is known in three comets: Halley, Hyakutake and Hale-Bopp (HHH). This work on the D/H ratio suggests that cometary impacts have contributed significantly to the water in the Earth's oceans. However, because the D/H ratio observed so far in comets is twice the value for Earth's oceans, it may be argued that comets cannot be the only source of ocean water. This is explained by the fact that HHH are comets that come from Oort's cloud, enriched in D, due to the low-temperature regime in that part of interstellar space. On the other hand the comets that brought the water to the primitive Earth were comets from Jupiter's region that had lower D-values, as in the D/H content of our oceans Delsemme (2000).

2 Constraints of the Ancient Sun on the Early Evolution of Life

The early Earth was much more dynamic geologically and most of the records of large impacts were deleted, but the same geological activity was most likely responsible for partial out gassing of a secondary atmosphere, the exact nature of which can be inferred from the isotopic composition of the noble gases: It has been shown that comets are capable by themselves of providing noble gases in the correct proportions provided that the laboratory experiments duplicate the conditions for cometary formation Owen & Bar (1995). Besides the temperatures had descended to about 1000 C, or below, by about 4.4 Gyr before the present (BP). This scenario for planetary origin allows the possibility of an early origin and evolution of life on Earth. However, it should be remembered that the lunar record demonstrates that some difficulties may arise in this scenario since the Imbrium basin on the Moon was formed by a large impact as late as 3.8 Gyr BP. This implies the persistence of catastrophic impacts for life on Earth, since our planet has a larger effective cross section than our satellite Sleep et al. (1989).

Yet, in this harsh environment photosynthesis of prokaryotes did arise. It is evident from fossils of the stromatolitic-forming cyanobacteria. But the best evidence comes from geo-chemical analyses of the ancient rocks that militate in favor of the presence of bacterial ecosystems in the period that we are discussing in this section, namely 3.8-3.9 Gyr BP. The question of the metamorphism to which the Isua samples have been subjected remains controversial Schidlowski et al. (1983). Stromatolites consist of laminated columns and domes, essentially layered rocks. Prokaryotic cells called cyanobacteria form them. In addition, they

are users of chlorophyll-a to capture the light energy that will drive the photosynthetic process. We remind the reader that chlorophyll is a pigment that is present in chloroplasts that captures the light energy necessary for photosynthesis. Chlorophyll-a is the most common of five such pigments absorbing well at a wavelength of about 400-450 nm and at 650-700 nm. The reason that there are so many pigments in photosynthesis is that each pigment absorbs light more efficiently in a different part of the spectrum. Cyanobacteria are mat-building communities. Right back into ancient times such mats covered some undermat formation of green sulphur and purple bacteria. Such underlying microorganisms are (and were) anaerobes that can actually use the light that impinges on the mat above them by using bacteriochlorophylls that absorb wavelengths of light that pass through the mat above them Schopf (1999). Stromatolites have persevered practically without changes for over 3 billion years. The exact date for the earliest stromatolitic fossils is at present under discussion Basier et al. (2002); Schopf et al. (2002). They have been dated at around 3.5 Gyr BP Schopf (1993). If the fossils are accepted, life's origin must be in the Archean, or even earlier, considering the complexity of a cyanobacterium itself.

Another signature of the early Sun is provided by isotopic fractionation of the five stable noble gas elements, namely, He, Ne, Ar, Kr, and Xe. The early atmosphere arose from collisions during the accretion period, the so-called heavy bombardment of the surface of the Earth. Planetesimal impacts increase the surface temperature affecting the formation of either a proto-atmosphere or a proto-hydrosphere by degassing of volatiles Matsui & Abe (1986).

Thus, life emerged on Earth, during the Archean (3.8 - 2.5 Gyr BP). From the point of view of SpW, we should first of all appreciate the magnitude of the ionizing radiation that may have been present at that time. According to some theoretical arguments the origin of life may be traced back to the most remote times of this eon (3.8 Gyr BP). Indeed, isotopic and geologic evidence suggest that photosynthesis may have been already viable by analysis of the biogeochemical parameter delta 13 C Schidlowski et al. (1983). Besides in the Archean the atmosphere was to a large extent anoxic. As a result the abundance of ozone would not have acted as a UV defense mechanism for the potential emergence of life. UVB (280-315 nm) radiation as well as UVC (190-280 nm) radiation could have penetrated to the Earth's surface with their associated biological consequences Cockell (1998); Elster (1999). If the distribution of life in the Solar System took place by transfer of microorganisms between planets, or satellites, knowledge of SpW becomes fundamental during the early stages of its evolution, to have some constraints on the possible transfer of microorganisms, as investigated extensively Horneck & Cockell (2001). The most radiation resistant organismknown at present exhibits a remarkable capacity to resist the lethal effects of ionizing radiation. The specific microorganism is a non-spore forming extremophile found in a small family known as the Deinococcaceae. In fact, Deinococcus radiodurans is a Gram-positive, red-pigmented, non-motile bacterium. It is resistant to ionizing and UV radiation. Various groups have studied these microorganisms Battista (1997); Daly et al. (2004); Levin-Zaidman et al. (2003). Members of this bacteria taxon can grow under large doses of radiation [up to 50 grays (Gy) per hour]. They are also known to recover from acute doses of gamma-radiation greater than 10,000 Gy without loss of viability. Such microorganisms demonstrate that life could have survived at earlier times when the Earth surface was more exposed to solar radiation.

3 Deeper Insights Into the Origin of Life From Solar Missions

Space climate and space weather are also fundamental for understanding the early evolution of life. The DNA repair mechanisms that extremophilic organisms evolved in response to a continuously changing space environment. The Sun changed considerably in time its temperature and luminosity, key factors for astrobiology that require better understanding, so that we would be in a position to *predict* with a certain degree of confidence what were the conditions like during the first Gyr of the evolution of the Solar System. The violent eruptions of solar flares during its earliest stage (T-Tauri), soon gave way to a very broad range of physical conditions that have to be clarified by further research. There are several reasons to raise the question: Why do we need improved understanding, and predictions of solar activity? One reason arises from theoretical modeling of the earliest organisms. Predictions range broadly in their claims. Improved understanding of solar activity in the first billion years of the Earth would provide essential clues. Additional aspects of astrobiology, such as the question of the distribution of life in the Solar System, also depend on further research outside the frontier of astrobiology, namely by acquiring improved understanding of solar activity, such as the preliminary information that has been possible to retrieve from the ISS.

Much progress has been achieved since the 1990s missions for studying the Sun. Firstly, remarkable progress has been possible with the Solar and Heliospheric Observatory (SOHO), a joint NASA-ESA spacecraft. SOHO is concerned with the physical processes that form and heat the Sun's corona, maintain it and give rise to the expanding solar wind. A second mission launched in the last decade is Ulysses with measurements of the Sun from a polar orbit. It is also dedicated to interplanetary research especially with interplanetary-physics investigations, including close (1992) and distant (2004) Jupiter encounters. More recently, the Transition Region and Coronal Explorer (TRACE) is giving us information on the three-dimensional magnetic structures that emerge through the photosphere, defining both the geometry and dynamics of the upper solar atmosphere. In this respect, the Solar Terrestrial Relations Observatory (STEREO) launched in February 2006 will study the nature of coronal mass ejections (CME), which in spite their significant effect on the Earth, their origin, evolution or extent in interplanetary space remains as a challenge. Persevering with the solar missions like Ulysses should be useful, especially in the future when we should address an important question: whether in the past 2 - 3 Gyrs similar events may have produced space climate and weather harmful, or beneficial for the evolution of life in the solar system. There is another reason for persevering with Ulysses-type of missions. The focus of space weather from the point of view of astrobiology gives us a hint. Jupiter's moon Io is emitting volcanic particles at passing spacecraft. The dominant source of the jovian dust streams is Io's volcanoes Graps et al. (2000). In September 2004 Io emitted dust particles whose impact rate was recorded by the Cosmic Dust Analyzer on board of Ulysses. The discovery of this phenomenon dates back to 1992 when, a stream of volcano dust hit Ulysses as it approached within 1 AU from Jupiter Grun et al. (1993). Cassini's dust detector is more capable than the instrumentation on Ulysses when faced with a similar event Srama et al. (2000). In addition to mass, speed, charge and trajectory, Cassini measured elemental composition finding sulfur, silicon, sodium and potassium, whose origin is volcanic. This raises a question that will deserve further attention in the future.

4 Solar and Extra-solar Imprints On the Lunar Regolith and Fossils

Preliminary modelling of the Sun does not allow useful extrapolations into the distant past in order to study in detail the solar physics influences on the emergence and early evolution of life on Earth Jerse (2006). The difficulty encountered in the simultaneous study of astrobiology and SpW is not insurmountable. Fortunately, considerable information can be retrieved from observations of extraterrestrial samples, either meteorites, or lunar material. We will consider the fossils that represent an imprint of anomalous conditions in our environment since the Proterozoic. We have studied with special attention the records that may give some information about the factors favorable for life. Such data may be retrieved from the Sun during a period when fossils of animals were not available, during or at the end of the Archean. Such imprints are available in the upper layer of the lunar surface, on its regolith. The Moon is depleted of volatile elements such as hydrogen, carbon, nitrogen and the noble gases, possibly due to the fact that the most widely accepted theory of its formation is the impact of the Earth by a Mars-sized body during the accretion period. The expulsion of a large amount of matter from the embryonic Earth gave rise to the Moon Canup & Asphaug (2001). The satellite cooled quickly, but did not form an atmosphere, possibly due to the smaller cross section than the Earth. Ions from the solar wind are directly implanted into the lunar surface Kerridge et al. (1991). This component was detected during the Apollo missions. The isotopic composition of the noble gases in lunar soils has been established as being subsequent to the formation of the Moon itself. But nitrogen has a special place in the research for the nature of the astrochemistry of the early solar system. Unlike some of the other CHNOPS elements, in lunar soils it is estimated that between 1.5 and 3 Gyr BP there was an increment of some 50% in the ratio ^{15}N/^{14}N. This result has been abundantly confirmed. By performing single grain analyses Wieler and co-workers have searched for evidence of a predominantly non-solar origin of nitrogen in the lunar regolith Wieler et al. (1999). There have also been attempts to analyze trapped N in the lunar regolith Hishizume et al. (2000). Ozima and co-workers propose that most of the N and some of the other volatile elements in lunar soils may actually have come from the Earth's atmosphere rather than the solar wind Ozima et al. (2005). Hopefully with the availability of new missions, such STEREO involving two spacecraft in heliocentric orbit to study coronal mass ejections (CMEs), further measurements of the isotopic N-abundances may contribute to sorting out the astrochemical signatures of the early solar system that are awaiting to be deciphered. Such knowledge of nitrogen will represent considerable progress in the study of the origin of life on Earth.

Gamma ray bursts (GRBs) are powerful explosions that produce a flux of radiation detectable across the observable Universe. These events possibly originate in distant galaxies, and a large percentage likely arises from explosions of stars over 15 times more massive than our Sun. A burst creates two oppositely directed beams of gamma rays that race off into space. Mass extinctions have eliminated a significant fraction of life on Earth. GRB, together with meteoritic collisions, or an atmosphere that has gone through a transition unfavorable to the Earth biota are three likely causes that need to be discussed together, as we have attempted to do in the present review. The Ordovician is the second oldest period of the Paleozoic Era, thought to have covered the span of time between 505 and 440 million years BP (Myrs BP). The late Ordovician mass extinction took place at approximately 440 Myrs BP may be at least partly the result of a GRB. Due to expected depletion of the ozone layer arising from the

incoming energetic flux, the solar UV radiation that is normally shielded would give rise to a severely modified ecosystem. All marine animals suffered mass mortalities during the Late Ordovician. Mass mortalities at the close of the Cambrian and late in the Ordovician resulted in the unique aspects of the Ordovician fauna. The Swift mission, launched in November 2004, contributes to determine recent burst rates. During evolution of life certain events triggered large-scale extinctions. We consider one of the most remarkable possible candidates. Radiation during post-Ordovician glaciation led to many new taxa typical of the Silurian. GRBs within our Galaxy have been suggested to be a possible threat to life on Earth Scalo & Wheeler (2002). Some effects similar to those due to a nearby supernova should be expected. GRBs are less frequent than supernovae, but their greater energy output results in a larger region of influence, and hence they may pose a greater threat. Alternatively extinctions may have been triggered by impacts (asteroids, comets) or by geochemical activity Chela-Flores et al. (2007).

5 Concluding Remarks

The Sun exhibits a stable radiation output, which is expected to endure for a long time scale, a subject that is extensively reviewed, for example in several papers in Ref.Sonett et al. (1991). This stable output is called space climate. On the other hand, on a short-time scale solar activity may perturb the heliosphere by originating the above-mentioned radiation outbursts, characterizing SpW Messerotti (2004). The main thesis that we have presented in this paper is that the long-term solar influence (space climate) does affect the evolution of life on Earth, but the evolution of the Earth itself gradually accommodates itself to the gradual adaptation of life to a changing environment. One evident example is the gradual emergence of an ozone layer in the Proterozoic, long after the first prokaryotic cells (cyanobacteria) emerged in the lower Achaean. On the other hand, SpW, a short-term influence, may have in the past been a factor in the origin, evolution, distribution and eventual destiny of life on Earth, namely a factor in the main topics that concern the new science of astrobiology. In our recent collaboration we have provided several examples that argue in favour of solar activity, space weather and astrobiology being brought within a unified framework Messerotti & Chela-Flores (2007a,b); Chela-Flores & Messerotti (2007); Chela-Flores et al. (2007). This approach naturally leads us to the suggestion of exploiting instrumentation from somewhat dissimilar sciences (astronomy and astrobiology) with a unified objective. We have attempted a preliminary comprehensive discussion of how research in the conditions of the early Sun combine with observations in several disciplines to give us insights into the factors that lead to the emergence of life in a given solar system (biogeochemistry, lunar science, micropaleontology and chemical evolution). These considerations are necessary to approach the conditions that will allow life to emerge anywhere in the universe.

Acknowledgements: This work has been carried out in the framework of COST Action 724 Working Group 1. MM acknowledges the support from the Italian Space Agency (ASI).

References

Socas-Navarro, H., Norton, A.A.: The Solar Oxygen Crisis: Probably Not the Last Word. The Astrophysical Journal, **660**, L153–L156 (2007)

Messerotti, M.: Space weather and space climate. In: Life in the Universe From the Miller Experiment to the Search for Life on Other Worlds. Seckbach, J.; Chela-Flores, J. Owen, T. Raulin, F. (eds.), Series: Cellular Origin, Life in Extreme Habitats and Astrobiology, 177–180 (2004)

Messerotti, M., Chela-Flores, J.: Solar activity and solar weather in the framework of life origin and evolution on Earth, ESA's Publication Division, Special Publication, in press (2007)

Messerotti, M., Chela-Flores, J.: Signatures of the ancient Sun constraining the early emergence of life on Earth. In: Space Weather. Research towards Applications in Europe, Jean Lilensten, ed., Springer, Dordrecht, The Netherlands, Astrophysics and Space Science Library (ASSL) Series, Vol. 344 (2007)

Chela-Flores, J., Messerotti, M.: Constraints on the origin of life due to the physics of the ancient Sun. IV Convegno della Ricerca Italiana in Fisica Solare e Relazione Sole-Terra, Memorie della Societ Astronomica Italiana Supplementi (in press, in electronic form) (2007)

Chela-Flores, J., Jerse, G., Messerotti, M., Tuniz, C.: Astronomical and astrobiological imprints on the fossil record. A review. "From Fossils to Astrobiology" Ed. J. Seckbach, Cellular Origins, Life in Extreme Habitats and Astrobiology, Springer, Dordrecht, The Netherlands, submitted for publication (2007)

Oparin(1953) Oparin, A.I.: Origin of Life, New York, Dover (1953)

Ponnamperuma, C., Chela-Flores, J., (eds.): Chemical Evolution: The Structure and Model of the First Cell. The Alexander Ivanovich Oparin 100th Anniversary Conference, Kluwer Academic Publishers, Dordrecht, The Netherlands (1995)

Goswami, J.N.: Solar flare heavy-ion tracks in extraterrestrial objects. In [43], Loc Cit., 426–444 (1991)

Lal, D., Ligenfelter, R.E.: History of the Sun during the past 4.5 Gyr as revealed by studies of energetic solar particles recorded in extraterrestrial and terrestrial samples. In [43], Loc Cit., 221–231 (1991)

Canuto, V.M., Levine, J.S., Augustsson, T.R., Imhoff, C.L., Giampapa, M.S.: Nature, **305**, 281–286 (1983)

Gold, T.: The Deep, Hot Biosphere, Proc. Natl. Acad. Sci. USA, **89**, 6045–6049 (1992)

Bernstein, M.P., Dworkin, J.P., Sandford, S.A., Cooper, G.W., Allamandola, L.J.: Racemic amino acids from the ultraviolet photolysis of interstellar ice analogues. Nature, **416**, 401–403 (2002)

Munoz Caro, G.M., Meierhenrich, U.J., Schutte, W., Barbier, B., Arcones Segovia, A., Rosenbauer, H., Thiemann, W., Brack, A., Greenberg, J.M.: Amino acids from ultraviolet irradiation of interstellar ice analogues. Nature, **416**, 403–406 (2002)

Ehrenfreund and Charnley, S.: Organic Molecules in the Interstellar Medium, Comets, and Meteorites: A Voyage from Dark Clouds to the Early Earth. Annu. Rev. Astron. Astrophys, **38**, 427–483 (2000)

Hoppe, P., Strebel, R., Eberhadt, P., Amari, S., Lewis, R.S.: Type II supernova matter in a silicon carbide grain from the Murchison meteorite. Science, **272**, 1314–1317 (1997)

Delsemme, A.H. Cometary Origin of the Biosphere (The 1999 Kuiper Prize Lecture), Icarus, **146**, 313–325 (2000)

Campins, H.: The chemical composition of comets. In: Chela-Flores, J., Lemarchand, G.A., Oro, J., (eds.). Astrobiology: Origins from the Big Bang to Civilization, Kluwer Academic Publishers: Dordrecht, The Netherlands (2000)

Owen T., Bar-Nun, A.: Comets, impacts and atmospheres. Icarus, **116**, 215–226 (1995)

Sleep, N., Zahnle, K., Kasting, J.F., Morowitz, H.J.: Annihilation of ecosystems by large asteroid impacts on the early Earth. Nature, **342**, 139–142 (1989)

Schidlowski, M., Hayes, J.M., Kaplan, I.R.: Isotopic Inferences of Ancient Biochemistries: Carbon, Sulfur, Hydrogen, and Nitrogen. In: Earth's Earliest Biosphere its Origin and Evolution. In: Schopf J.W. (ed.), Princeton University Press, Princeton, New Jersey, 149–186 (1983)

Schopf, J.W.: Cradle of Life: The Discovery of Earth's Earliest Fossils, Princeton University Press, Princeton, New Jersey (1999)

Brasier, M.D., Green, O.W., Jephcoat, A.P., Kleppe, A.K., Van Kranendonk, M.J., Lindsay, J.F., Steele, A., Grassineau, N.V.: Questioning the evidence for Earth's oldest fossils. Nature, **416**, 76–81 (2002)

Schopf, J.W., Kudryavtsev, A.B., Agresti, D.G., Wdowiak, T.J., Czaja, A.D.: Laser-Raman imagery of Earth's earliest fossils. Nature, **416**, 73–76 (2002)

Schopf, J.W.: Microfossils of the Earth Archaean Apex Chert: New evidence of the antiquity of life. Science, **260**, 640–646 (1993)

Matsui, T., Abe, Y.: Evolution of an impact-induced atmosphere and magma ocean on the accreting Earth. Nature, **319**, 303–305 (1986)

Cockell, C.S.: Biological Effects of High Ultraviolet Radiation on Early Earth - A Theoretical Evaluation. J. Theor. Biol., **193**, 717–729 (1998)

Elster, J.: Algal versatility in various extreme environments. In Enigmatic Microorganisms and Life in Extreme Environments. Ed. J. Seckbach, Kluwer Academic Publishers, Dordrecht, The Netherlands (1999)

Horneck, G., Cockell, C.S.: The History of the UV Radiation Climate of the Earth-Theoretical and Space-based Observations. Photochemistry and Photobiology, **73**, 447–451 (2001)

Battista, J.R.: Against all odds: The survival strategies of Deinococcus radiodurans. Ann. Rev. Microbiol., **51**, 203–224 (1997)

Daly, M.J., Gaidamakova, E.K., Matrosova, V.Y., Vasilenko, A., Zhai, M., Venkateswaran, A., Hess, M., Omelchenko, M.V., Kostandarithes, H.M., Makarova, K.S., Wackett, L.P., Fredrickso, J.K., Ghosal, D.: Accumulation of Mn(II) in Deinococcus radiodurans Facilitates Gamma-Radiation Resistance. Science, **306**, 1025–1028 (2004)

Levin-Zaidman, S., Englander, J., Shimoni, E., Sharma, A.K., Minton, K.W., Minsky, A.: Ringlike structure of the Deinococcus radiodurans genome: a key to radioresistance? Science, **299**, 254–256 (2003)

Graps, A.L., Grun, E., Svedhem, H., Kruger, H., Horanyi, M., Heck, A., Lammers, S.: Io as a source of the jovian dust streams. Nature, **405**, 48–50 (2000)

Grun, E., Zook, H.A., Baguhl, M., Balogh, A., Bame, S.J., Fechtig, H., Forsyth, R., Hanner, M.S., Hornyi, M., Khurana, K.K., Kissel, J., Kivelson, M., Lindblad, B.A., Linkert,

D., Linkert, G., Mann, I., McDonnell, J.A.M., Morfill, G.E., Phillips, J.L., Polanskey, C., Schwehm, G., Siddique, N., Staubach, P., Svestka, J., Taylor, A.: Discovery of jovian dust streams and interstellar grains by the ulysses spacecraft. Nature, **362**, 428–430 (1993)

Srama, R., Bradley, J., Burton, M., Dikarev, V., Graps, A., Grn, E., Heck, A., Helfert, S., Johnson, T., Kempf, S., Krger, H., Stbig, M.: Jupiter dust stream observations with Cassini. Max-Planck-Institut fr Kernphysik preprint, August 2 (2000)

Jerse, G.: Stima preliminare dei livelli di energia immessi nella Magnetosfera ed Atmosfera terrestri in diverse epoche da sorgenti di Space Weather, Diploma Thesis in Physics, University of Trieste (2006)

Canup, R.M., Asphaug, E.: Origin of the Moon in a giant impact near the end of the Earth's formation. Nature, **412**, 708–712 (2001)

Kerridge, J.F., Signer, P., Wieler, R., Becker, R.H., Pepin, R.O.: Long term changes in composition of solar particles implanted in extraterrestrial materials. In [43], Loc Cit., 389–412 (1991)

Wieler, R., Humbert, F., Marty, B.: Evidence for a predominantly non-solar origin of nitrogen in the lunar regolith revealed by single grain analyses. Earth and Planetary Science Letters, **167**, 47–60 (1999)

Hishizumi, K., Chaussidon, M., Marty, B., Robert, F.: Solar Wind Record on the Moon: Deciphering Presolar from Planetary Nitrogen. Science, **290**, 1142–1145 (2000)

Ozima, M., Seki, K., Terada, N., Miura, Y.N., Podosek, F.A., Shinagawa, H.: Terrestrial nitrogen and noble gases in lunar soils. Nature, **436**, 655–659 (2005)

Scalo, J., Wheeler, J.C.: ApJ, **566**, 723 (2002)

Sonett, C.P., Giampappa, M.S., Matthews, M.S.: (eds.) The Sun in Time. The University of Arizona, Tucston (1991)

Part III

Working Group 2:
The radiation environment of the Earth

Monitoring, modeling and forecasting of the Earth's radiation environment

R. Vainio[1] and D. Heynderickx[2,3]

[1] Department of Physical Sciences, University of Helsinki, Finland, rami.vainio@helsinki.fi
[2] Belgian Institute for Space Aeronomy, Brussels, Belgium
[3] Presently at: DH-Consultancy, Leuven, Belgium, DHConsultancy@skynet.be

1 Introduction

Working Group 2, *The Radiation Environment of the Earth*, of COST-724 Action concentrated on conducting observations and developing models of the dynamics of the Earth's radiation environment. The working group (WG) was a collaborative effort of more than 20 institutes in Europe (http://theory.physics.helsinki.fi/~space/cost724/).

When setting up the working group, the leaders of the WG-2 (R. Vainio and D. Heynderickx) did not formulate very detailed work package (WP) structure as a basis of work in WG-2. Instead, the WG was originally organized in four major WPs according to the goals of WG-2 expressed in the Memorandum of Understanding (MoU) of the action. These WPs were

WP2100: Interaction of solar energetic particles with the magnetosphere (leaders: J. Rodriguez-Pacheco, R. Vainio)
WP2200: Cosmic rays and space weather (leader: K. Kudela)
WP2300: Radiation belts: particles and plasma waves (leaders: H. Rothkaehl, D. Heynderickx)
WP2400: Radiation effects on the environment, technology, and human health (leader: Ts. Dachev)

The participating research groups each presented their research interests to the group as Expressions of Commitment (EoC) formulated on a common template, which outlined the work proposed to be undertaken in each research group during the action, and indicated the WPs that were to benefit from the proposed work. The EoCs were presented to the group in the first two WG-2 meetings, which took place in 2004 (in April and October, respectively). Some of the projects were already based on existing collaborations between the participating institutes while some others formed strong collaborations between the groups during the four years of the Action.

Most of the groups working on topics related to WP2100 were also working on WP2200, and in practice the two WPs constituted a single entity. The effects of the radiation on the Earth's atmosphere, originally included in WG2400, were also studied by the same groups. Thus, in practice the work was organized under the following broad topics

1. Solar and galactic cosmic rays and space weather
2. Radiation belts: particles and plasma waves
3. Radiation effects on the technology and human health

Under each topic, the work was organized roughly according to the same general scheme:

- Review of available models and data
- Model development
- Supporting experimental research

In the papers included in this chapter, the most important results achieved in WG-2 during the four years of the action are presented. In addition to these specific papers describing and reviewing the actual work, a summary of the basic physics behind the models developed in the WG is given in the first paper by *Vainio et al.* This paper is designed to provide the necessary tutorial background information for easier reading of the specific papers. It is, however, not aimed at providing a comprehensive review to the physics of the radiation environment.

The models and the available data sets being developed and maintained by the participating institutions are listed in the present paper, to give a quick-look summary to the models and data sets maintained within the Working Group.

In addition to the physical background presented in the first paper, the specific papers of the chapter are providing additional reviews and original results on the following topics (numbering follows the broad topics of the working group)

1. *Desorgher et al.* and *Usoskin et al.* describe the interaction of the cosmic radiation (both galactic and solar) with the Earth's magnetosphere and atmosphere; *Nymmik* and *Valtonen et al.* describe empirical models of solar particle fluences in the interplanetary medium and *Gabriel* and *Dorman* describe models designed for forecasting solar energetic particle events; *Kudela & Kuznetsov* summarize the observations of solar neutral radiation performed by the participating research groups; and *Hippler et al.*, *Dorman* and *Dudok de Wit & Chilingarian* describe observational techniques to use cosmic radiation to forecast large space weather events.
2. *Horne & Boscher* describe the recent modeling efforts on wave-particle interactions in the radiation belt regions and *Rothkaehl et al.* describe the observational aspects of the response of the ionospheric plasma to the physical processes in radiation belt region.
3. *McKenna-Lawlor* provides a review on the most important effects of radiation on technology in space and *Spurny & Dachev* review their comprehensive results on the effects of space radiation on human health.

As reflected by the number of papers falling under the topics 1–3, the most active collaborations inside the WG were formed in the fields related to solar and galactic cosmic rays.

2 Summary of models provided by WG-2

In the following, the models for the radiation environment developed by the members of COST724/WG2 are listed in two tables. Acronyms used in the table are listed in the end of the paper. Table 1 lists the models related to the cosmic-ray components of the radiation

environment. Table 2 lists models related to the geomagnetic field, to the plasma wave activity and to the radiation belts. Each row in the tables contains data for one model. The first column gives the name of the model (with a member of WG-2 participating in the model development in parentheses); the second column gives the domain of the model; the third indicates whether the model is a physical, empirical or a semi-empirical one; the fourth column gives the most important input parameters or data to the model; the fifth column describes the output of the model; and the sixth column gives some reference information – either a website or a scientific paper – about the model. Some of the models are also described in more detail in the specific papers of this chapter.

3 Summary of data provided by WG-2

Most of the monitoring work in WG-2 was performed by the CR stations taking part in the action. Table 3 provides a list of ground based CR detectors operated by participating institutions. The action significantly fostered the collaboration between these institutions and first steps were taken toward a real-time database of CR measurements in Europe (see next section).

A very extensive set of satellite data relevant to the radiation environment is provided by the Moscow State University's *Low Altitude Space Radiation Environment (LASRE) Database* (see, http://www.magnetosphere.ru/dataintr.html#LASRE). The database contains observations of energetic electrons and protons made on-board Cosmos-1686 and CORONAS satellites, and MIR Station. In addition, a large number of other data sets on, e.g., the geomagnetic field are available, and other databases, e.g., NASA's OMNI, are linked from the site.

Energetic particle data in the solar wind are provided by the ERNE/SOHO measurements (www.srl.utu.fi/erne_data/main_english.html). This website provides on-line, near-real-time access to spectral measurements of protons and He ions at energies 1–100 MeV/n with a 1-minute time resolution. Also heavy ions up to iron group are measured by the instrument. Contact E. Valtonen, eino.valtonen@utu.fi, for further information.

Other monitoring activities of the group include the HF wave diagnostics on-board the Coronas-I satellite. Wave measurements on-board CORONAS-I contained Solar Radio Spectrometer (SORS) within the range of 0.1–30 MHz with 25 kHz step and 15 kHz passband. Wave diagnostics in the frequency band 50–300 MHz were also available. Consecutive spectra were registered every 30 s with a sweep period of 6.4 s. The data is downloadable. For further information, contact: H. Rothkaehl (hrot@cbk.waw.pl).

4 Conclusions and Outlook

The specific objectives for WG-2 listed in the MoU are:

- *To develop a quantitative model of the interaction of solar energetic particle events with the Earth's magnetosphere.*
  - This task is fully completed by the successful implementation of the MAGNETOCOSMICS code to the European Space Weather Portal (ESWP). Also another magnetospheric CR propagation model by Kudela and Storini is available at ESWP.

Table 1. CR models submitted to COST724/WG2.

model	domain	type	objective (purpose)	input	output	ref.
PLANETOCOSMICS (L. Desorgher)	atmosphere	P	Atmospheric radiation environment	Primary CR spectrum at the top of the atmosphere	Secondary particles, flux, energy deposited	cosray.unibe.ch/~laurent/planetocosmics
MAGNETOCOSMICS (L. Desorgher)	magnetosphere	P	Geomagnetic effects (e.g., cutoffs) on CR.	position, time, geomagnetic indices Kp and Dst	cutoff rigidity, asymptotic direction of incidence	cosray.unibe.ch/~laurent/magnetocosmics/
CRII / Bern (L. Desorgher)	atmosphere	P	Atmospheric ionization	CR mod. strength Φ, position or cutoff rigidity	ionization rate (world grid or given location)	cosray.unibe.ch/~laurent/ionisation/ Contact: L. Desorgher desorgher@space.unibe.ch
CRII / Oulu (I. Usoskin)	atmosphere	P	Atmospheric ionization	CR mod. strength Φ, year. Opt: geograph. coords., altitude	Ionization rate or ion concentration (world grid or given location).	Usoskin et al. (2004). Contact: I. Usoskin ilya.usoskin@oulu.fi
CRII / Sofia (P. Velinov)	ionosphere and upper atmosphere	P	Atmospheric ionization	CR spectrum, cut-off rigidity	Ionization rate.	Velinov et al. (2005). Contact: P. Velinov, pvelinov@bas.bg
CR modulation / Oulu (I. Usoskin)	interplanetary	P	CR modulation	**1D**: CR mod. strength Φ. **2D** diff. coeffs. ($\parallel$ and $\perp$ to the field), SW speed $V(\lambda)$, HCS tilt angle, prop. of diff. barriers	Differential energy spectrum of GCR.	Usoskin et al. (2002). Contact: I. Usoskin ilya.usoskin@oulu.fi
Probabilistic SEP Model (R. Nymmik)	interplanetary	S-E	SEP fluence and peak flux	start and end time of the mission; probability level	diff. energy spectra of peak fluxes / fluences, exceeding with the given probability the calculated flux in the chosen time interval	elana.sinp.msu.ru/nymmik/models/sep.php

Table 2. Magnetic-field and radiation belt models submitted to COST724/WG2.

model	domain	type	objective (purpose)	input	output	ref.
Paraboloid Model of the Earth's Magnetosphere (V. Kalegaev)	magnetosphere	P	geomagnetic field	Solar wind density and velocity, IMF vector, al and Dst geomagn. indices	Magnetic field vector as a function of location	www.magnetosphere.ru/iso/
PADIE (R. Horne)	radiation belts	P	wave-particle interactions	wave mode, wave power, freq. bandwidth, plasma density distribution, angular spread of wave normal angles, magnetic field model	Pitch angle, energy, and mixed pitch angle-energy diffusion coefficients	Horne et al. (2003); Glauert and Horne (2005). Contact: R. Horne r.horne@bas.ac.uk
Salammbô (D. Boscher)	radiation belts	P	trapped particle flux	geomagn. indices Kp and Dst, SEPs at GEO; ext. models req.: IGRF, plasmapause model, wave model, PADIE, magnetic cutoff	Response of the radiation belts to magnetic storms and SEP events	Beutier and Boscher (1995). Contact: Daniel. Boscher@onecert.fr
SAMPEX/PET (D. Heynderickx)	radiation belts	S-E	trapped particle flux	F10.7 index, IGRF	trapped proton (20–500 MeV) flux below 600 km as a function of solar activity	Heynderickx et al. (1999)
POLE: Particle ONERA-LANL Electron (D. Boscher)	radiation belts	E	Trapped-particle flux	Year of the beginning of the mission, duration	0.03–2.5 MeV electron flux at GEO	Boscher et al. (2003). Contact: Daniel. Boscher@onecert.fr

Table 3. Ground based CR detectors operated by participating institutions. (Table kindly provided by E.O. Flückiger.)

Country	Station name Abbreviation	Type of detector	PI	Location [°] (lat, long)	Alt. [m]	$R_c^{\perp}$ [GV]	URL
Armenia	Mt. Aragats ERV3	18 NM64	Ashot A. Chilingarian, chili@aragats.am	(+40.50, +44.17)	3250	7.58	crdlx5.yerphi.am/
Armenia	Mt. Aragats AMMM	multidirectional muon monitor	Ashot A. Chilingarian, chili@aragats.am	(+40.50, +44.17)	3250	7.58	crdlx5.yerphi.am/
Armenia	Nor Amberd ERVN	-	Ashot A. Chilingarian, chili@aragats.am	(+40.50, +44.17)	2000	7.60	crdlx5.yerphi.am/
Finland	Oulu OULU	9NM64	Ilya G. Usoskin, Ilya.Usoskin@oulu.fi	(+65.06, +25.47)	0	0.78	cosmicrays.oulu.fi/
Germany	Kiel KIEL	18IQSY	Robert Wimmer-Schweingruber, wimmer@physik.uni-kiel.de	(+54.30, +10.10)	54	2.36	134.245.132.179/kiel/main.htm
Germany	Greifswald MuSTAnG	muon telescope	Rainer Hippler, Hippler@physik.uni-greifswald.de	(+54.09, + 13.37)	0	2.37	www.mustang.uni-greifswald.de/spaceweather.htm
Greece	Athens ATHN	6 NM64	Helen Mavromichalaki, emavromi@phys.uoa.gr	(+37.98, +23.78)	260	8.53	cosray.phys.uoa.gr/
Israel	Tel Aviv ESOI	6 NM64	Lev Dorman, lid@physics.technion.ac.il	(+33.30, +35.80)	2025	10.8	www.tau.ac.il/institutes/advanced/cosmic/
Italy	Rome ROME (SVIRCO)	20 NM64	Marisa Storini, marisa.storini@ifsi-roma.inaf.it	(+41.86, +12.47)	60	6.32	www.fis.uniroma3.it/~svirco/
Slovakia	Lomnicky Stit LMKS	12 NN64	Karel Kudela, kkudela@kosice.upsj.sk	(+49.20, +20.22)	2634	3.98	neutronmonitor.ta3.sk/
Switzerland	Jungfraujoch JUN1	18 IGY	Erwin Flueckiger, erwin.flueckiger@phim.unibe.ch	(+46.55, +7.98)	3570	4.50	cosray.unibe.ch/
Switzerland	Jungfraujoch JUNG	3 NM64	Erwin Flueckiger, erwin.flueckiger@phim.unibe.ch	(+46.55, +7.98)	3475	4.50	cosray.unibe.ch/

  - For a thorough description of the magnetospheric propagation of CR, see *Desorgher et al.*
  - The group has also developed models of the interaction of SEPs and GCRs with the Earth's atmosphere (see *Usoskin et al.*).
- *To develop a quantitative model of the development of trapped radiation in the Earth's magnetosphere during geomagnetic storms.*
  - This objective is addressed by the Salammbô and PADIE codes being developed by members of WG-2 (see, *Horne and Boscher*). The work is still in progress.
  - Analysis of observations on wave-particle interactions, supporting the model development, in the magnetosphere has also been performed by the group members (see *Rothkaehl et al.*, this volume).
- *To develop a quantitative model of the variation of galactic cosmic radiation in response to solar activity.*
  - For the long term modulation, several models exists and a few have been developed in WG-2 (e.g., the CR modulation model of Oulu, see Table 1 and *Vainio et al.*).
  - For the short-term effects (i.e., Forbush decreases), work to create a rigidity dependent model of Forbush decreases has been initiated as a collaboration between the Universities of Oulu and Helsinki. The groups have access to relevant CR data as well as numerical simulation tools needed to create the model. Results cannot be expected before the end of the year 2008.
- *To study how electronic technology in satellites, launchers and aircraft is affected by the Earth's radiation environment.*
  - Types of effects reported in the literature have been reviewed (see *McKenna-Lawlor*).
- *To study how humans are affected by solar and cosmic radiation in different activities (eg. astronauts, aircrew, air passengers, on the ground).*
  - A multi-year program of dosimetric measurements on-board spacecraft and aircraft by collaboration of WG-2 institutes has been carried out (see *Spurný and Dachev*).
- *To set up and maintain a database of recorded effects on electronic technology and human health.*
  - An extensive, albeit not complete, list of reported effects on electronic technology has been compiled (see *McKenna-Lawlor*, CD supplement of this volume).
  - Compiling a comprehensive database of the recorded effects was not considered feasible due to well-known difficulties in getting information of spacecraft failures from the commercial satellite operators.
- *Liaise with WG4 to ensure that relevant data and models are incorporated to a European Space Weather Network.*
  - Models ready for implementation have been incorporated to the ESWP.
  - The work is still in progress for some models.

In addition to the objectives listed in the MoU, the group has made significant progress other areas related to the radiation environment and its effects on the planet Earth and civilization. Four models for forecasting SEP events (*Gabriel*; *Dorman*), and peak fluxes and fluences of solar protons (*Nymmik*) and heavy ions (*Valtonen et al.*) have been under development under the umbrella of WG-2. Note that in addition, several teams in WG-1 (see *Storini et al.*, this volume) and WG-3 (see *Sanahuja et al.*, this volume) have been working on engineering-type

models for SEPs. An important application of CRs in space weather research is also their use as indicators of large interplanetary disturbances approaching the Earth (see *Dorman*; *Hippler et al.*; and *Dudok de Wit & Chilingarian*).

In conclusion, several new and existing models for describing the Earth's radiation environment have been developed during the four years of COST-724 action. The role of the action in enabling new collaborations has been a substantial one. As examples, we mention here some important developments: the atmospheric ionization codes maintained in three European institutes (Oulu, Bern and Sofia) were cross-calibrated and their ranges of validity were carefully studied (see *Usoskin et al.*). This collaboration was enabled by the working group meetigns and Short Term Scientific Missions by the teams. As another example of successful collaboration fostered by COST-724, we can list the successful FP7 proposal for a Real-time database of neutron monitor observations, to be established and maintained by the European cosmic-ray stations, most of which are members of WG-2. This database will create an opportunity for the provision of information of the atmospheric neutron component related to galactic and solar cosmic rays, which poses a radiation hazard to the aircraft crew and passengers on polar routes. The provision of such information in real-time can enable the rerouting of flights on high risk routes. This identified as one of the key application areas of the action in the MoU.

Some of the key areas of the dynamics of the radiation belts are still incompletely modeled. For example, work on replacing the empirical models of NASA for the radiation belts (AP-8 and AE-8 models) is long overdue. Forecasting of the SEP events is still in an unsatisfactory state although progress has been made during the action (see also *Storini et al.*, this volume). Probably one the most pressing needs is to bring the scientific models of the trapped particle radiation developed in Europe in the public domain. This would enable significant steps to be taken towards engineering models capable of adequately describing the dynamics of the radiation belts. Special efforts should also be directed toward obtaining failure reports from commercial satellite operators to enable a more complete view of the effects on technology to be acquired.

List of acronyms used in tables 1–3

CR	Cosmic ray
E	Empirical
GCR	Galactic cosmic ray
GEO	Geostationary orbit
HCS	Heliospheric current sheet
IGRF	International geomagnetic reference field
IMF	Interplanetary magnetic field
P	Physical
S-E	Semi-empirical
SCR	Solar cosmic ray
SEP	Solar energetic particle
SW	Solar wind

References

Beutier T., D. Boscher: A three-dimensional analysis of the electron radiation belt by the Salammbô code. J. Geophys. Res., **100**, 14853 (1995).

Boscher, D., S. Bourdarie, R. Friedel, and R. Belian: A model for the geostationary electron environment: POLE. IEEE Trans. Nuc. Sci., **50(6)**, 2278–2283 (2003).

Glauert, S. A., R. B. Horne: Calculation of pitch angle and energy diffusion coefficients with the PADIE code. J. Geophys. Res., **110**, A04206 (2005).

Heynderickx, D., M. Kruglanski, V. Pierrard, J. Lemaire, M. D. Looper, and J. B. Blake: A Low Altitude Trapped Proton Model for Solar Minimum Conditions Based on SAMPEX/PET Data. IEEE Trans. Nucl. Sci., **46**, 1475 (1999).

Horne, R.B., S.A. Glauert, and R.M. Thorne: Resonant diffusion of radiation belt electrons by whistler-mode chorus. Geophys. Res. Lett., **30(9)**, doi:10.1029/2003GL016963 (2003).

Usoskin, I.G., K. Alanko, K. Mursula, G.A. Kovaltsov: Heliospheric modulation strength during the neutron monitor era. Solar Phys., **207**, 389–399 (2002).

Usoskin, I.G., O.G. Gladysheva, G.A. Kovaltsov: Cosmic ray induced ionization in the atmosphere: Spatial and temporal changes. J. Atm. Solar-Terr. Phys., **66(18)**, 1791–1796, 2004.

Velinov, P. L. Y., L. Mateev, and N. Kilifarska: 3-D model for cosmic ray planetary ionisation in the middle atmosphere. Ann. Geophys., **23**, 3043–3046 (2005).

An overview of the physics of the Earth's radiation environment

R. Vainio[1], L. Desorgher[2], E. Flückiger[2], and I. Usoskin[3]

[1] University of Helsinki, Finland, rami.vainio@helsinki.fi
[2] University of Bern, Switzerland
[3] Sodankylä Geophysical Observatory, University of Oulu, Finland

1 Introduction

The Earth's radiation environment consists of three major components: the galactic cosmic rays (GCR), the solar energetic particles (SEPs) or solar cosmic rays (SCR), and the trapped particles of the Van Allen belts. In the following sections, we will briefly outline the physical processes that determine the evolution of these components. The level of the paper is designed to provide the necessary tutorial background information for getting familiar with the physics of the radiation environment. It is, however, not aimed at providing a comprehensive review to the subject.

2 Rationale – Physics behind the models

2.1 Cosmic-ray modulation

Before reaching the vicinity of Earth, Galactic cosmic rays (GCR) experience complicated transport in the heliosphere that leads to the GCR modulation, which determines the long-term variations of this component of the radiation environment. The CR transport is described by the Parker's equation (Parker, 1965; Toptygin, 1985):

$$\frac{\partial U}{\partial t} = \nabla \cdot (\mathbf{K^s} \cdot \nabla U) - \nabla \cdot (\mathbf{V_{sw}} U) - \nabla \cdot (\langle \mathbf{v_D} \rangle U) + \frac{1}{3} (\nabla \cdot \mathbf{V_{sw}}) \frac{\partial}{\partial T} (aTU) , \quad (1)$$

where $U(T, \mathbf{r}, t)$ is the CR number density per unit interval of particle kinetic energy, T; $\mathbf{V}_{\rm sw}$ is the solar wind (SW) speed; $a = (T + 2T_r)/(T + T_r)$ where T_r is the particle's rest energy; $\mathbf{K^s}$ is the symmetric part of the diffusion tensor. This equation describes the following basic processes affecting the CR transport in the heliosphere. The diffusion of particles due to their scattering on magnetic inhomogeneities is represented by the first term of the equation. The second term describes the convection of particles by the outblowing solar wind. Next term deals with drifts, via the average drift velocity $\langle \mathbf{v_D} \rangle$, that CR particles experience in the heliosphere. Two types of drifts are important: the gradient-curvature drift in the regular

heliospheric magnetic field, and the drift along the heliospheric current sheet (HCS), which is a thin magnetic interface between the two heliomagnetic hemispheres. Note that, although the drifts play an important role in the CR modulation (Jokipii and Thomas, 1981), they do not modify the CR spectrum *per se* but only in combination with other mechanisms. The last term in Eq. 1 accounts for the adiabatic energy losses in the expanding solar wind. The local interstellar spectrum (LIS) of CR forms the boundary condition for the heliospheric transport problem. Since the LIS is not measured directly, i.e. outside the heliosphere, it is not well know in the energy range affected by the CR modulation (below 100 GeV). In this energy range LIS is usually assumed basing on the modeled CR production and transport in the galaxy and/or on inverting the heliospheric modulation models. Presently used approximations for the LIS (e.g. Garcia-Munos et al., 1975; Burger et al., 2000; Moskalenko et al., 2002; Webber and Higbie, 2003) agree with each other for energies above 20 GeV but may contain uncertainties of up to a factor of 1.5 around 1 GeV. These uncertainties in the boundary conditions make the results of the modulation theory slightly model-dependent (see discussion in Usoskin et al., 2005) and require the used LIS model to be explicitly cited.

The transport equation (1) cannot be solved analytically, and a full numerical solution of the 3D time-dependent transport equation is a complicated task and requires knowledge of the heliospheric parameters which cannot be directly measured (e.g., the diffusion tensor – see Burger and Hattingh, 1998). Accordingly, the full solution (e.g. Kota and Jokipii, 1983; Kota, 1995) is usually applied to qualitative theoretical studies, while different simplifications are often used for practical purposes. Usual assumptions on the azimuthal symmetry and quasi-steady changes reduce the problem to a 2D time-independent problem, which can be successfully solved numerically (e.g. Langner et al., 2006; Alanko-Huotari et al., 2007). Note that these simplifications can be applied to time scales of longer than the solar rotation period. As next step one can assume that the heliosphere is spherically symmetric, thus reducing the problem to a 1D case (Gleeson and Axford, 1968). This approximation can be used only for rough estimates, since it eliminates the effect of the drifts, but it is useful for the long-term studies, when the heliospheric parameters cannot be evaluated (e.g., Usoskin et al., 2002; Caballero-Lopez and Moraal, 2004).

Using further but still reasonable assumptions (constant solar wind speed, roughly power-law CR energy spectrum, slow spatial changes of U), one can reduce the 1D equation to the force-field case (Gleeson and Axford, 1968), which can be solved analytically. The differential intensity J_i of cosmic ray nuclei of type i at 1 AU is given as

$$J_i(T,\phi) = J_{\mathrm{LIS},i}(T+\Phi_i)\frac{(T)(T+2T_\mathrm{r})}{(T+\Phi)(T+\Phi_i+2T_\mathrm{r})}, \tag{2}$$

where $\Phi_i = (Z_i e/A_i)\phi$ for a cosmic nuclei of i-th type (charge and mass numbers are Z_i and A_i), T and ϕ are expressed in MeV/nucleon and in MV, respectively, $T_\mathrm{r} = 938$ MeV, We stress again that this approach not only contains the explicit modulation potential ϕ, which corresponds to the mean rigidity losses of a CR particle in the heliosphere, but is also implicitly dependent on the LIS. We note that this approach gives the results at least dimensionally consistent with the full theory. Moreover, the spectrum of different GCR species measured at Earth can be perfectly fitted by Eq. 2 using the only parameter ϕ in a wide range of the solar activity level (see Fig. 1). Therefore, the force-field model provides a very useful and simple parametric approximation of the differential spectrum of GCR. This model contains only one

variable parameter and, therefore, the whole energy spectrum (in the energy range from 100 MeV/nucleon to 100 GeV/nucleon) for protons and $\alpha-$particles can be described by a single number, the modulation potential ϕ, within the framework of the adopted LIS. However, we warn again that ϕ is only a formal spectral index whose physical interpretation is not straightforward, especially on short time scales and during periods of active Sun (Caballero-Lopez and Moraal, 2004).

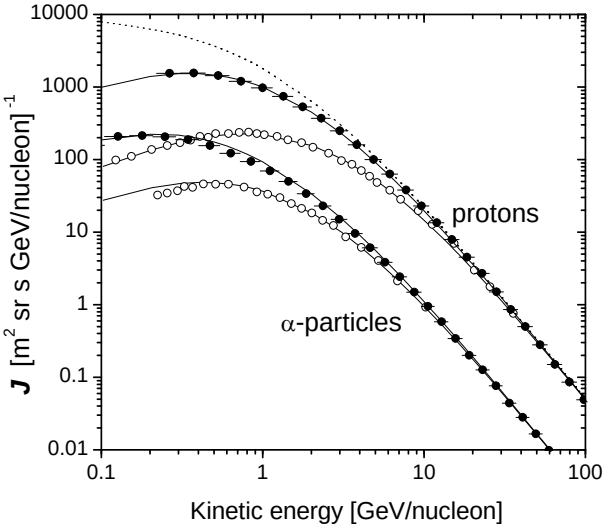

Fig. 1. Differential energy spectra of two most abundant components of GCR, protons (upper curves) and $\alpha-$particles (lower curves). Filled and open dots depict the results of direct measurements for a quite period of June 1998 (Alcaraz et al., 2000a,b) and a solar active period in September 1989 (Webber et al., 1991), respectively. The curves depict the best fit model results with $\phi = 530$ MV and $\phi = 1350$ MV, respectively (Usoskin et al., 2005). The dotted curve corresponds to the LIS ($\phi = 0$) for protons.

2.2 Solar energetic particle transport

Solar energetic particles (SEPs), i.e., solar cosmic rays (SCR), are observed as two major types of events: gradual and impulsive. The gradual events are intense proton-rich particle events lasting from some days to week and having an ion composition close to that of the coronal plasma. The maximum proton energies observed in these events extend up to a few GeV in the most extreme cases. Gradual events are related to coronal mass ejection and gradual X-ray flares. The impulsive events are electron-rich and their ion abundances show huge enhancements of minor ion species such as ^{3}He and heavies relative to the coronal abundances. They last from a few hours up to a day and have smaller proton intensities than the gradual flares. These events are related to impulsive X-ray flares. The two types of events are thought to be accelerated in coronal shocks driven by CMEs and in turbulent magnetized plasma of impulsive flares by wave-particle interactions, respectively. (Reames, 1999)

In principle, SEPs propagate in the interplanetary magnetic field (IMF) according to the same equations of motion as the galactic cosmic rays. Usually, however, effects such as adiabatic deceleration, convection with the solar wind, and drifts due to inhomogeneities in the magnetic field can be neglected in the inner heliosphere for particles of speeds $v \gtrsim 0.2\,c$, where c is the speed of light. In the simplest approach to the SEP transport, one can thus use the same diffusive transport equation (1) as with GCRs, but now with only two terms remaining

$$\frac{\partial U}{\partial t} = \nabla \cdot (\mathbf{K} \cdot \nabla U)\,, \tag{3}$$

where the diffusion tensor is usually taken to be of form $\mathbf{K} = K_{\parallel}(p, r)\mathbf{bb}$, i.e., only diffusion along the magnetic field, $\mathbf{B} = B\,\mathbf{b}$, is included. However, there is one important distinction relative to GCR that often invalidates the use of diffusive transport to describe SEP transport: unlike the GCR distribution with its quasi-stationary source outside the heliosphere, the SCR distribution has very anisotropic and rapidly evolving character.

The basic processes included in the non-diffusive SEP transport equation are streaming along the magnetic field lines, adiabatic focusing due to the decreasing magnetic field magnitude (by the conservation of the first adiabatic invariant), and pitch-angle diffusion due to the resonant interaction of the streaming energetic particles with the magnetic-field fluctuations (low-frequency plasma waves and/or turbulence), and the corresponding transport equation is known as the focused transport equation (Roelof, 1969; Ruffolo, 1991),

$$\frac{\partial f}{\partial t} + \mu v \frac{\partial f}{\partial s} + \frac{1-\mu^2}{2L} v \frac{\partial f}{\partial \mu} - \frac{\partial}{\partial \mu}\left(D_{\mu\mu} \frac{\partial f}{\partial \mu} \right) = Q, \tag{4}$$

where $f(s, v, \mu, t) = d^6N/(d^3x\, d^3p)$ is the distribution function of the SEPs on a given magnetic field line, s is the coordinate measured along the magnetic field, p is particle momentum, μ is the cosine of pitch angle (with $\mu = 1$ denoting outward propagation), $L = -B/(\partial B/\partial s)$ is the focusing length determined by the mean magnetic field, $B(s)$, as a function of distance, $D_{\mu\mu} = \frac{1}{2}\langle(\Delta\mu)^2\rangle/\Delta t$ is the pitch-angle diffusion coefficient, and $Q = Q(s, v, \mu, t)$ is the source function, determined by the processes that accelerate the particles in the solar corona and solar wind.

Later versions of the focused transport equation have included the effects of adiabatic deceleration and convection (Ruffolo, 1995) and partly even the effects of drift motions due to field inhomogeneities (le Roux et al., 2007). These are necessary especially if the energy changes of the particles in the solar wind, including particle acceleration in interplanetary shock waves, are to be modeled self-consistently. However, in the context of space weather engineering models, like SOLPENCO (see Sanahuja et al., this volume), the acceleration processes are typically handled in a phenomenological manner though an appropriately formulated source function Q. (SOLPENCO can be accessed on-line through http://www.spaceweather.eu .)

The most important unknown parameter in the focused transport equation is the pitch-angle diffusion coefficient. Usually, this parameter, $D_{\mu\mu} = \frac{1}{2}(1-\mu^2)\nu(v, \mu, s)$, is modeled by choosing the scattering frequency, $\nu \equiv \langle(\Delta\alpha)^2\rangle/\Delta t$ (where $\alpha = \arccos\mu$), to be of a power-law form $\nu = A(v, s)|\mu|^{q-1}$. The power-law index is, thus, determined by the spectral index, q, of the intensity of magnetic field fluctuations, $I(k) = I_0|k_0/k|^q$, through the quasi-linear theory (Jokipii, 1966). The magnitude, $A \sim \Omega(k_0 I_0/B^2)|k_0 v/\Omega|^{1-q}$, is related to

the gyrofrequency Ω of the particle and to the intensity I_0 of the magnetic fluctuations at a reference wavenumber, k_0, but since the intensity is not known as a function of distance throughout the inner heliosphere, modelers usually fix A by introducing the parallel mean free path, $\lambda_\parallel$, through

$$\lambda_\parallel \equiv \frac{3v}{4}\int_{-1}^{+1}\frac{1-\mu^2}{\nu}d\mu = \frac{3v}{A(2-q)(4-q)}, \tag{5}$$

and adopting a spatial dependence for this parameter. (The rigidity dependence of the mean free path is usually taken to be fixed by q as $\lambda_\parallel \propto R^{2-q}$, consistently with the quasi-linear result.)

The physical meaning of $\lambda_\parallel$ is that under strong scattering, i.e., $\lambda_\parallel \ll L$, particle transport in the interplanetary medium becomes diffusive with the spatial diffusion coefficient along the mean magnetic field given by $K_\parallel = \frac{1}{3}v\lambda_\parallel$. In this case, we can write

$$\frac{\partial U}{\partial t} = \frac{1}{r^2}\frac{\partial}{\partial r}\left(r^2 K_{rr}\frac{\partial U}{\partial r}\right), \tag{6}$$

where $K_{rr} = K_\parallel \cos^2\psi$, $\cos\psi = dr/ds$, ψ is the angle between the radial direction and the magnetic field, and r is the radial distance from the Sun. The attractive feature of this equation is that it can be solved analytically for reasonable assumptions of the spatial dependence of the diffusion coefficient. (See Dorman, this volume, for an example of using this equation to develop a forecasting model of SEP event evolution.)

The focused transport equation cannot be solved analytically in any realistic magnetic field geometry. Several simulation codes exist, however, to provide the numerical solutions, and they fall into two main types of solvers: (i) finite difference (FD) schemes (e.g., Ruffolo, 1991, 1995; Lario et al., 1998) and (ii) Monte Carlo (MC) simulations (e.g., Kocharov et al., 1998; Vainio et al., 2000). In FD schemes, one solves the focused transport equation directly on a grid, and in MC simulations one traces individual particles that follow the stochastic equations of motion equivalent to the focused transport equation. Both numerical methods have some attractive features and some drawbacks. The FD schemes are numerically very efficient and provide the solution for smoothly-behaving initial and boundary conditions very rapidly, but they are not ideally suited for δ-function-like particle injections, like for computing Green's functions of particle transport. The MC schemes, on the other hand are very easy to implement and update, because including a physical transport process to the code usually means a few lines of additional code. They can also easily handle any initial conditions and any boundary conditions that can be specified on a microscopic level, i.e., as rules of particle behavior at the boundaries of the simulation. As a downside, however, MC simulations usually require a large amount of CPU time to collect a large enough number of statistics for the reconstruction of the particle distribution.

2.3 Geomagnetic cutoff

The Earth's magnetosphere represents a natural shield against galactic and solar cosmic rays. The lower energy limit needed for a charged particle to cross the Earth's magnetosphere and

access a specific position at the top of the atmosphere decreases with the geomagnetic latitude of the observer, resulting in a cosmic ray flux on Earth increasing poleward.

For the study of the interaction of cosmic rays with the Earth's environment it is important to quantify the cutoff rigidity, which represents roughly the a lower bound of the CR particle's rigidity needed to reach a position from a given direction (Cooke et al., 1991). For the purpose of the study of solar energetic particles observed on Earth during Ground Level Enhancement (GLE) or for the study of cosmic ray anisotropy, it is also important to determine the asymptotic direction of a cosmic ray particle, which represents its direction of motion before entering into the magnetosphere.

Cutoff rigidities and asymptotic directions of incidence are computed by using backward trajectory tracing codes, which combine an internal model of the Earth magnetic field and a magnetospheric magnetic field model (Smart et al., 2000; Flückiger & Kobel, 1990; Bobik et al., 2003). In these codes the trajectories of cosmic rays with different rigidities, arriving at the same observing position and from the same direction of incidence, are computed backward in time as illustrated in the main picture in Fig. 2. The curves represent the trajectories of positively charged particles with a rigidity of 20, 10, 5, and 4.45 GV. In this case all the trajectories are initiated in the vertical direction at 20 km altitude above Jungfraujoch Switzerland. Particles with 20 and 10 GV rigidities have small trajectory bending before escaping the Earth's magnetosphere. The particle with 5 GV rigidity is bent stronger but can still escape the Earth's magnetosphere. The 4.45 GV trajectory makes several complex loops before reaching another point on the Earth's surface, illustrating that for this specific rigidity a cosmic ray can not reach the Jungfraujoch location. Some trajectories not shown here, which neither go back to the Earth nor leave the magnetosphere, can also be observed. Trajectories that do not leave the Earth's magnetosphere are called forbidden trajectories while those of particles escaping the Earth's magnetosphere are called allowed trajectories. The direction of motion at the position where an allowed trajectory crosses the magnetopause represents the asymptotic direction of incidence.

Backward trajectories are computed generally for a set of rigidities spanning a large range of values with a constant rigidity interval δR (usually 0.01 GV). The results of such computation for the case of Jungfraujoch is plotted in the right panel of Fig. 2. Three rigidity regions are identified:

i a high rigidity region where all trajectories are allowed;
ii a low rigidity region where all trajectories are forbidden;
iii an intermediate region called the penumbra where bands of allowed trajectories are separated by bands of forbidden ones.

The rigidity of the last allowed computed trajectory before the first forbidden one is called the upper cutoff rigidity R_U. The rigidity of the last allowed trajectory, below which all trajectories are forbidden, is called the lower cut-off rigidity R_L. Finally, the effective cutoff rigidity R_C is given by $R_C = R_U - n\delta R$, where n represents the number of allowed trajectories in the penumbra. The reader will find a complete description of the asymptotic direction computation method and cosmic ray cutoff terminology in Cooke et al. (1991).

For the analysis of the measurements of most ground-based cosmic ray experiments, where mostly vertically incident particles contribute to the counting rate, it is usually assumed that only cosmic rays with rigidity higher than the vertical effective cutoff rigidity R_C

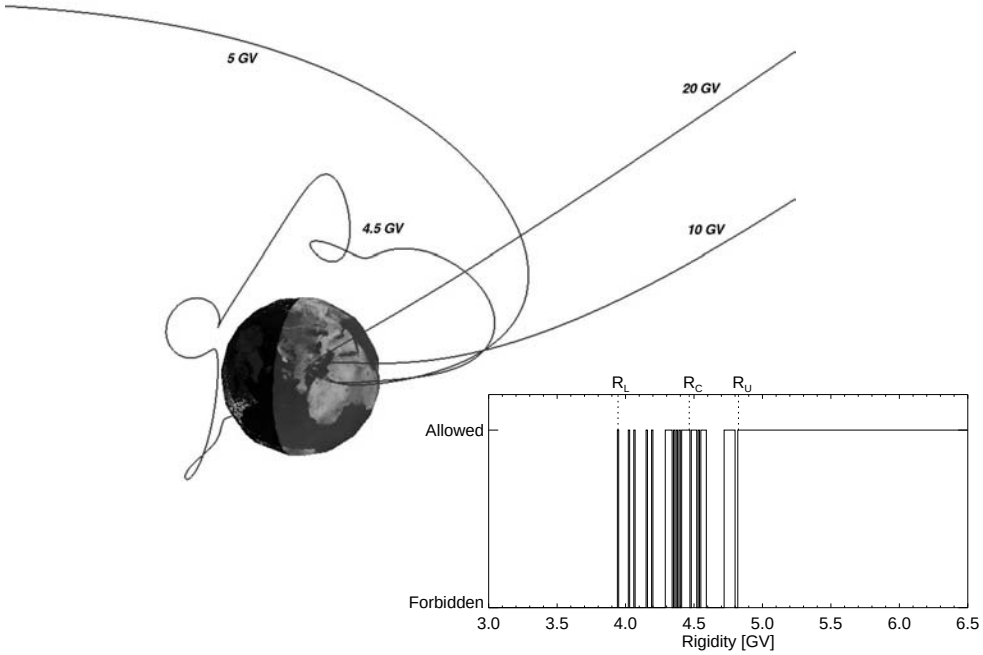

Fig. 2. Illustration of the backward trajectory technique used for computing cutoff rigidities and asymptotic directions. See the text for details.

can reach the top of the Earth's atmosphere from all directions of incidence. However at high altitude and for positions with high cutoff rigidity or in space, the contribution of non vertical particles becomes important and the variation of R_C with the direction of incidence must be taken into account (Clem et al., 1997; Dorman et al., 2007). The effective cutoff rigidity gives only a rough approximation of the complex structure of the penumbra. Different authors have treated more precisely the geomagnetic transmission in the penumbra region than just by using R_c (e.g., Boberg et al., 1995). In their work, Kudela and co-workers quantify the access of a CR of rigidity R to a given position by the geomagnetic transmissivity $T(R)$ that represents the percentage of allowed trajectories over the rigidity interval $[R, R + dR]$ (Kudela and Usoskin, 2003; Kudela et al., 2007).

The cutoff rigidity and asymptotic direction of incidence vary on different time scales following the variability of the geomagnetic field. The long term variation is due to the secular variation of the internal field. The diurnal variation in the geomagnetic cutoff is the effect of the rotation of the Earth in the magnetosphere, that is oriented in the solar wind flow. A semi seasonal variation is also observed reflecting the seasonal variation of the orientation of the internal field with the solar wind . The geomagnetic transmission depends also strongly on the geomagnetic activity. Different authors have study the variation of cutoff rigidity in function of substorm and storm activity. Flückiger et al. (1981); Flückiger & Kobel (1990) have studied

the dependence of cutoff rigidity on magnetospheric current systems during magnetic storms. Smart et al. (1999) have calculated the changes of vertical R_c in function of magnetic activity. Belov et al. (2005) have studied the variation of vertical R_c during the big magnetic storm of November 2003. Kudela et al. (2007) have studied the variation of geomagnetic transmissivity and asymptotic direction during big magnetic storms using different magnetic field models (see also Desorgher et al. in this issue).

A significant limiting factor in the precision achieved by computation of cutoff rigidity and asymptotic direction is the accuracy of magnetic field model. Over the last two decades models of the Earth's magnetospheric magnetic field have been continuously improved to describe more precisely the different magnetospheric current systems (magnetopause current, symmetric and partial ring currents, tail currents and field aligned currents) and their time variation during magnetic storms. In the joint paper of Desorgher et al. some of these models are compared in the context of cosmic ray physics.

Different possibilities are available today for computing cutoff rigidity and asymptotic direction for space weather purpose. Some groups have made their source code available (e.g., Desorgher, 2005). World grid of vertical R_c on Earth and at low Earth orbit can be found in the literature (e.g., Smart and Shea, 1997). Different web sites have been developed to offer the possibility to compute on-line the cutoff rigidity in function of position, time and magnetic activity (e.g., http://www.spaceweather.eu). For a rapid first order estimate of the cutoff rigidity analytical approximations exist. By approximating the geomagnetic field by a dipole, the cutoff rigidity is expressed by the Størmer cutoff formula

$$R_c = \frac{M \cos^4 \lambda}{r^2(1 + (1 - \cos^3 \lambda \cos \epsilon \sin \eta)^{1/2})^2} \tag{7}$$

where M is the dipole moment, r is the distance from the dipole center, λ is the geomagnetic latitude, ϵ is the azimuthal angle measured clockwise from the geomagnetic east direction (for positive particles), and η is the angle from the local magnetic zenith direction (Cooke et al., 1991). Shea et al. (1987) have shown that the vertical effective cutoff rigidity $R_c^{\perp}$ and the McIlwain L shell parameter are linked approximately by the relation

$$R_c^{\perp} = KL^{-\alpha} \tag{8}$$

where K and α depend on the epoch considered. Recently Storini et al. (2007) have extended this study and have found that the Eq. (8), with $K = 16.293$ GV and $\alpha = 2.073$ provides the best fit to compute cutoff rigidity at low and mid latitudes for the period 1955–1995. (Note that for a geocentric dipole field, the field line equation, $r = Lr_{\mathrm{E}} \cos^2 \lambda$ where r_{E} is the Earth's radius, predicts that $\alpha = 2$.) They have shown that for the epoch of 1990, this formula reproduces the computed R_C within an accuracy of 0.05 GV for 21 out of 31 sites over Europe. It is important to mention that while this formula allows a quick computation of the cutoff rigidity it should be used only for quiet geomagnetic time and for low and mid geomagnetic latitudes.

2.4 Atmospheric cascade

Cosmic rays that penetrate into the Earth's atmosphere interact by electromagnetic and hadronic processes with the atoms of the atmosphere. This interaction results in a cascade of

secondary particles also called cosmic ray shower (Grieder, 2001). The lowest energy needed for a cosmic ray particle to produce a cascade of secondary particles that can be observed on ground is roughly 500 MeV nucleon^{-1} and is referred as the atmospheric cutoff. The maximum flux of secondaries in an atmospheric cascade, referred as the Pfotzer maximum, takes place typically around 100–200 g/cm^{-2} of atmospheric depth.

Hadronic interactions of high energy primary and secondary nucleons and ions with atoms of the atmosphere produce mainly pions, but also nucleons, nuclear fragments and gammas. Neutral pions decay rapidly into energetic gammas that initiate electromagnetic cascades made of positrons, electrons and secondary gammas. The development of these electromagnetic cascades is controlled by the gamma pair production, photo electric, Compton scattering, and bremsstrahlung processes. Gamma nuclear interactions can also take place but these processes are not dominant in the development of an atmospheric cascade.

Charged pions decay into muons and neutrinos. These muons will either survive all their way through the atmosphere and be observed on ground and underground, or decay before and produce neutrinos, electrons and positrons which themselves are the source of electromagnetic cascades. Muons are also produced by the decay of kaons and charmed particles at higher energy. The flux of muons is higher than the protons and electronic flux at low altitude and is therefore a dominant source of ionization close to the ground.

Nucleons and nuclear fragments are produced at all energy and are the main product of hadronic interaction below the energy threshold of pion productions. Protons and ions with energy smaller than 100 MeV are rapidly stopped by coulomb interactions while the neutrons continue to interact. Below 10 MeV neutrons decelerate continuously by enduring elastic scattering on atmospheric nuclei, before being captured at thermal energy.

Following the description given above an atmospheric shower can be divided in three principal components:

i the electromagnetic or soft part made of gammas, electrons and positrons;
ii the hard component produced by the muons;
iii the nucleonic component made of secondaries neutrons and protons.

Below 40 km the shower particles are the main source of the ionization of the atmosphere. The impact of this ionization on the ozone layer and on the formation of clouds in the troposphere is the object of intense actual researches (Ermakov, 1997; Jackman, 2001; Marsh and Svensmark, 2000; Arnold, 2006). Some balloon experiments allow to measure the atmospheric ionization locally (Neher, 1971; Ermakov, 1997). However today a coordinated continuous world wide measurement of this ionization rate is still missing and computing codes have to be used to quantify it. The paper by Usoskin et al. (this volume) presents new achievements in cosmic ray induced ionization modeling, that have been obtained during this COST action.

Secondary albedo particles refer to shower secondaries produced at high altitude that escape the atmosphere upward. Albedo particles are an important source of space radiation at low altitude. Protons produced by the decay of albedo neutrons close to the Earth may be trapped in the Earth's magnetic field. This so called cosmic ray albedo neutron (CRAND) process represents the major source of the inner radiation belt proton. Energetic albedo protons can be shortly trapped in the magnetic field of the Earth before re-entering into the atmo-

sphere. These particles also known as sub-cutoff particles were observed for the first time by the AMS experiment (Alcaraz et al., 2000c).

2.5 Particle transport in the radiation belts

A very dangerous source of radiation in near-Earth space is constituted by the radiation belts. The radiation belts are ions (mainly protons) and electrons in an energy range from roughly a few tens of keV up to hundreds of MeV (10 MeV for electrons) trapped in the magnetosphere between an altitude of roughly 200 km and $7\,r_{\rm E}$.

The mean motion of radiation belt particles is characterized by a very rapid gyration around magnetic field lines, a slower bouncing of the gyration center along magnetic field lines between the northern and southern mirror points, and finally a very slow drift motion around the Earth (Roederer, 1970). The bouncing and drift motion of the gyration center make that particles in a static magnetic field move on so-called magnetic shells surrounding the Earth.

The gyration, bounce and drift motion are each quantified by a an adiabatic invariant that remains constant in time as far as the magnetic field varies slower than their typical time scales. The dynamics of the radiation belt is modeled by the Fokker-Plank diffusion equation in the adiabatic invariant phase space, where radial, pitch angle and energy diffusion, energy loss by friction with the atmosphere and the plasmasphere, and particle sources are considered (Shultz and Lanzerotti, 1974; Bourdarie et al., 1996). Radial diffusion represents the diffusion of the particles across the magnetic shells and is caused by variations of the magnetic field and electric field on a time scale shorter than the drift period (e.g., ULF waves, variation of the large scale convection electric field). Pitch angle diffusion spreads and mixes the particle mirror point distribution along magnetic field lines. It is produced by particle wave interactions and coulomb collision with the atmosphere. It is generally invoked as a loss process as it is the source of precipitation of the particles in the atmosphere, but can be also the source of particle acceleration. Indeed pitch angle and energy diffusion by whistler waves, combined with radial diffusion seems to be the most promising mechanism to explain the acceleration of electrons during magnetic storms inside the magnetosphere (Varotsou et al., 2005; Horne et al., 2005). For a more detailed description of the radiation belt dynamics and modeling we refer to the specific paper of Horne and Boscher (this volume).

3 Conclusion

A short description of physical processes governing the dynamics of the earth's radiation environment was given. The review is not a comprehensive one but will give necessary background information for the upcoming specific papers of this report.

References

Alanko-Huotari, K., I.G. Usoskin, K. Mursula, G.A. Kovaltsov: Stochastic simulation of cosmic ray modulation including a wavy HCS. J. Geophys. Res., **112**, A08101, (2007).

Alcaraz, J., et al. (The AMS collaboration): Cosmic protons. Phys. Lett. B, 490, **27** (2000a).
Alcaraz, J., et al. (The AMS collaboration): Helium in near Earth orbit. Phys. Lett. B, **494**, 193 (2000b).
Alcaraz, J., et al. (The AMS collaboration): Protons in near Earth orbit. Phys. Lett. B, **472**, 215–226 (2000).
Arnold, F.: Atmospheric Aerosol and Cloud Condensation Nuclei Formation: A Possible Influence of Cosmic Rays? Space Sci. Rev., **125**, 169–186 (2006).
Belov, A., L. Baisultanova, E. Eroshenko, H. Mavromichalaki, V. Yanke, V. Pchelkin, C. Plainaki, and G. Mariatos: Magnetospheric Effects in Cosmic Rays During the Unique Magnetic Storm of November 2003. J. Geophys. Res., **110**, A09S20, doi:10.1029/2005JA011067 (2005).
Boberg, P. R., A. J. Tylka, J. H. Adams, E. O. Flückiger, and E. O. Kobel: Geomagnetic Transmission of Solar Energetic Protons during the Geomagnetic Disturbances of October 1989. Geophys. Res. Lett., **22**, 1133–1136 (1995).
Bobik, P., M. Storini, K. Kudela, and E. G. Cordaro: Cosmic-Ray transparency for a medium latitude observatory. Il Nuovo Cimento, **26 C**, 2, 177–189 (2003).
Bourdarie, S., D. Boscher, T. Beutier, J. A. Sauvaud, and M. Blanc: Magnetic storm modelling in the Earth's electron belt by the Salammbo code. J. Geophys. Res., **100**, 14853 (1996).
Burger, R.A., and M. Hattingh: Toward a Realistic Diffusion Tensor for Galactic Cosmic Rays. Astrophys. J., **505**, 244–251 (1998).
Burger, R.A., M.S. Potgieter, B. Heber: Rigidity dependence of cosmic ray proton latitudinal gradients measured by the Ulysses spacecraft: Implication for the diffusion tensor. J. Geophys. Res., **105**, 27447 (2000).
Caballero-Lopez, R. A., and H. Moraal: Limitations of the force field equation to describe cosmic ray modulation. J. Geophys. Res., **109**, A01101 (2004).
Clem, J. M., J. W. Bieber, M. Duldig, P. Evenson, D. Hall, and J. Humble: Contribution of Obliquely Incident Particles to NM Counting Rate. J. Geophys. Res., **102**, 26919-26926 (1997).
Cooke, D.J., J. E. Humble, M. A. Shea, D. F. Smart, N. Lund, I. L. Rasmussen, B. Byrnak, P. Goret, and N. Petrou: On Cosmic-Ray Cutoff Terminology. Il Nuovo Centimento, **14 C**, 213–234 (1991).
Desorgher, L.: The MAGNETOCOSMICS code. http://cosray.unibe.ch/~laurent/magnetocosmics (2005).
Dorman L.I., O. A. Danilova, N. Iucci, M. Parisi, N.G. Ptitsyna, M. I. Tyasto, and G. Villoresi: Effective non-Vertical and Apparent Cutoff Rigidities for a Cosmic Ray Latitude Survey form Antarctica to Italy in Minimum of Solar Activity. Adv. Space Res., in press (2007).
Ermakov, V. I., G. A. Bazilevskaya, P. E. Pokrevski, and Yu. I. Stozhkov: Ion Balance equation in atmosphere. J. Geophys. Res., **102(D19)**, 23413–23419 (1997)
Flückiger, E. O., D. F. Smart, and M. A. Shea: On the effect of magnetospheric current systems on cosmic ray cutoff rigidities. in Proc. 17th Internat. Cosmic Ray Conf.,**4**, 244 (1981).
Flückiger, E. O., and E. Kobel: Aspects of Combining Models of the Earth's Internal and External Magnetic Fields. J. Geomag. Geoelectr., **42**, 1123–1136 (1990).
Flückiger, E. O., D. F. Smart, and M. A. Shea: Determining the strength of the ring current and the magnetopause currents during the initial phase of a geomagnetic storm using cosmic ray data. J. Geophys. Res., **95**, 1113 (1990).

Garcia-Munoz, M., G.M. Mason, J.A. Simpson: The anomalous ^{4}He component in the cosmic-ray spectrum at $\leq$50 MeV per nucleon during 1972–1974. Astrophys. J., **202**, 265 (1975).

Gleeson L.J., and Axford, W.I.: Solar Modulation of Galactic Cosmic Rays. Astrophys. J., **154**, 1011 (1968).

Grieder, P. K. F.: Cosmic rays at Earth – Researcher's reference manual and data book. Elsevier (2001).

Horne R. B., R. M. Thorne, S. A. Glauert, J. M. Albert, N. P. Meredith, and R. R. Anderson: Timescale for radiation belt electrons acceleration by Whistler mode chorus waves. J. Geophys. Res., **110**, A03225 (2005).

Jackman, C.H., R.D. McPeters, G.J. Labow, E.L. Fleming, C.J. Praderas, and J.M. Russell: Northern hemisphere atmospheric effects due to the July 2000 solar proton event. Geophys. Res. Lett., **28**, 2883 (2001).

Jokipii, J.R.: Cosmic-ray propagation. I. Charged particles in a random magnetic field. Astrophys. J., **146**, 480 (1966).

Jokipii, J.R., and B. Thomas: Effects of drift on the transport of cosmic rays. IV - Modulation by a wavy interplanetary current sheet. Astrophys. J., **243**, 1115–1122 (1981).

Kocharov, L., R. Vainio, G. A. Kovaltsov, J. Torsti: Adiabatic deceleration of solar energetic particles as deduced from Monte Carlo simulations of interplanetary transport. Solar Phys., **182**, 195 (1998).

Kota, J.: Three-dimensional transport of cosmic rays in the heliosphere. Nucl. Phys. B Proc. Suppl., **39 A**, 111–120 (1995).

Kota, J., and J. R. Jokipii: Effects of drifts on the transport of cosmic rays. VI. A three-dimensional model including diffusion. Astrophys. J., **265**, 573–581 (1983).

Kudela, K., and I. Usoskin: On Magnetic Transmissivity of Cosmic Rays. Czechoslovak J. Phys.,**54**,2, 239–253 (2003).

Kudela, K., R. Bucik, and P. Bobik: Transmissivity of low energy cosmic rays in the disturbed magnetosphere. To be published in Proc. European Cosmic Ray Symposium, Lisbon, Portugal (2007).

Langner, U.W., M.S. Potgieter, H. Fichtner, and T. Borrmann: Effects of Different Solar Wind Speed Profiles in the Heliosheath on the Modulation of Cosmic-Ray Protons. Astrophys. J., **640**, 1119–1134 (2006).

Lario, D., B. Sanahuja and A. M. Heras: Energetic particle events: efficiency of interplanetary shocks as 50 keV $< E <$ 100 MeV proton accelerators. Astrophys. J., **509**, 415–434 (1998).

le Roux, J. A., G. M. Webb, V. Florinski, and G. P. Zank: A Focused Transport Approach to Pickup Ion Shock Acceleration: Implications for the Termination Shock. Astrophys. J., **662**, 350–371 (2007).

Marsh, N., H. Svensmark: Low cloud properties influenced by cosmic rays. Phys. Rev. Lett., **85**, 5004–5007 (2000).

Moskalenko, I.V., A.W. Strong, J.F. Ormes, and M.S. Potgieter: Secondary antiprotons and propagation of cosmic rays in the galaxy and heliosphere. Astrophys. J., **565**, 280 (2002).

Neher, H.V.: Cosmic rays at high latitude and altitudes covering four solar maxima. J. Geophys. Res., **76**, 1637–1651 (1971).

Parker, E. N.: The passage of energetic charged particles through interplanetary space. Planet. Space Sci., **13(1)**, 9–49 (1965).

Reames, D.V.: Particle acceleration at the Sun and in the heliosphere, Space Sci. Rev., **90**, 413–491 (1999).

Roederer, J. G.: Dynamics of Geomagnetically Trapped Radiation, Springer: New York (1970).

Roelof, E. C.: Propagation of Solar Cosmic Rays in the Interplanetary Magnetic Field. In H. Ögelman and J. R. Wayland: Lectures in High-Energy Astrophysics, NASA SP-199, p. 111 (1969).

Ruffolo, D.: Interplanetary transport of decay protons from solar flare neutrons. Astrophys. J., **382**, 688–698 (1991).

Ruffolo, D.: Effect of adiabatic deceleration on the focused transport of solar cosmic rays. Astrophys. J., **442**, 861–874 (1995).

Shea, M. A., D. F. Smart, and L. C. Gentile: Estimating cosmic ray vertical cutoff rigidities as a function of the McIlwain L-parameter for different epochs of the Geomagnetic Field. Phys. Earth Plan. Int., **48**, 200–205 (1987).

Shultz, M., and L. J. Lanzerotti: Particle Diffusion in the Radiation Belt, Springer: New York (1974).

Smart D. F., and M. A. Shea: World Grid of Calculated Cosmic Ray Vertical Cutoff Rigidities for Epoch 1990. Proc. 25th Int. Cosmic Ray Conf., **2**, 401–404 (1997).

Smart D. F., M. A. Shea, E. O. Flückiger, A. J. Tylka, and P. R. Boberg: Changes in Calculated Vertical Cutoff Rigidities at the Altitude of the International Space Station as a Function of Magnetic Activity. Proc. 26th Int. Cosmic Ray Conf., **7**, 398–401 (1999).

Smart D. F., M. A. Shea, and E. O. Flückiger: Magnetospheric Models and Trajectory Computation. Space Sci. Rev., **93**, 305–333 (2000).

Storini, M., P. Metteo, and G. Moreno: Effects of the Geomagnetic Secular Variations on Cosmic Rays Access to the Terrestrial Environment. Adv. Space Res., in press (2007).

Toptygin, I.N.: Cosmic rays in interplanetary magnetic fields. Dordrecht, Kluwer (1985).

Usoskin, I.G., K. Alanko, K. Mursula, G.A. Kovaltsov: Heliospheric modulation strength during the neutron monitor era. Solar Phys., **207**, 389–399 (2002).

Usoskin, I.G., K. Alanko-Huotari, G.A. Kovaltsov, and K. Mursula: Heliospheric modulation of cosmic rays: Monthly reconstruction for 1951–2004. J. Geophys. Res., **110**, A12108 (2005).

Vainio, R., L. Kocharov, and T. Laitinen: Interplanetary and interacting protons accelerated in a parallel shock wave. Astrophys. J., **528**, 1015 (2000).

Varotsou A., D. Boscher, S. Bourdarie, R. B. Horne, S. A. Glauert, and N. P. Meredith: Simulation of the outer radiation belt electrons near geosynchronous orbit including both radial diffusion and resonant interaction with Whistler-mode chorus, Geophys. Let., **32**, L19106 (2005).

Velinov, P. L. Y., L. Mateev, and N. Kilifarska: 3-D model for cosmic ray planetary ionisation in the middle atmosphere. Ann. Geophys., **23**, 3043–3046 (2005).

Webber, W. R., and P.R. Higbie: Production of cosmogenic Be nuclei in the Earth's atmosphere by cosmic rays: Its dependence on solar modulation and the interstellar cosmic ray spectrum. J. Geophys. Res., **108(A9)**, 1355 (2003).

Webber W.R., et al.: A measurement of the cosmic-ray H-2 and He-3 spectra and H-2/He-4 and He-3/He-4 ratios in 1989. Astrophys. J., **380**, 230 (1991).

High energy solar neutron and γ-ray emissions: from the first ground level event to CORONAS-F results

K. Kudela[1], S.N. Kuznetsov[2,†]

[1] Institute of Experimental Physics, Slovak Academy of Sciences, Watsonova 47, 04001, Kosice, Slovakia; kkudela@kosice.upjs.sk
[2] Skobeltsyn Institute of Nuclear Physics, Moscow State University, Moscow, Russia
[†] Deceased in May 2007

Summary. The first part of the paper provides a short review of earlier observations of high energy neutrons and gamma rays from the Sun on satellites and on the ground, with a special emphasis on the contributions of Institute of Experimental Physics, Slovak Academy of Sciences, Kosice, to the topic. The second part of the paper illustrates measurements of solar gamma rays and neutrons on the Russian CORONAS-F satellite from August 2001 to December 2005. High energy neutral emissions from the Sun for three of solar flares, namely August 25, 2001, October 28, 2003, and November 4, 2003, are discussed in detail.

1 Introduction: Short survey of earlier observations and of IEP SAS contribution to the study.

The first detection of solar neutron signal at Earth's orbit, proposed in the paper by Bierman et al. (1953), was done on June 21, 1980 (Chupp, 1982b). Before that the presence of neutrons at the sites of solar flares was reported by the observation of 2.23 MeV neutron capture γ-ray line (Chupp et al., 1973). Basic considerations about the production of solar neutrons are reported, for example, by Lingenfelter and Ramaty (1967).

Gamma- and hard X-rays from the Sun were measured earlier on satellites such as OSO-7, SMM, CGRO, YOHKOH, GAMMA, GRANAT, and others (e.g., Chupp et al., 1982, 1987, 1993, 2003, and references therein). The hard electromagnetic spectral range has been observed also by satellites RHESSI (Lin et al., 2002; Smith et al., 2002, and others), INTEGRAL and, until December 2005, by CORONAS-F.

The efforts of several groups in the seventies to nineties of the 20$^{\text{th}}$ century were devoted to experimental studies of solar neutron response near Earth. One of such groups was the Department of Space Physics in Institute of Experimental Physics, Slovak Academy of Sciences (IEP SAS), Košice, Slovakia, engaged in the ground based observations of cosmic rays with the neutron monitor (NM) at Lomnický Štít (LŠ) as well as in satellite observations of energetic particles. Measurements started from a balloon experiment (Dubinský et al., 1977) and continued on the low-altitude polar orbiting satellite IK-17. Pulse shape discrimination technique in separating neutrons and γ-rays (Michaeli, 1983; Gusev et al., 1989) was used.

The detector system has been described by Efimov et al. (1983b). Although no solar neutrons were observed during the IK-17 mission, the study contributed to the description of latitudinal profile of albedo neutron and γ-ray flux in energy range 1–30 MeV at 500 km (Efimov et al., 1985).

CORONAS-I satellite, launched in Russia in March 1994, continued the measurements with similar instrumentation. One of the detectors on-board was SOlar Neutron and Gamma (SONG) experiment, described in paper (Baláž et al., 1994), a joint effort of Skobeltsyn Institute of Nuclear Physics, Moscow State University (SINP MSU) and IEP SAS. The detector was a CsI(Tl) crystal with anticoincidence shielding. Gamma-rays at 0.1–100 MeV and neutrons at 1–60 MeV have been detected. Detailed maps of γ-ray flux at different energies were obtained, and two components, (1) that due to interactions of primary cosmic rays with residual atmosphere and (2) that due to bremsstrahlung by high energy magnetospheric electrons, were identified (Bučík et al., 2000; Bučík, 2004).

In parallel, observations at ground-level, especially those by high-mountain NMs were checked for high-energy solar neutron response. One of those is at LŠ (2634 m, 49.40°N and 20.22°E, vertical cutoff rigidity $R_c \sim 4$ GV, measurements started during the IGY in 1957–1958; average counting rate now is 440 s^{-1}). Review of solar flare responses at that NM is in papers by Kudela et al. (1993) and Kudela and Storini (2002). On June 3, 1982, the gamma ray spectrometer on SMM recorded an extremely intense γ-ray line flare with the onset at ∼11:40 UT with the counting rates at the high energy channels remained high, which is characteristic for a flux of high energy solar neutrons at the satellite (Chupp, 1982a, personal communication). LŠ was in a proper position to observe solar neutrons from that flare and the result was positive. A ∼3-% increase was observed at 11:45–11:50 UT, corresponding to the arrival time of ∼1 GeV – ∼100 MeV neutrons. The estimate was ∼4000 counts from solar neutrons, corresponding to a fluence of ∼200 cm^{-2} at the top of atmosphere. This number was consistent with the ratio of neutron to 2.23-MeV γ-ray emission (Chupp, 1982b; Chupp et al., 1982) if characteristic rigidity of accelerated particles is $P_0 \sim 200 - 250$ MV (Efimov et al., 1983a). The solar neutron response, observed for the first time at the surface of Earth, was reported from NM at Jungfraujoch with 1-minute time resolution (Debrunner et al., 1983). Although LŠ NM had at that time only 5 min resolution, its measurement (883 g cm^{-2}, excess 2.7 ± 0.3 % in 1145–1150 UT) confirmed clearly, with high statistical accuracy, the increase at Jungfraujoch (745 g cm^{-2}, excess 3.9 ± 0.6 %). The increase from the same event was reported in the data of the Rome NM (Iucci et al., 1984). Protons produced by the decay of solar neutrons were discovered from the same flare also in satellite measurements (Evenson et al., 1983).

The efforts to increase the counting rate and to improve temporal resolution of existing NMs, as well as to develop new devices for the high mountain stations, were motivated by the event of June 3, 1982. Search of candidates of solar neutrons in LŠ data was performed (Kudela, 1990). Based on the list by Vestrand et al. (1987) and selecting the events with the depth $<$1020 g cm^{-2}, the superposed epoch analysis has indicated a possibility of anisotropic solar neutron production. Data of two NMs, namely Alma Ata and LŠ examined for the period 1980–1984 around the emissions of solar γ-rays have shown that the distribution of counting rates during the time of solar γ-ray emissions is significantly different from those before and after the flare for both stations (Belov et al., 1987).

2 SONG experiment on-board CORONAS-F satellite

CORONAS-F satellite was launched on July 31, 2001, in Russia, into a circular orbit with altitude 507$\pm$21 km, 82.5° inclination and an orbital period of 94.5 min. It was oriented towards the Sun. One of the instruments of a complex SKL (or SCR, Solar Cosmic Rays, PI S.N. Kuznetsov) coordinated by MSU is SONG, an improved version of SONG on-board CORONAS-I (description given by Kuznetsov et al., 1995). It is a joint instrument of SINP MSU and IEP SAS. Detector system consists of CsI(Tl) in active plastic shielding. SONG is able to detect hard X-rays and γ-rays at 0.03–200 MeV (12 energy channels, effective area $\sim$270 cm^2); neutrons at 3–100 MeV (effective area $\sim$38 cm^2); electrons at 8–100 MeV (5 energy channels, effective area $\sim$620 cm^2), and two channels measuring high-energy charged particles (first one responding to $>$75 MeV protons and $>$55 MeV electrons; the second one to 100–200 MeV protons). The instrument was operating from August 2001 until December 2005. More details about the SONG can be found in papers by Kuznetsov et al. (2003a,b, 2004).

SONG is capable of observing hard X-rays and γ-rays of solar origin when the satellite is outside the radiation belts or not shadowed by Earth. The background is due to local γ-rays produced by the interactions of CR either with the instrument, with the satellite body, or with the atmosphere. The increases due to bremsstrahlung by relativistic electrons of the radiation belts are discarded from the flare emission analysis. Review plots, i.e., light curves of the counting rates of different energy channels, are available at http://space.saske.sk/projects/songm/data.php?lang=1.

3 Solar flare measurements by SONG on CORONAS-F

SONG instrument on-board CORONAS-F observed several tens of hard X-ray events during solar flares. Table 1 shows a selection of these events with significant increases at $>$6 MeV.

Table 1. Solar γ-ray flares detected by SONG (CORONAS-F) from August, 2001, to September, 2005.

#	Date	UT of flare, SXR/GOES	SXR class/ GOES	Flare coords.	AR	UT of flare, HXR/SONG	$E_{\max}{}^{\star}$ [MeV]	γ-ray† fluence [m^{-2}]
1	25/08/01	16:23 – 16:45 – 17:04	X5.3	S17E34	9591	16:29 – 16:39	60–100	7150
2	11/12/01	07:58 – 08:14 – 08:08	X2.8	N16E41	9733	08:04 – 08:08	7–15	78
3	20/05/02	15:21 – 15:27 – 15:31	X2.1	S21E65	9961	15:25 – 15:29	7.7–16.5	87
4	28/10/03	09:51 – 11:10 – 11:24	X17.2	S16E08	0486	11:02 – 11:13	150–300	¿9200
5	29/10/03	20:37 – 20:49 – 21:01	X10.0	S15W02	0486	20:40 – 20:55	6–10	1270
6	04/11/03	19:29 – 19:53 – 20:06	X28	S19W83	0486	19:40 – 19:57	150–300	¿8100
7	20/01/05	06:36 – 07:01 – 07:26	X7.1	N14W61	0720	06:44 – 06:56	90–150	3620

* SONG Energy channel.
† Energy $>$ 500 keV.

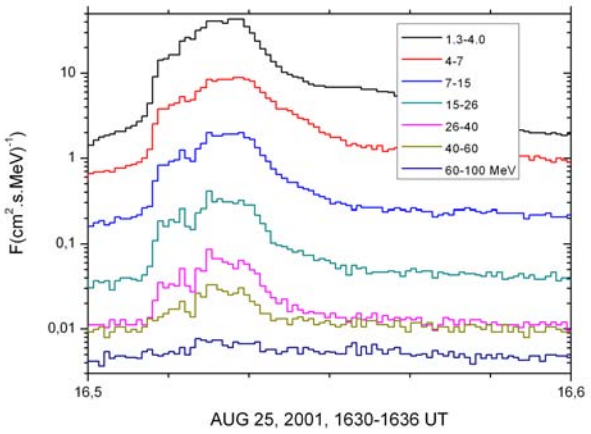

Fig. 1. Flux of gamma rays at various energy channels observed by SONG on-board CORONAS-F during the solar flare on August 25, 2001. The ticks on the horizontal axis correspond to 1-min intervals.

3.1 Event on August 25, 2001

A uniquely strong emission of solar γ-rays up to very high energies was observed on August 25, 2001 (Kuznetsov et al., 2003c). The parent solar flare is of the importance X5.3 and ball 3' in the active region NOAA 9591, coordinates S17° E34° at 16:23 UT. The index of the power-law energy spectrum at the time of maximum flux is estimated as -2.8 ± 0.1. The event was identified as the event with the highest energy emission of γ-rays, and a clear signal in neutron channels was detected in coincidence with the ground based observations by neutron monitor in proper local time (Watanabe et al., 2003). Gamma-rays up to $>$60 MeV were observed well above the background (see Fig. 1). Since it was before the launch of RHESSI it is impossible to compare the fluxes with another experiment. The event is not accompanied by any significant charged particle flux. It is not in the NOAA list of Solar Proton Events (http://umbra.nascom.nasa.gov/SEP/seps.html). There are no energetic proton or electron enhancements in polar caps detected by the MKL instrument on board CORONAS-F. The event is listed at http://www.harvard.edu/SSXG/kathy/flares/xflares.html as well as at http://isass1.solar.isas.ac.jp/sxt_co/sxt_trace_flares/list.html among flares jointly observed by SXT and TRACE, as an X5.4 flare, with the times of the first and the last flare mode SXT images. The latter one coincides with the observed very hard gamma emission by SONG-M. Note that nominal threshold energies of the energy channels are indicated in Table 1. (There was some evolution of the energy thresholds during the flight of SONG instrument.)

3.2 Event on October 28, 2003

In late October and early November 2003, SONG on-board CORONAS-F observed several X-ray and γ-ray events. The time history of the high-energy emission from the flare on October 28 is plotted in Figure 2. The parent solar flare is of the importance X17.2 and ball 4B, coordinates S16° E08°. During this solar flare, the increase above the background in the energy channel 60–100 MeV, is apparent.

There are several different spectral episodes observed during this flare. Gros et al. (2004) and Kiener et al. (2006) present results of γ-ray measurement from the flare, as observed by

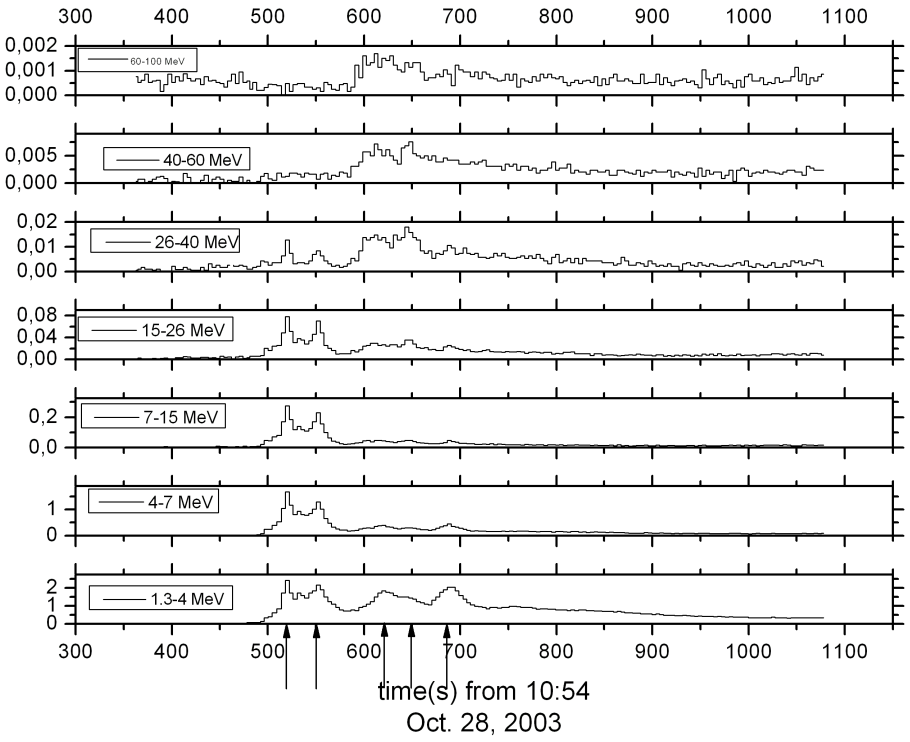

Fig. 2. Counting rate of gamma rays at various energy channels by SONG during the solar flare on October 28, 2003. The units of the vertical axes are #/(cm^2 s MeV). The effective surface of the detector is taken as 270 cm^2. The arrows depict time intervals with different energy spectra.

the INTEGRAL satellite. The RHESSI satellite measurements from the flare are presented, e.g., by Share et al. (2004). Acceleration of protons from this flare to unusually high energies is reported by Nonaka et al. (2006). Connection of broadband coherent synchrotron radiation in THz range, produced by a beam of ultrarelativistic flare electrons, with the observations of hard X-rays and γ-rays observed from the flare is discussed recently by Kaufmann and Raulin (2006). The time interval between the first two arrows in Figure 2, namely between 520 and 550 s from 10:54:00 UT, indicates the flux increases below 40 MeV. In this interval the first high-energy photon component thus, appears to have energies up to 40 MeV.

Gros et al. (2004) show the first impulse during the same time in continuum up to 10 MeV. CORONAS-F extends the energy of that emission up to 40 MeV. The third arrow ($\sim$620 s) depicts the maximum seen on CORONAS-F in 1.3–4 MeV, less pronounced in 4–7 MeV energy band and only slightly in 7–15 MeV. This is consistent with INTEGRAL profile of the continuum observed up to 10 MeV. While during the first interval (between arrows 1 and 2) there was no indication about high-energy continuum from π^0 decay, it appears with the onset $\sim$620 s on SONG. Most probably accelerated protons at $\sim$620–650 s produced π^0 mesons in nuclear interactions and, subsequently via their decay, the continuum of γ-quanta extending to higher energies than in the first interval (520–550 s). Most probably the variation of the spectra

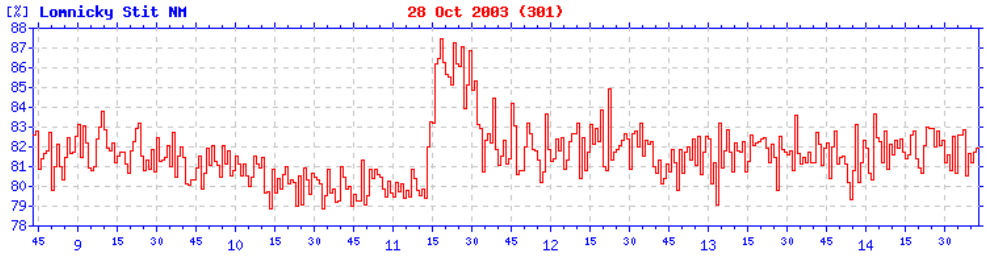

Fig. 3. 1-minute NM data at LŠ. 100% corresponds to $1.745 \cdot 10^6$ counts per hour. The onset is at 11:15 UT. Located in the southern hemisphere on approximately the same meridian, Tsumeb NM, with vertical cut-off of 9.2 GV, observes the onset earlier, at 11:04 UT with a 5 % peak increase (Stoker, 2005, personal communication). While Tsumeb had a zenith distance of 11° for that period, LŠ had a much larger distance, 51°.

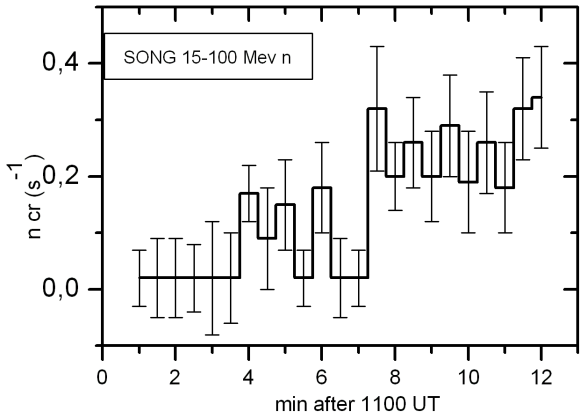

Fig. 4. SONG on CORONAS-F observed an increase of neutron channels 15–100 MeV above the background starting from ∼11:04 UT on October 28, 2003. The time coincidences with the onset on Tsumeb station (Fig. by Watanabe et al., 2006).

is due to two separate effects, (i) proton (or ion) acceleration to high energies and consequent pion decay and de-excitation of nuclei producing gamma ray lines, (ii) electron acceleration with consequent bremsstrahlung. A slight tendency of hardening of the spectra after 11:07 UT, consistent with RHESSI (Share and Murphy, 2005), is seen below 7 MeV. Above 7 MeV, a more complicated evolution of the spectra is apparent with two episodes of softening of the high-energy continuum spectra, namely at ∼520 s and 550 s after 10:54 UT. The spectral slope with a value close to -2 reported by RHESSI measurements at lower energies (0.46–8 MeV) is, within errors, consistent with the spectral shape obtained by CORONAS-F after 11:08 UT at energies above 7 MeV and also, within errors, with the shape at 1.3–4 MeV. Particles accelerated to relativistic energies produced the ground level event in cosmic rays, seen at several NMs. The increase on LŠ implies particle acceleration to at least 4 GV (Figure 3) and production of high energy γ-rays due to pion decay.

More discussion on the event can be found, e.g., in papers by Bieber et al. (2005), Miroshnichenko et al. (2005), and Watanabe et al. (2006).

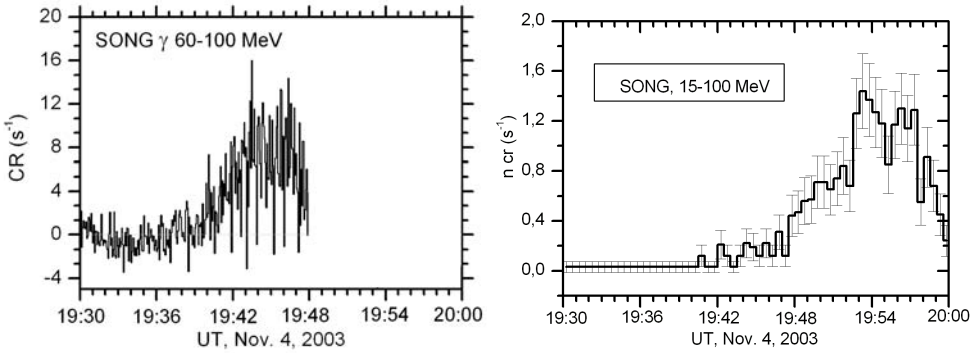

Fig. 5. The increases of high-energy γ-ray channel (left) and the neutron channel (right) of SONG (proton recoil, energy deposite 15–100 MeV) during the solar flare on November 4, 2003. The effective area for γ-ray channel 60–100 MeV is $\sim$60 cm^2.

3.3 Event on November 4, 2003

According to Watanabe et al. (2006), the largest flux of high energy neutrons from the flares in 23rd solar cycle was observed on November 4, 2003. SONG on CORONAS-F observed a γ-ray increase at least up to 60–100 MeV above the background. The neutron signal was also seen quite clearly by SONG. It is apparent from Figure 5. There is also possible signature of high energy neutrons in the Earth orbit from that flare, as deduced from a comparison of measurements of two NMs in different local-time sectors, namely those in Mexico (Valdes-Galicia, 2006, personal comminucation) and LŠ. The increase is observed after 19:45 UT at Mexico NM (vertical cut-off $\sim$9 GV), while at LŠ, with a lower geomagnetic cutoff (4 GV), the increase is not apparent.

4 Summary

The SONG instrument on-board CORONAS-F observed γ-ray emission at $>$6 MeV in at least 7 solar flares from August 2001 until September 2005. The most intensive flares in γ-rays were observed on August 25, 2001; October 28 and November 4, 2003; and January 20, 2005, which is discussed also elsewhere (Kuznetsov et al., 2006a,b). In these events, the γ-ray emission is seen to extend at least up to 60 MeV, and neutron channels at 15–100 MeV indicate increases as well. The flare of October 28, 2003, is characterized by time-variable energy spectra of γ-rays. Variations below 15 MeV are qualitatively consistent with those obtained by RHESSI and by INTEGRAL. Thus, SONG measurements extend the description of spectra to high energies, up to 100 MeV. At high energies, two episodes were observed with the softening of the spectrum of continuum emission not accompanied by a change at lower energies. Protons up to a rigidity of at least 4 GV were produced. Increases on neutron channels of SONG during the three events are accompanied by simultaneous NM increases in favourable local-time sectors, providing another confirmation of solar neutron events reported by Watanabe et al. (2005).

Measurements of solar neutrons closer to the Sun are a subject of discussion since the first observation of solar neutron signal at Earth from solar flare on June 3, 1982. In addition to space-probe and satellite observations, continuous measurements on the ground, especially at high mountains, are important for understanding the solar neutron spectra at high energies. A novel solar neutron detector described in papers by Tsuchiya et al. (2001) and Flückiger et al. (2001) is capable of measuring energy of incident neutrons and their arrival direction. During the solar cycle 23, sixteen remarkable solar neutron events were observed by the worldwide network of solar neutron telescopes and NMs (Flückiger et al., 2005). Relatively strong signals from solar neutrons were observed by solar neutron telescopes on October 28, and November 4, 2003 (Watanabe et al., 2006). Also the new ground based detectors, as described recently, e.g., by Chilingarian et al. (2007), may improve the knowledge about solar neutron production near the Sun.

Acknowledgements

This work was supported by the Slovak Research and Development Agency under the contract No. APVV-51-053805. KK acknowledges many colleagues and technicians in IEP SAS who were working on experimental devices for gamma and neutron measurements. The authors thank the referee for the suggestions on how to improve the paper. KK wishes to thank to Rami Vainio for important corrections and preparing the final version of the paper.

References

Baláž, J. et al., in IAU Colloquium 144, VEDA, Bratislava, p. 635, 1994
Belov, A.V. et al., Geomagn. Aeron., 27, 375, 1987
Bieber, J.W. et al., Geophys. Res. Let., 32, L03S02, 2005
Bierman, L. et al., Z. Naturforsch. 6a, 47, 1953
Bučík, R. et al., Acta Phys. Slovaca, 50, 267, 2000
Bučík, R., PhD thesis, P.J. Safarik U., Kosice, 2004
Chilingaryan, A., L. et al., Nuclear Instrum. Meth. In Phys. Res. A, 574, 255–263, 2007
Chupp, E.L. et al., Nature 241, 333–335, 1973
Chupp, E.L., personnal communication, June 20, 1982a
Chupp, E.L., paper presented at Seminar "Recent advances in the understanding of solar flares," Oct. 5–8, Tokyo, 1982b
Chupp, E.L. et al., Ap. J. Lett., 263, L95, 1982
Chupp, E.L. et al. Ap. J., 318, 913, 1987
Chupp, E.L. et al., Proc. of 23rd ICRC, Calgary, 3, 87, 1993
Chupp, E.L. et al., Proc. 28th ICRC, Tsukuba, 3171–3174, 2003
Debrunner, H. et al., 1983, Proc. 18th ICRC, Bangalore, 4, 75–78, 1983
Dubinský, J., et al., Bull. Astron. Inst. Czech., 28, 241, 1977
Efimov, Y.E. et al., Proc. 18th ICRC, Bangalore, 10, 276–279, 1983a
Efimov, Y.E. et al., Scientific space instrumentation (in Russian), Moscow, 1983b
Efimov, Y.E. et al., Czech. J. Phys., B 35, 1371, 1985

Evenson, P. et al., Proc. 18th ICRC, Bangalore 4, 97, 1983
Flückiger, E.O. et al., Proc. 27th ICRC, Hamburg, 3044–3047, 2001
Flückiger, E.O. et al., Int. J. Modern Phys. A, vol. 20, No 29, 6646–6649, 2005
Gros, M. et al., Proc. 5th INTEGRAL Workshop, ESA-SP 552, Noordwijk, ESA, 2004
Gusev, A.A., et al., Izv. Moscow University, ser. 3, Physics and Astronomy, 30, No 6, p. 126, 1989
Iucci, N. et al., Il Nuovo Cimento 7C, 732, 1984
Kaufmann, P. and J.-P. Raulin, Phys. Plasmas 13, 070701, 2006
Kiener, J. et al., Astronomy and Astrophysics, 445, 725–733, 2006
Kudela, K. Ap. J. Suppl. vol.73, no.2, June 1990, pp.297–301, 1990
Kudela, K. et al., Proc. 23rd ICRC, Calgary, 3, 71, 1993
Kudela, K. and M. Storini , ESA SP-477, 289, 2002
Kuznetsov, S.N. et al., Izv. Rus. Acad. Sci., ser. Fiz., 59, 2, 1995
Kuznetsov, S.N. et al., Solar System Res. 37, 121, 2003a
Kuznetsov, S.N. et al., Proc. 28th ICRC, Tsukuba, 3183, 2003b
Kuznetsov, S.N. et al., Proc. 28th ICRC, Tsukuba, p. 3183–3186, 2003c
Kuznetsov, S.N. et al., Indian J. Radio & Space Phys., 33, No 6, 353–357, 2004
Kuznetsov, S.N. et al., Solar System Res., 40, 2, 104–110, 2006a
Kuznetsov, S.N. et al., Contrib. Astron. Obs. Skalnate Pleso, 36, 85–92, 2006b
Lin, R.P. et al., Sol. Phys., 210, 3–32, 2002
Lingenfelter, R.E. and R. Ramaty, High Energy Nuclear Reactions in Astrophysics, W.A. Benjamin Inc., N. York, p. 99, 1967
Michaeli, L., in Scientific space instrumentation (in Russian), Metalurgia, 119, 1983
Miroshnichenko, L.I. et al., Adv. Space Res., 35, 1864–1870, 2005
Nonaka, T. et al. Physical Review D 74 (5), art. no. 052003, 2006
Ramaty, R. et al., Ap. J. Suppl., 487–526, 1979
Ryan, J.R. et al., Space Sci. Rev., 93, 35–53, 2000
Share, G.H. et al., The Astrophysical Journal, 615, L169–L172, 2004
Share, G.H. and J. Murphy, in Geophysical Monograph Series 162, AGU, doi:101029/162GM20, p. 13, 2005
Smith, D.M. et al., Sol. Phys., 210, issue 1–2, 33, 2002
Stoker, P., personnal communication, 2005
Tsuchiya, H. et al., Nucl. Instrum. & Methods in Physics Research A 463, 183–193, 2001
Valdes-Galicia, J., personnal communication, 2006
Vestrand, W.T. et al., Ap. J., 322, 1010, 1987
Watanabe, K. et al., Proc. 28th ICRC, Tsukuba, 3179–3182, 2003
Watanabe, K. et al., Proc.29th ICRC, Pune, 1, 37–40, 2005
Watanabe, K. et al., Ap. J., 636, 1135–1144, 2006

Comparison of Earth's magnetospheric magnetic field models in the context of cosmic ray physics

Desorgher L.[1], Kudela K.[2], Flückiger E. O.[1], Bütikofer R.[1], Storini M.[3], and Kalegaev V.[4]

[1] Physikalisches Institut, University of Bern, Sidlerstrase 5, 3012 Bern, Switzerland
[2] Institute of Experimental Physics, Slovak Academy of Sciences, Watsanova 47, 04001 Košice, Slovakia
[3] IFSI-Roma/INAF, Via del Fosso del Cavaliere 100, 00133 Roma, Italy
[4] Skobeltsyn Institute of Nuclear Physics, Moscow State University, Moscow 119992, Russia

Summary. Over the last two decades models of the Earth's magnetospheric magnetic field have been continuously improved to describe more precisely the different magnetospheric current systems (magnetopause current, symmetric and partial ring currents, tail currents and field aligned currents). In this paper we compare the different Tsyganenko models (Tsyganenko, 1989, 1995, 1996; Tsyganenko and Stinov, 2005) and the Alexeev A2000 model (Alexeev at al., 1996; Alexeev and Feldstein, 2001) in the context of cosmic ray physics. We compare the vertical cutoff rigidity and asymptotic direction of vertical incidence obtained with these models for the January 20, 2005 ground level enhancement and for the big magnetic storm of April 6, 2000. For the GLE of January 20, 2005, we study the impact of the differences in asymptotic direction obtained with the models on the radiation dose computation at aircraft altitude. For the magnetic storm of April 6, 2000, we discuss the importance of the different magnetospheric current systems in causing cutoff rigidity variations. Finally we summarise the advantages and drawbacks of the different models in the context of space weather.

1 Introduction

In most of the studies of the interaction of cosmic rays (CR) with the Earth's environment the effective vertical cutoff rigidity R_c at a given position is taken as the lower rigidity limit in the spectrum of CR particles reaching this position (Cooke et al., 1991; Smart et al., 2000). Asymptotic directions of vertical incidence are used in analysis of the relative variation of neutron monitor (NM) count rates for deducing the spectrum and pitch angle distribution of solar particles above 1 GV rigidity during ground level enhancements (GLEs), and for studying the anisotropy and flux variation of CR close to the Earth during Forbush effects. A good estimation of the cutoff rigidity and asymptotic direction in function of position, time, and geomagnetic activity is therefore important in the context of space weather. These quantities are computed by numerical integration of backward trajectories in a model of the geomagnetic field combining an internal part, usually represented by the International Geomagnetic Reference Field (IGRF) model (Langel, 1991), and a magnetospheric magnetic field model. During the last decades the magnetospheric magnetic field models have continuously evolved to describe more precisely the different magnetospheric current systems. While the model

developed by Tsyganenko (1989) provides six static mean states of the magnetosphere in function of the geomagnetic activity index Kp and considers only the symmetric ring current, the magnetopause current, and the tail current, the last generation of models developed by Alexeev and Feldstein (2001) and Tsyganenko and Stinov (2005) take into account also the partial ring current and the field aligned currents. Moreover the magnetopause currents are more precisely modeled as the field produced by the internal magnetospheric current systems is shielded in a magnetopause surface with its size and its shape being function of the solar wind conditions close to the Earth. Another improvement of these new models is that the amplitude, position and shape of the different magnetospheric currents are function of solar wind parameters and geomagnetic indices, and take also into account the prehistory of the coupling of the magnetosphere with the solar wind.

In this paper we compare the differences obtained in the computation of R_c and asymptotic direction when using the Tsyganenko (1989) model, the ring current extension of this model by Boberg et al. (1995), the Tsyganenko (1996) model, the Tsyganenko and Stinov (2005) model, and the Alexeev and Feldstein (2001) model. In the following of this paper we refer to these different models as the TSY89, TSY89BOB, TSY96, TSY05, and A2000 models respectively. In section 2 we present the effect of the difference in asymptotic direction of incidence on radiation dose computations for the January 20, 2005 GLE as well as the difference in R_c. In section 3 we compare the variation of R_c during the big magnetic storm of April 6, 2000, discuss the importance of the different current systems on this variation, and show the changes in asymptotic direction of incidence. In the last section we conclude and summarise the advantages and drawbacks of the different models in the context of space weather.

2 The ground level enhancement of January 20, 2005

We have investigated the level of variability that is to be expected in computation of radiation dose at aircraft altitude during GLEs when different magnetic field models are used for computing the asymptotic directions of vertical incidence. For this purpose we have computed the effective dose in the Earth's atmosphere induced by solar protons and galactic cosmic rays at 06:55 UT during the January 20, 2005 GLE. At this time the geomagnetic activity was relatively quiet (kp=2+). To describe the solar proton population above 1GV outside the magnetosphere we have considered the proton spectrum and the angular distribution computed from NM observations by Bütikofer et al. (2007). The obtained solar spectrum was highly anisotropic at this time. We have computed the flux of solar protons and galactic cosmic rays at the top of the atmosphere for a 5x5 degree world grid. The flux of solar protons at the top of the atmosphere was obtained from the flux outside the magnetosphere by computing asymptotic vertical directions of incidence. For the flux of galactic cosmic rays we have considered the model of Castagnoli and Lal (1980) with a solar modulation parameter of 700 MV. By using the PLANETOCOSMICS code we have computed for the whole grid, the flux of secondary particles at different atmospheric depth resulting from the interaction of the solar and galactic CRs with the Earth's atmosphere (Desorgher et al., 2005; Desorgher, 2005). Effective dose rates have been computed from particle fluxes by using flux to dose conversion factors published by Pelliccioni (2000).

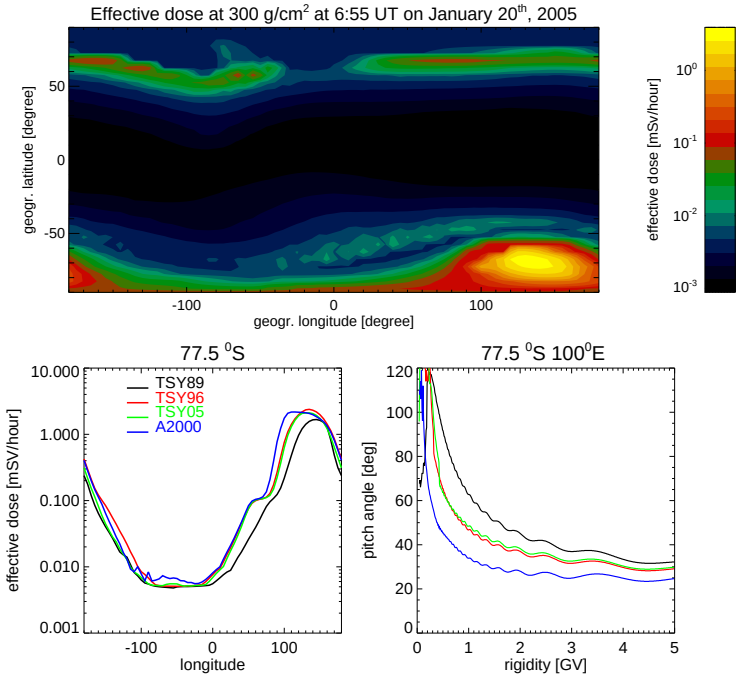

Fig. 1. The top panel represents the computed world map of radiation dose at 300 g/cm^2 induced by solar and galactic cosmic rays at 06:55 UT during the GLE of January 20, 2005. For these results the asymptotic directions of vertical incidence used for computing the flux of solar particles at the top of the atmosphere have been obtained by using the TSY89 model. The lower left panel represents the variation of the computed effective dose at 300 g/cm^2 for 77.5^o south latitude in function of longitude obtained by considering the TSY89 (black), TSY96 (red), TSY05 (green), and A2000 (blue) models. In the lower right panel, the pitch angle of the asymptotic direction of vertical incidence for the 77.5^o south latitude and 100^o east longitude position obtained with the same models is plotted in function of rigidity.

The upper panel of Figure 1 represents the computed radiation dose at 300 g/cm^2 atmospheric depth obtained by using the TSY89 model for the computation of the asymptotic direction of vertical incidence. We can see that the increase in the computed dose rate due to solar CRs is strongly dependent on location and can be larger by two order of magnitudes compared to the dose produced by galactic CRs in a very localised region around 70^o S and 140^o E. Some bands of increased dose are also obtained at high latitude both in north and south hemispheres. This is a direct consequence of the high anisotropy of the solar particles at this specific time.

While the general pattern of the dose maps obtained by considering different magnetic field models is similar (not shown here), significant local differences are observed. This is illustrated in the lower left panel of Figure 1 where we plot the variation with longitude at

77.5^o latitude south of the computed dose obtained with the TSY89 (black curve), TSY96 (red), TSY05 (green), and A2000 (blue) models. We see that the effective dose curves corresponding to the different magnetic field models reach comparable maxima around $120 - 140^o$ east longitude but are significantly shifted in the $0 - 120^o$ east longitude range. At 100^o east longitude the effective dose obtained with the TSY89 model is smaller by roughly an order of magnitude compared to other models. This difference reflects the difference between the pitch angles of computed asymptotic directions plotted in the lower right panel in function of rigidity for the 77.5^o south and 100^o east position.

We have also investigated the difference in R_c obtained with the various models. In Figure 2 R_c is plotted for the TSY89, TSY96, TSY05, and A2000 models in function of longitude for 77.5^o south and 47.5^o north latitudes. At mid latitude (47.5^oN) the differences in R_c are small, while at high latitude (77.5^oS) significant differences are observed. These differences have a small impact on the dose computation presented here.

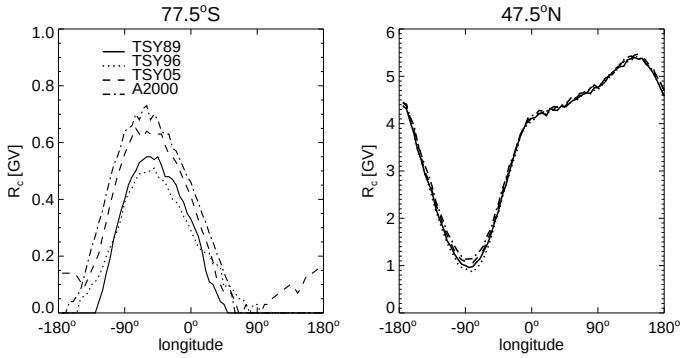

Fig. 2. Variation with longitude of R_c at 77.5^o south (left), and 47.5^o north (right) latitudes, at 6 UT on January 20, 2005 as obtained with the TSY89 (solid line), TSY96 (dotted line), TSY05 (dashed line) and A2000 (dashed dotted line) models.

3 The big magnetic storm of April 6, 2000

On April 4, 2000, a coronal mass ejection took place close to the western limb of the Sun and hits the Earth's magnetosphere on April 6 (Huttunen et al., 2002). It produced a big magnetic storm during which Dst reached a minimum value of -310 nT. We have computed the variation of R_c at Jungfraujoch and Lomnický Štít during this magnetic storm, using the TSY05, TSY89, TSY89BOB and TSY96 models. In this case the A2000 model has not been considered. By using NM response functions computed by Debrunner et al. (1982) and taking into account a realistic flux of galactic CRs outside the magnetosphere for this period, we have also computed the relative variation of the NM count rates induced by the change of the cutoff rigidity during the storm.

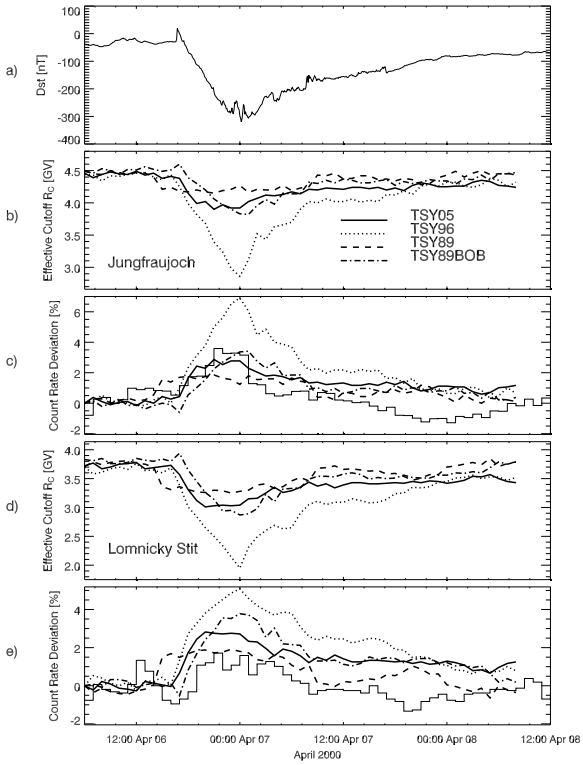

Fig. 3. a) Variation of the Dst index during the big magnetic storm of April 6, 2000. b) Variation for the same period of R_c at Jungfraujoch computed by using the TSY05 (solid), TSY96 (dotted), TSY89 (dashed), and TSY89BOB (dashed dotted) models. c) The bold lines represent the variation of NM count rates at Jungfraujoch estimated from the variation of R_c presented in b). The thin line represents the observed count rate variation. d) Same as b) but for Lomický Štít. e) Same as c) but for Lomnický Štít. For details see the text.

The results of our computations are presented in Figure 3. The panel a) represents the variation of the Dst index during the magnetic storm. The panels b) represents the variation of R_c for the same period computed by using the TSY05 (solid bold line), TSY96 (dotted line), TSY89 (dashed), and TSY89BOB (dashed dotted) models. The bold lines in panel c) represents the relative variation of NM count rates computed from the variation of R_c presented in the panel b). The thin solid line in the panel c) represents the observed relative variation of NM count rates. In the panels d) and e) the same information are plotted than in panel b) and c) but for Lomnický Štít. We see that the TSY05 and TSY89BOB models show the same magnitude of variation in R_c with some shift in time at both stations and reproduce quite

well the observed NM count rates increase at Jungfraujoch during the main phase of the magnetic storm, while they overestimate it at Lomnický Štít. The variation of R_c obtained with the TSY96 model is much bigger than with the other models leading to an overestimation of the count rate variation for both cases. The variation of the cutoff obtained with the TSY89 model is smaller than with other models, and does not follow the Dst variation. This is logical as the TSY89 model is only parametrised by the Kp index while the other models take into account the continuous variation of the Dst index. Despite this the maximum of NM count rates increase observed at Lomnický Štít is quite well reproduced.

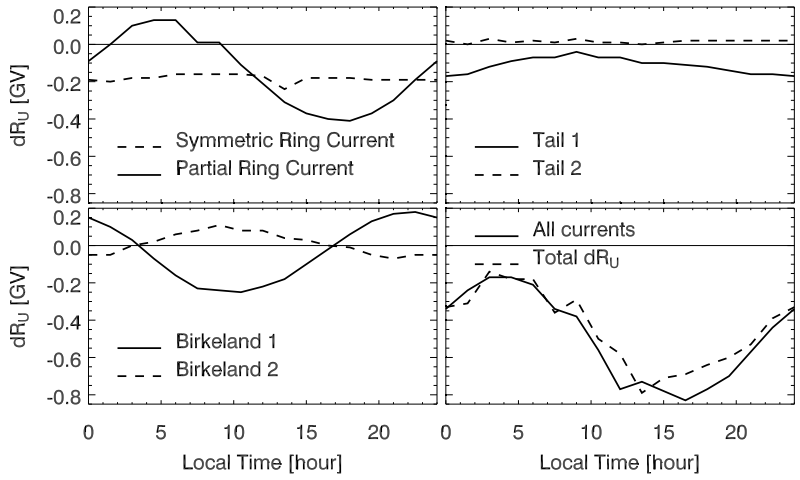

Fig. 4. Effect of the different magnetospheric current systems on the variation of the upper vertical cutoff rigidity during the magnetic storm of April 6, 2000, as simulated with the TSY05 model. For details see the text.

One aim of the computation presented above is to check if NM count rate variations during magnetic storms could be explained by computed cutoff changes and therefore be used to validate the magnetic field models. Recently Kudela et al. (2007) studied the variation of the magnetospheric transmitivity for low rigidity particles during different magnetic storms and discussed the possibility to use NM and muon telescope measurements for validating the magnetospheric magnetic field models. As mentioned in their study, this validation procedure should take into account the flux decrease and anisotropy increase of galactic CR outside the magnetosphere during magnetic storms. This has not been the case for our present analysis and the addition of this effect is foreseen in the future. However based on our first analysis we can say that the most realistic variation of the computed relative variation of NM count rates is produced by the TSY05 and TSY89BOB models. The TSY96 model can be clearly rejected as it overestimates the change in R_c. This is not surprising as the TSY96 model was developed to represent the magnetosphere for quite to moderate Dst activity. Indeed the TSY96 model

takes into account a linear variation of the ring current amplitude with Dst which is not valid in the case of intense storms.

We have also investigated the influence of the different magnetospheric currents in the variation of the cutoff rigidity during the April 6, 2000 magnetic storm. For this purpose we have used the TSY05 model as it allows to fix separately the strength of the symmetric ring current (SRC), of the partial ring current, of the Birkeland 1 and 2 currents, and of two different tail current systems (tail1, tail2). The amplitude of each current system has to be computed externally by the user from the prehistory of solar wind parameters, geomagnetic indices and combined indexes characterising the solar wind magnetosphere coupling. For our study we have considered that the amplitudes of the current systems before the storm at 12:00 UT on April 6, 2000 represent their quiet states while their amplitude obtained at 01:00 UT on April 7 defined their active states. We have then computed the variation of the cutoff rigidity in function of local time for Jungfraujoch in the case where each current system is set separately in its active state keeping the others in their quiet state. The differences obtained in upper vertical cutoff rigidity R_u (Smart et al., 2000), compared to the situation where all currents are quiet are plotted for each current system in Figure 4. We focus here on the changes in R_u rather than on the changes in R_c while the general effect of the current systems on the cutoff rigidity is somehow masked in R_c by the complex changes in the penumbra region. The top left panel shows the changes in R_u induced by the symmetric ring current (dashed) and partial ring current (solid). The second panels show the cutoff changes induced by the Birkeland 1 (dashed) and 2 (solid) current systems. The third panel shows the effect of the tail 1 (dashed) and tail 2 (dashed) current systems. We see that not only the symmetric ring current have a significant effect on the cutoff changes but also the partial ring current, Birkeland and tail currents. The azimuthal asymmetry of the current systems produces a significant local time variation of the changes in cutoff rigidity. These results are in agreement with previous studies of Flückiger et al. (1981, 1990). In the lower right panel the solid line represents the cutoff changes obtained when all the currents are set in their active state while the dashed line is the sum of the cutoff changes induced by the different currents. In this particular case the effect of the different current systems on the cutoff changes is additive. This is agreement with the study of Flückiger et al. (1986) who have found a relation of proportionality between the change in cutoff rigidity at low and mid latitude and the changes in the equatorial magnetic field in the vicinity of the position considered.

Finally we have studied the discrepancies between the magnetospheric models in term of asymptotic direction of vertical incidence at polar neutron monitor stations during the April 6, 2000 magnetic storm. In Figure 5 we present the differences between the asymptotic direction of vertical incidence obtained with the TSY05 and TSY89BOB models before the storm (thin solid line) and when Dst is minimum (thick solid line) for Barentsburg (upper left), Thule (upper right), McMurdo (lower left) and South Pole (lower right). We see that the differences in asymptotic direction increase significantly during the magnetic storm.

4 Conclusion and discussion

We have analysed the differences obtained in cutoff rigidity and asymptotic direction of vertical incidence by using different models of the Earth's magnetospheric magnetic field. We

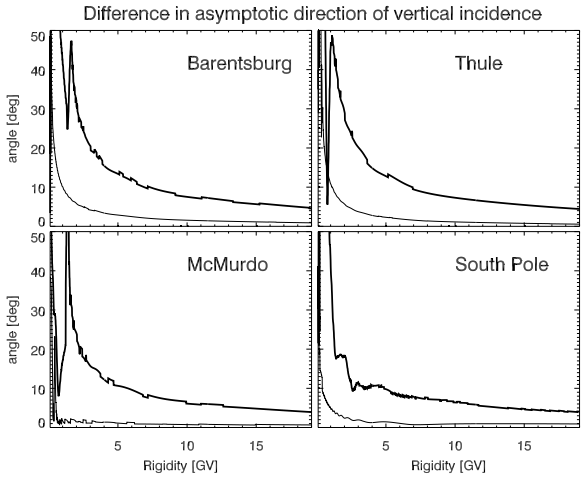

Fig. 5. Angular differences in asymptotic direction of incidence obtained with the TSY05 and TSY89BOB model, before the storm of April 6 2000 (thin solid line) and when the minimum of Dst was reached (bold solid line) for Barensburg (upper left), Thule (upper right), McMurdo (lower left) and South Pole (lower right) stations.

have found that for the GLE of January 20, 2005, at 06:55 UT the differences in asymptotic direction induce local differences in the radiation dose, but that the general patterns of the dose maps are identical. These local differences are significant for this specific case because the flux of solar particles in the vicinity of the Earth was highly anisotropic at this time. We have also shown that the differences in cutoff rigidity during January 20, 2005, between different magnetic field models are only significant at high latitude. We have shown that for the big magnetic storm of April 6, 2006 important differences in cutoff changes at Jungfraujoch and Lomnický Štít are obtained between the models. In order to validate the magnetic field models we have computed the relative variation of NM count rate resulting frome these cutoff changes and compared them to observations. From this comparison we can say that the TSY05 and TSY89BOB models show the best comparison with the observed NM count rate variations. However as the perturbation of the CR flux outside the magnetsophere has been neglected in our study some caution should be taken about this conclusion. In the future we plan to take this effect into account. We have also studied the separate effect of each magnetospheric current system during the same storm and have shown that not only the symmetric ring current but also the partial, Birkeland and tail currents have an important contribution to the cutoff changes. The azimuthal asymmetry of these current systems increase significantly the local time variation of the cutoff rigidity. We have shown that the effect of each separate current system can be added to roughly reproduce the total cutoff variation. This is of potential use for space weather applications, as this property could be used for a rapid estimation of the change of cutoff rigidity during magnetic storm. In this context we think that the procedure developed by Flückiger et al. (1986) for a rapid estimate of the cutoff change during enhanced

geomagnetic activity could be updated to the new generation model of the Earth's magnetosphere. Finally we have shown that the discrepancy between the TSY05 and TSY89BOB models in term of asymptotic direction of incidence is significant during big magnetic storms.

It is clear that the new generation of magnetospheric magnetic field models as the TSY05 and A2000 models allow a better investigation of the effect of the variation of magnetospheric currents on cutoff rigidity and asymptotic direction during times with enhanced geomagnetic activity. However these models have important drawbacks compared to the TSY89 and TSY89BOB models. Trajectory computations with these new models take roughly 20 times more computing time than with the TSY89 and TSy89BOB models. With todays personal computers a 5x5 degree world grid of R_c can be computed in roughly 1-3 hours with the TSY89 and TSY89BOB models, while for the TSY05 and A2000 1-3 days are needed. Moreover the TSY89 and TSYBOB89 models are much more easy to use than the other models as they have only Kp and Dst as input parameters. In conclusion for quiet geomagnetic activity we believe that the TSY89 and TSY89BOB are still valid for computing R_c and the asymptotic direction of vertical incidence while for precise study of the effect of magnetospheric currents during magnetic storm the TSY05 and A2000 models should be used. Our study have been focused only on cutoff rigidity and asymptotic direction changes on Earth. It would be interesting to reproduce the same study for satellite orbits.

Acknowledgement. All the authors acknowledge support by the COST724 action. LD, RB and EOF acknowledge support by the Swiss National Foundation (grants 2000020-105435/1, 200020-113704/1), and by the Swiss State Secretariat for Education and Research (grant COST-724/C05. 0034). Work of KK was supported by the Slovak Research and Development Agency under the contract No. APVV-51-053805. VK acknowledges support by RFBR grants 06-05-64508 and 07-05-00529. MS thanks support by INAF 2005-2007 grants.

References

Alexeev I. I., E. S. Belenkaya, V. V. Kalegaev, Ya. I. Feldstein, and A. Grafe, Magnetic storms and magnetotail currents, J. Geophys. Res., **101**, No4, 7737–7748 (1996).

Alexeev, I. I., and Y. I. Feldstein, Modeling of Geomagnetic Field During Magnetic Storms and Comparison with Observations, J. Atmos. Sol. Terr. Phys., **63**, 431–440 (2001).

Boberg, P. R., A. J. Tylka, J. H. Adams, E. O. Flückiger, and E. O. Kobel, Geomagnetic Transmission of Solar Energetic Protons during the Geomagnetic Disturbances of October 1989, Geophys. Res. Lett., **22**, 9, 1133–1136 (1995).

Bütikofer, R., E. O. Flückiger, L. Desorgher, and M. R. Moser, Analysis of the GLE on January 20, 2005: an Update, in Proc. of the 20th European Cosmic Ray Symposium, Lisbon, Portugal (2007).

Castagnoli, G. C., and D. Lal, Solar Modulation Effects in Terrestrial Production of Carbon-14, Radiocarbon, **22**, 133–158 (1980).

Cooke, D. J., J. E. Humble, M. A. Shea, D. F. Smart, N. Lund, I. L. Rasmussen, B. Byrnak, P. Goret, and N. Petrou, On Cosmic-Ray Cutoff Terminology, Il Nuovo Cimento, **14C**, 213–234 (1991).

Debrunner, H., E. O. Flückiger, and J. A. Lockwood, 8th Europ. Cosmic Ray Symp., Rome, 13 (1982).

Desorgher, L., E. O. Flückiger, M. Gurtner, M. R. Moser, and R. Bütikofer, Atmocosmics: a Geant4 Code for computing the interaction of cosmic rays with the Earth's atmosphere, Int. J. Mod. Phys. A, **20**, 6802–6804 (2005).

Desorgher, The PLANETOCOSMICS code, http://cosray.unibe.ch/∼laurent/planetocosmics (2005).

Flückiger, E. O., D. F. Smart, and M. A. Shea, On the effect of magnetospheric current systems on cosmic ray cutoff rigidities, in Proc. of the 17th International Cosmic Ray Conference, Paris, France, **4**, 244 (1981).

Flückiger, E. O., D. F. Smart, and M. A. Shea, A procedure for estimating the changes in cosmics ray cutoff rigidities and asymptotic directions at low and middle latitudes during periods of enhanced geomagnetic activity, J. Geophys. Res., **91**, 7925 (1986).

Flückiger, E. O., D. F. Smart, and M. A. Shea, Determining the strength of the ring current and the magnetopause currents duirng the initial phase of a geamagnetic storm using cosmic ray data, J. Geophys. Res., **95**, 1113 (1990).

Huttunen, K. E. J., H. E. J. Koskinen, T. I. Pulkkinen, A. Pulkkinen, M. Palmroth, E. G. D. Reeves, and H. J. Singer, April 2000 magnetic storm: Solar wind driver and magnetospheric response, J. Geophys. Res., **107 (A12)**, 1440 (2002).

Kudela, K., R. Bucik, P. Bobik, Transmissivity of low energy cosmic rays in the disturbed magnetosphere, in Proc. of the 20th European Cosmic Ray Symposium, Lisbon, Portugal (2007).

Langel, R. A., International Geomagnetic Reference Field: The sixth generation, J. Geomagn. Geoelectr., **44**, 679 (1991).

Pelliccioni, M., Overview of Fluence-to-Effective Dose and Fluence-to-Ambient Dose Equivalent Conversion Coefficients for High Energy Radiation Calculated Using the FLUKA Code, Rad. Prot. Dos., **88**, No 4, 279–297 (2000).

Smart D. F., M. A. Shea, and E. O. Flückiger, Magnetospheric Models and Trajectory Computation, Spac. Sci. Rev., **93**, 305–333 (2000).

Tsyganenko, N. A., A Magnetospheric Magnetic Field Model with a Warped Tail Current Sheet, Planet. Spac. Sci., **37**, 5–20 (1989).

Tsyganenko, N. A., Modeling the Earth's Magnetospheric Magnetic Field Confined within a Realistic Magnetopause, J. Geophys. Res., **100**, 5599–5612 (1995).

Tsyganenko, N. A., Effects of the Solar Wind Conditions on the Global Magnetospheric Configurations as Deduced from Data-Based Field Models. In Proceedings of 3rd International Conference on Substorms, Versailles, France, ESA SP-389, 181–185, Eur. Space Agency, Paris (1996).

Tsyganenko, N. A. and M. I. Sitnov, Modeling the Dynamics of the Inner Magnetosphere During Strong Geomagnetic Storms, J. Geophys. Res., **110 (A3)**, 3208 (2005).

Solar and galactic cosmic rays in the Earth's atmosphere

I. Usoskin[1], L. Desorgher[2], P. Velinov[3], M. Storini[4], E. O. Flückiger[2], R. Bütikofer[2], and G.A. Kovaltsov[5]

[1] Sodankylä Geophysical Observatory (Oulu unit), P.O.Box 3000, FIN-90014 University of Oulu, Finland, Ilya.Usoskin@oulu.fi,
[2] Physikalisches Institut, University of Bern, Sidlerstrasse 5, CH-3012 Bern, Switzerland
[3] Solar-Terrestrial Influences Laboratory, Bulgarian Academy of Sciences, Sofia 1113, Bulgaria
[4] IFSI-Roma/INAF, Via del Fosso del Cavaliere, 100 - 00133 Roma, Italy
[5] Ioffe Physical-Technical Institute, RU-194021 St. Petersburg, Russia

Summary. A brief review of the research of atmospheric effects of cosmic rays is presented. Numerical models are discussed, that are capable to compute the cosmic ray induced ionization at a given location and time. Intercomparison of the models, as well as comparison with fragmentary direct measurements of the atmospheric ionization, validates their applicability for the entire atmosphere and the whole range of the solar activity level variations. The effect of sporadic solar energetic particle events is shown to be limited on the global scale, even for for the most severe event, but can be very strong locally in polar regions, affecting the physical-chemical properties of the upper atmosphere, especially at high altitudes. Thus, a new methodology is presented to study cosmic ray induced ionization of the atmosphere in full detail using realistic numerical models calibrated to direct observations.

1 Introduction

Cosmic rays (CR) form an important outer space factor affecting physics and chemistry of the entire atmosphere. In particular, they are the main ionizing agent for the lower and middle atmosphere. For many practical purposes, e.g., for the impact of cosmic rays on the ozone layer and formation of clouds in the troposphere, it is important to know precisely the cosmic ray induced ionization (CRII) and its variations with the location, time, solar and geomagnetic activity. Two main components are important for CRII: (1) high energy galactic cosmic rays that are always present in the vicinity of the Earth and are subject of the solar modulation and (2) sporadic solar energetic particles of lower energy but high peak flux. The effect of both components is quantitatively studied here. Balloon experiments have been used in the past to measure the CRII at different locations and during several solar cycles (e.g., Neher, 1971; Lowder et al., 1972; Rosen et al., 1985; Ermakov et al., 1997), but a coordinated continuous world wide measurement of CRII is still missing. On the other hand, several physical models have been developed recently to compute CRII in the full range of physical parameters. In the framework of the COST-724 action, three numerical CRII models have been developed: Sofia model (Velinov and Mateev, 2005), Bern model (Desorgher et al., 2005; Scherer et al., 2006), and Oulu model (Usoskin et al., 2004; Usoskin and Kovaltsov, 2006). Here we present these

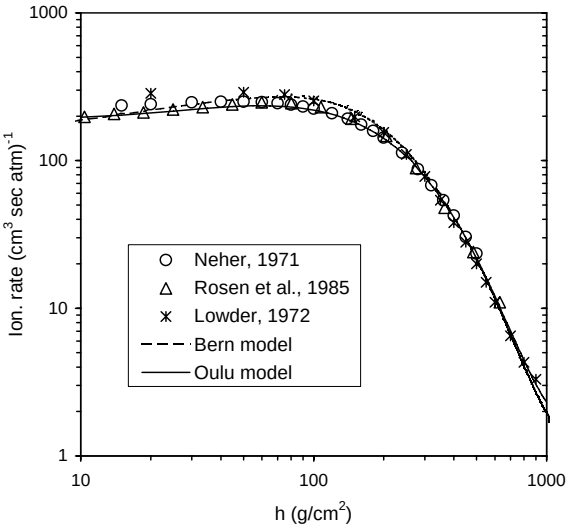

Fig. 1. Measured and calculated ionization rate in a high-latitude region during a solar maximum ($\phi \approx 1000$ MV). Symbols represent direct measurements as denoted in the legend, while curves correspond to the present calculations using the Bern (dashed) and Oulu (solid) models.

models, their validation and comparison with direct observations and other results. We also discuss effects caused by solar and galactic CR in the atmosphere.

2 Cosmic Ray Induced Ionization in the atmosphere

2.1 Galactic Cosmic Rays

The ionization due to galactic cosmic rays (GCR) is always present in the atmosphere, and it changes with the 11-year solar cycle due to the solar modulation. Primary cosmic rays initiate a nucleonic-electromagnetic cascade in the atmosphere, with the main energy losses at altitudes below 30 km resulting in ionization, dissociation and excitation of molecules (see, e.g., Dorman, 2004). The details of the cosmic ray initiated cascade are discussed in (Vainio et al., this volume). The CRII can be represented in numerical models in the following form:

$$Q(h, \phi, P_c) = \sum_i \int_{T_{c,i}}^{\infty} J_i(T, \phi)\, Y_i(h, T)\, dT, \qquad (1)$$

where the summation is performed over different i-th species of CR (protons, $\alpha-$particles, heavier species), $Y_i(h, T)$ is the ionization yield function (the number of ion pairs produced at altitude h in the atmosphere by one CR particle of the i-th type with kinetic energy T). The differential energy spectrum $J_i(T, \phi)$ of the i-th specie of GCR in space near Earth depends on solar activity and is often parameterized via the modulation potential ϕ (see, e.g., Usoskin et al., 2005). Integration is performed above $T_{c,i}$, which is the kinetic energy of a particle of $i-$th type, corresponding to the local geomagnetic rigidity cutoff P_c. Numerical CRII models presented here are based on detailed computations of $Y_i(h, T)$ by Monte-Carlo simulations of the nucleonic-electromagnetic cascade initiated by cosmic rays in the atmosphere. The Bern model (ATMOCOSMIC/PLANETOCOSMIC code - see Desorgher et al.,

2005) is based on the GEANT-4 Monte-Carlo simulation package. The PLANETOCOSMIC code is available at http://cosray.unibe.ch/~laurent/planetocosmics/. The Oulu model is based on the CORSIKA Monte-Carlo package extended by FLUKA package to simulate the low-energy nuclear interactions, and explicitly accounting for direct ionization by primary CR particles. A full numerical recipe along with the tabulated values of Y are given by Usoskin and Kovaltsov (2006). The Sofia model includes an analytical approximation of the direct ionization by CR primaries (Velinov et al., 2001) as well as CORSIKA/FLUKA Monte-Carlo simulations (Velinov and Mishev, 2007). Fig. 1 shows comparison of the CRII simulation results for Bern and Oulu model with fragmentary direct balloon-borne measurements of the ionization rate in a high latitude region ($P_{\rm c}$ <1.5 GV). Taking into account different location and dates of individual measurements, the agreement between calculated and measured CRII is pretty good (Scherer et al., 2006; Usoskin and Kovaltsov, 2006). Results of the simulations agree with each other within 10%, which is mainly attributed to the different atmospheric models used and, to a less extent, to different cross-section approximations in CORSIKA and GEANT-4 packages. The results of the CORSIKA-based Sofia model are very close to those of the Oulu model. Note that an analytical approximation model of CRII by O'Brien (2005) also shows a reasonable agreement with the present models.

Equation 1 separates the temporal variability of the cosmic ray flux impinging on the Earth (the $J(T,\phi)$ term) and local parameters (altitude and geomagnetic cutoff rigidity) via Y and $P_{\rm c}$. The CRII strongly depends on the altitude and geographical location, the latter via the geomagnetic rigidity cutoff $P_{\rm c}$. The CRII dependence on the solar modulation (ϕ) is relatively weak (10–50%), but it is responsible for the observed temporal variations. Some examples of the CRII at different altitudes and locations are shown in Fig. 2, while the lower panel of Fig. 4 depicts the geographical distribution of CRII for the atmospheric depth $h = 300$ g/cm^2.

2.2 The effect of solar energetic particle events

In addition to the permanent flux of GCR, sporadic solar energetic particle (SEP) events occur sometimes when strong fluxes of energetic particles are produced in solar flares or CMEs. Such SEPs (mostly protons) interacting with the Earth's atmosphere can produce an important increase of the atmosphere ionization (e.g. Schröter et al., 2006). Usually SEPs are accelerated up to hundreds of MeV, and the corresponding increase of the ionization is observed only at high altitude in the polar atmosphere. However, particles can be accelerated up to higher energies (a few GeV) during strong events called GLE (Ground Level Enhancement of cosmic rays). Ionization effects due to GLEs can extend down to the lower altitude. Here we quantitatively consider the ionization effect of a severe SEP/GLE event of 20/01/2005, which was one of the strongest GLEs ever observed (nearly 5-fold increase of the ground-level CR intensity at South Pole around 06:55-07:00 UT). We have computed the ionization of the Earth's atmosphere by SEPs at the peak of the event. We have considered the spectrum and the angular distribution of solar protons outside the magnetosphere computed by Bütikofer et al. (2006) from the neutron monitor network data. In contrast to GCR which impinge on Earth nearly isotropically, SEP have an anisotropic spatial distribution, especially during the main phase of the event, propagating mostly along the IMF line. An illustration of the method to account for the anisotropic SEP propagation is shown in Fig. 3 for two high-latitude sites on Earth, site I (57.5°N 60°W) and site II (67.5° S 140° E). The asymptotic directions, rep-

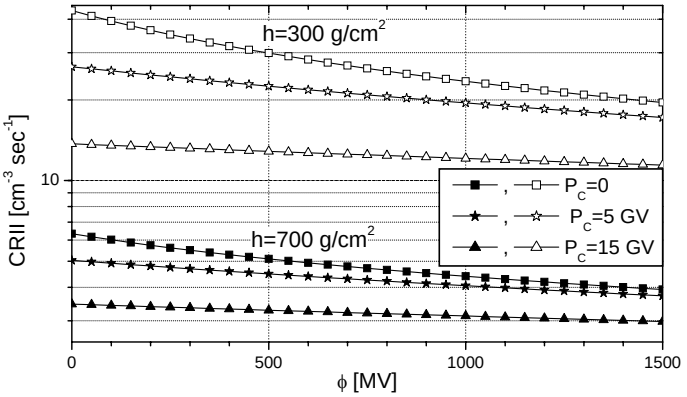

Fig. 2. CRII as a function of the modulation potential ϕ for different locations and altitudes (computations by Usoskin and Kovaltsov, 2006). Lower curves with solid symbols and upper curves with open symbols correspond to the atmospheric depths of 700 g/cm^2 (about 3 km altitude) and 300 g/cm^2 (about 9km), respectively. The results are shown for the geomagnetic pole (P_c=0), mid-latitude (P_c=5 GV, about 40° geomagnetic latitude) and equator ($P_c = 15$ GV).

resenting the particle arrival directions outside the magnetosphere, depend on the paticle's rigidity and are computed using the backward trajectory technique (Smart et al., 2000) and plotted in Fig. 3A. The geomagnetic field is described by a combination of the IGRF-2005 and Tsyganenko (1989) models. The main direction of the solar proton population outside the magnetosphere, also called the apparent source, is shown in Fig. 3A by the asterisk, together with the asymptotic directions corresponding to the pitch angles of 5°, 20°, 56° and 92°. For the peak time of this GLE the pitch angle distribution of the solar protons was very narrow with the flux at 55° pitch angle being only 10% of the flux in the main direction (IMF). Knowing the asymptotic directions, the enrgy spectrum, and the angular distribution of SEPs outside the magnetosphere, one can compute the flux of SEP at the top of the atmosphere as shown in Fig. 3B. The GCR proton spectrum for this specific time is also plotted for comparison. Because of the very narrow pitch-angle distribution of SEP in the peak phase of the event, the flux at the site II in the south hemisphere is an order of magnitude higher than at the site I in the northern hemisphere, since the former is close to the IMF direction (about 20°). Using the procedure described above we have computed the flux of SEP at the top of the atmosphere globally in a 5°x5° geographic grid. Next, the CRII over the globe was computed for the peak of the SEP event of 20/01/2005 using the Bern model (see Sect. 2.1). The resulting CRII is shown in Fig. 4 for the upper troposphere. The top panel represents the total ionization accounting for both SEP and GCR fluxes, while in the bottom panel the ionization induced only by GCR is plotted as reference. One can see that the increase in CRII due to solar cosmic rays strongly depends on the location and, for this particular event, can be as great as a factor of 100 in a very localised region around 70°S 140°E. This is a direct consequence of the high anisotropy of the solar particles at this specific time.

Thus, the ionization effect of SEP events is local and most important in the polar atmosphere. The global effect of CRII solar particles is tiny, even for the most severe events.

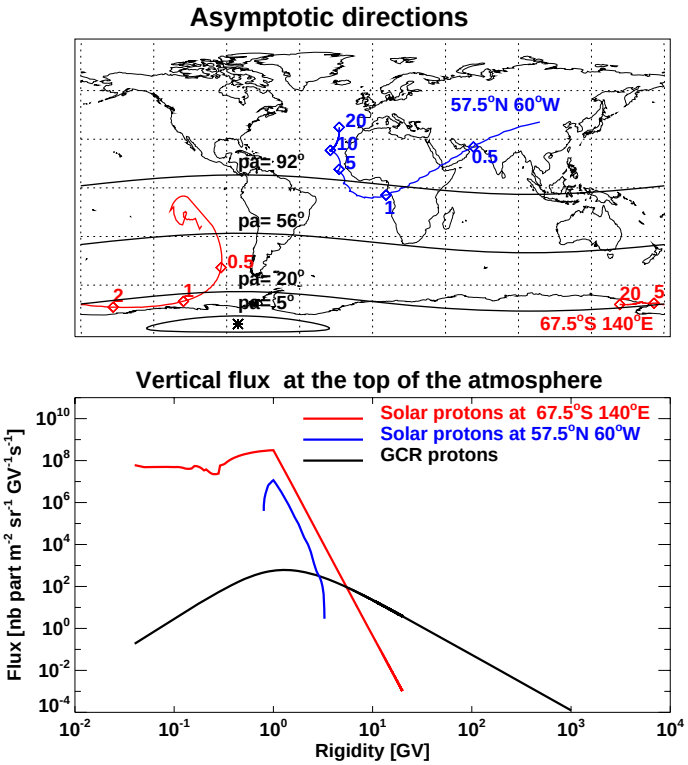

Fig. 3. Illustration of the method used for computing the solar proton flux at the top of the atmosphere from its spectrum and angular distribution outside the magnetosphere. A) Pitch angles and asymptotic directions for the two sites on Earth at 06:55 UT on 20/01/2005. The asterisk denotes the direction of the IMF. B) The corresponding flux of solar protons at the top of the atmosphere.

2.3 CR in the upper atmosphere

In contrast to the lower atmosphere, the ionization of the upper atmosphere, where the cascade is not developed, allows a relatively simple analytical solution. This is related to the fact that the atmospheric depth at the altitude of 35 km is about 6 g/cm^2 (< 1 g/cm^2 at 50 km), which is much less than the nuclear free path of protons and $\alpha-$particles (≈ 70 and 30 g/cm^2, respectively). Therefore, one can neglect nuclear interactions in the upper atmosphere (ionosphere and upper stratosphere) and consider only ionization losses of the primary CR particles. Moreover, for the altitude above 50 km, one can further neglect changes of the energy of energetic particles, thus reducing the CRII computation to an analytical *thin target* model (Velinov, 1966, 1968), where the electron production rate per g/cm^2 is computed as (cf. Eq. 1):

$$Q = \frac{1}{\Delta E} \sum_i \int_T \int_\Omega \left(\frac{dT}{dh}\right)_i J_i(T, \phi, \Omega)\, d\Omega\, dT, \tag{2}$$

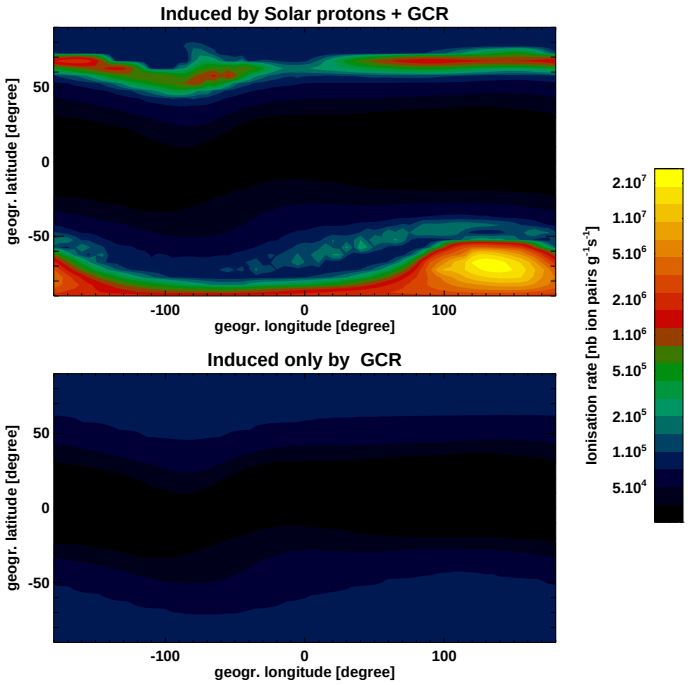

Fig. 4. Computed ionization rate of the upper troposphere (h =300 g/cm^2), at 06:55 UT on January 20, 2005: the total ionization rate (top panel) and that due to GCR only (bottom panel).

where $\Delta E = 35$ eV is the energy required for the formation of an electron-ion pair, $(dT/dh)_i$ are the ionization losses of a particle of type i. In the altitude range from 25-30 to 50 km, an *intermediate target* model needs to be used, that accounts also for the particle's deceleration due to ionization losses (e.g. Velinov and Mateev, 1990). This model was applied for calculation of atmospheric electrical conductivities in the middle atmosphere for different cases: GCR, solar CR, Forbush decreases, day and night conditions, etc. During a strong SEP event the conductivity at altitudes of 30-80 km may increase by two orders of magnitude comparing to the background of GCR. This may affect parameters of the global atmospheric electric circuit. The intermediate target ionization model was further developed to calculate also the effect of anomalous CR (Velinov and Mateev, 1992; Velinov et al., 2001) taking into account the Chapman function values for the spherical Earth environment (Velinov et al., 2004). Anomalous CR play an important role in the maintenance of the polar ionosphere and the ionosphere at the polar cusp (Velinov and Mateev, 1992; Mateev, 1997). This model has been recently upgraded using a more precise parameterization of the ionization loss function (Velinov and Mateev, 2005) and is valid for the altitude between 25-30 km and 120 km (see Fig. 5). At its lower bound this model agrees with the full-cascade models described above but systematically underestimate the ion production for the middle and low atmosphere. It can be generalized for a 3D case for the planetary environments.

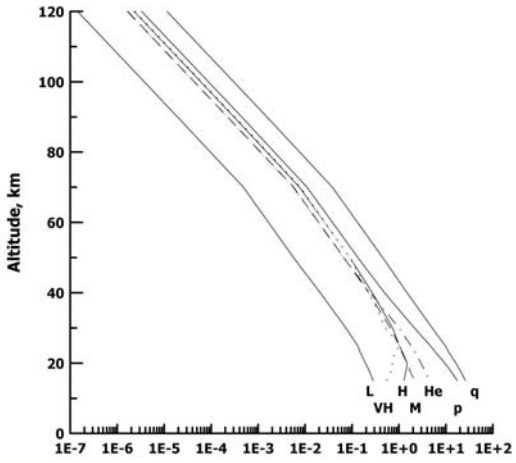

Fig. 5. Electron production rate q (cm^{-3} sec^{-1}) by cosmic rays, together with contributions from different groups of nuclei (p, He, L, M, H, VH) calculated for the solar minimum ($\phi = 400$ MV) by means of the intermediate target model (Velinov and Mateev, 2005).

We note that ionizing agents other than cosmic rays, such as solar electromagnetic radiation, precipitation of magnetospheric and quasi-trapped particles, become progressively more important at high altitudes. These processes should be also considered by realistic ionization models for the ionosphere. Below 30 km, the nucleonic-electromagnetic cascade becomes important and CRII should be computed using Monte-Carlo models discussed in Section 2.1.

3 CR and chemistry of the middle/upper atmosphere

Energetic CR affect chemistry of the middle/upper atmosphere, that can be both measured and modeled, e.g., SIC (Verronen et al., 2005), COMMA (Krivolutsky et al., 2006), TIME-GCM (Jackman et al., 2007). While GCR mostly affect the overall atmospheric environment, SEP result in ionizations, dissociations, etc. in the polar middle/upper atmosphere. SEP can produce minor atmospheric components (e.g., HOx and NOy) and trigger catalytic cycles with ozone destruction. Recent models and data show that: (i) SEPs deposit their energy in the Polar Cap regions; (ii) relevant O_3 depletions take place only after large SEP events; (iii) the day/night difference occurs in the chemical features, due to the different solar illumination, and (iv) SEPs can be related also to atmospheric dynamical changes, such as those involving temperature and wind. In the framework of the COST 724 action a number of SEP events were studied in details: 17/01/2005, 20/01/2005, 15/05/2005, 08/09/2005, 21/04/2002, and 14/07/2000. We used atmospheric data from satellite instruments: SAGE II (NASA Langley Atmospheric Sciences Data Center), POAM III (http://eosweb.larc.nasa.gov/PRODOCS/poam3/table_poam3.html), HALOE (http://haloedata.larc.nasa.gov/download/index.php) and MLS/EOS/AURA (http://mls.jpl.nasa.gov/data/). Proton fluxes were taken from the GOES satellite (http://www.ngdc.noaa.gov/stp/GOES/).

Studying the SEP events of Jan. 2005, Damiani et al. (2006) found two weak and short ($<$ 12 h) ozone depletions at the outer boundary of the Southern Polar Cap (Fig. 6- left panel). While the mesospheric ozone was greatly decreased in the Northern region (night), the ozone decrease was weak in the Southern region (day) (Damiani et al., 2007a). Furthermore, the

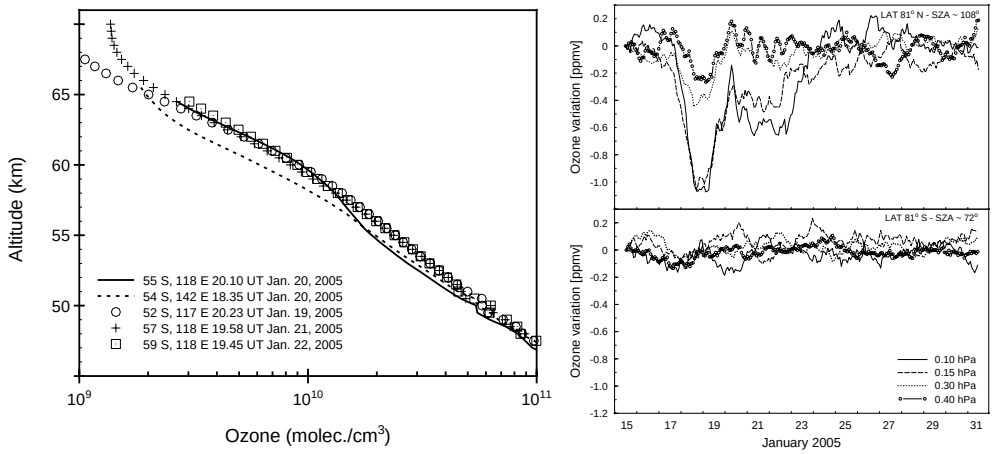

Fig. 6. Left: Atmospheric ozone profiles (SAGE II data) for similar locations during 19–22/01/2005; note the fast change during 20/01/2005 (after Damiani et al., 2006). **Right:** Ozone variability from MLS/AURA data for several atmospheric levels (after Damiani et al., 2007a).

ozone decrease in the Northern hemisphere lasted longer (several days) than in the Southern one, where only short depletions were found (Fig. 6- right panel). This is in agreement with the theoretical result based on intense photolysis processes in the summer hemisphere. Using the MLS measurements of nitric acid during January 2005, it was shown that, together with the ozone depletion, a HNO_3 increase (Damiani et al., 2007a) took place, lasting until the end of the month (Storini & Damiani, 2007). It was the first time when an increase of OH (proxy for HOx) could be highlighted. According to current models, the HOx increase during a SEP event may explain the observed mesospheric ozone depletion for the night condition. For example, the OH concentration raised by an order of magnitude in the North, whereas it remained almost constant in the South (Fig. 7). Note that the tertiary ozone peak in the winter mesosphere makes it easier to distinguish the O_3 decrease linked to the OHx component rise. The destruction of the ozone peak is clear on 18/01/2005, when the quantity of destroyed O_3 varied from $\sim 25\%$ (at ~ 55 km) to $\sim 75\%$ (at ~ 70 km) at Northern high latitudes.

Several other SEP events were similarly analyzed (Damiani et al., 2007b; Storini & Damiani, 2007). In spite of the lower SEP flux, they have also been able to produce intense variations mainly in the mesospheric chemistry. We found that SEP effects on the Earth's atmosphere are different for the night and day hemispheres at high latitudes. The response of odd hydrogen species to SEP events is very fast, almost contemporary, in both summer and winter hemispheres. However, it is difficult to separate the OH variability over the solar illumination changes since the high background concentration of hydrogen species depends on the H_2O concentration. On the other hand, reduced solar illumination facilitates highlight of atmospheric chemistry changes. We note that OH changes last longer in the winter hemisphere than in the summer one, because of the short life of OH components under solar light. This does not imply that seasons affect the possibility of odd hydrogen species to trigger catalytic cycles, but it only affects our capability to disentangle the true OH variability. In fact, the scenario of the middle/upper atmosphere response to the Sept. 2005 event reveals catalytic

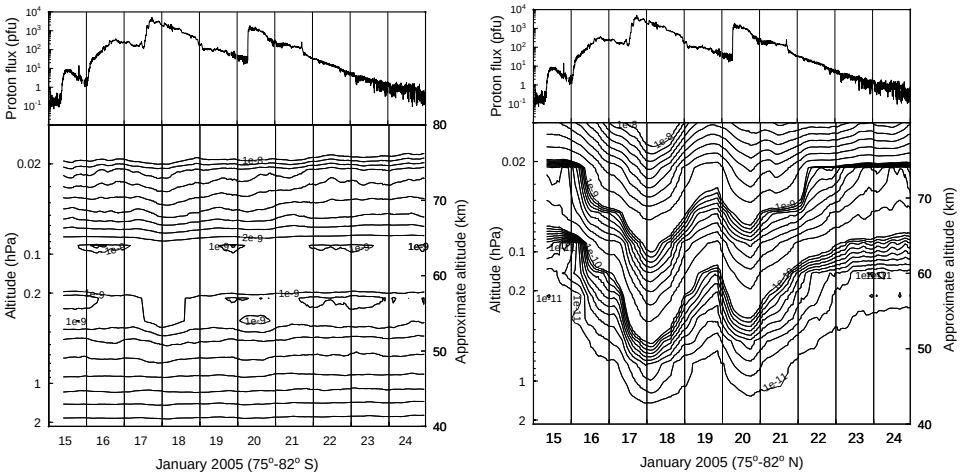

Fig. 7. Upper panels: Solar proton flux (E $>$ 10 MeV) from GOES. **Lower panels:** Contours of the OH increase (in volume mixing ratio) from MLS/EOS data for 75°-82° S (**left**) and 75°-82° N (**right**). (after Storini & Damiani, 2007).

triggering in both hemispheres, while the slightly less illuminated condition of the Southern hemisphere favors the presence of a third ozone peak in May 2005, and its subsequent destruction during/after the 15/05/2005 SEP event. The weak SEP fluence for the 16/05/2005 event led to an O_3 depletion of 10 % up to $\sim$ 60 km and reached 45 % at $\sim$ 70 km at 75°-82° S. The ozone depletion in the summer hemisphere is negligible for this event.

Although SEP result in the dominant destruction of ozone, it is possible that at certain altitudes ozone can be created as a result of chain ion reactions taking part in the stratosphere (see Tassev et al., 1999, 2003).

4 Conclusions

In this brief review we have summarized the results of the research, carried out in the framework of the COST-724 action, to study the atmospheric effect of cosmic rays. Three numerical models (Bern, Oulu and Sofia), that are capable to compute the cosmic ray induced ionization at a given location and time, are presented. The models agree with each other and with fragmentary direct measurements of the atmospheric ionization in different conditions. The models are validated for the entire atmosphere and the whole range of the solar activity level variations. The effect of sporadic solar energetic particle events is tiny on the global scale, even for a severe event, but can be very strong locally in polar regions, especially at high altitudes, leading to significant changes of the chemical properties in the upper atmosphere.

Thus, a new opportunity is presented to study cosmic ray induced effects of the atmosphere in full detail using realistic and calibrated to direct observations numerical models.

Acknowledgement. The authors are grateful to COST-724 action for support, especially for the Short Term Scientific Mission of IU and PV to Bern in 2005 that gave an opportunity to concentrate efforts on this topic. LD, RB and EOF acknowledge support by the Swiss National Foundation (grants 2000020-105435/1,200020-113704/1), and by the Swiss State Secretariat for Education and Research (grant COST-724/C05.0034). Research by PV was supported by NATO grant EAP.RIG. 981843. MS thanks the Antarctic Research Program of Italy for supporting the work. GK acknowledges support from the Academy of Finland and Finnish Academy of Sciences and Letters (Väisälä foundation).

References

Bütikofer, R., Flückiger, E.O., Desorgher, L., Moser, M.R., Analysis of the GLE on January 20, 2005: an update. in Proc. Europ. Cosmic Ray Symp., Lisbon (2007, in press)

Damiani, A., Storini, M., Laurenza, M., et al.: Southern ozone variations induced by solar particle events during 15 January - 5 February 2005. J. Atmos. Solar-Terr. Phys., **68**, 2042–2052 (2006) [errata corrige: **69**, 628-630, 2007].

Damiani, A., Storini, M., Laurenza, M., et al.: Search for the ozone variability related to SEP events during the current solar cycle. Adv. Space Res., (2007a, submitted).

Damiani, A., Storini, M., Laurenza, M., Rafanelli, C.: Solar particle effects on minor components of the Polar atmosphere. Annales Geophys., (2007b, in press)

Desorgher L., Flückiger E.O. , Gurtner M., et al.: ATMOCOSMICS: a GEANT4 code for computing the interaction of cosmic rays with the Earth's atmosphere, Internat. J. Modern Phys. A, 20, 6802-6804 (2005).

Dorman L. Cosmic Rays in the Earth's Atmosphere and Underground. Dordrecht, Kluwer Academic Publishers (2004).

Ermakov, V.I., Bazilevskaya, G.A., Pokrevsky, P.E., Stozhkov, Yu.I.: Ion balance equation in the atmosphere. J. Geophys. Res., 102(D19), 23413–23419 (1997).

Farman, J.C., Gardiner, B.G, Shanklin, J.D.: Large losses of total ozone in Antarctica reveal seasonal $ClO_x/NO/_x$ interaction. Nature, **315**, 207–210 (1985)

Jackman, C.H., Roble, R.G., Fleming, E.L.: Mesospheric dynamical changes induced by the solar proton events in October-November 2003. Geophys. Res. Lett., **34**, L04812, (2007)

Krivolutsky, A.A., Klyuchnikova, A.V., Zakharov, et al.: Dynamical response of the middle atmosphere to solar proton event of July 2000: Three-dimensional model simulations. Adv. Space Res., **37**, 1602–1613 (2006)

Lowder, W.M., P.D. Raft, nad H.L. Beck Experimental determination of cosmic-ray charged particle intensity profiles in the atmosphere, in: *Procs. National Symp. on Natural and Man-made Radiation in Space* (Eds. E.A. Warman), Las Vegas, 1971, NASA, 908-913 (1972).

Mateev, L.: An improved model of the cosmic ray ionization in the high latitude ionosphere considering the anomalous cosmic rays component, Bulg. Geophys. J., 23, 1/2, 87-95 (1997).

Neher, H.V, Cosmic rays at high latitude and altitudes covering four solar maxima, J. Geophys. Res., 76, 1637-1651 (1971).

O'Brien, K.: The theory of cosmic-ray and high-energy solar-particle transport in the atmosphere, in Procs. 7th Internat. Symp. on the Natural Radiation Environment (Eds. J.P. McLaughlin, S.E. Simopoulos, and F. Steinhusler), Elsevier, Amsterdam, pp. 29-44 (2005).

Rosen, J.M., D.J. Hofmann, and W. Gringel, Measurements of ion mobility to 30 km, J. Geophys. Res., 90(D4), 5876-5884 (1985).

Scherer, K., H. Fichtner, T. Borrmann, et al.: Interstellar-terrestrial relations: Variable cosmic environments, the dynamic heliosphere, and their imprints on terrestrial archives and climate, Space Sci. Rev., 127, 327–465 (2006).

Schröter, J., B. Heber, F. Steinhilber, M.B. Kallenrode: Energetic particles in the atmosphere: A Monte-carlo simulation. Adv. Space Res., 37, 1597-1601 (2006).

Smart, D.F., Shea, M.A., Flückiger, E.O.: Magnetospheric models and trajectory computations, Space Sci. Rev., 93, 305-333 (2000).

Storini M., Damiani, A.: Effects of the January 2005 GLE/SEP events on minor atmospheric components. Proc. 30th ICRC, Mexico, Abstract ID:1009 (2007)

Tassev Y., T. Yanev, P. Velinov, L. Mateev: Variations in the ozone profiles during the solar proton events from October 19–31, 1989. Adv. Space Res., 24, 649-655 (1999)

Tassev Y., P. Velinov, L. Mateev, and D. Tomova: A comparison between effects of solar proton events and geomagnetic storms on the ozone profiles. Adv. Space Res., 31, 2163-2168 (2003)

Tsyganenko, N.A.: A magnetospheric magnetic field model with a warped tail current sheet, Planet. Space Sci., 37, 5-20 (1989).

Usoskin, I. G., Gladysheva, O.G., Kovaltsov, G.A., Cosmic ray induced ionization in the atmosphere: spatial and temporal changes, J. Atmos. Sol. Terr. Phys., 66, 1791-1796 (2004).

Usoskin, I.G., Alanko-Huotari, K., Kovaltsov, G.A., Mursula, K.: Heliospheric modulation of cosmic rays: Monthly reconstruction for 1951-2004, J. Geophys. Res., 110, A12108 (2005).

Usoskin, I. G. and Kovaltsov, G.A.: Cosmic ray induced ionization in the atmosphere: full modeling and practical applications, J. Geophys. Res., 111, D21206 (2006).

Velinov P.: An expression for ionospheric electron production rate by cosmic rays. C. r. Acad. bulg. Sci., 19, 2, 109-112 (1966).

Velinov P.: On ionization in the ionospheric D region by galactic and solar cosmic rays, J. Atmos. Terr. Phys., 30, 1891-1905 (1968).

Velinov P., Mateev, L.: Response of the middle atmosphere on galactic cosmic ray influence, Geomag. Aeronom., 30, 593-598 (1990).

Velinov P., Mateev, L.: An improved model of the cosmic ray ionization in the high latitude ionosphere considering the anomalous cosmic ray component, C. r. Acad. bulg. Sci., 45, 2, 43-46 (1992).

Velinov, P., L.N. Mateev: Analytical approach for cosmic ray proton ionization in the lower ionosphere and middle atmosphere, C. r. Acad. bulg. Sci., 58, 5, 511-516 (2005).

Velinov P., A. Mishev: Cosmic ray induced ionization in the atmosphere estimated with CORSIKA code simulations, C. r. Acad. Bulg. Sci., 60, 5, 495-502 (2007).

Velinov P., M. Buchvarova, L. Mateev, H. Ruder.: Determination of electron production rates caused by cosmic ray particles in ionospheres of terrestrial planets, Adv. Space Res., 27, 1901-1908 (2001).

Velinov P., H. Ruder, L. Mateev, et al.: Method for calculation of ionization profiles caused by cosmic rays in giant planet ionospheres from jovian group, Adv. Space Res., 2004, 33, 232-239 (2004).

Verronen, P.T., Seppala, A., Clilverd, M.A. et al.: Diurnal variation of ozone depletion during the October-November 2003 solar proton events. J. Geophys. Res., **110**, A09S32 (2005)

The use of neutron monitor and muon telescope observations in monitoring and forecasting space weather

Lev I. Dorman[1,2]

[1] Israel Cosmic Ray & Space Weather Center and Emilio Ségre Observatory, affiliated to Tel Aviv University, Technion and Israel Space Agency, Qazrin 12900, Israel;
lid@physics.technion.ac.il

[2] Cosmic Ray Department of IZMIRAN, Russian Academy of Science, Troitsk 142092, Moscow Region, Russia

Summary. Cosmic rays (CR), as element of space weather, determine the radiation dose and radiation hazard for spacecraft (electronics, navigation system, and astronauts), aircraft (electronics, crew, and passengers), and affect high level technology on the ground for and even people's health (especially during great events). On the other hand the continuous observations of CR by neutron monitors (NM) may be used for automatically determining the onset of great solar energetic particle (SEP) events (§1). Then, on the basis of one-minute NM data, by the method of coupling functions, the time variation of the SEP energy spectrum in the space is determined (§2). For the next, much more complicated step, we need to solve the inverse problem of SEP generation and propagation. As a first approximation we consider the model of diffusive propagation. In the frame of this simple model we can determine the time of the ejection of SEPs from the solar corona, the source function and the parameters of propagation, and then forecast the expected SEP radiation (§3). To extend the obtained results to low energies we combine NM and satellite data and shortly describe how to organize alerts in the cases of expected dangerous hazard for objects in space, the magnetosphere, and the atmosphere. We show that the adopted model works well in the case of the September 29, 1989, SEP event (for both high- and low-energy particles), but the model is not universal. It can only account for prompt western-limb injections and does not generally explain events from the central part of the disk or from the eastern limb, and neither the cases related to particle acceleration by interplanetary shocks. For the present set of models, an Alert-system for dangerous SEP events to be developed by the NM stations involved in COST-724 is briefly described (§4).

Separately from the above modeling, we also consider the principles of using CR measurements to forecast at least 10–15 hours in advance the sudden commencement of great geomagnetic storms accompanied by Forbush decreases (FDs) – by using on-line hourly data of the world-wide network of NMs and muon telescopes (§5). We point out that for this kind of forecasting, the following features of the CR intensity variations connected to geomagnetic storms related to FDs may be useful: 1) CR pre-increase, 2) CR pre-decrease, 3) CR fluctuations, 4) change in the 3-D CR anisotropy.

1 The method of automatic search of the start of great SEP event

An increase of CR flux is determined by comparing the present Z-th one-minute data with the intensity averaged from 120 to 61 minutes before it. For each Z-th minute data the program

"SEP-Search" is started. This determines, for two independent channels A and B of the NM, the values

$$D_{A1Z} = \frac{1}{\sigma_1}\left[\ln I_{AZ} - \sum_{k=Z-120}^{Z-60} \frac{\ln I_{Ak}}{60}\right],\ D_{B1Z} = \frac{1}{\sigma_1}\left[\ln I_{BZ} - \sum_{k=Z-120}^{Z-60} \frac{\ln I_{Bk}}{60}\right], \quad (1)$$

where I_{Ak} and I_{Bk} are the one-minute total intensities in sections A and B and σ_1 is the standard deviation of the logarithmic intensity in a single channel. If simultaneously

$$D_{A1Z} \geq 2.5 \text{ and } D_{B1Z} \geq 2.5, \quad (2)$$

the program "SEP-Search" repeats the calculation for the next $Z + 1$-th minute and if Eq. (2) is satisfied again, the onset of a great SEP event is established and the program "SEP-Research/Spectrum" starts.

1.1 The probability of false alarms

Because the probability function $\Phi(2.5) = 0.9876$, the probability of an accidental increase with an amplitude larger than 2.5σ in one channel is $[1-\Phi(2.5)]/2 = 0.0062$ min^{-1}, i.e., one in 161.3 minutes. (Thus, in one day we expect 8.93 accidental increases in one channel.) The probability of accidental increases simultaneously in both channels is $\{[1 - \Phi(2.5)]/2\}^2 = 3.845 \cdot 10^{-5}$ min^{-1}, i.e., one in 26007 minutes or ∼18 days. The probability that the increases of more than 2.5σ is accidental in both channels in two successive minutes is equal to $\{[1 - \Phi(2.5)]/2\}^4 = 1.478 \cdot 10^{-9}$ min^{-1}, i.e., one in $6.76 \cdot 10^8$ minutes or ∼1286 years. Sending out false alarms at this rate (one in about 1300 years) is not dangerous, because the first alarm is only preliminary and it can be cancelled if in the third successive minute there is no increase in both channels larger than 2.5σ. (It is not excluded that in the third minute there is also an accidental increase, but the probability of this false alarm is negligible: one in $3.34 \cdot 10^7$ years.) Let us note that the false alarm can be sent also in the case of a solar neutron event (which is actually not dangerous for electronics in spacecrafts or for the astronauts' health), but this event usually is very short (only a few minutes) and this alarm will be automatically canceled in the successive minute after the end of a solar neutron event.

1.2 The probability of missed triggers

The probability of missed triggers depends very strongly on the amplitude of the increase. Let us suppose, for example, that we have a real increase of 7σ. (For the Italian–Israeli Emilio Segré Observatory (ESO) that corresponds to an increase of about 9.8 %.) The trigger will be missed if in either of the two channels and in either of the two successive minutes the increase of intensity is less than 2.5σ as a result of statistical fluctuations. For this scenario to occur the statistical fluctuation must be negative with an amplitude of more than 4.5σ. The probability of this negative fluctuation in one channel in one minute is equal to $[1 - \Phi(4.5)]/2 = 3.39 \cdot 10^{-6}$, and the probability of a missed trigger for two successive minutes of observation simultaneously in two channels is 4 times larger: $1.36 \cdot 10^{-6}$. This means that a missed trigger is expected only once per about 70000 SEP events with real increases of 7σ.

2 On-line determination of the SEP spectrum

Let the SEP rigidity spectrum out of the magnetosphere, $\Delta D(R,t)$, be described by the relation $\Delta D(R,t)/D_0(R) = b(t)R^{-\gamma(t)}$, where $D_0(R)$ is the spectrum of galactic CR before the SEP event. In this case, the observed CR variation, $\delta I_m(R_c,t) \equiv \Delta I_m(R_c,t)/I_{m0}(R_c)$, will be determined by using the method of coupling functions as:

$$\delta I_m(R_c,t) = b(t)F_m(R_c,\gamma(t)), \tag{3}$$

where $m =$ tot, 1, 2, 3, 4, 5, 6, 7, $\geq$8 typically gives the multiplicity of the NM data channel (but can denote also the data obtained by muon telescopes at different zenith angles, data for electron-photon component, data from balloons and satellites, etc.), and

$$F_m(R_c,\gamma) = a_m k_m (1-\exp(-a_m R_c^{-k_m}))^{-1} \int_{R_c}^{\infty} R^{-(k_m+1+\gamma)} \exp(-a_m R^{-k_m}) dR \tag{4}$$

is a known function (a_m and k_m are parameters of the Dorman function, see §3.8 in Dorman, 2004). Let us compare the data for two components, m and n. According to Eq. (3), we obtain

$$\delta I_m(R_c,t)/\delta I_n(R_c,t) = \Psi_{nm}(R_c,\gamma), \tag{5}$$

where

$$\Psi_{nm}(R_c,\gamma) = F_m(R_c,\gamma)/F_n(R_c,\gamma) \tag{6}$$

are calculated using Eq. (4). Comparison of the experimental results with the function $\Psi_{nm}(R_c,\gamma)$, according to Eq. (5), gives the value of $\gamma(t)$, and then from Eq. (3) the value of the parameter $b(t)$: $b(t) = \delta I_m(R_c,t)/F_m(R_c,\gamma(t)) = \delta I_n(R_c,t)/F_n(R_c,\gamma(t))$.

3 On-line determination of the time of ejection, diffusion coefficient and the SEP spectrum at the source

3.1 Forecasting by using NM data

We suppose that the time variation of the SEP flux and the SEP energy spectrum can be described in a first approximation by radial diffusion from a instantaneous point source described by the function $Q(R,r,t) = N_0(R)\delta(t)\delta(r)$, where r denotes the radial distance from the Sun.

Let us suppose that the diffusion coefficient $K(R,r) = K_1(R)(r/r_1)^{\beta}$, where $r_1 = 1$ AU. In this case, the density of the SEPs at r and at time t after the ejection of the SEPs into the solar wind is (Parker, 1963):

$$n(R,r,t) = \frac{N_0(R) r_1^{3\beta/(2-\beta)} [K_1(R)t]^{-3/(2-\beta)}}{(2-\beta)^{(4+\beta)/(2-\beta)} \Gamma(3/(2-\beta))} \exp\left(-\frac{r_1^{\beta} r^{2-\beta}}{(2-\beta)^2 K_1(R) t}\right), \tag{7}$$

where $N_0(r)$ is the rigidity spectrum of the total number of SEPs in the source. Let us suppose that the time of the ejection T_e, the parameters of diffusion coefficient, $K_1(R)$ and β, and

the source spectrum, $N_0(R)$, are unknown. In this case, for determining on-line these four unknown variables, we need information on the observed SEP spectrum in at least four moments of time, T_1, T_2, T_3 and T_4. (All times T are in UT, so in Eq. (7), $t_i = T_i - T_e$, where i = 1, 2, 3, 4.) The details of the solution of the inverse problem for SEP generation and propagation are described in Section 2.42.3 of the monograph by Dorman (2006). By the deduced values of T_e, $K_1(R)$, β, and $N_0(R)$, on the basis of Eq. (7), we can forecast the evolution of the SEP flux and spectrum for many hours ahead, and determine the expected radiation hazard. Really, after using the first four minutes of data, we then use five, six, seven and so on one-minute data, and the optimum solution is obtained by the least-squares fit of the model to the experimental data. Thus, with time the solution becomes more and more accurate. This can be seen in Fig. 1, where we show results of the analysis described above and the forecasting for the historical event on 29 September 1989 by using only Gran Sasso NM data (the total intensity and different multiplicities). From Fig. 1 it can be seen that using only the first few minutes of NM data (t = 10 min, i.e., 5 minutes after the start of the event) is not enough: the obtained curve forecasts too low an intensity. Only for t = 20 min (15 minutes after the event started) and later, we obtain a stable forecast in good agreement with the observed CR intensity.

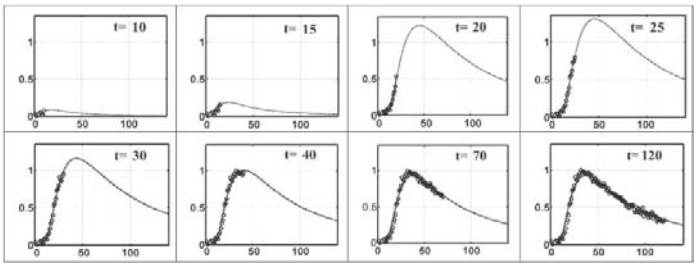

Fig. 1. Calculation at each new minute parameters T_e, $K_1(R)$, β, and $N_0(R)$ and forecasting of total neutron intensity (time t is in minutes after 11.40 UT of September 29, 1989; curves – forecasting, circles – observed total neutron intensity).

3.2 Forecasting by using both NM and satellite data

All the results described above, based on on-line NM data, reflect the situation in SEP behavior in the high energy (more than a few GeV) region. For extrapolation of these results to the low-energy interval (bu still dangerous for space-probes and satellites), we use on-line satellite data available through the Internet. We suppose that the time of ejection in both energy ranges is the same and that Eq. (7) describes the SEP time variation. The source function relative to time and space is a δ-function, and relative to the energy it is a power-law with an energy-dependent index:

$$N_0(R,t) = \delta(t - t_e)\, R^{-(\gamma_0 + \ln(E_k/E_{k0}))}. \tag{8}$$

In Fig. 2 we show results based on the NM and satellite data of forecasting expected SEP fluxes also at low energies and a comparison with the observed satellite data.

From Fig. 2 it can be seen that, by using on-line data from NMs in the high-energy range and from satellites in the low-energy range during the first 30–40 minutes after the start of the SEP event, it is possible to predict the expected SEP integral fluxes for different energies

up to a few days ahead. We point out, however, that the considered event of September 29, 1989, is particularly suitable for the analysis because it occurred at the west limb and had, therefore, only a limited contribution of particles accelerated at the interplanetary shock wave related to the event. For this reason, a radial diffusion model with a coronal source provides a reasonable scenario for the event. For other events occuring on the disk or at the east limb, we do not expect such a good performance of the forecast.

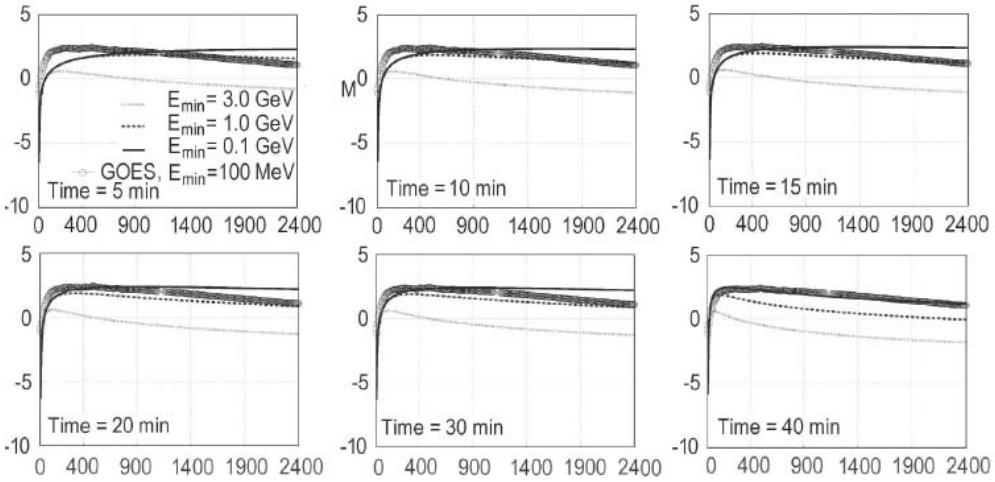

Fig. 2. Predicted SEP integral fluxes for $E_k \geq E_{\min}$ =3.0, 1.0, and 0.1 GeV. The forecasted integral flux for $E_{\min}$ =0.1 GeV we compare with observed fluxes for $E_k \geq$ 100 MeV on GOES satellite. The ordinate is $\log_{10}$ of SEP integral flux (in cm^{-2} s^{-1} sr^{-1}), and the Time (as well as abscissa) is in minutes from 11:40 UT of September 29, 1989.

4 Alerts to be issued in case dangerous SEP fluxes are expected

Using the above-described set of analysis methods, an alert system to warn about the dangerous SEP events could be deviced. If the predicted fluxes are expected to be dangerous, a preliminary "SEP-Alert-1/Space", "SEP-Alert-1/Magnetosphere", "SEP-Alert-1/Atmosphere" can be issued in the few minutes after the event onset. As more data become available, better predictions of the expected fluxes are made and more definitive alerts, Alert-2, Alert-3 and so on, can be automatically issued. Alerts give information on the expected time and the level of danger for different objects in space, in the magnetosphere, in the atmosphere on different altitudes and at different cut-off rigidities.

5 CR phenomena used for forecasting of great space storms

For a practical realization of forecasting hazardous space storms by means of CR, it will be necessary to get data from most CR stations in real-time (Dorman, 1993; Dorman et al., 1993). The main features observed in CR intensity variations before the beginning of major geomagnetic storms (caused by coronal mass ejections and interplanetary shock waves) can be used for forecasting, are the following (Dorman et al., 1995a,b, 1997, 1999; Munakata et al., 2000; considered in detail by Dorman, 2004):

1. CR pre-increase. The discovery of this effect in 1959 (Blokh et al., 1959) stimulated the development of the mechanism of galactic CR drift acceleration by interplanetary shock waves (Dorman, 1959; Dorman and Freidman, 1959) and further analyses (Dorman et al., 1995a,b; Belov et al., 1995a,b) show that this effect is related to particle interaction and acceleration by interplanetary shock waves;

2. CR pre-decrease was discovered by McCracken and Parsons (1958) and Fenton et al. (1959). (See also review by Dorman, 1963a,b.) This effect was analyzed recently both theoretically (Dorman et al., 1995a) and experimentally on the basis of the network of CR stations (Belov et al. 1995a,b). The pre-decrease effect can be due to a magnetic connection of the Earth with regions (moving from the Sun) with reduced CR density; this lower density can be observed at the Earth along the actual direction of interplanetary magnetic field (IMF) lines (Nagashima et al. 1990).

3. CR fluctuations. Many authors found some peculiarities in the behavior of CR fluctuations before FD: changes in the frequency spectrum; appearances of peaks in the spectrum at some frequencies; variations in some special parameter introduced for characterizing the variability of fluctuations. Though the obtained results are often contradictory (Dorman et al., 1995b), sometimes CR fluctuations appear as a reliable phenomenon for FD prediction, as expected from additional Alfvénic turbulence produced by the kinetic streaming instability of low-energy particles accelerated by shock waves (Berezhko et al., 1987);

4. Change in 3-D CR anisotropy. The CR longitudinal dependence changes abruptly in directions close to the usual directions of the IMF and depends on the character and source of the disturbance (Belov et al., 1995b, Dorman et al., 1995b). These effects, appearing long before FDs (up to 1 day), may be considered as predictors of FDs. Estimates of the CR anisotropy vector may be obtained by the global survey method described in short detail in Dorman (1974), and more recently in Chapter 3 of Dorman (2004).

In Fig. 3 shows an example result obtained for the geomagnetic storm of 9 September 1992, and represents asymptotic longitude vs. universal time CR intensity distribution. From Fig. 3 it can be seen that the pre-increase, as well as the pre-decrease, occurs 15–20 hours before the sudden commencement of the geomagnetic storm. (Many more examples were considered in Dorman et al., 2003.)

Conclusions

1. By using on-line one-min data from ground NM in the high energy range and from satellites in the low energy range during the first 30-40 minutes after the start of an SEP event,

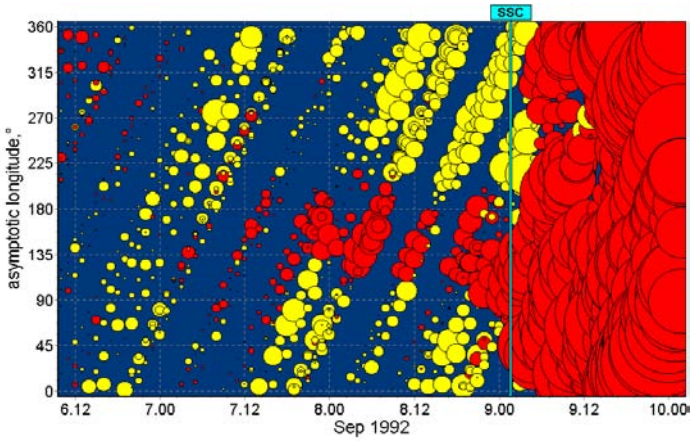

Fig. 3. Galactic CR intensity pre-increase (yellow circles) and pre-decrease and FD (red circles) before and after the Sudden Storm Commencement (SSC) of great magnetic storm at 9-th September 1992. The bigger diameter of circle means bigger amplitude of CR intensity variation.

it is possible to predict the expected SEP fluxes for different energies up to a few days ahead.

2. A strong space storm accompanied with a FD in CR intensity has clear pre-cursor effects, which can be used by the NM network for forecasting about 10–15 hours before the SSC. As was shown by Munakata et al. (2000), the CR pre-increase and pre-decrease effects can be observed very clearly also by the world-wide multi-directional muon telescope network. They investigated 14 major geomagnetic storms (characterized by $K_p \geq 8-$) and 25 large storms (characterized by $K_p \geq 7-$) observed in 1992–1998. It was shown that 89% of the major geomagnetic storms have clear precursor effects, which can be used for forecasting (the probability of exact forecasting increases with increasing storm strength).

It is foreseen that in the near future a continuous Alert-service can be organized for monitoring of major SEP events and large magnetic storms and for forecasting the dangerous situations on the basis of several CR stations involved in COST-724, including stations managed by I. Usoskin (Finland), E. Fluckiger (Switzerland), K. Kudela (Slovakia), M. Storini and M. Parisi (Italy), A. Chilingarian (Armenia), H. Mavromichalaki (Greece), and L. Dorman (Israel). In the next step, it will be very important to use also the available on-line data of CR stations managed by V. Vashenuk, V. Yanke, and E. Berezhko in Russia, and J. Bieber in the USA, Canada, Antarctic, as well as other stations from the worldwide network of CR stations.

Acknowledgements

Our great thanks to Prof. Yuval Ne'eman, Dr. Abraham Sternlieb, Prof. Izhak Ben Israel, and Dr. Zvi Kaplan for constant interest and support of the work of Israel Cosmic Ray & Space Weather Center and Emilio Ségre' Observatory, and A.V. Belov, A. Chlingarian, E.A. Eroshenko, E. Fluckiger, N. Iucci, K. Kudela, J. Lilensten, K.G. McCracken, M. Murat, M. Parisi, N. Ptitsina, L.A. Pustil'nik, M.A. Shea, D.F. Smart, M. Storini, M. Tyasto, I. Usoskin,

R. Vainio, P. Velinov, G. Villoresi, V.G. Yanke, and I.G. Zukerman for collaboration and interesting discussions. The work of neutron monitor in Emilio Ségre Observatory on Mt. Hermon is supported by Tel Aviv University, UNI Roma-Tre, and IFSI-CNR Collaboration.

References

Belov A.V., L.I. Dorman, E.A. Eroshenko, N. Iucci, G. Villoresi, and V.G. Yanke "Search for predictors of Forbush-decreases", *Proc. 24-th ICRC,* Rome, **4**, 888-891, 1995a.

Belov A.V., L.I. Dorman, E.A. Eroshenko, N. Iucci, G. Villoresi, and V.G. Yanke "Anisotropy of cosmic rays and Forbush-decreases in 1991", *Proc. 24-th ICRC*, Rome, **4**, 912-915, 1995b.

Berezhko E. B., V.I. Kozlov, A.I. Kuzmin, and N.N. Tugolukov "Cosmic ray intensity micropulsations assotiated with disturbances of electromagnetic conditions in the Heliosphere", *Proc. 20-th ICRC*, Moscow, **4**, 99-102, 1987.

Blokh Ya.L., E.S. Glokova, L.I. Dorman, and O.I. Inozemtseva "Electromagnetic conditions in interplanetary space in the period from August 29 to September 10, 1957 determined by cosmic ray variation data", *Proc. 6-th ICRC*, Moscow, **4**, 172-177, 1959.

Dorman L.I. "On the energetic spectrum and lengthy of cosmic ray intensity increase on the Earth caused by shock wave and albedo from magnetized front of corpuscular stream", *Proc. 6-th ICRC*, Moscow, **4**, 132-139, 1959.

Dorman L.I., *Cosmic Ray Variations and Space Research,* Nauka, Moscow, 1963a.

Dorman L.I., G*eophysical and Astrophysical Aspects of Cosmic Rays,* North-Holland Publ. Co., Amsterdam (In series "Progress in Physics of Cosmic Ray and Elementary Particles", ed. by J.G.Wilson and S.A.Wouthuysen, Vol. 7), 1963b.

Dorman L.I., *Cosmic Rays: Variations and Space Exploration.* North-Holland, Amsterdam, 1974.

Dorman L.I. "On the Cosmic Ray World Service", *Izvestia Academy of Science of USSR*, Ser. Phys., **57**, No. 7, 149-152, 1993.

Dorman L.I., *Cosmic Rays in the Earth's Atmosphere and Underground,* Kluwer Acad. Publishers, Dordrecht/Boston/London, 2004.

Dorman L.I., *Cosmic Ray Interactions, Propagation, and Acceleration in Space Plasmas*, Springer, Netherlands, 2006.

Dorman L.I. and G.I. Freidman "On the possibility of charged particle acceleration by shock waves in the magnetized plasma", *Proc. of All-Union Conf. on Magneto-Hydrodynamics and Plasma Physics*, Latvia SSR Academy of Sciences Press, Riga, 77-81, 1959.

Dorman L.I, N. Iucci, and G. Villoresi "The use of cosmic rays for continues monitoring and prediction of some dangerous phenomena for the Earth's civilization", *Astrophysics and Space Science*, **208**, 55-68, 1993.

Dorman L.I., N. Iucci, and G. Villoresi "The nature of cosmic ray Forbush-decrease and precursory effects", *Proc. 24- ICRC*, Rome, **4**, 892-895, 1995a.

Dorman L.I., G. Villoresi, A.V. Belov, E.A. Eroshenko, N. Iucci, V.G. Yanke, K.F. Yudakhin, B. Bavassano, N.G. Ptitsyna, and M.I. Tyasto "Cosmic-ray forecasting features for big Forbush-decreases", *Nuclear Physics B*,. **49A**, 136-144, 1995b.

Dorman L.I., N. Iucci, and G. Villoresi "Auto-model solution for non-stationary problem described the cosmic ray pre-increase effect and Forbush-decrease", *Proc. of 25-th ICRC,* Durban (South Africa), **1**, 413-416, 1997.

Dorman L.I., N. Iucci, N.G. Ptitsyna, and G. Villoresi "Cosmic ray Forbush-decrease as indicators of space dangerous phenomenon and possible use of cosmic ray data for their prediction", *Proc. 26-th ICRC*, Salt Lake City, **6**, 476-479, 1999.

Dorman L.I., A.V. Belov, E.A. Eroshenko, L.A. Pustil'nik, A. Sternlieb, V.G. Yanke, and I.G. Zukerman "Possible cosmic ray using for forecasting of major geomagnetic storms, accompanied by Forbush-effects", *Proc. 28-th ICRC*, Tsukuba (Japan), **6**, 3553-3556, 2003.

Fenton A.G., K.G. McCracken, D.C. Rose, and B.G. Wilson "The onset times of Forbush-type cosmic ray intensity decreases", *Canad. J. Phys*., **37**, 970, 1959.

McCracken K.G. and N.R. Parsons "Unusual Cosmic-Ray Intensity Fluctuations Observed at Southern Stations during October 21-24, 1957", *Phys. Rev.*, **112**, No. 5, 1798-1801, 1958.

Munakata K., J.W. Bieber, S.-I. Yasue, C. Kato, M. Koyama, S. Akahane, K. Fujimoto, Z. Fujii, J.E. Humble, and M.L. Duldig "Precursors of geomagnetic storms observed by the muon detector network*", J. Geophys. Res*., **105**, No. A12, 27457-27468, 2000.

Nagashima K., S. Sakakibara, K. Fujimoto, R. Tatsuoka, and I. Morishita "Localized pits and peaks in Forbush decrease, associated with stratified structure of disturbed and undisturbed magnetic fields", *Nuovo Cimento C,* Serie 1, **13C**, 551-587, 1990.

Parker E.N., *Interplanetary Dynamical Processes,* New York, Interscience Publ., 1963.

MuSTAnG — Muon Spaceweather Telescope for Anisotropies at Greifswald

R. Hippler[1], A. Mengel[1], F. Jansen[2], G. Bartling[2], W. Göhler[3], S. Brunner[3], and K. Kudela[4]

[1] Institute for Physics, University of Greifswald, Felix-Hausdorff-Str. 6, 17487 Greifswald, Germany, hippler@physik.uni-greifswald.de
[2] 1A Greifswald, Postfach, 17461 Greifswald, Germany
[3] HTS GmbH, Am Glaswerk 6, 01640 Coswig, Germany
[4] Institute of Experimental Physics, Slovak Academy of Science, Kosice, Slovakia

Summary. First results of the Muon Spaceweather Telescope for Anisotropies at Greifswald (MuSTAnG) that is dedicated to spaceweather forecasting are reported.

1 Introduction

The near Earth space is normally surrounded by a nearly isotropic intensity of primary cosmic rays from the Galaxy. Apart from particles associated with solar flares, the cosmic radiation comes from outside the solar system and it is mainly composed of protons and helium ions, other heavy nuclei, and electrons. The incoming charged particles interact with and are slightly modulated by the solar wind. A further modulation of Sun-ward directed anisotropy of cosmic ray intensity occurs in the case of a plasma cloud moving between Sun and Earth. These plasma clouds are caused by coronal mass ejections (CMEs) originating at the Sun and producing a shock wave on the Earth-ward directed side of the cloud. It has been noted that those interplanetary CMEs accompanied by a strong interplanetary shock often form a depleted region of primary galactic cosmic rays behind the shock front during its propagation between the Sun and Earth. Since primary cosmic ray particles travel close to the speed of light and thus much faster than the interplanetary shock front (velocities in the order of up to about 2000 km/s), it carries the information about the CME and the shock region to Earth far ahead of the shock. The CME/shock affected primary cosmic ray particles thus arrive at Earth much earlier than the Earth approaching CME and thus may be used to forecast the approaching space weather hazard.

2 Muon telescope set-up

The Muon Spaceweather Telescope for Anisotropies at Greifswald (MuSTAnG) is a multi-directional muon telescope dedicated to spaceweather forecasting. The phase 1 telescope consists of a set of suitably arranged and coupled muon detector units in two (upper and lower)

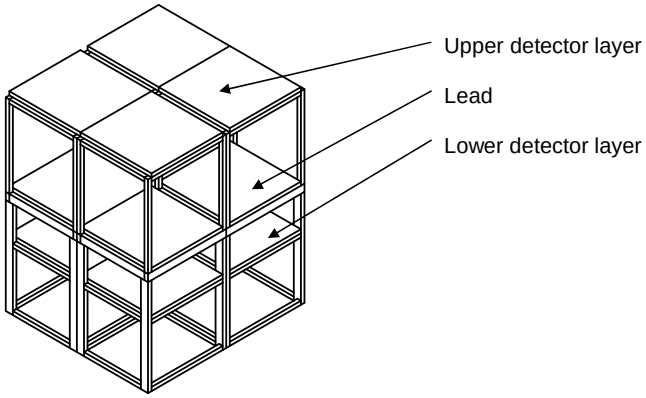

Fig. 1. Muon telescope construction (schematic). Each of the displayed 2×4 detectors boxes is approximately 1.05 m $\times$ 1.05 m tall (see text).

layers (Fig. 1). Directional information is derived from the passage of muons through two, one upper and one lower, detectors. In phase 1, MuSTAnG will be composed of 4×4 detectors of 0.25 m^2 area in each layer, i.e., a total of $2 \times 16 = 32$ detectors. Thus the full size of the detector area as shown in Fig. 1 is 2 m $\times$ 2 m = 4 m^2. An upgrade of MuSTAnG to a larger telescope is foreseen in phase 2.

The muon detectors are arranged in detector units containing 4 detectors each. Each detector unit, hence, consists of four scintillator plates of 5 cm thickness and 0.25 m^2 size. MuSTAnG is presently set-up with a distance of 0.95 m between the upper and lower de-

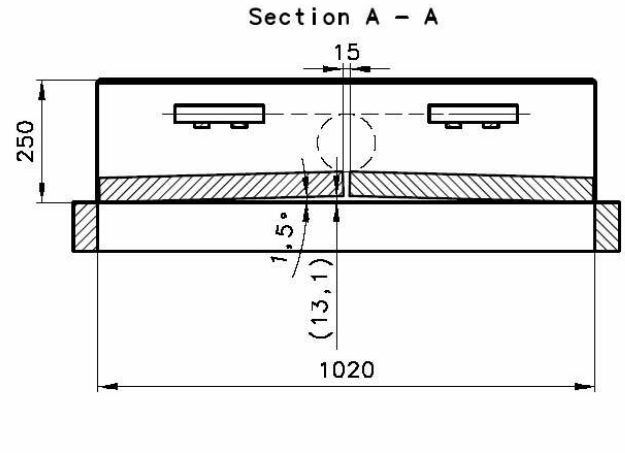

Fig. 2. Cross sectional view of scintillator box showing positions of scintillator plates, wavelength-shifting fibres, and photomultiplier modules (schematic).

Table 1. Mean zenith and azimuthal angles θ and ϕ, respectively, for the different upper layer/lower layer detector combinations. Distance between upper and lower layer 0.95 m, detector size 0.25 m^2.

$\pm\Delta$m	$\pm\Delta$n	0	1	2	3
0	θ	0.0	30.0	49.1	60.0
	ϕ	0.0	0.0	0.0	0.0
1	θ	30.0	39.3	52.3	61.3
	ϕ	90.0	45.0	26.6	18.4
2	θ	49.1	52.3	58.5	64.4
	ϕ	90.0	63.4	45.0	33.7
3	θ	60.0	61.3	64.4	67.8
	ϕ	90.0	71.6	56.3	45.0

tector planes; the corresponding zenith and azimuthal angles are displayed in table 1. The scintillator plates are coupled via 1 mm diameter wavelength-shifting (WLS) optical fibres to photomultiplier (PMT) modules (Fig. 2). Each scintillator plate is read-out by 17 WLS fibres that are spaced about 2.5 cm away from each other in keyhole-shaped grooves right beneath the top surface. In order to maximize the light output each scintilliator plate is painted with white reflective paint. The PMT modules are equipped with a bi-alkali photocathode of 25 mm active diameter having a quantum efficiency of 10–12 % at 500 nm. The PMT modules possess an integrated preamplifier and a high voltage supply. The passage of a single muon produces about 10,000 blue photons per MeV energy loss inside a scintillator plate, at an en-

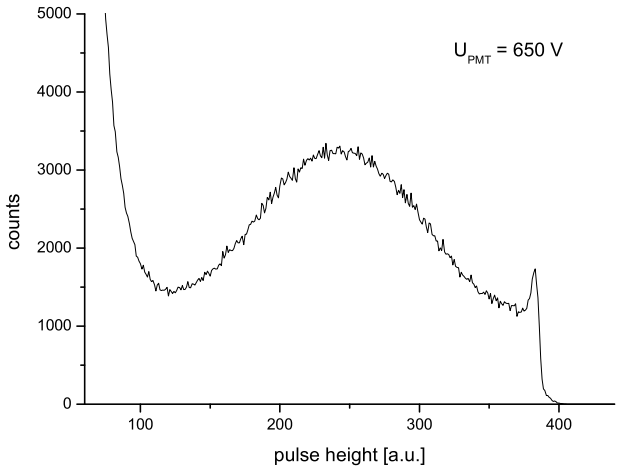

Fig. 3. Pulse height distribution of muon detector pulses.

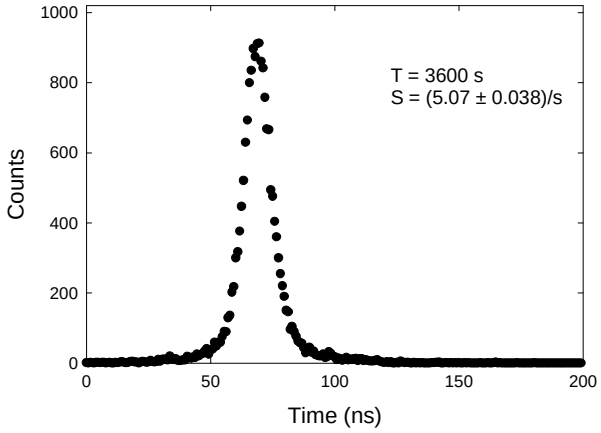

Fig. 4. Time correlation between one upper and one lower muon detector.

ergy loss of 1.8 MeV/cm (Achenbach et al., 2005). A fraction of typically 15 % of produced photons is absorbed by wavelength-shifting fibres and re-emitted as green photons. About 3 % of the re-emitted green photons are captured within the acceptance cone of the fibre and transmitted by internal reflections to the photomultiplier tube. The quantum efficiency of a bi-alkali photocathode is typically 10 % for green photons. The total yield of such a system is 7–8 photoelectrons/cm, and for a 5 cm thick plastic scintillator an average signal of 35–40 photoelectrons per incident muon may be expected.

Fig. 3 displays the pulse height distribution at the output of the photomultiplier tube. The distribution is composed of two contributions due to single photoelectron events (including dark current pulses) at small output amplitudes and a broad distribution at large output amplitudes due to muons.

Output pulses from the PMT tube are further amplified, discriminated and, after suitable pulse-shaping, fed into the coincidence electronics consisting of a field-programmable gate array (FPGA) logic (Yasue et al., 2003). The FPGA operates at 10 MHz and provides a time resolution of 100 ns.

The time correlation arising from the passage of a single muon through two (one upper and one lower) detector unit (0.25 m^2 each, typical count rate 40–50/s) has been separately investigated with a standard coincidence set-up. The test set-up consists of a commercial time-to-amplitude converter (TAC) converting the time difference between two (start and stop) signals into an output pulse with an output voltage that is proportional to the elapsed time span, and a PC-based pulse-height-analyzer card employing a built-in analogue-digital-converter (typical dead time 80 μs) to record the TAC output signal. Start and stop signals are derived from upper and the lower detectors, respectively. In order to facilitate operation of the TAC, a conveniently chosen cable delay of 13 m length corresponding to a time delay of about 65 ns was inserted into the lower (stop) detector signal line.

A time spectrum displaying a pronounced time peak with a full width at half maximum of about 12 ns containing about 18,200 correlated (true) events (recording time 1 hour) is obtained (Fig. 4). The background of uncorrelated (random) coincidences as estimated from

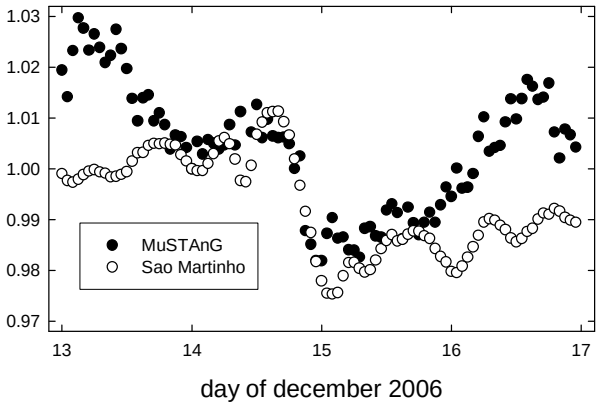

Fig. 5. Normalized muon count rate during 13–17 December 2006. MuSTAnG results (•) are compared to data of another muon space weather telescope at Sao Martinho (○).

the number of events in the time regime 150–200 ns is only about 36. The statistical accuracy calculated from these numbers is ~ 0.7 %. Multiple events, e.g., detector responses in either upper or lower detector occurring within the electronics dead time are not recorded.

3 Results

MuSTAnG test phase began end of November 2006. At the time, only $2 \times 8 = 16$ detectors totaling 2 m^2 in each of the two layers were mounted. GOES-11 satellite on 13 December 2006 recorded at 2:20 hours UT an increase of solar x-ray intensity by almost 4 orders of magnitude, followed by a ground level enhancement (GLE) that was recorded by several neutron monitors at 02:50 hours UT (Bartol, 2006).

These recordings, hence, provided the earliest alerts for the upcoming space weather event caused by a coronal mass ejection (CME). Fig. 5 shows the muon count rate variation of MuSTAnG during 13-17 December 2006. A clear drop of the muon intensity on 14 December 2006 is noted, indicating the arrival of interplanetary shocks and the associated interplanetary CME at Earth. The drop began around 17:00 hours UT and reached the 1 % level at 20:00 hours UT. It is confirmed by similar observations of other muon telescopes around the world, e.g., at Sao Martinho (Brazil), Nagoya (Japan), Hobart (Australia), and Kuwait (Bartol, 2006), and coincides with a pronounced enhancement of the estimated (3-hourly) geomagnetic K_p index reaching values of 7 during 15–18 hours and of 8 during 21–24 hours (GOES-11, 2006).

MuSTAnG construction in the new physics building (54° 5.51' N, 13° 24.24' E, vertical cut-off rigidity 2.35 GV) was completed end of April 2007. MuSTAnG is presently in its test phase with full operation foreseen during the second half of 2007.

4 Conclusions

The Muon Spaceweather Telescope for Anisotropies at Greifswald (MuSTAnG) began its test phase end of November 2006. The first space weather event was recorded during 14 December 2006. The measurements demonstrate the forecast potential of a network of muon and neutron telescopes as was recently emphasized by (Kuwabara et al., 2006).

Acknowledgements

The authors thank their colleagues for continuing support and discussions. This work was financially supported by the European Space Agency (ESA) and by Deutsches Zentrum für Luft- und Raumfahrt (DLR) through ESTEC contract 18835/04/NL/MV, and by the Slovak Research and Development Agency under contract No. APVV-51-053805.

References

Achenbach C P, Cobb J H, Wahl D, Nucl. Instr. Meth. Phys. Res. A 539, 112 (2005)

Bartol Research Institute, University of Delaware, `http://neutronm.bartol.udel.edu/spaceweather/` (2006)

GOES-11 Integral Proton Flux, GOES-11 Solar X-ray Flux, and Daily Geomagnetic Data: Estimated Planetary K-indices, U.S. Dept. of Commerce, NOAA, Space Environment Center, `http://www.sec.noaa.gov/Data/index.html` (2006)

Kuwabara T, Bieber J W, Clem J, Evenson P, Pyle R, Munakata K, Yasue S, Kato C, Akahane S, Koyama M, Fujii Z, Duldig M L, Humble J E, Silva M R, Trivedi N B, Gonzalez W D, and Schuch N J, Space Weather 4, S08001 (2006)

Munakata K, private communication (2006)

Yasue S, Munakata K, Kato C, Kuwabara T, Akahane S, Koyama M, Fujii Z, Evenson P, and Bieber J W, Proc. 28th Internat. Cosmic Ray Conf. (Tsukuba), Vol. 6, 3461-3464 (2003)

Using neutron monitor network data to improve the detection of space weather events

T. Dudok de Wit[1] and A. A. Chilingarian[2]

[1] LPCE, CNRS and University of Orléans, 3A av. de la Recherche Scientifique, 45071 Orléans cedex 2, France, ddwit@cnrs-orleans.fr

[2] Yerevan Physics Institute, Cosmic Ray Division, 2 Alikhanyan Brothers St., Yerevan 375036, Armenia, chili@aragats.am

Summary. We present two multivariate statistical methods for improving the real-time detection of space weather events from neutron monitor network data. Both exploit the similarity in the evolution of the count rates, as recorded by different monitors. The same methods can also be used as a simple and yet robust tool for filling data gaps.

Neutron and muon monitor networks can be used as single multidirectional spectrograph, thereby improving the detection of Ground Level Enhancements (GLEs) and of signatures from approaching interplanetary disturbances (Usoskin et al., 1997; Mavromichalaki et al., 2004). The real-time analysis of such network data, however, is often hampered by a number of practical difficulties such as data gaps and noise. Here we show how multivariate statistical analysis methods known as blind source separation methods can help rapidly characterize network data while alleviating some of these problems.

The blind source separation approach

Let us illustrate our approach using one year of hourly pressure-corrected neutron monitor data, downloaded from the website of the Solar-Terrestrial Division at Izmiran (ftp://cr0.izmiran.rssi.ru/Cosray!/). The neutron count rate measured at a location x and time t is $c(x,t)$. After eliminating all stations that exhibit large data gaps (more than 30% of the time) or experience stability problems, we are left with 43 stations. Small data gaps and spurious values are eliminated using the technique that will be described below.

Our working hypothesis is that all count rates can be expressed as a linear combination of a few common regimes. This idea is supported by the remarkable similarity between count rate evolutions as observed at different stations. For that reason, we express the count rate as a linear combination of separable functions of space and time, hereafter called "modes": $c(x,t) = \sum_{i=1}^{N} A_i f_i(t) g_i(x)$ with the orthonormality constraint $\langle f_i(t) f_j(t) \rangle = \langle g_i(x) g_j(x) \rangle = \delta_{ij}$, where δ_{ij} is the Kronecker symbol and $\langle . \rangle$ meaning ensemble averaging. This empirical decomposition is unique and is provided directly by the Singular Value Decomposition (SVD) (Chatfield & Collins, 1995). The weights are conventionally sorted in

decreasing order $A_1 \geq A_2 \cdots \geq A_N \geq 0$. The number of modes N equals the number of stations. Heavily weighted modes describe features that are observed coherently by many stations and so they are of prime interest. Detector and statistical noise on the contrary tends to be deferred to the last modes, because it is incoherent in time and in space. Since the method is data-adaptive, the same temporal modes are recovered regardless of the number of monitors, provided that these capture different aspects of dynamics.

A recent generalisation of the SVD, called Independent Component Analysis (ICA), regards the decomposition of multivariate data into a linear combination of modes that are not orthonormal, but independent (Hyvärinen & Oja, 2000). ICA is today often preferred to the SVD when it comes to handling blind source separation problems, in which a small number of "source" terms must be recovered from array data. Indeed, statistical independence generally is a more realistic assumption for disentangling different physical processes than decorrelation. The number of observables must of course exceed the number or modes.

Application to neutron monitor data

The fraction of the variance that is described by the i-th mode of the SVD is given by $V_i = A_i^2 / \sum_{j=1}^{N} A_j^2$. These values are plotted in Fig. 1, showing a characteristic distribution with a steep falloff followed by a flat tail. The largest modes capture salient features of the observed variability; three of them describe over 98.2% of the variance of the data. Modes from the tail in the contrary describe incoherent fluctuations that occur locally in time or at one particular station. The modes that are most likely to capture interesting physical features thus are the largest ones (Dudok de Wit, 1995). The number of such modes here is about 3 to 5.

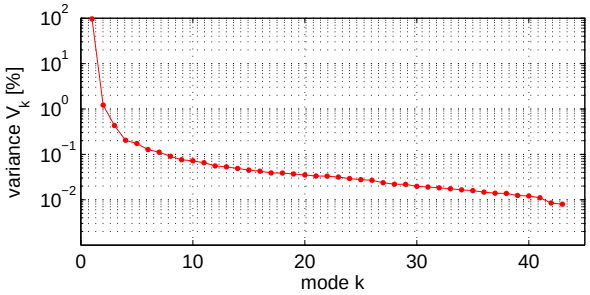

Fig. 1. Fraction of the variance (in %) that is explained by each of the 43 modes obtained by SVD.

Preprocessing is an important issue. Since we are interested in fluctuations only, for each station we subtract the time average and normalise with respect to the standard deviation.

The spatial structure of the first 4 modes obtained by ICA is shown in Fig. 2. Mode 1 is a mere weighted average of stations (with weights ranging from 0.94 to 1) whereas mode 2 extracts the difference between low and high rigidity stations, with no longitudinal dependence. Mode 1 can therefore be interpreted as a large-scale flux (Belov, 2000) whereas mode 2 expresses a rigidity dependence. Modes 3 and 4 on the contrary exhibit a strong longitudinal dependence; they are also in quadrature, which means that they describe longitudinally

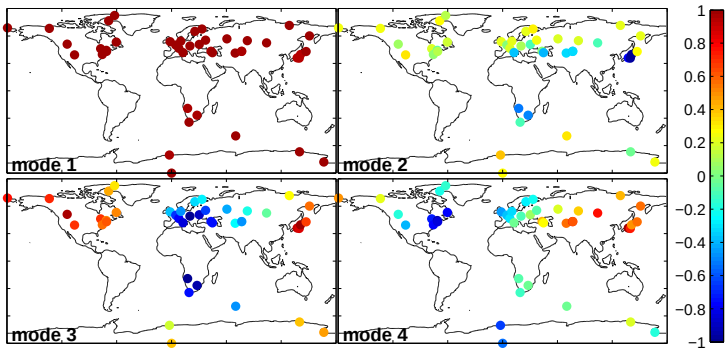

Fig. 2. Spatial structure of ICA modes 1 to 4. Each dot represents a monitor; the colour expresses the value of the k'th spatial mode $g_k(x)$ at that location, normalised to the maximum value of $|g_k(x)|$.

moving patterns (Aubry & Lima, 1995). Higher order modes in comparison have much less spatial coherence and are more difficult to interpret. The modes obtained by SVD are quite similar but their separating power is not as good.

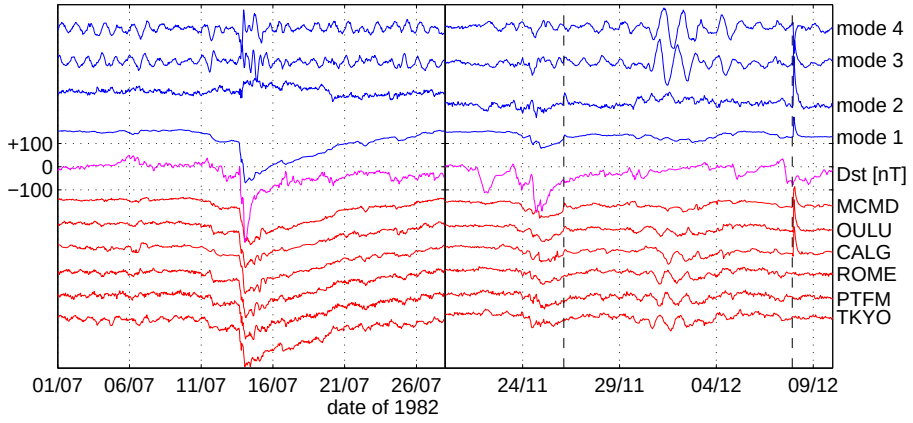

Fig. 3. From top to bottom, temporal profiles of ICA modes 1 to 4, the D_{st} index and count rates of 6 stations with increasing rigidity. All but the D_{st} index are plotted with arbitrary units. Two GLEs are indicated with dashed lines.

The temporal structure of the first four ICA modes is shown in Fig. 3 for a large storm in July 1982 and two GLEs in November and December 1982. A first small Forbush decrease occurs on July 11th around 10:00 UT and a much larger one on July 13th at 16:00. The exact timing of their onset times is affected by the omnipresent solar diurnal variation. However, this modulation of the cosmic ray flux, which travels longitudinally as the Earth rotates, is almost entirely captured by modes 3 and 4. By reconstructing the data from the all but modes

3 and 4, the onset comes out more evidently, especially for high rigidity stations. Since in addition the solar diurnal variation is well captured by modes 3 and 4, one can determine its amplitude (defined as $a(t) = \sqrt{f_3^2(t) + f_4^2(t)}$) and check that it drops before sudden storm commencements. Note that modes 3 and 4 are not equivalent to bandpass filtered count rates, since they exhibit occasional sharp transients. In particular, anisotropies associated with arriving shocks disrupt the regular oscillatory behaviour of these two modes and provide another criterion for detecting anomalous events. Such modes could therefore serve as an input for more elaborate cosmic-ray indices for space weather (Kudela & Storini, 2006).

GLEs manifest themselves as a short increase in modes 1 and 2. Two events (a weak one a strong one) are marked by dashed lines in Fig. 3. The increase observed in mode 2 implies that the contribution of GLEs versus that of the cosmic ray background is relatively more important at higher latitudes. A weak signature can also be found in modes 3 and 4 because the impact is not isotropic in longitude.

Interestingly, the power spectral density of temporal modes 1 and 2 reveals a power law scaling over more than two decades, which is almost totally devoid of the 24-hour modulation that dominates in modes 3 and 4. These two power laws have distinct spectral indices: $\alpha_1 = -2.30 \pm 0.03$ for mode 1 and $\alpha_2 = -1.30 \pm 0.03$ for mode 2. The first value is similar to the one found for the D_{st} index and attests a predominance of large-scale transients. Mode 2 in comparison has a much higher level of short-scale fluctuations; our interpretation is that this reflects the local conditions of the terrestrial environment. These two different spectral indices support the idea that modes 1 and 2 truly capture two different physical processes.

Filling data gaps

Another potentially important application is filling the data gaps that plague neutron observations. The idea, which is further developed in (Kondrashov & Ghil, 2006), consists in exploiting the redundancy of the observations to replace missing or corrupted samples with values obtained from the most significant modes. First, all corrupted samples are flagged and replaced by some reasonable estimate. The SVD is then computed. The strongest modes are used to replace the flagged values with a new estimate, and the SVD is then computed again. Convergence usually occurs after 5 to 20 iterations. Two advantages of this method are its extreme simplicity (the number of significant modes is the only tunable parameter) and its excellent performance with measurements that exhibit coherent regimes. The result is illustrated in Fig. 4, in which one month of data from the Climax monitor were deliberately taken out and subsequently reconstructed by SVD. The good performance of the method is attested by the low variance of the residuals and their statistical independence.

Conclusion and outlooks

Blind source separation methods offer a simple and yet powerful empirical approach for preprocessing in real time data from neutron monitor networks. Even though these methods are statistical, their modes convey a physical interpretation. Independent Component Analysis is well suited for characterizing common regimes, thereby enabling the robust identification of Forbush decreases and GLEs. The Singular Value Decomposition is better adapted for filling data gaps and resampling data.

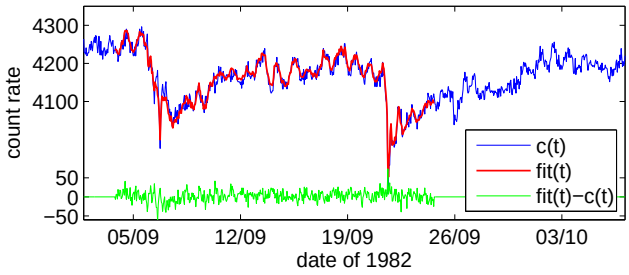

Fig. 4. Original count rate of the Climax neutron monitor ($c(t)$) and its value reconstructed by SVD ($fit(t)$), using four dominant modes out of the 43, and the residual error ($fit(t) - c(t)$).

These methods allow to investigate several other properties, and are presently being tested with data from the Aragats station (Chilingarian et al., 2005). First, due to the fact that both methods are linear, statistical hypothesis tests can be carried out on weak events. Another application is the correlated analysis of high-cadence data for the robust characterization of weak GLEs and anisotropic events. When using for example surface and underground detectors with different energy responses, differences in the amplitude of the spatial modes $g_k(x)$ are automatically adjusted by the method. Finally, we are using these methods to detect anomalous measurements (drifting count rates, offset errors). A station or a channel that behaves differently from the others often can readily be identified as this difference will tend to be picked up by one single mode.

References

Aubry, N., Lima, R.: Spatio-temporal and statistical symmetries. J. Stat. Phys. **81**, 793–828 (1995).

Belov, A.: Large-scale modulation: view from Earth. Space Science Rev. **93**, 79-105 (2000).

Chatfield, C., Collins, A. J., Introduction to Multivariate Analysis. Chapman and Hall, London (1995).

Chilingarian, A., Arakelyan, K., Avakyan, K. et al., Correlated measurements of secondary cosmic ray fluxes by the Aragats Space-Environmental Center monitors. Nuclear Instr. Methods Phys. Res. A. **543**, 483–496 (2005).

Dudok de Wit, T.: Enhancement of multichannel measurements in plasma physics by biorthogonal decomposition. Plasma Phys. Contr. Fusion, **37**, 117–135 (1995).

Hyvärinen, A., Oja, E.: Independent Component Analysis: algorithms and applications. Neural Networks, **13**, 411–430 (2000).

Kondrashov, D., Ghil, M.: Spatio-temporal filling of missing points in geophysical data sets. Nonl. Proc. Geoph. **13**, 151–159 (2006).

Kudela, K., Storini, M.: Possible tools for space weather issues from cosmic ray continuous records. Adv. Space Res. **37**, 1443-1449 (2006).

Mavromichalaki, H., Yanke, V., Dorman, L., Iucci, N., Chilingaryan, A., Kryakunova, O.: Neutron monitor network in real time and space weather. In: Daglis, I. A. (ed), Effects

of Space Weather on Technology Infrastructure. NATO Science Series II, **176**, 301–317 (2004).

Usoskin, I. G., Kovaltsov, G. A., Kananen, H., Tanskanen, P.: The World Neutron Monitor Network as a tool for the study of solar neutrons. Ann. Geoph., **15**, 375–386 (1997).

Prediction of Solar Energetic Particle Events

S. B. Gabriel

University of Southampton, sbg2@soton.ac.uk

Summary. This paper briefly addresses some of the issues associated with the prediction of solar energetic particle events, providing a definition of what is meant by the word prediction and succintly summarising the importance of this problem, in particular for manned space missions. Very little work has been done in this area and a very short precis of previous work is given, followed by some results from some research on the use of neural networks to predict events 24 to 48 hours in advance using x-ray fluxes as the inputs with the output being the occurence of an event or not. Finally, some other possible ideas, such as the analogy with self- organised criticality and turbulent plasma phenomena, are suggested which might be useful as starting points for new avenues of research.

1 Introduction

Future manned missions to the moon and Mars will require the prediction of large events with sufficient lead time to allow the astronauts enough time to get back to their shelter when they are on sorties. Currently, the same is true for extra-vehicular activity (EVA) from space stations but it is usual for the EVA not to take place if an event is predicted. If, for these future missions, the lead time is not sufficiently long then the astronauts may not be able to reach their shelters before the event peak flux resulting in exposure to potentially huge radiation doses. Since rise times of the very large events are typically of the order of 12 hours then lead times of one or two days are may be needed. Also, depending on exactly how long the astronauts are from their bases, the accuracy of the prediction of the start time of the event could be critical. Ideally, the prediction technique would be able to forecast all the key parameters, including flux spectra as a function of time from the event initiation.

So first what is meant by prediction? As discussed above, for certain applications, there is the need to be able to say what the proton fluxes, due to the occurrence of a solar energetic particle event (SEPE), are with lead times of the order of one of two days. The use of the word prediction is not always accepted in this context and sometimes people prefer to use the word forecast. Regardless, for the purposes of this paper, we will use the word prediction with the definition as follows:

Prediction of an SEPE is the ability to predict the occurrence of a rise in proton fluxes at any point in the heliosphere caused by an event on the sun, 24 to 48 hours before the

beginning of the SEPE at that same point in space. Ideally the characteristics of the SEPE (e.g., flux spectra at energies in the range of 1 to 500 MeV), as a function of time during the event as well as the event duration, should be predicted too.

2 Brief summary of previous work

There has been little work done on prediction (as defined above) of SEPEs. Current real-time prediction models (Balch, 1999; Garcia, 1994) assume a relation between SEPEs and discrete X-ray flares, and require a flare before a prediction can be made, inherently limiting lead time to several hours. The question arises as to whether one can predict an event without the need for a discrete X-ray flare. Recently, artificial intelligence techniques, using neural networks, have been used to predict SEPEs (Patrick, 2003) with lead times of the order of 48 hours. The inputs to the networks were the ratio of the GOES XL and XS X-ray fluxes. Overall success rates were about 65% and having tried many different input combinations, it has been concluded that this is probably the best that can be achieved with these inputs (Gabriel & Patrick, 2003).

2.1 Summary of Neural network results

Only a brief overview of the technique and some of the results which are presented in Patrick (2003) are presented in this section. The technique classifies the X-ray flux ratios (taken from the GOES XS and XL channels) preceding either an event or a quiet period (QP) and predicts the occurrence of an event 48 hours in advance. A real time model uses the majority decision of 10 separate neural networks. The total data set consisted of 97 SEPEs and 170 non SEPEs, which were divided into training (60 SEPEs/60 non SEPEs) and query sets (37 SEPEs/110 non SEPEs). A Principal component analysis (PCA) projected the training set onto non-real dimensions and the majority of variation was found in the first few principal axes. The least significant principal components (PCs) were discarded to reduce the dimensional complexity and noise. The number of PCs was varied and the training accuracy investigated with each configuration being tested with 10 random train/query combinations. Optimum performance was found when there were 12 PCs as inputs and 10,000 training epochs, giving 65% SEPEs classified successfully and 66% non SEPEs classified correctly.

A real time model, called POPE (Prediction of Proton Events) was developed and uses a majority voting system on the output from 10 different neural networks. Table 1 shows some of the SEPEs that were identified during the period from 26 December, 2001 till 9 November, 2002.

The predictions made by POPE over the past 12-months of operation have been assessed by breaking down the observed proton flux time series into a binary time series of SEPEs and Quiet Periods with 1-hour resolution. The observed series has then been compared against the POPE forecast. Within the training set the start times of SEPEs had been found to the nearest two hours, hence the predictions from the POPE model had a lead time of 48-hours, ± 2 hours.

Table 1. SEPEs identified during the period of real-time operation

ID	Start Time	Duration [h]	Fluence [p/cm^2]	POPE Output
1	26/12/01 06:00	49	$3.54{\cdot}10^8$	10
2	29/12/01 05:00	17	$2.35{\cdot}10^7$	10
3	30/12/01 21:00	119	$2.33{\cdot}10^8$	8
4	10/01/02 20:00	67	$1.03{\cdot}10^8$	9
5	18/03/02 13:00	32	$3.23{\cdot}10^7$	2
6	21/04/02 02:00	113	$2.84{\cdot}10^9$	6
7	22/05/02 18:00	44	$1.05{\cdot}10^8$	5
8	16/07/02 18:00	46	$1.02{\cdot}10^8$	1
9	22/07/02 07:00	97	$8.31{\cdot}10^7$	Model Down
10	22/08/02 04:00	20	$1.65{\cdot}10^7$	Model Down
11	24/08/02 01:00	60	$3.13{\cdot}10^8$	10
12	07/09/02 07:00	19	$2.55{\cdot}10^7$	10
13	09/11/02 19:00	34	$1.42{\cdot}10^8$	9

Method

The output from POPE that was used to assess its performance consisted of an integer of between 0 and 10, representing the number of networks from 10 which had an output of >50, i.e. the number of networks from 10 which were predicting an SEPE in 48-hours time.

Over the period of operation 1-hour resolution GOES-8 proton data was examined and an SEPE was defined as occurring if the hourly averaged >10 MeV integrated proton flux was greater than 1.0 p.f.u. for 12 consecutive hours. This is consistent with the way in which SEPEs were defined in the original training set. The start time of each SEPE was taken as the time at which the hourly averaged proton flux was first above 1.0 p.f.u. SEPEs were identified as ending when the hourly averaged >10 MeV integral proton flux fell below 1.0 p.f.u. for 12 consecutive hours. The POPE prediction for each SEPE was taken as the highest output from the model from within ± 2 hours of the SPE start time. Data collected during an ongoing SEPE was ignored, thus the POPE model was assessed on its ability to predict the initial onset of an SEPE.

Observed values with a >10 MeV hourly averaged proton flux of less than 1.0 p.f.u. which occurred at least 6 hours after the end of an SEPE were classed as instances of quiet periods. The prediction for each quiet period was taken as the highest output from the model from within ± 2 hours of the quiet period.

Outputs from the POPE model were only utilised if they were based on an input delay vector that did not contain a significant amount of missing data (due to data gaps from GOES). An input vector was deemed unsuitable if any of its component 3-hour averages contained more than 50% missing data.

The 48-hour forecast from the model was matched to each observed value of the hourly averaged >10 MeV integrated proton flux. The forecast consisted of an integer of between 0 and 10 and the threshold used to interpret the forecast was altered in order to examine the effect on SEPE and quiet period classification success rates.

Table 2. Classification success for real-time POPE model for different threshold interpretations of the multiple model output. Average success is shown in bold.

Threshold	>5 for SEPE	>6 for SEPE	>7 for SEPE	>8 for SEPE	>9 for SEPE
SEPEs from 11	8	7	7	6	4
QPs from 6249	2158	2711	3345	4120	5123
SEPEs [%]	72.7	63.6	63.6	54.5	36.4
QPs [%]	34.5	43.4	53.5	65.9	82.0
Average [%]	**53.6**	**53.5**	**58.6**	**60.2**	**59.2**

Changing the criterion for event prediction modifies the success rates and this can be seen in Table 2, where the threshold for an event has been varied from 5 to 9. Increasing the threshold decreases the success rate for event prediction but tends to increase the average success rate as the QP prediction success rate increases. Table 3 shows a contingency table for the POPE classification model using >8 as the decision threshold.

Table 3. Contingency table for real-time operation of POPE model, Dec 2001 – Dec 2002.

POPE Model		Event observed	
		Yes	No
Event Forecast	Yes	6	2129
	No	5	4120

3 Other techniques and comments

Dorman et al. (2004) have proposed the use of on line neutron monitor and muon telescope data at a one minute time resolution, for 20 to 30 minutes, to predict very large SEPEs with a lead time of up to about 2 days. But of course this will only work for events that have a hard event spectrum to produce neutrons observed on the ground.

Posner (2006) has proposed a method of forecasting SEPEs using relativistic electrons, having found that using a superposed epoch analysis:
i) Relativistic electrons always arrive before of non-relativistic SEPEs
ii) Early electron fluxes are highly correlated with proton fluxes
iii) Both proton and electron flux increases depend on the magnetic connection.

The question of predictability has been raised by Gabriel and Patrick (2003). By noting the intermittent or bursty behaviour of the >10-MeV proton fluxes over a period of about 10 years, they posed the question as to whether or not this behaviour might indicate that the sun is in a state of self-organised criticality (SOC), which has been observed or proposed to be present in other phenomena, e.g. X-ray flares and turbulent laboratory plasmas. If this is the case then it might be concluded that SEPEs are not predictable, at least based on time series analyses (rather than using pre-cursors and/or of course deterministic physics-based

methods). However, as they point out much more research is needed to be able to make this rather fundamental conclusion.

Finally as proposed by Joan Feynman (personal communication), if one could observe the back-side of the sun using spacecraft, then active regions or CMEs with the right parameters to cause SEPEs, could allow prediction with lead times of several days.

References

Balch, C. C.: SEC Proton Prediction Model: Verification and Analysis. Radiation Measurements **30**, 231–250 (1999)

Dorman, L. I., et al.: Monitoring and Forecasting of Great Solar Proton Events Using the Neutron Monitor Network in Real Time. IEEE Trans. Plasma Sci. **32**, 478–1488 (2004)

Gabriel, S. B., Patrick, G. J.: Solar Energetic Particle Events: Phenomenology and Prediction. Space Sci. Rev. **107**, 55–62 (2003)

Garcia, H. A.: Temperature and Hard X-Ray Signatures for Energetic Proton Events. Astrophys. J. **420**, 422–432 (1994)

Patrick, G. J.: The Development of a Solar Proton Event Prediction Model. PhD Thesis, University of Southampton (2003)

Posner, A.: Forecasting Solar Energetic Ion Events with Relativistic Electrons: Statistical and Superposed Epoch Analyses. 36th COSPAR Scientific Assembly, 16–23 July 2006, Beijing, China (2006)

Solar energetic particle fluences from SOHO/ERNE

E. Valtonen, E. Riihonen, and I.-V. Lehtinen

Space Research Laboratory, Department of Physics, University of Turku, FI-20014 Turku University
Eino.Valtonen@utu.fi

Summary. We have calculated integral fluences of solar protons and helium nuclei at 20 energy thresholds between 1.6 and 108 MeV/n from the SOHO/ERNE measurements during the years 1996-2005. We have also calculated fluences of oxygen and iron in the energy range from 10 MeV/n up to a few hundred MeV/n for 19 SEP events. These are the first results of the work aiming at a full employment of the ERNE data in investigating the fluence distributions of SEP events over the entire solar activity cycle and in deriving the total dose received on-board SOHO during its mission. Some instrumental problems are identified and future developments presented.

1 Introduction

Solar energetic particle (SEP) fluences have an important role in modelling space weather and its effects. By deriving SEP event fluence distributions from long-term measurements, probabilistic models can be created, which can be used for predicting cumulative and worst case fluences on a mission at a certain phase of the solar activity cycle (e.g., Feynman et al., 1993; Nymmik, 1999; Xapsos et al., 1998). As well, the measured data can be used for post-analysis of space weather effects on technology, e.g., analysing radiation effects on electronic components. Of specific interest is the fluence of protons at energies above $\sim$10 MeV, being capable of penetrating modest shielding. However, high-energy helium and heavier ions need also attention. These species can significantly contribute to displacement damage and single event effects in electronic components. Long-term observational results of high-energy solar heavy ions are, however, relatively scarce (Tylka et al., 1997; Mewaldt et al., 2001).

We have employed the SOHO/ERNE data from the years 1996-2005 to derive fluences of solar energetic protons, helium, oxygen, and iron at various energy thresholds. We describe in this report the current status of the work. In Section 2, a brief overview of the instrument is given. The available data and preliminary results are discussed in Sections 3 and 4, respectively. Known instrumental problems leading to uncertainties in the derived fluences are briefly discussed in Section 5. In Section 6 we present the conclusions and identify some future developments.

2 Instrument overview

SOHO is in a halo orbit around the Sun-Earth system's Lagrangian point L1 and thus observes environmental conditions in the interplanetary space. ERNE instrument (Torsti et al., 1995; Valtonen et al., 1997) consists of two sensors, one (LED) operating roughly between 1 and 12 MeV and the other (HED) between 12 and 130 MeV proton energies.

Both sensors are capable of identifying protons, helium, and heavy ions from carbon to iron. The operational upper energy limits for helium, oxygen, and iron are approximately 130 MeV/n, 350 MeV/n, and 550 MeV/n, respectively. The geometric factor of LED is $0.9\,\mathrm{cm}^2$ sr. The sensor has seven separate view cones with a total full opening angle of 64°. HED has a much larger geometric factor, varying from approximately $40\,\mathrm{cm}^2$ sr near the lower limit of operational energy range for each species to $25\,\mathrm{cm}^2$ sr at the upper limit. The full opening angle is 120°. Silicon strip detectors are used to achieve a good directional sensitivity within the view cone. The capability to determine the path lengths of incident particles in the detectors is also a prerequisite for precise identification of heavy ions. The large geometric factor of HED has both positive and negative effects on the performance of the instrument. Due to the large geometric factor, a high sensitivity is achieved, making it possible to observe even very small SEP events. However, the geometric factor of HED cannot be dynamically changed with flux conditions. Therefore, during very large SEP events the instrument has a tendency to saturate. From the point of view of using HED data in calculating, e.g., the total mission dose, this feature is very unfortunate, because a significant part of the total dose is received during the largest SEP events.

3 Available data

ERNE started measurements in December 1995 and data are available till the present time. Some data gaps exist both due to spacecraft and instrumental anomalies. The longest data gaps are from December 20, 1996 to March 3, 1997, from June 25 to October 8, 1998, from December 22, 1998 to February 7, 1999, and from March 13 to March 30, 2000. Calculated intensities of protons and helium at standard or user-selectable energy channels and time resolutions can be freely accessed through the internet (http://www.srl.utu.fi/erne_data/main_english.html). These data are available from May 8, 1996 and are continuously updated with a delay of a few days from the current time. Presently, intensities of heavy ions are not produced routinely, but have to be processed on case-by-case basis from the low-level pulse height data. The 24-hour averaged proton intensities measured by ERNE at two energy channels are presented in Figure 1. This figure illustrates the extremely dynamic nature of the interplanetary particle environment at low energies as well as the occurrence of high-energy protons, which also usually are related to largest SEP events, concentrating in the region of solar maximum activity.

4 Proton, helium, oxygen, and iron fluences

Proton and helium fluences are calculated from the data pre-analysed on-board the spacecraft. The on-board software identifies protons and helium nuclei and arranges the particles

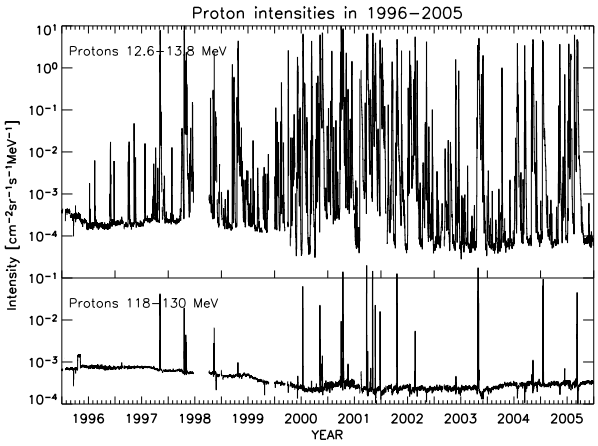

Fig. 1. Proton intensities at two energy channels observed by SOHO/ERNE during 1996-2005.

in energy bins. Corrections to the observed particle energies, which are too complicated to be taken into account on-board, are performed on-ground. Proton and helium intensities as a function of energy are then calculated by applying the energy and species dependent geometric factors. From these intensities, integral fluences are finally calculated at 20 approximately logarithmically spaced energy thresholds between 1.6 and 108 MeV/n. The fluences are given in units $\mathrm{cm}^{-2}\mathrm{sr}^{-1}$ representing the fluence of particles in the field of view of the instrument. In case of an isotropic flux, multiplication by the factor 4π gives the total fluence per cm^2. The basic time resolution of the instrument is one minute, but the calculated fluences have been archived as hourly averages. These archived data are then used for calculating, e.g., SEP event-averaged fluences.

Examples of SEP event-averaged integral fluences of protons and helium are shown in Figure 2. The figures illustrate the large variations in the total event fluences and the variability of the spectral shape from event to event. The behaviour of the helium fluence follows the general trends of the proton fluence in these events, but with slightly less variability, in particular at the highest observed energies.

Heavy ion data have to be fully processed on ground. Due to the complexity of the instrument, the processing is not done routinely for all the data received. It is usually done only for selected SEP events, which are of interest for various research goals. Therefore, ERNE heavy ion intensities covering continuous, long time periods are not currently available. In the course of this work, we have processed heavy ion data for the 19 SEP events shown in Table 1.

For oxygen and iron differential fluences have been calculated for the 19 events given in Table 1. Figure 3 shows the results for the same four events as presented in Figure 2 for protons and helium. The energy range for heavy ions is limited to > 10 MeV/n, because at lower energies the range is very small. The oxygen fluence is again highly variable in the studied events at low energies. At high energies, in the region of several tens of MeV/n and above the fluence is relatively constant reflecting a main contribution from galactic and anomalous cosmic rays. For iron, there are only two data points available from LED above 10 MeV/n followed by a relatively wide data gap between LED and HED. In most of the events studied, the fluences at high energies are very small and even with the high sensitivity of HED large

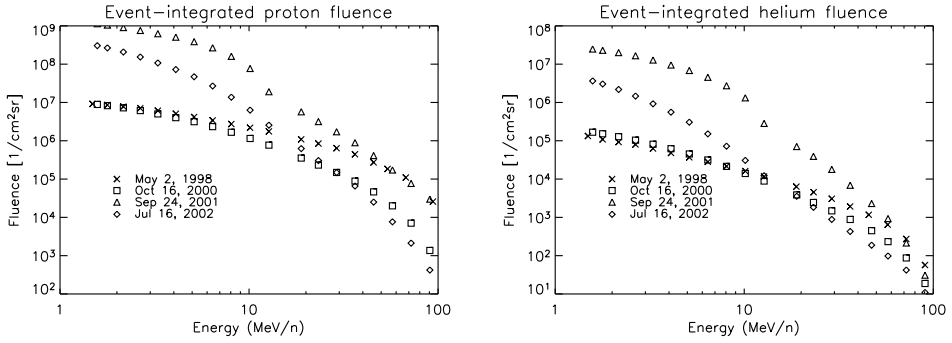

Fig. 2. Integral fluence of protons (left) and helium (right) as a function of energy for four SEP events.

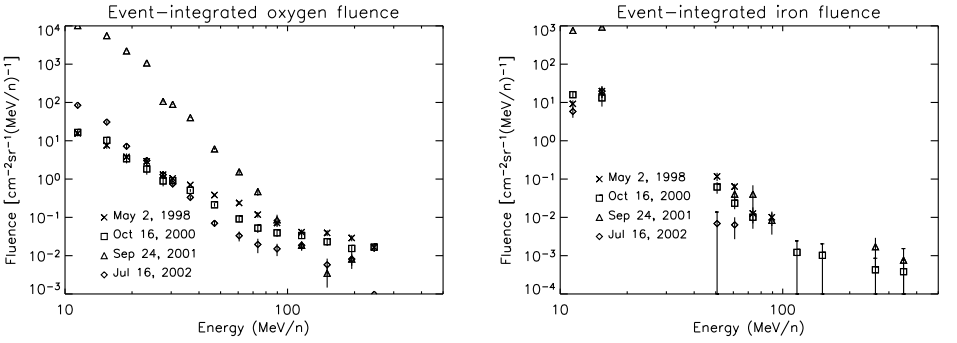

Fig. 3. Differential fluence of oxygen (left) and iron (right) as a function of energy for the same SEP events as in Figure 2.

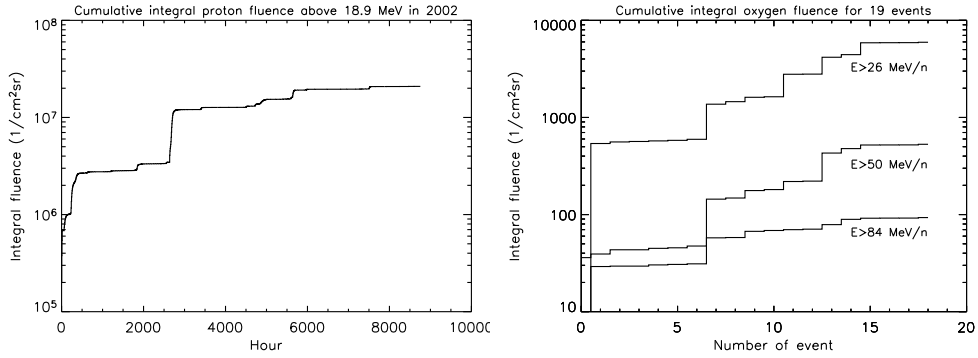

Fig. 4. Left: cumulative 1-hour averaged proton fluence above 18.9 MeV in the year 2002. Right: cumulative event-averaged integral oxygen fluence above three energy threshold for the 19 events of Table 1.

Table 1. SEP events for which oxygen and iron fluences have been calculated

Event	Start date and time	End date and time	Event	Start date and time	End date and time
1	1997-11-04 06:50	1997-11-06 12:00	11	2001-04-18 03:50	2001-04-22 00:00
2	1998-04-20 11:30	1998-04-25 20:00	12	2001-09-24 11:50	2001-09-26 06:00
3	1998-05-02 14:10	1998-05-04 00:00	13	2001-10-22 18:10	2001-10-26 06:00
4	1998-05-06 08:30	1998-05-08 19:00	14	2001-11-04 17:10	2001-11-09 00:00
5	2000-06-10 17:30	2000-06-13 09:00	15	2001-12-26 05:50	2001-12-29 09:00
6	2000-09-12 13:10	2000-09-15 19:00	16	2002-04-21 01:50	2002-04-24 00:00
7	2000-10-16 07:50	2000-10-20 10:00	17	2002-07-16 13:50	2002-07-19 00:00
8	2001-04-02 23:30	2001-04-05 23:00	18	2002-08-22 00:00	2002-08-24 01:00
9	2001-04-10 08:00	2001-04-12 12:00	19	2002-08-24 01:30	2002-08-27 06:00
10	2001-04-15 14:30	2001-04-18 00:00			

error bars have to be attached to the results and in some cases no iron nuclei were observed at the highest energies during the event.

Examples of cumulative integral fluences of protons and oxygen are shown in Figure 4. For protons, the hourly averages of integral fluence above 18.9 MeV are shown for the year 2002. The largest sudden step in the fluence comes from the April 21, 2002 SEP event. For oxygen, the event-averaged cumulative fluence above three energy thresholds is presented. The plot includes only the 19 events given in Table 1. The most prominent sudden steps in the fluence are caused by the April 2, 2001, September 24, 2001, and November 4, 2001 events.

5 Instrumental problems

As already mentioned in Section 2, due to the large geometric factor of HED this sensor tends to saturate during largest SEP events. This is the most significant drawback of the ERNE instrument. Saturation occurred, e.g., during the July 14, 2000 event, October 28-November 4, 2003 events, and January 20, 2005 event. When saturating, the live time of the instrument is not well known leading to large errors in the calculated fluence values. These errors are very difficult to estimate and correct. For this reason, ERNE fluences of the largest SEP events are presently not available.

Scintillators are employed in HED to reach the high upper limit of the operational energy range. The light collection from the scintillators is not fully uniform. The nonuniform response may also lead to some uncertainties in the derived fluences. This is not, however, considered very significant. HED also has a plastic scintillator anticoincidence shield. As from all the other scintillators, light from the plastic scintillators is read out by photodiodes. Due to the non-optimal match of the wavelength of the light from the plastic scintillator with the response function of the photodiodes, the capability of the anticoincidence shield to detect very high energy protons is limited. This again leads to uncertainties in precise measurements of the proton energies.

6 Conclusions and future developments

We have presented first results of the work aiming at deriving the fluences of protons, helium, and heavy ions from the long-term measurements of SOHO/ERNE. We have calculated the integral fluences of protons and helium at 20 energy thresholds for the period 1996-2005. We have also calculated differential fluences of oxygen and iron in several energy channels between 10 and a few hundred MeV/n. Some examples of the results were presented in this report.

The main drawback in employing SOHO/ERNE in deriving solar energetic particle fluences is the tendency of the instrument to saturate during largest SEP events. This is a serious difficulty, which presently has not yet been solved.

Currently, we are in the process of developing a simulation model of the instrument hardware to analyse possible methods, which could be used for solving the saturation problem. Once a successful solution is found, ERNE data are expected to be very valuable for many space weather related investigations. One of the major goals is to calculate the total dose that SOHO spacecraft and its components have received during the mission. The derived fluence and dose data will be made accessible through the internet.

The fluence data can also be used for space environment modelling. SEP event fluence distributions can be employed in creating probabilistic models of SEP event occurrence. Due to the high time resolution and high sensitivity of the instrument, even time-dependence of the fluences during particular events can be investigated.

References

Feynman, J., Spitale, G., Wang, J., Gabriel, S.: Interplanetary proton fluence model: JPL 1991. J. Geophys. Res., **98**, 13281–13294 (1993)

Mewaldt, R.A., Mason, G.M., Gloeckler, G., et al.: Fluences of solar, heliospheric, and galactic particles at 1 AU. Proc. 27th Int. Conf. Cosmic Rays, **10**, 3984–3987 (2001)

Nymmik, R.A.: Probabilistic model for fluences and peak fluxes of solar energetic particles. Rad. Measurements, **30**, 287–296 (1999)

Torsti, J., Valtonen, E., Lumme, M., et al.: Energetic particle experiment ERNE. Sol. Phys., **162**, 505–530 (1995)

Tylka, A.J., Dietrich, W.F., Boberg, P.R.: Probability distributions of high-energy solar-heavy-ion fluxes from IMP-8: 1973-1996. IEEE Trans. Nucl. Sci., **44**, 2140–2149 (1997)

Valtonen, E., Peltonen, J., Peltonen, P., et al.: Energetic and relativistic nuclei and electron experiment of the SOHO mission. Nucl. Instrum. and Meth. in Phys. Res., **A391**, 249–268 (1997)

Xapsos, M.A., Summers, G.P., Burke, E.A.: Probability model for peak fluxes of solar proton events. IEEE Trans. Nucl. Sci., **45**, 2948–2953 (1998)

Probabilistic model of solar energetic proton fluxes

Rikho A. Nymmik

Skobeltsyn Institute of Nuclear Physics, Moscow State University, 119899, Moscow, Russia
nymmik@srd.sinp.msu.ru

Summary. The occurrence of solar energetic particle (SEP) events over a long time scale is described by probability theory using regularities inherent in sets of SEP events. The most complete probabilistic model of SEP fluxes is based on successive utilization of these regularities. In this paper we present a short description of the technique of revealing the basic regularities for the probabilistic SEP model, used in the Skobeltsyn Institute of Nuclear Physics, Moscow State University (SINP/MSU).

1 Introduction

In developing a probabilistic model of any phenomenon, it is necessary to have, or to be able to compose, a quantitative picture of all possible situations of occurrence of the phenomenon being modeled. This is also applicable to the modeling of SEP fluxes, which in this work represents a purely probabilistic phenomenon with the systematic regularities inherent in SEP phenomena.

Any model can be based either on experimental data sets or on theoretical modeling of the phenomenon. For SEPs, theoretical models do not result in a satisfactory description of the whole phenomenon and, thus, models of SEP fluxes and fluences are usually based on generalized representations and analysis of the experimental data. The experimental data of SEPs possess, however, considerable statistical and systematic errors (Mottl and Nymmik, 2007). To avoid transferring such errors from the experimental data to the developed models, the statistical errors should be thoroughly analyzed, the results of various experiments should be compared with each other to reveal systematic errors, and the experimental data sets should be represented in the form of general mathematical regularities. Such a technique serves as a basis of the probabilistic model of SEP fluxes developed at the MSU.

The developed model answers the basic question, what is the probability of occurrence of any given value of peak flux or total (cumulative) fluence of particles during a given time interval, characterized by the known or the predicted level of solar activity.

The energy spectra of protons, for different values of occurrence probability, are determined from the characteristics of an artificial set of a number of realizations of particle fluxes calculated on the basis of the mathematical regularities obtained from the analysis of experimental data. Each realization of fluxes is determined in the following sequence:

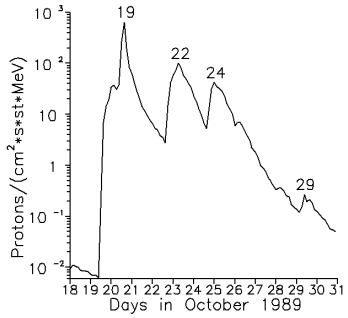

Fig. 1. Fluxes of solar protons within the interval of 15 MeV $\leq E \leq$ 40 MeV recorded on the GOES-7 satellite in October, 1989. According to the principles applied in the present work, the period contains four SEP events, and according to the principles accepted by NOAA (in a paper by Rosenqvist et al., 2005, in particular) the period contains only a single SEP event.

1. The random number of events for the given period of time is determined.
2. The random value of the peak flux or fluence for each event is determined.
3. The random parameters of energy spectra for each event are determined.
4. The values of differential and integrated fluxes for the chosen sequence of particle energies and for each random realization of the mission are calculated.
5. The probabilities of occurrence of the values of SEP fluxes and fluences are determined from the total set of calculated data.
6. The results are presented in the form of energy spectra of proton fluxes, which will be exceeded at the user-specified probability.

2 The SEP event concept and the random number of SEP events for the given period of time.

In the probabilistic SEP event modeling, several definitions of the concept of an SEP event are used. Here, we shall note two of them: In one of definitions, termed the technological definition and used, e.g., in the JPL91 (Feynman et al., 1993) and ESP (Xapsos et al., 1998) models, an SEP event is defined as the time period from the increase of the particle flux above a given threshold until the subsequent decrease of the flux below the same threshold (technique A). In the present model, each new increase of the flux of protons with energy higher than 30 MeV (with rare exceptions related to shock wave arrival from a preceding event) is assumed to constitute a new SEP event (technique B). The use of this technique leads to the same set of SEP events that was obtained by Bazilevskaya et al. (1986) by comparing the proton fluxes with X-ray bursts. Figure 1 presents the simplest example for selecting the events occurred in October, 1989: when separating the events from the data by technique A, this period contains only one event, but when separating them by technique B, the period contains four events.

However, it is also of importance that, irrespective of the technique of separating SEP events, we have an identical dependence of the rate of SEP events on the solar activity (monthly average smoothed Wolf numbers), i.e., that the mean rate of SEP events is proportional to the solar activity. This is demonstrated in Fig. 2, which presents these dependencies calculated for SEP events determined both by technique A (Rosenqvist et al., 2005) and by

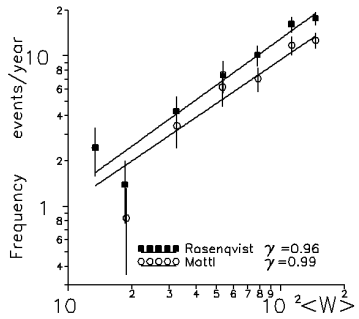

Fig. 2. Dependence of the rate of SEP events on the solar activity level. Circles represent the data from the paper by Rosenqvist et al. (2005) and the dark squares those corresponding to the data of Mottl (2005).

technique B (Mottl, 2005) for the set of SEP events with $E > 10$ MeV for proton fluences of $>10^7$ protons cm^{-2}, recorded during the period from Nov. 1973 to May 2003 on-board the satellites IMP-8 (the CPME instrument) and GOES (the DOME and TELESCOPE instruments). Note, that in the JPL91 and ESP models it is assumed, that for $W \geq 40$ the rate of events is invariable ($\nu \approx 7$ events per year), and for $W < 40$ the events can be neglected ($\nu \equiv 0$).

Taking into account that the event distribution function Ψ (see Fig. 3 below) for low values of peak fluxes and fluences (both denoted by Φ) has the form of $\Psi \sim \Phi^{-0.32}$ (see Eq. (2)), we can compute the average number $\langle n \rangle$ of events during m months, each with the monthly average Wolf numbers $\langle W_i \rangle$. With the threshold proton fluence at $\geq$30 MeV of $F_{30} \geq 10^5$ protons cm^{-2}, or with the threshold peak flux $f_{30} \geq 0.12$ protons cm^{-2} s^{-1} sr^{-1} the result is

$$\langle n \rangle = 1.35 \cdot 10^{-2} \sum_{i}^{m} \langle W_i \rangle \,. \tag{1}$$

Knowing the mean expected number of events, the number of events for each model realization can be calculated either according to the normal (Gaussian) or Poisson's distribution.

3 The event distribution function and its properties

Figure 3 presents the normalized distribution of SEP events, Ψ, as a function of $\geq$30-MeV proton fluence, i.e., Φ_{30}. The function, used in our model to arrive at the approximation (1) of the experimental data, is given as

$$\Psi(\geq \Phi_{30}) = \text{Const.} \cdot \Phi_{30}^{-\delta} \, \exp\left(-\frac{\Phi_{30}}{\Phi_0}\right) \tag{2}$$

where $\delta = 0.32$ and $\Phi_0 = 9 \cdot 10^9$ protons cm^{-2} are the distribution function parameters for proton fluences, and $\Phi_0 = 8.7 \cdot 10^3$ protons cm^{-2} sr^{-1} s^{-1} is the parameter for the peak proton fluxes (while δ remains the same for both distributions). Here, it is necessary to point out that in the JPL91 and ESP models the event distribution function is expressed, respectively, by the

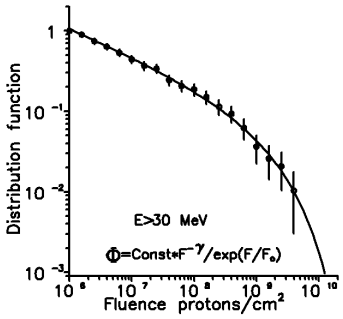

Fig. 3. Normalized distribution of SEP events in fluences of protons with $E \geq 30$ MeV based on SEP events recorded during 1974–1985 on-board the IMP-8 satellite and during 1986–2005 on-board the GOES series satellites.

lognormal function and by a function describing the maximum entropy principle applied to the power-law distribution. These functions noticeably differ from function (2) in the region of high values of particle fluxes, i.e., in the region of extreme SEP events. For a further discussion of the event distribution, see Nymmik (2007a,b).

The distribution functions, being determined for various periods (or phases) of solar activity and subsequently divided by a total number of sunspots for the corresponding period of observation, are identical within the limits of statistical accuracy. This implies that the shape of the SEP event distribution function is invariant with respect to solar activity, i.e., for any solar activity period one can make use of the same function (2); in particular, the relative probability of occurrence of extreme events is the same for any solar activity level. So, the random value of peak flux and/or fluence of each event is determined as a random quantity from the distribution (2) (see, for example Nymmik, 2007a,b).

4 Parametrizing the energy spectra

Having analyzed particle (protons and heavy ions) peak fluxes and fluences in hundreds of SEP events measured by various instruments, we have repeatedly demonstrated (Nymmik, 1993; Mottl et al., 2001) that a power-law function in particle rigidity (R [MV]),

$$\frac{d\Phi}{dE} = \frac{C}{\beta}\left(\frac{R}{R_0}\right)^{-\gamma}, \tag{3}$$

most successfully describes all SEP energy spectra at energies $\geq$ 30 MeV. Here $R = \sqrt{E(E+2mc^2)}$ is the proton rigidity, $\beta = R/\sqrt{R^2+m^2}$ is the relativistic velocity; $R_0 = 239$ MV corresponds to $E = 30$ MeV for solar energetic protons. Function (3) was shown to be also valid at energies <30 MeV ($R < 239$ MV) under the assumption that in this energy range the spectral index depends on the energy (the droop effect):

$$\gamma = \gamma_0\left(\frac{E}{30}\right)^{\alpha} \tag{4}$$

where α is the spectral droop index and γ_0 is the spectral index at $E \geq 30$ MeV.

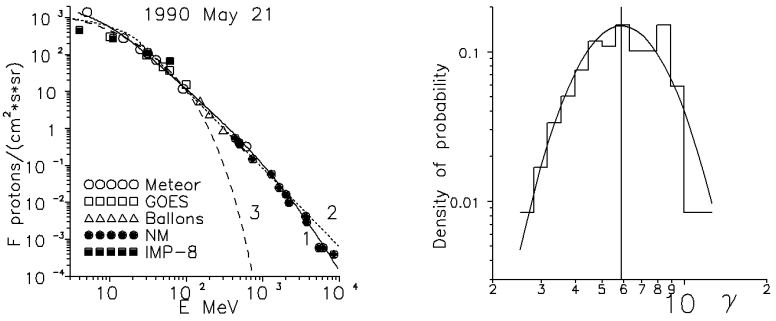

Fig. 4. (left). The integrated peak proton fluxes for the SEP event on May 21, 1990. The markers denote the METEOR data (circles), the GOES data (squares), the IMP-8 data (black squares), the balloon data (triangles), and the neutron monitor data (black circles). The energy spectra are shown as power-law functions of momentum (rigidity) (curve 1) and energy (curve 2), and as a rigidity exponent (curve 3).

Fig. 5. (right). Distribution of SEP events in spectral indices.

Figure 4 shows the spectrum of peak proton fluxes for a typical SEP event (May 21, 1990). The data have been measured by various instruments and are well approximated by functions (3) and (4).

The spectral indices of the proton fluence or peak flux energy spectra are distributed according to the log-normal, rather than normal law, namely (see Fig. 5):

$$\Psi[\log\gamma_0] = \frac{1}{\sqrt{2\pi}\sigma_\gamma} \cdot \exp\left(-\frac{(\log\gamma_0 - \langle\log\gamma_0\rangle)^2}{2\sigma_\gamma^2}\right) \tag{5}$$

The mean spectral index γ, independent of the SEP event fluence or peak flux value, is $\langle\gamma_0\rangle = 5.9$ or $\langle\log\gamma_0\rangle = 0.77$, and $\sigma_\gamma = 0.15$.

If the spectral index γ_0 and the fluence F_{30} or the peak flux f_{30} are known, the spectral coefficient C of the differential SEP event proton fluence or peak flux spectrum (Eq. (3)) is determined as:

$$C = \frac{\Phi_{30} \cdot (\gamma_0 - 1)}{239} \tag{6}$$

The random values of parameters α, which are required for determining the random fluxes of protons in the region $E < 30$ MeV, have been determined each time also by using the graph of the random values of the log-normal distribution. However, in this case the mean value depends both on the considered value of the quantity Φ (peak flux or fluence) and on the spectral index γ_0, i.e. $\langle\alpha\rangle = \mathrm{funct}(\Phi, \gamma_0)$. The form of this function and the methods of drawing the random values α can be found at the author's website.[1]

[1] http://srd.sinp.msu.ru/nymmik/

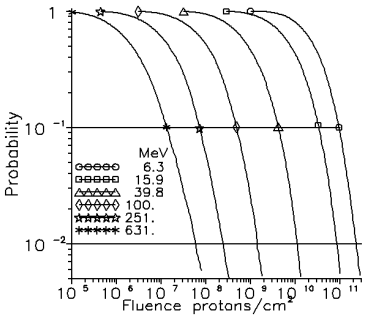

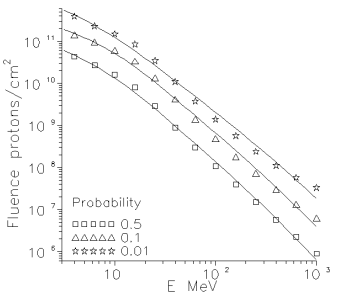

Fig. 6. (left) The selected energy probability functions for proton fluences in the case, where the model parameter is $\langle n \rangle = 32$.

Fig. 7. (right) The model output energy spectra for the proton fluence in the case of model $\langle n \rangle = 32$ for various probabilities of the fluences to exceed the given values.

5 Determination of the distribution of the possible values of fluxes

In the process of determination of energy spectra of the events, the data on peak fluxes and/or fluences of protons are accumulated for some sequence of threshold energy values. After performing calculations for the total set of realizations – N (the "conditions of the certain time period with a certain solar activity – $\sum_i W_i$"), the distributions of all possible values of expected fluxes are constructed for each energy (in Fig. 6) from the sets of values of fluxes. As an example,the figure presents such distribution functions calculated for the period, for which the mean number of events (with $\Phi \geq 30$ MeV $\geq 10^5$ cm^{-2}) is $\langle n \rangle = 32$.

6 Calculation of energy spectra of fluxes exceeding the spectra at the given probability

Such families are expedient to be re-calculated into energy spectra, the fluxes in which occur at the same probability (horizontal lines, Fig. 6). The particle fluxes, calculated in such a manner, can be expressed using formulas (3) and (4) in the analytical form, that facilitates using the results of the model in subsequent applied calculations. Fig. 7 gives the final model output for the probability distributions shown in Fig. 6, i.e., the SEP fluence energy spectra for various probabilities of the fluences to exceed the given spectra.

The users of the model are not obliged to carry out the whole set of calculations of energy spectra parameters. The parameters of these spectra are pre-calculated and tabulated in the model for the sequence of expected mean numbers of events ($\langle n \rangle = 1$, 2, 4, 8, 16, 32, 64, 128, and 256), and the sequences of most frequently used values of probability ($\psi = 0.9$, 0.84, 0.5, 0.16, 0.1, and 0.01). The energy-spectral parameters for $\langle n \rangle$ and ψ values, which are intermediate to the tabulated values, can be calculated by interpolating the tabulated data.

Therefore, it is sufficient for a user of the model to calculate the expected mean number of events by formula (1) and to specify the level of probability.

7 Conclusion

The present paper presents a technique for the calculation of SEP fluxes and fluences, whose occurrence during the given time period is expected at the given probability, under the forecasted level of solar activity. The results of the model calculations are the parameters of differential energy spectra, which allow on-line calculations of the characteristics effect of SEP fluxes on a substance, on instruments and on living organisms in the space environment to be performed. Interested users can carry out all calculations they wish through an interactive user interface at the author's website, http://srd.sinp.msu.ru/nymmik/.

References

Bazilevskaya G.A., Vashtsenyuk E.V., Ishkov V.N., et al.: Catalogue of Energy Spectra of Solar Proton Events of 1970–1979. IZMIRAN, Moscow, 1986.

Feynman J., Spitale G., and Wang J.: Interplanetary Proton Fluence Model: JPL 1991. JGR, 98(A8), 13281–13294, 1993

Mottl D.A.: Energy spectra of the fluxes of Solar energetic protons and the problem of the experimental data reliability. Thesis, Moscow State University, 2005.

Mottl D.A. and Nymmik R.A., The issues of reliability of solar energetic proton flux databases and models. Advances in Space Research, 39, 1355–1361, 2007.

Mottl D.A., Nymmik R.A., Sladkova A.I.: Spectra of solar energetic protons derived from statistical analysis of experimental data on large set of events. in Proc. of ICRC 2001, 3185, 2001.

Nymmik R.A.: Averaged Energy Spectra of Peak Flux and Fluence Values in Solar Cosmic Ray Events. Proc. 23rd ICRC, Calgary, 29, 1993.

Nymmik R.A., Regularities of solar energetic particle events and fluxes. Bulletin of the Russian Academy of Sciences: Physics, 71(4), 9270929, 2007a.

Nymmik R.A., To the problem on the regularities of solar energetic particle events occurrence. Advances in Space Research (in press), doi:10.1016/j.asr.2007.02.013.

Rosenqvist L., Hilgers A., Evans H., et al.: Toolkit for updating interplanetary proton-cumulated fluence models. J. of Spacecraft and Rockets, 42 (6), 1077-1090, 2005

Xapsos M.A., Summers G.P., Burke E.A., et al.: Probability model for peak fluxes of solar proton events. IEEE Trans. on Nuclear Science, 45 (6), 2948-2953, 1998

Wave Acceleration and Loss in the Earth's Radiation Belts

Richard Horne[1] and Daniel Boscher[2]

[1] Brittish Antarctic Survey, Cambridge, UK
[2] ONERA/DESP, Toulouse, France

Summary. High energy electrons trapped inside the Van Allen radiation belts are a hazard for satellites and astronauts. During magnetic storms the electron flux can change by up to five orders of magnitude as a result of acceleration, transport and loss processes. Here we review recent work to understand the basic physical processes, and how they are being incorporated into global models to specify and predict variations in the Van Allen radiation belts.

1 Introduction

The electron flux variations in the outer radiation belt can vary by over five orders of magnitude on a time scales ranging for a few minutes to a few days (Baker and Kanekal, 2007). These variations have been linked to satellite malfunctions, and in some cases total loss, and are also a hazard for astronauts in space. Thus it is important to understand the physical processes responsible for these variations so that better models can be developed to specify the state of the radiation belts, and periods of high risk for satellite operators, designers and insurers.

2 Electron acceleration

Electron flux variations in the radiation belts are a result of an imbalance between acceleration, transport and loss processes. It has been established that electron acceleration occurs inside the magnetosphere (Li et al., 1997) and several acceleration mechanisms have been proposed (see the reviews by Li and Temerin, 2001; Friedel et al., 2002; Horne, 2002). Until recently betatron and Fermi acceleration as a result of transport across the magnetic field (radial diffusion) towards the Earth has been the most widely accepted theory for electron acceleration. This process is much more efficient when ULF waves at frequencies of a few Hz are present (Elkington et al., 1999), and there is a high correlation between the occurrence of ULF waves, flux increases, and the speed of the solar wind (Mathie and Mann, 2000). To diffuse electrons towards the Earth the electron phase space density must increase with increasing L. However, recent observations show that the particle phase space density peaks in the inner region near

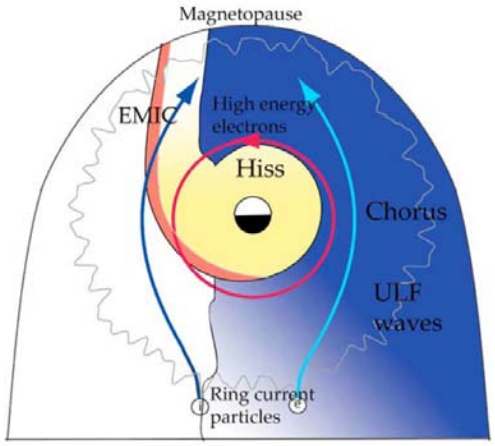

Fig. 1. Schematic diagram showing the regions in MLT where different types of waves can scatter relativistic electrons through resonant interactions. The light and dark blue lines show the convection of injected ring current electrons and ions. The coloured regions show different types of waves which scattere electrons via Doppler shifted cyclotron resonance, and the wavy lines refer to ULF waves. After Shprits et al. (2006a).

$L = 4.5$ and not in the outer region as required by inward radial transport (Green and Kivelson, 2004; Iles et al., 2006). This suggests that a local acceleration mechanism is required, and has opened up an exciting new research area.

Acceleration by wave-particle interactions is the leading candidate for local acceleration (Horne and Thorne, 1998; Summers et al., 1998). In this theory waves at frequencies comparable to the electron cyclotron frequency resonate with the electrons via Doppler shifted cyclotron resonance. The process breaks the first, and therefore all three, adiabatic invariants. There are five different wave modes that could contribute to local acceleration, but the most promising candidate so far is whistler mode chorus waves (Horne and Thorne, 1998; Horne et al., 2003a,b, 2005a,b, 2006; Shprits et al., 2006a,b; Summers et al., 1998, 2004). In this theory a source of low energy electrons ($\sim$10 keV) from the plasma sheet is injected into lower L shells by convective (and inductive) electric fields during substorms. These particles form the seed population. As the particles are injected into regions of higher magnetic field strength an anisotropic distribution develops, peaked perpendicular to the magnetic field, which excites whistler mode waves via Doppler shifted cyclotron resonance (See Fig. 1, after Shprits et al., 2006a). The waves grow by scattering low energy ($\sim$10 keV) electrons at small pitch angles into the atmosphere, but at the same time they are able to resonate with, and scatter, much higher energy electrons at large pitch angles which remain trapped inside the magnetic field. In effect there is a transfer of energy from a large number of low energy electrons at small pitch angles to accelerate a fraction of the population at large pitch angles to higher energies. Providing the wave power is enhanced for a sufficient amount of time the electrons can be diffused to higher energies and result in a net increase in flux.

Over the last few years several pieces of research support the idea of wave acceleration. First, chorus wave power is most intense between $L = 4 - 6$ from midnight MLT, through dawn to the early afternoon sector, corresponding to the peak of the outer radiation belt. Second, chorus wave power increases with magnetic activity outside the plasmapause (Meredith et al., 2001, 2003a,b,c) in regions where the ratio of the electron plasma frequency to gyrofrequency is low, which is the condition required for efficient electron diffusion to higher energies (Horne et al., 2003b). Third, wave acceleration predicts 'flat top' pitch angle dis-

tributions that are flat between about 60–90 degrees, and which are energy dependent. Such distributions have been observed during magnetic storms (Horne et al., 2003a). Fourth, careful modelling of the observed wave power which takes account of both bounce averaging and MLT variations gives a timescale for electron acceleration of the order of 1–2 days, which is comparable to the observed timescale for acceleration (Horne et al., 2005b).

Until now acceleration by whistler mode waves has been the most studied local acceleration process, and this has been treated in quasi-linear diffusion. However, highly non-linear interactions with individual chorus elements are also important for acceleration (Katoh and Omura, 2007) and require more research. Furthermore, other processes such as transit time damping may also be important (e.g., Summers and Ma, 2000).

3 Electron loss

As an electron drifts around the Earth it may encounter several different types of waves. Some waves, such as whistler mode chorus contribute, to acceleration but others, such as plasmaspheric hiss and electromagnetic ion cyclotron waves, contribute to electron loss to the atmosphere. In addition, outward radial diffusion onto open drift orbits as a result of changes in the outer magnetopause boundary may also contribute to electron loss.

Inside the high density plasmapause there are three types of waves that can contribute to electron loss via scattering into the loss cone. They are plasmaspheric hiss, lightning generated whistlers, and whistler mode waves from ground based transmitters (Abel and Thorne, 1998). Hiss tends to dominate the loss rates in the outer plasmapshere at energies of a fee hundred keV to a few MeV (Meredith et al., 2006), but lightning becomes more important for lower L. Transmitters tend to dominate at low L, typically less than $L = 2$.

In the region where the plasmasphere overlaps with the ring current, electromagnetic ion cyclotron waves, at frequencies between the proton gyro-frequency, and the Helium gyrofrequency, and between the Helium gyrofrequency and the Oxygen gyrofrequency are very effective in scattering radiation belt electrons into the loss cone (Summers and Thorne, 2003; Albert, 2003; Glauert and Horne, 2005). However, there is little observational evidence for these waves and more data is required to assess their importance on a global scale.

Outside the plasmapause, whistler mode chorus can also contribute to electron loss as well as acceleration. Whether loss exceeds acceleration depends on several factors, but losses tend to dominate when f_{pe}/f_{ce} is large. Thus information on the plasma density during magnetic storms is very important for determining losses to the atmosphere. EMIC waves are also observed outside the plasmapause, but they are then restricted to scattering electrons with higher energies, typically above 1 MeV, into the loss cone (Meredith et al., 2003b).

4 Global Modelling

For a long time a balance between inward radial transport and electron loss to the atmosphere has been recognised as an important process governing the structure of the quiet time radiation belts (Lyons and Thorne, 1973). Recently several models have been used to study flux variations in the radiation belts where loss due to wave-particle interactions is treated as a

simplified loss term. These models show that the flux in the heart of the radiation belts is underestimated when satellite data at geostationary orbit is used as an outer boundary (Brautigam and Albert, 2000; Shprits and Thorne, 2004; Shprits et al., 2006b), and thus additional local wave acceleration processes must be incorporated into radiation belt models.

One of the most comprehensive global models of the radiation belts is Salammbô (Beutier and Boscher, 1995; Bourdarie et al., 1997, see also Appendix A). This model is based on a Fokker-Planck equation where originally radial transport (radial diffusion), Coulomb collisions, and losses due to plasmaspheric hiss were included as diffusion processes. Wave acceleration and loss due to whistler mode chorus waves has now been included into Salammbô using diffusion coefficients from the PADIE code (Glauert and Horne, 2005), and a database of whistler mode chorus waves (Meredith et al., 2001, 2003c), and shows that wave acceleration is viable process to increase the flux on a global scale during magnetic storms (Varotsou et al., 2005). Salammbô has also been used to model the radiation belts as a co-rotating interaction region interacts with the Earth's magnetosphere, and also shows that wave acceleration can result in a major increase in the radiation belt electron flux during weak long duration magnetic storms (Horne et al., 2006).

Work on including wave processes into global models is at an early stage and there are many uncertainties over the distribution of wave power in MLT, the latitude distribution of the waves, and the effectiveness of different types of wave modes. It is essential that databases of all the different wave modes that can contribute to electron acceleration and loss are developed so that models can be improved. There is also a need to continue measuring the energetic particles and the seed population of electrons that power the waves. This in turn must be matched by developments in modelling to incorporate the data, and reproduce flux variations during magnetic storms and other disturbances more accurately. This is essential to develop a space weather prediction capability.

A Salammbô

Salammbô is a set of codes devoted to the understanding of radiation belt creation and dynamics, which occurs during magnetic activity periods. It solves the classical Fokker-Planck diffusion equation, either for proton or electron radiation belts, in the 3D phase space. The equation is written in terms of the three adiabatic invariants, corresponding to energy, pitch angle and L McIlwain parameter, so this version is a real 2D in space, where the results are averaged on the longitude (local time). There are two versions of the code, one for protons and the other for electrons.

For the proton version, sources are taken as plasma sheet night side injections and solar particle entrance occurring during magnetic storms or substorms, and the well known CRAND (Cosmic Ray Albedo Neutron Decay) phenomenon. Particle transport is assumed to be due to radial diffusion, either given by magnetic or electric perturbations, and to frictional process related to Coulomb interaction with neutrals from the exosphere and cold electrons from the plasmasphere. Losses correspond to the charge exchange phenomenon, a proton giving its energy to a cold hydrogen atom, the resulting cold proton being lost from the radiation belt point of view. Another loss taken into account is inelastic nuclear interactions with Other losses are efficient when the particle precipitates on the Earth (in fact, on the high atmosphere, near 100

km). All these processes are well known from the physical point of view, so they are exactly calculated in the code. Nevertheless, their inputs are less known and they come from different models. For the injections, distribution functions derived from plasma sheet populations are used at the boundary condition, set at $L = 8$. For the CRAND process, an incident cosmic neutron flux is derived from calculations. For the friction, the charge exchange and the inelastic nuclear interaction processes, exosphere neutral model is needed. From Mass-Spectrometer-Incoherent-Scatter neutral atmosphere model MSIS-86 (Hedin et al., 1987) – better at high altitudes than MSIS-90 – and using a hydrostatic model, all the neutral constituents are determined. As for the plasmasphere, we used the Carpenter model (Carpenter and Andersson, 1992), though difficult to extrapolate to non equatorial regions. For the solar particle entrance, a magnetic activity dependent magnetospheric shielding was determined from measurements and modelling. Finally, the most uncertain coefficients are the radial diffusion ones. They were in a first step derived from the work of Schulz and Lanzerotti (1974) and a magnetic activity dependence was added in a second step. Different advances were made with that code, from the influence of the magnetic field or the solar activity to the direct entrance of solar energetic particles during magnetic active periods (Vacaresse et al., 1999).

For the electrons, CRAND was determined to be not efficient, so the only source corresponds to storm and substorm injections. Frictions due to Coulomb interactions are once more used, derived from MSIS + hydrostatic model. Radial diffusion is also used here to transport particles across L shells. For electrons, pitch angle diffusion is here added. This can be due to Coulomb interactions with the neutral atoms or cold plasmaspheric electrons. These particles being many times lighter than protons, they can undergo changes in the pitch angles when interacting with electric field surrounding free electrons or bounded electrons from neutrals. They undergo also pitch angle diffusion when interacting with electromagnetic fields related to the presence of waves. These two pitch angle diffusions directly precipitate electrons into the loss cone. This is an efficient process for the electron loss, directly responsible for the slot region. In the current version, energy diffusion due to the interaction of electrons with whistler mode chorus waves present outside the plasmasphere are also considered (see the main body of the text). The different input models are also time dependent, like radial diffusion or characteristics of the wave, which vary with magnetic activity (Varotsou et al., 2005), and neutrals and the internal magnetic field, which vary with solar activity.

References

Abel, B., and R. M. Thorne (1998), Electron scattering loss in Earth's inner magnetosphere 1. Dominant physical processes, *J. Geophys. Res. 103*, 2385.

Albert, J. M. (2003), Evaluation of quasi-linear diffusion coefficients for EMIC waves in a multispecies plasma *J. Geophys. Res. 108*, doi:10.1029/2002JA009792.

Baker, D. N., and S. G. Kanekal (2007), Solar cycle changes, geomagnetic variations, and energetic particle properties in the inner magnetosphere, /it J. of Atmos. and Solar Terr. Phys., submitted.

Beutier, T., and D. Boscher (1995), A three-dimensional analysis of the electron radiation belt by the *Salammbô* code, *J. Geophys. Res. 100*, 14,853.

Bourdarie, S., D. Boscher, T. Beutier, J. A. Sauvaud, and M. Blanc (1997), Electron and proton radiation belt simulations during storm periods: A new asymmetric convection-diffusion model, *J. Geophys. Res. 102*, 17,541-17,552.

Brautigam, D. H. and J. M. Albert (2000), Radial diffusion analysis of outer radiation belt electrons during the October 9, 1990, magnetic storm *J. Geophys. Res. 105*, 291-309.

Carpenter, D., and R. Anderson (1992), An ISEE/whistler model of equatorial electron density in the magnetosphere, *J. Geophys. Res. 97*, 1097–1108.

Elkington, S. R., M. K. Hudson, and A. A. Chan (1999), Acceleration of relativistic electrons via drift resonant interactions with toroidal-mode Pc-5 ULF oscillations, *Geophys. Res. Lett. 26*, 3273-3276.

Friedel, R. H. W., G. D. Reeves, and T. Obara (2002), Relativistic electron dynamics in the inner magnetosphere–a review, *J. Atmos. Solar-Terr. Phys., 64*, 265.

Glauert, S. A., and R. B. Horne (2005), Calculation of pitch angle and energy diffusion coefficients with the PADIE code, *J. Geophys. Res. 110*, A04206, doi:10.1029/2004JA010851.

Green, J. C., and M. G. Kivelson (2004), Relativistic electrons in the outer radiation belt: Differentiating between acceleration mechanisms, *J. Geophys. Res. 109*, A03213, doi:10.1029/2003JA010153.

Hedin, A. E. (1987), MSIS-86 thermospheric model, *J. Geophys. Res. 92*, 4649.

Horne, R. B. (2002), The contribution of wave particle interactions to electron loss and acceleration in the Earth's radiation belts during geomagnetic storms, in *Review of Radio Science 1999-2002*, edited by W. R. Stone, pp. 801–828, John Wiley, Bognor Regis.

Horne, R. B., and R. M. Thorne (1998), Potential waves for relativistic electron scattering and stochastic acceleration during magnetic storms, *Geophys. Res. Lett. 25*, 3011.

Horne, R. B., N. P. Meredith, R. M. Thorne, D. Heynderickx, R. H. A. Iles, and R. R. Anderson (2003a), Evolution of energetic electron pitch angle distributions during storm time electron acceleration to MeV energies, *J. Geophys. Res. 108*A1, 1016, 10.1029/2002JA009468.

Horne, R. B., S. A. Glauert, and R. M. Thorne (2003b), Resonant diffusion of radiation belt electrons by whistler-mode chorus, *Geophys. Res. Lett. 30*, doi10.1029/2003GL016963.

Horne, R. B., R. M. Thorne, Y. Y. Shprits, N. P. Meredith, S. A. Glauert, A. J. Smith, S. G. Kanekal, D. N. Baker, M. J. Engebretson, J. L. Posch, M. Spasojevic, U. S. Inan, J. S. Pickett, and P. M. E. Decreau (2005a), Wave acceleration of electrons in the van Allen radiation belts, Nature, 437, 227-230.

Horne, R. B., R. M. Thorne, S. A. Glauert, J. M. Albert, N. P. Meredith, and R. R. Anderson (2005b), Timescale for radiation belt electron acceleration by whistler mode chorus waves, *J. Geophys. Res. 110*, A03225, doi:10.1029/2004JA010811.

Horne, R. B., N. P. Meredith, S. A. Glauert, A. Varotsou, D. Boscher, R. M. Thorne, Y. Y. Shprits, and R. R. Anderson (2006), Mechanisms for the acceleration of radiation belt electrons, in Recurrent Magnetic Storms: Corotating Solar Wind Streams, Geophys Monogr. Ser., vol 167, edited by B. T. Tsurutani, R. L. McPherron, W. D. Gonzalez, G. Lu, J. H. A. Sobral and N. Gopalswarmy, pp. 151-173, American Geophysical Union, Washington, D.C.

Iles, R. H. A., N. P. Meredith, A. N. Fazakerley, and R. B. Horne (2006), Phase space density analysis of the outer radiation belt energetic electron dynamics *J. Geophys. Res. 111*, A03204, doi:10.1029/2005JA011206.

Katoh, Y. and Y. Omura (2007), Computer simulation of chorus wave generation in the Earth's inner magnetosphere *Geophys. Res. Lett. 34*, L03102, doi:10.1029/2006GL028594.

Li, X., and M. A. Temerin (2001), The electron radiation belt, *Space Sci. Rev. 95*, 569.

Li, X., D. N. Baker, M. Temerin, D. Larson, R. P. Lin, G. D. Reeves, M. Looper, S. G. Kanekal, and R. A. Mewaldt (1997), Are energetic electrons in the solar wind the source of the outer radiation belt?, *Geophys. Res. Lett. 24*, 923-926.

Lyons, L. R., and R. M. Thorne (1973), Equilibrium structure of radiation belt electrons, *J. Geophys. Res. 78*, 2142-2149.

Mathie, R. A., and I. R. Mann (2000), A correlation between extended intervals of ULF wave power and storm-time geosynchronous relativistic electron flux enhancements, *Geophys. Res. Lett. 27*, 3261.

Meredith, N. P., R. B. Horne, and R. R. Anderson (2001), Substorm dependence of chorus amplitudes: implications for the acceleration of electrons to relativistic energies, *J. Geophys. Res. 106*, 13,165.

Meredith, N. P., M. Cain, R. B. Horne, R. M. Thorne, D. Summers, and R. R. Anderson, (2003a), Evidence for chorus driven electron acceleration to relativistic energies from a survey of geomagnetically disturbed periods, *J. Geophys. Res. 108(A6)*, 1248, doi:10.1029/2002JA009764.

Meredith, N. P., R. M. Thorne, R. B. Horne, D. Summers, B. J. Fraser and R. R. Anderson (2003b), Statistical analysis of relativistic electron energies for cyclotron resonance with EMIC waves observed on CRRES, *J. Geophys. Res. 108*, doi:10.1029/2002JA009700.

Meredith, N. P., R. B. Horne, R. M. Thorne, and R. R. Anderson, (2003c), Favored regions for chorus-driven electron acceleration to relativistic energies in the Earth's outer radiation belt, *Geophys. Res. Lett. 30*, 1871, doi:10.1029/2003GL017698.

Meredith, N. P., R. B. Horne, S. A. Glauert, R. M. Thorne, D. Summers, J. M. Albert, and R. R. Anderson (2006), Energetic outer zone electron loss timescales during low geomagnetic activity, *J. Geophys. Res. 101*, A05212, doi:10.1029/2005JA011516.

Schulz, M. and L. J. Lanzerotti (1974), Particle Diffusion in the Radiation Belts, Springer-Verlag.

Shprits, Y. Y., and R. M. Thorne (2004), Time dependent radial diffusion modeling of relativistic electrons with realistic loss rates, *Geophys. Res. Lett. 31*, doi:10.1029/2004GL019591.

Shprits, Y. Y., W. Li, and R. M. Thorne (2006a), Controlling effect of the pitch angle scattering rates near the edge of the loss cone on electron lifetimes, *J. Geophys. Res.111*, A12206, doi:10.1029/2006JA011758.

Shprits, Y. Y., R. M. Thorne, R. B. Horne, S. A. Glauert, M. Cartwright, C. T. Russell, D. N. Baker, and S. G. Kanekal (2006), Acceleration mechanism responsible for the formation of the new radiation belt during the 2003 Halloween Solar storm, *Geophys. Res. Lett. 33*, (L05104), doi:10.1029/2005GL024256.

Summers, D. and C. Ma, (2000), Rapid acceleration of electrons in the magnetosphere by fast-mode MHD waves, *J. Geophys. Res. 105*, 15,887.

Summers, D., and R. M. Thorne (2003), Relativistic electron pitch-angle scattering by electromagnetic ion cyclotron waves during geomagnetic storms, *J. Geophys. Res. 108*, doi:10.1029/2002JA009489.

Summers, D., R. M. Thorne, and F. Xiao (1998), Relativistic theory of wave-particle resonant diffusion with application to electron acceleration in the magnetosphere, *J. Geophys. Res. 103*, 20,487.

Summers, D., C. Ma, N. P. Meredith, R. B. Horne, R. M. Thorne, and R. R. Anderson (2004), Modeling outer-zone relativistic electron response to whistler mode chorus activity during substorms, *J. Atmos. Solar-Terr. Phys.*, *66*, 133-146.

Vacaresse, A., D. Boscher, S. Bourdarie, M. Blanc, and J.-A. Sauvaud (1999), Modeling the high energy proton belt, *J. Geophys. Res. 104*, 28,601.

Varotsou, A., D. Boscher, S. Bourdarie, R. B. Horne, S. A. Glauert, and N. P. Meredith (2005), Simulation of the outer radiation belt electrons near geosynchronous orbit including both radial diffusion and resonant interaction with whistler-mode chorus waves, *Geophys. Res. Lett. 32*, doi:10.1029/2005GL023282.

The response of ionospheric plasma to the physical processes in the radiation belt regions

H. Rothkaehl[1], K. Kudela[2], R. Bucik[2], and O. Grigoryan[3]

[1] Space Research Centre PAS, Bartycka 18a, 00-716 Warsaw, Poland
[2] Institute of Experimental Physics, SAS, Watsonova 47, 040 01 Kosice, Slovakia
[3] Institute of Nuclear Physics, Moscow State University, 119899 Moscow, Russia

Summary. Despite of the fact, that the analysis of the properties of the Earth's electromagnetic environment has a long history, the physical phenomena relevant to wave–particle interactions in the radiation-belt region and in the projected ionospheric region are still not sufficiently understood. In particular, a description of the energy transfer in the ionosphere–magnetosphere coupling processes should be a major task for investigations in the near future.

Using the wave and plasma diagnostics on-board past low-orbiting satellite missions AUREOL-3, APEX, MAGION-3, CORONAS-I and F, and the currently operating DEMETER satellite, selected physical processes taking place in the topside ionosphere are described. The aim of this paper is to analyze the ionospheric plasma response to the radiation belt particles. We present different types of ionospheric turbulence and instabilities generated by solar, anthropogenic, seismic and thunderstorm activities. The analysis of presented physical processes can enable new operational models for the Space Weather program to be developed.

1 Introduction

Wave particle interactions in the radiation-belt region are one of the key parameters in understanding the global physical processes governing the near-Earth environment. The fluxes of outer radiation belt electrons increase in response to changes in the solar wind and the interplanetary magnetic field, and decrease as a result of scattering into the loss cone and the subsequent absorption by the atmosphere. Recent observations and analyses show that in the radiation belt regions the ULF and VLF waves can accelerate particles up to relativistic energies (Horne and Thorne, 2003; Summers et al., 2007). The analysis carried out by O'Brien et al. (2003) indicates that electron acceleration for low L shell, less than 4.5, is mainly associated with ULF waves and microbursts, while for larger L, i.e., about 4.5, chorus waves are dominant. On the other hand, electromagnetic ion-cyclotron waves can be responsible for loss processes in the radiation belt regions (Meredith et al., 2003). Furthermore, the artificially generated VLF and ELF signals, lighting, and plasmaspheric hiss can contribute to the loss process in the inner belt and slot region of the magnetosphere (Imhof et al., 1984). The most important question in relation to the understanding of physical processes in the radiation belt regions concerns the estimation of the the ratio between acceleration and loss processes.

Moreover, the physical processes of wave-particle interactions in the inner and outer radiation belts can also trigger irregularities and turbulence in the topside ionosphere.

The aim of this paper is to present a review of different types of physical processes detected in ionospheric plasma driven by energetic particles, or by electromagnetic waves generated in the radiation belt regions. We discuss the effects of man-made noises registered in the ionosphere, correlations between seismic activity and bursts of gamma rays, and finally, the consequences of lighting discharge in the atmosphere for the acceleration processes in the radiation belt regions. In order to show an example of the coupling between inner magnetosphere and ionosphere, instabilities inside the main ionospheric trough during geomagnetic disturbances are analyzed.

2 Results

2.1 Electromagnetic pollutions detected in ionospheric plasma

The Earth's ionosphere is subjected to various man-made influences. Electromagnetic emissions observed in the nearest Earth environment are a superposition of natural emissions and various types of man-made noises.

The HF diagnostics on-board low-orbiting satellites in the topside ionosphere have detected increased intensities of about 20 dB/μV above the background radiation over the Euro-Asia region (Klos et al., 1997; Rothkaehl et al., 1997, 1999). As an example, in Fig. 1, the maps of HF noises before a strong geomagnetic storm on 31 March 1994 are presented for the 0.1–15 MHz band registered on-board CORONAS-I satellite. The figure shows natural plasma emissions as well as artificially generated plasma instabilities and electromagnetic fluxes transmitted primarily to the ionosphere by the network of broadcasting stations. Enhanced HF emissions are weaker in the southern hemisphere, but the observed correlation is still pronounced. These remarkable enhancements of the HF background emission are correlated with the position of the maximum flux of precipitating high-energy particles in the outer radiation belts, as observed in the 0.5–1.5 MeV energy range.

The enhancement of background radiation is prominent in the eastern hemisphere. The observed effect is markedly visible and stronger in the night-side ionosphere. Strong geomagnetic disturbances can broaden the area of the observed intensification of HF noises in comparison with the geomagnetic quiet time, but the intensity of the observed enhancement is not affected by geomagnetic disturbances.

The model proposed by Rothkaehl and Klos (2003) indicates that the observed broadband emissions in HF frequency range are a superposition of natural plasma emissions and man-made noises. Permanent pumping of the electromagnetic waves from the ground to the ionosphere and the penetration of energetic particles from the radiation belts can, as a consequence, disturb top-side ionosphere and lead to the generation of ionospheric plasma turbulence. Unfortunately, all HF frequency experiments were performed without good low frequency ionospheric plasma diagnostics. The examination of the data gathered on ARCAD-3 satellite helped to find the emissions in the VLF frequency range correlated it with broadband HF emissions detected over Europe and Asia region (Rothkaehl and Parrot, 2005). Assuming a

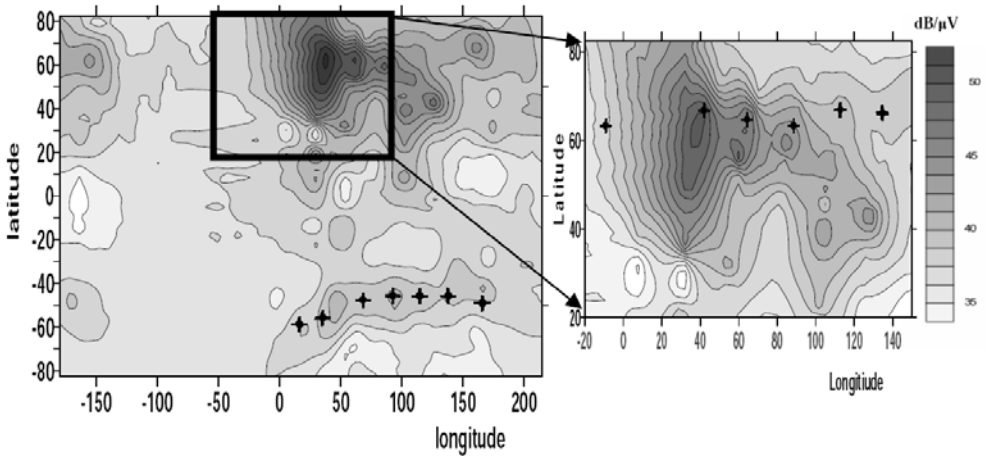

Fig. 1. The global distribution of the intensity of the electromagnetic emissions (integrated in the frequency range 0.1–15 MHz) recorded by SORS-1 instrument on board the Coronas-I satellite at 500 km altitude during night-time sector, under quiet geomagnetic conditions on 30 March 1994. The location of the maximum of the outer radiation belt determined by the high-energy particle detection in the 0.5–1.5 MeV energy range, on board Coronas-I satellite is marked by cross points.

simple model of two-component ionospheric plasma (cold background plasma and suprathermal electron beams) the coefficient of electromagnetic radiation created by the scattering of suprathermal electrons on the Langmuir or ion-acoustic turbulence was calculated. The theoretical analysis showed that this process is effective to create broadband emissions in the high frequency range. The consideration shows that the emitted power of observed broadband emission is in order of 10^{-18} W m^{-2} Hz^{-1}. Moreover, theoretical analysis shows that the generation of ion-acoustic turbulence is far more effective (Rothkaehl and Klos, 2003). The radiation belts can be a natural source of hot electrons, furthermore, the permanent pumping of strong electromagnetic waves into the atmosphere can cause an increased flux of precipitating energetic particles. The scattering of suprathermal electrons from the radiation belts on ion-acoustic or Langmuir turbulence is proposed as a mechanism of generation of broadband HF emissions.

2.2 The HF electromagnetic emissions and high energy electrons distribution

In the top-side ionosphere, the properties of ionospheric plasma can be affected by the domination of dense plasma (i.e., where the electron plasma frequency is greater than the electron cyclotron frequency). The analysed HF range covers high-frequency whistler waves, as well as Langmuir and upper hybrid modes of the natural plasma emissions. On the other hand, the non-linear plasma interaction can appear as a broadband turbulent spectrum.

Gamma-ray fluxes observed in the near-Earth space experiments are a superposition of atmospheric and local emissions produced in the interaction of primary and secondary cosmic rays, the Van Allen radiation, or the interaction of solar cosmic rays with the material of

the instrument and the satellite body. Atmospheric gamma rays are produced by interactions of cosmic ray protons, alpha particles, and electrons with oxygen and nitrogen nuclei in the atmosphere. At higher energies, gamma rays are created mainly by the decay of π^0 mesons from high energy nuclear interactions, while at lower energies the gamma rays are produced primarily by electron bremsstrahlung. (Bucik et al., 2000)

The analysis of electron fluxes with energy 30–500 keV registered on board ACTIVE satellite indicated two regions of flux maxima at $L = 1.3$ and $L = 1.6 - 1.8$ for different altitudes from 500 km up to 1100 km (Grigoryan et al., 2007). On the other hand, the analysis of the HF wave observations gathered on-board low-orbiting satellites APEX, ACTIVE, and CORONAS-I showed that the maximum of mean HF emissions, in the frequency band around the local gyrofrequency, mainly occurs during the night time and is related to the position of the radiation belts. Also, minor enhancements of these emissions are observed close to the geomagnetic equator (below the electron density equatorial anomaly) and close to the South-Atlantic Anomaly (SAA) region (Rothkaehl et al., 2006).

2.3 The ionospheric plasma response to seismic activity

Recent monitoring of the space plasma environment has shown that the electromagnetic noises detected at the ionospheric altitudes can also be caused by cataclysmic processes occurring on the surface of the Earth (Pulinets, 2007). A case study of HF-wave and gamma-ray measurements performed on-board CORONAS-I satellite shows enhancements of the whistler wave activity and soft gamma-ray fluxes, simultaneously, in ionospheric plasma over the seismic centre. One examples of such events is presented in Figure 2 (Rothkaehl et al., 2006).

Parallel to the well-known effects related to the seismic activity in the topside ionosphere, such as small-scale irregularities generated by acoustic waves and large-scale irregularities generated by anomalous electric fields, the modifications of magnetic flux tubes are also common features (Pulinets et al., 2002). The intensification of precipitating high-energy electrons and protons with simultaneous excitation of ELF and VLF noises above the earthquake epicentre was previously registered in the top side ionosphere as well. So it seems that changes in the magnetic flux tube topology can lead to increased precipitation of energetic electrons and, as a consequence, can yield excitation of the HF whistler mode very close to the local electron gyrofrequency. The precipitating energetic electrons generate the excitation of the HF whistler mode emission, via the incoherent Cherenkov mechanism. The proposed process has a cascade-like character (Rothkaehl et al., 2006).

2.4 The atmospheric discharge processes

Theoretical investigation and some observation campaigns show that whistler signals, generated by lightning discharges, can contribute significantly to the energetic balance in radiation belt regions. However, observations of hard X-rays associated with electron precipitation caused by lightning flashes are rare.

Electromagnetic energy originating in lightning discharges escapes into the magnetosphere and propagates as a whistler mode wave. The whistler mode pitch-angle scatters (and thus precipitates) energetic electrons, thereby generating bremsstrahlung hard X-rays. The theoretical investigation demonstrates that near the equatorial plane of the magnetosphere,

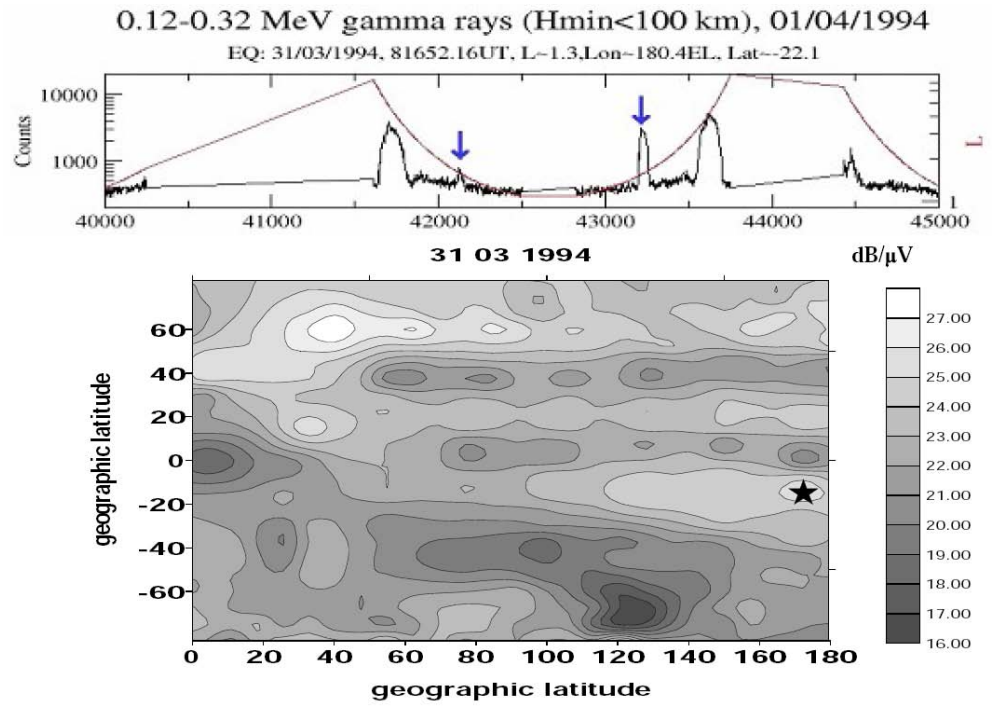

Fig. 2. Global distribution of spectral intensity integrated in the frequency range 0.1–2.0 MHz (up to the local electron gyrofrequency) during quiet geomagnetic conditions. The spectra were registered at various night times on 31 March 1994, by SORS instrument on board the CORONAS-I satellite. The position of maximum HF wave activity and the epicentre of the earthquake is marked by star, bottom panel. The upper panel presents gamma-ray fluxes in the 0.12–0.32-MeV energy range, detected 12 hours after the main shock of seismic activity (the earthquake occurs at 22:41 UT) by SORS instrument over the seismic epicentre. The arrows mark the enhancement of BLC electron fluxes over the seismic epicentre at $L \sim 1.56$ (two peaks on the same field line at $\sim$200 degrees), at 11:42 UT in the southern hemisphere and at 12:00 UT in the northern hemisphere.

whistler components above the nose frequency can accelerate energetic electrons. This acceleration takes place when the gyro-resonant electrons are trapped by the wave field. The acceleration rate in this regime is much larger than stochastic acceleration in the untrapped regime (Trakhtengerts et al., 2003). Highly anisotropic distributions of van Allen radiation belt electrons with 'pancake' pitch angle distributions can result from such an acceleration.

Examination of October–December 2002 SONG (SOlar Neutron and Gamma rays) data aboard CORONAS-F satellite has revealed many X-ray enhanced emissions (30–500 keV) in the slot region ($L \simeq 2$–3) between the Earth's radiation belts (Bucik et al., 2006). In one case, CORONAS-F data were analysed when the intense hard X-ray emissions were seen westward of the SAA in a rather wide L shell range from 1.7 to 2.6. Enhanced fluxes observed on 12 November were most likely associated with a Major Severe Weather Outbreak in Eastern USA, producing extensive lightning flashes, as was documented by simultaneous optical ob-

servations from space. We propose that whistler mode waves from these lightning discharges cause precipitation of energetic electrons from the radiation belts, which, in turn, produces atmospheric X-rays in the southern hemisphere. The future investigation and simultaneous registration of X-rays and HF waves can, thus, give us new information about the physics of radiation belt regions. The experiments devoted to the investigation of the relationship between thunderstorm activity and the appearance of highly anisotropic energetic electrons and wave activity can be a milestone towards understanding the physical processes of the near-Earth environment.

2.5 Links between the main ionospheric trough region and the plasmapause region

Mid-latitude trough region seems to be one of the regions where ionosphere–magnetosphere coupling processes can be observed, particularly during varying geomagnetic parameters. The mid-latitude electron density trough observed in the topside ionosphere has been shown to be the near-Earth signature of the magnetospheric plasmapause, and thus its behaviour can provide useful information about the magnetospheric dynamics, since its existence is dependent on magnetospherically induced motions (Quegan et al., 1982; Tulunay et al., 2003).

Main ionospheric trough is a night-side phenomenon. This depletion in electron density is very often inversely correlated with electron temperature. The main ionospheric trough feature is a very dynamic structure. It is well-known that the trough structure moves to lower altitudes with both the increasing level of geomagnetic activity and the increasing time interval from the local magnetic midnight. As is usually observed, the main ionospheric trough moves to lower latitudes during the main phase of a geomagnetic storm. The observations carried out on-board DEMETER satellite indicate an intensification of broadband VLF and LF waves inside the trough region during increased geomagnetic activity, see Fig. 3. The same effect, but only in HF and VLF frequency bands, was detected by wave experiments located on-board MAGION-3 satellite (Rothkaehl et al., 1997). The examination of HF radio emissions registered on-board MAGION-3 indicates an enhancement of HF emissions at frequencies higher than the local upper hybrid limit. These broadband emissions were detected very close to, but inside, the projected border of the plasmapause to the ionospheric level. Lingering broadband emissions inside the plasmasphere close to the plasmapause after strong geomagnetic disturbances have also been detected. They have been registered inside the trough up to the border of the auroral oval. These types of emissions are mainly correlated with low-frequency radiation, which is excited by the wave-particle interactions in the equatorial plasmapause and moves to the ionosphere along the geomagnetic field line heating the particles (mainly protons). As a consequence of this process we can observe the enhancements of electron acoustic or Langmuir turbulence in the topside ionosphere (Kazanov et al., 1994). Finally, suprathermal electrons can interact with such electrostatic waves and excite broadband HF emissions.

3 Summary

A description of near Earth space plasma behavior is a subject of investigation, both as a constituent of the geophysical environment, and as an element of physical processes in which

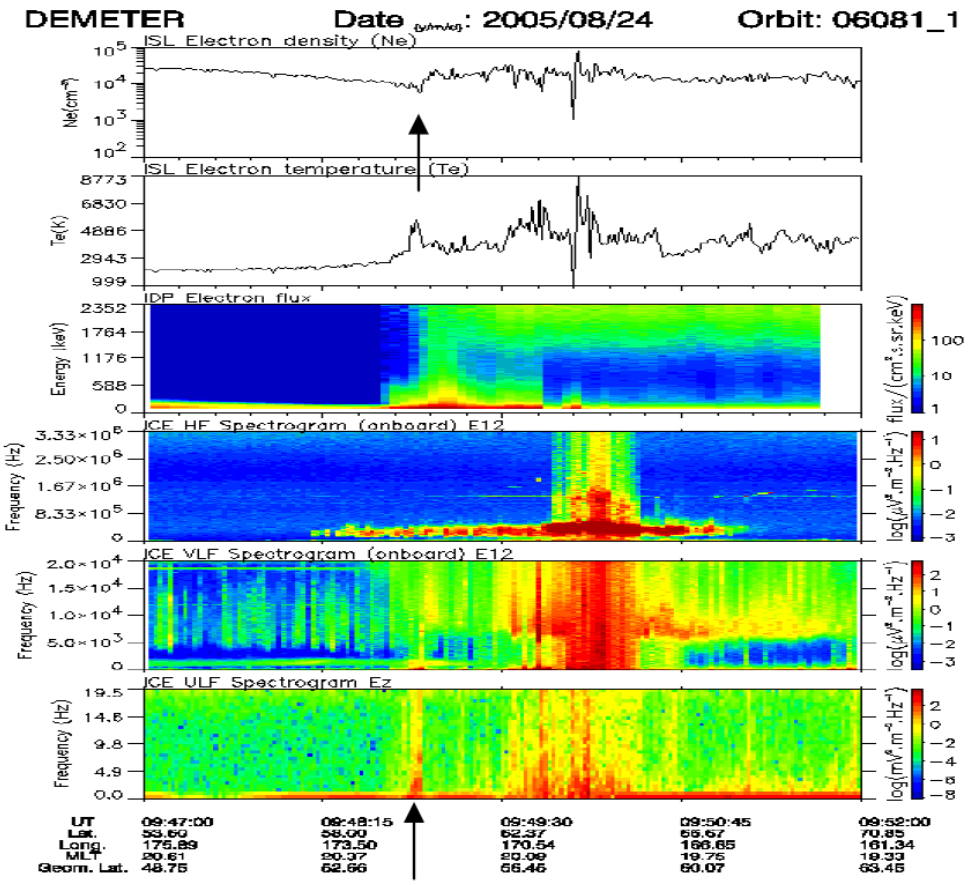

Fig. 3. The sequence of wave and plasma measurements was registered onboard Demeter satellite on 24 August 2005 during the growth phase of the geomagnetic storm. The arrow marks the position of the main ionospheric trough.

particles and waves participate. Whistler-mode hiss, chorus, and EMIC waves are now believed to act in processes of electron acceleration and loss in the radiation belts at rates greater than hitherto estimated. The feedback between the radiation belt region and the Earth atmosphere can be very important, although it is still not fully understood.

In order to mitigate the radiation hazards to space-borne experiments and space exploration programs, we need to elaborate on a new radiation belt model including, apart from a description of different types of physical processes driven by energetic particle fluxes, also a description of wave-particle interactions at ionospheric altitudes.

Recent investigations have shown that also human activity can perturb the near-Earth space environment. They indicate that the observed significant enhancements of electromagnetic turbulence over Europe and Asia are caused by permanent pumping of electromagnetic

waves into the ionosphere by a system of broadcasting stations. This effect can be intensified by precipitation of energetic particles from the radiation belts.

The correlation between earthquakes and anomalous bursts of trapped particles, precipitating from the lower boundary of inner radiation belt was observed as an intensification of HF wave activity by in-situ topside experiments. It seems that changes of the magnetic flux tube topology, correlated with seismic activity, can lead to an increase in the precipitation of energetic electron fluxes and, as a consequence, lead to an excitation of the HF whistler mode.

Theoretical investigations and some space-borne and ground-based experiments show that natural whistler waves generated by a lightning discharge in the Earth's atmosphere can accelerate the trapped radiation belt electrons.

The emissions detected inside the mid-latitude electron density trough, particularly during disturbed geomagnetic conditions are generated by local indicators as well as by remote physical processes localised on the equator of the plasmapause. In order to better understand the problems discussed above, we urgently need multi-point and multi-scale measurements carried out by newly designed instruments with an improved temporal and spatial resolution. This should help us to achieve a comprehensive understanding of the combined natural and anthropogenic plasma processes and their interactions with the geospace. The community of users potentially benefitting from these investigations is found in the civilian and the defence sectors and include the aviation industry, the satellite industry, the HF equipment manufacturers, the HF broadcast and communication services, and the trans-ionospheric radio operation (GPS, GLONASS, Galileo).

Acknowledgments

This research was supported by Polish Ministry of Sciences grant COST/43/2007. The authors wish to thank M. Parot, J.-J. Berthelier, and J.-P. Lebreton for the access to Demeter data.

References

Bucik, R., K. Kudela, A.V. Bogomolov, I.N. Myagkova, S.N. Kuznetsov, S.P. Ryumin: Distribution of gamma ray fluxes at altitude 500 km CORONAS-I data. Acta Phys. Slovaca 50 (1), 267–2742, 2000.

Bucik, R., K. Kudela, S.N. Kuznetsov: Satellite observations of lightning-induced hard X-ray flux enhancements in the conjugate region. Ann. Geophys., 24, 1969–1976, 2006.

Grigoryan, O., K. Kudela, H. Rothkaehl, V. Sheveleva: The electron formations under the radiation belts at L-shells 1.2–1.9. Adv Space Res., doi:10.1016/j.asr.2006.11.008, 2007.

Horne, R.B., R.M. Thorne: Relativistic electron acceleration and precipitation during resonant interactions with whistler-mode chorus. Geophys. Res. Lett., 30(10), 1527, 2003.

Imhof, W.L., J.B. Regan, E.F. Gaines, D.W. Datlowe: The L shell region of importance for wave emitted at ground level as a loss mechanism for trapped electron >68 keV, J. Geophys. Res., 89, 10827–10835, 1984.

Kazanov, G.V., T.I. Gombosi, O.A. Gorbachev, A.A. Trukhan, R.H. Miller: Thermodynamic Effect Of The Ion Sound Instability In The Ionosphere. J. Geophys. Res., 99, A4, 5721–5726, 1994.

Klos, Z., H. Rothkaehl, Z. Zbyszyński, S. Kuznetsov, O. Gregorian, N.I. Budko, I.S. Prutensky, S.A. Pulinets: The global distribution of HF emission in related to the high energy particle precipitation: in Plasma 97 – Research and applications of plasmas. Ed. M. Sadowski, H. Rothkaehl, 1, 1997.

Meredith, N.P., R.M. Thorne, R.B. Horne, D. Summers, B.J. Fraser, and R.R. Anderson: Statistical analysis of relativistic electron energies for cyclotron resonance with EMIC waves observed on CRRES. J. Geophys. Res., 108(A6), 1250, 2003.

O'Brien, T.P., K.R. Lorentzen, I.R. Mann, N.P. Meredith, J.B. Blake, J.F. Fennell, M.D. Looper, D.K. Milling, and R.R. Anderson: Energization of relativistic electrons in the presence of ULF power and MeV microbursts: Evidence for dual ULF and VLF acceleration. J. Geophys. Res., 108(A8), 1329, doi:10.1029/2002JA009784., 2003.

Pulinets, S.A., K.A. Boyarchuk, V.V. Hegai, A.V. Karelin: Conception and model of seismo-ionosphere-magnetosphere coupling. In: M. Hayakawa, O.A. Molchanov (eds.): Seismo Electromagnetics: Lithosphere–Atmosphere–Ionosphere coupling. (Terrapub: Tokyo) 353–361, 2002.

Pulinets, S.A.: Natural radioactivity, earthquakes and the ionosphere. EOS, 88(20), 217–218, 2007.

Rothkaehl, H., F. Jiříček, S. Šmilauer, M. Förster: Dynamic Changes in the Outer Ionosphere in the Region of the Ionospheric Trough During an Intense Magnetic Storm. Adv. Space Res., 20/3, 409–414, 1997.

Rothkaehl, H., Z. Klos, Z. Zbyszyński, S. Kuznetsov, O. Gregorian, J. Gotseljuk, N.I. Budko, I.S. Prutensky, S.A. Pulinets: The Global Distribution of RF Emission In The Topside Ionosphere and High Energy Particle Precipitation. J. Techn. Phys., 40, 313–316, 1999.

Rothkaehl, H., Z. Klos: Broadband HF emissions as an indicator of global changes within the ionosphere. Adv. Space Res., 31, 5, 2003.

Rothkaehl, H., and M. Parrot: Electromagnetic emission detected in the topside ionosphere related to human activity, J. Atm. Solar-Terr. Phys., 67, 821–828, 2005.

Rothkaehl, H., R. Bucik , K. Kudela: Ionospheric plasma response to the seismic activity. Physics and Chemistry of the Earth, 31,473–481, 2006.

Summers, D., N. Binbin, N.P. Meredith: Timescales for radiation belt electron acceleration, and loss due to resonant wave-particle interactions. J. Geophys. Res., 112, A04206, 2007.

Quegan, S., G.J. Bailey, R.J. Mofflett, T.J. Heelis, T.J. Fuller-Rowell, D. Rees, W. Spiro: A theoretical study of the distribution of ionisation in the high-latitude ionosphere and plasmasphere: first results on the mid-latitude trough and the light-ion trough. J. Atmosph. Terr. Phys., 44, 7, 1982.

Trakhtengerts, V.Y., M.J. Rycroft, D. Nunn, A.G. Demekhov: Cyclotron acceleration of radiation belt electrons by whistlers. J. Geophys. Res.,108(A3), 1138, 2003.

Tulunay, Y., I. Stanisawska, H. Rothkaehl: Revisiting the Ariel Trough Work for HF Telecommunication Purposes. Cosmic Res., 41(4), 319–331, 2003.

Radiation Effects Aboard Unmanned Earth Orbiting Spacecraft

Susan M. P. McKenna-Lawlor

Space Technology Ireland, National University of Ireland, Maynooth, Co. Kildare

Summary. Spacecraft responses to the ambient plasma environment are outlined including anomalous behaviour and failure following plasma induced charging (external and internal). Also sputtering effects; surface erosion due to oxidation; phantom commands; induced mode switching; loss of altitude control/orientation; loss of signal phase and amplitude lock; solar cell degradation and common electronic malfunctions are briefly described.

Surface Charging. The accumulation of electric charge on surfaces exposed to space constitutes the most significant cause of spacecraft anomalies leading to mission failure. Such charging is a consequence of interactions between spacecraft surfaces and space plasma, geomagnetic fields and solar electromagnetic radiation. The plasma environment of an Earth orbiting spacecraft depends on both its own gaseous products and location. Close to the Earth, plasma and EUV radiation constitute the major sources of charging currents. In a particular ambience, a spacecraft can accumulate charge until an equilibrium situation is reached at which the net current is zero. See the expression developed by Purvis et al. (1984) to approximate this current balance.

Spacecraft Charging in GEO. At $\sim$35,000 km where the ambient plasma is typically hot, tenuous and highly variable, the equilibrium potential of a spacecraft is typically a few volts positive as a result of the balancing pertaining between photoemission and charged particle collection. Electrons with several keV energies can precipitate during magnetic storms and, if the spacecraft then enters an eclipse so that the photoelectron current vanishes, surface charging to a negative potential of the same order of magnitude as the energies of the impacting electrons rapidly occurs. Such charging can occur differentially leading, thereby, to arcing which: causes physical damage to spacecraft materials; degradation of solar arrays and the generation of onboard noise. In such circumstances operational anomalies and even overall spacecraft failure can ensue.

The well known dawn-side drift of Earthward moving electrons in the geomagnetic field leads to circumstances that characterize most spacecraft anomalies that are related to surface charging in the midnight-to-dawn local time sector. On emerging from eclipse, the sunlit surfaces of a spacecraft charge up positively due to photoelectric emission. However, some parts of the structure may remain at a high negative potential through being in shadow. Also, in-

dividual surface materials may discharge at different rates, thereby creating large differential potentials. General guidelines concerning the assessment and control of spacecraft charging in GEO are contained in Purvis et al. (1984).

A relatively recent analysis based on *in situ* geosynchronous satellite data by Lai and Della-Rose (2001) indicates that spacecraft charging in a Maxwellian space environment depends solely on a critical (threshold) electron temperature. In this regard, whereas the electron-induced secondary-electron coefficient controls the onset of spacecraft charging from approximately -1 to -2 kV, the backscattered-electron emission coefficient and the ion-induced electron emission coefficient control the charging level at potentials beyond -3 to -4 kV.

Spacecraft Charging in LEO. At $\sim$100–1000 km (LEO) the plasma is dense, cool and rather stable so that low inclination orbits in this regime offer a relatively benign environment with regard to spacecraft charging. The spacecraft may be regarded as closely coupled to this dense ambient plasma and surface potentials of, at the most, a few volts are typically displayed. In high latitude polar orbits although the relevant plasma densities have similar values, intense fluxes of precipitating energetic (5–10 keV) electrons associated with auroral production can, in addition, be present. The impingement of these latter particles on spacecraft surfaces can produce differential surface charging. In LEO a spacecraft moves with a velocity that is in excess of the velocities of ambient thermal ions although somewhat lower than the velocities of ambient electrons. A plasma wake characterized by ion depletion can, accordingly, form behind the spacecraft and in the case of a structure where significant ram induced ion current collection occurs at the time when a large ion-free wake is created, onboard problems due to differential charging can become significant (Katz et al., 1985). Recent simulations of wake formation and their comparison with in situ spacecraft data are contained in Engwall and Eriksson (2005) and in Engwall et al. (2006).

If a large, energetic precipitating electron current impinges on wake related surfaces at a time when photoemission is blocked due to eclipse conditions, a catastrophic discharge can ensue. The consequences of such discharges range from transient operational anomalies to permanent failure. Discharges can occur via dielectric breakdown (punch through) or between particular surfaces (flash over). Broadband electromagnetic fields are associatively produced which can couple with the spacecraft electronics. Effects can include: physical damage to/degradation of surface materials (e.g. due to sputtering resulting from the attraction to the spacecraft surface of chemically active species); operational anomalies (such as telemetry glitches); logic upsets; component failures and spurious commands.

Investigations aboard DMSP spacecraft of charging in $\sim$840 km orbits at inclinations of $\sim 90^\circ$ suggest that vehicle size is an important factor with regard to charging. See the discussions of: circumstances that influence environmental interactions between a spacecraft and its surroundings; the several interaction mechanisms that can occur; consequences for particular spacecraft and mitigating strategies contained in Stevens and Kilpatrick (1986) and in Martin et al. (1990). It is noted that damage to surfaces and cables due to impinging micrometeroids/space debris can have a significant effect on arcing thresholds.

Internal Charging. Internal Charging occurs when impinging particles have sufficient energy to penetrate below the surface of a dielectric material and become trapped. Electrons with energies $\geq$100 keV can penetrate a surface metallization layer $\sim 100\ \mu$m thick. Such penetrating electrons become embedded in thermal blankets, coaxial cables, circuit boards and other in-

sulating materials. Energetic (1 MeV) electrons can penetrate a 2 mm thick aluminium layer. Protons require considerably higher energies to achieve similar penetration and since, in addition, their intensities fall off steeply with energy these latter particles are not perceived to pose a serious hazard with regard to internal charging.

High energy Van Allen belt electrons can penetrate the skin of a spacecraft and establish a negative potential on internal dielectric materials/floating conductors. A fluence of $10^{10}-10^{11}$ electrons/cm^2 with $E > 100$ keV over a period sufficient to dominate the pertaining dielectric leakage rate can, for instance, build up a charge on metalized areas of a circuit board that is sufficient to produce local arcing and associatively generate an electromagnetic pulse enduring for the order of tens of nanoseconds. Internal charging can affect: wire insulation; electrical connectors; feed throughs etc. Rapid/sustained internal discharge effects, including: arcing inside cables and Lichtenberg pattern arcs, give rise to onboard problems ranging from: the generation of electromagnetic interference, electronic damage; logic upsets; material degradation; optical emissions; spacecraft contamination and the generation of unforeseen forces and torques on individual spacecraft.

An internal discharge is potentially more damaging than an external one since it occurs in close proximity to sensitive, onboard, electronic circuitry. Studies made in GEO aboard the CRRES spacecraft indicate that "most environmentally induced spacecraft anomalies result from deep dielectric charging and resulting discharge pulses and not from surface insulator charging or single event upsets" (Gussenhoven et al., 1996). For a description of specific situations within that can potentially result in deleterious surface and internal charging see Stevens and Kilpatrick (1986) and Martin et al. (1990). A study of solar cycle and seasonal dependencies on spacecraft anomalies generated due to internal charging is presented in Wrenn et al. (2002).

Initial steps in the matter of taking existing NASA guidelines for preventing surface electrostatic charging (Purvis et al., 1984) and internal electrostatic charging (Whittlesey and Garrett, 1999) and combining these with recent laboratory and in orbit findings, have been made by Garrett and Whittlesey (2006). The necessary mitigation measures thus derived are thereafter discussed in terms of their implications for the engineering design and testing of future spacecraft.

Sputtering From Spacecraft Surfaces. Atmospheric constituents impinge on the surface of an Earth orbiting spacecraft with kinetic energies that vary according to the particle mass and spacecraft velocity concerned. Excited impacting species display, in addition to kinetic energy, excitation and ionization potential energies that can reach $\sim$25 keV/particle. The recombination of such atoms at the spacecraft surface to form diatomic molecules involves the release of energy and further energy is released through the formation of surface compounds. In LEO the majority of the collisional energies involved in gas-surface interactions have values similar to the surface binding energies of atoms in a solid. Thus, depending on the degree of surface localization concerned, it is possible for bond breaking to occur, resulting in the ejection of atoms and molecules. Early sputtering calculations (Laher and Megill, 1988) relevant to the most abundant atmospheric constituents indicate that significant surface degradation of cadmium, thalium, zinc, lead and indium can occur in LEO as a result of exposure times of the order of months. For magnesium tin, silver and gold corresponding degradation requires exposure times of years.

Atomic oxygen, which is formed when solar UV radiation dissociates molecular oxygen, is the dominant component in the Earth's atmosphere between ∼200 and 600 km. A solar cycle related variation results in a one to two orders of magnitude increase in the numerical density of atomic oxygen present at ∼300 km under solar maximum, quiet, geomagnetic conditions. The impingement of atomic oxygen on a spacecraft depends on the ambient density and relative spacecraft velocity (∼7.2 km/s in the case of an easterly orbit at 400 km altitude) and on the orientation of particular spacecraft surfaces (the worst case fluence occurs on a ram surface at sunspot maximum). Atomic oxygen is highly reactive and produces surface erosion due to oxidation. Also, as the spacecraft exits/enters Earth eclipse associated thermal cycling removes oxidized products from the surface, thereby exposing deeper layers to erosion. This process can, in the case of some materials, weaken structural elements and produce changes in surface properties that, gradually, adversely influence spacecraft thermal control. Mitigating design strategies include: judicious pre-selection of surface materials; minimizing the exposure of high voltage surface areas; choosing operating voltages that remain below possible onboard arcing thresholds and arranging spacecraft grounding to maintain sensitive surfaces near the plasma-electrical potential.

Phantom Commands. Disturbances due to electrical transients produced in association with surface and internal charging can appear to spacecraft systems like commands from the ground (*Phantom Commands*). These transients often occur in the local time period spanning dawn-midnight and midnight-dawn during magnetic storms. This is because during these transitions the photoelectric effect is abruptly rendered either absent or present, thereby potentially triggering an electrical discharge. Also, data recorded aboard GOES spacecraft indicate that there is a close correlation between Phantom Commands and occasions when electrons with $E > 2$ MeV penetrate the skin of a spacecraft. Further, thruster firings can produce changes in the local plasma environment that trigger arc discharges, in consequence of which control of spacecraft power and propulsion systems as well as control of individual scientific instruments can be lost. Also, *Induced Mode Switching* can occur, such that a spacecraft puts itself into standby mode, or otherwise changes its anticipated operational behaviour.

Loss of Altitude Control/Orientation. Variations in the pressure of the solar wind can cause the position of the sunward boundary of the magnetopause (normally located at $\sim 10\, R_E$ from the Earth's centre) to vary. Under conditions of high solar wind velocity and density and a strong southward directed component (Bz) of the Interplanetary Magnetic Field/IMF, the magnetopause can be compressed until it is inside GEO orbit (6.6 R_E). A spacecraft in GEO on the sunward side of the Earth can, under these conditions, be located outside the magnetopause for periods ranging from minutes to hours. When a spacecraft crosses the magnetopause and enters the magnetosheath its onboard sensors register a drop to near zero in the measured magnetic field. Also, the sign of the magnetic field tends to vary erratically and the spacecraft attitude control torques can, under these conditions, be inadvertently applied in the wrong direction. The design of the attitude control system should be such as to enable it to withstand magnetic field torques generated during disturbed conditions. It is noted that during *Solar Energetic Particle* (SEP) events photonic devices such as star trackers and CCDs display an increase in internal noise which can, *inter alia*, result in spacecraft orientation problems.

Loss of Signal Phase and Amplitude Lock. The ionosphere at times becomes highly irregular, thereby causing spacecraft signals traversing this disturbed medium to scintillate at the

receiver. Strong geomagnetic storms can lead to scintillation in the auroral zones. Scintillation effects may cause the phase tracking loops of a receiver to temporarily loose lock (Herox and Kleusberg, 1988), thereby introducing discontinuities in phase derived, biased pseudo ranges that can result in significant signal loss. In the case of the *Global Positioning System* (GPS) this effect not only interferes with telemetry but the system can associatively loose tracking contact with a number of spacecraft, thereby inhibiting precise location finding. The disturbances mentioned also introduce changes in the time it takes signals to traverse the ionosphere. These delays are proportional to the *Total Electron Content* (TEC) along the signal patch and inversely proportional to the square of the frequency of the signal. The pseudo range error accruing to variations in TEC can be up to about 16 m at the zenith and about three times that distance close to the horizon. Again these changes which can occur within times as short as 10 m at high latitudes and on diurnal time scales at mid-latitudes, reduce the accuracy and reliability of the GPS. See also the statistical study of Regar et al. (2006).

Solar Cell Degradation/Displacement Damage. Energetic particles can pass through the protective covers of solar cells on Earth orbiting spacecraft to produce ionization damage and crystal lattice defects (displacement damage). Thus, cell performance typically progressively degrades during the lifetime of a mission (made manifest through an ongoing measured reduction in voltage and current outputs) with implications for the ultimate survival of the concerned spacecraft. Accounts of current methods for calculating radiation damage to solar cells are contained in Messenger et al. (2001) and Morton et al. (2005).

Electronic Malfunctions. When a single particle causes a malfunction in onboard electronic components (e.g. in RAMs, microprocessors, HEX-FET power transistors), the outcome is called a *Single Event Effect* (SEE). These are main of three types, namely *Single Event Upsets* (SEUs), *Single Event Latch-ups* (SELs) and *Single Event Burnouts* (SEBs). An SEU is a soft error consisting of bit flips with no preference between 1 to 0 and 0 to 1. They are generated both by galactic cosmic rays and heavy ions produced during flaring. Particularly potent are ions in the CNO group and those with energies $\geq$2 MeV/n. Protons and heavier ions can also produce SEUs indirectly when they create particles characterized by high *Linear Energy Transfer* (LET) via nuclear reactions near, or within, the sensitive volume of an electronic device. SEUs do not damage the concerned component and a reset or rewriting of the device will restore normal behavior. Single high-Z particles, the application of an over voltage or a sudden flash of X-rays can turn on part of an integrated circuit to produce an SEL. The latched up system concerned must be powered down and switched on again to allow control of the circuit to be regained. However, the anomalous configuration may already have drawn down enough power through the chip to damage it, and even to associatively affect the power supply.

SEBs cause the device concerned to fail permanently. These events include, for instance, burnouts of n-channel power MOSFETs, gate rupture and frozen bits. An SEB may be triggered in a power MOSFET biased in the OFF state when a heavy ion passing through it deposits enough charge to turn the device ON (this susceptibility decreases with increasing temperature). A power MOSFET may undergo Single Event Gate Rupture (SEGR) due to localized dielectric breakdown in the gate oxide. Destruction of dipolar junction transistors can also occur *Single Event Dielectric Ruptures* (SEDRs) occur in CMOS devices and are similar to the SEGRs observed in power MOSFETs. *Total Ionizing Dose* (TID) is used in estimating

the effect produced on electronic components by charged particle radiation. TID is measured in terms of the absorbed dose, which is a measure of the energy absorbed by matter. It is quantified by the gray (Gy), where 1 Gy = 100 rads = 1 J/kg. Long term cumulative damage can cause electronic devices onboard a spacecraft to display increased leakage (with related changes in power consumption); threshold effects; timing changes; increased detector background noise etc. SEEs concern instant failure mechanisms and are expressed in terms of a *random failure rate* whereas TID is concerned with a *mean time to failure*. Spacecraft components can be manufactured to withstand high total doses of radiation. *Survivability* describes the ability of a system to perform its intended functions in space within a stressed environment. *Hardness* defines the environmental stress level which a system can survive. Recent studies to establish the sensitivities of candidate spacecraft electronics to heavy ion and proton induced SEEs are described in O'Bryan et al. (2005). A companion paper by Cochran et al. (2005) deals with the vulnerability of a variety of candidate spacecraft electronics to total ionizing dose and to displacement damage.

Conclusion. Conditions on the Sun, as well as in the solar wind, magnetosphere, thermosphere and ionosphere influence the performance and reliability of spacecraft in ways that are gradually becoming better understood, thereby allowing mitigating strategies to be developed and implemented.

References

Cochran, D. J. et al., Proc. IEEE Nucl. Space Rad. Effects Conf. (Rad. Effects Data Workshop), Seattle, Washington, 11–15 July, 2005

Engwall, E. and A. I. Eriksson, Proc. 7th Internat. School/Symp. Space Simulations, Kyoto, Japan, 26–31 March, 2005.

Engwall, E. et al., Phys. Plasmas, 13, 062904, doi: 10. 1063/1.2199207, 2006.

Garrett, H. D. and A. C. Whittlesey, AIAA-2006-569, Proc. 44th AIAA Aerospace Sci. Meeting & Exhibit. Reno Nevada, 9–12 January, 2006.

Gussenhoven, M. S. et al., IEEE Trans. Nucl. Sci., 43, 353–368, 1996.

Herox, P. and A. Kleusberg, Proc. 5th. Internat. Symp. on Satellite Positioning, Les Cruces, NM 13–17, 1988.

Katz, I. et al., IEEE Trans. Nucl. Sci., 32, 4092–4096, 1985.

Laher, R. R. and L. R. Megill, Planet. Space Sci. 36, 14971–1508, 1988.

Lai, S. T. and D. J. Della-Rose, J. Spacecraft & Rockets, 38, 922–928, 2001.

Martin, A. R. et al., ESA Report CR (P) No.. 3025, 1990.

Messenger, S. R. et al., Prog. in Photovoltaics, 9, No. 2, 103–121, 2001.

Morton, T. L. et al., Doc. ID20050203781.(Publ. NASA Center, Glenn Research Centre) 2005.

O'Bryan, M. V. et al., Proc. IEEE Nucl. Space Rad. Effects Conf. (Rad. Effects Data Workshop), Seattle, Washington, 11–15 July, 2005.

Purvis, C. K. et al., NASA Technical Paper 2361, 1984.

Regar, S. M. et al., Proc. 19th Internat. Tech. Meeting Instit. Nav. Sat. Div., Fort Worth, Texas, 25–26 Sept 2006.

Stevens, N. and M. Kilpatrick, Air Force Geophys. Lab. Publ., AFGL-TR 96-0214, 1986.

Whittlesey, A. and H. Garrett, NASA Hand Bk. 4002, Doc. ID, 20060033875, (Publ. NASA Centre JPL), 1999.
Wrenn, G. I. et al., Ann. Geophys. 20, 953–956. 2002

New results on radiation effects on human health

F. Spurný[1] and T. P. Dachev[2]

[1] Nuclear Physics Institute, Czech Acad. Sci., Prague, (NPI AS CR) Czech Republic;
spurny@ujf.cas.cz
[2] Solar Terrestrial Influence Laboratory, Bulg. Acad. Sci., (STIL-BAS), Sofia, Bulgaria;
tdachev@bas.bg

Summary. Humans are exposed to ionizing radiation all the time, and it is known that it can induce a variety of harmful biological effects. Consequently, it is necessary to quantitatively asses the level of exposure to this radiation as a base for estimating risks due to ionization radiation. During WP 2400 of WG 2 of COST 724 action, a number of spacecraft and aircraft experiments have been performed with both active and passive detectors. A large data base has been created. In this contribution we would like to stress results and their importance obtained in three particular directions: (i) simultaneous investigation of galactic cosmic rays on aircraft and on the International Space Station (ISS); (ii) onboard spacecraft neutron contribution as estimated on the basis of the comparison of results measured with MDU/Liulin equipment onboard ISS, Foton capsule and a commercial aircraft flying at subsonic altitudes; (iii) Complex analysis of the results of long term measurements onboard a Czech Airlines aircraft. The results obtained are presented, analyzed, and discussed, and their complementary nature is underlined. The contribution represents a version of the Final Report of the Work Package 2400 of the COST-724/WG-2: Radiation Environment of the Earth.

1 Introduction

Ionizing radiation is known to induce a variety of biological effects (cell killing, mutation, chromosome aberration, and carcinogenesis). Moreover, except for the various applications of radiation in medicine and industry, we are exposed to radiation all the time – cosmic radiation, nature radionuclides, etc. Consequently, it is necessary to qualitatively and quantitatively assess risks from ionizing radiation and to know patterns and mechanisms of biological effects.

Spacecraft and aircraft crews are exposed to elevated levels of cosmic radiation of galactic and solar origin and to secondary radiation produced in the atmosphere, the vehicle structure and its contents. Following recommendations of the International Commission on Radiological Protection (ICRP) in Publication 60 (ICRP, 1990), the European Union (EU) introduced a revised Basic Safety Standards Directive (EC, 1997) which, *inter alia*, included the exposure to cosmic radiation. This approach has been also adopted by other official documents (NCRP, 2002).

Quantities used to characterise the level of radiation protection of workers and/or humans in general are defined in ICRP Publication 60 (ICRP, 1990). The most basic of them is *effec-*

tive dose E, which considers the influence of radiation quality through *radiation weighting factor* w_R, and the influence of tissue sensitivity through the *tissue weighting factor for tissue or organ* w_T.

Operational quantities were designed by the International Commission on Radiological Units and Measurements (ICRU) to provide appropriate estimates of the protection quantities and to serve as calibration quantities for dosimetric devices. Operational quantities are based on the dose equivalent concept. The dose equivalent H is derived from the following relation:

$$H = Q \cdot D = \int Q(L) D_L dL \tag{1}$$

where D_L is the distribution of the dose D in linear energy transfer L and $Q(L)$ is the quality factor as a function of L in water.

For area monitoring of strongly penetrating radiation (as in space) ICRU recommends the quantity ambient dose equivalent, $H^*(d)$, defined at a point in a radiation field, "that would be produced by the corresponding aligned and expanded field, in the ICRU sphere at a depth, d, on the radius opposing the direction of the aligned field". The recommended depth, d, for monitoring in terms of $H^*(d)$ is 10 mm. Relevant reference conversion coefficients are available in ICRP Publication 74 and ICRU Report 57 (ICRP, 1996; ICRU, 1998).

The radiation fields onboard space- and/or aircraft are complex, with many types of ionizing radiation present with energies ranging up to many GeV.

There are three primary principal sources contributing to the radiation exposure close to the Earth (Kovalev and Vorobjov, 1983; Wilson et al., 1991):

1. Galactic cosmic radiation;
2. Radiation emitted during solar flares; and
3. Radiation of Earth's radiation belts.

While the first two can contribute to the exposure even at the Earth's surface, the third has to be considered only outside of the Earth's atmosphere. The levels of the exposure corresponding to these primary radiation sources can be briefly characterised as follows:

Galactic cosmic radiation (GCR) continuously impinges on the Earth by a nearly isotropic flux and consists of about 85% protons, 12.5% alphas, 1.5% heavier nuclei, and 1% electrons. The average energy of cosmic-ray particles outside of magnetosphere is about 1 GeV/nucleon, but particles with up to 10^{21} eV have been observed. The intensities and the components of the radiation field change with the geomagnetic latitude and altitude and with the solar activity. Typical annual values of the ambient dose equivalent due to this radiation in open space outside of the Earth's atmosphere and magnetosphere are presented in Table 1. These values diminish roughly three times behind the typical ($\sim$20 g cm^{-2}) shield thickness of a spacecraft, and the average quality factor decreases to about 2.0 – 3.0.

Solar particle events are not predictable either in their intensity nor in their energy spectrum. They consist mostly ($\sim$99%) of protons and are generally not isotropic. For the most energetic of known solar flares, which occurred February 23, 1956, the dose equivalent estimated in blood forming organs without a shield was about 1 Sv; for the others it was fortunately at least one or more orders of magnitude lower (O'Brien et al., 1996).

As far as **radiation belts** are concerned, doses due to them in open space are very high. However, due to their low energies ($\sim$ MeV for electrons, $\sim$ 100 MeV for protons), they

Table 1. Typical annual exposure levels due to GCR in open space at 1 AU

Dose quantity [unit]	Solar maximum	Solar minimum
D [Gy]	$\sim$0.06	$\sim$0.18
$H^*(10)$ [Sv]	$\sim$0.4	$\sim$1.0
Quality factor	$\sim$6	$\sim$5

are effectively shielded off by the spacecraft wall. Nevertheless their contribution is by far non-negligible for spacecraft orbit inclination of $\sim 50^\circ$ (as for ISS). In this case radiation belt protons contribute to the level of exposure a little more than 50% in the dose, a little less than 50% in the dose equivalent. They have to be seriously considered for planning of extra-vehicular-activities (EVA).

Fig. 1 presents an example of how the radiation from galactic and radiation belt sources are seen on real measurements at low-Earth orbiting satellites, such as Foton M2.

When compared with the Earth's surface, the specifics of onboard space- or air-craft radiation fields and their consequences can be summarized as:

- The exposure level is much higher, about 50 times onboard aircraft, up to 1000 times onboard spacecraft. Nevertheless, it is still a "low-dose" region when considering acute risk.
- However, solar flares can increase this level up to orders of magnitude in open space, and somewhat less onboard aircraft.
- The contribution to the effective dose from external exposure of radiation with high linear energy transfer (LET) is typically about 50% in these fields, compared to less than 10% for occupational exposures on Earth.
- About 50% of the personnel exposed onboard aircraft are women in reproductive age.

When summarized, radiation exposure in space could represent a barrier for particularly long term missions, such as to Mars. Reitz (2005) stated that the main task to be solved to improve the conditions for safe prolongation of human space activities is to diminish uncertainties related to the estimation of the risk. Main uncertainties are related to biological factors. Nevertheless, the improvement of physical knowledge, dosimetric as well as microdosimetric, could also bring an important contribution for diminishing uncertainties related to the estimation of the risk. For that it is necessary:

- to accumulate data on the actual level of exposure at different conditions and situations (flight altitude and other parameters, solar activity, shield thickness, etc.),
- to search for correlation between exposure levels in space and closer to Earth.

Actually, this task was one of the important objectives of WG-2 of the COST-724 activities. Selected examples of results obtained are presented in following chapters.

2 Examples of results obtained

2.1 Simultaneous Investigation of the Effects of Galactic Cosmic Rays on Aircrafts and on the Foton M2 satellite

Introduction

On 31 May 2005, the Foton M2 capsule, housing a payload of 39 experiments in physical sciences, biology, fluid physics, exobiology, materials science and technology, was launched aboard a Soyuz-U rocket from Baikonur Cosmodrome in Kazakhstan, It spent 15.6 days in Earth orbit. One of the instruments, R3D-B2, was developed in STILBAS, together with colleagues from Germany (Streb et al., 2002). It was able to register the ultraviolet radiation dose in 3 channels (UV-A, UV-B and UV-C), the photosynthetically available radiation (PAR), and the variation of the space radiation dose and flux outside of the Foton M2 capsule by means of MDU-Liulin equipment (see §2.2). This 256 channel space radiation spectrometer and the software had been fully developed in STIL-BAS. Another spectrometer with 4 visible and UV channels was also build by the Bulgarian team under the electronic schemes from German colleagues.

The solid state detectors of the R3D-B2 instrument were placed behind 1.0 mm aluminium, 0.1 mm copper, and 0.2 mm of plastic material. RADO experiment thermoluminescent detectors, devoted to estimate the protective properties of electrically-charged glass coatings against space radiation, were placed behind a layer of special glass. Totally, the thickness of this shielding was about 0.6–0.9 g cm^{-2}, i.e., about 10–30 times less than the shielding of Liulin-E094 experiment on ISS in 2001. The flight altitude of the Foton M2 satellite was 260–304 km, about 100 km less than that of ISS during the Liulin-E094 experiment.

MDU-Liulin equipment was simultaneously measuring onboard CSA aircraft. Data are available for the period 06/05 – 25/06/05, and a comparison between both data sets is presented.

Main results

Fig. 1 summarizes the distribution of the obtained dose and flux data and of the calculated dose to flux ratio in nGy cm^2/particle vs. the L-value. The dose and flux data show two obvious maxima – one at L-values of about 1.4 and another at about 3.8. The lower L-value maximum corresponds to the inner (proton) radiation belt, which is populated mainly by protons with energies from few tens to a few hundred MeV. The higher L value maximum corresponds to the outer (electron) radiation belt, which is populated mainly by electrons with energies from hundreds of keV to a few MeV. The large amount of points with low doses and fluxes are obtained at low and mid magnetic latitudes ($L < 1.2$) outside of the radiation belts and the South Atlantic magnetic Anomaly (SAA). This contribution originates mainly from galactic cosmic rays and shows a "knee" at L-values of about 2.5–3. The dose to flux ratio in the upper panel of the figure is provisionally divided into two parts – below and above 1 nGy cm^2/particle. According to [10] this value divides the range of doses delivered by electrons (below about 1 nGy cm^2/particle), and by protons above this value. Some more features are seen also in the upper panel. Points with specific doses at about 1–2 nGy cm^2/particle at $L = 1.2$ are generated by protons with energies of a few hundred MeV. Points with specific doses of about 2–5

nGy cm^2/particle around $L = 1.5$ are generated by protons with energies below 100 MeV. Points with specific doses of about 0.2–0.5 nGy cm^2/particle around $L = 2.5$ are generated by electrons and/or probably by bremsstrahlung. The absorbed doses deposited in the region of the inner radiation belt by protons are higher than those in the region of the outer radiation belt even though the outer belt fluxes are about 3 times (200 cm^{-2} s^{-1}) larger than those in the inner belt (70 cm^{-2} s^{-1}).

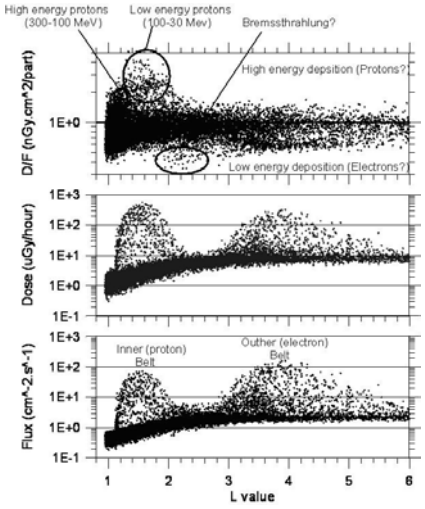

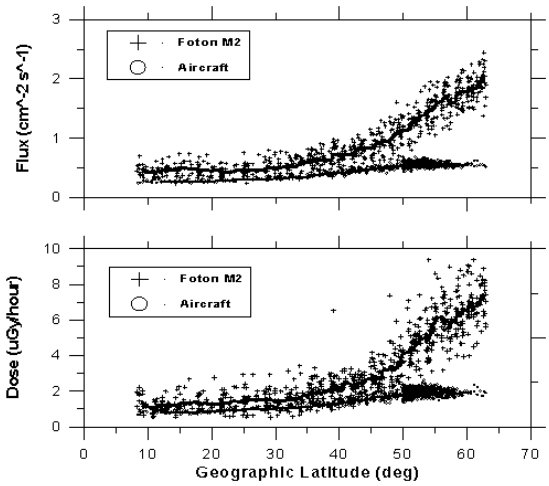

Fig. 1. Left: Distribution of dose and flux and dose to flux ratio data against the L value.

Fig. 2. Right: Comparison of dose and flux data obtained at Foton M2 satellite and on aircraft.

Comparison of the results obtained on the aircraft with these on Foton M2 satellite

Fig. 2 presents the results of the comparison of the data obtained on Foton M2 satellite and on CSA aircraft board. Data selection procedure is the following: for Foton M2 the altitudes are greater than 255 km and less than 265 km; the aircraft data are between 34500 feet (10.5 km) and 37500 feet (11.4 km); both data sets cover the geographic longitude range between -30° and 80°. Points present the measured data, while the heavy lines are the running average values over 21 points.

One can see on Fig. 2 that the absorbed doses and fluxes measured at the satellite are about twice as large as those on the aircraft at the same geographic latitude up to about 45° in northern hemisphere. For larger latitudes, satellite doses and fluxes rise faster with the latitude. This can be described by the fact that at latitudes below 45° only the effect of the galactic component of the radiation is registered in both cases. At higher latitudes and at the satellite altitudes additional radiation from radiation belts is present.

2.2 Onboard spacecraft neutron contribution as estimated on the basis of the results measured with MDU-Liulin onboard ISS, Foton M2, and commercial aircrafts

Materials and methods

Mobile Dosimetry Unit (MDU) Liulin is an energy deposition (E_{dep}) spectrometer based on pulse height analysis of energy deposited in a Si-diode. It has been used in NPI AS CR to estimate the level of aircraft crew exposure since the year 2000, and several long-term monitoring runs have already been performed (Spurný and Dachev, 2003; Dachev et al., 2005; Spurný and Dachev, 2005). Details of the use of that equipment for the estimation of the onboard exposure have been already described in previous publications (Spurný and Dachev, 2003; Dachev et al., 2005; Spurný and Dachev, 2005) and can be summarized as follows:

a Energy deposition spectra in Si detectors are transformed to the dose in Si, $D(\mathrm{Si})$.
b This dose is on the basis of calibrations performed in several on-Earth reference radiation fields divided into parts corresponding mostly to the energy deposited due to non-neutron and/or neutron (and neutron-like) component of the onboard radiation field.
c These partial $D(\mathrm{Si})$ are converted to the apparent ambient dose equivalent,$H_{\mathrm{app}}(\mathrm{MDU})$, due to components mentioned using conversion factors determined in the high-energy radiation field at CERN (Mitaroff and Silari, 2002) and during the direct onboard common measurements of MDU equipment with tissue equivalent proportional counters (Bottollier et al., 2004).

Results

Due to long-term onboard aircraft monitoring (2001–2005) and simultaneous onboard spacecraft measurements (ISS – 2001; Foton-M2 capsule – 2005) we were able to compare energy deposition spectra as registered with MDU-Liulin equipment. The examples of spectra are presented in Fig. 3. One can see that:

a Relative energy distributions for $E_{\mathrm{dep}} < 1$ MeV are similar for aircraft and spacecraft when flying out of the South Atlantic anomaly (SAA), i.e., for galactic cosmic rays (GCR);
b For $E_{\mathrm{dep}} > 1$ MeV, relatively more energy is deposited onboard spacecraft than aircraft;
c E_{dep} spectra inside SAA are quite different from both other cases.

We have tried to interpret these data suggesting that: events with $E_{\mathrm{dep}} < 1$ MeV correspond to low LET radiation; and events with $E_{\mathrm{dep}} > 1$ MeV correspond to the sum of neutron and heavier charged particles of GCR. Afterwards we have treated these data in this manner:

a For low LET component $D(\mathrm{Si}) \longrightarrow D(\mathrm{tissue}) \longrightarrow H^{*}(10)$;
b For neutrons in the region of $E_{\mathrm{dep}} > 1$ MeV we adopted the same procedure as onboard aircraft, considering that neutron spectra are in both cases similar; see Fig. 4 (Bartlett et al., 2005);
c For HECP we obtained $H^{*}(10)$ as: $D(\mathrm{Si}) = D(\mathrm{tissue})$; $5\,D(\mathrm{tissue}) \sim H^{*}(10)$;
d For inside SAA we assumed that all events are due to protons with average $QF \sim 1.3$.

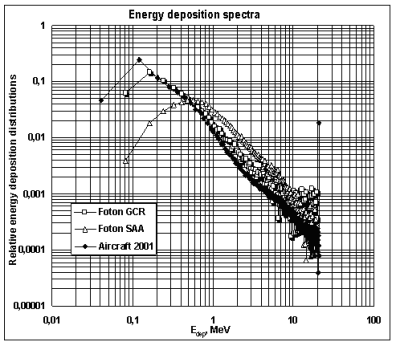

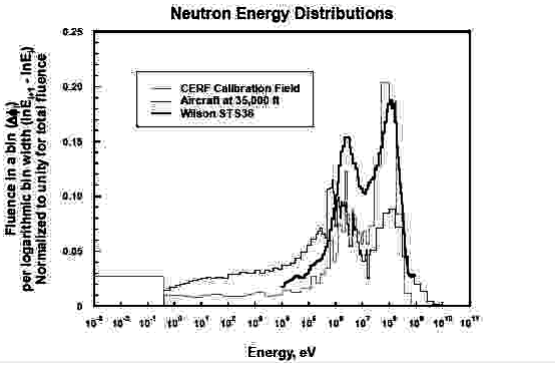

Fig. 3. Left: Comparison of full relative energy deposition spectra onboard aircraft, and FOTON capsule (inside SAA, or GCR).

Fig. 4. Right: Neutron spectra onboard aircraft, spacecraft, and at CERN.

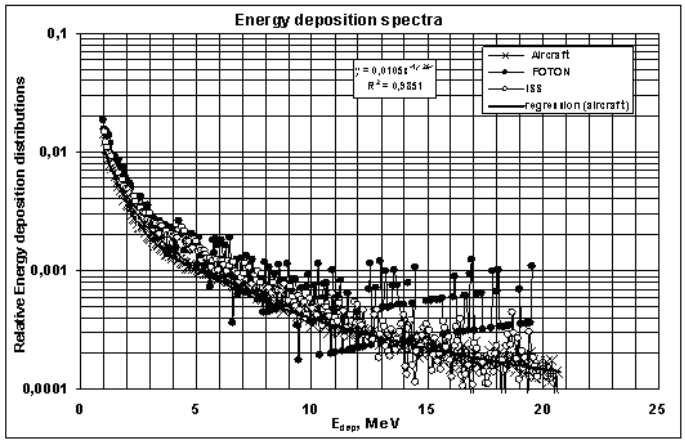

Fig. 5. Comparison of relative energy deposition spectra onboard aircraft, ISS, and FOTON in the region above 1 MeV.

To improve the statistical reliability we have integrated all available data from onboard aircraft ($D(\mathrm{Si})$ total $\sim$ 7 mGy) and/or ISS ($D(\mathrm{Si})$ total $\sim$ 1 mGy). E_{dep} spectra above 1 MeV are presented in Fig. 5. The daily values of dosimetry quantities obtained in this way are presented in Table 2 and are compared with the data obtained previously on the basis of combining data from thermoluminescent (TLD) and track etch detectors (TED).

One can see that the agreement of both sets of data is reasonable. They are also comparable with results of measurements performed at the beginning of 1997 (Benton et al., 2002). Total $H^*(10)$ between 620 and 680 μSv per day was found in this period of solar minimum, i.e., these values should be higher than those established during 2001, just after the solar maximum.

Table 2. Total daily values of dose quantities onboard space vehicles.

Quantity	ISS–MDU	ISS–TLD+TED	FOTON
D(Si) [μGy]	237	–	87
$H^*(10)$ high[1] [μSv]	284	316	115
$H^*(10)$ total[2] [μSv]	622	518	316
neutrons [%]	20.5	27	14.5

[1]high: HECP & neutrons; [2]total: high & low LET radiation

2.3 Further analysis of long-term measurements onboard of Czech Airlines Aircraft

Introduction

ICRP recommended in its Publication 60 to take the radiation exposure due to the cosmic radiation onboard aircraft into account as a part of occupational exposure. The recommendation was adopted into the Czech regulation in 1997. Several series of onboard measurements have been accomplished since that time, mostly onboard Czech Airlines (CSA) aircraft. This chapter brings the analysis of the database derived from dosimetric characteristics acquired with MDU-Liulin. It was placed onboard aircraft (A310-300) several times in years 2001, 2002, 2005, and 2006.

Transport codes

CARI-6 calculates the effective dose due to galactic cosmic radiation received by an adult on an aircraft flight during any month from January 1958 to the present (Frieberg and Snyder, 1992). It can also calculate the effective dose rate from galactic radiation at any specific location in the atmosphere at altitudes up to 60,000 feet. Routine monitoring of aircrew in the Czech Republic has been realized by means of this program since 1997.

The purpose of the program EPCARD (European Program Package for the Calculation of Aviation Route Doses) (Schraube et al., 2002) is also the calculation of the cosmic radiation dose to which an air crew is exposed during a flight, or the dose rate at a specific geographic position. The output of the program provides the ambient dose equivalent rate $H^*(10)$ and the effective dose rate E, giving the contribution from neutrons, protons and pions, electrons, muons, and photons, separately. Only total E values were used in this report.

Data-base information and statistics

Presently, the database contains more than 41,000 records. Each record consists of: dosimetric characteristics identified as $H_{\rm app}$(MDU), $H^*(10)$(EPCARD), E(EPCARD) and E(CARI-6); the spectra of pulses recorded in each of 256 channels of spectrometer; and following free variable parameters:

a date and time
b direction of flight (e.g. Prague – New York)
c geographic coordinates

d altitude in feet (1 foot = 30.48 cm)
e vertical cut-off rigidity in GV (based on an estimation made in 1990 for an altitude of 20 km)
f Apatity and Oulu neutron monitors (NM) records (to estimate actual solar activity).

More detailed information about some parameters of the database is given in Table 3.

Table 3. Total daily values of dose quantities onboard space vehicles.

Parameter	Minimum	Maximum	Most frequent value (frequency)
Altitude [feet]	20000	41000	35000 (25%)
Vertical cut-off rigidity [GV]	0	17	1–3 (70%)
Apatity NM [counts s^{-1}]	1020	1340	1130–1190 (50%)

Results and discussion

Integral values

An advantage of the database is that it permits a summary of values of measured and calculated long-term dosimetric characteristics. The average values are more statistically significant and easily comparable. We have studied these dependencies on the altitude (Fig. 6) and the rigidity (Fig. 7). The ratio of non-neutron and neutron components of ambient dose equivalent rates are compared in Fig. 8 and in Fig. 9. Vertical bars indicate standard deviation relative for an individual value. The uncertainty includes systematic and statistical uncertainties.

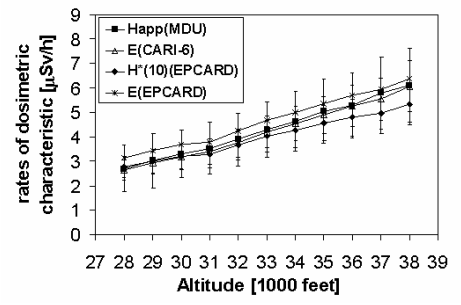

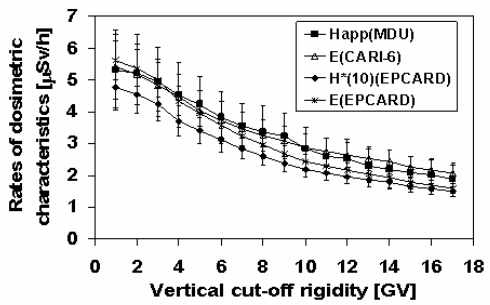

Fig. 6. Left: Altitude dependence of dosimetric characteristics.

Fig. 7. Right: Cut-off rigidity dependence of dosimetric characteristics.

One can see there that:

- Rates of dosimetric characteristics increase closely proportionally with altitude; they decrease with ascending rigidity;

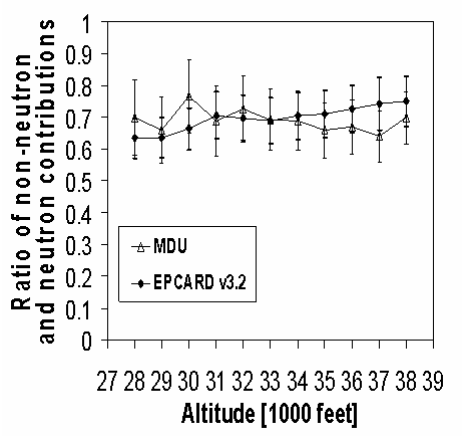

Fig. 8. Left: Ratio of non-neutron and neutron component of $H^*(10)$ measured with MDU and calculated with EPCARD v3.2 as a function of altitude (rigidity 1–3 GV).

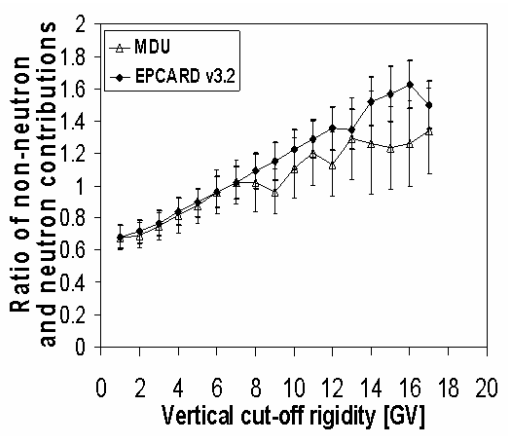

Fig. 9. Right: Ratio of non-neutron and neutron component of $H_{\rm app}$(MDU) and $H^*(10)$(EPCARD) as a function of rigidity (altitude 35 kfeet).

- $H_{\rm app}$(MDU) and E(CARI) values correlate well;
- $H^*(10)$(EPCARD) values are lower than measured; the difference increases with altitude (at 30 kfeet is 3%, at 38 kfeet is 13%) and does not depend on rigidity;
- E(EPCARD) values are higher than measured at 1–3 GV rigidities for all flight altitudes and lower for 5–17 GV;
- The ratio of non-neutron and neutron components does not depend on altitude but is highly dependent on rigidity; the neutron contribution is dominant at 7 GV and above;
- Measured and calculated values of the ratio agree well at all flight levels and for ridities of 1–7 GV; fluctuations above 7 GV are caused by lower statistics.

Spectral values

The database of recorded pulse height spectra enables us to evaluate also the relative $D(\mathrm{Si})$ spectrum as a function of different parameters. Fig. 10 shows the comparison of three relative energy deposition distributions at the same flight level 35,000 feet, at similar solar activity (1130–1190 counts/sec of Apatity NM), and different vertical cut-off rigidities. One can see that the relative contribution of $E_{\rm dep}$ between 0.2 and 0.6 MeV increases with increasing rigidity, that it is constant between 0.6 and 0.9 MeV, and that it decreases between 0.9 and 7.0 MeV. No distinct tendency can be estimated for $E_{\rm dep}$ above 7 MeV because of low statistics for rigidities above 4 GV. More measurements with MDU on aircraft flights in areas with rigidity from 4 GV up to 17 GV should be carried out to accumulate more data to obtain better statistics of integral and spectral values.

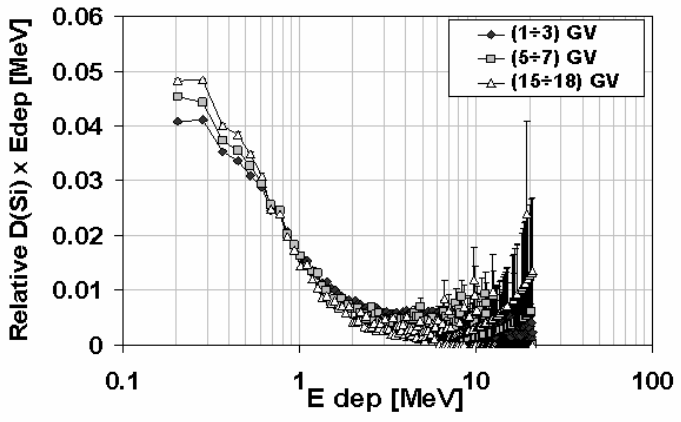

Fig. 10. Geomagnetic position dependence of E_{dep} distribution.

References

Bartlett, D., L. Hager, and R. Tanner: The use of passive personal neutron dosimeters to determine the neutron component of cosmic radiation fields in spacecraft – an update. 10th WRMISS,Chiba, Japan (2005).

Benton, E.R., E.V. Benton, A.L. Frank, V.V. Leonov, and J. Gastin: Dosimetric results from the MIR orbital station. Radiat. Prot. Dosim., **100**, 489–494 (2002).

Bottollier-Depois, J.-F., et al.: Exposure of aircrew to cosmic radiation: Onboard comparison of various dosimeters. Radiat. Prot. Dosim., **110**, 411–415 (2004).

Dachev, Ts., F. Spurný, G. Reitz, T. Tomov, P. Dimitrov, and Y. Matviichuk: Simultaneous investigation of galactic cosmic rays on aircraft and on International Space Station. Adv. Space Res., **36**, 1665–1670 (2005).

European Commission, Recommendations for the implementation of Title VII of the European Basic Safety Standards Directive (BSS) concerning significant increase in exposure due to natural radiation sources, EC Report Radiation Protection 88, European Commission, Luxembourg (1997).

Friedberg, W., W. Snyder, and D.N. Faulkner: US FAA. DOT/FAA/AM-92-2 (1992).

ICRP 1990 Recommendations of theInternational Commission on Radiological Protection, ICRP Publication 60, Annals of the ICRP 21, No. 1/3, Oxford (1991).

ICRP: Conversion Coefficients for Use in Radiological Protection against External Radiation. ICRP Publication 74, Annals of the ICRP, **26(3–4)**, Pergamon Press, Oxford (1996).

International Commission on Radiation Units and Measurements: Conversion Coefficients for use in Radiological Protection Against External Radiation. ICRU Report 57, ICRU, Bethesda, Maryland (1998).

Kovalev, J.J., E.I. Vorobjov: Radiacionnaja bezopasnost‘ ekipazhej letatelnych apparatov; (in Russian) Energoatomizdat, Moskva, 1–149 (1983)

Mitaroff, A., and M. Silari: The CERN-EU high-energy reference field (CERF) facility for dosimetry at commercial flight altitudes and in space. Radiat. Prot. Dosim., **102**, 7–22 (2002).

NCRP Publication 142: Operational radiation safety program for astronauts in low- Earth orbit: A basic framework. NCRP (2002).

O'Brien, K., W. Friedberg, H.H. Sauer, and D.F. Smart: Atmospheric Cosmic Rays and Solar Energetic Particles at Aircraft Altitudes. Environmental International, **22**, Suppl. 1, S9–S44 (1996).

Reitz, G.: Radiation – Limiting Human space flights? Invited talk presented during 15th Symp. Human in Space, Graz (2005).

Schraube, H., G. Leuthold, W. Heinrich, S. Roesler, V. Mares, and G. Schraube: EPCARD-European program package for the calculation of aviation route doses – Users manual. GSF-Bericht 08/02 ISSN 0721-1694 (2002).

Spurný, F., and Ts. Dachev: Long-term monitoring on the onboard aircraft crew exposure level with Si-diode based spectrometer. Adv. Space Res., **32**, 53–58 (2003).

Spurný, F., and Ts. Datchev: Aircrew exposure assessment by means of a Si-diode spectrometer. Radioactivity in the Environment, vol. 7, eds. McLanghlin J.P. et al., 871- 875 (2005).

Streb, C., P. Richter, M. Lebert, Ts. Dachev, and D.-P. Haeder: R3D-B, Radiation Risk Radiometer-Dosimeter on Biopan (Foton) and Expose on Intern. Space Station. Proc. 2nd Exo-Astrobiology Workshop, Graz, Austria, ESA SP-518, 71–74 (2002).

Wilson, J.W. et al.: Transport Methods and Interactions for Space Radiations. NASA Reference Publication 1257, NASA (1991).

Part IV

Working Group 3:
Interaction of solar wind disturbances with the Earth

The coupled system solar wind – magnetosphere – ionosphere – atmosphere – ground

Jurgen Watermann

Danish Meteorological Institute, Lyngbyvej 100, DK-2100 Copenhagen, Denmark jfw@dmi.dk

1 COST 724 in the context of European space weather activities

The COST Action 724 is science dominated but with an eye on the application of science. This means in practice that COST 724 attempts to enhance scientific understanding of space weather in order to enable interested people to generate value-added data (often derived from observations) and scientifically sound models for description and prediction of space weather. COST 724 WGs 1-3 are more oriented toward basic science than WG-4 which is more oriented toward service and public outreach. Space weather service providers rely on the science community as they adapt data and models to meet specific needs of space weather service users. The latter activity has been addressed by the European Space Agency (ESA) through the Space Weather Applications Pilot Project (SWAPP) which includes a range of Service Development Activities (SDA). The relation between COST 724 and SWAPP can be described by the following analogy scheme.

Science Community	⇔	Service Providers	⇔	Service Users
		COST 724 / WGs 1-3 WG 4		ESA-SWAPP SWENET

There is a certain overlap between the three groups. SWAPP has demonstrated that members of the science community can also be service providers or service users and users of one service can be providers of another. The close relation between COST 724 and SWAPP is demonstrated by the fact that several GIC servers which grew out of SWAPP are now in operation in Europe and northern America, and COST 724 member countries benefit from their existence (GIC = geomagnetically induced currents).

WG-3 of COST 724 deals with the interaction of solar wind disturbances with the Earth and is embedded in the COST 724 WG scheme with an obvious overlap with WG-1 and WG-2 as shown in Fig. 1.

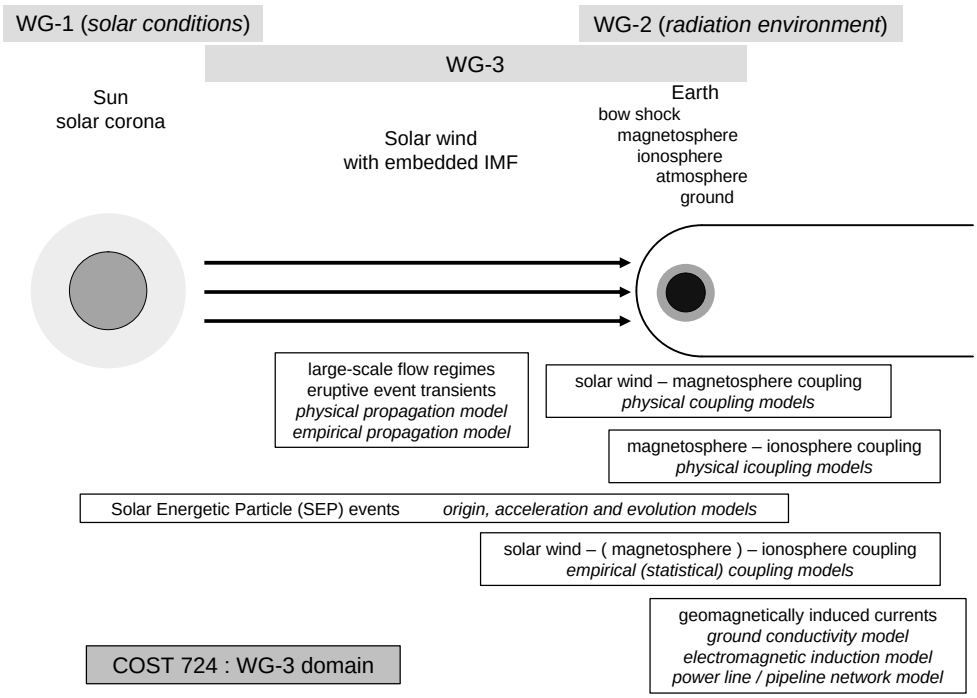

Fig. 1. Interrelations between WG-1, WG-2 and WG-3 physics domains

2 WG-3 and space weather related initiatives outside Europe

The conditions for space weather modelling in Europe differ distinctly from those in the USA where the Community Coordinated Modeling Center (CCMC, *http://ccmc.gsfc.nasa.gov/*) was established many years ago. The CCMC is a multi-agency partnership to enable, support and perform the research and development for next-generation space science and space weather models (CCMC Mission Statement). In addition to providing the scientific community with access to modern space research models the CCMC tests and evaluates models and supports operational space weather nowcasting and forecasting through the transition of research models to operational codes. The COST 724 initiated European Space Weather Portal provides only a limited number of research models (which is, however, expected to grow now that the portal has been established). The CCMC houses solar, heliospheric, magnetospheric and ionospheric models, similar to the European Space Weather Portal but on a larger scale and at a more sophisticated level (not least because the CCMC is well staffed).

An important future step concerns model integration. Specifically WG-3 models fill a wide range of space domains as WG-3 covers interplanetary space, the magnetosphere (with the exception of radiation belt physics), the ionosphere, the neutral atmosphere and the ground (induction fields). Also here have US research institutions taken the lead in a part of these domains with the establishment of the Geospace Environment Modeling program (GEM, *http://www-ssc.igpp.ucla.edu/gem/*). We recall that GEM was initated in 1987 as documented in

"The University of Washington Workshop" report (*http://www-ssc.igpp.ucla.edu/gem/pdf/gem_modeling.pdf*). GEM began its scientific activities with a "Theory Pre-Campaign" at the 1989 La Jolla workshop, has since continued with regular campaigns and is still active. GEM was designed to fill gaps in scientific understanding and provide modules for comprehensive modeling of geospace, coined "Geospace General Circulation Model" (GGCM). GEM enjoys lasting sponsorship from the US National Science Foundation.

A more recent US initiative was the creation of the Center for Integrated Space Weather Modeling (CISM, *http://www.bu.edu/cism/index.html*). According to the CISM web page it defines as its objective the understanding of the dynamic Sun-Earth system and the way life and society are affected, and it attempts to reach this objective through the creation of a physics-based numerical simulation model that describes the space environment from the Sun to the Earth. Also here is the situation quite different from the situation in Europe in that the CISM initiative benefits from substantial financial support provided by the US National Science Foundation.

3 The WG-3 work program

The COST 724 MoU identifies a number of specific tasks to be addressed by WG-3. During the course of the Action the list was expanded to include other topics which were deemed important but did not appear in the MoU. This resulted in the Work Package (WP) scheme shown in Fig. 2. The specific tasks listed in the MoU (regular font) and those added later (printed in italics) are listed below, preceded by the respective WP numbers. WP 3120 had to be suspended because of our failure to secure funding for doing research on this topic.

3110 $\equiv$ 3210 Create a catalogue of existing data sets and models relevant to WG-3

3120 *Develop models of the interaction of large-scale (recurrent) solar wind structures with the Earth's magnetosphere (suspended)*

3130 Develop models of the evolution of eruptive solar events (e.g., CME, SEP) propagating through interplanetary space and predict their arrival at the Earth's bow shock

3220 *Develop physical models of the response of the Earth's magnetosphere to solar wind disturbances and predict the resultant state of the magnetosphere*

3230 *Develop physical models of the response of the Earth's atmosphere to solar wind resp. magnetospheric disturbances*

3240 Develop empirical models of the response of the magnetosphere-ionosphere system to solar wind disturbances observed between Sun and Earth and predict the resultant magnetospheric-ionospheric current systems

3250 Develop models to describe and predict high-latitude ionospheric current systems and their temporal variations

3310 Review global, regional and local ground conductivity models and assess their role for geomagnetically induced currents

3320 Develop the capability to model electric fields induced in the ground during geomagnetic storms (geophysical step of GIC modeling)

3330 *Develop the capability to model electric currents induced in conducting grids during geomagnetic storms (engineering step of GIC modeling)*

3340 Set up and maintain a data base of recorded effects of geomagnetic storms on technological systems (shared with WG-4)

3400 Liaise with WG4 to ensure that relevant data and models are incorporated in a European Space Weather Network/Portal

3200 Liaise with COST Action 296 where modeling of the storm-time ionosphere is relevant to radio wave propagation

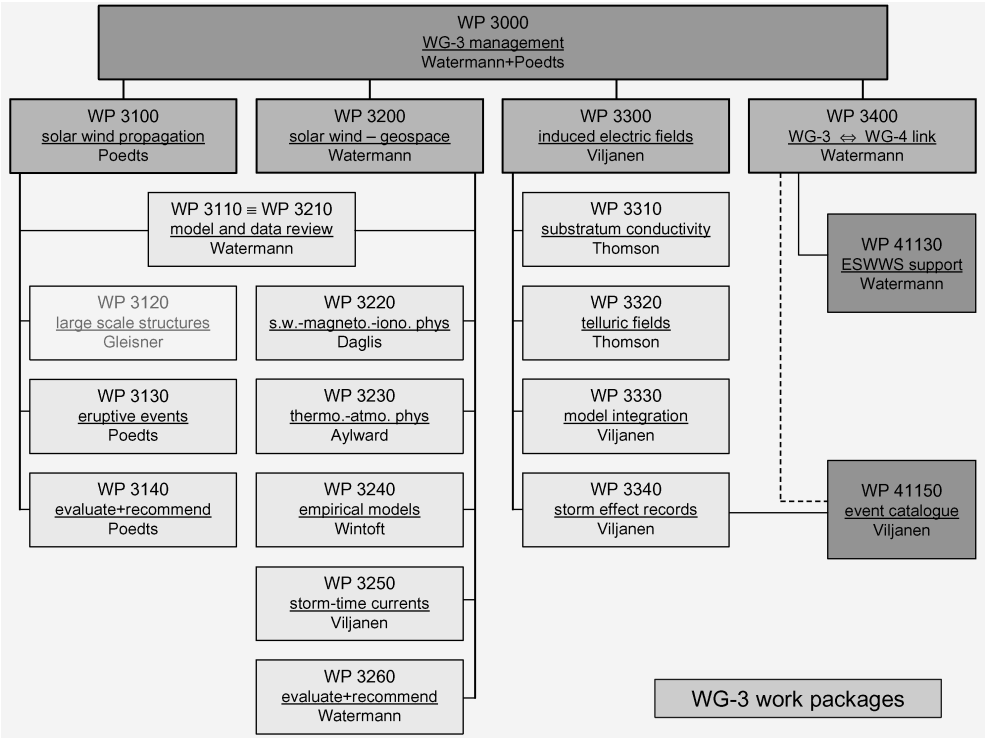

Fig. 2. WG-3 Work Package diagram

4 Introduction to topical contributions by WG-3 members

After a brief excursion on modeling efforts outside Europe we continue with a ”Model and Data Review” (WP 3110 ≡ WP 3210) of models and data sets relevant to WG-3 which were submitted via an interactive web site. Thereafter follows a suite of short reports on the themes

of individual WPs written by WG-3 members who were leading the respective WP or otherwise played an active role in WG-3.

Two contributions (both WP 3130) concern coronal mass ejections (CME) and solar energetic particles (SEP) in interplanetary space. "Modeling CME initiation and interplanetary evolution: recent progress" reviews progress made in simulating the evolution of CME propagating through interplanetary space under different background solar wind conditions. "SOLPENCO. The background physics" describes the physical foundation and the practical application and limitations of an operational code used to predict SEP fluxes and fluences up to 1 Astronomical Unit (AU).

Recent research advances concerning the interaction of solar wind disturbances with the Earth's magnetosphere are discussed in "Understanding the solar wind – magnetosphere – ionosphere coupling through the synergy of modeling, simulations and data analysis". Special emphasis is placed on understanding and modeling the dynamics of certain types of space weather relevant phenomena including the magnetospheric ring current, geomagnetic storms and substorms. An attempt to characterize ULF wave activity in near-Earth interplanetary space, the magnetosphere and the ionosphere by a newly developed set of ULF indices and to apply this to space weather research is described in "ULF wave power index for space weather applications". Both contributions relate to WP 3220.

A step toward coupling neutral and ionized atmospheric regions is made in "Recent advances in modelling space weather effects on the terrestrial upper and middle atmospheres" (WP 3230). This article reviews latest developments of upper atmosphere global circulation models and discusses to which extend the thermospheric response to space weather events can be simulated given the present and near-future density of observations.

Opportunities and caveats of empirical modeling of the effect of solar wind disturbances on the magnetosphere and ionosphere constitute the topic of WP 3240 and are discussed in four contributions. The focus of "Empirical modeling of the magnetospheric ring current" lies on the inner magnetospheric ion flux density and pitch angle distribution during quiet and disturbed periods. Several empirical models derived from in-situ satellite observations are discussed. "Empirical models of solar wind – magnetosphere – ionosphere coupling" compares empirical models which are available online and can be considered operational. Special attention is paid to an evaluation of the RWC-Lund model. A particular application of empirical modeling which is of interest to operational space weather warning services concerns forecasting geomagnetic indices. This is treated in "Forecasting Dst from solar wind data" and "Can the AE index be forecast?".

Aspects of the large-scale dynamics of high-latitude ionospheric convection, currents, electric fields and cross-polar electric potential with emphasis on the interplanetary magnetic field (IMF) control of these parameters is discussed in "Recent results on ionospheric convection based on SuperDARN". A summary of recent results of storm time high-latitude ionospheric currents with relevance to geomagnetically inducted currents (GIC) is the topic of "The complex spatiotemporal dynamics of ionospheric currents". Both papers fall into WP 3250.

The last part of the chain, electromagnetic fields induced in the ground as a result of magnetospheric and ionospheric disturbances associated with space weather events is treated in "A review of progress in modelling induced geoelectric and geomagnetic fields". The paper briefly reviews global and regional geological resp. geophysical models (with emphasis on

electric conductivity) and methods to compute induced electric fields, a prerequisite for computing GIC. This is often called the "geophyiscal step of GIC modeling". The paper falls under WP 3310 and WP 3320.

The current status of research and modeling capabilities of GIC in pipelines and power line networks (called the "engineering step of GIC modeling) including the status of operational codes is described in "Calculation of geomagnetically induced currents (GIC) in ground-based technological systems", enhanced by presenting numerical examples. Recent advances in this area have led to the establishment of several operational GIC servers as described in "Space Weather European Network GIC servers" which were developed under the ESA Space Weather Applications Pilot Project (SWAPP). Both articles are on outcome of work made in WP 3330.

Finally, a catalogue of records of geomagnetic storm effects on technological systems (WP 3340) is maintained jointly with WG-4 and is under continuous development. It is accessible via a link on the WG-3 menu item "Research Program" of the COST 724 homepage, *http://www.cost724.eu/*.

According to the COST 724 MoU the evaluation of models (possibly accompanied by recommendations) should form an important part of the work of the last year of the action (WP 3140 / WP 3260). This requirement has not been fulfilled in a rigorous way. Assessment of the quality and applicability of models is partially included in section 4 and in the individual reports. However, for a systematic evaluation certain ingredients are necessary which we failed to produce. Our action did not define clear and objective criteria which should be applied when conducting an evaluation. Our action did not define appropriate metrics needed to assign quantitative performance marks. As COST does not provide funding to conduct research it is unrealistic to expect that members of our action will have the time and resources to prepare and conduct a comprehensive evaluation of research and/or operational models.

5 Review of research models and data sets submitted to WG-3

5.1 Research models

Several WG-3 members submitted their research models to the collection of space weather relevant models. Some of them are purely physics based ("P") but with the option to assimilate space or ground based measurements as input (if available). They are often research models which are under continuous development and also computationally very demanding so that they are not fit for implementation as operational models. This is the case for GUMICS, CMAT and the more sophisticated ionospheric transport models such as TRANSCAR, TRANSCONVEC and TRANS4. Other models are empirical ("E") and are often used for fast computation if rapid nowcasting or forecasting is a major requirement. Some are hybrids (or semi-empirical models, "S-E") meaning that they are based on plasma physics principles but were subsequently simplified in order to facilitate nowcasting and forecasting via fast computation. Simplification can be achieved through interpolation between pre-calculated tables (e.g., SOLPENCO) or through calibration and training using past measurements (e.g., EFO and EDAM). Principally different types of hybrid models are GUMICS (which combines an MHD approach for the solar wind and magnetospheric domain with an electrostatic code for

the ionospheric part) and the TRANSCAR family which, in its basic form, merges a kinetic transport code to compute plasma production with a fluid code to compute plasma bulk parameters. A more extended version (TRANSCONVEC) considers also the electric convection field and the most recent version (TRANS4) adds a kinetic code for precipitation of solar wind protons.

A synoptic view of some of the main characteristics of the submitted models follows in Tables 1 and 2. It should be kept in mind that this is a selection of models for which WG-3 members were instrumental in the development phase. It is not meant to be a general list of models available in Europe or world-wide for the intended purposes.

5.2 Data sets

Nine data sets have been submitted to WG-3. Their main characteristics appear in synoptic form in Table 3. This is, of course, only a small and somewhat unsystematically collected subset of all available space weather relevant data. With the exception of one entry all of them concern observations recorded with ground-based sensors. Five of them contain magnetic field data sets or data directly derived from magnetic field observations (geomagnetic indices). Only one ionospheric radio sounder data base appears (the Grenoble-EISCAT data base), and this set can be considered historic (the data end in 1999). Many other ionospheric radar data sets exist in the scientific world. We only mention the international SuperDARN consortium (*http://superdarn.jhuapl.edu/*) which offers on its web site real-time and archived data in graphical form for download. EISCAT (*https://e7.eiscat.se/*) operates, besides the Tromsø and two Svalbard transmitters, additional receivers in Kiruna (SE) and Sodankylä (FI). Other major incoherent scatter radars potentially useful for space weather research include AMISR (*http://amisr.com/*), the MIT Haystack (*http://www.haystack.mit.edu/atm/mho/index.html*) and the Sondrestrom (Greenland) research facility (*http://isr.sri.com/*). Real-time and archived data can be viewed at or downloaded from the facilities' web sites, and many of their data are also ingested into the Madrigal data base (*http://www.openmadrigal.org/*) from where they can be downloaded by interested scientists with the help of sophisticated query schemes.

Here we do not consider the numerous digital ionospheric sounders (known as digisondes or dynasondes) because they (respectively their observations) are dealt with in considerable depth in COST action 296 (*http://www.cost296.rl.ac.uk/*) and by the European Digital Upper Atmosphere Server (DIAS, *http://www.iono.noa.gr/DIAS/*).

In order to give a flavor of the vast amount of data available for space research let us consider one single type, namely ground-based magnetometer data. They are provided by a large number of institutions and collected and further distributed by various organisations, sometimes along with a higher level numerically processed data and value-added products. The best known organisations include the World Data Centers for Geomagnetism, the International Service of Geomagnetic Indices (ISGI, *http://isgi.cetp.ipsl.fr/*) and the global network of geomagnetic observatories known as INTERMAGNET (*http://www.intermagnet.org/*).

The magnetometer data are often collected and distributed in an uncoordinated way, in contrast to many coherent scatter radar data which are collected, processed and distributed by a well-coordinated research community which has itself organised under the umbrella of SuperDARN (*http://superdarn.jhuapl.edu/*). In order to overcome the problems arising

from insufficiently coordinated magnetometer arrays a similar initiative has recently emerged which was inspired by SuperDARN and is named SuperMAG (*http://supermag.jhuapl.edu/*). It collects variometer data from collaborating partners and processes and displays them in a common way. As SuperMAG relies on archived data it is useful for the research community but not for operational purposes.

Table 4 lists the major subauroral, auroral and and polar cap arrays of ground-based magnetometers. The vast majority employs fluxgate sensors. They are mostly variometers, i.e., they are not absolutely calibrated but record only the deviation of the magnetic field vector from a fixed but usually unknown baseline. The table shows how many different magnetometer networks exist and how many different operation parameters need to be considered when using their data. The compilation of a catalogue of data sets is therefore a virtually infinite story.

6 Outlook

WG-3 has achieved most of the objectives stated in the MoU and has in some areas achieved even more, see Section 2. It has failed so far in two areas.

(1) We have not completed the evaluation of models (or ”modeling schemes” if we wish to use the language of the MoU), and we did not make recommendations, for the reasons mentioned in Section 2.

(2) We did not make sufficient progress toward the goal of integrating existing models into a scheme which covers the evolution of a space weather event from the Sun to the Earth. However, this step is a necessity if we want to design models or algorithms which are useful to and accepted and appreciated by potential space weather service users.

The shortcomings are, however, no surprise, given the complexity of this task and the limited resources available. COST kindly provides support for Management Committee meetings, sponsors space weather related workshops and co-finances scientific collaboration (the so-called Short Term Scientific Missions) but does not have the resources to allocate funds for conducting the basic scientific work which will end up as an element of a European comprehensive space weather modeling and prediction capability. The way forward is to continue taking small steps toward the final goal just like COST 724 has done so far.

Table 1. Solar wind and magnetosphere models submitted to WG-3

model	domain	objective (purpose)	type	input	output
SOLPENCO *www.am.ub.es/~blai*	interplanetary space	predict proton flux and fluences of SEP events associated with interplanetary shocks	S-E	heliolongitude of the solar activity, shock initial velocity at 18 solar radii	proton flux and fluencies at 0.4 AU and 1 AU for energies between 0.125 keV and 64 MeV
HIDALGO *www.srg.uah.es*	interplanetary space	magnetic clouds and their interaction with the Earth's magnetosphere	P	IMF and solar wind plasma pressure	prediction of the geomagnetic storms associated with magnetic clouds
GUMICS *www.space.fmi.fi/~pjanhune/gumics/*	magnetosphere	global solar wind – magnetosphere – ionosphere coupling	P	solar wind and IMF	magnetospheric and ionospheric plasma parameters
EFO *www.srg.uah.es/*	magnetosphere	magnetospheric ring current and Dst	P	solar wind V_x and B_z	Dst and storm alert
Ring current empirical model *anna.milillo@ifsi.rm.cnr.it*	inner magnetosphere	evolution of magnetospheric ion populations and their role for ring current development	E	equatorial plane proton spectra	global magnetospheric currents and ion fluxes
Event-oriented magnetospheric magnetic field *www.ava.fmi.fi/~nataly/*	inner magnetosphere	event-driven inner magnetosphere magnetic field	S-E	solar wind and IMF magnetic field from ground and space	real-time global magnetospheric magnetic field and Dst
Magnetospheric particle transport and acceleration *urlwww.ava.fmi.fi/ nataly/*	inner magnetosphere		P		

Table 2. Ionosphere, atmosphere and ground models submitted to WG-3

model	domain	objective (purpose)	type	input	output
EDAM *www.cpar.qinetiq.com*	ionosphere	plasma density distribution via data assimilation	S-E	various ionospheric observations	global electron density
TRANSSOLO *jean.lilensten@obs. ujf-grenoble.fr*	ionosphere	1-D height profiles of suprathermal electron flux between 90 and 1000 km	P	electron precipitation data if available	ionospheric ion and electron production
TRANSCAR *jean.lilensten@obs. ujf-grenoble.fr*	ionosphere	kinetic-fluid hybrid, plasma production and transport between 90 and 3000 km	P	particle precipitation data if available	time-dependent profiles of key plasma parameters
TRANSCONVEC *jean.lilensten@obs. ujf-grenoble.fr*	ionosphere	kinetic-fluid hybrid, plasma production and transport between 90 and 3000 km	P	particle precipitation data and convection maps if available	time-dependent profiles of key plasma parameters
TRANS4 *jean.lilensten@obs. ujf-grenoble.fr*	ionosphere	kinetic-fluid hybrid, plasma production and transport between 90 and 3000 km	P	particle precipitation data and convection maps if available	time-dependent profiles of key plasma parameters
CMAT *www.apl.ucl.ac.uk*	neutral atmosphere	neutral and ionised atmosphere coupling from 30 km to the exosphere	P	high-latitude convection and precipatation data and/or empirical models	neutral and ionized atmosphere parameters
GIC in pipelines *aurora.fmi.fi/gic_service/ english/index.html*	ground	compute GIC in pipeline systems	P	local geoelectric field and pipeline parameters	GIC and pipe-to-soil voltages
GIC in power systems	ground	compute GIC in power systems	P	local geoelectric field and DC parameters of the power system	GIC through transformers and along transmission lines

Table 3. Space weather relevant data sets submitted to WG-3

identification	monitor	spatial coverage	time resolution	real-time	availability	output format
aa, am, Kp, AE, Dst *www.cetp.ipsl.fr/~isgi/homepag1.htm*	geomagnetic indices	planetary	aa, am, Kp: 3 h AE: 2.5 min Dst: 1 h	yes	download	ASCII
IMAGE *www.ava.fmi.fi/image/*	fluxgate magnetometer	Fennoscandia and Svalbard	1 s or 10 s	most	download	ASCII, graphical
Greenland chain *www.dmi.dk/projects/chain/greenland.html*	fluxgate magnetometer	Greenland	1 s and 20 s	some	on request	ASCII, binary, graphical
SEGMA *massimo.vellante@aquila.infn.it*	fluxgate magnetometer	Southern Europe	1 s	no	on request	ASCII
ITACA[2] *sung3.ifsi.rm.cnr.it/~massetti/index.html*	auroral imager	Greenland-Svalbard	20 s or 1 min	no	download	graphical
ULF waves *umberto.villante@aquila.infn.it*	search coil magnetometer	Antarctica	1 s	no	on request	ASCII
GIC in the Finnish natural gas pipeline *www.ava.fmi.fi/gic/gicdata/gasum_index.html*	electric current meter	Mantsala (FI)	10 s	no	on request	graphical
Grenoble-EISCAT data base *www-eiscat.ujf-grenoble.fr*	incoherent scatter radar	Tromsø (NO) area	5 min	no	download	ASCII, binary, graphical
high-speed streams in the solar wind *venus.nipne.ro/new1/HSS_Catalogue.html*	spacecraft in-situ field and particle sensors	L1 point	3 h	no	download	ASCII

Table 4. Some ground-based magnetometer arrays used in space research

magnetometer array (contact)	availability	data distribution	coordinate system	real-time
AARI (Troshichev) *www.aari.nw.ru/clgmi/geophys/index.htm*		1 min	local magnetic (H,E,Z)	Arctic stations
AGO (Lanzerotti+Engebretson) *space.augsburg.edu/ago/*		1+10 s, 1 min	local magnetic (H,E,Z)	no
BAS-LPM (Freeman) *www.antarctica.ac.uk/bas_research/our_research/az/lpm/*		1 s	local magnetic (H,E,Z)	no
CARISMA (Mann) *www.carisma.ca/*		0.125+0.5+1 s, 1 min	geographic (X,Y,Z)	yes
MAGDAS (Yumoto) *magdas.serc.kyushu-u.ac.jp/index.html*		1s, 3 s, 1 min	local magnetic or geographic	some stations
Greenland (Watermann) *www.dmi.dk/projects/chain/greenland.html*	on request	1+20 s, 1+2+5 min	local magnetic	west coast stations
GIMA (Olson) *magnet.gi.alaska.edu/*		1 s, 1 min	local magnetic (H,E,Z)	some stations
IMAGE (Viljanen) *www.ava.fmi.fi/image/*	download	10 s, 1 min	geographic (X,Y,Z)	most stations
MACCS (Hughes+Engebretson) *space.augsburg.edu/space/MaccsHome*		0.5+5 s, 1 min	≈geographic (X,Y,Z)	CDR+NAN
SAMBA (Zesta) *samba.atmos.ucla.edu/index.html*		1 min	geographic (X,Y,Z)	no
SAMNET (Honary) *www.dcs.lancs.ac.uk/iono/samnet/*		1+5 s, user defined	local magnetic (H,E,Z)	LAN+CRK
SEGMA (Vellante) *sole-terra.aquila.infn.it/staz_segma.asp*	1 s	1 s	local magnetic (H,E,Z)	no
TGO (Hansen) *geo.phys.uit.no/geomag.html*		10 s	geographic (H, D, Z)	yes

Modelling CME initiation and interplanetary evolution: recent progress

C. Jacobs[1], B. van der Holst[1], and Stefaan Poedts[1]

Centrum voor Plasma-Astrofysica, Celestijnenlaan 200B, 3001 Leuven, Belgium
Carla.Jacobs@wis.kuleuven.be

Summary. An overview is given of the models currently in use for simulating coronal mass ejections (CMEs) and their interplanetary (IP) evolution up to the orbit of the Earth and beyond. Particular attention is given to the extensions and improvements of these models made in the last couple of years, the modelling of the background solar wind conditions, and to the numerical techniques involved.

1 Introduction

The theoretical modelling of the evolution of CMEs can be divided into different sub-problems. Such a sub-problem is, for instance, the observational study and modelling of the fast and slow solar wind where questions regarding the heating source(s) and acceleration mechanism(s) of the fast wind component need to be answered. Another sub-problem is the initiation of CMEs: why do CMEs occur and how are they triggered? Next, there is the sub-problem of the propagation of the CMEs, and, in particular, the observed time-height curves and arrival times at 1 AU need to be explained. Also the evolution and structure of the CMEs and the leading shock fronts during their propagation through the interplanetary space medium needs to be studied. The modification(s) of the CME shock structure may contain important clues to understanding the propagation properties of CMEs. The impact of the CME or magnetic clouds on the Earth's magnetosphere is another crucial sub-problem. The interaction of the CMEs with the bow shock of the Earth's magnetosphere drastically affects the characteristics of the magnetic field lines. Clearly, this affects the geo-effectiveness of magnetic storms.

Due to the complexity of the problem, numerical modelling of solar transients and prediction of the space weather is a challenging task which asks for a large amount of computational power and the continuous improvement of numerical techniques and physical models. Any physical model for solar eruptions has to be able to explain the fundamental cause of the eruption itself and the nature of morphological features associated with it. The ultimate goal is the modelling of solar eruptions from the onset of the eruptions up to the interaction with the Earth, and this on realistic time scales. During the last few years significant progress has been made in the field of computational magneto-fluid-dynamics applied to solar related phenomena. In this report an overview will be given of the latest developments in this field. The

next section deals with the first sub-problem, namely the modelling of the background conditions. In the third section the models currently used for CME initiation are discussed. Next, the progress concerning the third sub-problem is treated, i.e., modelling CME propagation and evolution.

2 Modelling the background solar wind

Since the first attempt to numerically model the solar corona by Pneuman & Kopp (1971), increasing progress has been made. Nowadays, thanks to the increment in computational power, the usage of 3D MHD models for reconstructing the solar corona and solar wind become more common. The availability of more detailed observations makes it possible to produce more realistic simulations via inclusion of observational data through the boundary conditions. Linker et al. (1999) performed a 3D MHD simulation of the solar corona during the Whole Sun Month campaign in which they used measurements of line-of-sight magnetic field as a boundary condition for the model. Riley et al. (2002) have developed an empirically driven MHD model for the solar corona and the inner heliosphere and investigated the evolution of the heliospheric current sheet during the course of the solar cycle. Their model is an extension of the previously mentioned model and is still employing a polytropic energy equation. The physics in the algorithm was improved (Lionello et al., 2001) by incorporating thermal conduction along the magnetic field, radiation losses and heating into the energy equation. A combination of an empirical and a physics based representation of the quasi steady global solar wind is the Wang-Sheeley-Arge model (Arge et al., 2004) which is an improved version of the Wang and Sheeley model (Wang & Sheeley, 1990), relating the magnetic field expansion factor to the solar wind speed. The model has been comprehensively validated with observations spanning nearly a full solar cycle (Owens et al., 2005) and is used as a boundary condition in several other models. One of them is the Hybrid Heliospheric Modeling System (Detman et al., 2006). It combines a source surface (potential field) current sheet model for the solar corona and a time dependent 3D MHD solar wind model to predict the solar wind conditions at the Earth. The empirical relationship of Wang & Sheeley (1990) is a crucial element in the model. Also Odstrcil et al. (2005) use the WSA model to derive the boundary conditions for their 3D MHD model calculating the solar wind parameters in the heliosphere. Roussev et al. (2003b) as well constructed a three-dimensional model for the solar wind incorporating solar magnetogram observations. In this model the solar wind is powered by the energy interchange between the coronal plasma and large-scale MHD turbulence. In order to reproduce the observed bimodal structure of the solar wind they impose a temperature variation on the solar surface depending on the strength of the magnetic field. Cohen et al. (2007) use the WSA model as an input for a 3D MHD code, in which the processes of turbulent heating in the solar wind are parametrised using a phenomenological, thermodynamical model with a varied polytropic index, as introduced by Roussev et al. (2003b). They employ the Bernoulli integral to bridge the observed solar wind speed at 1 AU with the assumed distribution of the polytropic index on the solar surface. Usmanov & Goldstein (2006) have developed a 3D steady state MHD model of the solar wind that covers the region from the coronal base to 100 AU and that accounts for the effect of pickup protons in the distant heliosphere. As initial condition for integrating the MHD equations from 1 AU to 100 AU they use the 1 AU output from

the tilted-dipole model of Usmanov & Goldstein (2003) which is appropriate for solar minimum conditions. Lionello et al. (2005, 2006) have developed a global MHD model to study the effect of differential rotation on the coronal magnetic field. They identified examples of reconnection and other changes of topology of the magnetic field.

3 CME initiation models

To date, there is no CME model sufficiently well developed to explain the real events of solar eruptions and related phenomena. The basic pre-eruption configuration and the topological changes in the magnetic field that result in the conversion of a large fraction of the magnetic energy into kinetic energy are not well known. Nevertheless, significant progress has been made in understanding the basic physical processes that are involved in those events. Reviews of CME initiation mechanisms can be found in Low (2001); Moore & Sterling (2006); Forbes et al. (2006). The current CME initiation models can be defined as storage and release models (Klimchuk, 2001) in which the energy to drive the CME is stored in the magnetic field. They can be categorised into two large groups depending on the state of the coronal magnetic field prior to the eruption.

The first group of models assumes that a flux rope exists prior to the eruption. Chen & Shibata (2000) proposed an emerging flux trigger mechanism for the onset of CMEs. They have performed two dimensional MHD simulations in a Cartesian box of a flux rope initially in equilibrium and driven unstable by the emergence of extra magnetic flux trough the lower boundary. A current sheet form below the flux rope and the flux rope are pushed upward by fast magnetic reconnection. Recently, Dubey et al. (2006) have extended this study in spherical geometry. The analytical flux rope model of Titov & Démoulin (1999), which had been proposed to explain flares and CMEs, was numerically studied in the context of CME initiation by Roussev et al. (2003a). These authors concluded that a highly twisted field at the surface of the flux rope was needed in order to produce the eruption. In the previous simulations the initial flux rope is suspended in the corona by a balance between magnetic compression and tension forces. Simulations of the evolution of a twisted magnetic flux rope from below the photosphere into the corona, was numerically simulated by several authors (e.g. Manchester et al., 2004b; Amari et al., 2004). The evolution of the flux rope is at first quasi statically and then undergoes a dynamic transition, driven by reconnection processes.

The second group of models relies on the existence of sheared magnetic arcades, which become unstable and erupt once some critical state is reached in the solar corona. Contrary to the previous class of models, here a flux rope does not exist prior to the eruption, it is formed in the course of the eruption by magnetic reconnection. Mikić & Linker (1994) had shown already that shearing motions energise the magnetic field and might cause the formation of a flux rope when the shearing motions continue for a sufficiently long time. Jacobs et al. (2006) performed a parameter study of the effect of the shear velocity and the background wind on the evolution of the flux rope formation. In the sheared arcade models two main sub-classes can be distinguished: flux-cancellation models and breakout-models.

The difference between the models are very subtle and are mainly in the location of the reconnection side driving the eruption. In the flux-cancellation models (e.g. Amari et al., 2000, 2003; Linker et al., 2003; Roussev et al., 2004; Riley et al., 2006) a flux rope is formed

by reconnecting the opposite polarity feet of a sheared magnetic arcade. In these models the reconnection takes place at the photosphere or near the base of the solar corona. In the breakout model (Antiochos et al., 1999; Lynch et al., 2005) the eruption is again triggered by magnetic reconnection, but here this process occurs in a current sheet sitting above the sheared arcade. This model asks for a specific multipolar magnetic topology to enable the eruption. Li & Luhmann (2006) have done an observational study of the magnetic field topology of CME source regions and found both bipolar and quadrupolar topology at the source regions, but the bipolar topology is more common overall and in each year. As of today, there is no convincing observational evidence that proves or disproves either class of CME models, and no model is advanced enough to explain real observations.

4 CME propagation and evolution

In the past, heliospheric disturbances were often modeled by driving the inner boundary conditions placed upstream of the critical point of the solar wind (at $> 20\, R_\odot$) (e.g. Vandas et al., 2002). These models provide basic physical insight into how a large solar disturbance propagates and interacts with the large-scale solar wind. However, there are little or no observable parameters at these distances to constrain the boundary conditions. Only recently has the propagation of a CME from the inner corona to 1 AU been modelled in two- and three-dimensional geometries. For example, Jacobs et al. (2005) and Chané et al. (2006) have done a parameter study to investigate the effect of the background wind and the polarity of the initial flux rope on the CME evolution in an axial symmetric set-up. An example of a 3D CME propagation model is the theoretical model of Gibson & Low (1998). This analytical model was used as a CME generation mechanism in numerical simulations (e.g. Manchester et al., 2004a; Lugaz et al., 2005), in which the dynamics of the CME are followed as it interacts with a bimodal background solar wind. The 12 May 1997 CME event was numerically simulated by Odstrcil et al. (2004b, 2005), who tried to reproduce the plasma parameters near Earth. The inner boundary in their model is placed at 0.14 AU. The ambient solar wind is derived from coronal models utilising photospheric magnetic field data and the transient disturbances are derived from geometrical and kinematic fitting of coronagraph observations of CMEs. Wu et al. (2006) have studied the detailed nature of interacting CME shocks with a 1-dimensional adaptive grid MHD code. An event study of three interacting CMEs was done by Lugaz et al. (2007). As model for the background solar wind the varying polytropic index model of Roussev et al. (2003b) was used. The CMEs are initiated using an out-of-equilibrium semicylindrical flux rope (Roussev et al., 2003a). The shocks generated by CMEs are important in the production of Solar Energetic Particles (SEPs). Sokolov et al. (2004) simulated the time-dependent transport and diffusive acceleration of particles at shock waves driven by CMEs. Aran et al. (2006) have developed SOLPENCO, a tool for rapid predictions of proton flux and fluence profiles observed during gradual SEP events. The geo-effectiveness of a CME event was simulated by Ridley et al. (2006), who investigated the magnetospheric and ionospheric response to a very strong interplanetary shock and associated CME.

Although idealised, these numerical simulations were able to reproduce many generic features of CMEs seen in observations.

5 Conclusions

In the last couple of years, the modelling of the solar wind and of CMEs superposed on this wind has advanced to a stage where individual events can be simulated rather realistically and then compared with observations. The current state-of-the-art 3D MHD models are beginning to apply magnetogram data as input boundary conditions and are starting to include non-MHD effects, such as solar particle acceleration and kinetic effects. Still, very few of them are sufficiently developed to explain the real events in detail, and most of them only consider one of the sub-problems involved in space weather modelling. Future models should aim to model the entire process from CME initiation to CME evolution. However, this is a difficult task as considerable variations of physical conditions in the solar photosphere, corona, and interplanetary space involve many physical processes occurring on vastly different spatial and temporal scales. One way to deal with this problem is to decouple the solar corona model from a model solving the inner heliosphere and to use the output of the coronal model as a boundary condition for the heliospheric model (Odstrcil et al., 2004a). Coronal models need to simulate more complex physical processes while heliospheric models can use simpler approximations over a much larger spatial domain. Computationally, it is also more efficient to advance the heliospheric portion of the simulation independently of the coronal time step. Another way to deal with the varying spatial scales is the use of adaptive mesh refinement techniques, as done in the BATS-R-US code (Powell et al., 1999), or in the AMR-VAC code (van der Holst & Keppens, in press). Currently, only two groups have developed advanced 3D coupled MHD models to model a CME event from its initiation up to the interaction with the magnetosphere of the Earth: the CORHEL model (Luhmann et al., 2004) at the University of Boston and the Space Weather Modeling Framework (SWMF) (Tóth et al., 2005) at the University of Michigan. In the SWMF one has the choice between different models for the solar background wind as well as different CME triggering models. Using reasonably high spatial resolutions in all of the coupled components, the SWMF runs significantly faster than real time on massive parallel supercomputers.

With new solar missions launched (e.g. STEREO), more detailed observations will become available, which in turn, will be used in more-realistic data-driven models. The continuous development of new numerical schemes, the improved computer facilities, and the more detailed observations, will undoubtedly lead us to a more realistic modelling of solar transients and will provide us more insight into the physics involved.

References

Amari, T., Luciani, J. F., & Aly, J. J., Coronal magnetohydrodynamic evolution driven by subphotospheric conditions, ApJ, **615**, L165–L168 (2004)

Amari, T., Luciani, J. F., Aly, J. J., Mikić, Z., & Linker, J. A., Coronal mass ejection: initiation, magnetic helicity, and flux ropes. I. Boundary motion-driven evolution, ApJ, **585**, 1073–1086 (2003)

Amari, T., Luciani, J. F., Mikić, Z., & Linker, J. A., a twisted flux rope model for coronal mass ejections and two-ribbon flares, ApJ, **529**, L49 – L52 (2000)

Antiochos, S., DeVore, C., & Klimchuk, J., A model for solar coronal mass ejections, ApJ, **510**, 485 – 493 (1999)

Aran, A., Sanahuja, B., & Lario, D., SOLPENCO: A solar particle engeneering code, Adv.Space.Res, **37**, 1240–1246 (2006)

Arge, C., Luhmann, J. G., Odstrcil, D., Schrijver, C. J., & Li, Y., Stream structure and coronal sources of the solar wind during the May 12th, 1997 CME, J. Atmosph. and Solar-Terrestrial Phys., **66**, 1295–1309 (2004)

Chané, E., van der Holst, B., Jacobs, C., Poedts, S., & Kimpe, D., Inverse and normal coronal mass ejections: evolution up to 1AU, A&A, **447**, 727 – 733 (2006)

Chen, P. & Shibata, K., An emerging flux trigger mechanism for coronal mass ejections, ApJ, **545**, 524 – 531 (2000)

Cohen, O., Sokolov, I. V., Roussev, I. I., et al., A semiempirical magnetohydrodynamical model of the solar wind, ApJ, **654**, L163–L166 (2007)

Detman, T., Smith, Z., Dryer, M., et al., A hybrid heliospheric modeling system: Bckground solar wind, J.Geophys.Res, **111**, A07102 (2006)

Dubey, G., van der Holst, B., & Poedts, S., The initiation of coronal mass ejections by magnetic flux emergence, A&A, **459**, 927–934 (2006)

Forbes, T. G., Linker, J. A., Chen, J., et al., CME Theory and Models, Space.Sc.Rev., **123**, 251–302 (2006)

Gibson, S. E. & Low, B. C., A time-dependent three-dimensional magnetohydrodynamic model of the coronal mass ejection, ApJ, **493**, 460 – 473 (1998)

Jacobs, C., Poedts, S., & van der Holst, B., The effect of the solar wind on CME triggering by magnetic foot point shearing, A&A, **450**, 793 – 803 (2006)

Jacobs, C., Poedts, S., van der Holst, B., & Chané, E., On the effect of the background wind on the evolution of interplanetary shocks, A&A, **430**, 1099 – 1107 (2005)

Klimchuk, J. A., in Geophys. Monograph Series, Vol. 125, Space Weather, ed. P. Song, H. J. Singer, & G. L. Siscoe (AGU), 143 (2001)

Li, Y. & Luhmann, J., Coronal magnetic field topology over filament channels: implication for coronal mass ejection initiations, ApJ, **648**, 732–740 (2006)

Linker, J., Mikić, Z., Biesecker, A., et al., Magnetohydrodynamic modeling of the solar corona during Whole Sun Month, J.Geophys.Res, **104**, 9809 – 9830 (1999)

Linker, J. A., Mikić, Z., Lionello, R., et al., Flux cancellation and coronal mass ejections, Phys. Plas., **10**, 1971–1978 (2003)

Lionello, R., Linker, J. A., & Mikić, Z., Including the transition region in models of the large-scale solar corona, ApJ, **546**, 542–551 (2001)

Lionello, R., Linker, J. A., Mikić, Z., & Riley, P., The latitudinal excursion of coronal magnetic field lines in response to differential rotation: MHD simulations, ApJ, **642**, L69–L72 (2006)

Lionello, R., Riley, P., Linker, J. A., & Mikić, Z., The effects of differential rotation on the magnetic structure of the solar corona: magnetohydrodynamic simulations, ApJ, **625**, 463–473 (2005)

Low, B. C., Coronal mass ejections, magnetic flux ropes, and solar magnetism, J.Geophys.Res, **106**, 25141–25163 (2001)

Lugaz, N., Manchester, W. B., & Gombosi, T. I., The evolution of coronal mass ejection density structures, ApJ, **627**, 1019–1030 (2005)

Lugaz, N., Manchester, W. B., Roussev, I. I., Tóth, G., & Gombosi, T. I., Numerical investigation of the homologous coronal mass ejection events from the active region 9236, ApJ, **659**, 788–800 (2007)

Luhmann, J. G., Solomon, S. C., Linker, J. A., et al., Coupled model simulation of a Sun-to-Earth space weather event, J. Atmosph. and Solar-Terrestrial Phys., **66**, 1243–1256 (2004)

Lynch, B. J., Antiochos, S. K., DeVore, C. R., & Zurbuchen, T. H., The breakout model for CME initiation in 3-dimensions, Proc. Solar Wind 11 - SOHO 16, **ESA SP-592** (2005)

Manchester, W., Gombosi, T., Roussev, I., et al., Modeling a space weather event from Sun to the Earth: CME generation and interplanetary evolution, J.Geophys.Res, **109**, A02107 (2004a)

Manchester, W. B., Gombosi, T. I., & DeZeeuw, D. L., Eruption of a buoyantly emerging magnetic flux rope, ApJ, **610**, 588–596 (2004b)

Mikić, Z. & Linker, J., Disruption of coronal magnetic field arcades, ApJ, **430**, 898 – 912 (1994)

Moore, R. L. & Sterling, A. C., in AGU Monograph Series, Vol. 165, Solar Eruptions and Energetic Particles, ed. N. Gopalswamy, R. Mewaldt, & J. Torsti, 43 (2006)

Odstrcil, D., Pizzo, V. J., & Arge, C. N., Propagation of the 12 May 1997 interplanetary coronal mass ejection in evolving solar wind structures, J.Geophys.Res, **110**, A02106 (2005)

Odstrcil, D., Pizzo, V. J., Linker, J. A., et al., Initial coupling of coronal and heliospheric numerical magnetohydrodynamics codes, J. Atmosph. and Solar-Terrestrial Phys., **66**, 1311–1320 (2004a)

Odstrcil, D., Riley, P., & Zhao, X. P., Numerical simulation of the 12 May 1997 interplanetary CME event, J.Geophys.Res, **109**, A02116 (2004b)

Owens, M. J., Arge, C. N., Spence, H. E., & Premboke, A., An event-based approach to validating solar wind speed predictions: High-speed enhancements in the Wang-Sheeley-Arge model, J.Geophys.Res, **110**, A12105 (2005)

Pneuman, G. W. & Kopp, R. A., Gas-magnetic field interactions in the solar corona, Sol.Phys., **18**, 258–270 (1971)

Powell, K. G., Roe, P. L., Linde, T. J., Gombosi, T. I., & DeZeeuw, D. L., A solution-adaptive upwind scheme for ideal magnetohydrodynamics, J. Comp. Phys., **154**, 284–309 (1999)

Ridley, A. J., DeZeeuw, D. L., Manchester, W. B., & Hansen, K. C., The magnetospheric and ionospheric response to a very strong interplanetary shock and coronal mass ejection, Adv.Space.Res, **38**, 263–272 (2006)

Riley, P., Linker, J. A., & Mikić, Z., Modeling the heliospheric current sheet: Solar cycle variations, J.Geophys.Res, **107**, A7 1136 (2002)

Riley, P., Linker, J. A., Mikić, Z., & Odstrcil, D., Modeling interplanetary coronal mass ejections, Adv.Space.Res, **38**, 535–546 (2006)

Roussev, I. I., Forbes, T. G., Gombosi, T. I., et al., A three-dimensional flux rope model for coronal mass ejections based on a loss of equilibrium, ApJ, **588**, L45 – L48 (2003a)

Roussev, I. I., Gombosi, T. I., Sokolov, I. V., et al., A three-dimensional model for the solar wind incorporating solar magnetogram observations, ApJ, **595**, L57 – L60 (2003b)

Roussev, I. I., Sokolov, I. V., Forbes, T. G., et al., A numerical model of a coronal mass ejection: shock development with implications for the acceleration of GeV protons, ApJ, **605**, L73–L76 (2004)

Sokolov, I. V., Roussev, I. I., Gombosi, T. I., et al., A new field line advection model for solar energetic particle acceleration, ApJ, **616**, L171–L174 (2004)

Titov, V. S. & Démoulin, P., Basic topology of twisted magnetic configurations in solar flares, A&A, **351**, 707–720 (1999)

Tóth, G., Sokolov, I. V., Gombosi, T. I., et al., Space Weather Modeling Framework: A new tool for the space science community, J.Geophys.Res, **110**, A12226 (2005)

Usmanov, A. V. & Goldstein, M. L., A tilted-dipole MHD model of the solar corona and solar wind, J.Geophys.Res, **108**, 1354 (2003)

Usmanov, A. V. & Goldstein, M. L., A three-dimensional MHD solar wind model with pickup protons, J.Geophys.Res, **111**, A07101 (2006)

van der Holst, B. & Keppens, R., Hybrid block-AMR in Cartesian and curvilinear coordinates: MHD applications, J. Comp. Phys. (in press)

Vandas, M., Odstrćil, D., & Watari, S., Three-dimensional MHD simulation of a loop-loke magnetic cloud in the solar wind, J.Geophys.Res, **107**, 1236 (2002)

Wang, Y.-M. & Sheeley, Jr., N. R., Solar wind speed and coronal flux-tube expansion, ApJ, **355**, 726–732 (1990)

Wu, C.-C., Feng, X. S., Wu, S. T., Dryer, M., & Fry, C. D., Effects of the interaction and evolution of interplanetary shocks on "background" solar wind speeds, J.Geophys.Res, **111**, A12104 (2006)

SOLPENCO. The background physics

B. Sanahuja[1,2], A. Aran[1], and D. Lario[3]

[1] Departament d'Astronomia i Meteorologia. Universitat de Barcelona. Spain
Blai.Sanahuja@ub.edu; aaran@am.ub.es
[2] Institut d'Estudis Espacials de Catalunya (ICC/UB). Spain
[3] Johns Hopkins University, Applied Physics Laboratory. Laurel, MD (USA)
David.Lario@jhuapl.edu

Summary. SOLPENCO is a code developed as a first step toward the prediction of flux and fluences of solar energetic particle (SEP) events. Its core is a data base that contains a large number of pre-calculated energetic particle flux profiles. This allows a rapid computation, by interpolation, of particle fluxes and fluences of other possible scenarios for gradual SEP events, under user's demand (within a given range of possibilities). SOLPENCO is based on the combined shock-and-particle transport simulation model built by Lario et al. (1998). We shortly review the background physics of this model, how the data base has been constructed, as well as the limitations of both the model and the code.

1 Introduction

Solar energetic particle (SEP) events are one of the most severe hazards of the solar induced space weather phenomena. SEP events are highly random in nature and can lead to large radiation doses, either in short time intervals or by accumulation in extended periods. SEP events produce most of the particle fluence measured over a solar cycle as well as the highest proton fluxes between 0.5 and 200 MeV. The radiation risks that SEP events represent to manned spaceflights and to spacecraft operations have been extensively reviewed (e.g. Feynman & Gabriel, 2000). Critical to the ability to design space missions is our capacity for predicting SEP fluxes and fluences. The "Space Radiation Hazards and the Vision for Space Exploration: Report of a Workshop" (Baker et al., 2006) summarises the state-of-the-art of our understanding about human health risks from space radiation exposure, and its monitoring and forecasting as related to exploration missions.

The most significant sources of SEP fluxes in the interplanetary (IP) medium are solar flares and shock waves driven by coronal mass ejections (CMEs). As observed from a heliocentric distance of 1 AU, the energetic particle flux enhancements produced by SEP events may last several days and, in terms of total radiation dose, protons are the primary hazard posed. The multiple processes involved in the development of SEP events include acceleration and transport of particles in a time dependent system formed by the propagating CME-driven shock, the associated evolving magnetic field topology, as well as the generation of magnetic field fluctuations. Increasingly detailed models of the evolving shock properties, wave-particle interactions and particle transport processes have been able to reproduce major features of the

shock-associated SEP events (e.g. Lee, 2005) However, such models include necessary simplifying assumptions that are not always constrained by observations (Lario, 2005).

In spite of these modelling efforts, the prediction of SEP events is still in its infancy. Two excerpts of the report "Radiation Environment Models and In-Orbit Monitoring" of ESA (Daly et al., 2005) illustrate the need for models that correctly describe the radiation environment for future missions: "*...New requirements include the assessment of the temporal behaviours (durations, peaks, threshold durations, spectral variations) and sounder treatment of heavy ions in solar particle events...*". "*...Helio-radial variations are therefore very difficult to derive without recourse to models of solar particle acceleration and propagation since a significant proportion of the energetic particles are produced in interplanetary shocks.*" The US National Space Weather Program: Implementation Plan, FCM-P31 (1997) estimated a period of ~ 15 years before a reliable scientific model can be achieved.

The process of predicting the flux and fluence of large SEP events, days or hours in advance of their occurrence, is a formidable challenge that should accomplish the following steps: (i) determine where, when and how a solar event will occur; (ii) specify the characteristics of the associated CME, such as location, size, speed, and its ability to drive a shock wave; (iii) determine the efficiency of the CME-driven shock at accelerating particles, as well as how they will be injected into the IP medium; and (iv) forecast how these particles and the associated shock will travel through IP space to reach spacecraft and/or astronauts.

2 Brief overview

SOLPENCO (SOLar Particle ENgineering COde) is a tool for predicting SEP fluxes and fluences that aims to be useful for space weather purposes (Aran et al., 2004, 2005). The core of SOLPENCO is a data base that contains a large number of pre-calculated particle flux profiles, assuming a given injection rate of shock-accelerated particles (Lario et al., 1998) for different solar-interplanetary scenarios. This allows a rapid computation of proton fluxes and fluences by interpolation of similar scenarios for gradual SEP events, under user's demand (within a given range of possibilities). SOLPENCO provides the flux and cumulative fluence profiles of SEP events characterised by the following parameters:

(1) the heliocentric distance of the spacecraft, either 1 AU or 0.4 AU;
(2) the initial speed of the shock, any value between 750 and 1800 km s^{-1};
(3) the heliolongitude of the solar parent activity, any value between W90 and E75;
(4) the mean free path, either 0.2 AU or 0.8 AU, for 0.5 MeV protons (scaled with particle rigidity);
(5) the presence of a foreshock region, Yes or No; and
(6) the proton energy: 0.125, 0.25, 0.5, 1, 2, 4, 8, 16, 32 or 64 MeV.

All these parameters are input variables that the user can select through a friendly interface. Therefore, the code provides at least, if only integer values of the initial speed and solar heliolongitude are considered, 697,864 possibilities for each proton energy and heliocentric distance. SOLPENCO can be run on-line at www.spaceweather.eu/es/model_access_interface (registration needed) and it is available under request.

The outputs provided by SOLPENCO are:

– the upstream duration of the event (i.e. the time from the onset of the activity at the Sun up to the shock arrival at the spacecraft);
– the shock transit speed;
– the upstream fluence, integrated for all the energies over that selected by the user;
– the peak intensity at the selected energy and the time when it is attained; and,
– the flux and the cumulative fluence profiles.

These outputs are provided in either a data ASCII file and/or in a Portable Network Graphics (PNG) display.

These outputs depend on the assumptions adopted in the model (Section 3) and the values used as input to describe the interplanetary scenario where the SEP event develops. By "interplanetary scenario" we mean both the conditions for injection and propagation of shock-accelerated particles (characterised by the input variables 2, 4, 5, and 6) and the relative position of the observer with respect to the Sun (i.e. the heliocentric radial distance of the observer and the heliolongitude of the parent solar activity characterised by the input variables 1 and 3). This heliolongitude also defines the direction of propagation of the shock in IP space by assuming that the nose of the shock is centred in the heliolongitude of the parent solar activity. For a given gradual SEP event, SOLPENCO interpolates among pre-calculated SEP profiles in the data base which have the closest angular positions and initial shock velocities to those chosen by the user.

3 Background physics

SOLPENCO is based on the combined shock-and-particle model developed by Lario et al. (1998). This model assumes that the injection of shock-accelerated particles takes place at the point on the front of the shock that magnetically connects with the observer (also known as cobpoint, or Connecting with the OBserver POINT; Heras et al., 1995). The cobpoint changes its location along the shock front and its properties as the shock expands in interplanetary space.

The evolution of the interplanetary shock is described by means of the 2.5D magnetohydrodynamic (MHD) time-dependent model of Wu et al. (1983). This MHD model simulates plasma disturbances that propagate through the IP medium, keeping symmetry with respect to the equatorial plane. The domain of the shock propagation simulation extends from close to the Sun (18 $R_\odot$) up to 1.1 AU (it can be extended up to Mars' orbit when necessary). Smith & Dryer (1990) details the method of computation, the input pulse and the steady-state medium where the shock propagates. For each SEP event, the model provides a simulation of the shock propagation; thus we can estimate the strength of the shock at each time and for every point along the shock front and in particular at the cobpoint. We mainly characterise this strength by the downstream/upstream normalised velocity ratio, $\mathrm{VR} = (V_{r_d} - V_{r_u})/V_{r_u}$ and the magnetic field ratio, $\mathrm{BR} = |B|_d/|B|_u$ (where subscripts u and d stand for upstream and downstream of the shock, respectively).

The simulation of the energetic particle propagation through the IP medium consists in solving the focused-diffusion transport derived by Ruffolo (1995) that includes the effects of focusing in the diverging magnetic field, pitch-angle scattering by magnetic field irregularities

and solar wind convection and adiabatic deceleration effects. The source of particles is mobile and located at the travelling shock front (see details in Lario et al., 1998). The pitch-angle scattering is described by a diffusion process with a diffusion coefficient defined in terms of the standard quasi-linear approximation for the interplanetary magnetic field (IMF) fluctuations (Jokipii, 1966). Thus, the energetic particle transport equation has two main parameters: the injection rate of shock-accelerated particles, Q, and their mean free path $\lambda_{\|}$ (that depends on the rigidity of the particles). These parameters are derived by comparing the output flux and first order anisotropy profiles with the corresponding observational profiles of actual SEP events by looking for the best possible simultaneous fit for all the considered energies.

The key point of the shock-and-particle model is that it allows us to compare the evolution of the MHD variables at the cobpoint with the injection rate of shock-accelerated particles derived from the transport model. Since both simulations are worked independently, any empirical relation found between the injection rate and the MHD variables is independent of the mechanism that accelerates particles at the shock. From modelling different SEP events (Lario et al., 1998), we have been able to derive an empirical relation between the injection rate of shock-accelerated particles, Q, and the MHD velocity jump across the front of the shock, VR, at the cobpoint: the $Q(\mathrm{VR})$-relation. At present, our knowledge of the acceleration mechanisms at the shock and the shock itself are still insufficient to perform accurate comparisons of theory and observations in individual gradual events. Therefore, transport modelling using phenomenological SEP source functions, as the one considered in SOLPENCO, is still an important tool for space weather studies.

Once such a functional dependence as $Q(\mathrm{VR})$ is derived, it is possible to invert the procedure. That is, for a given solar event that triggers an interplanetary shock, the MHD simulation of the shock propagation model provides the parameters of the shock (i.e. the velocity, density and magnetic field compression ratios) all along its front and throughout its travel time toward the observer, and in particular at the cobpoint. By adopting a $Q(\mathrm{VR})$ relation we can evaluate the number of particles to be injected onto the IMF line rooted at the cobpoint, and assuming average parameters for the IP propagation of energetic particles along the IMF we can predict the SEP intensities at any point in IP space.

To build up the data base of SOLPENCO we use the $Q(\mathrm{VR})$ relation derived from modelling several actual SEP events: $\log Q = \log Q_0 + k\mathrm{VR}$, when $\mathrm{VR} > 0.1$ (Lario et al., 1998). This expression allows us to relate the dynamic evolution of the shock strength at the cobpoint to the rate at which shock-accelerated particles are injected. The factor k has been taken as $k = 0.5$, the average value derived from modelling several SEP events for 0.5 MeV protons (Aran et al., 2004), and this value is assumed to be the same for all energies. Q_0 scales as a power law with energy, with a spectral index $\gamma = 2$ for $E < 2$ MeV and $\gamma = 3$ for $E \geq 2$ MeV. These are average values derived from the literature (e.g. van Nes et al., 1984; Cane et al., 1988) and from our modelled SEP events. The values of Q_0 are taken from those obtained from the simulation of the 24 – 26 April 1981 SEP event since this event presents an almost constant value of $k \sim 0.5$ (Lario, 1997; Aran et al., 2004).

Finally, we shortly comment four limitations of SOLPENCO that should be considered in future versions of the code. A limitation of the shock-and-particle model is that it can only be applied to the upstream part of SEP events. The shock front is a mobile source of particles that injects them into both the upstream and the downstream regions and that highly modifies the topology of the IP medium as it moves away from the Sun. A full description of

the rapidly changing compressed downstream region is difficult for MHD models and, as a consequence, a reasonable modelling of the energetic particle propagation in this region is not straightforward. Lario et al. (1999) started from the modelled draping of the downstream IMF around a magnetic cloud and described the focusing effects of the resulting IMF configuration. Lee (2005) pointed out that the e-folding decay time of SEP intensities usually observed after the shock passage can be explained in terms of the combination of two processes: the trapping of particles between the shock and the Sun, and the adiabatic deceleration due to the expansion of the downstream volume. This is a line to be worked out to model the downstream region of SEP events.

The formation of CME-driven shocks and their characteristics are poorly understood. The present available data and our observational capabilities do not allow us to discern when, where and how shocks form close to the Sun and how energetic particles are first injected into the IP medium. As a consequence, in our simulations we are forced to choose initial input shocks at the inner boundary of the MHD code that better reproduce the passage of the shock at the observer's location as well as the jump parameters measured by the spacecraft. Additionally, it is not possible yet to have quantified indicators of CME activity (initial shock speed, direction, for example) and, in general, of any solar activity suitable to be used as proxies of a shock formation.

It is important to adopt an MHD model for the description of the coronal/interplanetary shock that starts near the corona ($\sim$3 $R_\odot$) because the high-energy component ($>$10 MeV) of SEPs is usually generated in this region close to the Sun where the shock is still strong enough to accelerate particles to high energies.

The value of the coefficient k in the $Q(\mathrm{VR})$ relation varies with the energy of the particles and from event to event. As far as we know, the unique way to asses it (and probably extending it to BR) is modelling a large set of SEP events, mainly originated from solar longitudes between W50 and E10. In order to calibrate this dependence and to quantify it for operative purposes, these fittings must be compared to those synthesised by the code assuming the previous $Q(\mathrm{VR})$ relation. Finally, in order to extend this relation to higher energies (50–100 MeV), it would be also very useful to study the evolution of the anisotropy at these high energies, because of the further constraints that can impose on theoretical models and simulations.

4 Conclusions

SOLPENCO allows the user to obtain flux and fluence predictions of gradual SEP events originating from the western to far eastern locations, as seen at two heliocentric radial distances: 1 and 0.4 AU. The proton energy channels considered extend up to 90 MeV, to accommodate the range of energies relevant to space weather purposes. This is a first step toward a fully and reliable operational tool, but a large modelling effort is needed in order to fix the drawbacks of the shock-and-particle model and SOLPENCO itself. Furthermore, it is basic obtaining accurate particle, plasma and magnetic field data because without them, SEP event modelling will remain limited. The potential applications and later developments in the starting era of STEREO mission are appealing because, by the first time after the Helios-1 and -2, it will

be possible to perform multi-spacecraft analysis of SEP events in a systematic way. Nevertheless, STEREO will not be able to give insights into the variation of SEP events with the heliocentric distance. To estimate these variations, physics-based models and tools such as the shock-and-particle model and SOLPENCO are needed.

References

Aran, A., Sanahuja, B., & Lario, D.: An engineering model for solar energetic particles in interplanetary space, Final Report, ESA/ESTEC Contract 14098/99/NL/MM (2004)

Aran, A., Sanahuja, B., & Lario, D.: Fluxes and fluences of SEP events derived from SOLPENCO. Ann. Geophys., **23**, 3047–3053 (2005)

Baker, D. N., Braby, L. A., Curtis, S., & et al.: Space Radiation Hazards and the Vision for Space Exploration. Ad Hoc Committee on the Solar System Radiation Environment and NASA's Vision for Space Exploration: A Workshop. National Research Council. The National Academies Press. Washington DC (2006)

Cane, H. V., Reames, D. V., & von Rosenvinge, T. T.: The role of interplanetary shocks in the longitude distribution of solar energetic particles. J. Geophys. Res., **93**, 9555–9567 (1988)

Daly, E., Nieminen, P., Hilgers, A., & et al.: Radiation Environment models and in-orbit monitoring. Technical Note, TEC-EES/2005.265/ED, ESA (2005)

Feynman, J. & Gabriel, S. B.: On space weather consequences and predictions, J. Geophys. Res., **105**, 10543–10564 (2000)

Heras, A. M., Sanahuja, B., Lario, D., & et al.: Three low energy particle events: modeling the influence of the parent interplanetary shock, Astrophys. J., **445**, 497–508 (2005)

Jokipii, J. R.: Cosmic-Ray Propagation. I. Charged Particles in a Random Magnetic Field. Astrophys. J., **146**, 480–487 (1966)

Lario, D.: Propagation of Low-Energy Particles through the Interplanetary Medium: Modeling their Injection from Interplanetary Shocks. PhD thesis. University of Barcelona (1997)

Lario, D.: Advances in modeling gradual solar energetic particle events. Adv. in Space Res., **36**(12), 2279–2288 (2005)

Lario, D., Sanahuja, B., & Heras, A. M.: Energetic particle events: efficiency of interplanetary shocks as 50 keV $<$ E $<$ 100 MeV proton accelerators. Astrophys. J., **509**, 415–434 (1998)

Lario, D., Vandas, M., & Sanahuja, B.: Energetic Particle Propagation in the Downstream Region of Transient Interplanetary Shocks. In S. R. Habbal & et al. (ed) Solar Wind Nine. AIP Conf. Proc., **471**, 741–747 (1999)

Lee, M. A.: Coupled Hydromagnetic Wave Excitation and Ion Acceleration at and Evolving Coronal/Interplanetary Shock. Astrophys. J. Suppl., **158**, 38–67 (2005)

Ruffolo, D.: Effect of adiabatic deceleration on the focused transport of solar cosmic rays. Astrophys. J., **442**, 861–874 (1995)

Smith, Z. & Dryer, M.: MHD study of temporal and spatial evolution of simulated interplanetary shocks in the ecliptic plane within 1 AU. Solar Phys., **129**, 387–405 (1990)

US National Space Weather Program: Implementation Plan, FCM-P31. 8455 Colesville Road, Suite 1500, Silver Spring MD 20910 (1997)

van Nes, P., Reinhard, R., Sanderson, T. R., & et al.: The energy spectrum of 35- to 1600-keV protons associated with interplanetary shocks. J. Geophys. Res., **89**, 2122–2132 (1984)

Wu, S. T., Dryer, M., & Han, S. M.: Non-planar MHD model for solar flare-generated disturbances in the heliospheric equatorial plane, Solar Phys., **84**, 395–418 (1983)

Understanding the solar wind – magnetosphere – ionosphere coupling through the synergy of modeling, simulations and data analysis

Ioannis A. Daglis[1], Georgios Balasis[1], Natalia Ganushkina[2], Fiori-Anastasia Metallinou[1], Minna Palmroth[2], Risto Pirjola[2], and Ioanna Tsagouri[1]

[1] Institute for Space Applications and Remote Sensing, National Observatory of Athens, Metaxa and Vas. Pavlou, Penteli, 15236 Athens, Greece, daglis@space.noa.gr
[2] Finnish Meteorological Institute, Space Research Unit, P.O. Box 503, FIN-00101 Helsinki, Finland

Summary. Comprehensive understanding of the dynamics of the coupled solar wind – magnetosphere – ionosphere system is of utmost interest, both from the perspective of solar system astrophysics and geophysics research and from the perspective of space applications. The physical processes involved in the dynamical evolution of this complex coupled system are pertinent not only for the Sun-Earth connection, but also for major phenomena in other astrophysical systems. Furthermore, the conditions in geospace - collectively termed space weather - affect the ever increasing technological assets of mankind in space and therefore need to be understood, quantified and efficiently forecasted. The present collaborative paper communicates recent advances in geospace dynamic coupling research through modeling, simulations and data analysis and discusses future directions.

1 Introduction

The dynamic processes governing physical conditions in geospace, which have been collectively termed space weather in the course of the last decade, have strongly attracted the scientific community because they reflect the influence of a star on a planetary environment. The particular planetary environment not only is an accessible natural plasma laboratory but moreover happens to be the cradle of mankind.

However, key dynamic processes such as magnetic reconnection and charged particle acceleration, which are studied *in situ* in geospace, are also relevant for major universal phenomena in other astrophysical systems.

Accordingly, understanding the dynamics of the coupled solar wind - magnetosphere - ionosphere system is of broader astrophysical interest. Furthermore, this understanding has recently been gaining technological relevance because of the ever increasing technological assets of mankind in space, which are endangered by extreme space weather disturbances.

This paper is a collaborative communication of specific recent advances in geospace research and has the following structure. Section 2 gives a synoptic presentation of the currently sole European global magnetohydrodynamic (MHD) simulation modeling the geospace plasma environment using solar wind parameters as input, and reports some recent results.

Section 3 discusses the influence of convection and substorms on the build-up of the storm-time ring current and presents the relevant results of a three-dimensional dynamic ion-tracing model. Section 4 presents the results of recent comparative modeling studies, where the role of substorm-induced impulsive electric field on the build-up of the storm-time ring current is investigated. The paper concludes with a section on modeling of the ionospheric storm-time response at middle latitudes.

2 MHD simulations for modeling the entire solar wind - magnetosphere - ionosphere system

Currently, the only self-consistent method to model the entire solar wind - magnetosphere - ionosphere system is based on ideal MHD theory, where plasma is assumed to be fluid having electromagnetic properties. In principle, a computationally efficient code can describe the coupled solar wind - magnetosphere - ionosphere system in real time, using measurements in the solar wind as input. However, in practice there are several difficulties in building a fully operational simulation that can be used for forecasting the space environment. Even with the fastest computers the existing codes still have to make compromises with spatial resolution in order to speed up the code execution to the real-time limit.

GUMICS-4 (Janhunen, 1996), developed at the Finnish Meteorological Institute, is the only European global MHD simulation modeling the Earth's plasma environment using solar wind parameters as input. GUMICS-4 consists of two computational domains: The MHD domain including the solar wind and the magnetosphere and the electrostatic domain including the ionosphere. The two domains are linked together by electron precipitation and field-aligned currents from the magnetosphere, which together with the ionospheric conductivity define the ionospheric potential. This potential is mapped back to the magnetosphere where it is used as a boundary condition for the MHD solution. Like most global MHD simulations, GUMICS-4 predicts the system behavior well in the outer magnetosphere (e.g., magnetopause), whereas the inner magnetosphere with overlapping plasma populations having different temperatures is less well in accordance with in-situ measurements (Palmroth et al., 2003). In the ionosphere, GUMICS-4 is known to be temporally and spatially in agreement with different measurements, but the magnitude of the ionospheric effects is lower than expected (Palmroth et al., 2005, 2006a).

In the space weather point of view, GUMICS-4 has been used to develop a mathematic formula between the ionospheric total power dissipation and the solar wind parameters (Palmroth et al., 2004, 2006a). It was found that the formula using the solar wind parameters correlates with over 80% correlation coefficient with the GUMICS-4 power in the ionosphere, which in turn is temporally in agreement with measurements. The importance of this is that the formula may be found useful in predicting the ionospheric total power dissipation from the solar wind measurements. Assuming that the solar wind parameters are transmitted real-time from the first Lagrange point between the Sun and the Earth, this gives about one hour lead time to prepare for large energy dissipation creating harmful effects, such as increased friction on low-altitude spacecraft orbits.

The first attempt of quantitative investigation of energy transfer from the solar wind into the magnetosphere has been carried out with GUMICS-4 (Palmroth et al., 2003). Recently,

the initial results have been extended into more systematical direction. The energy and mass transfer appear to have a different spatial and temporal variation on the outer edge of the magnetospheric domain, the magnetopause (Palmroth et al., 2006b). The energy transfer was identified as being a consequence of the electromagnetic energy focusing towards the magnetopause, while the mass transfer preferably occurred during quiet geomagnetic conditions.

Clearly different from earlier speculations, it has been recently noticed that the energy transfer at the magnetopause depends on earlier enhanced magnetic activity, such that after strong driving the energy transfer remains enhanced (Palmroth et al., 2006c). This is demonstrated in Figure 1, where the results for the total power transferred through the magnetopause is depicted in four simulation runs, where the interplanetary magnetic field (IMF) was rotated 360° from north to south and north again. The IMF direction is shown on top of the panel. The time axis (run time, RT) is simulation time from the beginning of the rotation such that 00:00 RT is the time when the first change in the solar wind reaches the dayside magnetopause. The dashed line is the scaled function of IMF $sin^2(\theta/2)$, where θ is the angle of the IMF with respect to north. The function has been proposed to represent the effect of IMF direction in the energy transfer (e.g., Kan & Lee, 1979). Figure 1 suggests that while during the downleg phase (during rotation from north to south) the total power through the surface is rather well represented by $sin^2(\theta/2)$ function, during the upleg phase (rotation from south to north) the power input stays enhanced longer than the $sin^2(\theta/2)$ function indicates in all four runs.

3 Modeling storm-time substorms

Ring current development and the role of magnetospheric convection and substorm injections is one of the central issues of geospace storm dynamics. Modeling has been used extensively to support our effort to clarify the relative influence of convection and substorms on the ring current development.

A way to approach the problem is to examine temporal and spatial variations of ion energy densities in the inner magnetosphere during storms both with and without substorm occurrence. This is done with a a three-dimensional dynamic ion-tracing model. The geomagnetic field used is simulated through the Tsyganenko model (Tsyganenko, 1989), which gives a description of the average magnetic field configuration for 6 different levels of geomagnetic activity. It includes contributions from external sources such as the ring current, the magnetotail current system, the magnetopause currents and the large-scale system of field-aligned currents.

The large-scale steady convection electric field in the magnetosphere is calculated by the Volland-Stern model (Volland, 1973; Stern, 1975). It has been arranged to fit most general features of electric fields observed by polar orbiting satellites.

The electric field induced by a transition of the geomagnetic field, from an initial level to a final one, more or less disturbed, is derived by the vector potential technique of Delcourt (Delcourt & Sauvand, 1994).

The plasma sheet in the Earth's magnetotail plays a key role as a source of the ring current particles. We therefore traced plasma sheet particles under the scenarios described above. In order to reach substantial conclusions, we need to run a significant number of simulations for a large variety of initial conditions, and for a large number of test particles. Running the code

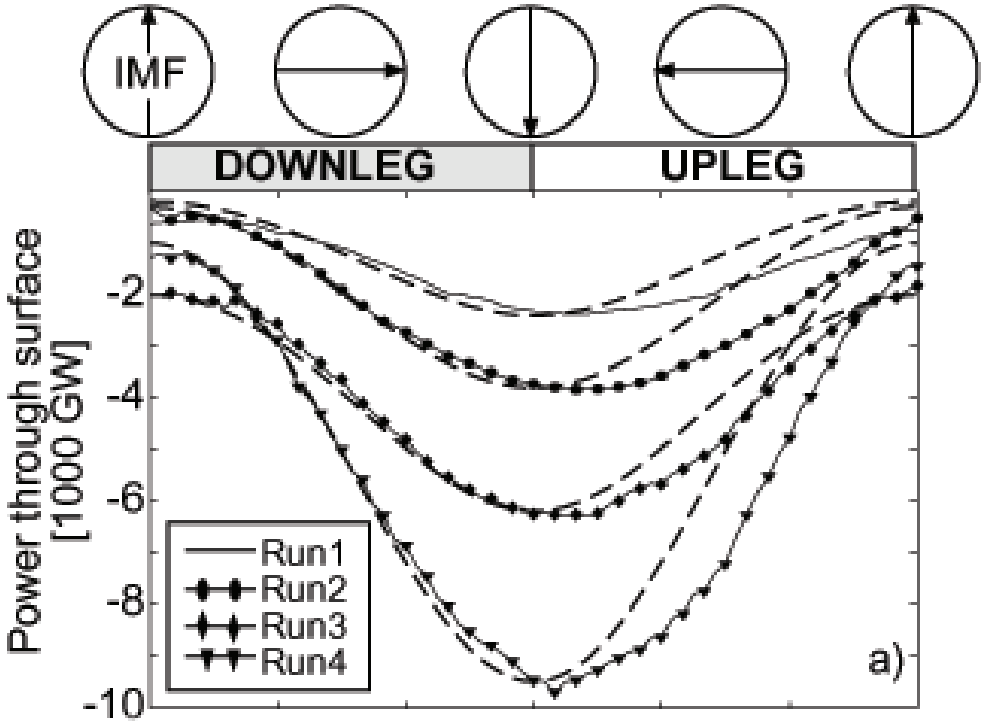

Fig. 1. Total power input through magnetopause (solid) in four runs with different solar wind pressure and magnetic field magnitude conditions. The IMF direction is shown above. The dashed lines are the scaled $sin^2(\theta/2)$ for each run. See Palmroth et al. (2006c) for details.

on parallel platforms has the potential of reducing the total computing time, making thus the investigation of a multitude of cases possible. Therefore we have parallelized the code and run it on the Hellas-Grid computing grid.

In Figures 2–3 we present temporal and spatial variations of the energy density of plasma sheet H^+ and O^+ particles respectively. During this particular run we traced 2000 particles with the following initial parameters: magnetic local time (MLT): near midnight, magnetic latitude: 5°–15°, pitch angle: 60°, energy: 1 keV.

This work addresses the importance of substorm-induced electric fields in the build-up of particle radiation during geospace magnetic storms. We do this through a test-particle approach of ion transport and energization, simulating a convection-only storm and a storm-with-substorms case.

The results of the simulation show that for both ion species the inclusion of substorm-induced electric fields renders ion acceleration much more efficient. The difference in energization is much more prominent for O^+ ions, which have been know to be preferentially accelerated by substorm-induced electric fields (e.g., Daglis & Axford, 1996).

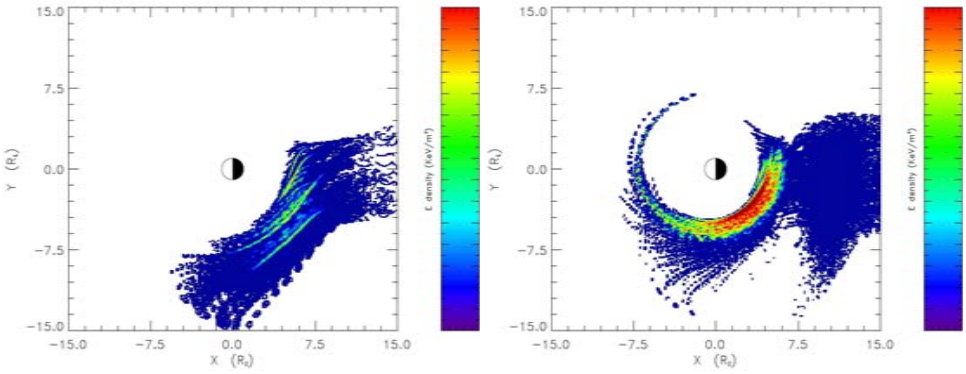

(a) (b)

Fig. 2. Temporal and spatial variations of energy densities of plasma-sheet H^+, in the equatorial plane, under the influence of (a) a large convection electric field only and (b) a storm-time substorm, during the growth phase.

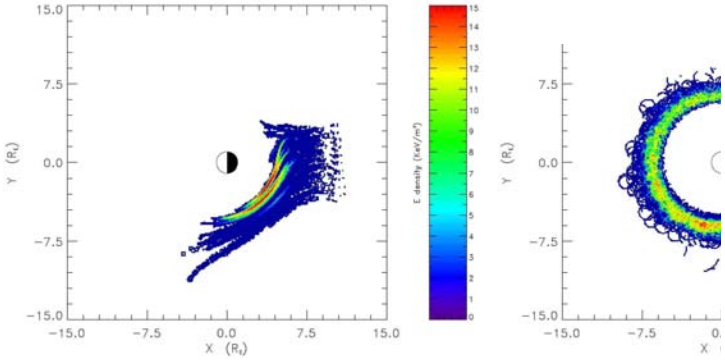

(a) (b)

Fig. 3. Temporal and spatial variations of energy densities of plasma-sheet O^+,in the equatorial plane, under the influence of (a) a large convection electric field only and (b) a storm-time substorm, during the growth phase.

4 The role of substorm-associated electric fields in the ring current development

It is clear that the relative importance of the large-scale convection electric field and the substorm-associated electric fields in the energization and transport of ions into the ring current is still an open question.

Observations show that substorm-associated electric fields usually display a very complicated behavior (Maynard, 1996). The enhanced electric fields are impulsive with amplitudes

of up to 20 mV/m, which is more than three times the largest convection electric field, and coincident with the braking of the fast flows and correlated with the magnetic field dipolarization in the inner central plasma sheet (Tu et al., 2000 and references therein).

Ganushkina et al. (2005) studied the role of electric field pulses in the ring current formation by tracing protons numerically in the guiding center approximation in Volland-Stern large-scale convection electric field and Tsyganenko T96 magnetic field models. In addition, they introduced substorm-associated variations as electric field pulses, similar to Li et al. (1998), at substorm onsets. It was shown that the large-scale convection alone can transport the ions to the observed ring current location, but that the electric field pulses were necessary to get the observed energy spectrum peaking at several tens of keV. The formation of the ring current is thus a combination of convection and pulsed inward shifts and consequent energization.

In order to evaluate the energy range, which is most important for the ring current energy content during storms, Ganushkina et al. (2005) analyzed Polar CAMMICE MICS particle data during 27 storms. The energy density and total energy of ring current protons were computed in the low (1–20 keV), medium (20–80 keV), and high (80–200 keV) energy ranges. The statistical results showed that the medium energy protons contributed most to the total ring current energy during the storm main phase. During the recovery phase, the high energy protons played a dominant role.

Further development of the particle tracing procedure made it possible to trace protons with arbitrary pitch angles, assuming conservation of the 1st and 2nd invariants, in different time-dependent magnetic and electric fields (Figure 4). For May 2–4, 1998 storm, using stationary Volland-Stern electric field model, the results showed that the main contribution to the ring current energy comes from protons with medium energies of 20-80 keV during the entire storm (Figure 4a). The contribution from the high energy protons was very small. Using other empirical electric field models, such as Boyle et al. (1997) polar cap potential applied to Volland-Stern type convection electric field, or varying the plasma sheet number density and/or temperature in the initial distribution showed similar results (Figure 4b). However, when the substorm activity was represented by incorporating the time varying fields associated with dipolarization in the magnetotail (similar to Sarris et al. (2002) pulse model), the contribution from the high energy protons became dominant during the storm recovery phase (Figure 4c).

Recently, three ring current models were used by Ganushkina et al. (2006) to follow the evolution of the proton ring current during the 2001-04-21–25 storm: The ring current model combined with tracing particles numerically in the drift approximation by Ganushkina et al. (2005), the empirical model of proton fluxes in the inner magnetosphere developed by Milillo et al. (2003), and the kinetic ring current-atmosphere interaction model (RAM) by Liemohn et al. (2001). It was found that (1) using more realistic magnetic field models leads to reduction of the ring current energy content by 30%; (2) details of the global convection field have little influence on the overall ring current evolution; (3) smaller-scale impulsive electric field have profound effects on the ring current evolution, particularly with regard to the acceleration of the higher-energy particles; and (4) in the ring current models, the choice of the initial and boundary conditions have significant effects on the modeled ring current intensity and energy spectrum.

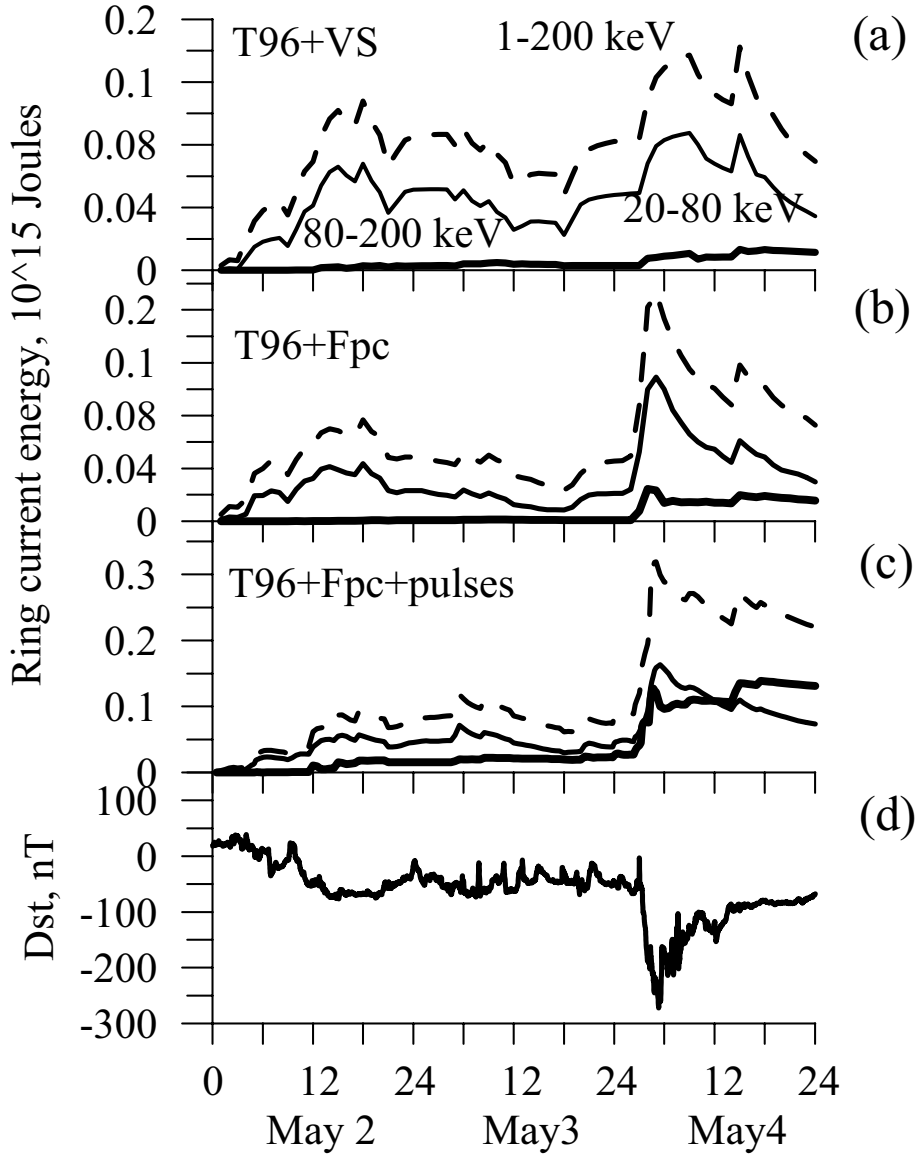

Fig. 4. Calculated proton ring current energy in Joule for total (1–200 keV, dashed lines), medium (20–80 keV, thin solid lines) and high energies (80–200 keV, thick solid lines) while tracing in (a) Tsyganenko T96 magnetic field and Volland-Stern electric field, (b) T96 and Boyle et al. (1997) polar cap potential applied to Volland-Stern model, and (c) with addition of electric field pulses at substorm onsets, together with the measured Dst index (d) for May 2–4, 1998.

As observations and modeling have shown, the substorm-associated electric fields are effective in the particle transport and energization. There is a great need to get more realistic models for the electric field. Likewise, there is an equal need for better and more comprehensive electric field observations that could be used to constrain such models both for the large-scale convection and smaller-scale temporally evolving structures.

As summarized above, the present state of our understanding of the magnetospheric dynamics is quite advanced. Thus, gaining new understanding will necessarily require complex models of the electromagnetic fields and particle motion. This will require combination and coupling of multiple sources as well as large-scale and small scale processes. The relative significance of these is still an open issue and calls for detailed as well as synoptic observations, preferably simultaneously.

5 Modeling of the ionospheric storm-time response at middle latitudes

The ionosphere is directly associated to the solar radiation and it strongly couples to the neutral atmosphere and the magnetosphere and therefore the forecasting and modeling of the ionospheric storm-time response is appeared to be a challenging scientific objective, while it is a strong requirement for state of the art space weather applications.

There have been several attempts to simulate the storm-time response of the thermosphere-ionosphere system using theoretical models, but the increasing demand for models suitable for real time applications turned the efforts in the development of empirical storm-time ionospheric models driven by geomagnetic activity indices. Such is the STORM Time Empirical Ionospheric Correction Model (Araujo-Pradere et al., 2002), which uses the 3-hour Ap index and the empirical model proposed by Kutiev & Muhtarov (2001), in which geomagnetic activity level is expressed by the kp index. A statistical approach to the problem was proposed by Muhtarov et al. (2002), in which the prediction efficiency of an autocorrelation model was improved by adding a synthetic geomagnetic index extracted from the predicted Ap in the Geomagnetically Correlated Autoregression Model (GCAM). Validation tests of the models' performance gave evidence for a limited improvement over climatology since the available geomagnetic activity indices either direct or transformed do not provide high enough correlation with ionospheric disturbances and there is no efficient geophysical index to predict the ionospheric storm onset, its magnitude and duration (Mikhailov et al., 2005).

Taking advantage from: i) recent studies that support the high correlation of ionospheric disturbances with Bz-IMF disturbances (Mikhailov et al., 2005) and the direct correlation of the IMF disturbances in terms of total IMF magnitude and Bz-IMF changes with the qualitative signature of ionospheric storm disturbances at middle latitudes (Belehaki & Tsagouri, 2002), ii) the availability of IMF observations in real-time from the NASA Advanced Composition Explorer (ACE) spacecraft from the vantage L1 point, and iii) recent advances in ionospheric storm dynamics (e.g., Proelss 1995; Tsagouri et al., 2000), an empirical storm-time model for nowcasting and forecasting ionospheric disturbances at middle latitudes, suitable for both scientific and operational purposes was recently suggested by Tsagouri & Belehaki (2006) driven by IMF conditions. The model was designed to introduce a storm time correction factor to the reference ionosphere level taking into account the IMF conditions and the local time of the observation point. Validation tests of the model's performance showed

significant improvement over climatology during storm days, while the model's predictions successfully capture the physical processes that governs the ionospheric storm onset and the ionospheric storm effects' temporal evolution during the first 24-hour, providing significant evidence for the close connection between solar wind disturbances and ionospheric storm effects at middle latitudes.

References

Araujo-Pradere, E.A., Fuller-Rowell, T.J., Codrescu, M.V.: STORM: An empirical storm-time ionospheric correction model - 1. Model description. Rad. Sc., **37**, (5), 1070, (2002)

Belehaki, A., Tsagouri, I.: On the occurrence of storm induced night time ionisation enhancements at ionospheric middle latitudes. J. Geophys. Res., doi:10.1029/2001JA005029 (2002)

Boyle, C.B., Reiff, P.H., Hairston, M.R.: Empirical polar cap potentials. J. Geophys. Res., **102**, 111–125 (1997)

Daglis, I.A., Axford, W.I.: Fast ionospheric response to enhanced activity in geospace: Ion feeding of the inner magnetotail. J. Geophys. Res., **101**, 5047–5065 (1996)

Delcourt, D.C., Sauvaud, J.-A., Pedersen, A.: Dynamics of single-particle orbits during substorm expansion phase. J. Geophys. Res., **95**, 20853–20865 (1990)

Ganushkina, N.Y., Pulkkinen, T.I., Fritz, T.: Role of substorm-associated impulsive electric fields in the ring current development during storms. Ann. Geophys., **23**, 579–591 (2005)

Janhunen, P.: GUMICS-3: A global ionosphere-magnetosphere coupling simulation with high ionospheric resolution. In Proceedings of Environmental Modeling for Space-Based Applications, Eur. Space Agency Spec. Publ., ESA SP-392 (1996)

Kan, J.R., Lee, L.C.: Energy coupling and the solar wind dynamo. Geophys. Res. Lett., **6**, 577 (1979)

Kutiev, I., Muhtarov, P.: Modeling of midlatitude F region response to geomagnetic activity. J. Geophys. Res., **106(A8)**, 15501–15509 (2001)

Li, X., Baker, D.N., Temerin, M. et al.: Simulation of dispersionless injections and drift echoes of energetic electrons associated with substorms. Geophys. Res. Lett., **25**, 3763–3766 (1998)

Liemohn, M.W., Kozyra, J.U., Thomsen, M.F. et al.: Dominant role of the asymmetric ring current in producing the stormtime Dst. J. Geophys. Res., **106**, 10883–10904 (2001)

Maynard, N.C., et al.: Dynamics of the inner magnetosphere near times of substorm onsets. J. Geophys. Res., **101**, 7705–7736 (1996)

McPherron, R.L.: The role of substorms in the generation of magnetic storms. In Tsurutani, B.T., Gonzalez, W.D., Kamide, Y., Arballo, J.K. Magnetic Storms, Geophys. Monogr. Ser., 98, AGU, Washington, DC (1997)

Mikhailov, A.V., Depuev, V.H., Depueva, A.H.: Short-term foF2 forecast: Present day state of art. In Space Weather: Research towards applications in Europe, Astrophysics and Space Science Library, **344**, 169–184 (2005)

Milillo, A., Orsini, S., Daglis, I.A.: Empirical model of proton fluxes in the equatorial inner magnetosphere: Development. J. Geophys. Res., **106**, 25713–25730 (2001)

Muhtarov, P., Kutiev, I., Cander L.: Geomagnetically correlated autoregression model for short-term prediction of ionospheric parameters. Inverse Problems, **18**, (1), 49–65 (2002)

Palmroth, M., Pulkkinen T.I., Janhunen P., Wu C.-C.: Stormtime energy transfer in global MHD simulation, J. Geophys. Res., 108(A1), 1048, doi: 101029/2002JA009446 (2003)

Palmroth, M., Janhunen, P., Pulkkinen, T. I., and Koskinen, H. E. J.: Ionospheric energy input as a function of solar wind parameters: global MHD simulation results, Ann. Geophys., 22, 549-566 (2004)

Palmroth, M., Janhunen, P., Pulkkinen, T. I., Aksnes, A., Lu, G., Ostgaard, N., Watermann, J., Reeves, G. D., and Germany, G. A.: Assessment of ionospheric Joule heating by GUMICS-4 MHD simulation, AMIE, and satellite-based statistics: Towards a synthesis, Ann. Geophys., 23, 2051-2068 (2005)

Palmroth, M., Janhunen, P., Germany, G. A., Lummerzheim, D., Liou, K., Baker, D. N., Barth, C., Weatherwax, A. T., Watermann, J.: Precipitation and total power consumption in the ionosphere: Global MHD simulation results compared with Polar and SNOE observations, Ann. Geophys., 24, 861-872 (2006a)

Palmroth, M., Laitinen, T. V., and Pulkkinen, T. I.: Magnetopause energy and mass transfer: Results from a global MHD simulation, Ann. Geophys., 24, 3467-3480 (2006b).

Palmroth, M., Janhunen, P., and Pulkkinen, T. I.: Hysteresis in solar wind power input to the magnetosphere, Geophys. Res. Lett., 33, L03107, doi: 10.1029/2005GL025188 (2006c)

Proelss, G.W.: Ionospheric F-region storms. In Handbook of Atmospheric Electrodynamics, 195–248, Volume II, CRC Press (1995)

Sarris, T.E, Li, X., Tsaggas, N., Paschalidis, N.: Modeling energetic particle injections in dynamic pulse fields with varying propagation speeds. J. Geophys. Res., **107**, doi:10.1029/2001JA900166 (2002)

Stern, D.P.: The motion of a proton in the equatorial magnetosphere. J. Geophys. Res., **80**, 595–599 (1975)

Tsagouri, I., Belehaki, A., Moraitis, G., Mavromihalaki, H.: Positive and negative ionospheric disturbances at middle latitudes during geomagnetic storms. Geophys. Res. Lett., **27**, (21), 3579–3582 (2000)

Tsagouri, I., Belehaki, A.: A new empirical model of middle latitude ionospheric response for space weather applications. Adv. Sp. Res., **37**, 420–425, (2006)

Tsyganenko, N.A.: A magnetospheric magnetic field model with a warped tail current sheet. Planet. Space Sci., **37**, 1, 5–20 (1989)

Tu, J.-N., Tsuruda, K., Hayakawa, H., Matsuoka, A., Mukai, T., Nagano, I., Yagitani, S.: Statistical nature of impulsive electric fields associated with fast ion flow in the near-Earth plasma sheet. J. Geophys. Res., **105**, 18901–18907 (2000)

Volland, H.: A semi-empirical model of large-scale magnetospheric electric field. J. Geophys. Res., **78**, 171–180 (1973)

ULF Wave Power Index for Space Weather Applications

Viacheslav Pilipenko[1], Natalia Romanova[2], and Laura Simms[3]

[1] Space Research Institute, Moscow pilipenk@augsburg.edu
[2] Institute of the Physics of the Earth, Moscow runatka@mail.ru
[3] Augsburg College, MN lsimms@augsburg.edu

Summary. The solar wind-magnetosphere interaction has a turbulent character which is not accounted for by commonly used geomagnetic indices and OMNI parameters. To quantify the level of low-frequency turbulence/variability of the geomagnetic field, IMF, and solar wind plasma, we have introduced a set of ULF wave power indices. These simple hourly indices are based on the band-integrated spectral power in the 2-7 mHz range. The ground geomagnetic wave index has been produced from data of ground-based magnetometer arrays in the northern hemisphere. The interplanetary and geostationary wave indices have been calculated using magnetometer and plasma data from interplanetary and geosynchronous satellites. The set of ULF wave indices has turned out to be an easy-to-use tool for the statistical analysis of various space weather problems. For example, these indices enables one to construct with the multi-regression analysis a path diagram which gives a complete description of the relative importance of interplanetary parameters in driving the ground ULF activity. The enhancements of relativistic electrons at the geosynchronous orbit correlate well with intervals of an elevated ground ULF wave index. This fact confirmed the importance of magnetospheric ULF turbulence in energizing electrons up to relativistic energies. The interplanetary index has revealed statistically the role of the interplanetary turbulence in IMF/solar wind driving of the magnetosphere. The application of this index to the analysis of conditions in the solar wind prior to magnetic storms has shown that a weak irregular increase of the solar wind density is observed on average 2 days before the storm commencement. The ULF index database for the period since 1991 is freely available via anonymous FTP for all interested researchers to further validation and statistical studies.

1 Introduction: the Necessity of Wave Indices

The interaction between the solar wind (SW) and the terrestrial magnetosphere is the primary driver of many magnetospheric plasma processes. This interaction has often been treated under the implicit assumption of quasi-steady and laminar plasma flow. However, many of the energy transfer processes in the magnetospheric boundary regions have a sporadic/bursty character, and observations have highlighted the importance of including the effects of turbulence (Borovsky et al., 2003). The turbulent character of SW drivers and the existence of natural MHD waveguides and resonators in near-terrestrial space in the lower ULF frequency range ($\sim$1-10 mHz) favours a quasi-periodic magnetic field response to SW forcing at the boundary layers. Much of the turbulent nature of plasma processes in SW-magnetosphere interaction can be observed in the ULF range with ground and space based sensors.

Progress in understanding and monitoring the turbulent processes in space physics is hampered by the lack of convenient tools for their characterization. The existing geomagnetic indices and OMNI hourly average parameters quantify the energy supply in certain regions of the coupled SW-magnetosphere-ionosphere system and are used as primary tools in statistical studies of solar-terrestrial relationships. However, these indices characterize the steady-state level of the electrodynamics of the near-Earth environment. Until recently there was no index characterizing the turbulent character of the energy transfer from the SW into the magnetosphere and the short-scale variability of near-Earth electromagnetic processes. However, for many space weather related problems a proxy for the level and character of low-frequency turbulence, even if a crude one, is of key importance. We will call it a "ULF turbulence index".

A new hourly turbulence index, based on the spectral ULF power in the Pc5 frequency band, was introduced by Kozyreva et al. (2006). The wave power index characterizes the ground ULF wave activity on a global scale and is calculated from northern hemisphere high-latitude ground-based magnetometer data. The ground power index is complemented by interplanetary and geostationary ULF wave indices as indicators of the turbulent state of the interplanetary space and the magnetosphere. The set of wave power indices derived from ground, geostationary, and interplanetary monitors provides scientists with a convenient and easy-to-use tool for the statistical study of the role of MHD turbulence in SW-magnetosphere interactions. In this paper we test the role of these ULF indices for statistical studies of various aspects of the solar-terrestrial relationships and demonstrate their merits and disadvantages.

2 Algorithm of the ULF Wave Index Construction

The algorithm for constructing the ULF wave index (Kozyreva et al., 2006) is based on an estimate of the ULF wave power $F_j = B_j(f)^2$ ($j = 1, 2, ...$) in the band Δf from f_L to f_H, averaged over N_c components:

$$T = \frac{1}{N_c}\left[\Delta f \sum_j \int_{fL}^{fH} F_j(f)df\right]^{1/2} \tag{1}$$

The signal component S of the spectral power is calculated similar to (1), but with the background spectral power $F^{(B)}(f)$ subtracted from the total spectral power $F(f)$, namely $F_j(f) \rightarrow F_j(f) - F_j^{(B)}(f)$. The background spectrum is determined as a least-square fit of the power-law spectral form $F^{(B)}(f) \propto f^{-\alpha}$ in a chosen frequency band. The spectral power below $F^{(B)}(f)$ is attributed to noise $N_j(f)$, so $T_j = S_j + N_j$. However, the statistical relationships obtained with the two indices T and S turned out to be very similar. The final product is composed from the suite of the following hourly ULF wave indices:

- The ground ULF wave index (T_{GR}, S_{GR}) is a proxy for global ULF activity. It is derived from the peak values of wave powers computed from 1-min samples of the horizontal components of all magnetometer stations in the 05 to 15 MLT sector (to exclude irregular nighttime disturbances), and in the latitudinal range from 60°to 70°geomagnetic latitude. An extension of the latitude range does not influence significantly the resultant index.

- The geostationary ULF wave index (T_{GEO}, S_{GEO}) is calculated from 1-min 3-component magnetic data from GOES satellites and quantifies magnetic fluctuations in the region of the geostationary orbit.

- The interplanetary ULF wave index (T_{IMF}, S_{IMF}) quantifies the short-term IMF variability and T_n the solar wind fluctuations. They are calculated from 1-min resolution data from the interplanetary spacecraft WIND and ACE. The data are time-shifted to the terrestrial bow shock ($\sim$15 R_E). Alternatively, the 1-min OMNI database may be used.

In this paper we demonstrate that a wide range of space physics studies may benefit from the introduction of the ULF wave index. The availability of a simple proxy for the near-Earth turbulence gives the possibility to visualize its role in solar-terrestrial relationships.

3 Solar Wind/Magnetosphere Coupling

The turbulent/eddy viscosity of the SW flow passing the magnetosphere is controlled to a considerable extent by the level of upstream turbulence. Therefore, the degree of global coupling of the SW flow to the magnetosphere appears to be influenced by the level of SW/IMF turbulence upstream of the Earth (Borovsky et al., 2003). The eddy viscosity concept predicts that the magnetosphere behaves as a turbulent high-Reynolds-number system, so the coupling lessens when the level of upstream turbulence lessens. Therefore, the presence of turbulence inside and outside the magnetosphere should have profound effects on the large-scale dynamics of the system through eddy viscosity and diffusion.

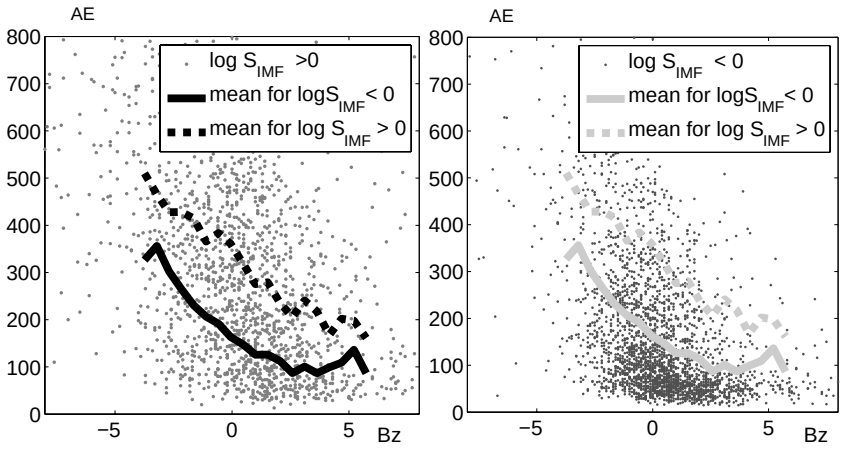

Fig. 1. The dependence of auroral activity, as characterized by AE index (in nT), on the IMF driver B_z (in nT) for quiet (log$T_{IMF} < 0$) and turbulent (log$T_{IMF} > 0$) IMF for the period 1994–1995.

With the help of the ULF index T_{IMF} we confirm that a more turbulent SW results in a higher effective degree of SW coupling to the magnetosphere (Borovsky et al., 2003; Gon-

charova et al., 2004). The auroral response, characterized by the hourly average of the AE index, is compared to the strength of the SW driver, characterized by the IMF B_z component, for laminar and turbulent IMF (Figure 1). The IMF is considered turbulent when $\log S_{IMF} > 0$ and steady when $\log S_{IMF} < 0$. Comparison of median curves shows that under southward IMF condition ($B_z < 0$) AE grows nearly linearly with an increase of the magnitude of B_z. For northward B_z the average AE values do not strongly depend on the SW driver. The auroral response to turbulent IMF is generally higher than to laminar IMF. The difference is most significant for IMF $B_z \geq 0$ when one expects viscous interaction to dominate over reconnection. Our comparison confirms that the magnetosphere is driven more weakly when the IMF turbulence level is low.

4 Which IMF Parameters Control the Ground ULF Wave Activity?

Numerous studies have shown that the SW velocity is the key parameter to control the ground ULF activity. However, these results were obtained using data from a few selected stations which were subject to diurnal variations owing to the Earth's rotation. The new global ground ULF index S_{GR} provides the opportunity to verify this result. The correspondence between the ground ULF wave power and the solar wind speed V is for slow SW ($V < 450$km/s) and fast SW ($V > 450$km/s), see Figure 2, left panel. The distribution has clear lower and upper boundaries (indicated by dashed lines), indicating that for any V the ground wave activity cannot exceed a V-independent saturation level. The occurrence of lower and upper boundaries signifies that the intensity of ground fluctuations is within certain limits for any given V. These statistical results should be explained by theories of ULF wave excitation through the Kelvin-Helmholtz instability.

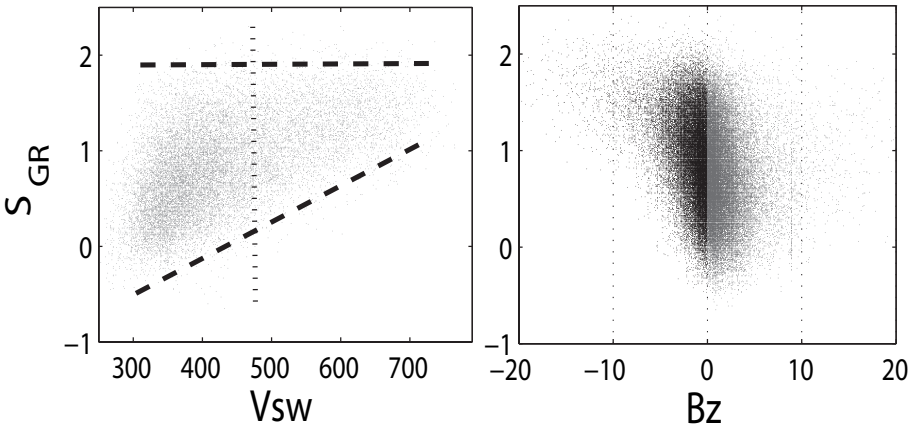

Fig. 2. Correspondence between the global ground ULF activity, as characterized by $\log S_{GR}$ index, and the SW velocity V (left panel) and IMF orientation Bz (right panel).

However, the SW velocity is not the only controlling factor of magnetospheric ULF wave activity. Figure 2 (right panel) shows different S_{GR} distribution patterns for northward ($Bz > 0$) and southward ($Bz < 0$) IMF. Statistically the ground ULF wave activity is somewhat higher under southward IMF. This may indicate that reconnection contributes to processes which stimulate ULF activity.

Ground and interplanetary ULF power indices provide a convenient tool not only for the visualization but also for the statistical analysis of the SW-magnetosphere interaction thereby accounting for the turbulence aspect. As an example we consider the path analysis of the possible drivers of ground ULF wave activity. Path analysis is a visualization of multiple regression - a diagram showing possible causal relationships between the variables. The relative strengths of the path coefficients (standardized regression coefficients) are used to determine which paths have the most influence on the dependent variable. In the path diagram solid lines represent positive and dashed lines negative correlations. The effect of each independent variable on the ground ULF activity, characterized by the T_{GR} index, is considered to be a combination of both direct and indirect paths.

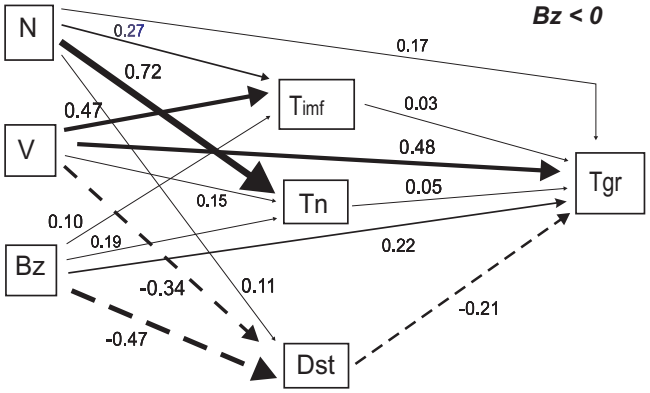

Fig. 3. Path diagram showing the direct and indirect influence of IMF/SW parameters on ground ULF activity under southward IMF conditions. The standardized regression coefficients attached to the arrows indicate the relative contribution of each controlling parameter to the magnitude of T_{GR}.

The diagram in Figure 3 shows that V has the greatest direct effect on ground ULF activity for southward IMF, with some contribution from Bz and N. There are also contributions from indirect paths via IMF/SW turbulence and ring current formation as characterized by the T_{IMF}, T_N, and Dst indices.

5 IMF and SW Variability Before Magnetic Storms

SW density fluctuations with time scales ∼2-250 min are often observed many hours before magnetic storm onsets (Khabarova et al., 2006). The change of the SW turbulence in the ULF frequency range is verified statistically using the new wave indices. We consider here the interplanetary ULF wave index T_n derived from the ACE plasma measurements. Figure 4 shows histograms of T_n distributions over all times of an entire year and during the 12-hour interval before storm onset, for solar minimum (1995, left panel) and solar maximum (2000, right panel). The samples include all storms with an intensity exceeding $Dst < -50$ nT. The

histograms show a shift of the T_n distributions to higher values in the 12 hours before storm onset both at solar minimum and maximum. The enhancement becomes less evident if a 2-day interval before onset is used (not shown). Thus, the SW density becomes more turbulent and irregular about at least 1/2 day before the arrival of solar stream causing a storm.

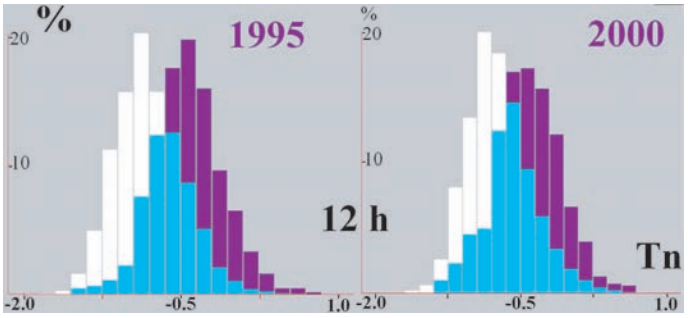

Fig. 4. Statistical distributions of the T_n index during solar minimum (left) and solar maximum (right) years: yearly distribution (white), distribution during 12-hour interval before storm onset (blue) and intersection between them (green).

This fact may be considered as an indication of a pre-conditioning of storm stimulation. The plasma density enhancement near the heliospheric current sheet (HCS) and high-speed corotating streams adjacent to the HCS plasma sheet may occur. The presence of naturally occurring irregular high densities and stream-stream compressive effects may indicate that both, an L1 spacecraft and the Earth, are approaching the HCS region The histogram may indicate that statistically the region of the corotating stream interaction with the HCS is favorable for triggering moderate storms.

6 ULF Wave Index and "Killer" Electrons

Here we consider the application of the ULF wave index to the problem of magnetospheric electron acceleration up to relativistic energies. The relativistic electron events are not merely a curiosity for scientists, they can have disruptive consequences for spacecrafts (Pilipenko et al., 2006). Commonly, relativistic electron enhancements in the outer radiation belt are associated with magnetic storms (Baker et al., 1998; Reeves, 1998), though the wide variability of the response and the puzzling time delay ($\sim$2 days) between storm main phase and the response has hampered the identification of responsible mechanisms. Moreover, some electron events may occur even without a magnetic storm or during a very mild storms ($|Dst| \sim$ 20-40 nT). An example of such an event on is shown in Figure 5. In this case a high-speed solar stream arrives without a favorable Bz and consequently does not trigger a substantial storm (as measured by the Dst index).

The efficiency of non-identified mechanisms of energetic electron acceleration is strongly enhanced upon increase of V. Because the SW does not interact directly with magnetospheric electrons, some intermediary must provide energy more directly to the electrons. Rather surprisingly, ULF waves in the Pc5 band (at a few mHz) have emerged as a possible energy reservoir: the presence of Pc5 wave power after minimum Dst was found to be a good indicator of relativistic electron response (O'Brien et al., 2001). In a laminar, non-turbulent

magnetosphere the "killer" electrons would not appear. The proposed mechanism of electron acceleration to ∼100 keV supplied by substorms is a revival of the idea of the magnetospheric geosynchrotron: pumping of energy into seed electrons is provided by large-scale MHD waves in a resonant way when the wave period matches an integer multiple of the electron drift period (Elkington et al., 1999; Ukhorsky et al., 2005). However, this mechanism is not the only one, a local resonant acceleration upon interaction with high-frequency chorus emissions was claimed to be responsible for the electron energization (Meredith et al., 2003).

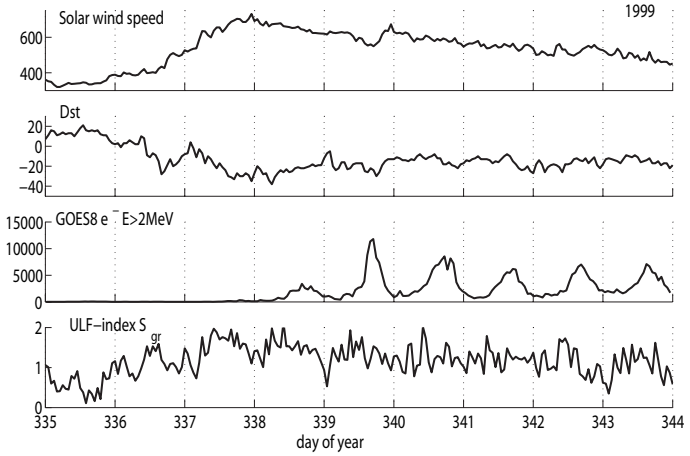

Fig. 5. The "electron event" without magnetic storm observed at GOES-8 on December, 1999.

The example shown in Figure 6 shows that an increase of the relativistic electron flux up to 2–3 orders occurs after weak storms, but the increase after strong storm was much shorter and less intense. At the same time, the correspondence with ULF wave activity is quite well for all events.

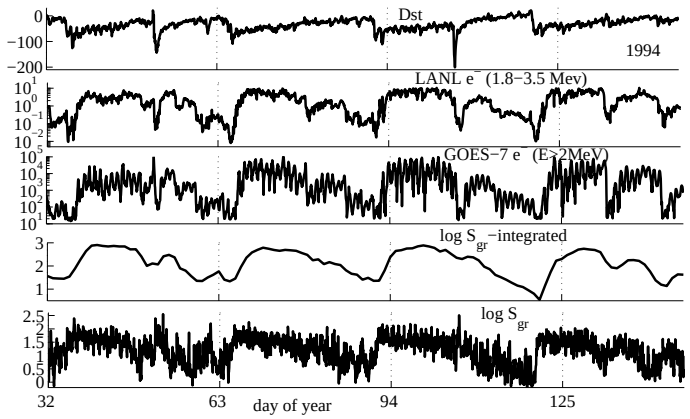

Fig. 6. Comparison between the Dst index, electron fluxes at geostationary orbit measured by LANL $J_e(\mathrm{cm}^2\mathrm{keV}\cdot\mathrm{s}\cdot\mathrm{str})^{-1}$ and GOES-7 $J_e(\mathrm{cm}^2\cdot\mathrm{s}\cdot\mathrm{str})^{-1}$, cumulative index $\langle S_{GR}\rangle$, and ULF index S_{GR} during 1994.

Figure 6 suggests that long persistent ULF activity is more important for electron acceleration than short-term ULF bursts even if intense. Thus, the cumulative ULF index

$$\langle S_{GR} \rangle = \tau^{-1} \int_{-\infty}^{t} S_{GR}(t) \exp(-t/\tau) dt \tag{2}$$

integrated over a time frame $\tau \sim 2 - 3$ days might be a more appropriate parameter than the standard ULF index. Indeed, the correlation of electron flux with integrated ULF-index increases substantially, from $\sim$0.5 to $\sim$0.8 (see Figure 7). The cross-correlation function shows that the elevated level of ULF wave activity precedes the peak of relativistic electron flux for about 2 days (Mann et al., 2004), whereas the same delay for the cumulative index is about 1 day. This increase of correlation, probably, implies the occurrence of a cumulative effect of some diffusion process.

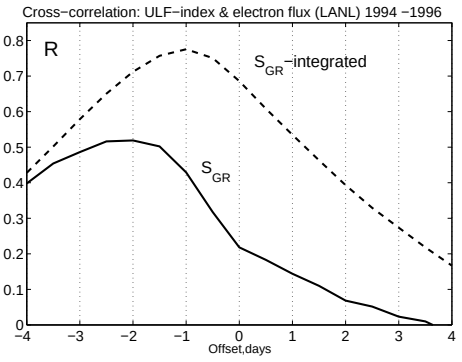

Fig. 7. Cross correlation between the electron flux $J_e(\text{cm}^2\text{keV}\cdot\text{s}\cdot\text{str})^{-1}$ at geostationary orbit measured by LANL and the cumulative, $\langle S_{GR} \rangle$, (dashed) and standard, S_{GR}, (solid) ULF indices during 1994.

7 Conclusions

The new ULF wave power index is a simple and convenient tool for the description of the turbulence of the SW-magnetosphere system. It can be applied to various space physics problems. If employed to examine the SW plasma structure in front of the Earth it may serve as a medium-term magnetic storm forecast. A preliminary analysis using these indices has elucidated the role of ULF turbulence in the magnetospheric field and particle response to SW/IMF forcing. The correlation between "killer" electron flux and time-integrated ULF power is high, which indicates that the mechanism of a "magnetospheric geosynchrotron" does contribute to the electron acceleration. Therefore, the ULF index should be taken into account by any adequate space radiation model. The ULF index database for the period since 1991 is freely available via anonymous FTP (*space.augsburg.edu/MACCS/ULF-index*) or may be requested on CD from authors for further validation and statistical studies.

Acknowledgments. This study is supported by the INTAS grants 05-1000008-7978 and YSF 05-109-4661, and NSF grant ATM-0305483. We appreciate the help of O. Kozyreva in the index production.

References

Borovsky, J.E., Funsten, H.O.: Role of solar wind turbulence in the coupling of the solar wind to the Earth's magnetosphere, J. Geophys. Res., **108**, 1246, doi:10.1029/2002JA009601 (2003)

Kozyreva, O.V., Pilipenko, V.A., Engebretson, M.J., Yumoto, K., Watermann, J., Romanova, N.: In search of new ULF wave index: Comparison of Pc5 power with dynamics of geostationary relativistic electrons, Planet. Space Science, **55**, 755–769 (2006)

Goncharova, M.Yu., Pilipenko V.A.: The IMF Bz variability - high-latitude magnetic activity index relationship, Proc. of Conf. in memory Yu. Galperin 3-7 Feb., 2003 "Auroral phenomena and solar-terrestrial relations", Boulder, SCOSTEP, 134–141 (2004)

Khabarova, O., Pilipenko V., Engebretson M.J., Rudenchik E.: Solar wind and interplanetary magnetic field features before magnetic storm onset, Proc. of the 8-th International Conference on Substorms, Canada, 127–132 (2006)

Pilipenko, V., Yagova, N., Romanova, N., Allen, J.: Statistical relationships between the satellite anomalies at geostationary orbits and high-energy particles, Advances in Space Res., **37**, 1192–1205 (2006)

Baker, D.N., et al.: Coronal mass ejections, magnetic clouds, and relativistic magnetospheric electron events: ISTP, J. Geophys. Res., **103**, 17279–17291 (1998)

Reeves, G.D., Relativistic electrons and magnetic storms: 1992-1995, Geophys. Res. Lett., **25**, 1817–1820 (1998).

O'Brien T.P., McPherron R.L., Sornette D., Reeves G.D., R. Friedel, Singer H.J.: Which magnetic storms produce relativistic electrons at geosynchronous orbit? J. Geophys. Res., **106**, 15533–15544 (2001)

Elkington, S.R., Hudson M.K., Chan A.A.: Acceleration of relativistic electrons via drift-resonant interaction with toroidal-mode Pc5 ULF oscillations, Geophys. Res. Lett., **26**, 3273–3276 (1999)

Ukhorskiy, A.Y., Takahashi K., Anderson B.J., Korth H.: Impact of toroidal ULF waves on the outer radiation belt electrons, J. Geophys. Res., **110**, A10202, doi:10.1029/2005JA011017 (2005)

Meredith N.P., et al.: Evidence for chorus-driven electron acceleration to relativistic energies from a survey of geomagnetically disturbed periods, J. Geophys. Res., **108**, 1248, doi:10.1029/2002JA009764 (2003)

Mann I.R., O'Brien, T.P., Milling, D.K.: Correlations between ULF wave power, solar wind speed, and relativistic electron flux in the magnetosphere: solar cycle dependence, J. Atmosph. Solar-Terr. Phys., **66**, 187–198 (2004)

Empirical modeling of the magnetospheric ring current

Anna Milillo and Stefano Orsini

INAF/IFSI, Rome, Italy
anna.milillo@ifsi-roma.inaf.it, stefano.orsini@ifsi-roma.inaf.it

Summary. By using theoretical models of plasma dynamics, it is possible to reconstruct the evolution of many magnetospheric processes; nevertheless, these models need the support of both electric and magnetic field models, and they can simulate only known processes. Conversely, the empirical models are mainly based on statistical analysis; hence, they start from observations, not from processes. Statistical analyses and the derived empirical models are important complements to theoretical models and simulations since the former represent the actual conditions. The empirical models of the inner magnetosphere ion distribution by Milillo et al. (2001) and of the pitch angle distribution by De Benedetti et al. (2005) have proved to be successful in deriving average features of the ring current as well as in obtaining the long-term development of the ion distributions during quiet and disturbed periods. The major goals of this approach are: 1) the description of the equatorial proton population during quiet times and the quantitative characterization of their spatial and energetic distribution; 2) the evidence of some key features of the proton distribution strictly connected to the solar wind characteristics; 3) the investigation of the evolution of magnetospheric ion populations during geomagnetic disturbances and their role in the ring current development. In this paper we review the above mentioned studies.

1 Introduction

Generally, theoretical models provide a useful tool for the understanding of the dynamics of the magnetospheric plasma. The models are based on known physical processes but require assumptions and approximations such as adiabaticity, electromagnetic configuration, active loss/source processes, boundary conditions, etc. (e.g., Ebihara and Ejiri (2000); Jordanova et al. (2001); Fok et al. (2001); Liemohn et al. (2001); Ganushkina et al. (2005)). Sometimes they are linked to observations used as boundary conditions (e.g., Fok et al. (1996)). But they cannot explain processes which are active in the magnetosphere and not included in the model. For this reason, statistical analyses and the derived empirical models are important complements to theoretical models and simulations since they represent the actual conditions.

Empirical models of the inner magnetospheric ion population were developed thanks to the ion data collected in a systematic way after the end of the 1980s by the AMPTE-CCE, Polar (Acuna et al., 1995) and LANL satellites. In fact, the AMPTE-CCE/CHEM data allowed to perform statistical studies in order to study both the quiet and storm time ring current (Kistler et al., 1989; Daglis et al., 1990; Sheldon and Hamilton, 1993; Orsini et al., 1994; Fok

et al., 1996; Jordanova et al., 1996). Sheldon and Hamilton (1993), for instance, compiled a quiet time data set from AMPTE-CCE/CHEM data. Their selection criteria were based on both *Dst* and *Kp* indexes. Fok et al. (1996) used the same data set as initial condition in order to compare specific storm-time AMPTE-CCE/CHEM data with theoretical simulations. Orsini et al. (1994) compiled a data set by ordering the H^+, He^+, and O^+AMPTE/CCE/CHEM observations according to three levels of the *AE* index. By using these data, the average plasma pressure at different geomagnetic activity levels was derived, (Lui and Hamilton, 1992; De Michelis et al., 1999; Milillo et al., 2003).

More recently, Roeder et al. (2005) used more than three years (between 1996-1999) of particle flux data by the Polar/CAMMICE/MICS (Wilken et al., 1992) and Hydra instruments to build empirical models of the plasma environment (H^+, $O^+$and electrons) at energies between 20 eV and 200 keV in the Earth's inner magnetosphere. The combination of the CAMMICE/MICS and Hydra models provides the average ion flux as a function of position in the magnetosphere regardless of geomagnetic activity. Korth et al. (1999), averaging one year of LANL/MPA data (Bame et al., 1993; McComas et al., 1993), performed a statistical analysis of the geosynchronous plasma in order to study the plasma sheet access.

Data collection and/or storage problems may be overcome when the experimental data are treated through an analytical approximation. Milillo et al. (1999, 2001) introduced the formulation of an empirical model capable of reproducing the inner magnetospheric distributions of the 90°pitch angle proton flux at low geomagnetic activity ($AE < 100$ nT) trough a functional form, directly derived from the average AMPTE-CCE/CHEM ion fluxes. The functional form of Milillo et al. (2001), referred to as MODEM (Milillo-Orsini-Daglis-Empirical-Model), is expressed as a function of the L-shell parameter (L), energy (E) and Magnetic Local Time (MLT). The same data set has been used to derive an H^+pitch angle distribution model (De Benedetti et al., 2005), referred to as PADEM (Pitch-Angle-Distribution-Empirical-Model). This model describes the pitch angle distribution of the proton flux as a function of geocentric distance, energy and MLT, normalized by the 90°pitch angle flux at low geomagnetic activity. By combining these two models a full description of the proton distribution is available.

By varying a few parameters of the MODEM according to local measurements, the general characteristics of the long-term evolution of the proton distributions during quiet as well as storm times are reproduced (Orsini et al., 2004; Milillo et al., 2006). This easy and quick approach (referred to as dynamic MODEM) proved to be a useful tool for global viewing magnetospheric dynamics from local measurements.

The empirical models are useful not only to obtain global average distributions but also for many other purposes. In fact, they can be used as initial and/or boundary conditions for the theoretical models (Ebihara et al., 2002). Furthermore, macroscopic quantities (such as energy density, total energy, perpendicular current density and so forth) which characterize the inner magnetosphere can be derived and compared to the results of theoretical models (Milillo et al., 2003; Ganushkina et al., 2006). Milillo et al. (2003) derived from MODEM an electric field model that can be used as input for theoretical particle circulation models.

The organization of this paper is as follows. The ion data base is briefly described in section 2. Section 3 summarizes the method followed in order to determine the functional forms of MODEM and PADEM. Some of the dynamic MODEM results are described in section 4.

2 Statistical Analysis

The the AMPTE-CCE/CHEM instrument (Gloeckler et al., 1985) measures energetic ions in 32 logarithmically equally spaced energy channels ranging from 1.5 keV to 316 keV. Data collected in the equatorial inner magnetosphere between L=3.0 and L=9.5 over the whole mission period (1985 through 1987) were analysed. Measurements of the three main species in the Earth's inner magnetosphere (H^+, $He^+$and O^+) were divided into three different classes according to geomagnetic activity (AE<100 nT, 100 nT<AE<600 nT and AE>600 nT) and averaged within bins of 0.25 (L), 1 hour (MLT), and 20°pitch angle (Orsini et al., 1994). An extract of the data set (proton fluxes at low geomagnetic activity) is shown in Fig. 1 in the form of an L-E diagram.

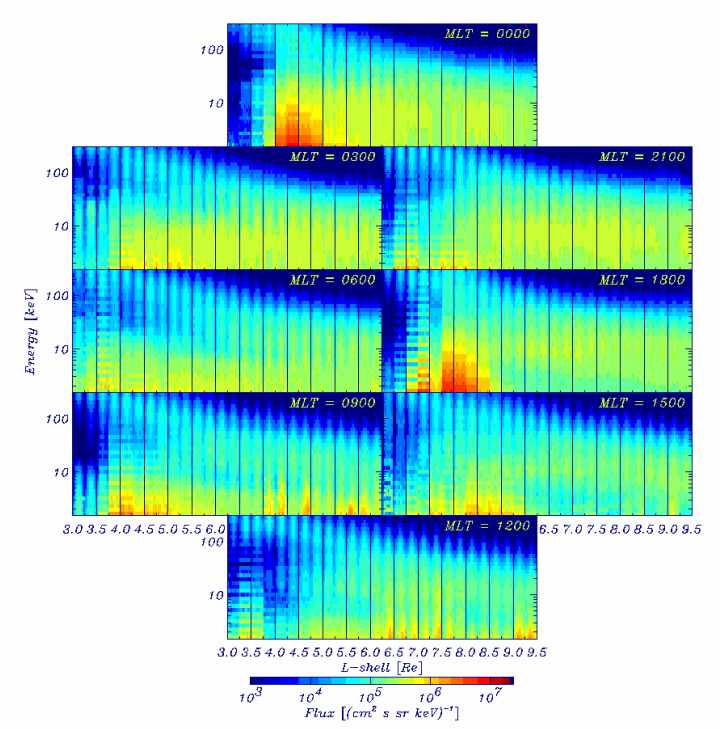

Fig. 1. Proton fluxes for AE<100 nT vs L and E (in keV). For each L-E bin the pitch angle distribution is color-coded. Different panels refer to different MLT: 0000, 0300, 0600, 0900, 1200, 1500, 1800, 2100 (from De Benedetti et al. (2005)). The H^+AMPTE-CCE/CHEM measurements at L<5 and E<30 keV are not guaranteed to be free from background noise, due to contamination by the radiation belt high energy ions/electrons.

The varoius panels of Fig. 1 evidence the presence of two main proton populations in the Earth's inner magnetosphere. One at energies lower than few tens of keV extends up to L=9 and is strongly asymmetric in azimuth, the other at higher energies is more symmetric in azimuth, but strongly energy-distance dependent, in fact, the flux increases in energy in the inner regions. This second population is not seen in the O^+distribution (see Fig. 2) as evidenced by Orsini et al. (1994) and Roeder et al. (2005).

The physical interpretation of these two populations is that lower energy proton fluxes are directly linked to the entry from the plasma sheet via convection and/or injection. These fluxes

are strongly influenced by electromagnetic fields; hence, they are subjected to the asymmetries that characterize these fields. The higher energy population is associated with particles which reside inside the magnetosphere for a longer period. The *L-E* behavior is in fact typical for low diffusion conditions (Ejiri, 1978). Since the proton life time (approximately the charge-exchange characteristic time, Orsini et al. (1994)) is longer than the O^+life time this population is evident only in the H^+data set.

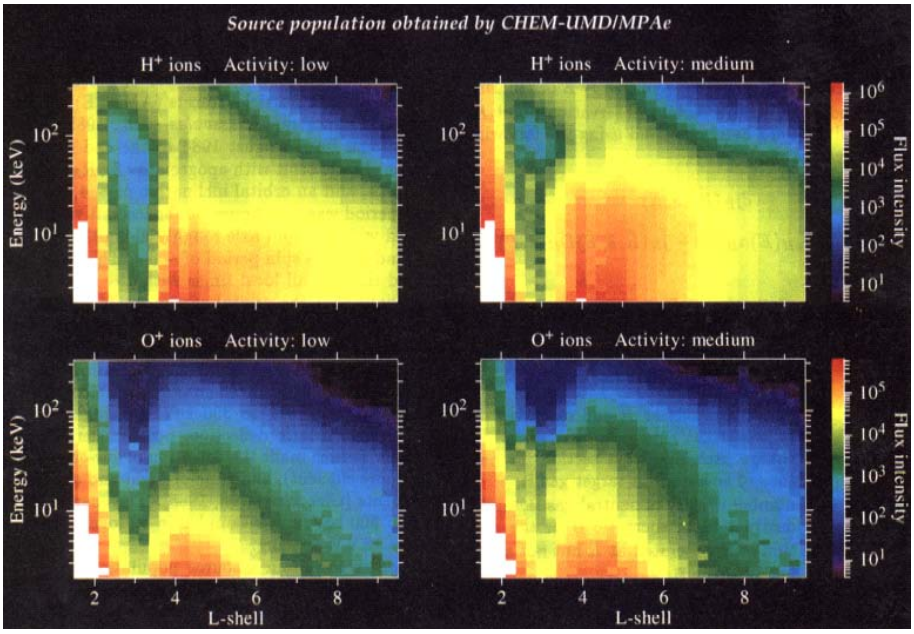

Fig. 2. Color-coded H^+(top) and O^+(bottom) differential flux as a function of *L* and *e* as derived by AMPTE-CCE/CHEM averaged observations (MLT 2300-0100). Left panels refer to periods when $AE<500$ nT, right panels refer to 500 nT$<AE<$1000 nT periods (from Orsini et al., 1994).

3 Stationary Empirical Models

3.1 MODEM

MODEM, describing the 90°pitch angle equatorial proton differential flux per energy and steradiant, *f*, consists of the composition of different empirical functions of *L*, *e*=log(*E*) and MLT (*h*). Some functions are probably the analytic description of contamination due to high-energy particles that affected the original data or of transient intense phenomena that affect the averaged fluxes; for example, they can be related to the dayside detached auroras (Zhang et al., 2003, 2004). Hence, the description of convected or injected population as well as diffused population is described by a subset of the model as stated in Milillo et al. (2003).

The considered subset is: 1) a wide Gaussian function in L that describes the basic ion flux at intermediate energies (5-60 keV); 2) a Gaussian function in L characterizing the high-energy population (E>20 keV). The first function is weighted by a step function due to the sharp flux cut-off below $L\approx3.5$.

One of the major outcomes from this stationary model is the relation between the characteristic energy of the convected/injected population and MLT. In Fig. 3, upper panel, the intensity of the strongest flux is displayed in an MLT-e frame. In fact, there is a clear linear relation between log(E) and MLT which is described by the MODEM parameter $COAG2_B$=-0.0318h+3.66. This relation is in good agreement with the relation concerning the characteristic energy of the nose structure during low Kp (Vallat et al., 2007), see Fig. 3, bottom panel. This effect is due to the combination of the convection of particles in the presence of the magnetic and electric field together with the loss processes acting in the inner magnetosphere that produce an energy dependent flux decrease resulting in a gap in the energy distribution depending on MLT (Milillo et al., 2003).

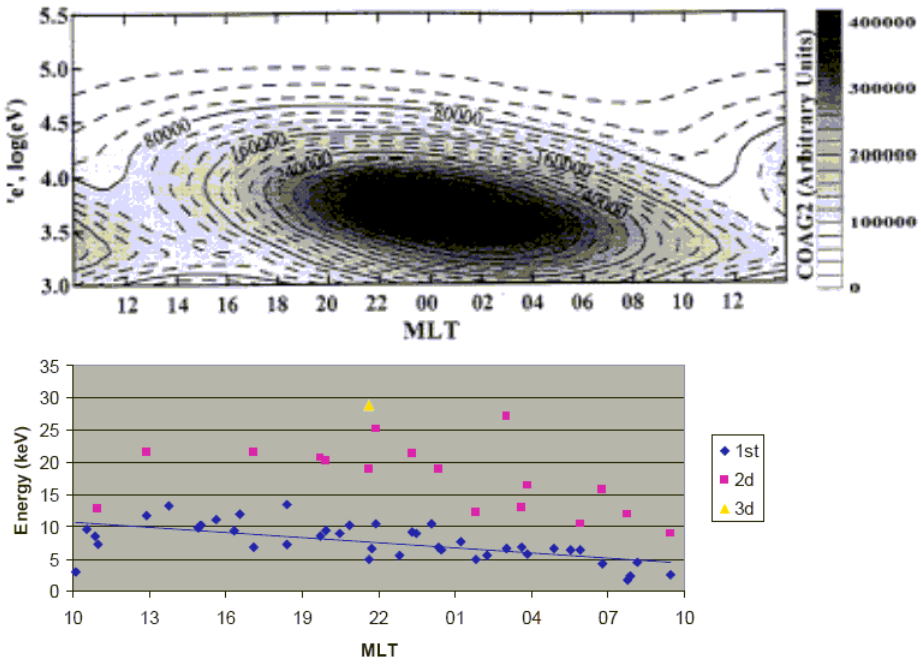

Fig. 3. Top panel: Contour plot in an MLT-e frame of the maximum flux of the convected/injected population at low geomagnetic activity (from Milillo et al. (2001)). The characteristic energy of the population increases from midnight toward dusk and decreases toward dawn. Bottom panel: Characteristic energy of the nose structure vs. MLT for Kp=0 and Kp=1 (Vallat et al., 2007). Note that the energy axis is logaritmic in the upper panel and linear in the second one.

3.2 PADEM

PADEM consists of a multi-parametric functional form that depends on pitch angle, energy, L-shell and a few independent factors. Different factors are determined for different MLT hours. This is the first model capable to accurately reproduce the average proton pitch angle distribution in the whole inner magnetosphere. It reveals interesting statistical features many of which confirm the results of previous studies related to magnetic field drift shell splitting (e.g., Roederer (1967)), electric field drift shell splitting (Korth et al., 1983) and magnetopause shadowing (e.g., West et al. (1973)). For example, pitch angle anisotropy is higher in the inner regions than in the outer regions (Fok et al., 1995). Generally, fresh particles, convected from the plasma sheet, have more isotropic PAD while long time resident particles exhibit anisotropic PAD essentially for two reasons: i) they have different trajectories in the inner magnetosphere according to their pitch angle, producing both butterfly and pancake PAD; ii) they are affected by charge-exchange loss processes (acting on low energy ions that reach high latitudes at low altitudes, where the geocoronal density is higher) or by pitch angle scattering and wave-particle interactions (acting on high-energy particles, see Fok et al. (1996), mainly at higher latitudes), thus generating pancake PAD.

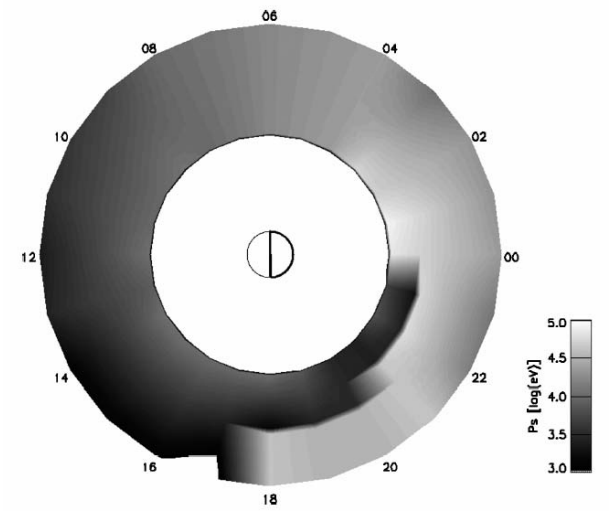

Fig. 4. Grey-scaled L-MLT polar map of the parameter describing the energy where the PAD becomes more isotropic defined for $5<L<9$. The circle at L=1 with the night side in bold is also indicated (from De Benedetti et al. (2005)).

De Benedetti et al. (2005) found that in the outer regions the PAD exhibit isotropic or less pronounced pancake profiles at a specific energy which exhibits a clear MLT dependence (Fig. 4). It increases clockwise giving the impression of a spiral shape. In fact, starting in the inner regions in the night-dusk sector at an energy of 3 keV, it reaches values close to 10 keV on the day side; it is almost constantly 20 keV between L=5 and L=9 in the dawn side and increases from 20 keV up to values close to 100 keV in the night side inner regions; finally, at dusk, after a complete circle, a second isotropization is noticeable at larger distances at energies of tens of keVs. This feature seems to be related to the last closed paths of the particles. In fact, the $E>30$ keV particles escape in the dusk flank while the 5 keV$<E<$30 keV particles

penetrate deeper and circulate around the Earth acquiring more energy by approaching intense magnetic field regions. Where the electric equipotential lines are closed in quiet conditions, fresh particles are not seen.

4 Dynamical Proton Distribution Model

Dynamic MODEM was used to derive a realistic global picture of the inner magnetosphere from in situ spacecraft measurements (Orsini et al., 2004; Milillo et al., 2006). The procedure is performed by tuning a subset of the model parameters in order to reconstruct the development of the measured data at a given location. The six selected parameters deal with the characteristics of the two plasma distributions described by MODEM: intensity, position and width of the two energy spectra. Orsini et al. (2004) showed that generally a good relation exists between the selected parameters and the *Dst* index. For instance, Fig. 5 shows that the width of the convected/injected population increases with geomagnetic activity.

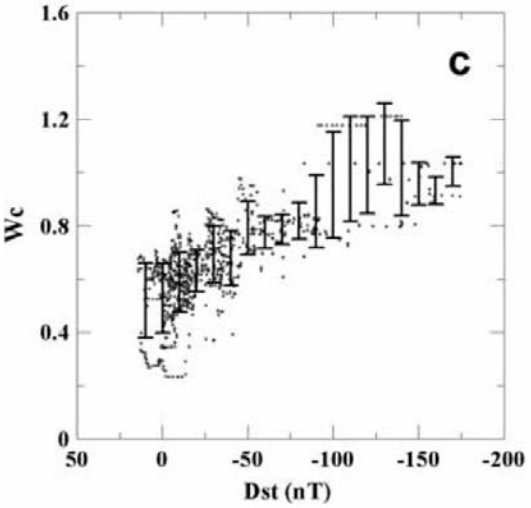

Fig. 5. Scatter-plot of the running averages of the parameter that describes the width of the convected/injected population versus averaged *Dst*. The average statistical uncertainties within 1 standard error are plotted in steps of 10 nT as solid bars (from Orsini et al. (2004))

Milillo et al. (2006) found that the same parameter increases according to the convection electric field, $V_s w B_z$, and this increase occurs simultaneously with the solar wind arrival at the magnetopause in the night sector while it has different time shifts proceeding clockwise (dusk, noon, dawn). This reflects the sudden response of the flux distribution to the electric field increase in the night side and the clockwise circulation of the "fresh" particles.

Ganushkina et al. (2006) compared the results of theoretical models with those from dynamic MODEM, evidencing that the contribution of different ring current populations to the total energy during storm time has a clear development. The empirical approach reveals a good agreement with the observed geomagnetic disturbances, as well as with the result evidenced by Ganushkina et al. (2005) which shows that the higher energy particles contribute mainly during recovery phase thanks to the effect of the electric field pulses during the storm. In

fact, the dynamic MODEM diffused population contributes mainly during the storm recovery phases.

References

Acuna, M.H., Ogilvie, K.W., Baker, D.N., Curtis, S.A., Fairfield, D.H., Mish, W.H. The Global Geospace Science Program and its investigations. Space Sci. Rev., **71**, 5–21 (1995)

Bame, S.J., et al.: Magnetospheric plasma analyzer for spacecraft with constrained resources. Rev. Sci. Instr., **64**, 1026 (1993)

Daglis I.A., Sarris, E.T., Kremser, G.: Indications for ionospheric participation in the substorm process from AMPTE/CCE observations. Geophys. Res. Lett., **17**, 57–60 (1990)

De Benedetti, J., Milillo, A., Orsini, S., Mura, A., De Angelis, E., Daglis, I.A.: Empirical Model of the Inner Magnetosphere H^+Pitch Angle Distributions. In: Pulkkinen, T., Friedel, R., Tsyganenko, N. (eds) The Inner Magnetosphere: Physics and Modelling. AGU Monograph series, **38**, 283–291 (2005)

De Michelis, P., Daglis, I.A., Consolini, G.: An average image of proton plasma pressure and of current systems in the equatorial plane derived from AMPTE/CCE/CHEM measurements. J. Geophys. Res., **104**, 28615–28624 (1999)

Ebihara, Y., Ejiri, M.: Simulation study on fundamental properties of the storm-time ring current. J. Geophys. Res., **105**, 15,843 (2000)

Ebihara, Y., Ejiri, M., Nilsson, H., Sandahl, I., Milillo, A., Grande, M., Fennel, J.F, Roeder,J.L.: Statistical distribution of the storm-time proton ring current: POLAR measurements. Geoph. Res. Letters, **29(20)**, doi:10.1029/2002GL015430 (2002)

Ejiri, M.: Trajectory traces of charged particles in the magnetosphere. J. Geophys. Res., **83**, 4798–4810 (1978)

Fok, M.-C., J.U. Kozyra, J.U., Ho, G.C., Hamilton, D.C.: Three-dimensional ring current decay model. J. Geophys. Res., **100**, 9619–9632 (1995)

Fok, M.-C., Moore, T.E., Greenspan, M.E.: Ring current development during storm main phase. J. Geophys. Res., **101**, 15311–15322 (1996)

Fok, M.-C., Wolf, R.A., Spiro, R.W., Moore, T.E.: Comprehensive computational model of the Earth's ring current. J. Geophys. Res., **106**, 8417 (2001)

Ganushkina, N.Y., Pulkkinen, T.I., Fritz, T.: Role of substormassociated impulsive electric fields in the ring current development during storms. Ann. Geophys., **23**, 579 (2005)

Ganushkina, N.Y., Pulkkinen, T.I., Milillo, A., Liemohn, M.: Evolution of the Proton Ring Current Energy Distribution during April 21-25, 2001 storm. J. of Geoph. Res, **111(A11)**, A11S08 (2006)

Gloeckler, G., et al.: The charge-energy-mass (CHEM) spectrometer for 0.3 to 300 keV/e ions on the AMPTE/CCE. IEEE Trans. Geosci. Remote Sens., **GE-23**, 234–240 (1985)

Jordanova, V.K., Kistler, L.M., Farrugia, C.J., Torbert, R.B.: Effects of inner magnetospheric convection on ring current dynamics: March 10-12, 1998. J. Geophys. Res., **106**, 29,705 (2001)

Jordanova, V.K., Kistler, L.M., Kozyra, J.U., Khazanov, G.V., Nagy: Collisional losses of ring current ions. J. Geophys. Res., **101**, 111–126, 1996

Kistler, L.M., Ipavich, F.M., Hamilton, D.C., Gloeckler, G., Wilken, B., Kremser, G., Studemann, W.: Energy spectra of the major ion species in the ring current during geomagnetic storms. J. Geophys. Res., **94**, 3579–35998 (1989)

Korth, A., Kremser, G., Roux, A., Perraut, S., Sauvaud, J.-A., Bosqued, J.-M., Pedersen, A., Aparicio, B.: Drift boundaries and ULF wave generation near noon at geostationary orbit. Geophys. Res. Lett., **10(8)**, 639–642 (1983)

Korth, H., Thomsen. M.F., Borovsky, J.E., McComas, D.J.: Plasma sheet access to geosynchronous orbit. J. Geophys. Res., **104**, 25,047–25,061 (1999)

Liemohn, M.W., et al.: Dominant role of the asymmetric ring current in producing the storm-time *Dst*: J. Geophys. Res., **106**, 10,883 (2001)

Lui, A.T.Y., Hamilton, D.C.: Radial profiles of quiet time magnetospheric parameters. J. Geophys. Res., **97**, 19325–19332 (1992)

McComas, D.J., Bame, S.J.,Barraclough, B.L., Donart, J.R., Elphic, R.C., Gosling, J.T., Moldwin, M.B., Moore, K.R., Thomsen, M.F.: Magnetospheric plasma analyser: Initial 3-spacecraft observations from geosyncronous orbit. J. Geophys. Res., **98**, 13453 (1993)

Milillo A., Orsini, S., Daglis, I.A., Livi, S.: An empirical model of the ion distributions in the equatorial inner magnetosphere. Phys. and Chem. of the Earth, **24(N1/3)**, 209 (1999)

Milillo, A., Orsini, S., Daglis, I.A.: Empirical model of proton fluxes in the equatorial inner magnetosphere. 1. Development. J. of Geoph. Res., **106**, 25713–25730 (2001)

Milillo A., Orsini, S., Delcourt, D.C., Mura, A., Massetti, S., De Angelis, E., Ebihara, Y.: Empirical model of proton fluxes in the equatorial inner magnetosphere: 2. Properties and applications. J. of Geoph. Res, **108(A5)**, 10.1029/2002JA009581 (2003)

Milillo, A., Orsini, S., Massetti, S., Mura, A.: Geomagnetic Activity dependence of the Inner Magnetospheric Proton Distribution: an Empirical Approach for the 21-25 April 2001 Storm. J. of Geoph. Res, **111**, A11S13, doi:10.1029/2006JA011956 (2006)

Orsini, S., Daglis, I.A., Candidi, M., Hsieh, K.C., Livi, S., Wilken, B.: Model calculation of energetic neutral atoms precipitation at low altitudes. J. Geophys. Res., **99**, 13489–13498 (1994)

Orsini, S., Milillo, A., Mura, A.: Modeling the time-evolving plasma in the inner magnetosphere: An empirical approach. J. of Geoph. Res., **109**, A11216, doi: 10.1029/2004JA010532 (2004)

Roederer, J.G.: On the adiabatic motion of energetic particles in a model magnetosphere. J. Geophys. Res., **72**, 981–992 (1967)

Roeder, J.L., Chen, M.W., Fennell, J.F., Friedel, R.: Empirical models of the low-energy plasma in the inner magnetosphere. Space Weather, **3**, S12B06, doi:10.1029/2005SW000161 (2005)

Sheldon, R.B., Hamilton, D.C.: Ion transport and loss in the Earth's quiet ring current 1. Data and standard model. J. Geophys. Res., **98**, 13491–13508 (1993)

Vallat et al. Ion multi-nose structures observed by CLUSTER in the inner Magnetosphere. Ann. Geophys., **25**, 171–190, 2007

West, H.I., Jr., Buck, R.M., Walton, J.R.: Electron pitch angle distributions throughout the magnetosphere as observed on OGO 5. J. Geophys. Res., **78**, 1064–1081 (1973)

Wilken, B., Weiss, W., Hall, D., Grande, M., Sorass, F., Fennell, J.F.: Magnetospheric ion composition spectrometer onboard the CRRES spacecraft. J. Spacecr. Rockets, **29**, 585 (1992)

Zhang, Y., Paxton, L.J., Immel, T.J., Frey, H.U., Mende, S.B.: Sudden solar wind dynamic pressure enhancements and dayside detached auroras: IMAGE and DMSP observations. J. Geophys. Res., **108 (A4)**, 8001, doi:10.1029/2002JA009355 (2003)

Zhang, Y., Paxton, L.J., Meng, C.-I., Morrison, D., Wolven, B., Kil, H., Christensen, A.B.: Double dayside detached auroras: TIMED//GUVI observations. Geophys. Res. Lett., **31**, L10801, doi:10.1029/2003GL018949 (2004)

Empirical models of solar wind - magnetosphere - ionosphere coupling

Peter Wintoft[1], Hans Gleisner[2], Magnus Wik[1], and Henrik Lundstedt[1]

[1] Swedish Institute of Space Physics, Scheelevägen 17, SE-223 70 Lund, Sweden
peter@lund.irf.se
[2] Danish Meteorological Institute, Lyngbyvej 100, DK-2100 Copenhagen, Denmark.

Summary. We here give a review of existing empirical models of solar wind, magnetosphere, and ionosphere coupling. We focus on models that have been implemented for real time operation and that are publicly available on the Internet. We discuss useful prediction lead time and how it can be studied using wavelet coherence. This analysis is applied to the *Dst* forecasts of the RWC-Sweden model and it is shown that although the forecasts are very accurate they are not accurate enough to provide true 1–2 hour forecasts. We believe this is a general result for the 1–2 hour forecast models. When predicting indices one should instead relate the lead time to the time scale of the process. This necessitates the use of solar observations or statistical models.

1 Introduction

The prime goal of empirical models is to make predictions of the future given information of the past (*Farmer and Sidorowich*, 1987). An empirical model extracts relations from data. The physical understanding of the problem, the generic form of the empirical model, and the amount and quality of the data that are of importance for the success of the model to predict the true system. The physical knowledge of the system is usually coded into the model, e.g. through selection of physical observables, transformations of observables, selection of data, and/or constraining the model. In Section 2 we list empirical models that are available through the Internet.

As we wish to make predictions of the future we need to decide on possible prediction lead time when constructing the model. Of course, one always wish to make as long a prediction as possible, however, the physics of the system sets an upper limit. Going past the physical limit will always lead to a statistical prediction, which may be useful, but it relies on that there is some static behaviour. Having a first idea on prediction lead time one may construct several models that explores different lead times. This leads to the importance of proper validation of the model with respect to lead time (Section 3).

2 Online empirical models

We have identified 18 models that run in real time operation that forecasts some magnetospheric or ionospheric parameter. In Table 1 we list the models ordered with respect to prediction lead time. We also try to give the physical explanation to the forecast lead time (*Physics* column). In the following we will focus on *Dst* models that predict a few hours ahead.

Table 1. Online empirical models. The *Physics* column indicates the reason for the lead time: "L1-Earth" means the solar wind advection time from L1 to Earth; "ring current" is the ring current dynamics; "mag.sph." is general magnetospheric dynamics; "statistics" means that there is no physical explanation, it is a statistical model. The *Model* column indicates either the model name or the provider of the forecast.

Parameter	Lead time	Physics	Model
foF2	0 hours	-	SEC (*Fuller-Rowell et al.*, 2001)
RMS dB/dt	30 min	L1-Earth	RWC-Sweden (*Wintoft et al.*, 2005)
AE	1 hour	L1-Earth	GIFINT (*Pallocchia et al.*, 2006)
Dst	1–2 hours	L1 + ring current	RWC-Sweden (*Lundstedt et al.*, 2002)
Dst	1–2 hours	L1 + ring current	GIFINT (*Pallocchia et al.*, 2006)
Dst	1–2 hours	L1 + ring current	LASP (*Temerin and Li*, 2006)
Kp	0–6 hours	L1+mag.sph.+statistics	RWC-Sweden (*Boberg et al.*, 2000)
Kp	30–90 min	L1 + mag.sph.	SEC (*Costello*, 1997)
Kp	1, 4 hours, 4 days	L1+mag.sph.+statistics	UPOS (*Wing et al.*, 2005)
Pseudo K	24 hours	Statistics	RWC-Canada (*Coles and Lam*, 1998)
foF2	24 hours	Statistics	STIF (*Muhtarov et al.*, 2002)
MUF	24 hours	Statistics	DIFS (*Butcher*, 2005)
$>$ 2 MeV el.	2 days	Radial diffusion of el.	LASP (*Li et al.*, 2001)
Ap	3 days	Statistics	GIFS (*Thomson et al.*, 1993)
Ap	3 days	Statistics	SEC
$>$ 2 MeV el.	3 days	Rad. difff.+statistics	SEC (*Baker et al.*, 1990)
$>$ 2 MeV el.	8 days	Above+Sun-solar wind model	SEC (*Baker et al.*, 1990)
Ap	27 days	Solar rotation + static	SEC (*SEC*, 2005)

There are several models for *Dst*. The LASP model (*Temerin and Li*, 2006) uses an ARMA-type filter with non-linear terms and is quite complex. *Dst* is calculated from a sum of six terms:

$$Dst = dst1^* + dst2^* + dst3^* + (\text{pressure term})^* + (\text{direct IMF Bz term})^* + (\text{offset term}) \quad (1)$$

where the $dstn$ terms, $n = 1, 2, 3$, contain a driver term that depends on the solar wind and a decay term. The star (*) indicates that these terms are also modulated by a function depending on season. There are about 150 coefficients in the model that are found through searching the space "by hand" in order to minimise the RMS error between predicted and observed *Dst*.

The *Dst* model at RWC-Lund (*Lundstedt et al.*, 2002) uses an Elman neural network. This type of network is a recurrent neural network (RNN) that contains feed-back connections that adds memory and complex behaviour

$$y_i(t) = \tanh\left(\sum_{j=1}^{3} w_{ij}x_j(t)) + \sum_{k=1}^{4} c_{ik}y_k(t-1) + b_i\right) \quad (2)$$

$$\overline{Dst}(t+1) = \sum_{i=1}^{4} v_i y_i(t) + a \quad (3)$$

$$(4)$$

where the inputs are $x_1 = B_z$, $x_2 = n$, and $x_3 = V$. Time t is in hours. The solar wind data were obtained from the OMNI data set which contains data from several different spacecraft. In that data set all data have been transformed as if they were measured at a sub-solar point at Earth. The 1-hour prediction lead time comes from ring current dynamics.When using data from and L1-spacecraft, like ACE, there is additional lead of 30-60 minutes due to the L1-Earth travel time.

The GIFINT model (*Pallocchia et al.*, 2006) is very similar to the RWC-Lund model but uses only solar wind IMF data as input. The model has also three inputs ($x_1 = B_z$, $x_2 = B^2$, and $x_3 = B_y^2$) and four context units ($k = 1, 2, 3, 4$). The main reason to use IMF only is that the magnetometer onboard ACE is not affected by proton events like the plasma instrument.

3 Evaluating prediction lead time

It is very difficult to decide which model is the optimal among all available models when only overall measures like RMS error or correlation is used. In Figure 1 we show the observed solar wind velocity V, magnetic field B_z, and *Dst* together with the predicted *Dst* (top three plots) from the model by *Lundstedt et al.* (2002) during a 1000-hour period starting in 4th May 1981. The linear correlation is 0.93 and the RMS error is 13 nT. The predicted *Dst* (red) follows the observed *Dst* (blue) well. However, evaluating the model by looking at the plotted *Dst* is misleading considering that we are doing 1-hour forecasts. To study the prediction in detail we apply a wavelet coherence algorithm (*Grinsted et al.*, 2004) to the observed and predicted *Dst* (middle of figure). Now it becomes evident when the model works and at what time scales it works. The red areas indicates a strong correlation, while the blue areas indicates a weak correlation. The thick black line marks areas with significant correlation. At time scales longer than 32 hours a strong correlation is seen most of the time. At shorter time scales the correlation varies significantly. It is only during the storm periods that the correlation exists down to scales of 3–4 hours. Thus, the 1-hour forecasts of *Dst* has limited use as the predictions only starts to work at scales of, in the best case, 3–4 hours, and more typically at 16 hours. This is also the time scales of the typical storms and these are the events caught by the eye when judging the *Dst* plot. However, it is also seen that when there is significant correlation the predicted and observed *Dst* are in phase as indicated by the horizontal rightward pointing arrows.

It is instructive to compare the wavelet coherence for a persistence model $\overline{Dst}(t+1) = Dst$ (bottom of Figure 1). There is a strong correlation at all times and all scales (red area) but looking at e.g. the 4-hour scale the arrows are pointing vertically upwards indicating a phase shift of 90 degrees which is consistent with the 1-hour shift introduced by the persistence model.

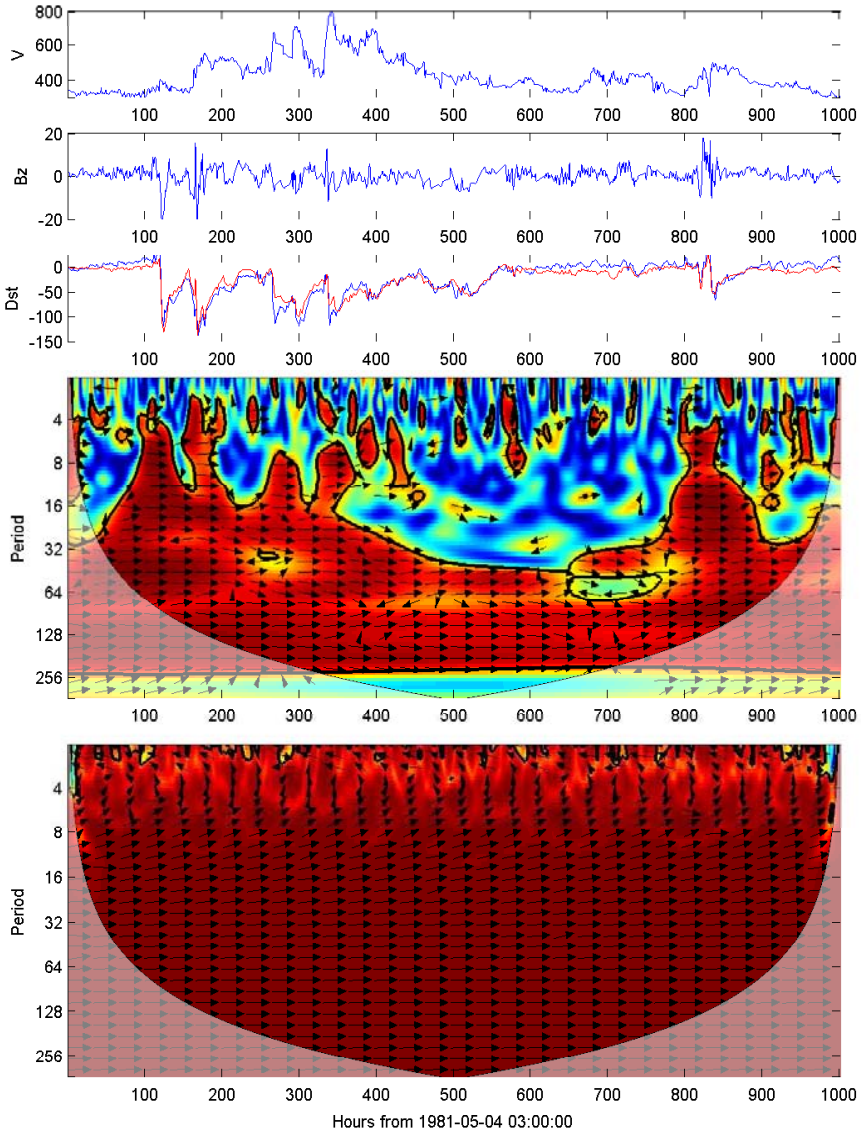

Fig. 1. From top to bottom: solar wind velocity (km/s), magnetic field component B_z (nT), observed *Dst* (blue) and predicted *Dst* (red) in nT, wavelet coherence between observed *Dst* and predicted *Dst* for the RWC-Sweden model, and wavelet coherence for the pesristence model. The period covers 1000 hours starting on 4th May 1981. In the wavelet coherence plots a strong correlation is coloured red and weak correlation is blue. The arrows indicates phase shifts so that rightward pointing horizontal means no shift and upward pointing means 90 degree lag. The period goes from 2 hours up to over 256 hours.

4 Discussion and conclusions

There are several successful models that have been implemented to forecast different space weather parameters. However, the demands put on a model for real time operation is different from that of a model for studying solar-terrestrial relations. The forecast lead time must be thoroughly analysed in order to judge the usefulness of the model. We showed here with one example, the *Dst* model by *Lundstedt et al.* (2002), that the accuracy of the 1–2 hour forecasts is not sufficient to be truly useful in a real time situation, a result that probably holds for other 1-hour forecast models. However, even if a model could be developed that truly forecasts *Dst* 1–2 hours in advance, such a model would probably have limited use for a space weather forecast application, as it would imply that there is an application that is highly correlated with *Dst*.As indices describe large scale processes and have specific limitations (*Baumjohann*, 1986; *Campbell*, 2004; *Kamide and Rostoker*, 2004) this is unlikely. These short term forecast models are more suited for nowcasting and post-event analysis. To forecast indices one should look at the time scale of the process to motivate a useful prediction lead time. For *Dst* storms this is about 20 hours, or possibly down to 4 hours if focusing on the main phase only. From a physical view point this is a problem when a solar wind monitor at L1 is used. The solution is to either use a model with solar observations as inputs (lead time $\sim$3 days) or to use a statistical model.

References

Baker, D. N., R. L. McPherron, T. E. Cayton, and R. W. Klebesadel, Linear prediction filter analysis of relativistic electron properties at 6.6 RE, *Journal of Gephysical Research*, *95*(A9), 15,133–15,140, doi:10.1029/90JA00856, 1990.

Baumjohann, W., Merits and limitations of the use of geomagnetic indices in solar wind-magnetosphere coupling studies, in *Solar Wind-Magnetosphere Coupling*, edited by Y. Kamide and J. A. Slavin, pp. 3–15, Terra Scientific Publishing Company, Tokyo, 1986.

Boberg, F., P. Wintoft, and H. Lundstedt, Real time kp predictions from solar wind data using neural networks, *Physics and Chemistry of the Earth*, *25*(4), 275–280, 2000.

Butcher, N., Daily ionospheric forecasting service (DIFS) III, *Annales Geophysicae*, *23*, 1–8, 2005.

Campbell, W. H., Failure of Dst index fields to represent a ring current, *Space Weather*, *2*, S08,002, doi:10.1029/2003SW000041, 2004.

Coles, R. L., and H.-L. Lam, Geomagnetic forecasting in Canada: a review, *Physics in Canada*, pp. 327–331, 1998.

Costello, K., Moving the Rice MSFM into real-time forecast mode using solar wind driven forecast models, Ph.D. thesis, Houston, Texas, 1997.

Farmer, J. D., and J. J. Sidorowich, Predicting chaotic time series, *Physics Review Letters*, *59*, 62–65, 1987.

Fuller-Rowell, T. J., M. V. Codrescu, and E. A. Araujo-Pradere, *Capturing the storm-time F-region ionospheric response in an empirical model*, pp. 393–401, 2001.

Grinsted, A., J. C. Moore, and S. Jevrejeva, Application of the cross wavelet transform and wavelet coherence to geophysical time series, *Nonlinear processes in geophysics*, *11*, 561–566, 2004.

Kamide, Y., and G. Rostoker, What is the physical meaning of the AE index?, *Eos Trans. AGU*, *85*(19), 188,192, 2004.

Li, X., M. Temerin, D. N. Baker, G. D. Reeves, and D. Larson, Quantitative prediction of radiation belt electrons at geostationary orbit based on solar wind measurements, *Geophysical Research Letters*, *28*(9), 1887–1890, 2001.

Lundstedt, H., H. Gleisner, and P. Wintoft, Operational forecasts of the geomagnetic *Dst* index, *Geophysical Research Letters*, *29*(24), 34–1–34–4, doi:10.1029/2002GL016151, 2002.

Muhtarov, P., I. Kutiev, and L. Cander, Geomagnetically correlated autoregression model for short-term prediction of ionospheric parameters, *Inverse Problems*, *18*, 49–65, 2002.

Pallocchia, G., E. A. G. Consolini, M. F. Marcucci, and I. Bertello, Geomagnetic Dst index forecast based on IMF data only, *Annales Geophysicae*, *24*, 989–999, 2006.

SEC, Users guide to emphThe preliminary report and forecast of solar geophysical data, *Tech. rep.*, NOAA, 2005.

Temerin, M., and X. Li, Dst model for 1995–2002, *Journal of Gephysical Research*, *111*, A04,221, doi:10.1029/2005JA011257, 2006.

Thomson, A. W. P., T. D. G. Clark, and D. J. Kerridge, Forecasting Ap in the Short-Term using Time Series Analysis, *Solar Terrestrial Predictions: Proceedings of a Workshop at Ottawa, Canada*, *3*, 269–283, 1993.

Wing, S., J. R. Johnson, J. Jen, C. I. Meng, D. G. Sibeck, K. Bechtold, J. Freeman, K. Costello, M. Balikhin, and K. Takahashi, Kp forecast models, *Journal of Gephysical Research*, *110*, A04,203, doi:10.1029/2004JA010500, 2005.

Wintoft, P., M. Wik, H. Lundstedt, and L. Eliasson, Predictions of local ground geomagnetic field fluctuations during the 7–10 November 2004 events studied with solar wind driven models, *Annales Geophysicae*, *23*, 3095–3101, 2005.

Forecasting *Dst* from solar wind data

C. Cid[1], E. Amata[2], E. Saiz[1], G. Pallocchia[2], Y. Cerrato[1], and G. Consolini[2]

[1] Space Research Group-Science, Universidad de Alcala, Alcala de Henares, Spain
consuelo.cid@uah.es
[2] Istituto di Fisica dello Spazio Interplanetario, INAF, Roma, Italy
ermanno.amata@ifsi-roma.inaf.it

Summary. This paper is focused on forecasting the *Dst* index from solar wind data in two different ways. In a first stage, we briefly recall a recent Artificial Neural Network (ANN) algorithm for the Dst prediction called EDDA Pallocchia et al. (2006), based on IMF inputs only and compare its performance, over a two and half years period, with that of the Lundstedt et al. (2002) algorithm and the Wang et al. (2003) algorithm, which both make use of both IMF and plasma inputs. We show that: 1) all three algorithms perform similarly for "small" and "moderate" storms; 2) the EDDA and Wang algorithms perform similarly and considerably better than the Lundstedt et al. (2002) algorithm for "intense" and for "severe" storms; 3) the EDDA algorithm has the clear advantage, for space weather operational applications, that it makes use of IMF inputs only.

In a second stage, we analyze the different ways of alerting of severe geomagnetic activity. After a description of the state of the art of warning using IMF and solar wind plasma, we compare using OMNIweb database the results obtained with previous methods and that proposed by Saiz et al. (2007) using only IMF as input for a new forecasting tool. The results presented evidence, not only that this new tool is a proper one for technological purposes, but also that solar wind-magnetosphere interaction involves more physical mechanisms than magnetic reconnection.

The advantage of forecasting *Dst* from IMF only lies in the fact that plasma data are at times less reliable and display data gaps more often than IMF measurements, especially during large solar disturbances, i.e during periods when space weather forecast are most important.

1 Introduction

In the past years, many studies have been devoted to the relation between *Dst* and solar wind conditions. Among them we recall Gonzalez et al. (1994), who studied extensively the storm time profile and intensity in relation with the solar wind structures associated with CME's and Corotating Interaction Regions (CIR's), and Gonzalez et al. (2005), who studied the relationship between peak *Dst* and peak negative B_z during intense geomagnetic storms; moreover, we recall the recent review by Yermolaev et al. (2005) and all references therein. In a complementary way several authors tried to forecast *Dst* from measurements of the Interplanetary Magnetic Field (IMF) and solar wind plasma parameters. As a result, a number of empirical models has been developed, based on differential equations (see e.g. Burton et al. (1975), Fenrich and Luhman (1998), O'Brien and McPherron (2000), Temerin and Li (2006), Wang

et al. (2003)), statistical correlative analysis (Baker , 1986), linear filtering (McPherron et al., 1988), nonlinear filtering (Klimas et al., 1992) and on artificial neural networks (see Lundstedt et al. (2002) and references therein). All of them have, as their inputs, both magnetic and solar wind data. Pallocchia et al. (2006) remarked that plasma instruments can be affected by enhanced solar X-ray and energetic particle fluxes and can fail more often than magnetometers; moreover, the solar wind speed exceeds at times the upper instrumental limits of plasma detectors. On the other hand, during these events a reliable *Dst* forecast is most needed, as such disturbances can be accompanied by very large geomagnetic storms. Therefore, operational *Dst* forecasting services cannot neglect the failures of L1 plasma monitors. In this paper we report on two new approaches to the forecasting of geomagnetic storms, both based on IMF data only: the first one based on an ANN algorithm ((Pallocchia et al., 2006), and (Amata et al., 2007)); the second one consisting in a tool which does not reconstruct the individual *Dst* values as a function of time, but warns on real time of severe geomagnetic activity ((Saiz et al., 2007)).

2 The EDDA ANN algorithm based on IMF only

Pallocchia et al. (2006) developed a new ANN algorithm based on L1 IMF inputs only, called EDDA (Empirical *Dst* Data Algorithm) and Amata et al. (2007) described a comparison of its performance with that of two previous algorithms: the first one also based on the ANN technique and developed by Lundstedt et al. (2002); the second one based on differential equations and is due to Wang et al. (2003). In the following we will refer to them as "Lund" and "Wang", while we will refer to the Kyoto World Data Centre *Dst* data as the "Kyoto" *Dst*.

Both EDDA and Lund are based on Elman networks (Elman, 1990) with 4 hidden neurons. Lund has three inputs: solar wind density, n, and speed, V, and the B_s parameter (defined as $B_s = |B_z|$, for $B_z < 0$, and B_s = 0, otherwise). EDDA has three inputs: B^2, B_z and B_y^2. Wang is a first order differential equation algorithm, which calculates $Dst(t)$ from plasma density, $n(t)$, the x component of plasma velocity, $V_x(t)$, and IMF $B_z(t)$ at the time t, dynamical pressure $P_{dyn}(t+1)$ at the time $t+1$ (in hours) and a starting value of Dst at the time t_0, where $t_0 < t$. The EDDA, Lund and the Wang algorithms were trained and tested over periods up to 2002, 2001 and 2002 respectively and were compared for the period January 2003 - 15 May 2005. Amata et al. (2007) examined all storm periods for that period and found that in general all three algorithms perform reasonably well and in a similar fashion for small and moderate storms, while Wang and EDDA perfomed similarly and better than Lund for larger storms. We discuss hereafter in some detail a moderate storm and a severe storms pertaining to the selected period.

The left panel of Figure 1 shows EDDA, Lund, Wang and Kyoto data (red, blue, green and black lines, respectively) from 00 UT on 7 to 00 UT on 11 May 2005. The Kyoto *Dst* shows two storms, the first starting around 18 UT on 7 May with a broad minimum of $\simeq -95nT$ between 3 and 7 UT on 8 May, and the second starting around 11 UT of 8 May, during the recovery phase of the first storm, when the *Dst* had risen back to $\simeq -50nT$, and reaching its minimun of $\simeq -120nT$ around 17 UT on 8 May. After that, the recovery lasted more than two days. All three algorithms roughly reproduced the duration of the first minimum but at a higher level by $\simeq -75nT$. The second storm was reproduced correctly as regards its initial

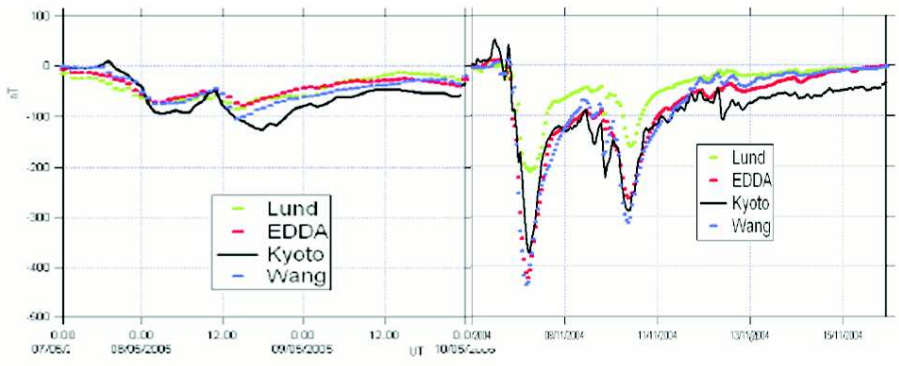

Fig. 1. EDDA (red dashed line), Wang (blue dashed line), Lund (green dashed line) and Kyoto (black solid line) *Dst* index plotted for 07 – 11 May 2005 (left panel) period and 07–16 November 2004 (right panel).

phase, especially by Wang which displayed a drop from $\simeq -50nT$ to $\simeq -100nT$ between 11 UT and 13 UT on 8 May. After that time the recovery started for all three algorithms, several hours in advance with respect to the Kyoto *Dst*, Wang performing better than EDDA and Lund by $\simeq 20nT$.

The right panel of Figure 1 shows EDDA, Lund, Wang and Kyoto data from 00 UT on 7 to 00 UT on 16 November 2004. The Kyoto *Dst* displays a very deep minimum of $\simeq -375nT$ at $\simeq 07UT$. This is followed by a recovery to $\simeq -100nT$ over 18 hours and by two storms, with minima of $\simeq -150nT$ and $\simeq -215nT$, at 20 UT and 23 UT, respectively, on 9 November, and a larger storm with a minimum of $\simeq -295nT$ at 10 UT on November 10. The final recovery lasts more than 6 days. Lund follows the time sequence of events displayed by the Kyoto *Dst*, but fails to reproduce the minima, as it falls to $\simeq -200nT$ for the first storm and to $\simeq -160nT$ for the fourth one (while it misses altogether the second and the third smaller ones). Conversely, both Wang and EDDA display a dip which closely resembles that of the Kyoto *Dst* with a minimum at $\simeq 07UT$, although the minimum value is somewhat lower being $\simeq -440nT$, i.e. 117 per cent of the Kyoto minimum.The recovery is better reproduced by EDDA, while the third storm is better forecast by Wang; the second storm is underestimated by both algorithms, while the fourth one is well reproduced by both, apart from a lower (higher) minimum seen by Wang (EDDA). Finally, from 12 UT on 12 November onwards the levels of the Wang and EDDA *Dst* approach the Lund rather than the Kyoto *Dst*.

3 Forecasting severe geomagnetic activity

Several authors have concluded that there is a high probability for intense storms to be triggered during the southward IMF passage (see Tsurutani (2001) and references therein). Gonzalez and Tsurutani (1987) found that duskward interplanetary electric fields greater than 5 mV/m over periods exceeding 3 hours were related to intense storms ($Dst < -100nT$).

Tsurutani (1995) found that this electric field condition was approximately equivalent to $B_z < -10nT$.

Instead of looking at *Dst* peak value as the magnitude considered in quantifying geoeffectiveness, Saiz et al. (2007) considered that significant variations in this index were at least as dangerous as the lowest values of it. Then, they developped a new tool for real time warning of these events. This real time forecasting tool has been developped to forecast those events where Dst index variations are less than $-50nT$ per hour. Different conditions have been used inside the tool: the first order differential equation of Burton et al. (1975) and Wang et al. (2003) or the new proposal of Saiz et al. (2007). In this last case the tool has only the z component of IMF as input, although in the previous ones, also solar wind density and velocity are required as input parameters.

For the validation of the tool, data from the OMNIweb database were used. This database provides one-hour resolution data for the years 1963 to 2006. Five-minute resolution data are also available for 1995 to 2005. There are 96 events from 1963 to 2006 where Kyto *Dst* varies more than $-50nT$ per hour, although from 1995 to 2005 the number of events is reduced to 30, which the tool should forecast. To select these events, we have considered that in the case of multiple-step storms, only the first warning was considered, and then, only one event appears. This set of events selected includes in it the most severe geomagnetic storms.

3.1 Warning with solar wind plasma and IMF

The first attemp of forecasting with the tool was made using the first order differential equation of Burton et al. (1975). After a correction of dynamic pressure effects, the Dst variation was obtained with this equation as a combination of a source term, or injection function, and a loss term proportional to own Dst index. Several authors have considered this model providing different expressions for the injection function and the recovery time [e.g. Fenrich and Luhman (1998), O'Brien and McPherron (2000), Wang et al. (2003)]. In the tool, we have considered the injection function from Burton et al. (1975) and Wang et al. (2003)(after 'case of Burton' or 'case of Wang'). We have regarded as a warning when the injection function is over $-50nT$ for one hour. With this criterion, we have disregarded the decay term in the differential equation. The inputs of the tool are in both cases, Burton and Wang, solar wind density, n, and speed, V, and the B_s parameter (see above). In both cases the results are very similar. Only 32 per cent of events with data available were predicted on time in the case of Burton and only 37 per cent in the case of Wang. By other hand, the number of 'late warning' events (this term means that the tool achieves a warning but after the event happens at terrestrial surface) is comparable to the number of hits in both cases. Moreover, the number of false alarms (that is, the tool achieves a warning but variation of *Dst* is less than $-50nT$ per hour) and the total number of on time and late hits are somewhat similar. These results indicate that the forecasting tool is not accurate enough for technological purposes.

3.2 Warning only with B_z

Highly varying IMF is observed at the begining of severe geomagnetic storms, in such a way that when variation of B_z increases, then, the Dst index decreases. These large changes in B_z use to happen at interplanetary shocks or sheaths followed by ICMEs. Daglis et al. (2003)

pointed out that, when a northward turning of the IMF and a dynamic pressure enhancement occur simultaneously during a long interval of southward IMF, a major substorm is triggered. These facts guided to Saiz et al. (2007) to relate significant variations on B_z and *Dst*. Then, the second attemp of forecasting was done implementing in the tool the proposal of Saiz et al. (2007). In this case the tool needs only one input, B_z. This fact avoids the failures in plasma instruments in L1 refered before (Pallocchia et al., 2006).

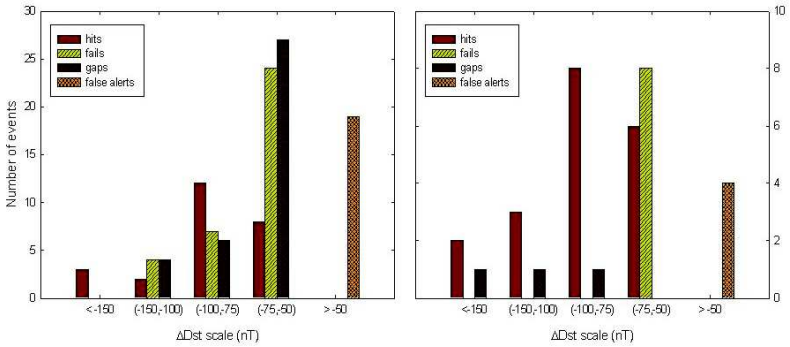

Fig. 2. Results of forecasting using the proposal of Saiz et al. (2007) with hourly (left) and five-minutes (right) resolution data as a function of the variation of *Dst*

The condition of the tool to achieve a warning is based on the variations of B_z for a certain time interval. First, it is computed the difference between the maximum and the minimum value of B_z in that time interval. If this variation is over a threshold, then the tool gets a warning of severe geomagnetic activity. The tool has to be trained with historical data sets in order to get the best time interval value and the threshold value before being useful to forecast in real time. We have trained the tool with one hour resolution data and the best results are obtained for a time interval of 3 hours and a threshold of $30nT$, meanwhile for five minute resolution data the threshold is shifted to $44nT$. The results using this tool as a real time tool are shown in Figure 2. In both cases, hourly and five-minutes resolution, we can forewarn of every event with variations of *Dst* less than $-150nT$ per hour and data available. In the case of one hour resolution data, results for other intervals of variations of *Dst* are comparable to those of the cases of Burton and Wang, but in this case only B_z was used, in contrast to previous tool where solar wind density and velocity data were used to determine the warning signs.

In the case of five minutes resolution, the number of 'false alarms' is reduced to only four events. This fact, along with 70.4 per cent of hits relative to events without data gaps, and 100 per cent of hits for variations of *Dst* less than $-75nT$ per hour, indicates that our tool is successful. On the other hand, all the 'fail events' (those that the tool misses) presented variations of *Dst* in the interval $(-60, -50)nT$ per hour, that is, they were the less geoeffective events. Moreover, every one of them presented also a variation of B_z value in the interval $(30, 40)nT$. Thus, these events let us estimate the accuracy range of our forecasting tool.

4 Conclusions

In this paper we briefly reviewed two new approaches to the problem of geomagnetic storms forecasting, both based on IMF data only.

The first approach lead to the development of an ANN algorithm called EDDA (Pallocchia et al., 2006). Amata et al. (2007) performed a quantitative comparison between the EDDA, Lund (Lundstedt et al., 2002) and Wang (Wang et al., 2003) algorithms from the beginning of 2003 to 15 May 2005. In conclusion, Amata et al. (2007) found that the EDDA and Wang algorithms, based on an ANN network and on differential equations respectively, perform better than the ANN Lund algorithm for "large" and for "severe" storms. On a statistical basis, it appears that the Wang algorithm performs better for small positive *Dst* values, while the EDDA and Wang perform in a similar way for "moderate", "large" and "severe" storms. As regards small *Dst*'s, the Wang algorithm might better reproduce the initial compression than EDDA. This is not surprising as EDDA does not include among its input parameters the plasma density nor the plasma speed and relies upon the IMF only.

As regards the relevance of the EDDA and Wang algorithms to operational space weather services, it is to be remarked that, as discussed by Pallocchia et al. (2006), the two algorithms are not equivalent, as EDDA uses the IMF only, while Wang uses also plasma data and an initial Dst value. Pallocchia et al. (2006) also comment on the ability of EDDA to predict the *Dst* index on the basis of the IMF only by referring to the Akasofu ϵ parameter, which is defined as $\epsilon = VB^2 sin^4(\theta/2) l_0^2$, where B is the IMF magnitude, V is the solar wind speed, θ is the IMF clock angle and $l_0 \simeq 7$ Earth radii. We notice that ϵ contains the square of the magnetic field intensity, i.e. the second EDDA input, and the θ clock angle, which is calculated from B_z, i.e. the first EDDA input, and B_y, the square of which is the third EDDA input. To comment on the fact that the ϵ parameter contains V, we notice that this dependence is linear, whereas that on B is quadratic.

The second approach presents a forecasting tool of significative variations of *Dst* (Saiz et al., 2007) concluded that large variations of the *Dst* index are related to significant changes in B_z, instead of to southern B_z, duskward E_y or high pressure. To find a physical explanation to this result, is necesary to consider that *Dst* index is related to the ring current around the Earth. It is believed that this current is only related to the duskward electric field. In this case, only one term of the Faraday law has been considered, neglecting variations of magnetic field with time. We suggest that, changes of B_z with time in a time scale of the order of the time of answer of the magnetosphere need to be considered in order to determine the ring current and then, the *Dst* index. These results should be considered in upcoming models of solar wind-magnetosphere interaction.

Acknowledgements. The authors thank the ACE spacecraft team and SEC for making the real time and verified data available, and the Kyoto World Data Centre and OMNIweb service for making their data sets available too. This work was partially supported by the ESA contract N. 17032/03/NL/LvH, in the framework of the Pilot Project on Space Weather Applications and by ASI contract N. I/035/05/0, and by grants from the Comisión Internacional de Ciencia y Tecnología (CICYT) of Spain (ESP 2005-07290-C02-01 and ESP 2006-08459).

References

Amata, E., Pallocchia, G., Consolini, G., Marcucci, M. F., Bertello, I.: Comparison between three algorithms for *Dst* predictions over the 2003-2005 period. JASTP, Accepted for publication, (2007)

Baker, D.N.: Statistical Analyses in the Study of Solar Wind / Magnetosphere Coupling, Solar Wind-Magnetosphere Coupling. Kamide,Y. and Slavin, J.A. (eds) D. Reidel Publishing Company, Dordrecht, Holland, 17, (1986)

Burton, R. K., McPherron, R. L., and Russell, C. T.: An empirical relationship between interplanetary conditions and Dst. J. Geophys. Res., **80**, 4204-4214, (1975)

Daglis, I. A., Kozyra, J. U., Kamide, Y., Vassiliadis, D., Sharma, A. S., Liemohn, M. W., Gonzalez, W. D., Tsurutani, B. T. and Lu, G.: Intense space storms: Critical issues and open disputes. J. Geophys. Res., **108**, 1208, doi: 10.1029/2002JA009722, (2003)

Elman, J. L.: Finding structure in time, Cognitive Sci.,**14**, 179-211, (1990)

Fenrich, F. R. and Luhmann, J. G.: Geomagnetic response to magnetic clouds of different polarity. Geophys. Res. Lett., **25**, 2999-3002, (1998)

Gonzalez, W. D., and Tsurutani B. T.: Criteria of interplanetary parameters causing intense magnetic storms ($Dst < -100nT$). Planet. Space Sci., **35**, 1101.(1987)

Gonzalez, W. D., Joselyn, J. A., Kamide, Y., Kroehl, H. W., Rostoker, G., Tsurutani, B. T., and Vasyliunas, V. M.: What is a geomagnetic storm? J. Geophys. Res., **99**, 5771-5792, (1994)

Gonzalez, W. D. and Echer, E.: A study on the peak Dst and peak negative Bz relationship during intense geomagnetic storms. Geophys. Res. Lett., **32**, L18103, (2005)

Klimas, A. J., Baker, D. N., Roberts, D. A., Fairfield, D. H., Buechner, J.: A nonlinear dynamical analogue model of geomagnetic activity. J. Geophys. Res., **97**, 12253-12266, (1992)

Koskinen, H. E. J. and Tanskanen, E. I.: Magnetospheric energy budget and the epsilon parameter. J. Geophys. Res., **107**, 42-1, (2002)

Lundstedt, H., Gleisner, H., and Wintoft, P.: Operational forecasts of the geomagnetic Dst index. Geophys. Res. Lett., **29**, 34-1, (2002)

McPherron, R. L., Bargatze, L. F., Holzer, R. E., Baker, D. N., Clauer, C. R.: IMF control of geomagnetic activity. Advances in Space Research, **8**, 71-86, (1988)

Pallocchia, G., Amata, E., Consolini, G., Marcucci, M.F., Bertello, I.: Geomagnetic Dst index forecast based on IMF data only. Ann. Geoph., **24**, 989-999, (2006)

O'Brien, T. P. and McPherron, R. L.: Forecasting the ring current index Dst in real time. J. Atmos. Terr. Phys., **62**, 1295-1299, (2000)

Saiz, E., Cid and C. Cerrato, Y.: Forecasting intense geomagnetic activity using interplanetary magnetic field data. *Submitted* (2007)

Temerin, M. and Li, X.: A new model for the prediction of Dst on the basis of the solar wind. J. Geophys. Res., **107**, 31-1, (2006)

Tsurutani, B. T.: The interplanetary causes of magnetic storms, substorms and geomagnetic quiet in Space Storms and Space Weather Hazards, by Daglis, I. A. (ed.), 103, Kluwer Acad.,(2001)

Tsurutani, B. T. and Gonzalez, W. D.: The future of geomagnetic storm predictions: implications from recent solar and interplanetary observations. J. Atmosph. Sol. Terr. Phys., **57**, 1369, (1995)

Yermolaev, Yu. I., Yermolaev, M. Yu., Zastenker, G. N., Zelenyi, L. M., Petrukovich, A. A., Sauvaud, J.-A.: Statistical studies of geomagnetic storm dependencies on solar and interplanetary events: a review. Plan. Sp. Sci., **53**, 189-196, (2005)

Wang, C. B., Chao, J. K., and Lin, C.-H.: Influence of the solar wind dynamic pressure on the decay and injection of the ring current. J. Geophys. Res., **108**, 5-1, (2003)

Can the AE index be forecast?

E. Amata[1], G. Pallocchia[1], G. Consolini[1]

Istituto di Fisica dello Spazio Interplanetario, INAF, Roma, Italy
ermanno.amata@ifsi-roma.inaf.it

1 Introduction

The AE index is defined as AE = AU - AL, where AU and AL estimate the eastward and westward auroral electrojets from a chain of magnetometers located at northern geomagnetic latitudes between 60 and 70 degrees over all longitudes (Davies & Sugiura, 1966).

Tsurutani et al. (1990) found that the AE spectral index was -1 at low frequency, as for the solar wind driver, and was -2.2 at time scales longer than 5 hours. In this respect, it is now accepted that two main components of the auroral electrojet can be identified, each with its own characteristic distribution and timescale, one directly driven by the solar wind and the other due to the loading-unloading process in solar wind-magnetosphere coupling (Kamide & Baumjohann (1993); Kamide & Kokubun (1996); Freeman et al. (2000); Consolini & De Michelis (2005)). The auroral electrojet associated with the direct solar wind energy flows primarily in the dusk and dawn sectors and increases as convection enhances. This enhancement characterises the substorm growth phase, but lasts for the entire substorm, though with highly varying strength. On the other hand, the unloading of energy stored in the tail during the growth phase leads to the formation of an intensive westward electrojet during the successive substorm expansion phase, localized in the midnight sector.

Different methods were used to separate the directly driven from the unloading components of AE, ranging from differential techniques (Clauer & Kamide, 1985) to the method of natural orthogonal components (Sun et al., 1998). More recently, (Freeman et al., 2000) employed the threshold crossing method to highlight the unloading component and to show that it was stronger in AL than AU. Then Uritsky et al. (2001) from a burst analysis method, again based on threshold crossings, found that on short time scales AE is not well predicted. Finally, Consolini & De Michelis (2005) separated the two components by the Local Intermittency Measure method based on wavelet technique.

Other authors devoted their efforts to forecast the AE index from solar wind IMF and plasma measurements. To this regard, a very important conclusion was reached by Bargatze et al. (1985), who found that the response of the magnetosphere to solar wind forcing is essentially non-linear. However, it is worth recalling that Kamide & Baumjohann (1993) noted that "if one ... uses hourly or threehourly values of the solar wind parameters and the auroral electrojet indices, the second component, i.e. the substorm expansion component, tends to be

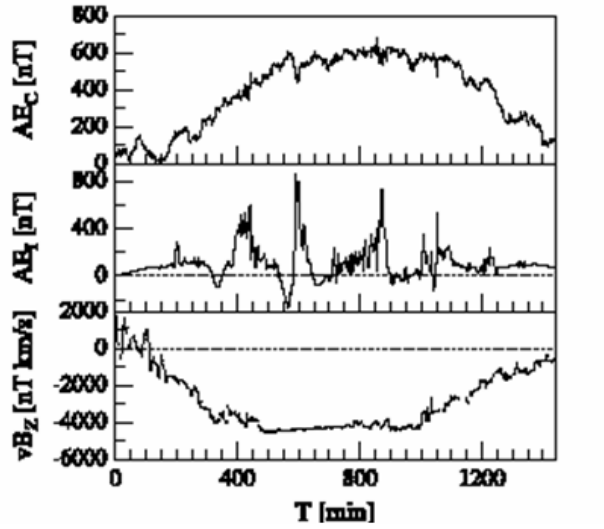

Fig. 1. The two AE components, solar wind driven (top panel) and intermittent (central panel) separated by means of the LIM method for 30 October 1978; the bottom panel displays the solar wind VB_z electric field (Consolini & De Michelis, 2005).

blotted out, making the correlation high. This may be the reason why significant portions of the slowly varying component of high latitude magnetic variations are predictable by the linear filter technique". Many authors attempted to reproduce the AE index by various methods. Price & Prichard (1993) used linear filtering; Vassiliadis et al. (1995) used the local linear prediction technique to reproduce the bursty character of the AE evolution; Ukhorskiy et al. (2004 and references therein) discussed the failure of the center-of-mass approximation to the local-linear technique to produce a bursty representation of the AE data; Chen & Sharma (2006), in a recent follow-on to the Ukhorskiy et al. work, corrected to some degree this aspect of the center-of-mass approximation, while Klimas et al. (1998) applied an entirely different technique to obtain a good representation of both the directly driven and the bursty loading-unloading aspects of the electrojet index data. Finally, Artificial Neural Networks (ANN) were used by several authors. For example, Takalo & Timonen (1997) used as inputs both solar wind VB_s and previously observed AE values and obtained a reliable prediction of the next AE value, but noticed that their algorithm "cannot be used for realistic prediction purposes as AE is not immediately available". On the other hand, Gleisner & Lundstedt (2001) developed an Elman network algorithm based only on solar wind data and comprising of three inputs, n (solar wind density), V (solar wind speed), and B_z (z GSM component of the IMF).

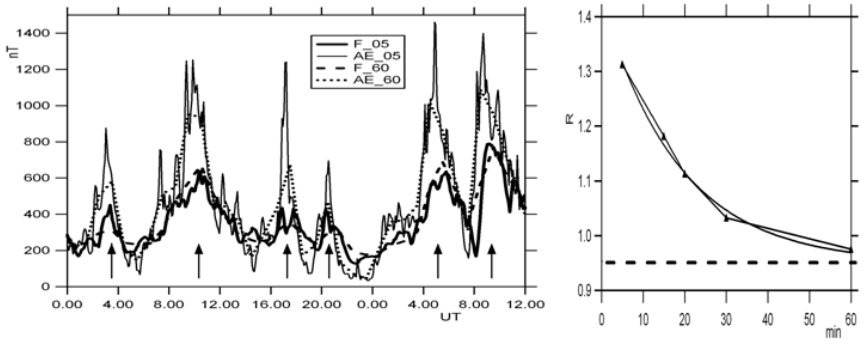

Fig. 2. a) AE_{05} (thin line) and F_{05} (thick line), AE_{60} (dotted line) and F_{60} (dashed line) plotted against time from 00 UT on 07 September 1995 to 12 UT on 08 September 1995 (see text for details). b) Normalised standard deviation for 5, 15, 20, 30 and 60 min ANN AE algorithms (see text for details).

2 An example of AE forecasting

Pallocchia et al. (2007) trained 5 ANN algorithms (with inputs GSM B_z and V_x), based on 5, 15, 20, 30 and 60 min averages of AE and solar wind data for 1995. Panel a of figure 2 displays 5 min AE averages and forecasts (AE_{05} and F_{05}, thin and thick lines, respectively) and 60 min AE averages and forecasts (AE_{60}, dotted line; F_{60}, dashed line) for 36 hours starting on 00 UT on 07 September 1995. AE_{60} plot displays 6 main enhancements (vertical arrows) with smaller peak values (by a factor of 1.6 – 1.8, due to the averaging process) with respect to the AE_{05} enhancements. We notice that the 60 min forecast AE, F_{60}, resembles closely F_{05}, both in the timing of the enhancements and in the peak values, apart for some small variations on scales < 60 min; moreover, F_{60} reproduces AE_{60} better than F_{05} reproduces AE_{05}, as all main enhancements are matched in time (exception made again for some time delays) and the F_{60} peaks are smaller than the corresponding AE_{60} ones by a factor of 1.5 – 2.

Panel b of figure 2 shows that the total normalised standard deviation, R, between the forecast and the Kyoto AE decreases with averaging time. Supposing that this decrease follows an exponential law, we can fit the R points through the dotted curve. It appears that $R(60min)$ differs from the asymptotous (horizontal dashed line) by $\simeq 3\%$.

These results can be interpreted in terms of the contribution of the two AE components: the unloading component could be responsible for the smaller scale large peaks, which fail to be reproduced by the AE ANN algorithms, while the directly driven component could be responsible for the broader enhancements. However, the fact that the peaks of the broader enhancements are not exactly reproduced suggests that the separation between the two components is not complete at these time scales. A large level of uncertainty in the AE prediction from solar wind data cannot be avoided, whatever time scale is chosen for the AE calculation. A better AE forecasting should require an input capable of quantifying the internal magnetotail state, as indirectly done by Takalo & Timonen (1997) by adding to the inputs at a given time the previous AE experimental value. In conclusion, it is possible to qualitatively forecast AE enhancements on time scales of a few hours bearing in mind that an underestimate by a

factor of 1.5–2 is very probable, while faster variations of AE, over time scales below 60 min, cannot be reproduced.

References

Bargatze, L.F., Baker, D.N., McPherron, R.L., Hones, E.W.: Magnetospheric impulse response for many levels of geomagnetic activity. J. Geophys. Res., **90**, 6387 (1985)

Chen, J., Sharma, A. S.: Modeling and prediction of the magnetospheric dynamics during intense geospace storms. J. Geophys. Res., **111 (A4)**, A04209, doi:10.1029/2005JA011359 (2006)

Clauer, C. R., Kamide, Y.: DP1 and DP2 current systems for the March 22, 1979, substorms. J. Geophys. Res., **90**, 1343 (1985)

Consolini, G., De Michelis, P.: Local intermittency measure analysis of AE index: The directly driven and unloading component. Geophys. Res. Letters, **32**, doi:10.1029/2004GL022063 (2005)

Davies, T. N., Sugiura, M.: Auroral electrojet activity index AE and its universal time variations. J. Geophys. Res., **71**, 785 (1966)

Elman, J. L.: Finding structure in time. Cognitive Sci., **14**, 179-211 (1990)

Freeman, M. P., Watkins, N. W., Riley, D. J.: Evidence for a solar origin of the power law burst lifetime distribution of the AE index. Geophys. Res. Lett., **27**, 1087 (2000)

Gleisner, H., Lundstedt, H.: Auroral electrojet predictions with dynamic neural networks.J. Geophys. Res., **106**, 24541-24549 (2001)

Kamide, Y., Baumjohann, W.: Magnetosphere-Ionosphere Coupling. Springer-Verlag, New York (1993)

Kamide, Y., Kokubun, S.: Two-component auroral electrojet: Importance for substorm studies. Geophys. Res., **101**, 13027 (1996)

Klimas, A. J., Valdivia, J. A., Vassiliadis, D., Baker, D. N.: AL index prediction using data-derived nonlinear prediction filters. In: Chang, T., and Jasperse, J. R. (eds) Physics of Space Plasmas. MIT Center for Theoretical Geo/Cosmo Plasma Physics, Cambridge, Massachusetts (1998)

Pallocchia, G., Amata, E. Consolini, G., Marcucci, M.F., Bertello, I.: AE index forecast at different time scales through an ANN algorithm based on L1 IMF and plasma measurements. JASTP, Accepted for publication (2007)

Price, C. P., Prichard, D.: The non-linear response of the magnetosphere: 30 October 1978. Geophys. Res. Lett., **20**, 771 (1993)

Sun, W., Xu, W.-Y., Akasofu, S.-I., Mathematical separation of directly driven and unloading components in the ionospheric equivalent currents during substorms. J. Geophys. Res., **103**, 11695 (1998)

Takalo, J., Timonen, J.: Neural network prediction of AE data. Geophys. Res. Lett., **24**, 2403 (1997)

Tsurutani, B. T., Sugiura, M., Iyemori, T., Goldstein, B. E., Gonzalez, W. D., Akasofu, S. I., Smith, E. J., Siscoe, G. L.: The nonlinear response of AE to the IMF BS driver: A spectral break at 5 hours. Geophys. Res. Lett., **17**, 279 (1990)

Ukhorskiy, A. Y., M. I. Sitnov, A. S. Sharma, Papadopoulos, K.: Global and multiscale features of solar wind-magnetosphere coupling: From modeling to forecasting. Geophys. Res. Lett., **31 (8)**, L08802, doi:10.1029/2003GL018932 (2004)

Uritsky, V., Klimas, A. J., Vassiliadis, D.: Comparative study of dynamical critical scaling in the auroral electrojet index versus solar wind fluctuations. Geophys. Res. Lett., **28**, 3809 (2001)

Vassiliadis, D., A. J. Klimas, D. N. Baker, Roberts, D. A.: A description of the solarwind magnetosphere coupling based on nonlinear filters. J. Geophys. Res., **100 (A3)**, 3495-3512 (1995)

Recent Advances in Modelling Space Weather effects on the terrestrial upper and middle atmospheres

A.D. Aylward, G.J.Millward, A.Lotinga, A.Dobbin and M.J.Harris

Atmospheric Physics Laboratory, Dept of Physics and Astronomy, University College London, Gower Street, London WC1E 6BT, UK alan@apl.ucl.ac.uk

Summary. As Global Circulation Models of the terrestrial upper atmosphere have evolved in recent years, they have been able to better simulate the observed physical effects of the penetration of space weather effects into and through the thermosphere. Although much of the physics is understood and can be demonstrated with the models not all the details can be predicted - or even reproduced - at even medium resolution (50-100km). The effects seen are complex and result from spatially and temporally variable inputs for which there is insufficient density of measurements. A major obstacle to obtaining sufficient resolution is the fact that energy and momentum inputs are global and have a complex 3-D structure linked back to the magnetosphere.

1 Introduction

The development of coupled atmosphere-thermosphere-ionosphere-plasmasphere models has a long history which eventually led to those like CMAT (Coupled Mesosphere And Thermosphere) and CMAT2, the latter representing the current state of the art in coupled atmospheric modelling. CMAT2 is written in Fortran 90/95 and modularizes the code into small logical parts which can be swapped around allowing different combinations of sub-systems. If, for example, only a simple, non-coupled ionosphere is required then the model can be run with a parameterized ionosphere like the Chiu ionosphere (Chiu, 1975) or the PIM (Parameterised Ionosphere Model). If a coupled ionosphere-neutral atmosphere is needed then the self-consistent GIP (Global Ionosphere Plasmasphere) model is used. GIP is a combination of the high-latitude ions, plasmasphere and molecular ions routines from the CTIP (Coupled Thermosphere, Ionosphere, Plasmasphere) and CMAT models. CMAT2 takes the lower boundary down to 15km altitude. It allows for a variety of lower boundary conditions – MSIS, NCEP and fixed – and can be used with three different gravity wave parameterizations. It has variable resolution grid-spacing. It can be compiled and run with virtually any useful latitude-longitude and height spacing, so that one can trade off resolution against system usage. The magnetic field configuration used in GIP is an “Apex” system, that is one that traces the field lines from equatorial apex to ground, rather than approximating them analytically .

2 Simple state structure of the thermosphere

The global circulation models developed so far are built around a ”core” thermosphere. Because of its viscosity the thermosphere has a fairly uniform large scale structure, so it is easy to model its basic cyclical behaviour, and all the models do this well. Fig. 1, for example, shows the wind and temperature structure for equinox and the solstices under magnetically quiet conditions. Because of the time constants involved the temperature peaks in the afternoon. The equinox temperature pattern is more or less symmetric, and the two solstices are more or less mirror images with the temperature maximum now shifted to the summer hemisphere. The winds blow more or less from the temperature maximum to the minimum. The ”more or less” is to recognize that there are small distortions to the temperature and wind patterns due to the effects of auroral heating which is not symmetric due to the offset tilted dipole of the Earth’s magnetic field. Not shown here, but part of the overall seasonal behaviour, the model successfully reproduces many of the seasonal effects due to the change of the O:N_2 ratio such as the winter anomaly in electron density (Yonezawa, 1959), and the fact there is an annual variation of thermospheric temperature at mid-latitudes but a semi-annual variation at equatorial latitudes. These examples show the models’ ”steady-state” behaviour – that is the result of it being run through the same conditions again and again until it settles into an unchanging state.

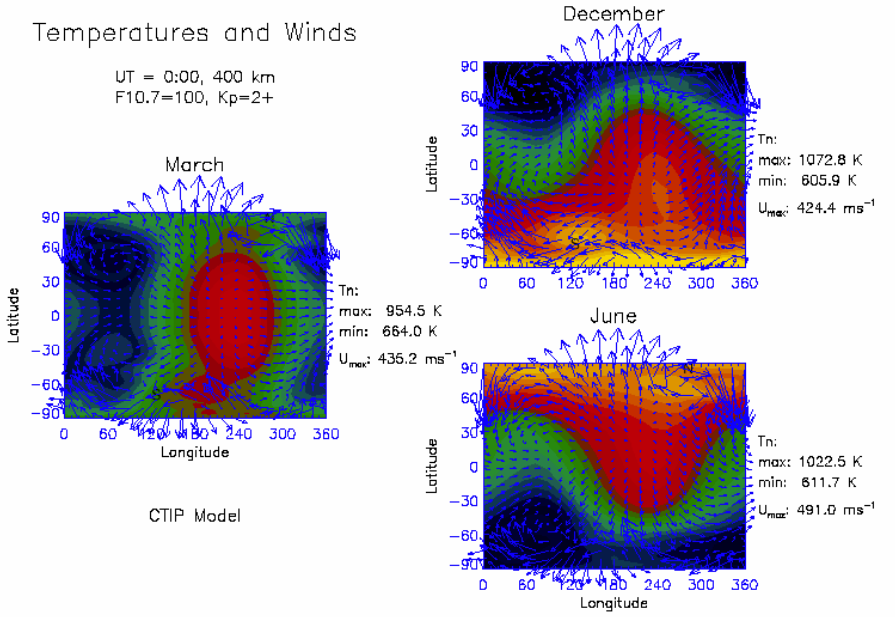

Fig. 1. Thermospheric seasonal behaviour under quiet geomagnetic conditions. Colour coded temperature and overplotted neutral velocities (arrows) for equinox (left) and solstices (right)

3 Dynamic situations

The models can also be run dynamically in that the drivers – such as the auroral convection pattern and precipitation – can be continually changed as the model runs. This is closer to the "real" Earth, but the physics is less easy to follow. The models exhibit wave behaviour, as the thermosphere does if the energy inputs are "pulsed" (Millward et al., 1993).

The fact the Earth has a magnetic field means the electrodynamics must be treated globally. It produces, for example, some interesting behaviour at the equator. CTIP illustrates the linkage between the ionospheric E- and F-regions via the geomagnetic field in showing that auroral disturbances have an effect at the equator faster than it takes for a wind disturbance to travel from auroral to equatorial zones, simply because low altitude mid-latitude field lines cross the equator at F-region altitudes and so wind effects on the plasma in the E-region at mid-latitude is transmitted to the equatorial region by electrodynamic coupling.

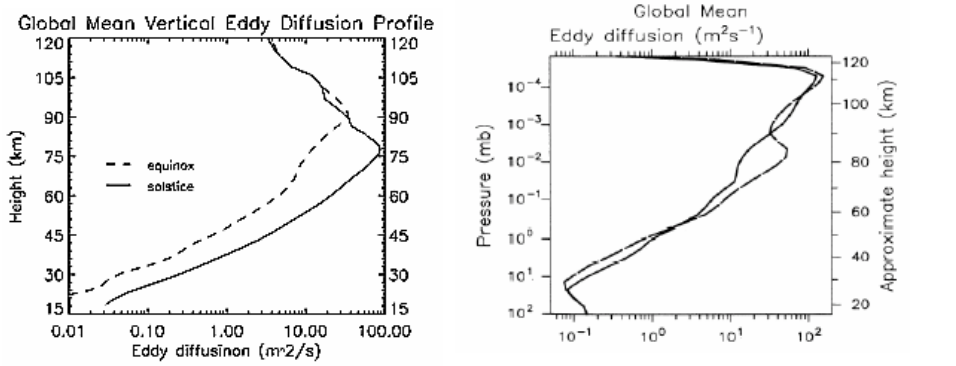

Fig. 2. The effect of different gravity wave parameterisations on the Global Mean Eddy diffusion coefficient altitude profile. On the left CMAT2 has been run with a hybrid Lindzen Matsuno scheme, on the right with a Doppler Spread parameterisation. Dashed line is January solstice, full line is April. F10.7=80 and Ap=6 were used as activity parameters

The most important tides seen in the terrestrial atmosphere are thermal tides. These are heat and pressure oscillations generated by solar illumination – infra-red and visible wavelengths at the ground, UV radiation in the stratospheric ozone layer and EUV in the thermosphere. As the sun rises and sets in the course of a day, a basic diurnal driver is established. In the lower atmosphere and thermosphere the response, too, is primarily diurnal, though non-sinusoidal components in the heating profiles and asymmetries in the terrestrial response function mean that other harmonics can be strong: in the ozone layer the response seems to be mainly a semi-diurnal oscillation. The tides are important to the coupling between upper and lower atmosphere, as they provide a mixing influence and can couple non-linearly with other effects such as the chemistry or gravity waves.

Atmospheric gravity waves (AGWs) are implemented in GCMs as parameterisations since individual AGWs are too small to be resolved by the global model grids. The AGWs are small-scale oscillations in the lower atmosphere (fed by any turbulence such as weather fronts, lee waves from mountains etc.) which grow as they propagate vertically until they break when their amplitudes have become unsustainable. The effect of this breaking is to deposit momentum - and the combined result of this in the mesosphere is to reverse the meridional flow and the north-south temperature gradient. This is again an obvious source of vertical coupling in the atmosphere, and a complex one that it is not easy to measure or treat theoretically. For CMAT2 there are several alternative parameterisations, and Fig. 2 shows the effect on the eddy diffusion coefficient of the choice of parameterisation.

4 Model applicability in ”Space Weather” studies

To study how Space Weather effects propagate from space to ground at the Earth one can either take the CMAT approach and extend a thermospheric model – already ”space-coupled” – downwards, or extend a meteorological model upwards. The advantage of the former is that thermosphere-ionosphere GCMs already include a number of effects which are not present in meteorological models and are more than just a matter of extending the dynamics. CMAT2, for example, has atomic oxygen and Nitric Oxide chemistry and transport from the upper atmosphere built in, and so the source functions for these and other chemical species would not need to be parameterised. Thermosphere ionosphere GCMs also have coupled auroral zones which supply a momentum input and a particle input, and hence via this a chemical variability to the middle – and potentially lower – atmosphere. That these effects propagate down at all is controversial, but there is strong statistical evidence that some effects get through, if only by intermediary action.
The features in the upper atmosphere GCMs useful for studying Space Weather effects are:
- energetic and particle coupling from the magnetosphere to the lower atmosphere,
- solar radiation variation at the resolution of Solar2000 - and varying with time,
- wave coupling to the troposphere parameterised or using empirical models,
- detailed chemistry at all levels, with dynamical coupling between layers,
- increased spatial resolution to look at small-scale structures,
- increased time resolution to look at impulsive events.

The most obvious space weather input is at the auroral zone. This comprises both an energy effect (particle precipitation and heating) and a momentum effect (plasma convection). Both effects have a spatially and temporally complex dynamic behaviour which is the result of the complex and highly variable nature of the interaction between the solar wind and the magnetosphere. The basic physics of most of the components of this interaction are known. We can simulate the auroral input as a plasma flow pattern (momentum) and a particle precipitation pattern (energy). Given these, we can show, individually, how most known effects come about. In Fig. 3 we show a time vs latitude plot of the modelled response of the atmosphere equatorward of the geomagnetic storm of April 9-12 1997, and we see three basic responses to the aurorae – positive and negative storm effects and in-situ precipitation. All these effects seen in the modelling were present in TEC measurements and radar data, but at slightly differ-

ent times, intensities or positions. It is understandable that we do not have a perfect match. In thermosphere-ionosphere studies we do not have an input of spatial and temporal resolution as high as is common in meteorology. Our input convection and precipitation models are the result of accumulating lots of satellite data and hence are only accurate on average and not for a specific period.

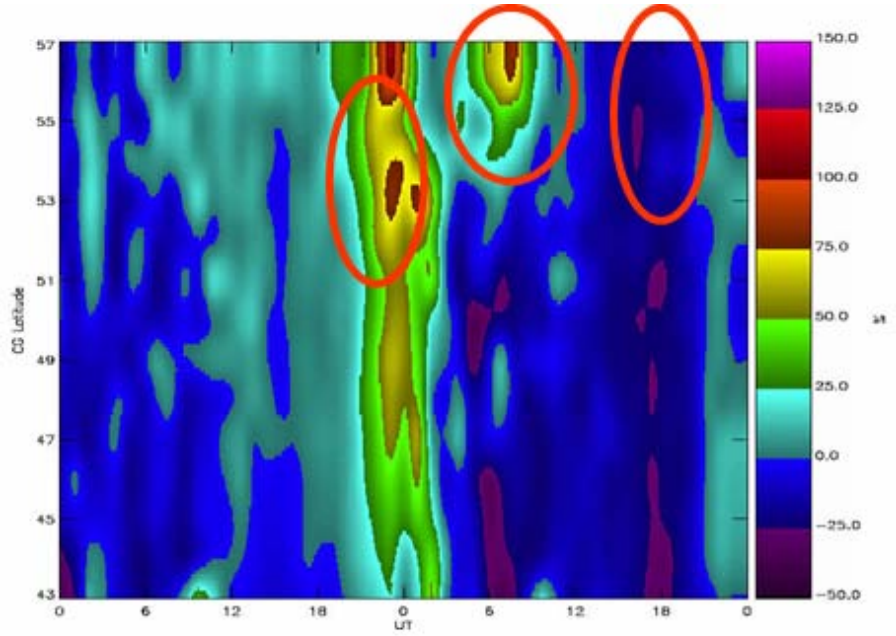

Fig. 3. Simulation of TEC for the April 9-12th 1997 storm period. The run shows three distinct types of response to the auroral activity. In the leftmost ring we see the so-called "dusk effect" where neutral winds cause an increase of ionization. The middle ring shows direct precipitation, while the right ring shows a depletion caused by electrodynamical lowering of the ionization due to electric fields. All these effects were observed but with slightly different magnitudes and morphology.

Some progress is possible in improving the resolution of the simulations in limited areas: it is possible to use current GPS TEC networks to get fairly dense electron density maps. Ionospheric (non-coupled) models can, therefore, do a good job with the right application of data assimilation techniques, of fitting to and "near-casting" ionospheric conditions. However, the ionosphere depends on the neutral atmosphere, and a change of neutral composition would soon feed through into electron density changes, so that a lack of measurements of the neutral atmosphere would soon render the simulation invalid. With little chance that thermospheric wind, temperature and composition data is ever going to be taken at the same resolution as the TEC, it is difficult to see how predictions could be improved. However, better convection maps for the high-latitude atmosphere are becoming available, thanks chiefly to the SUPER-

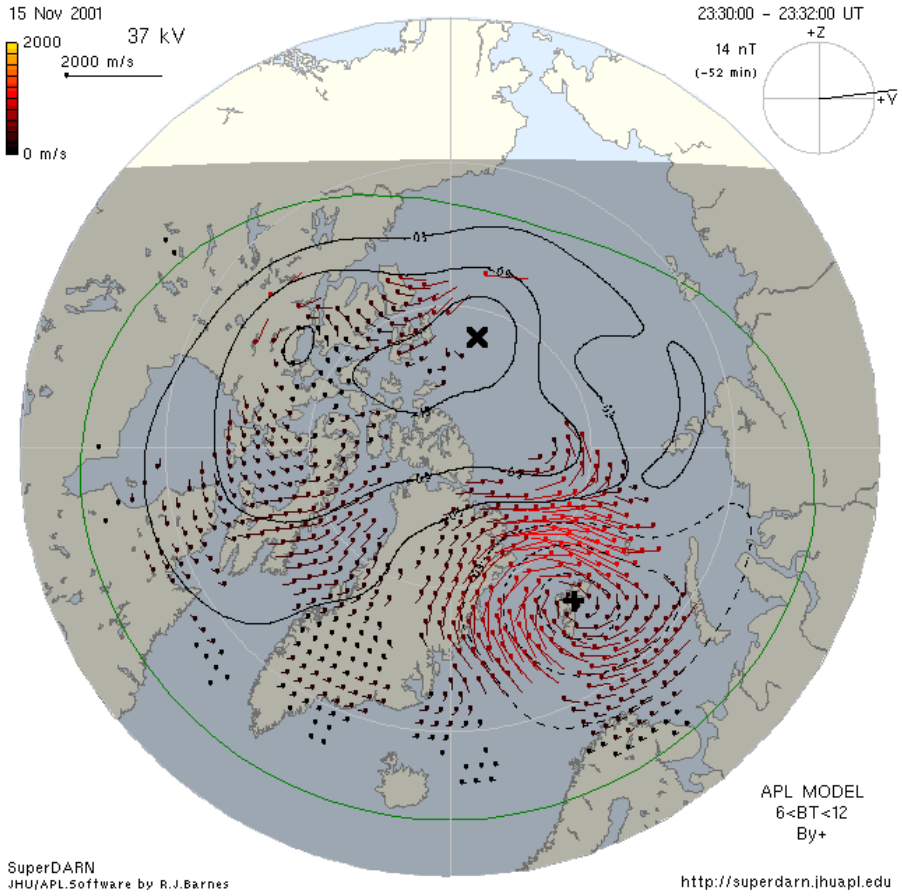

Fig. 4. SUPERDARN high-latitude convection pattern. This is generated by a model which is constrained by any actual data taken by the radars (taken from *http://superdarn.jhuapl.edu/*).

DARN radars. The complexity of the true pattern, as opposed to the older averaged models, becomes apparent in Fig. 4 where we see the global fit of convection velocities to the northern hemisphere SUPERDARN radars. Using this as an input to models like CTIP gives a significantly different neutral winds and Joule heating pattern to the ”traditional” (highly averaged) convection models. What is now needed is a precipitation model that (a) fits onto the complex SUPERDARN convection pattern and (b) is of a similar spatial resolution. The OVATIONS model (Newell et al., 2002) is a step towards this goal, and we might expect nowcasting to get better with this. But there are many other parameters – e.g. the initial state of the atmosphere, the small-scale structure of the dynamics etc. – which will still limit the accuracy of our forecasting. There have been recent advances, though, in areas where the effects are more averaged globally - i.e. where the effects are smoothed out in a way equivalent to the

smoothing seen in the empirical input models. Thus Fig. 5 shows the penetration of NO to low latitudes following substorm activity.

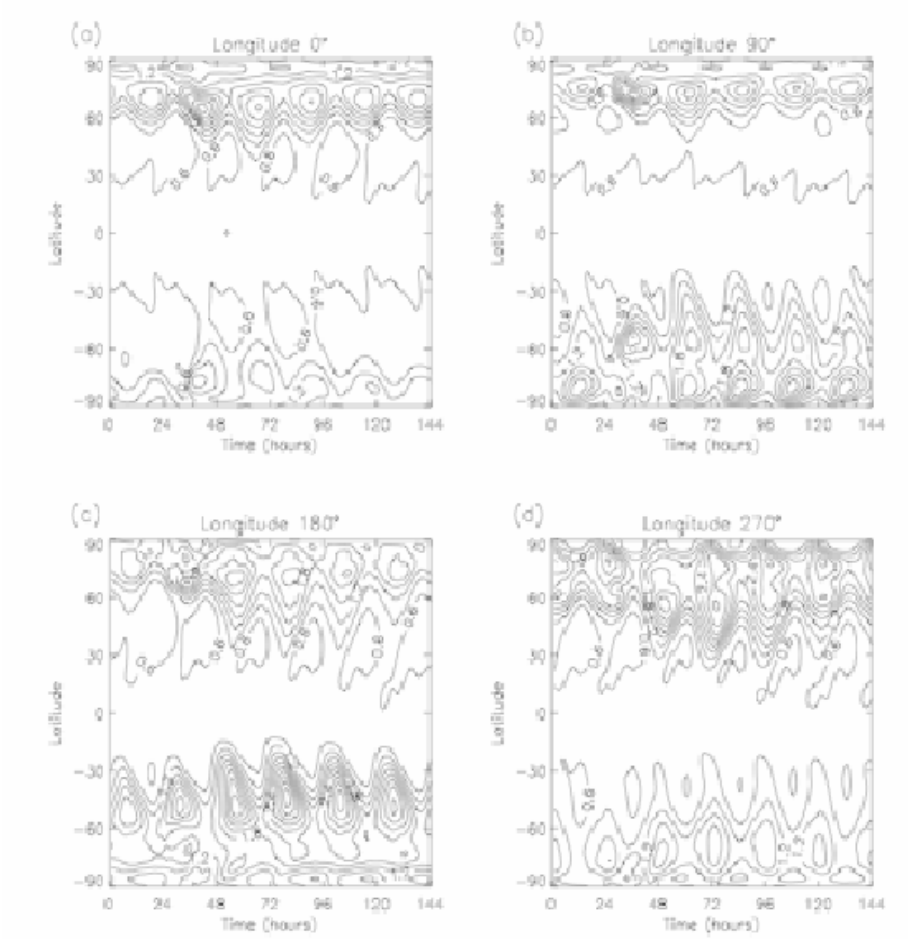

Fig. 5. Nitric Oxide response at four different longitudes during a simulated 6-day storm period. The contours show Nitric Oxide densities (see Dobbin et al 2006 for details of scaling).

5 Latest developments with CMAT2

In creating CMAT2 from CMAT, on-the-fly graphics and simple web access to the model was built in as it runs. This improves significantly the chance to detect at an early stage problems and errors made in the early phases of model runs. We have not yet reached the level where

a run can be modified on the fly, but this is an obvious next step. Some progress is being made in the area of data assimilation from data sets such as the GPS TEC data and from other instruments that can give information to constrain the simulations. These techniques have been perfected in (tropopause) meteorology, and this expertise can be used higher up.

However, progress in atmospheric science is not merely a question of higher observational resolution – new phenomena were also discovered. For instance, in 1989 "upward going lightning" above a large thundercloud region was photographed and christened "sprites" (Franz et al., 1990). This discovery started a whole new area of atmospheric science. The discovery of the sprites was followed by a host of other new discoveries such as "elves", "blue jets" and Gamma ray bursts above thunderstorms. All these phenomena show that the lower atmosphere is coupled to the ionosphere in ways we had not previously suspected. This brought the global electric circuit into the focus of the discussion and the question of how it might be implemented into GCMs. It is difficult to see how immediate progress can be made given the resolution and dynamic range of current GCMs, but this seems to be an area where future work will concentrate.

6 Conclusions

Models of the Earth's upper atmosphere have become increasingly complex and more tightly coupled to the regions above and below. There is a move to more flexibility in the resolution and increasing modularity which allows code-sharing between models. The lower boundary can be as low as the ground, with a choice of boundary models. Such models are already useful for a range of studies on the coupling between atmospheric layers, and are being used increasingly to couple to other models in the Sun-Earth chain. Developments continue, but some elements are still unclear, in particular, how to extend the representation of electric fields to include the global electric circuit.

References

Chiu T.T.: Chiu ionospheric model. Planet. Space Sci. **40**, 544 (1975).

Dobbin A.L., Aylward A.D. and Griffin E.M: 3D GCM modelling of Thermospheric Nitric Oxide During the 2003 Halloween Storm. Ann. Geophys. **24**, 2403–2412 (2006).

Franz, R.C., Nemzek, R.J., Winckler, J.R.: Television image of a large upward electrical discharge above a thunderstorm system. Science, **249**, 48–51 (1990).

Millward, G.H., Quegan, S., Moffett, R.J., Fuller-Rowell, T.J., Rees, D.: A modelling study of the coupled ionospheric and thermospheric response to an enhanced high-latitude electric-field event. Planet.Space Sci., **41**, 45–56 (1993).

Newell, P.T., Sotirelis, T., Ruohoniemi, J.M., Carbary, J.F., Liou, K., Skura, J.P., Meng, C.-I., Deehr, C., Wilkinson, D., and Rich, F.J.: OVATION: Oval variation, assessment, tracking, intensity, and online nowcasting. Ann. Geophys., **20**, 1039–1047 (2002).

Yonezawa T.: On the Seasonal and non-seasonal variations of the F-layer at middle latitudes. J. Rad. Res. Lab. Japan, **6**, 651 (1959).

Recent results on ionospheric convection based on SuperDARN

E. Amata[1], C. Hanuise[2], M. Lester[3], and M.F. Marcucci[1]

[1] IFSI-INAF, Rome, Italy Ermanno.Amata@ifsi-roma.inaf.it
[2] LPCE-CNRS, Orleans, France
[3] Leicester University, Leicester, UK

1 Introduction

The large-scale morphology of ionospheric convection in the auroral and polar regions has been studied for many years using low-altitude spacecraft (Heppner & Maynard (1987); Weimer (1995)), ground magnetometers (Kamide et al. (1994); Papitashvili et al. (1994)) and, more recently, SuperDARN convection measurements (Ruohoniemi & Greenwald (2005) and references therein). The SuperDARN data allow to evaluate, both in near real time and for historical data, two space weather products: the high latitude ionospheric convection patterns and the associated cross polar cap electric potential (CPCP). In this paper we discuss how CPCP and convection patterns are calculated and how they depend in general on the IMF orientation. Further on, we briefly describe some recent observations made during different periods of northern IMF which provided evidence, for the first time, of dual lobe reconnection.

2 High latitude convection patterns and CPCP

The SuperDARN network comprises of 12 HF radars in the Northern Hemisphere (NH) and 7 radars in the Southern Hemisphere (SH), each consisting of a primary array of 16 antennae and an interferometer array of 4 antennae. Each radar is electronically steered into one of sixteen different beam directions covering a fan of 52°. The radars transmit a short sequence of pulses, referred to as a multi-pulse sequence, and sample the returning echoes. The Auto-Correlation Function of the echoes allows to calculate the back-scattered power, spectral width and Doppler velocity of the plasma density irregularities in the ionosphere. In the standard operating mode, for each 3.25° beam 75 spatial ranges are resolved with a 45 km separation (Greenwald et al.,1995; Chisham et al.,2007).

The reconstruction of convection patterns by using SuperDARN data is based on finding a functional form for the distribution of electrostatic potential in the ionosphere that best fits all the line-of-sight velocity measurements available at the time of interest. The convection velocity v is related to ϕ through the relationships $\mathbf{E} = -\delta\phi$ and $\mathbf{v} = \mathbf{E}x\mathbf{B}/B^2$. The algorithm for the implementation of this method is fully described by Ruohoniemi & Baker (1998). The first step is to map the line-of-sight velocity measurements onto a global grid of nearly equal

area grid cells measuring 1° in geomagnetic latitude. In the next step of the analysis the gridded velocity data are fitted to an expansion of ϕ in terms of spherical harmonic functions

$$\phi = \sum_{l=0}^{L} \sum_{m=0}^{Min(L,M)} (A_{(l,m)} cos(m\phi) + B_{(l,m)} sin(m\phi)) P_l^m cos(m\phi). \quad (1)$$

where the P_l^m are the associated Legendre functions. L and M, which express the order and degree of the expansion, respectively, determine the resolution available in the fitting. The coefficients of the expansion $A_{(l,m)}$ and $B_{(l,m)}$ express the physical content of the solution and are found by performing a singular-value decomposition. The global fitting is implemented with a package of software known as "Map Potential", which is also used as a name for the technique.

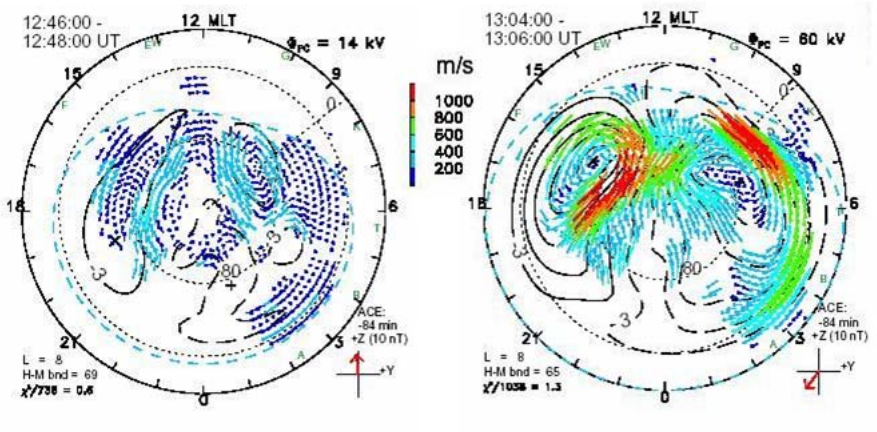

Fig. 1. SuperDARN NH convection patterns for southward (left panel) and northward (right panel) IMF.

An example of such a reconstruction for the NH is shown in Figure 1, where the contours of constant electrostatic potential (solid and dashed black lines) also represent flow streamlines. The left panel is characterised by a relatively weak convection characterized by a cross polar cap potential (CPCP) $\simeq 15$ kV. This occurred at the end of a long period of northward IMF. The convection pattern shows reverse (sunward) convection in the high latitude dayside ionosphere and evidence of viscous convection cells on the flanks. Near 12.56 UT an abrupt southward turning of the IMF reached the magnetopause. A two-cell convection pattern, typical of southward IMF conditions, is established very quickly ($\simeq$ mins) over the entire high-latitude region. The convection then rapidly intensifes, with CPCP reaching values near to 60 kV within $\simeq 10$ mins, as shown in the right hand panel. By combining the data from all northern hemisphere SuperDARN radars, Figure 1 effectively images the global convection electric field, obtaining a result that is analogous to space-based images of the global distribution of auroral luminosity. The line-of-sight velocity dataset used as input for the convection maps is often spatially extensive but not truly global. To ensure that the solution is

realistic over areas of sparse radar coverage, the velocity data are supplemented with data from the statistical model by Ruohoniemi & Greenwald (1996), who combined many years of SuperDARN line-of-sight velocity data to produce global ionospheric maps of electrostatic potential sorted by IMF strength and direction. The selection of model data is keyed to the IMF conditions presumed to prevail at the magnetopause at the time of interest using suitably time-lagged data from spacecraft situated in the solar wind. The model data are weighted in the fitting so as to just stabilize the solution while minimizing the impact of the statistical model. Improvements in the statistical model aspect of the convection mapping technique are continually under development and the continued expansion of the SuperDARN network reduces the reliance of the maps on the model data. It is also useful to downweight line-of-sight velocity data outside the equatorward boundary of the convection zone that derives from the work of Heppner & Maynard (1987). In Figure 1 the Heppner-Maynard boundary is depicted as a dashed cyan line. The latitude of this boundary in the midnight meridian characterizes the size of the convection zone. The coverage provided by the radars is sometimes sufficient to effectively determine the entire global convection pattern, i.e., the solution becomes independent of the selection of statistical model data. For each convection pattern the CPCP is evaluated providing a measure of the coupling of the solar wind electric field to the high latitude ionosphere. CPCP values corresponding to high solar wind electric fields must be considered with caution as there is evidence that, for very large values of CPCP (above $\simeq 70$ kV), they may saturate (Shepherd et al., 2002).

Global convection maps can be generated at the 1- or 2-min resolution of the radar scans, which is suitable for observing the response of ionospheric convection to changes in the solar wind and the IMF. Using internet links to many of the radars, a near real-time mapping of the ionospheric convection pattern is now possible for the NH and is displayed at the SuperDARN JHU/APL web site (http://superdarn.jhuapl.edu/). With the planned extension of the internet links to all of the SH SuperDARN network, global convection mapping in both hemispheres is likely to become a routine SuperDARN data product. To this regard, limitations to the ability of the system to produce reliable convection maps exist due to a gap in the azimuthal coverage of the NH high latitude ionosphere over Siberia and to two similar gaps in the SH coverage. However, in 2008 the SH gaps should be filled by the installation of two radars at Dome C and the NH gaps by the installation of 4 radars at three different locations in Siberia.

3 Ionospheric convection as a function of IMF

It is now well accepted that the high latitude ionospheric convection results mainly from the transfer of magnetic flux from the day side to the night side due to reconnection at the magnetopause and from the transfer of flux from the night side to the day side at lower latitudes as the result of reconnection in the magnetotail central plasma.

For a purely southward IMF, reconnection takes place at the low latitude dayside magnetopause, so that newly opened flux is transferred to the night side and two convection cells are set up in both hemispheres with anti-sunward flow in the polar cap. The relative dimensions and orientations of the two cells depends upon the relative importance of the IMF Bz and By components or, more precisely, on the magnetic clock angle defined as $\theta = arctang(By/Bz)$. For $\theta = 180^\circ$ two symmetric cells are observed (see the righ panel

of Figure 1), while for $\theta = 90^\circ$ the dusk and dawn cells dominate in the Northern and in the Southern Hemisphere respectively and the opposite situation occurs when $\theta = -90^\circ$. For strongly northward IMF (i.e. for $\theta \simeq 0^\circ$) , reconnection is thought to occur tailward of the cusps (lobe reconnection) thus generating two reverse cells with sunward flow over the polar cap (see the left panel of Figure 1).

There has been disagreement for a long time over the detailed patterns of ionospheric convection resulting from strongly southward IMF. Early studies (Burke et al. (1979); Reiff & Burch (1985)) suggested the existence of four convection cells during northward IMF conditions: two "reverse" cells at high latitudes driven by lobe reconnection antisunward of the cusp regions, and two "normal" cells at lower latitudes driven by viscous processes at the magnetopause. On the contrary, Heppner & Maynard (1987) suggested that only two highly-distorted cells would develop, while Rich & Hairstone (1994) performed a statistical study and found four-cell convection to occur very rarely. Conversely, the statistical study of ionospheric convection by Ruohoniemi & Greenwald (1996) using SuperDARN data showed that, at least statistically, a four-cell structure existed for strong northward IMF. Their statistical convection pattern clearly showed two reverse convection cells poleward of 80° magnetic latitude near the noon meridian, which were almost completely contained within the dayside ionosphere. The work of Ruohoniemi & Greenwald (1996), further detailed by Ruohoniemi & Greenwald (2005), provides a complete picture of the statistical dependence of high-latitude convection on the IMF. Significant features in their statistical maps include the transition of the dawn and dusk convection cells into more rounded or crescent shapes depending on the sign of IMF By, the intensifcation of the two-cell pattern with increasing magnitude of southward IMF, and the emergence of sunward convection in the dayside ionosphere for increasingly positive IMF Bz. Although the statistical maps derived by Ruohoniemi & Greenwald (2005) cannot account for the full range of possible convection configurations they do define a zero-order solution of the global convection. For most IMF conditions the patterns are very similar to those derived from satellite-based statistical studies (e.g. Weimer (1995)). These statistical convection maps have also been used in comparison with statistical maps of particle precipitation (Newell et al., 2004), helping to place both sets of observations into context.

4 Recent results on lobe reconnection

Huang et al. (2000) provided the first evidence of the two reverse convection cells in a 30-min averaged SuperDARN vector velocity map of the dayside northern ionosphere during steady northward IMF conditions. This study further showed that the four cell convection configuration was stable as long as the IMF conditions remained stable and that the reverse convection cells were typically of size $\simeq 1000$ km with a potential drop of $\simeq 5$ kV in each cell. Such cells are typically totally contained in the polar cap and their convection stirs the open field lines within the polar cap itself. If the northward IMF condition persists, the Open Closed field line Boundary (OCB) may move poleward as magnetic flux is convected back to the day side due to reconnection in the plasma sheet. At the same time the lobe merging gap is located poleward with respect to the OCB. Moreover, the OCB may be forced to move poleward very quickly in both hemispheres. This is the case of the so called dual lobe reconnection, i.e. the simultaneous reconnection of an IMF field line at two locations on the magnetopause, tailward

of both the northern and the southern cusp. Figure 2 (from Imber et al., 2006) provides an illustration of what schematically happens when the IMF is southward (left panel), northward but with single lobe reconnection (central panel) and northward with dual lobe reconnection (right panel). As the figure shows (top right hand panel), the dual lobe reconnection yields the formation of a newly closed field line in the day side, while the magnetosheath solar wind sweeps away two disconnected field lines tailward of the cusps; at the same time, the reverse cells are no longer confined within the polar cap and the merging gap lies along the OCB (bottom right hand panel).

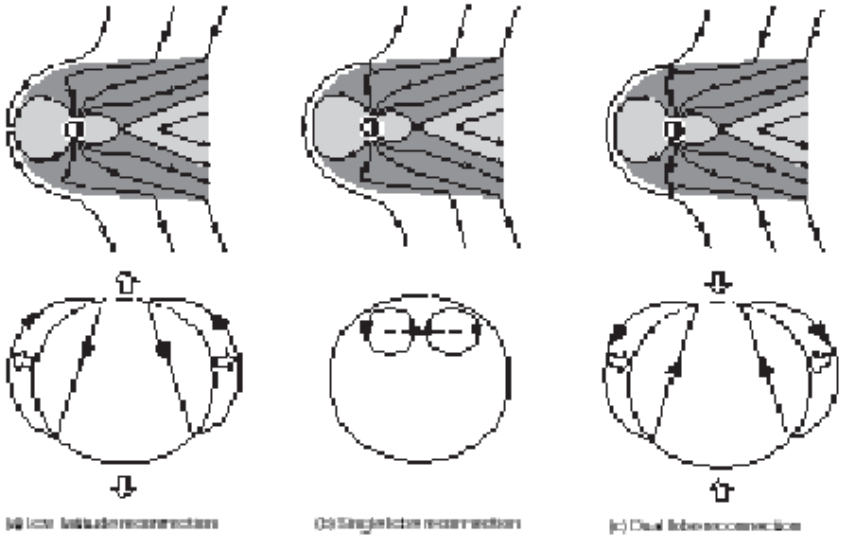

Fig. 2. Schematic representations of the magnetosphere in the GSM X-Z plane and ionospheric convection patterns during single, low latitude and dual lobe reconnection. The solid circle is the OCB, encircling the polar cap. The dashed portion of the OCB is the merging gap, the arrowed lines are flow streamlines and the large arrows indicate expansion or contraction of the polar cap. Local noon is directed towards the top of the figure.

Three papers appeared recently on dual lobe reconnection as observed by SuperDARN with the complement of various spacecraft observations.Imber et al. (2006) first presented substantial evidence for the occurrence of dual lobe reconnection during a period of strongly northward IMF, when they identified two bursts of sunward plasma flow across the noon portion of the open/closed field line boundary (OCB), indicating magnetic flux closure at the dayside. They also estimated that, in order for dual reconnection to occur, the interplanetary magnetic field clock angle must be within 10° of zero (North) and that the total flux crossing the OCB during each burst was small (1.8 and 0.6 per cent of the flux contained within the polar cap for the two flows). Moreover, they observed a brightening of the noon portion of the northern auroral oval, thought to be due to enhanced precipitating particle fluxes due to the

occurrence of reconnection at two locations along the field line. Finally, they estimated that 2.510^{30} solar wind protons (4 tonnes by mass) were captured by the flux closure process, sufficient to populate the cold, dense plasma sheet observed following the dual lobe reconnection interval.

The second paper on dual reconnection was by Imber et al. (2007), who performed a new case study using SuperDARN measurements of the ionospheric convection flow and observations of the aurora by the IMAGE spacecraft. In this case they used the noon-midnight and dawndusk keograms of the aurora to show that the polar cap shrinked during the interval and calculated, using the SuperDARN potential maps, that the amount of flux closed during the interval was 0.13GWb, i.e. approximately 10 per cent of the pre-existing polar cap.

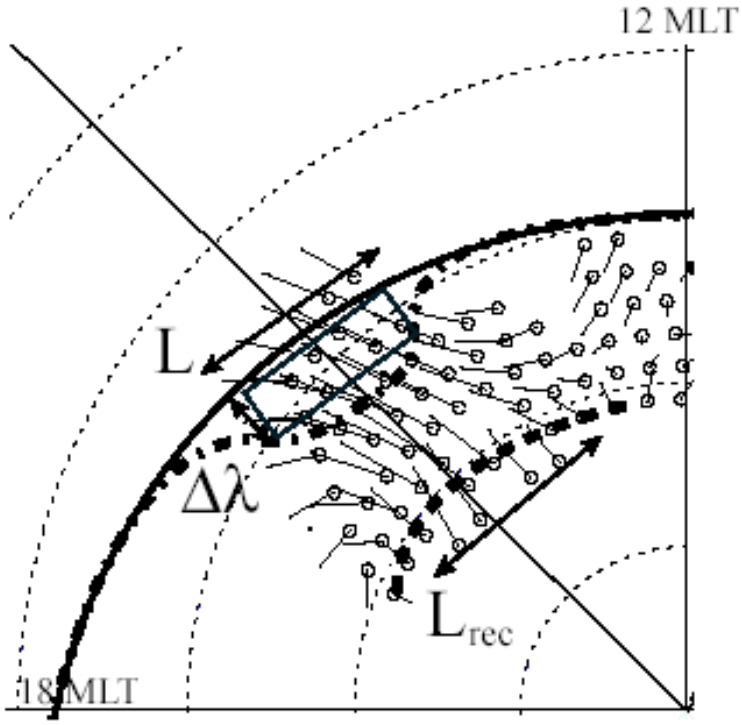

Fig. 3. The sketch refers to the case studied by Marcucci et al. (2007) and shows the OCB before the occurrence of dual lobe reconnection (heavy line), the new position of the OCB when dual reconnection has been going on for some time (dot-dashed line) and the projection of the northern lobe reconnection line (dashed line). The SuperDARN flow vectors for a 2 min interval are overplotted on the drawing.

Finally, Marcucci et al. (2007) presented a detailed study of SuperDARN data and IMAGE FUV observations of the aurora in the NH for a period when the IMF was predominately

northward with the By component changing from positive to slightly negative. Cluster plasma and magnetic field observations, during the same period, show that lobe reconnection is continuously going on in the Southern Hemisphere at dusk. Moreover, Cluster observations show evidence that dual lobe reconnection is occurring at particular time intervals. SuperDARN convection maps throughout the period of study show that that lobe reconnection is occurring at the Northern Hemisphere despite the fact that the dipole tilt is unfavorable and Bx is positive. DMSP, IMAGE S13 and SuperDARN observations show that, during the 2 hours, four poleward movements of the OCB are associated with enhanced sunward/westward velocity flows crossing the OCB itself. Marcucci et al. (2007) interpret this as the result of lobe flux re-closure occurring sporadically in the dusk sector, with at least one poleward movement of the OCB coinciding with Cluster in situ observations of dual lobe reconnection. Figure 3 shows a sketch drawn by from Marcucci et al. (2007) for their case study. The sketch shows the OCB before the occurrence of dual lobe reconnection (heavy line), the new position of the OCB when dual reconnection has been going on for some time (dot-dashed line) and the projection of the northern lobe reconnection line (dashed line). The SuperDARN flow vectors for a 2 min interval are overplotted on the drawing clearly showing the flow across the OCB.

References

Burke, W. J., Kelley, M. C., Sagalyn, R. C., Smiddy, M., Lai, S. T.: Polar cap electric field structures with a northward interplanetary magnetic field. Geophys. Res. Lett., **6**, 6, 21-24 (1979)

Chisham, G., Lester, M., Milan, S.E., Freeman, M.P., Bristow, W.A., Grocott, A., MacWilliams, K.A., Ruohoniemi, J.M., Yeoman, T.K.,Dyson, P., Greenwald,R. A., Kikuchi, T., Pinnock, M., Rash, J., Sato, N., Sofko, G., Villain J.-P., Walker, A.D.M.: A decade of the Super Dual Auroral Radar Network (SuperDARN): Scientific achievements, new techniques and future directions. Surveys in Geophysics, **28**, 33 - 109, doi:10.1007/s10712-007-9017-8 (2007)

Greenwald, R. A., Baker, K. B., Dudeney, J. R., Pinnock, M., Jones, T. B., Thomas, E. C., Villain, J. -P., Cerisier, J. -C., Senior, C., Hanuise, C., Hunsucker, R. D., Sofko, G., Koehler, J., Nielsen, E., Pellinen, R., Walker, A. D. M., Sato, N., Yamagishi, H.: DARN/SUPERDARN: A Global View of the Dynamics of High–Latitude Convection. Space Sci. Rev., **71**, 761–796 (1995)

Heppner, J. P., Maynard, N. C.: Empirical high-latitude electric field models. J. Geophys. Res., **92**, 4467-4489 (1987)

Huang, C.-S., Murr, D., Sofko, G. J., Hughes, W. J., Moretto, T.: Ionospheric convection response to changes of interplanetary magnetic field Bz component during strong By component, J. Geophys. Res., **105**, 5231-5243 (2000)

Imber, S. M., Milan, S. E., Hubert, B.: The auroral and ionospheric flow signatures of dual lobe reconnection. Ann. Geophys., **24**, 3115-3129 (2006)

Imber, S. M., Milan, S. E., Hubert, B.: Observations of significant flux closure by dual lobe reconnection. Ann. Geophys., **25**, 1617-1627 (2007)

Kamide, Y., Richmond, A. D., Emery, B. A., Hutchins, C. F., Ahn, B. H., de la Beaujardire, O., Foster, J. C., Heelis, R. A., Kroehl, H. W., Rich, F. J., Slavin, J. A.: Groundbased studies of

ionospheric convection associated with substorm expansion. J. Geophys. Res., **99**, 19451-19466 (1994)

Marcucci, M. F., Coco, I., Ambrosino, D., Amata, E., Milan, S. E., Bavassano Cattaneo, M. B., Retino, A.: Extended SuperDARN and IMAGE observations for northward IMF: evidence for dual lobe reconnection. J. Geophys. Res., accepted for publication (2007)

Newell, P. T., Ruohoniemi, J. M., Meng, C.-I.: Maps of precipitation by source region, binned by IMF, with inertial convection streamlines. J. Geophys. Res., **109**, A10206, doi:10.1029/2004JA010499 (2004)

Papitashvili, V. O., Belov, B. A., Faermark, D. S., Feldstein, Y. I., Golyshev, S. A., Gromova, L. I., Levitin, A. E.: Electric-potential patterns in the northern and southern polar-regions paramaterized by the interplanetary magnetic field. J. Geophys. Res., textbf99, 13251-13262 (1994)

Reiff, P. H., Burch, J. L.: IMF B_y-dependent flow and Birkeland currents in the dayside magnetosphere. 2. A global model for northward and southward IMF. J. Geophys. Res., textbf90, 1595–1609 (1985)

Rich, F. J., Hairston, M.: Large-scale convection patterns observed by DMSP. J. Geophys. Res. **99**, 3827-3844 (1994)

Ruohoniemi, J. M., Greenwald, R. A.: Statistical patterns of high-latitude convection obtained from Goose Bay HF radar observations. J. Geophys. Res., **101**, 21743-21763 (1996)

Ruohoniemi, J. M., Baker, K. B.: Large-scale imaging of high-latitude convection with Super Dual Auroral Radar Network HF radar observations. J. Geophys. Res., **103**, 20797–20811 (1998)

Ruohoniemi, J. M., Greenwald, R. A.: Dependencies of high-latitude plasma convection: Consideration of interplanetary magnetic field, seasonal, and universal time factors in statistical patterns. J. Geophys. Res., **110**, A09204, doi:10.1029/2004JA010815 (2005)

Shepherd, S. G., R. A. Greenwald, Ruohoniemi, J. M.: Cross polar cap potentials measured with Super Dual Auroral Radar Network during quasi-steady solar wind and interplanetary magnetic field conditions. J. Geophys. Res., **107**, 1-9, doi 10.1029/2001JA000152 (2002)

Weimer, D. R.: Models of high-latitude electric potentials derived with a least error fit of spherical harmonic coefficients. J. Geophys. Res., **100**, 19595-19608 (1995)

The complex spatiotemporal dynamics of ionospheric currents

Antti Pulkkinen[1] and Ari Viljanen[2]

[1] University of Maryland & NASA/GSFC, United States antti.pulkkinen@gsfc.nasa.gov
[2] Finnish Meteorological Institute, Helsinki, Finland ari.viljanen@fmi.fi

Summary. We summarise recent studies of high-latitude magnetic variations from the viewpoint of geomagnetically induced currents. A comprehensive analysis of geomagnetic data from northern Europe using spatiotemporal structure functions has revealed several new features:
(1) There is a significant change in the dynamics of the field fluctuations in the range 80-100 s where the time derivative of the magnetic field (dB/dt) undergoes a transition from correlated to uncorrelated temporal behaviour.
(2) The spatiotemporal behaviour of dB/dt above temporal scales of 100 s resembles that of uncorrelated white noise.
(3) The spatial symmetry of the field fluctuations increases during substorms, indicating the presence of spatially less ordered ionospheric currents.
(4) The spatial scaling properties of the field fluctuations may explain why the magnetotelluric sounding method works better than expected in auroral regions.

1 Background

Estimation of geomagnetically induced currents (GIC) in power systems and pipelines requires a model of ionospheric currents. The simplest example is an infinitely wide uniform sheet current creating a plane wave. Although this is clearly not the real physical situation at high latitudes, an appropriate modification allowing for spatial field variations yields satisfactory results in practical GIC calculations (Viljanen et al., 2004). However, accurate forecasting of GIC is still an unobtainable goal, whose fundamental difficulty has been realized only during the latest years.

The main features of ionospheric current systems and the related magnetic variations ($\mathbf{B}$) are relatively well-known (Kamide & Baumjohann, 1993). However, the key quantity in GIC studies is the time derivative of the magnetic field ($d\mathbf{B}/dt$), or more specifically, the derivative of the horizontal field vector ($d\mathbf{H}/dt$). Viljanen (1997) and Viljanen et al. (2001) showed that large $d\mathbf{H}/dt$ (exceeding 1 nT/s) primarily occur during events governed by westward ionospheric currents. However, the directional distributions of $d\mathbf{H}/dt$ are much more scattered than those of the simultaneous horizontal variation field vector $\mathbf{H}$ (Fig. 1). A pronounced difference between $\mathbf{H}$ and $d\mathbf{H}/dt$ takes place at about 02-06 MLT in the auroral region when $d\mathbf{H}/dt$ prefers an east-west orientation, whereas $\mathbf{H}$ points to the south. In the auroral region,

the occurrence of large $d\mathbf{H}/dt$ has two daily maxima, one around the local magnetic midnight, and another in the morning. There is a single maximum around the midnight at subauroral latitudes. This implies the importance of substorms as a major cause of GIC (Viljanen et al., 2006). The scattering of $d\mathbf{H}/dt$ distributions is smaller during the descending phase of the sunspot cycle. Seasonal variations are also seen, especially in winter when $d\mathbf{H}/dt$ is more concentrated to the north-south direction than at other times.

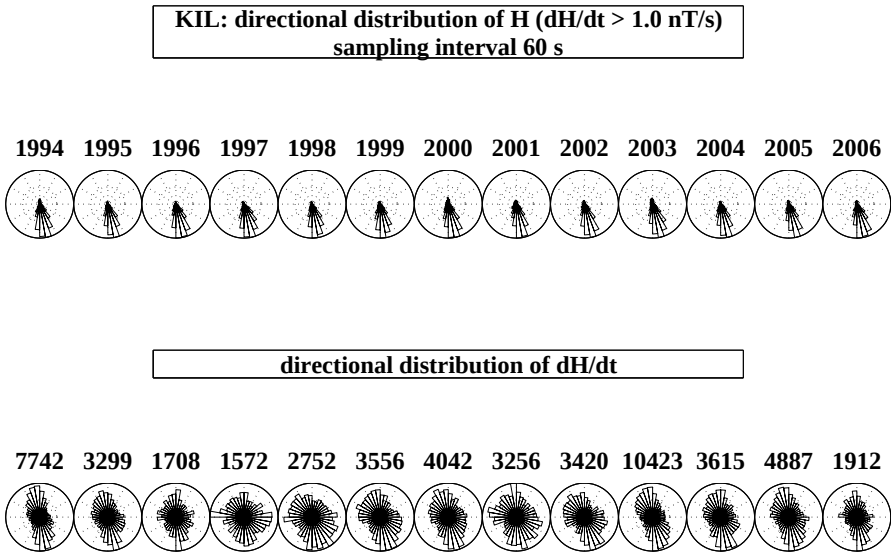

Fig. 1. Directional distribution of $\mathbf{H}$ (upper row) and $d\mathbf{H}/dt$ (lower row) at Kilpisjärvi (geomagnetic latitude 66 deg) from 1994 to 2006, as calculated from one minute values. Only timesteps fulfilling the condition $|d\mathbf{H}/dt| > 1$ nT/s are included. The distribution patterns are normalized separately for each subplot. The total number of timesteps are given as title texts in the lower row. Geographic north is upwards. Figure extended from Viljanen et al. (2001) with new data of 2001-2006.

2 Spatiotemporal scaling properties

The spatiotemporal scaling properties of the auroral region ground horizontal magnetic field fluctuations have been investigated in terms of structure function analysis by Pulkkinen et al. (2006a). The distorting effects of the continuation of the magnetic field from the ionosphere to the ground level and the effects of the geomagnetic induction on the derived scalings were first studied. It was found that the spatial fluctuations of the magnetic field and its time derivative are distorted by the field continuation in the ranges of scales of the data, i.e., 100-2400 km and 10-10000 s. Specifically, the extent of the distortion was found to depend on the original ionospheric level scaling of the fluctuations. The effect of geomagnetic induction was found

to be negligible in the ranges of scales of the data. The main findings of this study were
(1) There is a significant change in the dynamics of the field fluctuations in the range 80-100 s where the time derivative of the magnetic field undergoes a transition from correlated to uncorrelated temporal behaviour.
(2) The spatiotemporal behaviour of the time derivative of the magnetic field above temporal scales of 100 s resembles that of uncorrelated white noise.
(3) The spatial symmetry of the field fluctuations increases during substorms, indicating the presence of spatially less ordered ionospheric equivalent currents.
(4) The spatial scaling properties of the field fluctuations may explain why the magnetotelluric sounding method works better than expected in auroral regions.

These results manifest the importance of small-scale structures of ionospheric currents, as illustrated schematically in Fig. 2. The distribution patterns of $d\mathbf{H}/dt$ cannot be explained by any simple sheet-type model of east-west ionospheric currents, but rapidly changing north-south currents and field-aligned currents must play an important role.

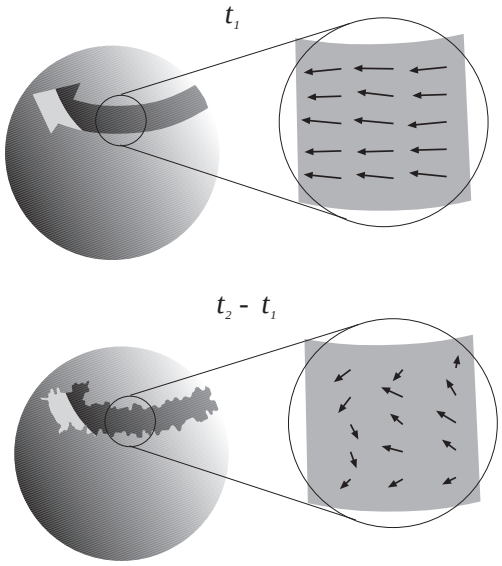

Fig. 2. Graphical illustration of typical auroral ionospheric current characteristics behind large GIC (Pulkkinen, 2003). Top: intensified electrojet at time $t = t_1$. Generally $|J_y| \gg |J_x|$, i.e. on the ground $|B_x| \gg |B_y|$. Bottom: differential currents $(t_2 - t_1)$ producing the surface geoelectric field. Generally $|dJ_y/dt| \approx |dJ_x/dt|$, i.e. on the ground $|dB_x/dt| \approx |dB_y/dt|$.

The complexity of the auroral phenomena described above implies that stochastic processes may play an important role in the spatiotemporal structure of the field fluctuations. Accordingly, the role of stochastic processes in the coupled magnetosphere-ionosphere system was investigated by Pulkkinen et al. (2006b). It was found that the introduced stochastic model was able to reproduce some central elements of the auroral ionospheric current fluctuations

expressed in terms of the AE-index. Possible stochasticity of the spatiotemporal dynamics of ionospheric currents sets certain limitations for the predictability of the phenomenon. The limitations on the predictability of GIC are discussed more in-depth by Pulkkinen (2007).

The complexity of the auroral ionospheric current fluctuations is intimately coupled with the multiscale property of auroral emissions (Uritsky et al. (2006), and references therein). Although the identification of the processes in the solar wind-magnetosphere-ionosphere system responsible for the complex multiscale behaviour of the auroral ionospheric phenomena is a very challenging task, localized reconnection in the plasma sheet has been proposed as a possible candidate (e.g., Pulkkinen et al. (2006b); Uritsky et al. (2006)). The collective effects of localized reconnection events in the plasma sheet have been studied in detail by Klimas et al. (2005) who found that their partially non-MHD model can reproduce some complex observed characteristics of the ionosphere-magnetosphere system.

References

Kamide, Y., Baumjohann, W.: Magnetosphere-ionosphere coupling. Physics and Chemistry in Space, **23**, 178 p. (1993).

Klimas A. J., Uritsky, V.M., Vassiliadis, D., Baker, D. N.: A mechanism for the loading-unloading substorm cycle missing in MHD global magnetospheric simulation models. Geophys. Res. Lett., **32**, L14108, doi:10.1029/2005GL022916 (2005).

Pulkkinen, A.: Geomagnetic induction during highly disturbed space weather conditions: Studies of ground effects. Finnish Meteorological Institute Contributions, **42** (2003).

Pulkkinen, A., Klimas, A. Vassiliadis, D., Uritsky, V., Tanskanen, E.: Spatiotemporal scaling properties of the ground geomagnetic field variations. J. Geophys. Res., **111**, No. A3, A03305, doi:10.1029/2005JA011294 (2006a).

Pulkkinen, A., Klimas, A. Vassiliadis, D., Uritsky, V.: The role of stochastic fluctuations in the magnetosphere-ionosphere system: a stochastic model for the AE-index variations, J. Geophys. Res., **111**, A10218, doi:10.1029/2006JA011661 (2006b).

Pulkkinen, A.: Spatiotemporal characteristics of the ground electromagnetic field fluctuations in the auroral region and implications on the predictability of geomagnetically induced currents. In: Lilensten, J. (ed.) Space Weather, Research towards Applications in Europe, Series: Astrophysics and Space Science Library, **344**, XII, Springer (2007).

Uritsky, V. M., Klimas, A.J., Vassiliadis, D.: Critical finite-size scaling of energy and lifetime probability distributions of auroral emissions. Geophys. Res. Lett., **33**, L08102, doi:10.1029/2005GL025330 (2006).

Viljanen, A.: The relation between geomagnetic variations and their time derivatives and implications for estimation of induction risks. Geophys. Res. Lett., **24**, 631–634 (1997).

Viljanen, A., Nevanlinna, H., Pajunpää, K., Pulkkinen, A.: Time derivative of the horizontal geomagnetic field as an activity indicator. Ann. Geophys., 19, 1107–1118 (2001).

Viljanen, A., Pulkkinen, A., Amm, O., Pirjola, R., Korja, T., BEAR Working Group: Fast computation of the geoelectric field using the method of elementary current systems and planar Earth models. Ann. Geophys., **22**, 101–113 (2004).

Viljanen, A., Tanskanen, E.I., Pulkkinen, A.: Relation between substorm characteristics and rapid temporal variations of the ground magnetic field. Ann. Geophys., 24, 725–733 (2006).

A Review of Progress in Modelling Induced Geoelectric and Geomagnetic Fields

Alan W. P. Thomson[1], Allan J. McKay[1] and Ari Viljanen[2]

[1] British Geological Survey, Murchsion House, West Mains Road, Edinburgh, EH9 3LA
awpt@bgs.ac.uk, aljm@bgs.ac.uk
[2] Finnish Meteorological Institute, Helsinki, Finland. ari.viljanen@fmi.fi

Summary. The Earth's lithosphere and mantle responds to Space Weather through time-varying, depth-dependent induced magnetic and electric fields. Understanding the properties of these electromagnetic fields is a key consideration in modelling the hazard to technological systems from Space Weather. In this paper we review current understanding of these fields, in terms of regional and global scale geology and geophysics. We highlight progress towards integrated European-scale models of geomagnetic and geoelectric fields, specifically for the purposes of modelling geomagnetically induced currents in power grids and pipelines.

1 Introduction

Geomagnetically Induced Currents (GIC) flow in grounded conducting networks, such as power grids and pipelines, during geomagnetic storms. GIC are near-DC electrical currents that are a consequence of the induced geoelectric field that follows from Faraday's law of electromagnetic (EM) induction. To fully understand the flow of GIC in networks we need to first understand how the geoelectric field responds to a given geomagnetic disturbance. This geophysical response depends on three main factors: the spatial structure and variation periods of the primary geomagnetic field and the three-dimensional conductivity structure of the Earth. Given a surface distribution of the geoelectric field, electrical network analysis can then be used to determine the flow of GIC in conducting networks (e.g. Lehtinen and Pirjola, 1985; Pulkkinen et al., 2001).

In this review we will report on recent progress on the geophysical problem, particularly in the understanding of the three-dimensional electrical conductivity structure of the Earth from both global and regional EM surveys, and from technical (modelling) innovations. We summarise major recent discoveries and provide, for the reader, references to the major papers. We concentrate on papers published in the last ten years or so and therefore refer the reader to the reviews of Schwarz, 1990, and Hjelt, 1988, for the status of the scientific literature prior to this time.

The structure of the paper is as follows. In Section 2 we discuss recent global induction studies that reveal current 'best estimates' of the electrical conductivity of the Earth's mantle and lithosphere. In Section 3 we highlight studies that provide resources relevant to deriving

regional conductivity models, for example on the European continental scale. In Section 4 we outline various techniques that are, or could be, employed to model the EM fields relevant to GIC.

2 Global Induction

The Earth surface 'footprint' of Space Weather can be large: both continental-scale and global-scale EM fields can be induced in the Earth, depending on the scale size and period of external magnetic variations, these being subject to solar wind control. The global scale response occurs primarily in the deep mantle. In this section we highlight recent global induction studies that provide deep mantle conductivity models. These models typically have a simple radial dependence and are used to underly various crustal/ upper mantle models required to model EM fields at periods relevant to GIC.

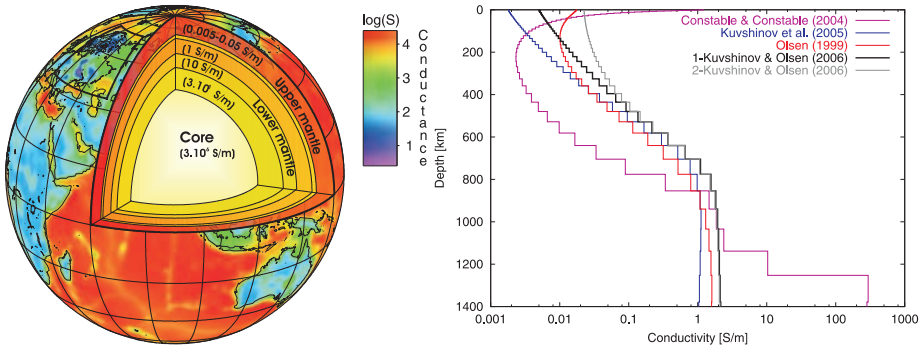

Fig. 1. Left - Global map of surface conductance with the cutaway showing the Eurasian mantle conductivity model of Semenov and Jozwiak (1999); after Vozár et al. (2006). Right - Mantle conductivity profiles of various studies; see Kuvshinov and Olsen (2006) for full details and references.

2.1 Radial Conductivity Models

Magnetic satellite missions such as CHAMP (2001 to present), Ørsted (1999 to present), and SAC-C (2002 to present) offer global uniform data coverage. These data sources have been used to derive deep (to a depth of 1500 km) radial conductivity models (e.g. Kuvshinov and Olsen, 2006). At depths greater than 400 km the models consistently show a monotonic increase in conductivity from about 0.03-0.08 S/m to 1-2 S/m at 900 km depth; see Figure 1 for example.

2.2 Three Dimensional Conductivity Models

The importance of 3D analysis regarding the interpretation of satellite induction observations in the longer period range of hours to days is now recognised (e.g. Everett et al., 2003). Global

surface conductance (conductivity-thickness product) maps (S-Maps) (see Figure 1) are often formulated using a combination of bathymetric data, and the global sediment thickness compilation of Laske and Masters (1997); see Everett et al. (2003) for example. However, Vozár et al. (2006), for example, are refining a global S-map using a combination of Magnetotelluric (MT) and Geomagnetic Deep Sounding (GDS) data. If successful, this will prove to be a valuable resource.

Compilations such as the world geological map (http://ccgm.free.fr) and world magnetic anomaly map (Purucker, 2007) provide insights into global (and regional) tectonics. The planned ESA Swarm mission should provide information about electrical conductivity heterogeneities in the Earth's mantle (Kuvshinov et al., 2006)

3 Regional Conductivity Models

The main sources of regional conductivity models stem from MT and GDS surveys; a comprehensive review of which is outwith the scope of this paper (but see Haak (1985) for an earlier review, continent by continent). We restrict ourselves therefore to a summary of regional conductivity studies of relevance to modelling GIC within Europe and North America. However we note that studies reported in Schwarz (1990) provide valuable detail for regions such as New Zealand, South Africa, Australia, and Japan.

Recent European investigations of the electrical conductivity of the lithosphere and asthenosphere have been reviewed comprehensively by Korja (2007). Fennoscandia is well-covered in respect of recent MT and GDS studies following the completion of the Baltic Electromagnetic Array (BEAR) project. Korja et al. (2002) compiled a map of the crustal conductance for the Fennoscandian Shield and its surrounding ocean and seas, and continental areas using the BEAR array data, and numerous other studies. The crustal conductance compilation of Korja et al. (2002) has been utilized by Engels et al. (2002) to model electric and magnetic fields at the Earth's surface.

The electrical conductivity structure of the UK landmass is complex and it is surrounded by shallow shelf seas along with the deep ocean a few hundred kilometers to the west. These factors are all known to influence the EM fields observed on land in a period range appropriate to GIC (McKay and Whaler, 2006). Thus, the geological setting, and geomagnetic latitude, of the UK has influenced the approach to modelling the EM fields. For example, Thomson et al. (2005) used a quasi 3D thin-sheet model to calculate the geo-electric field at the peak (as determined by the time of maximum GIC in the Scottish Power grid) of the October 2003 geomagnetic storm; see Figure 2. They noted the regional variation of the electric field and strong electric field enhancements due to the coastal conductivity contrast.

The Pre-Cambrian Shield is a highly resistive feature of Canadian geology. MT soundings have been made at many sites throughout Canada as part of the Lithoprobe project (e.g. Ferguson et al., 2005). Boteler (2001) used published MT soundings to determine regional conductivity models applicable to determining GIC in the five largest power systems in Canada. Fernberg et al. (2007) attributed anomalously large pipe to soil potentials to the lateral boundary between the shield and the relatively conductive Paleozoic rocks on the shield's eastern margin.

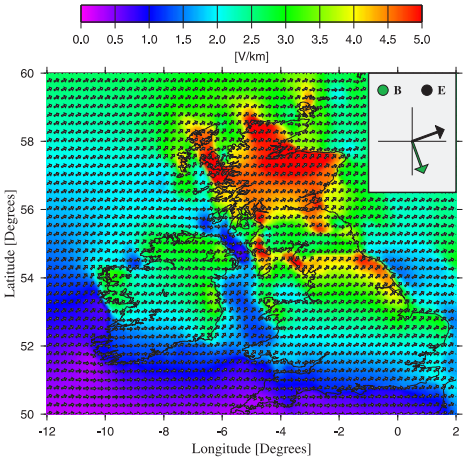

Fig. 2. Surface electric field throughout the UK estimated at 21:20UT assuming a driving period of 360 s. The colour and arrows represent the E-field amplitude [V/km] and azimuth respectively. The inset shows the azimuth of the primary geomagnetic field, and secondary electric field for a simple 1D model. After Thomson et al. (2005).

4 EM Field Modelling

The calculation of the geoelectric field at the Earth's surface normally comprises two main steps. First, specifying or determining the primary geomagnetic field responsible for induction. Second, calculation of the induced EM fields.

The characteristic feature of high geomagnetic latitudes is large and rapid temporal change, and strong spatial inhomogeneity, in the rate of change of the primary geomagnetic field (e.g. Pulkkinen and Viljanen, 2007). For example, Figure 3 illustrates the strong spatial inhomogeneity of the horizontal magnetic field rate of change just prior (20:06:30UT) to the power grid blackout experienced in Sweden at 20:07UT (Pulkkinen et al., 2005b) while the ground magnetic field is relatively smooth at 20:07:00UT.

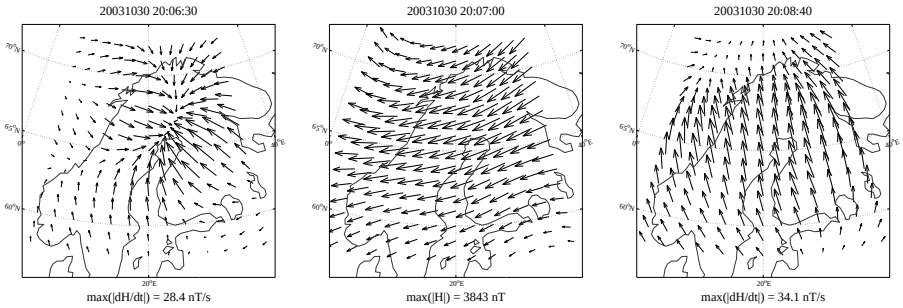

Fig. 3. The time derivative of the horizontal ground magnetic field at 20:06:30UT (left), equivalent ground currents formed by rotating the ground magnetic field at 20:07:00UT (middle) and the time derivative of the horizontal ground magnetic field at 20:08:40UT (right). The sampling rate of the geomagnetic field was 10s, and the measurements were interpolated onto a uniform grid using the SECS method.

The geomagnetic disturbance field is primarily of ionospheric origin. Geomagnetic disturbances are often represented using ionospheric equivalent currents. However, it is possible to try to predict the geomagnetic field at the Earth's surface directly from solar wind data (e.g. Gleisner and Lundstedt, 2001a,b; Weigel et al., 2003).

Models of idealized geomagnetic disturbances (e.g. a westward traveling surge) have been used to investigate the occurrence of GIC (e.g. Viljanen et al., 1999). The representation of the geomagnetic field using Spherical Elementary Currents Systems (SECS), introduced and validated by Amm (1997) and Pulkkinen et al. (2003a) respectively, means that recent studies have considered particular geomagnetic storm events and used ground based magnetometer data to derive equivalent ionospheric currents (e.g. Pulkkinen et al., 2003b) or interpolated maps of the ground magnetic field; see Figure 3 for example. SECS can also be used with a single magnetometer chain (Vanhamaki et al., 2003).

4.1 Determining the geoelectric field

The 'plane-wave' model (which forms the basis of the MT method) is commonly employed to calculate the geoelectric field. The simplest realization of the plane-wave method is a primary field that propagates vertically downward into an Earth of uniform or layered conductivity. The appeal is its simplicity, and its remarkable success (e.g. Viljanen et al., 2004).

The Complex Image Method (CIM) is an approximate method for calculating the EM fields at the Earth's surface (e.g. Boteler and Pirjola, 1998). Pulkkinen et al. (2003a) combined SECS and CIM; Viljanen et al. (2004) demonstrated the applicability to calculating the geoelectric field. Therefore, it is now possible to calculate quickly, and accurately, the geoelectric field using realistic representations of ionospheric current sources over a given region despite using the plane-wave surface impedance.

McKay and Whaler (2006) have shown that it is possible to use MT and GDS response functions to estimate directly the electric and magnetic fields throughout a region, rather than relying solely on conductivity models. Their study was limited to a single central period, however, where array (or the spatial coverage is good) MT and/or GDS data are available then the method is applicable to GIC.

3D Earth conductivity models have been applied in GIC research, but they have yet to be implemented in a practical sense; see for example Beamish et al. (2002) and Thomson et al. (2005). Pulkkinen and Engels (2005) used the 3D volume code of Avdeev et al. (2002), and the method of SECS to include both a non-uniform time-varying source field and 3D conductivity variations to study the effect of induction in the Earth on estimates of ionospheric equivalent currents. Significant induction effects were observed e.g. overestimation of up to 30% of the main ionospheric current flow amplitude, which increases away from the main current flow.

Pulkkinen et al. (2007) show that it is possible to estimate the MT surface impedance using GIC and geomagnetic observatory data. Therefore, Earth conductivity models which optimally describe the link between magnetic variations and GIC are being developed.

5 Summary

Significant progress in both Earth conductivity and EM modelling has been made in the last ten years, much of it relevant to the problem of the space weather impact on technological

systems such as power networks and pipelines. In this short review we have summarised new findings on the geophysics relevant to the ground effects of space weather, and provided a reference list for more detailed reading. Future challenges with particular regard to GIC are the fast calculation of the EM fields using 3D Earth models, and developing an understanding of the level of model detail required. In conclusion we note that future planned satellite magnetometry missions, in particular the ESA mission SWARM, will likely provide even greater insights into the geophysical properties of the Earth and its environs, with clear benefit to the scientific and engineering communities interested in the ground effects of space weather.

References

Amm, O.: Ionospheric elementary current systems in spherical coordinates and their application. **49**, 947–955 (1997).

Avdeev, D.B., Kuvshinov, A.V., Pankratov, O.V. and Newman, O.: Three dimensional induction logging problems, Part 1: an integral equation solution and model comparisons. Geophysics, **67(2)**,412–426 (2002).

Beamish D., Clark, T.D.G., Clarke E., and Thomson A.W.P.: Geomagnetically induced currents in the UK: geomagnetic variations and surface electric fields. J. Atmos. Sol. Terr. Phys., **64**,1779–1792 (2002).

Boteler, D.H.: Assessment of geomagnetic hazard to power systems in Canada. Natural Hazards, **23**, 101-120 (2001).

Boteler, D. and Pirjola, R.J.: The complex-image method for calculating the magnetic and electric fields produced at the surface of the Earth by the auroral electrojet. Geophys. J. Int., **132**,31–40 (1998).

Engels, M., Korja, T., and the Bear Working Group: Multisheet modelling of the electrical conductivity structure in the Fennoscandian Shield. Earth Planets Space, **54**, 559–573 (2002).

Everett M.E., Constable, S. and Constable, C.G.: Effects of near surface conductance on global satellite induction responses, Geophys. J. Int., **153**, 277–286 (2003).

Ferguson I.J., Craven, J.A., Kurtz, R.D., Boerner, D.C., Bailey, R.C., Wu, X., Orellana, M.R., Spratt, J., Wennberg, G. and Norton A.: Geoelectric response of Archean lithosphere in the western Superior Province, central Canada, Phys. Earth Planet. Int., **150**, 123–143 (2005).

Fernberg, P. A., Samson, C., Boteler, D. H., Trichtchenko, L. and Larocca, P.: Earth conductivity structures and their effects on geomagnetic induction in pipelines. Annales Geophysicae, **25**, 207–218 (2007).

Gleisner, H., and Lundstedt, H.: A neural network-based local model for prediction of geomagnetic disturbances, J. Geophys. Res., **106**, 8425–8434 (2001a).

Gleisner, H., and Lundstedt, H.: Auroral electrojet predictions with dynamic neural networks, J. Geophys. Res., **106**, 24541–24550 (2001b).

Haak, V.: Anomalies of electrical conductivity in the Earth's crust and upper Mantle. In: Fuchs, K. and Soffel, H. (ed), Landolt-Bornstein, New Series, 5/2b pp 397–436, Springer-Verlag, Berlin Heidelberg (1985)

Hjelt, S. E.: Regional EM studies in the 80s. Surv. Geophys., **9**, 349-387 (1988)

Korja, T.: How is the European lithosphere imaged by Magnetotellurics? submitted Surv. Geophys., (2007)

Korja, T., Engels, M., Zhamaletdinov, A.A., Kovtun, A.A., Palshin, N.A., Smirnov, M.Y., Tokarev, A.D., Asming, V.E., Vanyan, L.L., Vardaniants, I.L., and the Bear Working Group: Crustal conductivity in Fennoscandia–a compilation of a databse on crustal conductance in the Fennoscandian Shield. Earth Planets Space, **54**, 535–558 (2002)

Kuvshinov, A. and Olsen, N.: A global model of mantle conductivity derived from 5 years of CHAMP, Ørsted and SAC-C magnetic data, Geophys. Res. Lett., **33**, L18301, (2006).

Kuvshinov, A., Sabaka, T. and Olsen, N.: 3-D electromagnetic induction studies using the Swarm constellation: Mapping conductivity anoamlies in the Earth's mantle, Earth Planets Space, **58**, 417–427 (2006).

Laske, G. and Masters, G., A global digital map of sediment thickness. EOS Trans. AGU, **78(46)** (1997).

Lehtinen, M. and Pirjola, R., Currents produced in earthed conductor networks by geomagnetically induced currents. Annales Geophysicae, **3**,4,479–484 (1985).

McKay, A.J. and Whaler, K.A.: The electric field in northern England and southern Scotland: implications for geomagnetically induced currents. Geophys. J. Int., **167**, 613–625 (2006).

Pulkkinen, A., Pirjola, R., Boteler, D., Viljanen, A. and Yegerov, I: Modelling of space weather effects on pipelines. J. Appl. Geophys., **48**, 233-256 (2001).

Pulkkinen, A., Amm, O., Viljanen, A. and the Bear Working group: Ionospheric equivalent current distributions determined with the method of spherical elementary current systems. J. Geophys. Res., **108(A2)**, 1053 (2003a).

Pulkkinen, A., Amm, O., Viljanen, A. and the Bear Working group: Separation of the geomagnetic variation field into parts of external and internal parts using the spherical elecmenatry currents system method. Earth Planets Space, **55**, 117–129 (2003b).

Pulkkinen, A. and Engels, M.: The role of 3D geomagnetic induction in the determination of the ionospheric currents fom ground-based data. Annales Geophysicae, **23**, 909–917 (2005).

Pulkkinen, A., Lindahl, S., Viljanen, A. and Pirjola, P.: Geomagnetic storm of 29-31 October 2003: Geomagnetically induced currents and their relation to problems in the Swedish high-voltage power transmission system. Space Weather, **3**, doi: 10.1029/2004SW000123 (2005b).

Pulkkinen, A., Viljanen, A. and Pirjola, P.: Determination of ground conductivity and system parameters for optimal modeling of geomagnetically induced current flow in technological systems. Earth Planets Space, submitted (2007).

Pulkkinen, A. and Viljanen, A.: The complex spatiotemporal dynamics of ionospheric currents. This volume.

Purucker, M.: Magnetic anomaly map of the world. EOS Trans. AGU, **88(25)**, (2007).

Schwarz, G.: Electrical conductivity of the Earth's crust and upper mantle. Surv. Geophys., **11**, 133-161 (1990)

Semenov, V. Yu and Jozwiak W.: Model of the geoelectrical structure of the mid and lower mantle in the Europe-Asia region. Geophys. J. Int., 138, 549-552 (1999).

Thomson, A.W.P., McKay, A.J., Clarke, E., Reay, S.J.: Surface electric fields and geomagnetically induced currents in the Scottish Power grid during the 30 October 2003 geomagnetic

storm.Space Weather - The International Journal of Research and Applications, **3**, Art. No. S11002 (2005).

Vanhamaki H, Amm O, Viljanen A: One-dimensional upward continuation of the ground magnetic field disturbance using spherical elementary current systems. Earth Planets Space, **55**, 613–625 (2003).

Viljanen, A. and Amm, O. and Pirjola, R.: Modelling geomagnetically induced currents during different ionospheric situations. J. Geophys. Res., **104**, 29,059–28,071 (1999).

Viljanen, A., A. Pulkkinen, O. Amm, R. Pirjola, T. Korja and BEAR Working Group: Fast computation of the geoelectric field using the method of elementary current systems and planar Earth models, Ann. Geophys., **22**, 101–113, (2004)

Vozár, J., Semenov, V.Y., Kuvshinov, A.V. and Manoj, C.: Updating the map of Earth's surface conductance. EOS Trans. AGU, **33(15)**, (2006).

Weigel, R. S., Klimas, A.J. and Vassiliadis,D.: Solar wind coupling to and predictability of ground magnetic fields and their time derivatives, J. Geophys. Res., **108**, 1298 (2003).

Calculation of geomagnetically induced currents (GIC) in ground-based technological systems

Risto Pirjola

Finnish Meteorological Institute, Space Research Unit, P.O. Box 503, FIN-00101 Helsinki, Finland
risto.pirjola@fmi.fi

Summary. Geomagnetically induced currents (GIC) in ground-based technological conductor networks, e.g. power grids and pipelines, are a ground manifestation of Space Weather. GIC are a potential source of problems to the systems, and so GIC constitute a research topic that is of scientific and practical importance. Theoretical calculation of GIC in a given network is convenient to perform in two steps: determination of the geoelectric field and computation of GIC driven by this field. In this paper, we outline the implementation of both steps, and provide some numerical examples about a fictitious discretely-earthed network describing a power system. The effect of uncertainties in the earthing resistances of the network is shown to be small. It is also seen that large enough additional resistances in the earthings provide a possible means to decrease GIC risks.

1 Introduction

Geomagnetically induced currents (GIC) flowing in ground-based technological networks such as electric power transmission grids, oil and gas pipelines, telecommunication cables and railway systems, are the ground end of the Space Weather chain whose origin is solar activity (e.g., Pirjola (2000)). Although the chain as a whole includes complicated plasmaphysical and electromagnetic processes the basic physical principle of GIC is easy to understand based on Faraday's and Ohm's laws: Rapidly-varying space currents produce temporal disturbances (or storms) in the geomagnetic field accompanied by an induced (geo)electric field, which drives currents in conductors. Besides technological networks, which experience GIC, the Earth itself is also a conductor. Thus, currents induced in the ground also much affect the geomagnetic disturbance field and the geoelectric field observed at the Earth's surface (see, e.g., Watermann (2007)).

GIC are a source of possible trouble to the systems. The first effects were already noted in the telegraph equipment in the 1840s (e.g., Boteler et al. (1998) and references therein). Today, power systems and pipelines constitute the most significant networks regarding GIC. In the former, the dc-like GIC may saturate transformers leading to different problems, even to a collapse of the whole network or to permanent damage of transformers (e.g. Molinski (2002)). In buried oil and gas pipelines, GIC and the associated pipe-to-soil voltages may enhance corrosion and disturb corrosion control (Gummow, 2002).

Geomagnetic disturbances are the largest in auroral regions located at high latitudes. This means that GIC are especially a problem in the same areas. However, during major geomagnetic storms, the auroral oval can extend substantially towards lower latitudes. GIC magnitudes also depend on the grid topology, configuration and resistances and much vary from site to site in a network. It should also be noted that the sensitivities of systems to GIC also depend on many engineering details, so that a small GIC that does not disturb one grid at all may be problematic to another. These facts mean that lower-latitude networks may be affected by GIC as well. The increasing sizes of high-voltage power grids, the complex interconnections and the extensive transport of energy make GIC issues more and more important at all latitudes (Kappenman, 2004).

GIC have produced problems in Sweden several times (Boteler et al., 1998; Pulkkinen et al., 2005). The high-latitude location, together with a high ground resistivity, provides an explanation for GIC observations in Sweden. Finland, lying at the same latitudes and having a similar geology, has practically never experienced GIC problems. However, extensive research on GIC in the Finnish high-voltage power grid and in the Finnish natural gas pipeline has been carried out for about thirty years (Pirjola et al., 2003), and it is still considered worth being continued. The work, which is done as collaboration between the Finnish Meteorological Institute (FMI) and the power and pipeline companies has included theoretical modelling, recordings of GIC and derivation of statistics on expected GIC occurrence. Elovaara (2007) provides an up-dated engineering summary of studies of GIC in the Finnish high-voltage power system.

2 Theoretical Modelling

A calculation of GIC in a given ground-based system is convenient to perform in two steps: (i) determination of the horizontal geoelectric field at the Earth's surface ("geophysical step"), (ii) computation of GIC produced by the geoelectric field ("engineering step"). The input of the geophysical step consists of ground conductivity information and of ionospheric current or ground-based magnetic data, and this step is independent of the technological system considered. The engineering step utilises the geoelectric field and the network topology, configuration and resistances for the determination of GIC at each site of the system considered.

Different techniques and software for both steps have been investigated and developed (for a review, see, e.g., Pirjola (2002) and references therein). The determination of the geoelectric field necessarily includes assumptions and idealisations. In particular, the vicinity of the ionospheric auroral electrojet current system makes the situation complicated. The "local plane wave method" has been shown to be very appropriate in practical calculations for the first step (Viljanen et al., 2004). It is important to note that, in general, the geoelectric field is rotational, i.e. no single-valued geopotential exists, which means that geovoltages affecting conductors are path-dependent (Pirjola, 2000). This also implies that theoretically GIC may also flow in horizontal loops with no earthings.

The second step can in principle be performed exactly provided that all connections and resistances of the system are (considered) known. In the case of a discretely-earthed network, e.g. a power grid having earthings at transformer neutrals at (sub)stations, matrix formulas are available (Lehtinen and Pirjola, 1985). For a buried pipeline, which is continuously earthed

by leakage through the coating covering the pipe, the "distributed-source transmission line theory" (DSTL) has been shown to be useful (Pulkkinen et al., 2001).

The software developed, for example at FMI, for the two steps are readily available for any network at any location. This naturally requires that detailed information about the grid parameters is available (which has sometimes appeared to be a problem in practice). To get an idea of the magnitude of the horizontal geoelectric component associated with the time derivative of the perpendicular horizontal geomagnetic component, a simple integral formula based on a uniform-Earth assumption is available that clearly shows that the electric field at a given moment depends on past values of the derivative but with a weighting factor decreasing with the time lag (e.g., Pirjola (2002)). For determining the sites in a network that probably experience the largest GIC, an assumption that the affecting geoelectric field is uniform all over the grid is advisable to be made first. It helps identify where special concern about GIC impacts is needed and how GIC measurements should be located.

3 Examples

We now consider a fictitious discretely-earthed network as depicted in Fig. 1. The geometry and the resistance values used resemble (but are not equal to) the Finnish 400 kV power grid. The average earthing resistance and the average line resistance per length unit are 0.62 Ω and 7.2 mΩ/km, respectively. Details of the modelling of a complicated three-phase power transmission grid with transformers for GIC calculation purposes are described by Pirjola (2005a).

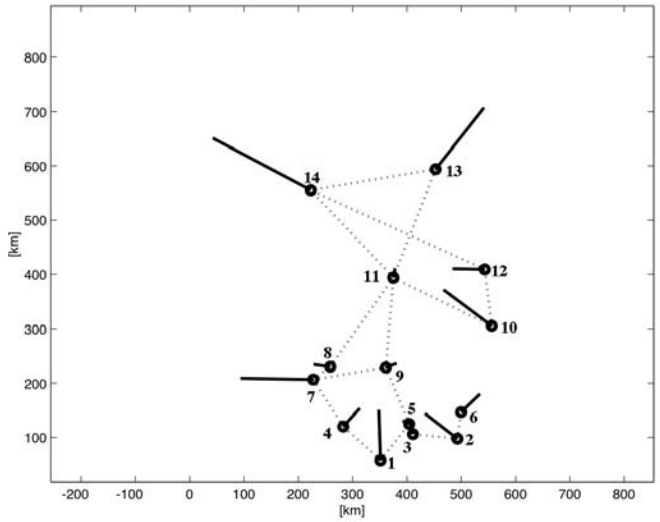

Fig. 1. Fictitious discretely-earthed network. The fourteen circles denote the stations earthed to the ground and connected to each other by conductors (dotted lines). The line segments associated with the stations indicate the directions of a uniform horizontal geoelectric field that give the largest absolute values of GIC into (or from) the ground at different stations,and the length of the line segment is proportional to the largest GIC magnitude at the particular station.

We assume that the network is impacted by a uniform horizontal geoelectric field of 1 V/km. This magnitude represents a typical situation during a geomagnetic storm, but it should also be noted that GIC are proportional to the electric field, so GIC for other uniform

electric field values can be obtained by a simple scaling. The line segments associated with the stations indicate the directions of the geoelectric field that give the largest absolute values of GIC into (or from) the ground at different stations, and the length of the line segment is proportional to the largest GIC magnitude at the particular station. (Note that reversing the direction of the geoelectric field only inverts the directions of GIC but the absolute values remain unchanged.) Fig. 1 clearly shows the well-known "corner effect" that the largest GIC occur in the corners and ends of a network. Transformers at Stations 3, 5, 9 and 11 are not probable candidates for suffering from GIC problems, and they are less interesting sites for GIC recordings, too.

Table 1. Averages of the absolute values of GIC into (or from) the ground at the stations of the network shown in Fig. 1 for a uniform eastward ("E") and northward ("N") electric field of 1 V/km for the various cases considered in this study.

	bs	p10	m10	r20	nr
E	61.0	58.2	64.1	60.1	21.1
N	44.5	42.9	46.3	45.0	19.5

Although the second step of the calculation of GIC is in principle straightforward and exact, an accurate description of connections and resistances met by GIC, e.g., in a high-voltage power system is difficult in practice. One reason is that the grid parameters are usually only known for the 50/60 Hz ac frequencies. In order to understand how much uncertainties may affect calculated GIC data, tests of the sensitivity of GIC values to changes of the parameters should be made. We have performed the following computations by using the network shown in Fig. 1 and a uniform horizontal geoelectric field of 1 V/km to the east ("E") and to the north

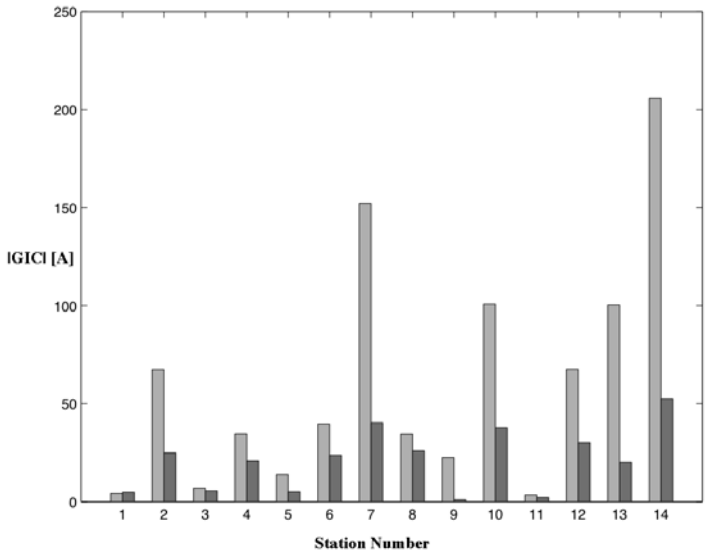

Fig. 2. Absolute values of GIC into (or from) the ground at individual stations of the network shown in Fig. 1 for an eastward electric field of 1 V/km. The lighter left-hand column and the darker right-hand column refer to the basic situation ("bs") and to the case in which all earthing resistances are increased by 2.5 Ω ("nr"), respectively.

("N"): basic situation ("bs"), all earthing resistances increased by 10% ("p10"), all earthing resistances decreased by 10% ("m10"), all earthing resistances changed randomly between -20% and +20% ("r20"), and all earthing resistances increased by 2.5 Ω ("nr"). The last case corresponds to the installation of a neutral point reactor in the earthing lead of every transformer commonly used in the Finnish 400 kV system (Pirjola, 2005b), and it also provides a hint about possibilities of using additional resistances as a means to decrease GIC. Table 1 gives the averages of the absolute values of GIC into (or from) the ground at the fourteen stations in each case considered. Fig. 2 shows the absolute values of GIC at individual stations for an eastward electric field of 1 V/km in the cases "bs" and "nr". Table 1 supports the conclusion that variations of about 10–20% of the resistance values do not much change GIC and are thus insignificant in connection with GIC risk estimates. As seen from both Table 1 and Fig. 2, a substantial increase of all earthing resistances clearly decreases GIC magnitudes and may thus be regarded as a technique to mitigate possible GIC problems. It has to be emphasised that in this study the additional resistance was assumed to be installed at all stations. Pirjola (2005b) demonstrates that an increase of the earthing resistance at some stations generally tends to increase GIC at other stations, then possibly even enhancing the overall GIC risk.

4 Concluding Remarks

Geomagnetically induced currents (GIC) in electric power transmission grids, in oil and gas pipelines, and in other technological conductor networks at the Earth's surface result from solar activity. GIC may seriously affect the systems. Consequently, research of GIC is, besides scientifically, lso practically important. GIC are a particular high-latitude problem but since GIC magnitudes and possible effects also depend on technical details of the systems they cannot be ignored at lower latitudes either. Theoretical calculation techniques of GIC in a network discussed in this paper can easily be applied to any grid provided that the configuration and resistances of the system are known. By numerical examples, we demonstrate in this paper that small uncertainties in resistance values of a network do not seem to be critical for GIC estimations. It is also indicated that large enough additional resistances to be met by the GIC flow may provide a possible means to reduce GIC risks.

References

Boteler, D.H., Pirjola, R.J., Nevanlinna, H.: The effects of geomagnetic disturbances on electrical systems at the Earth's surface. Adv. Space Res., **22**, 17-28 (1998)

Elovaara, J.: Finnish experiences with grid effects of GIC's. In: Lilensten, J. (ed) Space Weather - Research Towards Applications in Europe. Springer, Dordrecht, The Netherlands (2007)

Gummow, R.A.: GIC effects on pipeline corrosion and corrosion control systems. J. Atmos. Solar-Terr. Physics, **64**, 1755–1764 (2002)

Kappenman, J.G.: An overview of the increasing vulnerability trends of modern electric power grid infrastructures and the potential consequences of extreme space weather environments.

In: I.A. Daglis (ed) Effects of Space Weather on Technology Infrastructure. NATO Science Series, II. Mathematics, Physics and Chemistry **176**, Kluwer Academic Publishers (2004)

Lehtinen, M., Pirjola, R.: Currents produced in earthed conductor networks by geomagnetically-induced electric fields. Ann. Geophys., **3**, 479–484 (1985)

Molinski, T.S., 2002: Why utilities respect geomagnetically induced currents. J. Atmos. Solar-Terr. Physics, **64**, 1765–1778 (2002)

Pirjola, R.: Geomagnetically Induced Currents During Magnetic Storms. IEEE Trans. Plasma Science, **28**, 1867–1873 (2000)

Pirjola, R.: Review on the calculation of surface electric and magnetic fields and of geomagnetically induced currents in ground-based technological systems. Surveys in Geophysics, **23**, 71–90 (2002)

Pirjola, R.: Effects of space weather on high-latitude ground systems. Adv. Space Res., **36**, 2231–2240 (2005a)

Pirjola, R.: Averages of geomagnetically induced currents (GIC) in the Finnish 400 kV electric power transmission system and the effect of neutral point reactors on GIC. J. Atmos. Solar-Terr. Phys., **67**, 701–708 (2005b)

Pirjola, R., Pulkkinen, A., Viljanen, A.: Studies of space weather effects on the Finnish natural gas pipeline and on the Finnish high-voltage power system. Adv. Space Res., **31**, 795–805 (2003)

Pulkkinen, A., Lindahl, S., Viljanen, A., Pirjola, R.: Geomagnetic storm of 29-31 October 2003: Geomagnetically induced currents and their relation to problems in the Swedish high-voltage power transmission system. Space Weather, **3**, S08C03, doi:10.1029/2004SW000123 (2005)

Pulkkinen, A., Pirjola, R., Boteler, D., Viljanen, A., Yegorov, I.: Modelling of space weather effects on pipelines. J. App. Geophys., **48**, 233–256 (2001)

Viljanen, A., Pulkkinen, A., Amm, O., Pirjola, R., Korja, T., BEAR Working Group: Fast computation of the geoelectric field using the method of elementary current systems and planar Earth models. Ann. Geophys., **22**, 101–113 (2004)

Watermann, J.: The magnetic environment - GIC and other ground effects. In: Lilensten, J. (ed) Space Weather - Research Towards Applications in Europe. Springer, Dordrecht, The Netherlands (2007)

Space Weather European Network GIC servers

Ari Viljanen[1], Risto Pirjola[1], Antti Pulkkinen[2], David Boteler[3], Henrik Lundstedt[4], Larisa Trichtchenko[3], and Alan Thomson[5]

[1] Finnish Meteorological Institute, Helsinki, Finland ari.viljanen@fmi.fi, risto.pirjola@fmi.fi
[2] University of Maryland & NASA/GSFC, United States antti.pulkkinen@gsfc.nasa.gov
[3] Natural Resources Canada, Geomagnetic Laboratory, Ottawa, Canada DBoteler@NRCan.gc.ca, LTrichtc@NRCan.gc.ca
[4] Swedish Institute of Space Physics, IRF Lund, Sweden henrik@lund.irf.se
[5] British Geological Survey, Edinburgh, United Kingdom awpt@bgs.ac.uk

Summary. Studies of geomagnetically induced currents (GIC) culminated during the European Space Weather Applications Pilot Project in 2003-2006. Based on the previous experience, five operative GIC servers were established in Finland, Sweden, UK and Canada. They provide real-time information of geomagnetic activity and nowcast estimation of GIC in power systems (Canada, Sweden, UK) or in pipelines (Canada, Finland).

1 Status of GIC modelling

The basic procedure to calculate geomagnetically induced currents (GIC) consists of two steps:
1) Determine the horizontal geoelectric field at the earth's surface.
2) Apply a DC model of the conductor system in which the electric field causes GIC.
The first step is independent of the technological conductor system, and requires assumptions of ionospheric currents and of the earth's conductivity. In practice, use of the measured magnetic field at the earth's surface and a local layered-earth model yield satisfactory results (Viljanen et al., 2004). More advanced earth modelling takes into account lateral variations of the conductivity (Thomson & McKay, 2007). Analysis of ionospheric currents is discussed by Pulkkinen & Viljanen (2007).

Applicability of a DC model of the conductor systems is based on the relatively slow variations of the geomagnetic field. Two kind of conductor systems have been considered: discretely grounded (power system) and continuously grounded (buried pipeline). A power system GIC model was derived by Lehtinen & Pirjola (1985). The pipeline model based on the distributed-source transmission line (DSTL) theory was first discussed by Boteler & Cookson (1986), and finally extended by Pulkkinen et al. (2001) for a general pipeline network. Consequently, step 2 mentioned above has reached a mature status.

2 European Space Weather Applications Pilot Project

During the European Space Weather Applications Pilot Project in 2003-2006, five service development activities (SDA) dealt with GIC (http://www.esa-spaceweather.net/swenet/). Three of them were prepared for European and two for Canadian companies. The methodology in all SDA's is based on the two-step procedure outlined above. We give here a brief description of each service.

GIC Forecast

Contractor: Swedish Institute of Space Physics
Subcontractor: Finnish Meteorological Institute
Industrial partner: Elforsk AB
Server website: http://www.lund.irf.se/gicpilot/
Description: The service forecasts GIC in the southern part of the Swedish high-voltage power grid. It also provides general information about ground effects of space weather to the general public and educates the public and decision makers about GIC and how forecasts can help mitigate the effects. Real-time forecasts of dB/dt at Uppsala and Brorfelde and of GIC at one station are open to the public. Real-time forecasts for several stations are a restricted part of the service.

GIC Now!

Contractor: Finnish Meteorological Institute
Industrial partner: Gasum Oy
Server website: http://aurora.fmi.fi/gic_service/english/
Description: GIC Now! and the restricted part Gasum Now! services are is a sister product of Auroras Now! (Viljanen et al., 2006) The purpose of GIC Now! is to provide general information about ground effects of space weather. This is made both via popular texts about impacts of space weather and via practical examples of the phenomena. The elementary parts of the public service are a real-time view to the present GIC activity in terms of geomagnetic activity indicators and quick-look images of the induced current recordings carried out in the Finnish natural gas pipeline. The restricted part of the service, Gasum Now!, is a service providing real-time estimates of the space weather impact on the Finnish pipeline (Fig. 1).

Pipeline Space Weather Service

Contractor: Natural Resources Canada
Industrial Partner: Correng, Corrosion Service International
Server website: http://www.spaceweather.gc.ca/apps/pipeline_operations_e.php
Description: The service uses geomagnetic field variations at the geomagnetic observatory closest to the pipeline location. Geoelectric field variations are determined by converting the magnetic field data to the electric field using a 1-D layered earth conductivity model. Pipe-to-soil potential (PSP) difference variations for a sample pipeline are obtained by applying the distributed source transmission line model (DSTL) for pre-defined pipeline topologies with the geoelectric field as a driving source. Calculations of PSP variations for user-defined pipeline topologies are also available.

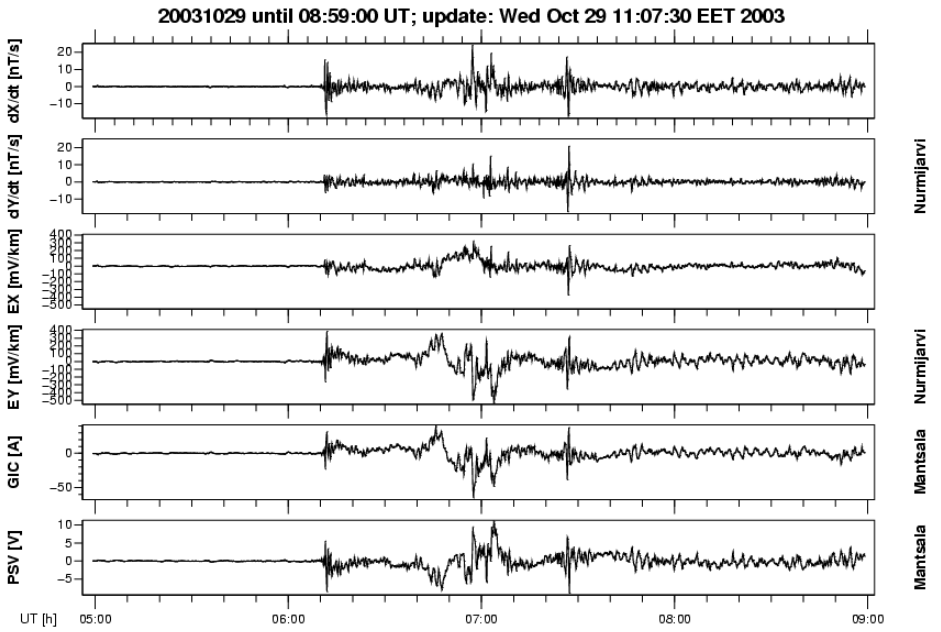

Fig. 1. Screen snapshot of the nowcasted GIC and pipe-to-soil voltage at Mäntsälä in the Finnish natural gas pipeline in the beginning of the Halloween storm in October 2003.

Real-Time GIC Simulator

Contractor: Natural Resources Canada
Subcontractor: Finnish Meteorological Institute
Industrial partner: Hydro One
Server website: http://www.spaceweather.gc.ca/gic_simulator_e.php
Description: The GIC Simulator uses real-time geomagnetic data feeding into earth and power system models to produce real-time displays of GIC flow throughout the power system. A layered ground conductivity model is used to calculate the surface impedance of the earth. It is applied with the incoming magnetic field data to calculate the electric fields at the earth's surface. The next stage of the process is to use the calculated electric field as input to a power system model, which is automatically updated when power lines or equipment are taken in or out of service. The model output are GIC values for all the high voltage lines and transformers throughout the network. The GIC information is provided to the system operators in such a way that all the relevant information is readily available without overloading the operators with extra data.

Solar Wind Monitoring and Induction Modeling for GIC

Contractor: British Geological Survey
Industrial partner: Scottish Power
Server website: http://www.geomag.bgs.ac.uk/gicpublic/
Description: This service is a webpage system that provides daily forecasts of geomagnetic activity, advanced warning of geomagnetic storm onset, monitoring data during storms and analysis of GIC in the Scottish part of the UK power grid. Real-time geomagnetic data are illustrated in the form of UK observatory hourly standard deviations in the north and east components. Daily magnetic activity forecast is given to three days ahead. A solar wind shock monitor provides advanced warning of magnetic storm onset. The Scottish Power grid network model is used to estimate GIC.

References

Boteler, D., Cookson, M.J.: Telluric currents and their effects on pipelines in the Cook Strait region of New Zealand. Materials Performance, March, 27–32 (1986).

Lehtinen, M., Pirjola, R.: Currents produced in earthed conductor networks by geomagnetically-induced electric fields. Ann. Geophys., **3**, 479–484 (1985).

Pulkkinen, A., Pirjola, R., Boteler, D., Viljanen, A., Yegorov, I.: Modelling of space weather effects on pipelines. J. Appl. Geophys., **48**, 233–256 (2001).

Pulkkinen, A., Viljanen, A: The complex spatiotemporal dynamics of ionospheric currents. In: COST724 Final Report. This volume (2007).

Thomson, A.W.P., McKay, A.J.: A Review of Progress in Modelling Induced Geoelectric and Geomagnetic Fields. In: COST724 Final Report. This volume (2007).

Viljanen, A., Pulkkinen, A., Amm, O., Pirjola, R., Korja, T., BEAR Working Group: Fast computation of the geoelectric field using the method of elementary current systems and planar Earth models. Ann. Geophys., **22**, 101–113 (2004).

Viljanen, A., Pulkkinen, A., Pirjola, R., Pajunpää, K., Posio, P., Koistinen, A.: Recordings of geomagnetically induced currents and a nowcasting service of the Finnish natural gas pipeline system. Space Weather, **4**, S10004, doi:10.1029/2006SW000234 (2006).

Part V

Working Group 4:
Space Weather Observations and Services

Synthesis of working Group 4 activities

Jean Lilensten (WG4 chairman)[1], Maurizio Candidi (vice-chairman)[2], Anna Belehaki[3], Iwona Stanislavska[4], Daniel Heynderickx[5], Paul Gille[6], Ermanno Amata[2], Mauro Messerotti[7], Frank Jansen[8], and Yurdanur Tulunay[9]

[1] Laboratoire de Planetologie de Grenoble, Observatoire des Sciences de l Univers de Grenoble, CNRS-UJF, France jean.lilensten@obs.ujf-grenoble.fr
[2] Istituto di Fisica dello Spazio Interplanetario, INAF, Roma, Italy Maurizio.Candidi@ifsi.rm.cnr.it Ermanno.Amata@ifsi-roma.inaf.it
[3] Ionospheric Group, Institute for Space Applications and Remote Sensing, National Observatory of Athens, Metaxa and Vas. Pavlou, 15236 Palaia Penteli, Greece belehaki@space.noa.gr
[4] Polish Academy of Sciences Space research center Bartycka 18 A 00 716 Warsaw Poland stanis@cbk.waw.pl
[5] DH Consultancy, Diestsestraat 133/3, B-3000 Leuven, Belgium DHConsultancy@skynet.be
[6] CNRS - LPCE - Relations extérieures, 3A, avenue de la Recherche Scientifique, 45071 Orléans cedex 2, France Paul.Gille@cnrs-orleans.fr
[7] INAF-Trieste Astronomical Observatory, Basovizza Observing Station, Loc. Basovizza n. 302, 34012 Trieste, Italy messerotti@oats.inaf.it
[8] 1A, Greifswald, Germany jansen@1a-firstapplications.com
[9] FDepartment of Aerospace Engineering, ODTU/METU, 06531, Ankara, Turkey ytulunay@metu.edu.tr

1 Introduction

As stated in the Memorandum of Understanding of the action, the tasks of WG4 consisted of:

- Coordinate a network of European websites relevant to data, models, prediction and public outreach;
- Develop methods and standards for data exchange to enable coupling of different space weather models (e.g. using Spacegrid) and to disseminate relevant information to users;
- Liaise with COST Action 271 to let COST 271 benefit from space weather model development and to incorporate COST 271 output where it will be of benefit to other space weather services;
- Maintain databases of users and statistics about the service.

The main task of WG4 was defined as to implement the basis of the European Space Weather Network. WG4 consisted of representatives of working groups 1-3, as well as experts on the

design of web based communication systems. WG4 was responsible for maintaining close links with SEC in the USA, and active participation in the development of a European Space Weather Service at ensuring the best balance between providing redundancy and complementarity of US and European space weather services. WG4 was also responsible for promoting the science and benefits of Space Weather in COST member states that have not participated in setting up this Action, liaising with Eumetsat and the Global Monitoring for Environment and Security (GMES) initiative of ESA and the EU.
Many of these objectives were attained with much greater succes than expected, but a few failed. They will be discussed thereafter.

2 Where did we succeed?

2.1 Service to users

On top of the space weather portal, we wanted to address the users services directly (requirements to the users will be addressed later). However, several of us were already working on such aim through the ”Space Weather European NETwork” (SWENET) held by ESTEC. It was not only useless to duplicate the efforts. It was also not ethically possible to do the same work for two different entities. Fortunately, our relationships with ESTEC are excellent, so that the SWENET people agreed to have their service provider web server directly accessible through our portal. In counterpart, we kept supplying information to the SWENET people, and the colleagues working for the 2 entities felt much more comfortable.

2.2 Models and tools for the study, forecast and prediction

One of the most important contributions of any space weather service is its ability to provide forecasts and predictions of space weather conditions and/or effects on technological systems. Indeed, as space weather is an application driven discipline, a key measure of its success and usefulness is the existence or development of services that allow some form of mitigation for the effects that make up the field of space weather. As the driver of space weather is the Sun, prediction of the state of the Sun on various time scales would be the ultimate goal. However, although substantial progress is being made, our current understanding of the processes occurring on the Sun’s surface and corona is far from sufficient to be able to provide even basic predictions of phenomena such as coronal mass ejections. For now, prediction is limited to the early detection of these events and providing estimates on the effects they may cause on the interplanetary medium and, ultimately, the Earth’s magnetosphere, ionosphere and ground systems. Similarly, methods have been developed to provide some measure of forecast for quantities such as magnetospheric indices, TEC, or ionospheric scintillation, often based on neural networks or other analyses of time series of these observed quantities. As the historical data series become longer, the quality of these forecasts will improve. However, the goal of more physics based predictions still seems a distant prospect.

2.3 Requirements of the users - including the European industry

After the two ESA contract studies (see the introduction of this report), an extended list of areas were identified where public and private users could take benefit of the coordination of a European framework for all space weather developments, e.g. : hazards to people and systems, aviation and spacecraft security, satellite navigation, satellite telecommunications, ground effects.
These actual or potential users are of many types : international agencies (ESA, Eumetsat), national agencies (CNES, DASA), defence bodies (NATO), power distribution authorities (EDF), aeronautic and space industries (Alcatel, EADS, DLR), small service business (CLS, IEAA, Noveltis, EtaMax), insurance (SWissRe), etc. The ways of exchanges and coordinated actions start from common participations or meetings, like the ESA Pilot projects, the European Space Weather weeks, the ESA info days on cost/benefit analysis, the SWENET data base, the other participations to the COST system. Even if these common actions between such heterogeneous entities is not yet always formal, it presently takes the shape of proposal submission to ESA EMITS calls or towards the European Framework Programme (FP6 then FP7), eg in Space thematics (GMES, Galileo) or in Research Infrastructures. The Space Weather "user community" is just now a reality.

3 Where did we go still further? A European frame of space weather

There are two points that merit to be emphasized. The first one is that we built a community in Europe. 28 countries participated to the action. We had 15 short term scientific missions, 11 management committee and scientific meetings, where we learnt to collaborate with each other. This is the main success of the action.
Furthermore, there are also concrete realizations. What we have made is to built a European frame for the discipline. That goes through different initiatives.

3.1 A European school

Promoted by COST Action 724 and funded by ICTP, COST, United States National Space Weather Program, CAWSES, National Institute for Astrophysics and National Institute for Nuclear Physics, an international advanced school on space weather was held at the Abdus Salam International Centre for Theoretical Physics (ICTP) in Trieste (Italy) from 2 to 19 May 2006. Originally the directors were J. Forbes (Univ. of Colorado, USA), J. Lilensten (Univ. of Grenoble, France; Chairman of COST Action 724) and S. Radicella (ICTP; Local Organizer), but due to unexpected personal problems occurred during the preparation of the School, J. Lilensten was forced to leave his activity as co-director. He suggested M. Messerotti (INAF-Trieste and Dept. of Physics/Univ. of Trieste; Italian Representative in COST Action 724 and Leader of Working Group 1) to take over such responsibility, but he continued to collaborate with the organization of the activity. The main topics elaborated in the theoretical lectures were respectively: a) Introduction to Space Weather; b) Basic physics of magnetoplasmas;

c) The Sun: the physics behind; d) The Sun: Space Weather applications; e) The Interplanetary Medium; f) Earth Magnetosphere: the physics behind; g) Earth Magnetosphere: Space Weather applications; h) Ionosphere-Thermosphere basics; i) Thermosphere-Ionosphere coupling in a global models; j) Solar Radiophysics and Space Weather; k) Space Weather and Radiocommunications; l) Photochemistry of Earth's atmosphere; m) Solar influences on ozone and climate; n) Influence of Space Weather on life emergence and evolution on Earth and at other planets. Practical sessions in the computer laboratory were focused on the topics illustrated in the theoretical lectures, whereas practical sessions at the ICTP Microprocessor Lab were aimed at experimenting with a Terrella device. The school was organized in three weeks for a total of 15 days of lectures. Due to the extended range of topics covering a significant part of Space Weather theory and applications, the lecturers were 29 experts in different fields, who covered 60 hours of theoretical lectures and 55 hours of practical lectures for a total of 115 hours of lectures. The participants could benefit of additional 15 hours of free computer laboratory activities. A number of participants presented their research work in special sessions of the school. The registered participants were 54 from Europe and developing countries, selected from 180 applications according to scientific excellence criteria.

3.2 An annual European meeting: ESWW

As stated in the introduction of this report, ESTEC has maintained a key role in structuring the field in Europe, primarily by organising a yearly workshop from 1998 to 2003. In 2003, the COST 724 action started. Taking advantage of the enthusiasm around this new action, it was immediately decided that the annual ESA Space Weather Workshop become known as a European Space Weather Week with two main partners, ESA and COST. The first two years, this meeting took place in Noordwijk (NL) at the ESTEC center. The attendance increased from about 120 to 150. We decided then to move to Brussels. The Royal Observatory of Belgium became member of the Organizing Committee along with us and with ESA. The attendance raised to 210. Finally, we expect still more participants for the fourth edition since the number of contributions increased (this is writen 2 monthes before the meeting date). This meeting is a European counterpart of the US equivalent. Our US colleagues start recognizing its importance and increase their presence. We also start having contributors from Japan and Autralia. There is little doubt that this meeting is now secured for the years to come.
Each European Space Weather Week is divided into plenary and splinter sessions. Plenary sessions mainly focus on the science-to-applications topics of radiation environment of the Earth, spacecraft and aircraft environments, ionosphere, positioning and telecommunication, magnetic environment and ground induced currents and other ground effects, atmospheres and drag, global change and solar weather versus solar activity forecast and predictions. An additional two sessions address business aspects in the context of agencies activities and outreach to communities, emerging markets and education. Every year, a large number of splinter meetings take place, which cover both scientific and operational themes. Overall, it is felt that this annual European Space Weather Week clearly demonstrates the presence of an active space weather community in Europe.

3.3 Regular European publications

The only systematic scientific publications on Space Weather are currently available through *Space Weather*, the international journal of research and applications published in the US by the American Geophysical Union. Space Weather Journal is an online publication devoted to the emerging field of space weather and its impact on technical systems, including telecommunications, electric power, and satellite navigation.
In Europe, research papers on space weather are mainly published by two scientific journals, Annales Geophysicae and Journal of Atmospheric and Solar Terrestrial Physics. Nevertheless these are multi- and inter- disciplinary scientific journals for the publications on the Sun-Earth system, including not only the science of Space Weather, but covering the broader scientific field of Solar-Terrestrial plasma physics, and Earth's atmosphere and oceans.
COST724 Action managed for the first time to release in Europe regular publications devoted to Space Weather through two special issues in Annales Geophysicae and one Volume in Astrophysics and Space Science Library of Springer. These three volumes present the research contributions and the invited review talks from the First, Second and Third European Space Weather Weeks organized by our Action and ESA. The aim was to disseminate the Action's results to the international scientific community; but most importantly the aim was to demonstrate the European state of the art in the science underpinning space weather and on science-to-applications topics of the spacecraft and aircraft environment, positioning and telecommunication, satellite drag, and GICs and other ground effects.
As modern societies are more and more depended on the technological systems operating in geospace, systematic research on space weather effects and prompt dissemination of the recent advances through peer review publications is becoming a demand. To address this need, it is our perspective to continue regular space weather publication activities through close collaboration with the ESA SWWT and related COST Actions. Through these publications the numerous European scientists and engineers working on space weather basic research and applications will find the forum to present the latest advances on the emerging and exciting field of space weather.

3.4 An integrated European portal including services

The European Space Weather Portal is an integrated website that was developed under the COST 724 action, in the frame of Working Group 4 - Space Weather Observations and Services. It provides a centralized access point for the members of the space weather community to share their knowledge and results. The services provided by the portal include the possibility to access space weather data, both in graphical and various numerical forms. The portal also provides a platform to run both local and remote models, and access the results of these model runs. As a service for the general public, a large section is devoted to education and outreach, which invites children as young as five years to get involved with science. In recognition of the diversity of the action's members and their efforts in creating online space weather resources, the portal also provides cross-links to existing websites. To allow geographically disperse members to contribute, content may be created from anywhere in the world, using only a web browser. Support on the use of the portal is provided by e-mail or by live demonstrations at scientific conferences.

Along with COST 724, the European Space Weather Portal is being jointly developed by the Belgian Institute for Space Aeronomy, which is also funding its hosting.

3.5 Education and outreach activities

Since 1980 a paradigm emerged in geosciences, which is called "Earth System Science (ESS)" or "Earth System (ES)". Earth system science views the Earth as a synergistic physical system of interrelated phenomena, processes and cycles which remain largely unexplored in traditional disciplinary Earth science course offerings. In the present day society, there is a vital need for setting up education activities in parallel to outreach activities.
As ESS emerged a framework for addressing the scientific dimensions of global change, the COST 724 Action has initiated the scientific collaboration between scientists of the universities, governmental and industrial bodies in Europe, concerning the Space Weather education. The university offers the unique opportunity to develop knowledge and understanding about Space Weather that can then be applied, as graduates enter the main stream society. In this context, it is expected that the initiative taken by the COST 724 Action would create firmly a university based cooperative effort in Space Weather under the ESS curriculum development. The basic users of a Space Weather Education Program may be summarized as in the following areas: communications, satellite operations, power grids, manned spaceflight, navigation, etc. Scientific and technological developments are achieved as the results of research, observations, models and education. Forecasting and warning services use the technology developed and disseminate the results to the basic users mentioned above. Comments of users are returned back to the education program via feedback mechanisms. Thus, the quality and efficiency of the education system are sustained at satisfactory levels.
COST 724 maintained many outreach activities. In this report, one paper is dedicated to the *Space Weather and Europe - an Educational Tool with the Sun* (SWEETS) project. One to a space weather experiment. But a simple visit to the European web portal will prove that we had many more activities, including outreach publications and kids drawings on space weather.

4 Where did we fail?

The main task that we did not fulfill is in establishing strong relationships with the US different agencies involved in space weather. At first when our action started, we analyzed that the urgency was to exist as a strong European entity before starting collaboration with SEC or other agencies. Several colleagues of our Management Committee participated to the US space weather week and presented our action. There are of course individual collaborations between COST 724 participants and US colleagues. But we did not devote enough efforts to have structural relationships for mutual benefits.
Although we did address the users needs and the users services, we did not manage to have industrials coming to our meetings, at the noticeable exception of German aircraft industry the 1st year of action. Industrials joined the European space weather week, and connections were established through this way.

5 Conclusion

Although this Working Group was not scientific *per se*, it was a link between all of us, between the researchers, between the working groups. After having developed this project, we can conclude that it would not have been possible to reach all our objectives without this additional working group. The single bureau would not have been sufficient to maintain this level of activity.

A European definition for Space Weather

J. Lilensten[1], B. Sanahuja[2], and M. Messerotti[3]

[1] Laboratoire de Planetologie de Grenoble, OSUG-CNRS, France
jean.lilensten@obs.ujf-grenoble.fr
[2] Dept. Astronomica i Meteorologia, Universitat de Barcelona, Spain Blai.Sanahuja@ub.edu
[3] INAF Trieste and Dept. of Physics, Univ. of Trieste, Italy messerotti@oats.inaf.it

Summary. Our action has devoted a lot of efforts to define properly space weather and get one -or several- European definitions. In this paper, we will explain how we handled the task, what difficulties we came with, and how we managed to converge toward the following European space weather definition:
Space weather is the physical and phenomenological state of natural space environments. The associated discipline aims, through observation, monitoring, analysis and modelling, at understanding and predicting the state of the sun, the interplanetary and planetary environments, and the solar and non-solar driven perturbations that affect them; and also at forecasting and nowcasting the possible impacts on biological and technological systems.

1 Why a new 'Space weather' definition?

During the 3rd Management Committee (MC) meeting in Trieste, on November 2004, the MC considered that there were two main problems with this unofficially but widely accepted USNSWP definition of Space Weather:

1. The statement that it "can endanger human life or health" which is true under certain (exceptional) circumstances, it is often felt too strong and not at the same level of relevancy than the other effects.
2. The fact that this definition is much oriented toward effects instead of science.

The preparatory work and the debate at the MC meeting could not lead immediately to a consensual definition. Therefore, it was decided to set-up a working group which would summarise the issue, analyse the problems and propose a procedure.

2 The working group. The procedure.

The members of the working group specifically dedicated to work on a new space weather definition included 6 colleagues from our action and from ESTEC, under chairmanship of Blai Sanahuja (coordinator). The MC asked the working group to try to the reach a space

weather definition, or a reasonably space weather definition draft with qualifications to be presented and discussed in a MC meeting. To reach this issue, the following actions were programmed:

- To produce a document summarizing the relevant points of discussion on the subject.
- To make a list of constraints we put in the SW definition.
- To define a procedure that can lead to the SWDf (with possible alternatives).

3 To produce a document summarizing the relevant points of discussion on the subject

The important issues identified by the working group, with respect the USNSWP definition are: (1) It is the most widely used so far (including in COST programme of work and ESA space weather pilot project). In addition, it seems that COST community will be in practice working on a concept which is not fundamentally different from the US agencies and from the ESA pilot project. (2) It is criticised for its excessive emphasis on hazardous SW effect on human health. (3) It is criticised for the lack of reference to scientific activities.

To solve problems regarding point (1) the only requirement is that effort is made such that the new definition is compatible with the definition of USNSWP. From the discussions that took place at MC meeting the technical problems with the definitions are points (2) and (3) above. Regarding point (2), it seems that the statement that space weather can endanger human life or health is considered to be too strong. It is recognised, however, that ionising radiation has statistically health impact on astronauts and air crew if certain threshold are exceeded. So the statement is not wrong but it should be softened. Regarding point (3), the working group examined the analogy with atmospheric weather and found out that in all definitions the weather is defined by its effect on human activities and that there is no need to make reference to any of the related science (e.g., atmospheric science, meteorology, climatology, etc.). The working group decided that an equivalent approach should be used for the definition of space weather which is a concept which can be the subject of scientific study but is not a scientific activity per se.

From the above discussion, the working group identified the following constraints and set of guidelines for the definition of space weather to be elaborated.

4 Proposed constraints by the working group for the definition of space weather

Constraint 1. It should be compatible with the USNSWP definition (i.e., it must appear clearly that they describe the same concept). Constraint 2. It should soften the statement that Space weather can endanger human life or health but must be compatible with it. Constraint 3. The definition must have an analogy with the ‘weather’ definition hereby reflecting the analogy of the two concepts. This implies the following points 5 and 6 below. Constraint 4. It should mention effects on human activity and technology. Constraint 5. The space weather should be made as a concept independent of the scientific research.

Furthermore, the working group recommended the following additional constraints on the definition: Constraint 6. It must be compatible with all well recognised space weather effects. Constraint 7. It should not mention only negative effects of space weather. Constraint 8. It should refer to the solar variability. Constraint 9. It should be understandable by an audience broader than the scientific community.

5 Procedure to perform to present and, eventually, to approve a definition of space weather.

The working group approved to prepare a list of twelve definitions, divided in two groups, to be presented in the 5th MC meeting in Vienna, on April 2005. The idea was to reduce the number of potential definitions in order to simplify and speed up the final discussion. The first group (six items) contained the most suitable definitions, as understood by the working group, while the second subset gathers the definition of space weather finally discarded.

The working group approved to propose a procedure to select a definition of space weather, subject to the approval of the MC and to the decision by the MC to go ahead with such selection. There were three steps: (1) After discussion, approval by the MC of the list of constraints presented by the working group (2) After discussion, approval by the MC of the list of possible definitions of SWDf (3) After discussion, if proceeds, selection of a definition from the list previously approved, with a final voting by the MC members.

This procedure had to be approved by the MC. The working group understood that if at the end of the process there were an extended consensus was reached on a given definition, the form of this definition could be modified in order to improve it or to make it more understandable.

Based on these criteria, 5 definitions were approved by the working group.

- *SWDf2*: Space Weather describes physical conditions in the Earth's environment which are ultimately determined by the variable solar activity. Space weather manifests itself through various physical phenomena which are observed in the Earth's environment comprising space and ground.
- *SWDf8*: Space Weather describes the physical processes induced by solar activity that have impact on our terrestrial and space environment, on ground based and space technological systems, and on human activities and health. The main goals of space weather are establishing the scientific basis to understand such phenomena and developing operational tools to predict and forecast them.
- *SWDf10*: The conditions and processes occurring in space which have the potential to affect the near Earth environment. Space Weather processes can include changes in the interplanetary magnetic field, coronal mass ejections from the sun, and disturbances in the Earth's magnetic field. The effects can range from damage to satellites to disruption of power grids on Earth.
- *SWDf11*: Space Weather describes physical conditions in the Earth's environment which are ultimately determined by the variable solar activity and which may affect human activities in space and on Earth. Space weather activities include: scientific research, operational observations and modeling, forecast and specification services.

- *SWDf12*: Processes in the solar wind and Earth environment induced by solar variability (variable conditions on the Sun). Particular consideration is given to their impact on space-born and ground-based technological systems and human healthProcesses in the solar wind and Earth environment induced by solar variability (variable conditions on the Sun). Particular consideration is given to their impact on space-born and ground-based technological systems and human health

The definitions that were discarded are

- *SWDf1*: Space Weather describes physical conditions in the Earth's environment which are ultimately determined by the variable solar activity.
- *SWDf3*: Space Weather Research aims at the understanding and quantification of physical processes associated with solar activity which affect the coupled Sun-Earth system in all aspects.
- *SWDf4*: The goal of space weather research is the establishment of the scientific basis needed to develop the capability to forecast solar activity and its effect on geospace, the biological manifold, and technological systems.
- *SWDf5*: Space environment changes (essentially electromagnetic and particulates with natural origin) and their related effects (especially on human activities in space and on Earth).
- *SWDf6*: Space Weather is the physical and phenomenological state of Ecospace, the region where human activities interact with the terrestrial and space environments. Space Meteorology is aimed at the observation, the study and the prediction of Sun- and non-Sun-driven perturbations in Ecospace, which affect both biological and technological systems.
- *SWDf7*: Space Weather is the science of the composition and dynamics of the space environment of the Earth, from its upper atmosphere to the heliosphere. It aims at understanding the mostly solar origin of the space environment and all the interactions inside the space environment predicting and quantifying the energy inputs due to solar activity and cosmic radiations and their impact on the space environment predicting and quantifying the consequences of these variations on the ecospace, defined as the region where human activities interact with the terrestrial and space environments
- *SWDf9*: Sun activity that acts on the biosystem

6 Development and discussion at the 5th MC meeting

The discussion was very warm. Discarded definitions were considered by some colleagues as the bests, some wanted to have more emphasis on science, some on technology. In spite of the working group efforts to set up a rationale working way, the criteria were soon forgotten. The reactions reflected in many ways our cultural differences, showing how interesting, but how difficult it is to build Europe! The working group tried to convince the Management Committee that we can even come with three definitions adapted to different tasks: it turned out to be totally impossible. It looked very much as a dead end.

7 A European definition for space weather

During the 9th MCM in Sofia (May 2007), we decided to restart the process. Dr. Messerotti gave a semantic grid to analyse our definitions. We restarted the discussion from SWDf6. We understood that there should not be a definition inside of a definition (ecospace must not be explained inside of the space weather definition), and that there is a difference between the space weather itself and the associated discipline. We created a discussion group that gathered 30 participants. Each word was discussed. Finally, we converged to the following definition, which constitutes therefore the European definition for Space Weather:
Space weather is the physical and phenomenological state of natural space environments. The associated discipline aims, through observation, monitoring, analysis and modelling, at understanding and predicting the state of the sun, the interplanetary and planetary environments, and the solar and non-solar driven perturbations that affect them; and also at forecasting and nowcasting the possible impacts on biological and technological systems.

References

US National Space Weather Program: Implementation Plan, FCM-P31-1997, Office of the Federal Coordinator For Meteorological Services and Supporting Research, Silver Spring, Md., 1997; http://www.ofcm.gov/nswp-sp/text/a-cover.htm

European space weather forecasting service

H. Lundstedt[1], P. Wintoft,[2], I. Stanislawska[3], and A. Belehaki[4]

[1] ISES and Swedish Institute of Space Physics, Scheelev. 17, 223 70 Lund, Sweden, henrik@lund.irf.se
[2] Swedish Institute of Space Physics, Scheelev. 17, 223 70 Lund, Sweden, peter@lund.irf.se
[3] Polish Academy of Sciences Space research center Bartycka 18 A 00 716 Warsaw Poland stanis@cbk.waw.pl
[4] Ionospheric Group Inst. for Space Appl. and Remote Sensing National Observatory of Athens Metaxa and Vas. Pavlou str. Palaia Penteli 15236 Greece, belehaki@space.noa.gr

Summary. Forecasting service is offered by several organizations in Europe, though Regional Warning Centers (RWC) of the International Space Environment Service (ISES) are the main distributers. However, even ISES associate centers (commercial CLS) and collaborative expert centers such as ESA exist. There are also providers of forecast service as an ESA Service Development Activity (SDA).

1 Introduction

The International Space Environment Service (ISES) is a permanent service of the Federations of Astronomical and Geophysical Data Analysis Services (FAGS), under the support of the International Union of Radio Science (URSI) in association with the International Astronomical Union (IAU) and the International Union of Geodesy and Geophysics (IUGG). ISES was called IUWDS (International URSIgram and World Days Service) until 1996. The IUWDS was formed in 1962 as a combination of the former International World Days Service, initiated in 1959 as part of the IGY, and the former URSI Central Committee of URSIgrams which initiated rapid international data interchange service in 1928. The first forecast broadcast from Eiffel Tower URSIgram was sent 1928. The mission of ISES is to encourage and facilitate near-real-time international monitoring and prediction of the space environment, to assist users in reducing the impact of space weather on activities of human interest. Currently there are eleven RWCs (Figure 1). However, South Africa is becoming the twelfth and Brazil is next. RWC-USA in Boulder plays a special role as "World Warning Agency", acting as a hub for data exchange and forecasts (Poppe & Jordan, 2006).

2 Service offered by Regional Warning Centers

According to ISES Bylaws, the main tasks of the RWC is to provide users with near-realtime space weather forecasts, provide timely and free exchange of data, information and techniques with other RWCs, as well as to collect space environment data from local regions.

Four of the current eleven full member RWCs are located in Europe. A brief description of each center's service follows.

Fig. 1. Regional Warning Centers of ISES. Soon the Southern hemisphere will also be covered by Regional Warning Center South Africa and Regional Warning Center Brazil and not just by Regional Warning Center Australia.

2.1 RWC-Belgium (Brussels)

The Solar Influences Data Analysis Center (SIDC) is a research group for solar physics at the Royal Observatory of Belgium. Its operational activities include the World Data Center for the sunspot index (Vanlommel et al., 2004) and the RWC-Belgium for space weather forecasting (Berghmans et al., 2005). (http://sidc/oma.be/)

The RWC-Belgium has very extensive web pages consisting of most solar-terrestrial data available, both ground and space-based. They also offer many visualization tools and tools for detecting solar phenomena, such as coronal mass ejections.An overview of the space weather and sunspot products can be found on http://sidc.oma.be/registration/registration_ main.php.

2.2 RWC-Czech Republic (Prague)

RWC-Czech Republic provides both solar, ionospheric and geomagnetic data.

Astronomical Observatory Ondrejov delivers solar white-light and H-alpha images which are observed on a daily bases. Ionospheric Observatory Pruhonice provides ionogram every

2 minutes. Ionospheric Observatory Panska Ves provides telemetry data for the following projects: ACTIVE, APEX, INTERBALL-TAIL and INTERBALL-AURORAL.

Geomagnetic Observatory Budkov delivers measurements and forecasts of the K geomagnetic index and has done that since 1967. (http://rwcprague.ufa.cas.cz/)

2.3 RWC-Poland (Warsaw)

In Poland, optical observations are continued in Bialkow (Wroclaw University), radio observations come from Krakow (Jagiellonian University) and Piwnice (Torunian University).

Geophysical Observatory in Belsk (about 40 kilometers apart from Warsaw) gives information about geomagnetic K indices. Ionospheric disturbances are monitored by ionosondes. One of them is the Warsaw's ionosonde. (http://www.cbk.waw.pl/rwc/rwc.html)

2.4 RWC-Sweden (Lund)

RWC-Sweden in Lund offers several self-developed real-time forecasts based on solar wind data, downloaded from the NASA ACE satellite (Lundstedt, 2005). Neural networks have been trained to forecast geomagnetic indices Dst (Lundstedt et al., 2002) and Kp (Boberg et al., 2000). RWC in Lund is also offering local geomagnetically induced currents (GIC) predictions, of interest to the power companies in Sweden (Lundstedt, 2006).

Geomagnetic data from a magnetometer at Risinge (Lundmark, 2007) will soon be available from RWC-Sweden web site in Lund. (http://www.lund.irf.se/rwc/)

3 Service offered by other organizations

3.1 ESA (Noordwijk)

ESA is a so called collaborative expert center. ESA has coordinated much of the space weather activities in Europe since 1996 and has a very extensive space weather web server. ESA has developed SWENET (Space Weather European Network) that has links to 31 Service Development Activities (SDA) though ESA does not develop their own operational forecasts. (http://www.esa-spaceweather.net/spweather/index.html)

3.2 Collecte Localisation Satellites (CLS) and CERCLe - Observatoire de Paris

CLS is a commercial site and provides only limited public service: Solar images from SOHO, Observatoire d'Astrophysique de Catania (Italy), Nobeyama - Japon Radio - Heliogramme and Wingst geomagnetic magnetogram. (http://www.cls.fr/previsol/)

Cycle Eruptions et Rayonnement Cosmique au Lesia (CERLe) of Observatoire de Paris, partner of CLS, provides however, public solar service and information about aircrew dosimetry. (http://venus.obspm.fr/previ/)

3.3 Rutherford Appleton Laboratory (RAL)

Short-Term Ionospheric Forecasting (STIF): Ionospheric forecasts are provided up to 24 hours ahead, using an autoregressive procedure developed jointly by the Radio Communications Research Unit and the Geophysical Institute of the Bulgarian Academy of Science.

The latest European forecast maps of the critical frequency in the ionospheric F2 layer for ordinary waves (foF2) and the Maximum Usable Frequency (MUF(3000)F2) are available. The latest European derived Total Electron Content (TEC) forecast maps are also available. STIF has been adopted as the short-term forecasting tool of the European collaborative project COST 251.

4 Digital Upper Atmosphere Server (DIAS)

The aim of the European Digital Upper Atmosphere Server (DIAS) (Belehaki et al., 2005), funded by the eContent programme of European Comission, is to provide a European service for the specification and the prediction of the state of the ionosphere. DIAS consortium consists of National Observatory of Athens, Greece; BAE System, UK; National Institute of Geophysics and Volcanology, Italy; Leibniz-Institute of Atmospheric Physics, Germany; University of Athens, Greece; Rutherford Appleton Laboratory, UK; Swedish Institute of Space Physics; Space Research Center, Poland; Blustaff, Italy; Institute of Atmospheric Physics, Czech Republic; Observatoire de L*f*bre, Spain; INTA/CEDEA, Spain.

The objectives of DIAS are: To develop a pan-European digital data collection on the state of the upper atmosphere based on historical data collections and on the real-time information provided by several European ionospheric stations; To develop a new digital server for the management and distribution of this collection, based on cutting edge technology; To develop added value products and services for ionospheric specification and forecasting that best fit the need of the market and to perform all necessary actions for the efficient promotion of this pan-European digital data collection to the European and worldwide market. DIAS products and services of ionospheric specification and forecast are: Ionogram, Ionospheric scale parameters (foF2, MUF(3000)F2); Electron density profiles, maps, daily plot of the effective sunspot number; Long-term ionospheric predictions (maps of foF2, MUF(3000)F2 and MUF over Europe); Short-term ionospheric forecasting (one-24 hours); Ionospheric activity index. (http://dias.space.noa.gr)

5 British Geological Survey (BGS)

Daily global geomagnetic activity (Ap index) forecasted for up to 3 days ahead, using neural networks, (Thompson, 1993) are available from British Geological Survey. The forecasts were developed as a Service Development Activity (SDA) (BINCAST = BGS Indices, Nowcasts and Forecasts) of the ESA Space Weather Pilot Projects. (http://www.geomag.bgs.ac.uk/gifs/)

6 Conclusion

A great number of European space weather service providers exist. ISES plays the role of international providers of both local and global service. Coordination of European service, with respect to ISES, would therefore be advisable. Without coordination there is a risk for duplication. ISES has many years of experience of delivering forecast service to customers. ISES has also a so called Forecast Forum, within which forecasts of an upcoming or ongoing event can be discussed between the RWCs. Finally, coordination makes it also easier for the customers to find the service they are looking for.

References

Belehaki, A., Cander L.R., Zolesi, B., Bremer, J., Juren, C., Stanislawska, I., Dialetis, D., Hatzopoulos, M.: DIAS project: The establishment of a European digital upper atmosphere server, J. Atmos. Sol. Terr. Phys., 67, 1092-1099 (2005).

Berghmans, D., Van der Linden, R.A.M., Vanlommel, P., Warnant, R., Zhukov, A., Robbrecht, E., Clette, F., Podladchikova, O., Nicula, B., Hocheedez, J.-F, Wauters, L., Willems, S.: Solar activity: nowcasting and forecasting at the SIDC, Ann., Geophys., **23**, 3115-3128 (2005).

Boberg, F., Wintoft, P., Lundstedt, H.: Real time Kp predictions from solar wind data using neural networks, Phys. Chem. Earth, Pt C 25 **4**, 275-280, (2000).

Lundmark, A.: Geomagnetic measurements - The magnetometer in Risinge, Diploma work at Swedish Institute of Space Physics and Umeå University (2007).

Lundstedt.H, Gleisner, H., Wintoft, P.: Operational forecasts of the geomagnetic Dst index, Geophys. Res. Lett., **29**, 34-1–34-4 (2002).

Lundstedt, H.: Progress in space weather predictions and applications, Adv. Space Res., **36**, 2516-2523 (2005).

Lundstedt, H.: The sun, space weather and GIC effects in Sweden, Adv. Space Res., **37**, 1182-1191 (2006).

Poppe, B. and Jordan, K.P.: Sintinels of the Sun, Forecasting Space Weather, Johnson Books, Boulder (2006).

Thompson, A.W.P.: Neural networks and non-linear prediction of geomagnetic activity, Proceedings of the International Workshop on Artificial Intelligence Applications in Solar-Terrestrial Physics, Lund, Sweden, 22-24 September, 1993 (1993).

Vanlommel, P., Cugnon, P., Berghmans, D., Van der Linden, R.A.: Cletter, F.: The SIDC: World Data Center for the sunspot index, Solar Physics, **224**, 1-2, 133 (2004).

Real-time space weather forecasts based on neural networks

H. Lundstedt[1] P. Wintoft[2], Y. Tulunay[3], and E. Tulunay[4]

[1] ISES and Swedish Institute of Space Physics, Scheelv. 17, 223 70 Lund, Sweden, henrik@lund.irf.se
[2] Swedish Institute of Space Physics, Scheelv. 17, 223 70 Lund, Sweden, peter@lund.irf.se
[3] Faculty of Aeronautics and Astronautics Istanbul Technical University Ayazaga Campus 80626 Maslak Istanbul Turkey ytulunay@ae.metu.edu.tr
[4] ODTU/METU, Turkey ersintul@metu.edu.tr

Summary. Within solar-terrestrial physics there are numerous neural network applications and many predictions of solar-terrestrial effects have been developed. However, few solar-terrestrial predictions have been transitioned into operational real-time forecasts of space weather and effects. In this article we give a short overview of these operational forecasts.

1 Introduction

Previously several neural methods have been applied to solar-terrestrial physics data (Lundstedt, 2005). The real challenge, however, is to transfer the model into operational real-time forecasts using real world data (Lundstedt et al., 2002). Validation then plays an important role (Wintoft et al., 2007).

A breakthrough for the real-time forecasts of space weather and effects came with availability of real-time solar wind data from the NASA spacecraft Advanced Composition Explorer (ACE). A real-time solar wind monitor is therefore crucial.

STEREO and upcoming SDO mission are foreseen to become a breakthrough for forecasts days ahead.

The delivering of the real-time forecasts is an important issue. -Where can the user get access to the forecasts? In (Lundstedt et al., 2007) we describe forecast service in Europe and determine that International Space Environment Service (ISES) plays a key role in data and forecast exchange through its Regional Warning Centers (RWC). ISES space weather website (http://www.ises-spaceweather.org/) has the ability and the aspiration to be the international site to access global and regional forecasts of space weather and effects.

2 Neural networks

Neural networks (Haykin, 1994) can deal with information that is chaotic, fuzzy, probabilistic, and noisy. They are highly parallell and differ by how the neurons (process units) work, how the neurons are connected (topology) and by which learning algorithm that has been chosen.

Neural networks can also be combined with other Artificial Intelligence (AI) techniques, such as expert system, fuzzy system and genetic algorithm, into so called Intelligent Hybrid System (IHS) (Lundstedt, 2001); (Lundstedt, 2006b). Data presented to neural networks are first preprocessed, often using wavelet methods (Lundstedt et al., 2006) and Principal Component Analysis (PCA). Various techniques have then been developed to extract the knowledge the neural networks have learned. Weights of the neural networks can be compared with terms of the differential equations describing the physics. Multi-layer back-propagation (MLBP), recurrent neural networks, radial-base networks and self-organizing maps have been applied to predictions of solar activity and space weather effects. Today real-time predictions of the space weather and effects are available, based on recurrent neural networks and using solar wind data as input (Lundstedt, 2005).

3 Real-time operational space weather forecasts

A breakthrough for the real-time forecasts of space weather and effects came with availability of real-time solar wind data from the NASA spacecraft Advanced Composition Explorer (ACE). Most of the operational forecasts are based on ACE data as input and the existence of solar wind monitor at L1 is therefore crucial. "Kuafu solar wind monitor mission of China" is planned to be launched 2012.

3.1 Solar activity and solar wind velocity

Forecasts of flares, based on solar vector magnetograms, using neural networks are available from RWC-China. The complexity and non-potentiality of the solar magnetic field, and herewith likelihood of causing solar flares, are described by the maximum horizontal gradient, length of neutral line and number of singularities (Cui et al., 2006).

Predictions of the solar wind velocity 1-3 days ahead, based the photospheric magnetic expansion factor and using a radial bases neural network has been developed (Wintoft & Lundstedt, 1997), though it has not yet been implemented for operational use.

3.2 Magnetosphere and ionosphere conditions

The Magnetospheric Specification and Forecast Model (MSFM) was developed by Rice University in USA (Freeman et al., 1993). It uses as input neural network predictions of geomagnetic activity index based on real-time ACE solar wind data to forecast the magnetospheric environment of satellites ($\approx 6R_{Earth}$). These forecasts are used by the US Air Force.

Many predictions of ionospheric conditions, e.g. of foF2 (Tulunay et al., 2000), MUF, TEC (Tulunay et al., 2006), have been developed using neural networks and they are expected to soon be transitioned into operational forecasts.

3.3 Geomagnetic indices and local geomagnetic field

Daily global geomagnetic activity (Ap index) for up to 3 days ahead, using neural networks, (Thompson, 1993) are available from British Geological Survey

(http://www.geomag.bgs.ac.uk/gifs/). The forecasts were developed as a Service Development Activity (SDA) (BINCAST = BGS Indices, Nowcasts and Forecasts) of the ESA Space Weather Pilot Projects.

Following forecasts are based on real-time ACE solar wind input. Predictions of Dst index are available from Instituto di Fisica dello Spazio Interplanetario (Roma) (http://gifint.ifsi.rm.cnr.it/). They also offer predictions of AE index. Both developed as an ESA SDA (Geomagnetic Indices Forecasting and Ionospheric Nowcasting Tools = GIFINT). Dst and Kp forecasts are also available from RWC-Sweden (http://www.lund.irf.se/se/rwc/) (Boberg et al., 2000), (Lundstedt, 2002). Operational forecasts of Dst are also available from NICT Space Environment Information Service, RWC-Japan in Tokyo (http://hirweb.nict.go.jp/index.html).

Forecasts of local geomagnetic fields (dB/dt) for two locations Uppsala (Sweden) and Brorfelde (Denmark), based on ACE solar wind data and neural networks are also available from RWC-Sweden in Lund (http://www.lund.irf.se/gicpilot/gicforecast/forecastdb.html).

3.4 Effects on technological systems

There are three main areas of effects: On satellite systems, on communication, navigation, and on electrical systems (Lundstedt et al., 2006). Much has been developed as service development activity (SDA) of the ESA Space Weather Pilot Projects. An extensive web site SWENET (http://esa-spaceweather.net/sda/) is available. However, few services are running and even fewer based on neural networks.

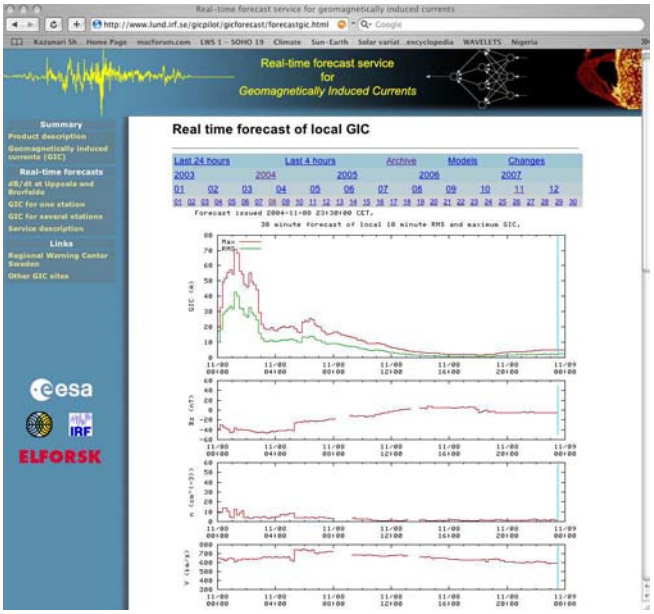

Fig. 1. GIC forecast web page.

Forecasts of local geomagnetically induced currents (GIC) in power systems is one of many operational service that are running and are available from RWC-Sweden in Lund (http://www.lund.irf.se/gicpilot/gicforecast/). The forecasts were developed within the ESA GIC pilot project (GIC forecast) together with Finish Meteorological Institute (FMI) and the power industry (Elforsk in Sweden). Fig. 1 shows the forecasts of GIC for the storm event in November 8, 2004 as well as the solar wind values of the velocity, density and southward IMF component.

4 Conclusions

Many predictions have been developed within solar-terrestrial physics, based on neural networks. However, few have been transferred into operational forecasts of the space weather and effects.

References

Boberg, F., Wintoft, P., Lundstedt, H.: Real time Kp predictions from solar wind data using neural networks, Phys. Chem. Earth, Pt C, 25(4), 275-280 (2000).

Cui, Y., Li R., Zhang, L., He, Y., Wang, H.: Correlation Between Solar Flare Productivity and Photospheric Magnetic Field Properties, Solar Phys. **237**, 1 August (2006).

Freeman, J., Nagai, A., Reiff, P., Denig, W., Gussenhoven-Shea, S., Henemann, M., Rich, F., Hairston, M.: The use of neural networks to predict magnetospheric parameters for input to a magnetospheric forecast model, in Proceedings of the International Workshop on Artificial Intelligence Applications in Solar-Terrestrial Physics, Lund, Sweden, 22-24 September, 1993 (1993).

Haykin, S.: Neural Networks – A Comprehensive Foundation, Macmillan College Publ. Comp., Inc., New York (1994).

Lundstedt, H.: Predicting Solar Activity with Artificial Intelligence, in AGU Chapman Monograph 125, Space Weather (2001).

Lundstedt, H.: ESA Space Weather Programme Study (Alcatel team) WP 3110, TN, Space Weather Service (50 pages) (2002).

Lundstedt. H, Gleisner, H., Wintoft, P.: Operational forecasts of the geomagnetic Dst index, Geophys. Res. Lett., **29**, 34-1–34-4 (2002).

Lundstedt, H.: Progress in space weather predictions and applications, Adv. Space Res., **36**, 2516-2523 (2005).

Lundstedt, H.: The sun, space weather and GIC effects in Sweden, Adv. Space Res., **37**, 1182-1191 (2006a).

Lundstedt, H.: Solar activity modelled and forecasted: A new approach, Adv. Space Res., **38**, 862-867 (2006b).

Lundstedt, H., Liszka, L., Lundin, R., and Muscheler,R.: Long-Term Solar Activity Explored with Wavelet Methods, Ann. Geophys., **24**, 1-9 (2006c).

Lundstedt, H., Stanislawska, I., Belehaki. A.: European forecasting service, ISSI, (2007).

Thompson, A.W.P.: Neural networks and non-linear prediction of geomagnetic activity, Proceedings of the International Workshop on Artificial Intelligence Applications in Solar-Terrestrial Physics, Lund, Sweden, 22-24 September, 1993 (1993).

Tulunay, E., Ozkaptan, C., Tulunay, Y.: Temporal and Spatial Forecasting of the foF2 Values up to Twenty four Hours in Advance, Phys. Chem. Earth, 25(4), 281-285 (2000).

Tulunay, E., Senalp, E.T., Radicella, S.M., Tulunay, Y.: Forecasting Total Electron Content Maps by Neural Network Techniques, Radio Science, **41**, RS4016, AGU, Washington, USA (2006).

Wintoft, P., Gleisner, H., Wik, M, Lundstedt, H.: Empirical models of solar wind - magnetosphere - ionosphere coupling, ISSI (2007).

Wintoft, P., Lundstedt, H.: Prediction of Daily Average Solar Wind Velocity from Solar Magnetic Field Observations using Hybrid Intelligent Systems, Phys. Chem. Earth, **22**, (7-8), 617-622 (1997).

Development of the European Space Weather Portal

Heynderickx Daniel[1], Stegen Koen[2], and Wera Jan[3]

[1] BIRA, Ringlaan 3, B-1180 Ukkel, Belgium daniel.heynderickx@oma.be
[2] BIRA, Ringlaan 3, B-1180 Ukkel, Belgium koen.stegen@oma.be
[3] BIRA, Ringlaan 3, B-1180 Ukkel, Belgium jan.wera@oma.be

Summary. The *European Space Weather Portal* is an integrated website that was developed under the COST 724 action, in the frame of Working Group 4 – Space Weather Observations and Services. It provides a centralized access point for the members of the space weather community to share their knowledge and results. The services provided by the portal include the possibility to access space weather data, both in graphical and various numerical forms. The portal also provides a platform to run both local and remote models, and access the results of these model runs. As a service for the general public, a large section is devoted to education and outreach, which invites children as young as five years to get involved with science. In recognition of the diversity of the action's members and their efforts in creating online space weather resources, the portal also provides cross-links to existing websites. To allow geographically disperse members to contribute, content may be created from anywhere in the world, using only a web browser. Support on the use of the portal is provided by e-mail or by live demonstrations at scientific conferences. The *European Space Weather Portal* is being developed by the Belgian Institute for Space Aeronomy, which is also funding its hosting.

This document describes the technical development of the software system that provides the functionality available at the portal's URL: http://www.spaceweather.eu.

1 Rationale

The COST 724 members realized from the beginning that the community needed a website to share their results, so in the frame of Working Group 4 – Space Weather Observations and Services – it was decided to build a website where contributions could be centralized. To fulfill this need, the development team at the Belgian Institute for Space Aeronomy started in the summer of 2006 with a portal website to allow the COST 724 members to provide feedback on this website well before the COST 724 action ended.

Because the COST actions are largely based on voluntary cooperation, and under the pressure of a looming European Space Weather Week where a first demonstration of the portal system would be most appropriate, the development team decided that a formal questionnaire to collect requirements from members and possible users would take too much time, and it was decided to set out some self-defined aims and objectives which seemed appropriate for a scientific portal in general. As a baseline the following aims and objectives were used.

1.1 Collaborative content creation

To implement the COST objective to support co-operation across Europe, a major objective of the system was that it would facilitate the collaborative creation of content. At the time the development started, the COST 724 action already included 27 different countries, with over 50 national representatives, who would be actively contributing content to the *European Space Weather Portal*. This large number of authors could only succeed in creating something coherent if they all would work together, and share their little piece of the larger jigsaw. The system should provide a remotely accessible platform to support this collaboration as much as possible.

1.2 Multi-Lingual

A website that includes contributions from a large number of countries, would without the slightest doubt include content in multiple languages. Also, if the site was to do outreach for the general public, having the possibility to support different languages was not merely content-provider driven, but also content-requester driven; people getting acquainted with a new subject feel more comfortable reading in their mother tongue, than reading in a foreign language – which English is for most of those 27 countries.

1.3 Database independence

As the portal system was designed with the possibility for growth, it was anticipated that the choice for a particular database management system could be regretted afterwards. For this reason the selection of the portal system was decided with a requirement that it should be possible to choose the vendor for the back-end database on which all content would be stored – either open source or closed source.

1.4 Extensibility

To be useful to the scientific community, the system should be extensible from the beginning, otherwise, the system would have to be rebuilt from scratch exactly at the moment when it becomes a success, and the increasing number of users caused an increased amount of feature requests. Only an extensible system would be flexible enough to cope with a multitude of features requested by and aimed at such a wide variety of users as from layman (including children) to expert scientists.

1.5 Open Source

Many systems such as described above exist, both closed source and open source. Open source systems are usually free of charge, closed source variants generally require licensing fees. The combination of desired features and flexibility in commercial applications easily costs in excess of 10,000 Euro, so due to the limited funds for the COST 724 action, a free open source system was chosen, knowing that some missing features would have to be included by hand.

2 Methodology and Implementation

Because there are hundreds of different content management systems, a survey was done to find a content-management system (CMS) that provides most of the desired functionality off-the-shelf in order to minimise the required amount of custom code. The first CMS tested was *TikiWiki* (http://tikiwiki.org). It was installed on a server at BIRA, filled with some content and published to selected users for evaluation.

Despite positive feedback from the users, the development team quickly realised that for most modules that provide additional functionality, the module or *TikiWiki* itself required the administrator to edit the source code merely to get the module working. The availability of the source code is a great advantage when something doesn't work, but when hardly anything works, the amount of effort necessary to edit the source code frequently would severely limit the progress of the portal as a whole. Therefore it was decided to abandon *TikiWiki*.

Given the experience gained with *TikiWiki*, another CMS named *Drupal* (http://drupal-.org/) was evaluated. Initially the *TikiWiki* mindset made *Drupal* administration a little bit awkward, but the system was given a fair chance and after a while it became clear that not only the system itself was better than *TikiWiki*, but also the available modules could be activated without too much trouble. In fact it is still this second test system that operates the current *European Space Weather Portal*.

3 Output

The most visible output is obviously the website itself, which is accessible at *http://www.-spaceweather.eu*. The *.eu* domain name was chosen to emphasize the European roots of the COST actions, and at the same time make all participating countries feel equally represented, regardless of their geographical location.

The main features of the portal are access to space weather data and models, glossaries of acronyms, an introduction to space weather translated in several languages, and an extensive section on public outreach.

Comments, both e-mails and posts on the portal itself, show that the *European Space Weather Portal* is greatly appreciated by both the scientific community and the children who made drawings. Both teachers and children are very proud to see their images on line.

4 Conclusion

The combined efforts of the COST 724 members resulted in an integrated portal built on collaboration as the cornerstone of success. No single partner on its own could have developed this variety of features in such a small amount of time. The joined forces aimed at a common goal culminated in a tool to be used for a long time to come.

In the future, the development team would like to extend the functionality of the portal by providing access to more space weather related data, wherever possible in real-time. Simplified integration of models and processing tools into the portal, and a way to connect the output of one model/tool to the input of another, combined with improved data visualisation

will lead to an integrated framework for event analysis. This, together with an extension of the outreach section should cover the needs of the entire spectrum of the space weather community, including the general public.

5 Acknowledgements

The development team of the *European Space Weather Portal* wishes to acknowledge following persons and organisations for their significant contribution in the development of the *European Space Weather Portal*.

The COST 724 chair members, for their continuous motivation of both the development team and the COST 724 members to push forward and make the best system possible.

The COST 724 community as a whole for the trust they have had in the development team, and the following members in specific for contributing translations and pictures: Alain Corbeau, Alan Aylward, Bart Declercq, Blai Sanahuja, Nicolas Fuller, Jan Wera, Jean Lilensten, Jurgen Watermann, Koen Stegen, Lev Dorman, Magdalena Stavinschi, Maja Mitic, Mauro Messerotti, Monique Pick, Natalia Romanova, Norbert Jakowski, Norma Crosby, Patrick Guio, Pavel Hejda, Rami Vainio, Risto Pirjola, Sarah Hansson, Susan McKenna-Lawlor, Ioanna Tsagouri, Tsevetan Dachev, Vida Zigman, Vincent Génot, Ersin and Yurdanur Tulunay.

The Belgian Institute for Space Aeronomy for kindly funding the development team, the acquisition of the domain name and for funding the ongoing costs associated with the operation of this portal.

The young European artists and their teachers for making beautiful drawings.

Last but not least, ESA-ESTEC for their support.

COST 724: a springboard for industries

J. Lilensten[1], L. Desorgher[2], D. Heynderickx[3], F. Jansen[4]

[1] Laboratoire de Planétologie de Grenoble, OSUG-CNRS, France
[2] SpaceIT GmbH, Bern, Switzerland
[3] DH Consultancy BVBA, Leuven, Belgium
[4] 1A, Greifswald, Germany

Summary. Our action has devoted a lot of efforts to create relationships with industry. This resulted in catalogue available on the space weather web portal of industrials related to space weather applications. But maybe more important in our point of view, it also resulted in succesfull creation of one private company and in the kick off of two pre-existing companies owned by 3 of our COST 724 members. In this paper, we describe these three companies and analyse how COST and these private companies benefit from each other.

1 Introduction

COST is aimed at coordinating the scientific and technological activities over Europe in different domains. Although purely a public system funded by the DG research, COST is open to all kinds of relationships with industry. In the space weather domain and maybe more than in many other disciplines, industry is a fundamental parameter. Not only industrials can benefit from the outputs of the space weather activities (i.e. to protect spacecrafts, pipe lines, communications a.s.o.), but industrials can also provide services that are not the aim of public research laboratories. In the frame of our action, we have been delighted to serve as ground for three companies from three participants of this COST action. In the following we will describe these companies and show how a COST action can be usefull in such activities.

2 DH Consultancy BVBA

DH Consultancy BVBA is a one-man company based in Leuven, Belgium. The company was founded by Dr. Daniel Heynderickx in June 2007. D. Heynderickx has a long-standing experience in several ESA projects, including project management, coordination and follow-up of contracts, and participation in the technical work. He has had key roles in ESTEC Contracts Space Environment Information System (SPENVIS), Trapped Radiation Environment Development (TREND), Radiation Environment Research from Multiple Monitors (RERMM), Space Weather Network (SWENET), and Solar Energetic Particle Environment Modelling (SEPEM).

He is also one of the Belgian National Representatives for COST 724 action "Developing the Scientific Basis for Monitoring, Modelling and Predicting Space Weather". As such, he played a key role in starting up the European Space Weather Portal (http://www.spaceweather.eu), the European gateway to space weather resources. The portal is a product of the COST action, and is being developed and maintained by the Belgian institute for Space Aeronomy, in the framework of the Belgian Solar Terrestrial Centre of Excellence.

DH Consultancy is building on the experience gained in these various projects. It offers expertise in the following domains:

- radiation environment modelling
- space environment effects on spacecraft and components
- processing, storing and accessing spacecraft and ground based data
- space weather models and predictions
- tailored services combining data, models and custom built processing tools

After only a few months of experience, a number of prototype demonstrator services are already available on a server which can be reached through http://www.dhconsultancy.net. The tools and services currently under development include:

- a mirror of the Izmiran 1 hour average neutron monitor data archive, converted into an SQL data base, with data retrieval and plotting tools
- an SQL database of a number of geomagnetic and solar wind indices, with retrieval and plotting tools
- an SQL database of the 5 minute averaged particle, X-ray and magnetic field measurements made by the NOAA GOES satellite series, with retrieval and plotting tools
- an application to calculate real-time geomagnetic cut-off values for neutron monitor stations, using real time Kp values (from Regional Warning Center Sweden) and the MAGNETOCOSMICS code developed by the University of Bern.

In the future, more data and services will be added, including a platform for remote running of computer models.

Company information:
DH Consultancy BVBA, Diestsestraat 133/3, 3000 Leuven, Belgium
Tel: +32-16-225860
E-mail: `DHConsultancy@skynet.be`
url: `http://www.dhconsultancy.net`

3 Space IT GmbH

SpaceIT GmbH is a SME that provides expertise in the field of space radiation. It is specialised in the development of softwares for modelling and forecasting the radiation environment in space and on Earth, and for quantifying its effect on technologies, planets, and biology. It was founded in March 2006 by Dr. L. Desorgher.
During its PhD and its research work in Cosmic Rays at the University of Bern, L. Desorgher was involved in several ESA projects and did also take part actively to the COST 724 action.

He his the developer of the MAGNETOCOSMICS and PLANETOCOSMICS code on base of which he did develop during this COST action a code for computing the ionisation of the Earth's atmosphere by galactic and solar cosmic rays. During his different past activities he could gather the following expertise that he his now offering through is own company:

- Analysis of space instrument data
- Modeling of space radiation environment
- Space weather modeling
- Modeling the effect of energetic particles on planets, on biology and on infrastructure (electronics,...)
- Important knowledge in the electromagnetic and nuclear processes involved in the interaction of energetic particles with matter
- Important knowledge on magnetosphere and space physics
- Use of MonteCarlo techniques (Geant4) for modeling the interaction of energetic particles with matter
- Development of software according to software engineering standard

Company information:
SpaceIT GmbH, Sennweg 15, CH 3012 Bern, Switzerland
Tel: +41 31 301 45 22
E-mail: desorgher@space.unibe.ch

4 1A First Applications and Management Consultancy for Space Weather Service, Research, Education and Culture

1A was established in 2001 a few years before the action started. His chairman is Dr. Frank Jansen, who is one of the German National representative of the COST 724 action. 1A is located at the Technology Centre Vorpommern at the Hanse and University town Greifswald in Germany. 1A offers the following products and services:

- construction and marketing of space weather related hardware products like space weather forecast radio and cosmic ray telescopes and monitors, aircraft dosimeter, current monitors for power lines and pipelines, forecast and nowcast operation centres
- development, installation and service for space weather related software for the following applications: satellites, Galileo satellites navigation, long / short distance and wireless telecommunication, aircraft and aircrew protection, pipelines, power lines and car electronic,
- simulations on space weather forecast and nowcast of solar and cosmic ray origin, for the nearby Earth environment, magnetosphere, ionosphere, atmosphere, ground based effects and global warming
- world-wide realization of ESA space house
- European wide promotion via interactive exhibit in a space weather bus for shopping and science centres, industrial fair organisation, conferences and space weather dance show for social events

- consultancy for board of directors, for security organisations, training of employees on space weather user, science and benefits related aspects

Amongst the clients and partners, one finds the European Commission Brussels, the European Space Agency, the German Aerospace DLR, the Max-Planck-Institute or the Austrian Research Centers Seibersdorf, Austria. One finds also the Swiss reinsurance (Switzerland) company, Ruhrgas AG, Essen, Germany, O2 / Telefonica Nrnberg, Germany, several universities such as Bern (Switzerland), Delaware (USA), Greifswald (Germany), Shinshu (Japan) and Yerevan (Armenia) or several institutes such as the Space Weather Observatory WWW Greifswald, Germany, the Australian Antartic Division Hobart, the Bulgarian Academy of Sciences Sofia, or the Slovak Academy of Sciences Kosice

Company information:
Dr. Frank Jansen, 1A Greifswald, Brandteichstr. 20, 17489 Greifswald, Germany
Tel: +49 3834 762463, +49 176 24267648
Skype connection: lieven130597
Fax: +493834 550222
www.1A-FirstApplications.com

5 Discussion and conclusion

How did the action and these companies benefit from each other ? The benefit for COST 724 is obvious: these three colleagues irrigated our action with their dynamism. What about the other way round ?

In June 2006, a short term scientific mission was dedicated to further arrangements for the European Space Weather Portal and the modification-implementation of current models in the field of Space Physics. The implementation was carried out together with the model providers so they could understand better how exactly it works and how they can modify the code themselves. After the implementation, a working model access server and an interface were available so the model providers had a test environment. Taking the advantage of flexibility of computer tools, it was decided to implement several other models concerning the topics of COST724. This was made through public laboratory facilities (BIRA, Belgium). In April 2007, a second STSM followed with twenty experts from nine countries:, with the aim of using the facility developed in the first STSM to give access to neutron monitor data. In the words of the organisers themselves, this workshop was a historical occasion in the sense that for the first time neutron monitor station representatives and scientists were gathered for a dedicated meeting on standardisation and collaboration to establish a common platform for data exchange and for future developments.
The main outcomes of the workshop were a concrete plan for a set of action items on the data providers to send extensive descriptions of their instrumentation, data content and processing. On top of it, a database was foreseen. As DH Consultancy is already providing data base services, it could become a partner for the COST 724 (and related) service activities.
Space IT GmbH had been created before the start of the COST 724 action. At that time, its purpose was for Dr. Desorgher to be able to continue the works that he was doing at the University of Bern on a private basis. During the COST724 action Dr. Desorgher was responsible

for the development of a code that computes the ionisation of the Earth's atmosphere by cosmic rays. During a STSM we managed to gather in Bern all the colleagues that had created such cosmic radiation codes in Europe. To our surprise, this had never been made before.The involvement of Dr. Desorgher in the COST724 action had a positive influence on the development of SpaceIT. During the different COST meetings that he did attend, he could initiate or strengthen contacts with different collaborators for future projects and more specially with DH Consultancy. But in order to better understand what COST offered to Space IT, let us listen to L. Desorgher himslef: "COST allowed me to realize more strongly that there is a need for companies such as mine in space weather in space radiation activities. This motivates me quite a while ! It is also very motivating to meet colleagues such as me who, coming from academic institutes, create small size companies. But the most important for me is that COST allowed me to take contacts, and to learn more on the future european prospectives.

The case of the 1A company is quite different. This company had been created two years before the action started. A difficult question arose: should the European Space Weather Web Portal be developed under the umbrella of this company? This was not possible because most of the data provided in the portal were from public institutes, and 1A would not have been allowed to make money out of them. But an other way of collaborating soon raised up. Dr. Jansen was already known for his internationally recognized outreach activities. He had created a CDrom devoted to space weather, had participated to creating a dance show on the solar storms. In the case of the CD rom, Dr. Jansen did benefit from the international aspect of our action (26 countries) to have it translated in different languages. Along with other colleagues, Dr. Jansen decided to run for a FP7 funding on a space weather outreach program (described in this book). He needed of course to have a good knowledge of the current outreach activities in different countries. The first STSM of the action was devoted to this task. In December 2004, Dr. Frank Jansen visited the Finnish Meteorological Institute (FMI) / Space Research Unit in Helsinki in order to write a paper about space weather and insurance aspects, to study the "Aurora Now" system developed by the FMI for touristic purposes at Finnish Lapland hotels and to visit the National Finnish Science Centre Heureka in Vantaa nearby Helsinki.
Dr. Jansen was then given the task to develop outreach activities for our action, which was the topics of his working package. He could soon participate to a proposal to the European Commission. It was not easy to get funded. In spite of our support, the first application was rejected. We therefore decided to write as many letters as possible and to support 1A in all our meetings. This was certainly a strong help, and Dr. Jansen and his 1A company were finally funded for this outreach activity.
It is obvious that these activities did benefit to all partners, COST 724 and the three companies described above. It shows that public and private activities are not contradictory when they are thought for a mutual benefit.

Education: discussion and case studies

Yurdanur Tulunay

Middle East Technical University, 06531, Ankara, Turkey ytulunay@ae.metu.edu.tr

Summary. Since 1980 a paradigm emerged in geosciences, which is called "Earth System Science (ESS)" or "Earth System (ES)". "There is no process or phenomenon within the ES that occurs in complete isolation from other elements of the system"(Johnson et al., 2000). As ESS emerged a framework for addressing the scientific dimensions of global change, the COST 724 Action has initiated the scientific collaboration towards education between scientists of the universities, governmental and industrial bodies in Europe, concerning the Space Weather education. The university offers the unique opportunity to develop knowledge and understanding about Space Weather that can then be applied as graduates enter the main stream society. In short, it is expected that the initiative taken by the COST 724 Action would create a university based cooperative effort in Space Weather under the ESS curriculum development firmly.

Since 1980 a paradigm emerged in geosciences, which is called "Earth System Science (ESS)" or "Earth System (ES)". "There is no process or phenomenon within the ES that occurs in complete isolation from other elements of the system. While this interconnectedness is elegant and satisfying philosophically, it presents an enormous challenge to researchers attempting to quantify various elements, states and processes within the system" (Johnson et al., 2000). Figure 1 illustrates the concept of a pyramidal structure relating ESS and global change education in the larger interest of society. Broadly based and orderly higher-level responses address the goals and constraints of global sustain ability. Future of our planet and destiny of humankind are dependent upon the interdisciplinary pyramid of ES as illustrated by Johnson et al. (2000) in their paper.

In 1991, NASA and the Universities Space Research Association (USRA) initiated a program to introduce college undergraduates to the interdisciplinary challenges of an emerging Earth system science approach to understanding our planet. Earth system science views the Earth as a synergistic physical system of interrelated phenomena, processes and cycles which remain largely unexplored in traditional disciplinary Earth science course offerings. The ongoing Cooperative University-based Program for Earth System Science Education (ESSE) challenges colleges and universities to develop and offer classroom courses which examine the Earth as a system and to share their progress, course materials and learning modules. Concurrent with the development of the ESSE community and its shared learning resources has been the exponential growth of the Internet and its suite of communication tools, which

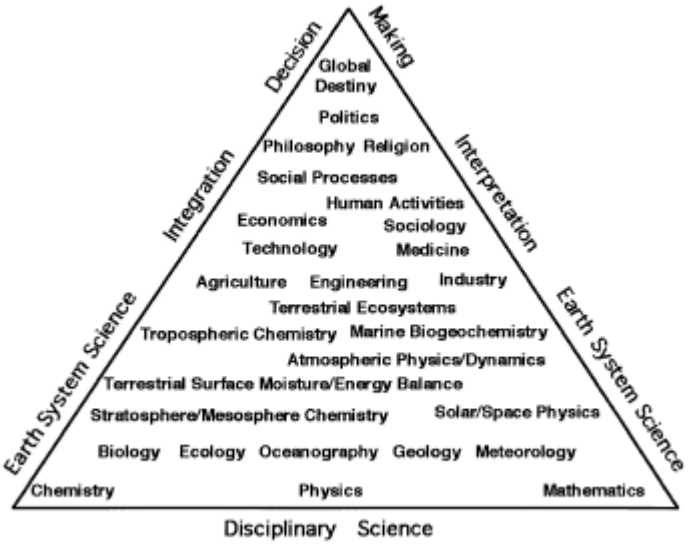

Fig. 1. "Conceptually the pyramidal structure illustrates relation of Earth System Science and global change education to larger interests of society. Broadly based higher-level education in Earth System Science and global change provides foundation for societal activities and response that addresses goals and constraints of global sustainability. Development of Earth System Science and global change curriculum requires joining of basic and applied disciplinary interests to create this foundation." (Johnson et al., 2000)

are central resources for the ESSE Program. The Internet has enabled the rapid deployment of information and resources through shared repositories of learning materials and general Earth system science knowledge, all of which serve to create and maintain an active informed education community (Johnson et al., 2000).

In the present day society, there is a vital need for setting up education and outreach activities in the Space Weather field for creating a healthy environment for the proper development of Space Weather markets along with the fundamental and applied research activities. The Space Weather, concretely, must provide value added services for the end user that has to be the driving motivation. Last, but not the least, a portal financial support for the Space Weather service providers is the formation of the competent human resources (Crosby et al., 2006; Siscoe G., 2000; Tulunay Y. and Tulunay E., 2005). Sufficient financial support for the Space Weather service providers is required for the information of competent teaching (scientific and technical personnel) and, hence, for research and education in the subject.

"In Europe, as in North America and Japan, several private Space Weather initiatives have been launched in recent years, but daunting constraints-including the high cost of space-based monitoring and the vast complexity of space weather systems-make it imperative that large agencies coordinate the actions of researchers, data providers, users, and military organiza-

tions. In Europe, this role has begun to be filled by the COST 724 Action" (Lilensten et al., 2004).

As ESS emerged a framework for addressing the scientific dimensions of global change, the COST 724 Action has initiated the scientific collaboration towards education between scientists of the universities, governmental and industrial bodies in Europe, concerning the Space Weather education. The university offers the unique opportunity to develop knowledge and understanding about Space Weather that can then be applied as graduates enter the main stream society. In short, it is expected that the initiative taken by the COST 724 Action would create a university based cooperative effort in Space Weather under the ESS curriculum development firmly.

The basic users of a Space Weather Education Program may be summarized as in the following areas: communications, satellite operations, power grids, manned spaceflight, navigation, etc. Scientific and technological developments are achieved as the results of research, observations, models and education. Forecasting and warning services use the technology developed and disseminates the results to the basic users mentioned above. Comments of users are returned back to the education program via feedback mechanisms. Thus, the quality and efficiency of the education system are sustained at satisfactory levels.

The following case studies illustrate the beginning of such a task towards a coherent and concrete unifying Space Weather education for the science and engineering curricula in Europe:

- Case 1: Books

1. Space Weather, Research towards Applications in Europe Series, Lilensten, J. (Ed.), Astrophysics and Space Science Library, Vol. 344, 2007, XII, 332 p., ISBN: 978-1-4020-5445-7
   This book shows the state of the art in Europe on a very new discipline, Space Weather. This discipline lies at the edge between science and industry.
2. Space Weather, Environment and Societies, Lilensten, Jean, Bornarel, Jean, 2006, XIII, 242 p., ISBN: 978-1-4020-4331-4
   Our planet exists within a space environment affected by constantly changing solar atmosphere producing cosmic particles and electromagnetic waves. This "space weather" profoundly influences the performance of our technology because we primarily use two means for transmitting information and energy; namely, electromagnetic waves and electricity.
   (Retrieved from http://www.springer.com/, 2007)
3. "From the Sun - Auroras, Magnetic Storms, Solar Flares", Cosmic Rays, S.T. Suees and B.T. Tsurutani eds., American Geophysical Union, Washington, DC, USA, ISBN 0-87590-292-8, 1998
   This book is appropriate for high school graduates and scientists unfamiliar with space physics.
4. "Space Weather - Physics and Effects", Eds. Volker Bothmer and Ioannis A. Daglis, Praxis Publishing Ltd, Chichester, UK, 2007, ISBN 3-540-23907-3
   This is a very recent comprehensive book on the physics of space weather and on space

weather impacts on human technology (for readers with some scientific and technical background)

- Case 2: Formal Education
  Formal education on the Near Earth Space at the Middle East Technical University, Department of Aerospace Engineering in Ankara has been offering some courses towards the Near Earth Space medium since 1990, that is,
  AE453 "Introduction to Atmospheric Physics",
  AE454 "Introduction to Atmospheric Physics II",
  AE551 "Introduction to Space Sciences",
  AE552 "Selected Topics on Space Sciences",
  AE552 "Applied Orbital Mechanics".
  (for more detailed information, please visit http://www.ae.metu.edu.tr).
  With the COST 724 Action initiative, the syllabi of these courses have been re-interpreted under the philosophy of the ESS with Space Weather flavour.
  In parallel to the course work with emphasize on Space Weather approach, the subjects of the graduate theses have been directed towards the objectives of the COST 724 at the METU Department of Aerospace Engineering.
- Case 3: Summer School The State Planning Organization (DPT) and Turkish Scientific and Technical Research Council (TÜBİTAK) have been issuing strategic programs periodically to list the priority areas in research and technical developments to promote activities in selected disciplines. Space Research and related technologies are two of the items that have systematically been short listed. However, initiatives in the Near Earth Space Science, or ESS, and technologies had not yet become part of the system in practice until the beginning of the COST 724 Action. Under the spirit of the COST 724 Action, there was a graduate course delivered in Turkey emphasizing "Solar-Terrestrial Physics and Space Weather" (Crosby et. al., 2006). This Feza Gürsey Institute graduate course was an initiative to promote the Near-Earth Space Physics in relation to the Space Weather principles in Turkey the first time.
  The enthusiasm of the students during this course to learn about this subject matter has shown that there is a need for the next generation of scientists and engineers to appreciate the applicability of the Space Weather on the technology and life on planet Earth that the world relies upon in the third millennium.

References

Crosby N. B., M. J. Rycroft, Y. Tulunay, Overview of a Graduate Course Delivered in Turkey, Emphasizing Solar Terrestrial Physics and Space Weather, Surveys in Geophysics, Springer Netherlands, DOI: 10.1007/s10712-005-6204-3, **27 /3**, pp. 319-364 (2006)

Johnson D. R., M. Ruzek, M. Kalb, Earth System Science and the Internet, Computers & Geosciences, **26**, 669-676 (2000)

Lilensten J., T. Clark, A. Belehaki, Europe's First Space Weather Think Tank, Space Weather, **2**, S04001, doi:10.1029/2003SW000021 (2004)

NASA, Earth System Science Advisory Committee Earth System Science: a closer view, NASA, Washington, DC. 208. (1988)

Siscoe, G., The space-weather enterprise: past, present, and future, J. Atm & Solar-Terrestrial Phys, **62**, pp. 1223-1232 (2000)

Tulunay Y., E. Tulunay, A Case Study of Curriculum Development Related to the Space Environment and Emerging Space Weather Markets, Advances in Geosciences, **3**, pp. 29-33 (2005)

The Planeterrella, an outreach space weather experiment in COST 724

Jean Lilensten[1] and Mauro Messerotti[2]

[1] Laboratoire de Planetologie de Grenoble, Observatoire des Sciences de l Univers de Grenoble, CNRS-UJF, France jean.lilensten@obs.ujf-grenoble.fr
[2] INAF-Trieste Astronomical Observatory, Basovizza Observing Station, Loc. Basovizza n. 302, 34012 Trieste, Italy messerotti@oats.inaf.it

1 Introduction

We present here a plasma space weather experiment which makes it possible to simulate most of the phenomena leading to the formation of polar lights. It consists in shooting electrons on a magnetized sphere placed in a vacuum chamber. This experiment, inspired by the Terrella of K. Birkeland built at the turn of 19th century, allows the visualization of very many geophysical and astrophysical situations. Although delicate, it is feasible at undergraduate level

2 The Terrella: Kristian Birkeland's historical experiment

In 1733, in the first treatise on the aurora borealis (or polar lights), Jean-Jacques Dortous de Mairan describes in an intuitive but visionary way the bond between the aurorae and the Sun: *It is certain, as we shall demonstrate from a great number of observations which are not ambiguous, that the atmosphere of the Sun [. . .] reaches sometimes the terrestrial Orbit. At that time the matter which composes this atmosphere suddenly meets the higher parts of our air, below the limits where universal gravity, whatever the cause, starts to act with more force towards the center of the Earth than towards the Sun, falls into the Earth's atmosphere to more or less depth, according to whether specific gravity is more or less large, with regards to the layers of air which it crosses, or which it survives*. A few years later, in 1747, the Swedish astronomer Anders Celsius and his assistant Olof Hiorter discover that the magnetic field is an essential ingredient of the physics of aurorae borealis. During the 19th century, geographers establish that the polar lights occur preferentially around the magnetic poles, drawing what will be called the "auroral ovals". Parallel works in electromagnetism also result in postulating the existence of charged particles, the electrons, soon discovered by Thomson in 1901. These charged particles were at that time given the name "cathode rays".
At the end of the 19th century, the Norwegian physicist Kristian Birkeland, a brilliant experimenter, had the original idea to shoot cathode rays on a magnetized sphere suspended in

a vacuum chamber. This sphere was connected to the anode of the power generator. Birkeland imagined the cathode to represent the Sun with the cathode rays simulating the solar atmosphere (for which Parker will coin the term "solar wind" in 1958), and the suspended magnetized sphere representing the Earth. He built up to fourteen different versions of his experiment during the course of his life. This experiment is called "Terrella". It made it possible to make the first laboratory demonstration of the mechanism of the polar lights by reconstructing and visualizing the auroral ovals. The notes of Birkeland are not very precise, but his experiment was recently rebuilt at the University of Tromsø (Norway) by the engineer Terje Bruntdland starting from the original experiment. This new experiment determined the necessary vacuum conditions to be about a few pascals, while the electric tension should be of a few hundred volts.
By reversing the polarities of his experiment between the sphere and the dusk, Birkeland was also the first to visualize the ring currents. The radiation belts associated to these currents were later discovered in 1958 during the first US space flights by James Van Allen, a result which earned him the Crafoord prize in 1989. Unfortunately, Birkeland gave a bad interpretation to his observation, comparing the rings he saw to Saturn's rings.

3 A new experiment: The Planeterrella

In the frame of the COST 724 action, we started by building a Terrella experiment for the space weather school that we organized at the Abdus Salam International Centre for Theoretical Physics (ICTP) along with the US National Science Foundation. This was a very successful experiment, reproducing all feature explored by Birkeland one century ago. Figure 1 shows the Terrella experiment with the students gathered around. This experiment was developed by the technical staff of ICTP and INAF-Trieste Astronomical Observatory.

Fig. 1. The ICTP Terrella experiment (credit: Gosain Sanjay, space weather school student).

Based on the past experience, we realized that Birkeland had done something triky, and we reshaped his experiment in order to build a totally new one. Instead of Birkeland's hanging globe, which made his experimental setting very difficult to modify, we thought of a new way.

In the experimental setting proposed here, the sphere is put on a base which one can freely move. It can be adjusted in height, such as the mount supporting a parasol. With this configuration, the magnetic axis can be pointed in any desired direction. The electrode is attached to a wheel inserted into a notch, embedded in a bent plastic structure. Thus, it can be moved at will and positioned in all directions around its axis. In the Terrella configuration, it is not possible to have two spheres, as they attract each other because of the strong magnetic fields. In our new experiment, one can multiply the number of spheres and thus look at interactions in multiple configurations.
We use a vacuum chamber of 50 liters with a diameter of 50 cm. It is built out of plexiglas. Plexiglas is opaque to UV radiations and it is cheaper than glass. As a corollary, one cannot make a spectral analysis in UV from the outside of the vacuum chamber; the spectrometer should be inserted inside. The two spheres have a diameter respectively of 10 and 5 cm. They are manufactured in a non-magnetic metal (aluminium). Birkeland used copper. The vacuum must be about 10 Pa, and can thus be obtained with a primary pump. The tension is higher than approximately 500 V for an intensity of an order of 0.1 to 1 mA. Thereafter, we will take a value of 1000 V and 0.1 mA. The emitted electrons have then an energy of 1 keV, or 1.609 ? 10-16 J. At the moment, we use rare earth permanent magnets in the spheres. The intensity is approximately 0.5 T at the surface of the magnets, which have a size of a half centimeter. Their positioning is done simply by using a base of modeling clay inside the spheres.

4 Observations

The electrons emitted by the cathode collide with the ambient gas, creating ions and molecules in excited states. Some desexcitations lead to visible light emissions, which we will describe in the part devoted to the physics of the phenomenon. The light is more intense in the areas of greater electron density. It is this light which was observed by Birkeland, and which is visible on the images which follow.

4.1 Birkeland's observation reproduced

All the configurations observed by Birkeland are reproducible in this new configuration. In figure 2, one sees the two auroral ovals. Here, the sphere is the anode and the electrode is the cathode.
In Figure 3, the setting is reversed and the electrode becomes the anode while the small sphere acts as the cathode. The electrons are emitted in a plane perpendicular to both the magnetic and electric fields, creating the radiation belt in the shape of a ring. This ring can also be observed in the configuration where the tube is cathode, but is less luminous than the auroral ovals; therefore this ring is difficult to see and photograph. It is the ring that Birkeland had taken for Saturn's rings.
What does this new experiment offer in terms of additional possibilities?

4.2 A better visualization of the phenomena

Rather than using the electrode duct as an electron gun, one can now use one sphere as the cathode (the star) and another as the anode (the planet). This is shown in figure 4. In the

Fig. 2. Visualisation of the auroral ovals (credit: C. Simon, LPG/ESTEC)

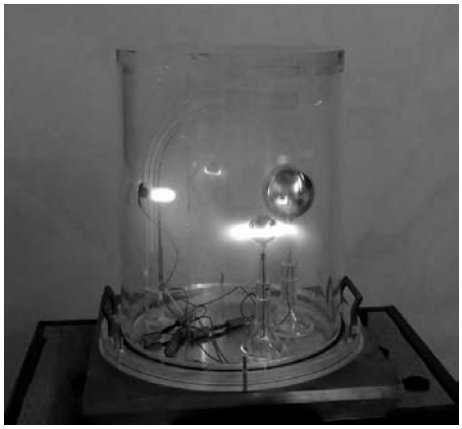

Fig. 3. Visualisation of the radiation belt (credit: C. Simon, LPG/ESTEC)

foreground, the auroral ovals are formed on a magnetized planet. In the background, the star-cathode is also magnetized. Here one sees the coronal halo with the coronal holes around the poles which are comparable with those observed on the Sun. This is independant of the presence of the magnetized planet and may be observed anyway. It is however necessary to take care not to push the analogy too far: the coronal holes are of course related to the solar magnetic field, but also to the dynamics of the star.

4.3 Planets with tilted magnetic axes

The fact that the magnetic and geographic poles of Saturn are aligned represent a curiosity in the Solar system: at the moment, there is no aggreement on the process to create a planetary magnetic field, and nothing implies such an alignement. The Earth and Jupiter have magnetic declinations of about 10 degrees. It is this configuration that Birkeland always privileged. The simple fact of being able to position the spheres as needed and to allow the electrode to move makes it very easy the incline the magnetic field inside the sphere (see technical details in the third part). One can thus simulate the configurations of Neptune and Uranus, which magnetic angles are about 50 degrees. The geographical North Pole of Uranus points towards the Sun,

Fig. 4. Interaction between a magnetized star and a magnetized planet (credit: C. Simon, LPG/ESTEC)

so that its magnetic axis is almost directed like that of the Earth with respect to the solar wind. The Voyager probe has already detected a night aurora on Uranus, close to its magnetic pole. The angle of inclination of the axis of rotation of Neptune on the ecliptic is 29 degrees, with an angle of 45 degrees between the magnetic and geographical axes. Thus the solar wind enters directly into the polar cap.

4.4 Interaction between a magnetized planet and a magnetized satellite

On December 12, 1996, Nature published the discovery of Dr Kivelson and his colleagues of the magnetic field of Ganymede, satellite of Jupiter . The magnetic fields of Io and Europa were discovered shortly after. The configuration with several spheres makes it possible to quantitatively approach the auroral interactions of these bodies. It goes without saying that scaling problems can arise, and that it is therefore necessary to be very careful with the interpretation of the observations. In Figure 5, the electrons are emitted by the electrode duct (on the right side in the image), and the two spheres are connected to the anode. The small sphere, with a stronger magnet, represents Jupiter with a significant current belt and auroral phenomena at the poles while the large sphere represents a magnetized satellite.

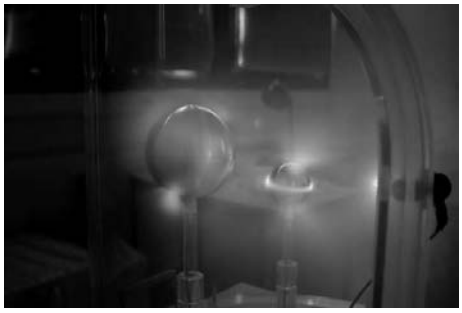

Fig. 5. A magnetized planet with a magnetized satellite (credit: C. Simon, LPG/ESTEC).

4.5 Interaction between a magnetized exoplanet and a near magnetized star

More than a hundred exoplanets have been discovered since 1995 (http://exoplanet.eu/catalog.php). Because of the methods of detection most are "Jupiter-like" planets in term of size, with very short distances from their star (for example 0.04 astronomical units for HD179949b). Nothing excludes that these planets, like their star, can be magnetized. In this case, the short distance between them implies direct magnetic interactions, their fields recombining without the generation of a magnetosphere. This case can also be approached in a qualitative way in the current configuration of the experiment.

4.6 The polar caps

The physical link between the radiation belts and the auroral ovals is represented by the polar caps. Inside the caps the Earth's magnetic field opens to the plasma mantle and to space. Although difficult to photograph, the caps can nevertheless be seen in the current experiment.

4.7 Binary systems

Since each sphere and the electrode are connected to an electric plug, we can also easily simulate the electromagnetic interaction of two-star systems (binary stars) with planets in all magnetic configurations.

4.8 The Planeterrella

The configurations of the experiment suggested here are very numerous. It is now possible to simulate the majority of the cases encountered in planetology. This is why we named this experiment "Planeterrella".

5 Conclusion

This experiment is a little delicate to implement, but could be performed at a highschool level with materials from the school. The great difficulty comes from the manufacture of the spheres. Those must have a good surface quality, because any irregularity can deviate the electric field. We used the end balls of a staircase ramp with varied success. The cheapest and easiest way to manufacture the spheres is to order them from a company working in metallurgy. This experiment allows developing a very high level physics involving plasma physics, quantum mechanics, radiation physics... This is developed elsewhere Lilensten et al. (2007) and is not the topics of this paper. This new Planeterrella experiment, although largely inspired from the Birkeland's Terrella, would not have been thought without the COST 724 frame and its European Space Weather school. Starting from scratch, the overall cost is high (approximately 20.000 euros). The design and concept are obviously a significant part of the cost of the project. This is why the experimental designs we conceived are freely available on request for cultural uses and teaching for non profit, with the condition of quoting the CNRS and the

designer of this experiment (J. Lilensten). Several programs are under study. In the first one, with the support of UNESCO, we aim at building Planeterrellas in developing countries in order to reach a unit cost lower than 1000 euros. The goal is to allow the scientific universities in these countries to acquire a model for practical work of plasma physics. The second program consists in the spreading of this experiment in high schools and universities in France.

Acknowledgements We thank CNRS-SERAS group for their assistance in the engineering and design, and O. Brissaud for his assistance in the assembly of the experiment. We thank G. Gronoff for his enthusiasm and assistance. For profit-making applications, the CNRS Alps delegation is the only partner entitled to negotiate the terms of collaboration.

References

Jean-Jacques Dortous de Mairan, in Traité historique et physique de l'aurore boréale,1733.

Lilensten J., Barthelemy M., Simon C. and Jeanjeacquot P., The Planeterrella, a pedagogic experiment in planetology and plasma physics, submitted to *Amer. Journ. Phys., 2007.*

Collaboration among COST actions. Ionosphere and space weather

J. Lilensten[1], B. Zolesi[2], A. Belehaki[3], I. Stanislawska[4], and L. Perrone[2]

[1] Laboratoire de Planetologie de Grenoble, OSUG-CNRS, France
jean.lilensten@obs.ujf-grenoble.fr
[2] Istituto Nazionale di Geofisica e Vulcanologia Via di Vigna Murata, 605 00143 Roma Italy
zolesi@ingv.it
[3] Ionospheric Group, Institute for Space Applications and Remote Sensing, National Observatory of Athens, Metaxa and Vas. Pavlou, 15236 Palaia Penteli, Greece belehaki@space.noa.gr
[4] Polish Academy of Sciences Space research center Bartycka 18 A 00 716 Warsaw Poland
stanis@cbk.waw.pl

Summary. In this paper, we describe the collaboration between two COST action: COST 724 devoted to space weather and COST 296 (formerly COST 271) devoted to the study of the ionosphere and its impact on communication and positionning. Several colleagues work in the two actions. This resulted in an important input provided by the COST 296 action to COST 724 based on the ionospheric models developed during the last COST actions(COST 238, 251, 271 and 296) for space weather applications.

1 Introduction

The objectives of the COST 724 action are to develop within a European framework the science underpinning space weather applications, as well as exploring methods for providing a comprehensive range of space weather services to a variety of users, based on modelling and monitoring of the Sun-Earth system.
The objectives of the COST 296 action, continuing the studies of COST 238, COST 251 and COST 271, are to develop an increased knowledge of the effects imposed by the ionosphere on practical radio systems, and for the development and implementation of techniques to mitigate the deleterious effects of the ionosphere on such systems.
The two actions oughted to work complementary in order to avoid duplication of efforts. Indeed, the ionosphere is a major actor of space weather studies which have applications on positionning and radiocommunications. This is why several colleagues belong to the two actions, COST 724 and COST 296. Thanks to their enthusiasm and will to collaborate, COST 296 prepared a list of ionospheric models to be included in the space weather portal that COST 724 had created. In this paper, we will shortly describe this list. Then, we will describe a pan-European ionospheric server (DIAS) that, although an idependant European project, beneficiated to the two actions.

2 Report on ionospheric models developed during the last COST actions in ionospheric science

There are different approaches to describe the ionosphere for space weather purposes:

- Based on the goals: long term prediction, forecasting, nowcating or specific phenomena modeling
- Based on the parameter that is being described: electron density profile (*Ne*), total electron content (*TEC*), the maximum value of the electron density in the F region and its associated plasma frequency(*foF2*), or the maximum useable frequency (*MUF*) for short wave communications
- Finally, they can also be classified versus their approach: they may use statitics, physics, fitted laws or a mixture of them.

Fourty ionospheric models have been presented. A brief description of some selected models is given in the table. All the references about the models in Tab. 1 are given in Perrone et al. The long term prediction chapter includes the analysis of nine different models; nine models deal with ionospheric forecasting and nine with nowcasting; nine are able to provide electron density profiles and /or total electron content. Finally, eight models are more specific, dealing for example with the F1 region, or with scintillations. Those are not less important though for dedicated applications.
The modeling was carried out by collaborative groups, where individuals from different countries worked together to achieve a common goal. From this huge amount of work, it was realized that Europe is satisfactory equiped for ionospheric space weather applications even if further developments are always requested. The skill sits here. Coordination is a major requirement for future applications in space weather.

3 DIAS

DIAS is a pan-European distributed information server providing information on the ionospheric conditions over Europe (http://www.iono.noa.gr/DIAS/Default.htm). The action officially finished in May 2006 but is still maintained and very active since then. The system is capable of supporting the acquisition, elaboration, evaluation, dissemination and archiving of the ionospheric observations currently obtained from seven European ionospheric stations operating in Athens, Rome, Juliusruh, Chilton, Ebre, Pruhonice, and Lycksele, serving the development of value added products and services which concern: i) the ionospheric specification in real time, at single-station locations (ionograms, f-plots and electron density profiles) and whole Europe (daily plots of the effective sunspot number and ionospheric nowcasting maps of foF2, M(3000)F2, MUF and electron density), ii) short-term ionospheric forecasting up to 24h ahead for foF2 at single-station locations and for the whole area in terms of European maps and iii) long-term ionospheric prediction maps of foF2, M(3000)F2 and MUF for the European area. More details on the system operation can be found in Belehaki et al., (2005; 2006; 2007).
DIAS products and services are designed to support the continuous and reliable performance of applications that use radio propagation and are affected by space weather. In particular

ionospheric disturbances affect mainly the following systems: the VLF-LF Communication and Navigation, HF Communications, HF Broadcasting, OTH Radar Surveillance, Satellite Communication, Satellite Navigation, Spaced-based Radar and Imaging. Considering the range of applications influenced by ionospheric effects, the community of DIAS potential users is quite extensive. The main users of DIAS are the Defense Industry, the Aviation Industry (both civil and military), the Civil HF Broadcast Operators, the Upper Atmosphere Researchers and Amateur Radio Operators

DIAS has important applications both in space weather and in the ionosphere. This is therefore no surprise that this project has irrigated our two actions: data and code contributors have been suppoorted by the COST actions and in return, the efforts of COST contributors could have a direct application thanks to the DIAS server. The DIAS chair is also vice-chair of the COST 724 action.

Model and Reference	Description
The Empirical Orthogonal Functions (EOF) method (Dvinskikh, 1988; Dvinskikh and Naiedova, 1989; 1991; Singer and Dvinskikh, 1991)	Global and regional long-term mapping of ionospheric characteristics.
KGRID (Bradley and Dick, 1993)	Long term prediction of ionospheric characteristics over a limited geographic area using krigging technique.
LINLAT (Bradley and Dick, 1993)	Linear latitude and common diurnal variation procedure LINLAT provides estimates of monthly median foF2 and M(3000)F2 within the PRIME area as a function of geographic latitude and longitude, month and UT.
MQMF2R (Mikhailov and Mikhailov, 1993; 1995 ; Mikhailov and Teryokhin, 1992)	The mu1tiquadric (MQ) method was first developed for world-wide monthly median mapping but has subsequently been adapted for regional mapping and for instantaneous mapping. Then the MQMF2R was the COST 251 method for month1y median foF2, based on Sing1e Station Models (SSM) and on the multiquadric method for spatial approximation.
PASHA (Predicted Adjusted Spherical Cap Harmonic Analysis) (De Franceschi and De Santis, 1993a, 1993b; Bradley, 1995)	PASHA was developed during the Cost 238 action . This model is based on the Spherical Cap Harmonic Analysis (SCHA) that is a technique for modelling the geomagnetic field over a limited region of the Earth's globe.
SIRM (Simplified Ionospheric Regional Model) (Zolesi et al., 1993, 1996)	The Improved SIRM is a regional ionospheric model of the standard vertical incidence ionospheric characteristics, evolved from the original SIRM developed under the EU COST 238 project, and applied to a more extended area taking into account the consequences of high latitude regions.
SWILM (Space Weighted Ionospheric Local Model) (Hanbaba, 1999; De Franceschi et al., 2000)	SWILM was introduced during the COST 251 action for the regional long-term prediction of foF2 and M3000(F2) over the European area.
UNDIV (Bradley, 1995)	UNDIV a method for the long term mapping of the monthly median ionospheric chararcteristics foF2 and M(3000)F2 was first presented in the COST238 action and then was developed during the COST251 action.
Autocovariance method (Stanislawska and Zbyszynski, 2001; 2002)	The autocovariance method was developed during the COST271 action. It is a statistical approach for single-station forecasting of the critical frequency of the F2 layer (foF2).

CORLPREV (Muhtarov and Kutiev 1998a; 1998b; 1999)	CORLPREV was developed during the COST 251 action. The model is based on the auto-correlation procedure applied for the short-term prediction of ionospheric characteristics.
DERA (Hanbaba, R. and Zolesi B., 2000)	The DERA Ionospheric Forecasting Service (IFS) neural network model can provide predictions of the hourly variation of the ionospheric parameter foF2 from l to 24 hours ahead. However, the operational package of the model has been designed in such a way that it would be a simple matter to incorporate predictive models for additional geophysical parameters into the same framework.
Empirical modeling of global foF2 ionospheric response to geomagnetic activity Kutiev, I. and P. Muhtarov (2003)	The empirical model was developed during the COST 271 action. This empirical model describes the variations of F2 region ionization induced by geomagnetic activity .
Multiregression method (Mikhailov et al. 1999; Marin et al., 2000)	The Multiregression method was developed during the COST 251 action. This method is based on a multi-regression of deviation of hourly dev(foF2) from foF2 running median with the previous observations and Ap index
METU-NN foF2 Forecast model (Tulunay, 1991; Altinay et al., 1997; Tulunay et al., 2000; Tulunay et al., 2001).	The METU-NN foF2 Forecast Model is employed to forecast the ionospheric foF2 values up to 24-hour in advance. It is a data-driven approach applying the Neural Network (NN) based modelling.
STIF (Short-Term Ionospheric Forecasting) (Cander, 2003; Muhtarov and Kutiev 1998)	STIF an operational tool for the European region based on continuous monitoring of the ionosphere has been developed and is available on the World Wide Web for interactive use (http://www.chilbolton.rl.ac.uk/weather/tec.htm). It provides forecasts for up to 24 hours ahead and archive measurement maps of the critical frequency foF2, the Maximum Usable Frequency for a 3000 km range MUF(3000)F2, total electron content (TEC) and FOT (Frequency of Optimum Traffic) for the area of interest at an each UT hour.
IMASHA (Instantaneous Mapping Adjusted Spherical Cap Harmonic Analysis) (Bradley, 1995)	IMASHA was developed during the COST 238 action. IMASHA is the same method of adjusted spherical cap harmonic analysis (ASHA) developed for long-term ionospheric mapping and app1ied to the instantaneous mapping of the hourly values of ionospheric characteristics over a restricted area .
ISWIRM (Instantaneous Space Weighted Ionospheric Regional Model) (De Franceschi et al., 2000; Perrone et al., 2002; Stamper et al., 2004; Pietrella and Perrone, 2005)	ISWIRM a regional model for the now-casting of the critical frequency of the F2 layer (foF2) over Europe has been developed during the COST271 action. Inside this region the hourly values of foF2 are obtained, correcting the monthly medians values of foF2 predicted by the space-weighted ionospheric local model (SWILM) on the basis of hourly observations of foF2 coming from four reference stations (Rome, Chilton, Lycksele, and Loparskaya or Sodankyla).
K2 (Kriging 2) (Stanislawska et al. 1995, 1996)	K2 was developed during the COST 238 action as an alternative Kriging procedure. In particular, it was introduced a separate latitude scaling factor which allows for differences in NS and EW correlation distances.
KGRID (Bradley and Dick, 1993b; Samardjiev et al, 1993a).	KGRID, a computer-based procedure for instantaneous ionospheric mapping developed by M I Dick of RAL for implementation with the NEW ionospheric measurement data set (Bradley and Dick, 1993b), is an implementation of the method of Kriging (Samardjiev et al, 1993a).
KIM/KIMS (Bradley et al, 1994a; 1994c, 1995a).	Two specific instantaneous mapping procedures have been developed known as KIM, which is based on Kriging alone, and KIMS in which synthetic 'screen-point' values are added in remote areas to constrain mappings to physically realistic figures, rather than to let these be determined by the mathematical expressions which are optimised to the measurement data from elsewhere.
MQMF2-IM (MultiQuadratic method with ionospheric index MF2 for Istantaneous Mapping) (Mikhailov et al 1994, 1995; Hanbaba 1999; Hanbaba and Zolesi, 2000).	MQMF2-IM was developed during the COST 238(PRIME) and COST251 Action. The method MQMF2-IM was recommended for instantaneous mapping within the PRIME area. MQMF2-IM for foF2 and M(3000)F2 uses the following: (1) Single Station Model(SSM) for foF2 and M(3000)F2, (2) screen points inside the area, (3) effective hourly MF2eff and R12eff indexes, (4) buffer zone, (5) main ionospheric through model and (6) multiquadratic method for spatial approximation

PLES (Poland PL, Spain ES) (Stanslawska et al. 1999, 2000; Hanbaba 1999; Hanbaba and Zolesi, 2000)	PLES was developed during COST251 action . PLES for instantaneous values of foF2 and M(3000)F2, combines monthly median maps of ionospheric characteristics and a set of screen points-measurements for a single moment of time of different origin using two interpolation methods modified for ionospheric purposes: Kriging and “fitting”.
SAIM (Eliseyev and Besprozvannaya, 1998; Hanbaba, 1999)	SAIM was developed during the COST 251 action. The objective was to provide maps of foF2 even in extreme situations when foF2 observations are not available or available only from 1-3 ionosondes, using the effective Kp-index.
SIRMUP SIRM UPdating method (Zolesi et al., 2004)	SIRMUP is based on the idea that real time values of foF2 at one location can be determined from the SIRM model by using an effective sunspot number, Reff, instead of the 12-month smoothed sunspot number, R12. The final output from the SIRMUP now-casting method are maps of foF2 and M(3000)F2 covering the European area from 5oW to 40oE in longitude and 34oN to 60oN in latitude.
NeQuick (Di Giovanni and Radicella, 1990; Radicella and Zhang, 1995; Leitinger et al., 2001)	NeQuick is a quick-run ionospheric electron density model designed for transionospheric propagation applications. It has been developed at the Aeronomy and Radiopropagation Laboratory of The Abdus Salam International Centre for Theoretical Physics (ICTP), Trieste, Italy, and at the Institute for Geophysics, Astrophysics and Meteorology (IGAM) of the University of Graz, Austria. To describe the electron density of the ionosphere above 100 km and up to the peak of the F2 layer, the NeQuick uses a modified DGR profile formulation, which includes five semi-Epstein layers with modeled thickness parameters.
NTCM (Neustrelitz TEC Content Model) (Jakowski, 1998, 1999)	The regional TEC model NTCM was developed during the COST 251 action. Two versions of the model were developed and applied to map construction: NTCM 1 algorithm includes fundamental ionospheric variations and solar activity dependence. NTCM 2 version compared with NTCM l includes additionally a geomagnetic latitude dependence term.
COSTTEC Leitinger and Hochegger (1999)	The COST 251 model for TEC, known as COSTTEC, is based on monthly and hourly medians of electron content derived from the Differential Doppler effect on the signals of the polar orbiting NNSS satellites for three solar activity interval. The medians were gained for the latitudes 45, 50, 55 and 600N from latitudinal profiles of electron content.
COST 251 recommended model COSTPROF for the electron-density height profile (Hanbaba, 1999; Hanbaba, R. and Zolesi B., 2000)	The COST 251 recommended model COSTPROF for the electron-density height profile consists of two parts: 1) A bottom side model for the height region below the F2-layer peak based on the ionospheric characteristics foE, foF1, foF2 and M(3000)F2 and on rocket soundings. 2) A topside model for the height region above the F2-layer peak based on O+-H+ diffusive equilibrium with built-in maps for three parameters: the oxygen scale height at the F2-layer peak, its height gradient and the 0+- H+ transition height. The model is continuous in all spatial first derivatives, a necessity in applications e.g. ray tracing and location finding.
METU-NN GPS TEC Forecast Model METU-NN GPS TEC Forecast Map Model (Tulunay, 1991; Tulunay et al., 2002; Tulunay et al., 2004a; 2004b)	Highly nonlinear and complex processes in the Near-Earth Space can be modeled by the METU-NN models, which have been developed by the Group since 1990. The METU-NN, Neural Network, has one input one hidden and one output layer. Levenberg-Marquardt Backpropagation algorithms with validation stop are used for training the METU-NN. The METU-NN GPS TEC Forecast Model is employed to forecast the Total Electron Content (TEC) values up to 24-hour in advance.
RAL-MQP Dyson and Bennett (1988) Baker and Lambert (1988) Dick and Bradley (1993)	This model composes a height profile as a combination of quasi-parabolic (QP) and inverted QP segments. In this way, continuity of gradient is preserved throughout all segment interfaces. The model is completely specified by means of empirical formulations in terms of the standard ionospheric characteristics foF2, foF1, foE, and M(3000)F2, together with a knowledge of the solar-zenith angle.
TEC Monthly Median Mapping (Leitinger and Feichter, 1992, 1993; Leitinger and Spalla , 1994)	A monthly median mapping was developed during the COST 238 action giving TEC up to a nominal height of 1000 km for the whole PRIME area. The adopted mapping is based on the differential Doppler data sets for Lindau/Germany calibrated with the Graz/Austria measurements and grouped into latitude bands centred on 45, 50, 55 and 60deg. N for a nominal geographic longitude of 15deg. E.
The Brussels Meteorogical Institute Physical Models (DYMEK)	This is a photochemical equilibrium mid-Latitude daytime model using Chapman function production terms and the continuity equations for positive and negative ion production and losses (Dymek, 1989). In its initial form vertical transport by neutral winds and diffusion was excluded. Likewise, there was no allowance for day-to-day changes in solar EUV flux with production taken to be governed solely by solar-zenith angle. However, further model development (Dymek and Jodogne, 1993) has led to incorporation of the latest MSISE-90 model of neutral composition and temperature.

DANILOV D-Region modeling Danilov and Smirnova (1994) Danilov et al, 1995	This is a model for the D-region electron density developed based in comparisons with rocket measurements. A new four-classes model has been formulated for day-time winter conditions with electron densities separately given in tabular form at 5 km intervals over the 60-90 km height range for quiet, major stratospheric warming, weak and strong winter-anomaly conditions. The model is based on comparisons with extensive sets of rocket measurements and takes account of two chemically distinct cluster ions including hydrated protons. It incorporates a dependence on solar-zenith angle X and is defined for the range X = 40-90°. No changes with solar activity have been detected or are included.
Prediction of the F1 layer occurrence and L-condition (Scotto, 1999, 1998,1997)	The critical frequency foF1 predicted by the Du Charme formula assumes limits for the presence of the layer as a function of the solar zenith angle and of the solar activity given by the R12 index. In the study undertaken in the frame of COST 251, a new probability function to evaluate the occurrence of the F1 layer and "L condition" (cases where electron density profiles on the ionograms traces show a ledge rather than a remarkable cusp, so no critical frequency can be assigned to the layer) was proposed.
Long-term trends of ionospheric changes (Bencze et al., 1998; Bremer, 1998, 1999a,b; Danilov and Mikhailov, 1998; Lastovicka, 1997).	Studies in the area dealt with long-term trends observations of different ionospheric parameters. It has been shown that the detected ionospheric trends are relatively small compared with the solar and geomagnetic influences. Therefore, during the next years it is not necessary to take into account their influences on the ionospheric HP radio propagation. Neverthe1essthis effect has to be carefully monitored in the future. Especially it should be noticed that the scientific problem of a possible increasing atmospheric greenhouse effect requires further investigations. Mainly in the F2 region the results of the trend analyses are partly controversial and cannot be explained by the greenhouse effect.
Trough modeling (Mitchell et al., 1997) (Mitchell et al., 1999a,b)	A new approach to modelling the trough has been demonstrated. This method is based on a tomographic image of the ionosphere over United Kingdom that is extrapolated to other longitudes across the European sector. Initial results from the mapping were shown to compare well with observations from ionosondes east of the tomography receiver chain. In a separate study a seasonal variation has been revealed in the latitudinal position of the trough, showing the trough to be further south during the winter than the summer.
GISM and Hybrid Scintillation models Beniguel, 2002 Forte and Radicella; 2002 Gherm et al., 2000; 2002	GISM model developed at IEEA uses the Multiple Phase Screen technique (MPS). It consists in a resolution of the Parabolic Equation (PE) for a medium divided into successive layers, each of them acting as a phase screen. Within the scope of the activities of COST271 relevant to the problem of transionospheric propagation a second model for scintillation on transionospheric links (such as employed for satellite navigation) has been developed in co-operation between the University of St.Petersburg, Russia and the School of Electronic and Electrical Engineering, the University of Leeds, United Kingdom. The Abdus Salam ICTP, Italy also collaborated with both the teams providing the experimental data on scintillation, ideas for proper processing of the scintillation data and necessary expertise and data on the ionosphere modeling. The developed technique is based on a hybrid method and it is extended to combine the complex phase method and the technique of a random screen.
LCNN	LCNN makes use of a neural network to model the monthly median ionospheric foF2 frequencies in order to establish a new long-term prediction procedure to support radiowave propagation at frequencies above 2 MHz.
NNARX	A neural network based auto-regressive model with additional inputs is one possible approach that uses the hybrid time-delay multi-layer percepton with only the critical frequency of the F2 layer as input parameter to produce one output foF2 value.
The ap(τ) model	To forecast the ionospheric response to geomagnetic storms, geomagnetic indices have been introduced taking into account their past history. One of these is ap(?) derived with a time weighted series accumulation from the geomagnetic planetary index ap
Definitions and limits of ionospheric variabilities	Specification of the disturbed ionosphere based on a "casual" mechanism as for instance response to geomagnetic perturbations is rather inadequate to describe the current state of the ionosphere and plasmasphere. An ionospheric definition could specify disturbed ionospheric conditions much better than any geophysical since there is not a one to one correspondence.
Trough model for HF propagation assessments (Bradley et al., 1998)	A first order trhough model is introduced to the instantaneous maps created for HF propagation assessments, as a correction to the mapped values on the equatorial side of the auroral oval by night. Maps of the European ionosphere generated by means of this model demonstrate the lack of spatial structure particularly for the higher latitudes, with consequential reasonable smaller errors when applied to propagation assessments.

4 Conclusion

Meteorology is not a unified discipline. It includes several very different domains. Such is space weather. During the last years, we had this great opportunity to have two actions that were complementary in the *ESSEM* domain. This has given very important deliverables in our two actions and right support for their future developments for a mutual benefit.

References

Perrone L., B. Zolesi and L. Cander, Ionospheric models developed during the last COST actions for space weather applications, submitted Annals of Geophysics

Space Weather and Europe — an Education Tool with the Sun (SWEETS)

R. Hippler[1], M. Wolfgram[3], A. Glover[2], F. Jansen[4], M. Kokowsky[5], B. Schmieder[6], S. Poedts[7], I. Stanislawska[8], J. Stelmach[9], K. Kudela[10], R. Reis[11], R. Nakamura[12], W. Denne[13], M. Gausa[14], P. Beck[15], Y. Tulunay[16], and B. Ryabov[17]

[1] Institut für Physik, Universität Greifswald, Felix-Hausdorff-Str. 6, 17487 Greifswald, Germany, e-mail: hippler@physik.uni-greifswald.de
[2] Sternwarte Greifswald, Domstr. 10a, Greifswald, Germany
[3] European Space Agency, Keplerlaan 1, Noordwijk, The Netherlands
[4] 1A–First Applications for Space Weather Service, Research, Education, and Culture, Greifswald, Germany
[5] Technologiezentrum Vorpommern, Brandteichstr. 20, Greifswald, Germany
[6] Observatoire de Paris, 61 Avenue de L'Observatoire, Paris, France,
[7] Katholieke Universiteit Leuven, Oude Markt 13, Leuven, Belgium
[8] Center for Plasma Astrophysics, Space Research Centre, Polish Academy of Sciences, Bartycka 18a, 00-716 Warszawa, Poland
[9] University of Szczecin, Wielkoploska 15, 70-451 Szczecin, Poland
[10] Institute of Experimental Physics, Slovak Academy of Science, Watsonova 47, 04001 Kosice, Slovakia
[11] Centro de Astrofísica da Universidade do Porto, Rua das Estrelas, 4150-762 Porto, Portugal
[12] Institut für Weltraumforschung, Österreichische Akademie der Wissenschaften, Dr. Ignaz Seipel-Platz 2, 1010 Graz, Austria
[13] Deutsche Tanzkompanie, Wilhelm-Riefstahl-Platz 7, 17235 Neustrelitz, Germany
[14] Andoya Rocket Range and Alomar Observatory, 8483 Andenes, Norway
[15] Austrian Research Centers, 2444 Seibersdorf, Austria
[16] Middle East Technical University, Department of Aerospace Engineering, ODTU Inonu Bulvari, 06531 Ankara, Turkey and
[17] Institute of Astronomy of the University of Latvia, Rainis boulevard 19, 1586 Riga, Latvia.

Summary. Space Weather and Europe – an Education Tool with the Sun (SWEETS) is a public outreach activity and funded in 2007 by the European Commission within the 6th framework programme. SWEETS has several main elements, e.g., a space-weather-on-tour bus, a web quiz, production of a space weather DVD, and organization of space weather science festivals and forums in Europe.

1 Introduction

Space weather is primarily an astronomical phenomenon due to solar activity and cosmic rays but its study is by nature interdisciplinary and encompasses various fields of physics, engineering, and human activity. Space weather describes the conditions in space that affect Earth

and its technological systems. Our space weather is a consequence of the behavior of the Sun, the nature of Earth's magnetic field, and our location in the solar system. It is the popular name for energy-releasing phenomena in the magnetosphere, associated with magnetic storms, substorms and shocks. Space weather storms disturb satellite navigation and telecommunication, cause satellite failures and losses, electronics failure, electricity cut-off, pipeline corrosion, and can enhance radiation exposure to aircraft crew and passengers and to astronauts.

The purpose of Space Weather and Europe — an Education Tool with the Sun (SWEETS) is to demonstrate the beauty and significance of the Sun, solar activities, cosmic rays and space weather to Europe (Fig. 1). SWEETS also encompasses and supports some of the activities of the International Heliophysical Year (IHY). The solar aspect of the space weather phenomenon becomes more and more known to decision makers and to the public. The SWEETS project aims to promote and raise public awareness by means of attractive and high quality deliverables, e.g., a space weather mobile bus tour, web quiz, a space weather Digital Versatile Disc (DVD), science festivals including a space weather and Earth environment technology fair, a rocket & balloon campaign, and a space weather TV movie, during science weeks and festivals in 27 countries all over Europe. The main space weather forum/festival will take place during the European Science Week between in November 2007 at Schwerin castle in Germany followed by a participation of SWEETS in the finals of the European Science Week end of November 2007 in Lisbon.

2 SWEETS Members

SWEETS has 17 consortium members from all over Europe including Austria, Belgium, France, Germany, Latvia, Norway, Poland, Portugal, Slovakia, and Turkey. Consortium members are University of Greifswald (Germany), Sternwarte Greifswald (Germany), European Space Agency, 1A–First Applications Greifswald (Germany), Technologiezentrum Vorpommern Greifswald (Germany), Observatoire de Paris (France), Katholieke Universiteit Leuven (Belgium), Center for Plasma Astrophysics, Space Research Centre of the Polish Academy of Sciences (Poland), University of Szczecin (Poland), Institute of Experimental Physics of the Slovak Academy of Sciences in Kosice (Slovakia), Centro de Astrofísica da Universidade do Porto (Portugal), Institut für Weltraumforschung of the Austrian Academy of Science in Graz (Austria), Deutsche Tanzkompanie Neustrelitz (Germany), Andoya Rocket Range and Alomar Observatory in Andenes (Norway), Austrian Research Centers in Seibersdorf (Austria), Middle East Technical University Ankara (Turkey), and Institute of Astronomy of the University of Latvia in Riga (Latvia).

3 SWEETS Activities

Main activities of SWEETS are a space-weather-on-tour media bus touring Europe, informing about origin and hazards of space weather events, support of local science festivals on space weather all over Europe, organization of a web quiz on space weather. Local winners will be invited by participating institutions, the main winner was invited to a rocket launch at Andoya Rocket Range (Norway) in August 2007, organization of a science festival on space

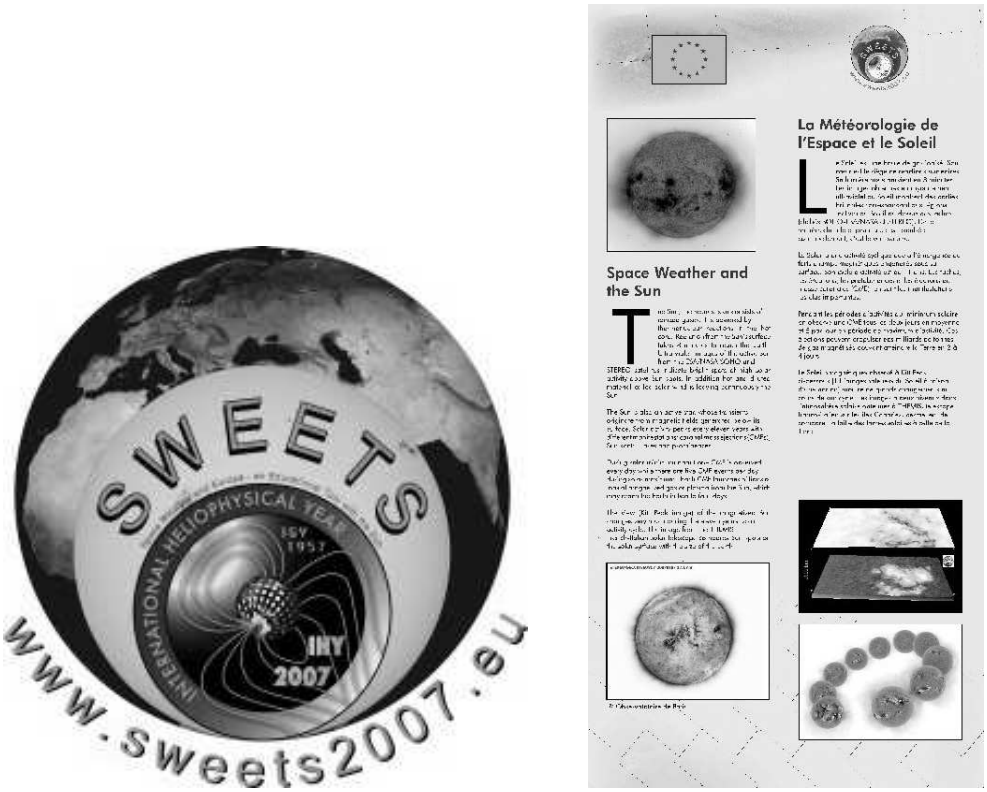

Fig. 1. SWEETS logo (left) and a typical poster exhibition panel(right).

weather during the European Science Week in November 2007, an European space weather and environment technology fair during 19-20 November 2007 in Greifswald, a space weather planetarium show, and a space weather DVD.

3.1 Spaceweather-on-tour bus and support of local science festivals.

SWEETS is organising a space-weather-on-tour bus tour through Austria, Belgium, France, Germany, Latvia, The Netherlands, Norway, Poland, Slovakia, and Portugal.

The bus is operated by Personenverkehr GmbH Müritz in Waren (Germany); it contains a space weather poster exhibition (Fig. 1), an interactive exhibition including a video presentation of the first CD-ROM on space weather (Jansen and Hippler, 2002), personal computers with near real time access to space weather observing satellites, an optical telescope and a radio telescope for solar observations by visitors. The tour through the bus is guided by different high-level and outreach-educated European space weather scientists.

Thus far (September 2007), the space-weather-on-tour bus has made its way from Greifswald via Vienna, where it stopped at the Vienna International Center during the SWEETS-supported Symposium on *Radiation Exposure to Aircraft Crew due to Space Weather Effects*

Fig. 2. Space-weather-on-tour bus in fort of the Observatoire Paris at Meudon.

and the Fiftieth session of the *Committee on the Peaceful Uses of Outer Space (COPUOS)*, to Paris, Copenhagen, Oslo, Andenes, Riga, and Kosice back to Germany. The tour will further continue through Poland, Belgium, The Netherlands, Austria, and Germany, ending in Portugal during the European Science Week in November 2007.

3.2 Web quiz

SWEETS has organized a space weather web-based quiz with participants coming from all over Europe. The main quiz winner was been invited to Andoya Rocket Range in northern Norway in August 2007 participating in a scientific rocket launch.

3.3 Spaceweather Forum/Festival, European Space Weather and Earth Environment Technology Fair

Sweets will organize a science festival/forum on space weather during the European Science Week in November 2007 (Fig. 3) that includes a *space weather storm* dance show, a *space-weather-on-tour* movie, presentation of a new space weather DVD, and video links connecting the Muon Spaceweather Telescope for Anisotropies at Greifswald (MuSTAnG) to other space weather observatories all over the world. The first European space weather and Earth environment technology fair will take in Greifswald during the following days (19-20 November 2007).

3.4 DVD and Movie

SWEETS consortium will produce a space weather Digital Versatile Disc (DVD) for education and promotion purposes. The contents of this DVD will be based on the popular and suc-

Fig. 3. Announcement of the First European Space Weather and Earth Environment Technology Fair 2007.

cessful, space weather CD-Rom published in 2002/2003 (Jansen and Hippler, 2002). High resolution movies and simulations, updated new images, text and descriptions of space weather activities will guarantee an excellent quality of the new DVD.

SWEETS is also producing a TV film about European and international space weather activities.

Acknowledgements

SWEETS is funded by the European Commission within the 6th framework programme and supported by COST 724 action.

References

F. Jansen, R. Hippler, Weltraumwetter - Space Weather - Meteorologie de L'Espace, CD-ROM, Greifswald: Institut für Physik der Ernst-Moritz-Arndt-Universität, Edition I, English version (2002); Edition II, updated English, French and German version (2003)

The State of the Art in space weather observational activities and data management in Europe

I. Stanislawska[1] and A. Belehaki[2]

[1] Space Research Centre PAS, 00-718 Warsaw, Bartycka 18a, Poland
[2] National Observatory of Athens, Metaxa and Vas. Pavlou, 15236 Palaia Penteli, Greece

Summary. One of the primary scientific and technical goals of space weather is to produce data in order to investigate the Sun impact on the Earth and its environment. Studies based on data mining philosophy yield increase the knowledge of space weather physical properties, modelling capabilities and gain applications of various procedures in space weather monitoring and forecasting. Exchanging tailored individually and/or jointly data between different entities, storing of the databases and making data accessible for the users is the most important task undertaken by investigators. National activities spread over Europe is currently consolidated pursuant to the terms of effectiveness and individual contributions embedded in joint integrated efforts. The role of COST 724 Action in animation of such a movement is essential. The paper focuses on the analysis of the European availability in the Internet near-real time and historical collections of the European ground based and satellite observations, operational indices and parameters. A detailed description of data delivered is included. The structure of the content is supplied according to the following selection: (1) observations, raw and/or corrected, updated data, (2) resolution, availability of real-time and historical data, (3) products, as the results of models and theory including (a) maps, forecasts and alerts, (b) resolution, availability of real-time and historical data, (4) platforms to deliver data. Characterization of the networking of stations, observatories and space related monitoring systems of data collections is integrated part of the paper. According to these provisions operational systems developed for these purposes is presented and analysed. It concerns measurements, observations and parameters from the theory and models referred to local, regional collections, European and worldwide networks. Techniques used by these organizations to generate the digital content are identified. As the reference pan-European and some national data centres and bases are described and compared with currently available data information provided worldwide and by relevant entities outside Europe. Current, follow up and expected future European space weather observational activities and data management perspectives in respect to European main lines of policy is the subject of the conclusions.

1 Introduction

By the definition:*space weather is the physical and phenomenological state of natural space environments. The associated discipline aims, through observation, monitoring, analysis and modelling, at understanding and predicting the state of the sun, the interplanetary and planetary environments, and the solar and non-solar driven perturbations that affect them; and also at forecasting and nowcasting the possible impacts on biological and technological systems (COST724 Final Report, 2007).*

Thus, any track of activity related to space weather (observational data collection, management structure, modelling and prediction, definition of services) may be the subject of a unified system approach.
On the track of such approach, Geospace General Circulation Model (GGCM), a numerical research model developed by American National Science Foundation (NSF) Division of Atmospheric Sciences aimed at strengthening predictive capability of the dynamical and structural properties of geospace. GGCM is fully modular and progressive as the geospace system was divided into a set of discrete but mutually interacting numerical elements, each representing either a physical domain or a boundary between domains. The system is designed to be progressive and adaptable to new physical models and numerical techniques. The system approach is also applicable to system measurement requirements defined as the parameters to be measured, the location of these measurement, time and spatial resolution of the monitoring (Hapgood, 2001); reasonable data bases construction. Historically, the different observatories and institutes performed observations of characteristic parameters of Earths environment according to their scientific research interests. However to build the marked oriented space weather services the clear specification of product is required. Thus, the supply of different services by selected observational data is needed and specific measurements can service broad user interests. In effect the system of observations based on scientific knowledge of space weather is based on space segment and related its ground support as well as ground-based segment. Finally, the consolidated system of systems on different levels (European, worldwide etc.) is defined.
The management of data gathered in the frame of observational system needs the different tools. Networking of observational activities, observational grids, data exchange programs, European area servers as well as international cooperation are implemented together to help the decision-maker institutions manage the data dissemination. To identify and extract the data required to generate the specified products, the broad spectrum of data assessment and processing methods like data mining, mapping, artificial neural networks is explored. Thus, data providers who not only distribute but also process the data stored are the important partners in space weather services.
Generally, the philosophy of space weather data organisation has take into account the following:

- The system approach - system measurement requirements.
- The space weather data have to be integrated with other environmental European services and data system management like GMES and INSPIRE.
- The mix-policy is applied with respect to space segment in space weather domain.
- The European space weather data management architecture has to be similar to that of GMES.
- European Space Weather activity has to be one of the GMES service element.

2 Space weather related observation in Europe

As advanced technological systems require space weather knowledge to function efficiently, a quantitative, predictive understanding of the complex system of systems as Earth‘s environment, is needed. The ground-based gathered space weather data have the same value as in situ

data collected for environmental monitoring. The European space weather monitoring and forecasting is crucial. There are the needs for a continuously operating and reliable service to support regular society demands as well as natural hazard monitoring and risk management operations.
In that context it is natural that space weather data have to be integrated with other environmental European services and data system management like GMES and INSPIRE. In this way space weather data and services will contribute to the Group on Earth Observation (GEO) process and other relevant international initiatives. Such policies will optimize the use of data and services, and can make them readily accessible in the most efficient and effective way to the widest possible range of users and applications.

Ground-based monitoring of Earth environment

Many space weather parameters are measured by the astronomical and geophysical observatories. The continuous increase of such measurements will contribute towards advances in scientific understanding and technological development. Among the practical advantages of these ground-based measurements are their easy maintenance and upgrade and the capability to continuously patrol a selected region of the geospace environment. The existence of long series of archive data from ground-based observatories and stations is also very important factor.
Europe has a wealth of ground-based solar, magnetic and ionospheric measurements related to space weather. Historically, the regularly published monthly Zurich sunspot numbers as well as the magnetic storm information broadcasted from the Eiffel tower were the first space weather services in the world (1928). The current European space weather resources were survey by ESA Report(Hapgood, 2001). This assessment identified some 180 resources of which 105 were related to ground measurements. These mainly focus on observations of the Sun (23%), the ionosphere (34%) and ground-effects (37%). This activity is spread over many European countries but the strongest national element is in France, Germany, Italy, Scandinavia and the UK. A strong Pan-European element is also present and it is a good base for further European collaboration, co-ordination and integration. The ground-based observations which at present days are used in space research practice are:
- solar observations
- galactic cosmic rays monitoring,
- aurora and north sky observation,
- geomagnetic field registration,
- ionosonde and GPS sounding of the ionosphere.

Satellite monitoring of the Sun-Earth system

Space Segment is the important component of space weather data gathering. However, until now the space European missions performed the ”dual use” programs: exploring and monitoring solar-terrestrial space (SOHO). Thus, the space weather monitoring has to use the existing and planed Earth exploring missions and install space experiments on the board spacecrafts

(SWARM Earth magnetic field dedicated explorer). The appropriate satellite and orbits have to be selected by instrument definition. Thus, in space weather domain the mix-policy is applied i.e. whether to use the existing and planned missions, piggy back space weather instruments on other spacecraft, or dedicated space weather missions. All three options have to be taken into consideration in practice by space weather data providers.
Satellite monitoring of the Sun-Earth system may be shown as:
- solar monitoring (Ulysses ,Soho, STEREO)
- magnetosphere and interplanetary space (Cluster),
- ionosphere and geomagnetic field monitoring (ISS, Freja, Demeter, CHAMP, SWARM)
Analysis of the availability in the Internet near-real time and historical collections of the European ground based and satellite observations, operational indices and parameters is the necessary task for organizing the SW platform. The collections contain: measurements, observations and parameters from the theory and models from local, regional, European area and worldwide. Data delivered are observations, raw and/or corrected data with well defined resolution, description about their availability of real-time and historical data. Bases include products, as the results of models and theory, also, as well as maps, forecasts and alerts. The important issue are techniques used to generate the digital content and platforms to deliver data. Some forms of delivered products, specifically if issued in the form of maps, might be problematic due to their fast evolution and the sparseness of data in some regions (Trishchenko et al., 2006). The forms of the deliverables should answer t o the continuously discussed with the users issues.

3 Management of observational data useable in space weather practice

To preserve compatibility with GMES data management, it seems that European space weather data management architecture has to be similar to that of GMES.
First of all, we have to define what elements of observational infrastructure would be similar and to whom the services will be addressed. The observational infrastructure has to be organized in data grids, and networking of observational activities. The nodes and communication links of the grid has to be defined.
To construct Space Weather activity as one of the GMES service element, its content will have to be broken down into discrete ”Space Weather (SW) services” and Space weather scenarios. SW services and SW scenarios should be identified to avoid duplication of user requirement collection. Each ”SW scenario” has to be related to observational grid component ”nodes” and ”links”. The role of SW data providers has to be defined as well. On the other side the SW service providers apply data mining, statistical and physical modelling creating the SW server for European area.

Data management architecture

The general architecture of data management can be described according to the layer structure:

- Layer 1 Data Collection

- Layer 2 SW data standardisation
- Layer 3 SW added value product generation
- Layer 4 SW product distribution to users
- Layer 5 Product assessment by end users

Description of layers

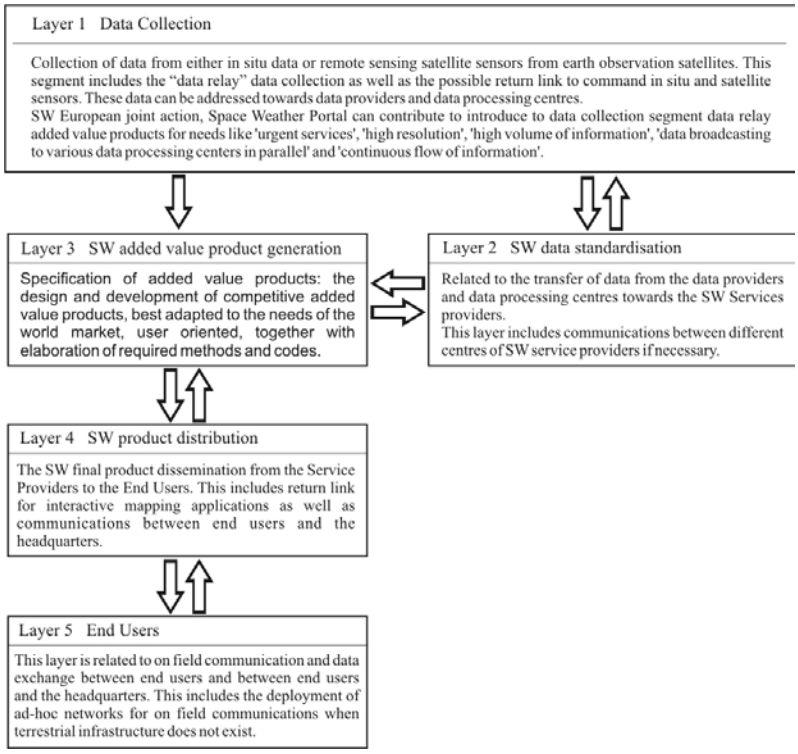

Networking of observational activities

Observational activity is realised by means of:

- observation grids,
- data exchange programs,
- European area servers including activity outside Europe (North and South polar regions)
- international co-operation

Some examples of the entities and organisations managering in European area and worldwide are: ESA, EUMETSAT, ISES, Intermagnet (International Real-time Magnetic Observatory Network), WDCs, COST, MM100 magnetometer network (an European magnetometer network for geomagnetic pulsation studies), DIAS, SuperDARN, Louis/Lofar, EISCAT.

Data mining, statistical and physical modelling

The operational needs to predict the solar-terrestrial variability determined the architecture of space weather data management. The geomagnetic and ionospheric storms, chemical composition of the thermosphere response for solar activity are usually chaotic, and it is impossible to relate them to an simple empirical models, or much more advanced statistical and physical ones. In this domain modelling provides additional data for operational indices and parameters. The understanding the cause-effect relations in this domain involve an investigation of data gathered, methodology of data processing and specific analysis procedures. Space weather related science research problems have to be a guide for any methods applied to integrate modules and tools of numerous analysis techniques. Thus, the data mining which uses the verity of techniques to get out the essential information from large data set is preferable instrument to support space weather architecture target.
The example is the SPIDR-the Space Physics Interactive Data Resource, a distributed network of database and application servers implementing interactive data mining technologies, physical modeling and delivery of selected data (Zhizhin, et al., 2000). The project is developing together and locating its nodes at NGDC in Boulder as well as at Center of Geophysical Data Studies in Moscow. The interoperation architecture of the SPIDR consists many modules which try to support the main target of the system-useful manage of solar-terrestrial data set.
In Europe the similar tasks are developed. Some examples are elaborated within the frame of programs conducted by the co-operational entities: EU Framework Programmes, ESA, COST, DIAS, ISES, national agencies and organizations. The important guide for this activity are the procedures of the International Standard Organisation (ISO) defined by the requirements concerning the end products, as well as all needed input to their purchase by users. However, leading role for European design of space weather products to serve needs of society will be allocated to European Space Weather Portal.

Organizations involved in the generation of digital information - general description

Some of World Data Centers (WDCs) are located in Europe, as WDC for Solar Terrestrial Physics in Chilton operated by RAL, $http://www.wdc.rl.ac.uk/$, World Data Center for the Sunspot Index Brussels $http://sidc.oma.be/$. Convenient access and management of historical space physics data gives Russian mirror of SPIDR (Space Physics Interactive Data Resorce) http://spidr.ngdc.noaa.gov/spidr located in $(http://clust1.wdcb.ru/spidr/)$. The International Space Environment Service (ISES) $http://www.ises-spaceweather.org/$ has to be mentioned here. Other European and national activities can be reached by European Portal and its Navigator $http://www.cbk.waw.pl/sw_europe$. European organization of future SW information management is based upon the European Space Weather Portal. Its operating modules the web pages maintenance and information management consists of European Space Weather Portal $(http://gauss.oma.be/COST724/ESWWS/)$, and its integral parts located at different serve rs over Europe. The actual configuration consists of: model interface (http://gauss.oma.be/COST724/ESWWS/remote_access/), European space weather related web pages Navigator http://www.cbk.waw.pl/sw_europe/ with its ionospheric and telecommunication part http://www.cbk.waw.pl/cost296/, and server for measurements data and models provider (http://ca724wg1.ts.astro.it/mod_data.php).

4 Conclusion

The importance of the space weather observational activities and data management is the important issue in a European Space Policy. The objective of the FP7 space work programme is to support it focusing on applications such as GMES (Global Monitoring for Environment and Security), but also in other programmes devoted to science and to more application oriented areas as, increasing application potential, technical development of Europe that increases competitiveness of its industry, and to social sustainable development that is the base for future existence.
In our practice - Space weather observational activities and data management according to the EU priorities and requirements for new researches and operational issue mainly are assessment of the risk after space weather phenomena, including impact on biological and technical systems and providing appropriate services through European Space Weather Portal by all available Pan-European and national activities.

5 References

Hapgood, M., Road map for European co-ordination in space weather, ESWS-RAL-RP-0003, Issue1.0, 19 November 2001.
L. Trichtchenko, L., A. Zhukov, R. van der Linden, S. M. Stankov, N. Jakowski, I. Stanislawska, G. Juchnikowski, P. Wilkinson, G. Patterson, and A. W. P. Thomson: November 2004, Space Weather Events: Real-Time Observations and Forecast, Space Weather, 5, S06001, doi:10.1029/2006SW000281.
Zhizhin, M., A. Burtsev, A. Gvishiani, E. Kihn, H. Kroel, Interactive intelligent space physics

data mining and visualization via Internet, Computer Graphics and Geometry, Internet Journal, 2, 3, 2000.

International Years Initiatives and COST Action 724

M. Candidi[1] and M. Messerotti[2,3]

[1] INAF-IFSI Institute of Interplanetary Space Physics, Via del Fosso del Cavaliere, 00133 Rome, Italy
candidi@ifsi-roma.inaf.it
[2] INAF-Astronomical Observatory of Trieste, Loc. Basovizza n. 302, 34012 Trieste, Italy
messerotti@oats.inaf.it
[3] Department of Physics, University of Trieste, Via A. Valerio n. 2, 34127 Trieste, Italy
Mauro.Messerotti@ts.infn.it

Summary. Space weather is at the core of several activities in various international programs and initiatives. A review of the scientific and operational objectives of the groups working on space weather in such framework will be given. The IPY, the IHY, the eGY initiatives, and programs like ICESTAR within SCAR, and the Theme 2 of CAWSES will be addressed. The integration of COST724 with all other initiatives will be described, and perspectives for future better cooperation will be outlined, in order to achieve maximum synergy.

1 Introduction

Several initiatives have been recently taken by several scientific organisms, to celebrate the 50^{th} anniversary of the International Geophysical Year (IGY, http://www.nas.edu/history/igy/). The IGY was declared when ICSU, the International Council of Scientific Unions, in 1952 proposed a comprehensive series of global geophysical activities to span the period July 1957-December 1958. The IGY was modelled on the International Polar Years of 1882-1883 and 1932-1933 and was intended to allow scientists from around the world to take part in a series of coordinated observations of various geophysical phenomena. Although representatives of 46 countries originally agreed to participate in the IGY, by the close of the activity, 67 countries had become involved. The IGY was initiated as a worldwide event, to observe geophysical phenomena and to secure data from all parts of the world; to conduct this effort on a coordinated basis by fields, and in space and time, so that results could be collated in a meaningful manner. Its main goal was to learn more about the Earth's fluid envelope - its atmosphere and oceans - at all heights and depths. This type of research demanded widespread coordinated observations. The IGY was the scenario upon which various history making steps were taken: most eminent of which was the launch of the first artificial satellites. The IGY satellites carried simple instrumentation, with respect to the sophisticated payloads that modern missions carry into space; they were low orbit satellites, and nevertheless led to discoveries of relevance to science, and in particular to "space weather"; the radiation belts were discovered (Van Allen is reported to have said: "Space is radioactive!). These are so important to space weather effects that we may say that the main result of the first artificial satellites

was crucial to the very establishment of the scientific discipline of space weather. The Special Committee for the IGY became the model on which three post-IGY Scientific Committees developed, for Antarctic (SCAR), Oceanic (SCOR), and Space Research (COSPAR). The IGY encompassed eleven research fields of the Earth sciences: aurora and airglow, cosmic rays, geomagnetism, gravity, ionospheric physics, longitude and latitude determinations (precision mapping), meteorology, oceanography, seismology and solar activity. We can see that five out of eleven had to do with subjects that we would now label as "elements of space weather". The programs aimed at celebrating the 50^{th} anniversary of the IGY take different names depending on the attitude of the initiators of the different initiatives, and concentrate on different regional territories to which the initiative is devoted, or to the specific technology called upon by the initiative itself. We will see that the various celebrations are aimed at a very much more extended series of scientific objectives than the IGY. In the following the initiatives will be described and the regions or technologies highlighted will be detailed.

2 IPY (http://classic.ipy.org/about/)

It is to be noted that the IGY started out as the $3rd$ International Polar Year, and developed into a research effort that was directed to the whole world. It had anyhow much to do with the continent of Antarctica. A notable political result founded on the IGY was the ratification of the Antarctic Treaty in 1961. The IPY, the fourth International Polar Year, was initiated as a proposal of SCAR to ICSU, eminently on the grounds that SCAR recognizes the importance of the IGY in advancing Antarctic research. The International Polar Year, i.e. the 4th Polar Year, is a large scientific programme focused on the Arctic and the Antarctic. The IPY is organized through the International Council for Science (ICSU) and the World Meteorological Organization (WMO). In order to have full and equal coverage of both the Arctic and the Antarctic, IPY 2007-8 covers two full annual cycles from March 2007 to March 2009 and will involve over 200 projects, with thousands of scientists from over 60 nations examining a wide range of physical, biological and social research topics. It is also an unprecedented opportunity to demonstrate, follow, and get involved with, cutting edge science in real-time. It is envisioned that the International Polar Year (IPY) 2007-2008 will be an intense, internationally coordinated campaign of research that will initiate a new era in polar science. IPY 2007-2008 will include research in both polar regions and recognise the strong links these regions have with the rest of the globe. It will involve a wide range of research disciplines, including the social sciences, but the emphasis will be interdisciplinary in its approach and truly international in participation. It aims to educate and involve the public, and to help train the next generation of engineers, scientists, and leaders. The International Council for Science (ICSU) formally agreed to establish an International Polar Year in 2007-2008 and formed an International Planning Group to direct the development of an IPY programme. The World Meteorological Organization (WMO) agreed to co-sponsor the Polar Year with ICSU and contributed to the Planning Group activities in 2003-2004. In September 2004 the Planning Group completed its brief and handed over leadership of the Polar Year planning to the ICSU-WMO Joint Committee. The IPY has been designed ever since the beginning around several themes of focus:

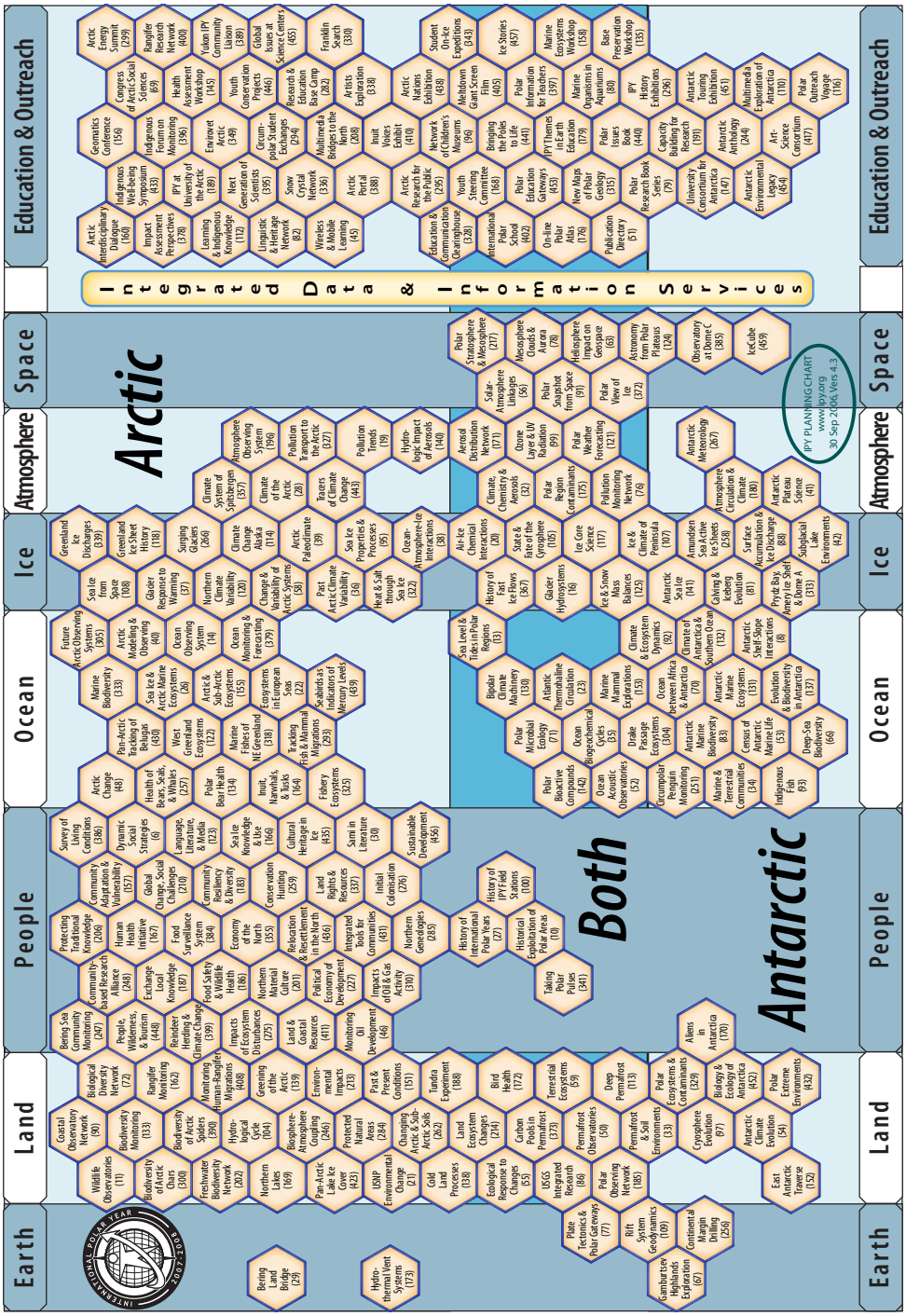

Fig. 1. Honeycomb diagram of the IPY research activities

1. To determine the present environmental status of the polar regions by quantifying their spatial and temporal variability.
2. To quantify, and understand, past and present environmental and human change in the polar regions in order to improve predictions.
3. To advance our understanding of polar - global interactions by studying teleconnections on all scales.
4. To investigate the unknowns at the frontiers of science in the polar regions.
5. To use the unique vantage point of the polar regions to develop and enhance observatories studying the Earth's inner core, the Earth's magnetic field, geospace, the Sun and beyond.
6. To investigate the cultural, historical, and social processes that shape the resilience and sustainability of circumpolar human societies, and to identify their unique contributions to global cultural diversity and citizenship.

The number of scientific disciplines involved in the IPY is clearly much larger than during the IGY, extending to social aspects, and including astronomy and astrophysics, as an example of disciplines that were not focussed on by the IGY. The proposals aimed at conducting research in the framework of the IPY have been written in the spirit of the themes listed above. After an initial period of expression of interest, and the presentation of the formal proposals, the Organising Committee has grouped them under the various themes, and several proposals have accepted the suggestion to be merged into more complete clusters, which are now officially recognised as the "IPY research activities". They are shown in the "honeycomb diagram" in Fig. 1.

3 IHY (http://ihy.gsfc.nasa.gov/)

The International Heliophysical Year carries in its title the word "Heliophysical": A broadening of the concept "geophysical," extending the connections of the Earth to the Sun & to interplanetary space. On the 50th anniversary of the International Geophysical Year, the 2007 IHY activities will build on the success of IGY 1957 by continuing its legacy of system-wide studies of the extended heliophysical domain. Approaching its 50th anniversary, NASA has established an extensive suite of spacecraft and observatories, our "Great Observatory," which places mankind on the verge of a system-wide understanding of the entire interconnected heliophysical system. Fifty years after the IGY, the world's science community will again come together for an international program of scientific collaboration: the International Heliophysical Year (IHY) 2007. As we approach the limit of human exploration and prepare for humanity's first encounter with interstellar space, we have expanded our concept of "geophysics" to embrace other planets, interplanetary space, and the Sun itself. The term "heliophysical" is an extension of the term "geophysical," where the Earth, Sun & Solar System are studied not as separate domains but through the universal processes governing the human realm of space. The IHY has three primary objectives:

- Advancing our Understanding of the Fundamental Heliophysical Processes that Govern the Sun, Earth and Heliosphere.
- Continuing the tradition of international research and advancing the legacy on the 50th anniversary of the International Geophysical Year.

- Demonstrating the Beauty, Relevance and Significance of Space and Earth Science to the World.

The five IHY Science Themes are:

Theme 1 Evolution and Generation of Magnetic Structures and Transients.
Theme 2 Energy Transfer and Coupling Processes.
Theme 3 Flows and Circulations.
Theme 4 Boundaries and Interfaces.
Theme 5 Synoptic Studies of the 3-D Coupled Solar-Planetary-Heliospheric System.

4 eGY (http://www.egy.org/)

The electronic Geophysical Year (eGY) (2007-2008) is an initiative of the International Union of Geodesy and Geophysics and it is led by the International Association of Geomagnetism and Aeronomy (IAGA), conceived to celebrate the 50th anniversary of the International Geophysical Year (1957-1958). In fact, eGY embraces and extends the IGY principles by pursuing the following goals in the framework of data and information handling via a cooperative international efforts:

- International cooperation and data sharing.
- Universal access to data and information.
- Timely and convenient access to data.
- Global, cross-disciplinary scope.
- Data preservation.
- Capacity building, especially in developing countries.
- Education, public outreach, information for decision making.

The role of eGY is aimed at facilitating, encouraging and promoting:

- Modern data access and services (“e-Science for Geoscience”).
- Responsible data stewardship.
- Cooperation among bodies/initiatives to reduce duplication and proliferation of standards, and share expertise.
- Establishment of virtual observatories throughout the geosciences.
- Establishment of criteria to determine optimal and minimum funding for data activities supporting research.

eGY also serves to provide a link between programs with related data and information requirements - IPY, IHY, Planet Earth, and initiatives such as GEOSS (Global Earth Observing System of Systems; http://www.epa.gov/geoss/). The eGY activities are managed by a Secretariat, an International Committee promotes and liaises with worldwide interested organizations and individuals and five thematic Working Groups are devoted respectively to the following topics:

- Virtual Observatories.
- Data Integration & Knowledge Discovery.

- Best Practice (joint with CODATA, Committe on Data for Science and Technology, http://www.codata.org).
- Data Rescue and Preservation.
- Education and Public Outreach.

5 ICESTAR (http://scar-icestar.org/)

ICESTAR (Interhemispheric Conjugacy Effects in the Solar Terrestrial and Aeronomy Research), is a research program approved and supported by SCAR (the Scientific Committee for Antarctic Research). It concentrates efforts in the analysis of solar terrestrial interactions as observed from Antarctica. It focuses on scientific objectives that stem from the assumption that near-Earth space (geospace) is an integral part of the Earth system, providing the material link between the Sun and Earth, primarily through the polar regions. A goal of the ICESTAR Programme is to create an integrated, quantitative description of the upper atmosphere over Antarctica, and its coupling to the geospace environment. The research program is organised around several Thematic Action Groups (TAGs) as follows:

TAG A Quantification of the coupling between the polar ionosphere and neutral atmosphere from the ”bottom-to-top” and the global electric circuit.

TAG B Quantification of the inner magnetospheric dynamics using remote sensing techniques.

TAG C Quantification of the state of the upper atmosphere, ionosphere, and magnetosphere over the Antarctic continent and how it differs from the Northern hemisphere during a wide range of geophysical conditions.

TAG C.1 Quantify the atmospheric consequences of the global electric circuit and further understand the electric circuit in the middle atmosphere as guided by the electric fields generated at the solar wind-magnetosphere interface. Contact: Nikolai Østgaard (University of Bergen, Norway).

TAG C.2 Quantify the thermal and dynamical structure of the middle and upper atmosphere over the Antarctic continent and how it differs from the Northern hemisphere during a wide range of geophysical conditions. Contact: Scott Palo (University of Colorado, USA).

TAG D Creation and management of the data portal to enable the ICESTAR programme and SCAR’s SSG/PS.

6 CAWSES (http://www.bu.edu/cawses/)

CAWSES (Climate And Weather in the Sun Earth System) is an international program sponsored by SCOSTEP (Scientific Committee on Solar-Terrestrial Physics) established with an aim of significantly enhancing our understanding of the space environment and its impacts on life and society. The main functions of CAWSES are to help coordinate international activities in observations, modelling, and applications crucial to achieving this understanding, to involve scientists in both developed and developing countries, and to provide educational opportunities for students of all levels. The work of the CAWSES program is organised in

four research themes, of which Theme 2 is especially close to the objectives of COST 724. In the following the titles of the four themes are listed. The specific objectives of Theme 2 are also reported, since Theme 2 is the closest to the objectives of COST 724:

Theme 1 Solar Influence on Climate.

Theme 2 Space Weather: Science and Applications: "Space Weather" is a term that encompasses the science and applications arising from short-term variations of the Sun, propagation of energetic particles and electromagnetic emissions through interplanetary space, and effects on technology and humans orbiting in geospace and on the Earth's surface. It includes rapid phenomena such as solar flares and coronal mass ejections, effects of shock waves at the magnetosphere, short-lived magnetic substorms at auroral latitudes and longer-lasting global magnetic storms, as ell as large and small scale ionospheric structures driven by internal atmospheric processes. These can affect satellites and humans in orbit, interrupt telecommunications, and degrade power distributions systems. The goals of the project are to develop dependable, robust deterministic end-to-end models that predict conditions in geospace from a quantitative understanding of the observed phenomena including multi-scale coupling between different plasma regions of the Sun-Earth system. A desired outcome will be identification of critical inputs to specify the geospace environment to minimize impacts of solar disturbances and geomagnetic storms on technology, human society, and all life.

Theme 3 Atmospheric Coupling Processes.

Theme 4 Space Climatology.

7 Connections with COST 724 and perspectives for the future

COST 724 has progressed without connections, at least explicit connections, to the other programs. This approach is justified in the initial steps of the COST 724 action, which has now established itself as a core activity of the countries that have signed the agreement, mostly European countries. It will be necessary and appropriate that efforts are spent towards connecting much more closely in the future, between European efforts and international initiatives. The individual, innovative approach taken by COST 724 will greatly benefit from parallel initiatives with the other programs, which are internationally broader. This connection is favoured by the evolution of the other programs, which are close to being renewed by the relevant institutions, SCOSTEP in the first place (CAWSES is going to be completed in 2008, and SCOSTEP is examining the continuation into a "CAWSES2" program). A different connection may be sought with IPY, eGY and IHY, which are a burst of activities to be completed by February 2009. The legacy of these programs will result in extensive data analysis phases, after the official end of the field initiatives that are active during the Years themselves. Connection to the official programs that will result will be of utmost importance for COST 724 and the activities that will follow in the European framework.

Acknowledgements: The text in this presentation is largely drawn from the web pages of the various programs, and from the web sites of the institutions that maintain them. This work has been carried out in the framework of COST Action 724 WG4.

Concept Maps for a Space Weather Ontology

M. Messerotti[1,2]

[1] INAF-Astronomical Observatory of Trieste, Loc. Basovizza n. 302, 34012 Trieste, Italy
messerotti@oats.inaf.it
[2] Deptartment of Physics, University of Trieste, Via A. Valerio n. 2, 34127 Trieste, Italy
Mauro.Messerotti@ts.infn.it

Summary. We present a first attempt aimed at building an ontology for Space Weather based on a graphical representation of knowledge. For this purpose, the IHMC Concept Maps sofware toolkit was used as a quite flexible and effective development environment. The preliminary set of Concept Maps is shown and briefly commented as well as the future perspectives.

1 Introduction

A clear definition of the concepts relevant to Space Weather and its operational field is needed due to many conceptual ambiguities introduced by the common practice. Therefore the construction of an ontology is the appropriate way to solve ambiguities, to emphasize relationships and to set the basis for defining a Space Weather knowledge model. In Section 2 we outline a semantic model for knowledge and in Section 3 we explain how knowledge can be represented in graphical form by Concept Maps. In Section 4 we define the foundation ontology and in Section 5 we outline the Space Weather ontology building process and we comment the basic Cmaps. The conclusions are drawn in Section 6.

2 A Semantic Model for Knowledge

A semantic model for knowledge is based on a set of propositions, each one expressing the relationship between concepts. A concept is a pattern of regularities in objects which are descriptive knowledge elements. A relationships is a logical action link, i.e., an inferencing knowledge element. It is therefore possible to graphically represent a certain knowledge on a topic or sub-topic by drawing a graph with blocks connected by lines to describe the relevant propositions. A similar representation is defined as a Concept Map (Cmap) (Messerotti (2002) and references therein).

3 Representing Knowledge via Concept Maps

The knowledge representation outlined in the previous section can be achieved by constructing Cmaps as graphical schemes of knowledge in organized form. Various software tools exist for

this purpose, but we claim that the most user-friendly and, at the same time, the most advanced for its capabilities to export knowledge in machine-readable format is the Cmap Tools Knowledge Modelling Kit, a multi-platform client developed by the Institute for Human and Machine Cognition (IHMC, Florida, USA) that allows the interactive drawing of a Cmap and its eventual publication on a local or remote Cmap server. In the latter case, the published Cmaps become accessible: (a) at human level via a conventional web client (like e.g. Microsoft Internet Explorer or Mozilla Firefox) for reading only or for remote collaborative editing upon authentication; (b) at machine level via specific web services for knowledge manipulation, as a Cmap can be parsed and exported as an XML file which codes the concepts and their relationships (Messerotti, 2006, 2007). This software tool is freely available for non-commmercial purposes and can be downloaded upon registration at the URL http://cmap.ihmc.us/. A Cmap is a quite flexible representation as external resources such as other Cmaps, hyperlinks, scripts, etc, can be associated with concepts, so that a set of Cmaps published on a Cmap server can be navigated to explore the coded knowledge.

For the publication of the Cmaps developed in the framework of CA724, a dedicated Cmap server was installed and active at the INAF-Astronomical Observatory of Trieste. It is reachable at the URL http://imhotep.oats.inaf.it:3000/.

A sample Cmap is shown in Fig. 1. By selecting an adequate layout, the vertical location of the concept blocks with respect to each other can rank the conceptual hierarchy in terms of inclusivity, being the most inclusive concepts at the top of the graph and the less inclusive ones at the bottom. Similarly, the relative horizontal location can be associated with the generalization level. The adoption of such layout schemes is not mandatory and it depends on the specific nature of the Cmap, i.e., on the knowledge framework it describes.

4 Definition of a Foundation Ontology

An ontology describes the knowledge on a general subject (foundation ontology) or on a specific topic (domain ontology) and it is the formulation of a conceptual scheme about e.g. a domain that is constructed by:

- Defining the precise meaning of domain entities (Semantics).
- Identifying the relationships between entities (Associativity).
- Stating the rules between entities and set of entities (Operativity).

The formulation of a foundation ontology for Space Weather is needed for a series of reasons:

- There is no clear definition of the terminology and many ambiguities exist.
- There is no clear definition of the physical domains.
- The interrelationships are defined only on a fragmentary basis and are typically limited to subdomains. 1item The development of Semantic Virtual Observatories need the existence of ontologies to incorporate the relevant knowledge models and to properly operate knowledge handling and knowledge discovery on data sets.

5 Ontology of Space Meteorology

For the reasons considered in the previous section, we preliminarily started the process of building a foundation ontology for Space Weather (Messerotti, 2007) by: (a) identifying the elementary concepts

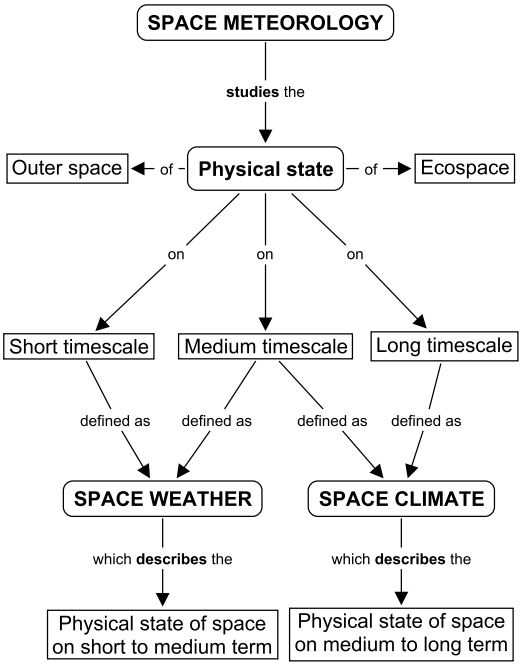

Fig. 1. Cmap that defines the domain of Space Meteorology

according to the available knowledge and performing a careful analysis of the related terminology to define the semantics ; (b) identifying the relationships among elementary concepts according to the available knowledge of the underpinning physics, that characterize the associativity and (c) stating the rules between concepts and set of concepts to define the operativity framework.

The Cmap at the highest generalization level, which describe the basic definitions of Space Weather and Space Climate according to their operational framework, is shown in Fig. 1. A terminology issue becomes immediately evident and it is related to the term ”Space Meteorology”, which is used with different meanings in different contexts. In fact, it can be interpreted e.g. either in terms of ”terrestrial meteorology from space” or ”meteorology of space”. We claim that a detailed analysis of the semantics leads to the selection of the second meaning for close analogy with the terrestrial meteorology, whereas the first meaning, notwithstanding its large use in some scientific communities, should be rejected in the construction of the foundation semantics, which has, in fact, the role to operate disambiguation where needed as in this case. In fact, a fundamental rule is that the common use of a term cannot bias its correct definition in a domain, as this would propagate throughout the whole domain semantics having eventually unpredictable conceptual side effects.

Definition of outer space, whose physical conditions are studied by Space Meteorology, and its physical environments (galactic, local and interplanetary) with their own population properties is reported in Fig. 2.

Fig. 3 shows the typical drivers which characterize the physical state of space at different spatial scales.

Fig. 4 shows the typical timescales on which the drivers are known to operate.

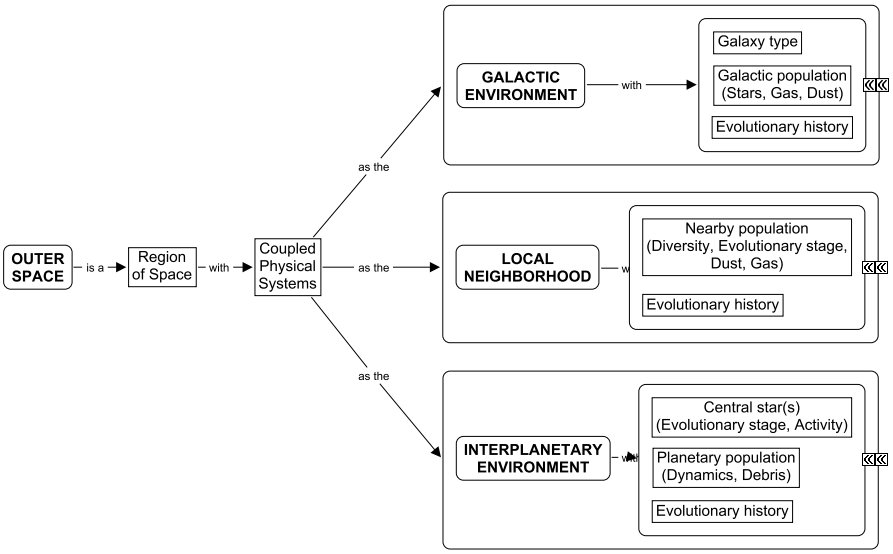

Fig. 2. Cmap that defines the outer space and its physical constituents

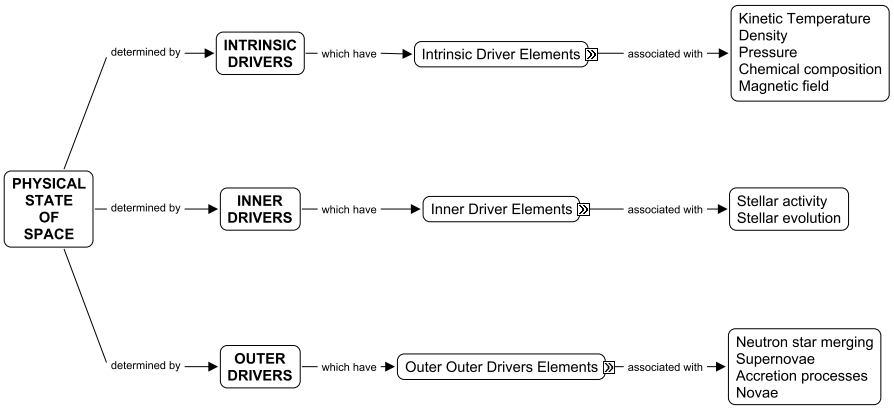

Fig. 3. Cmap that show the intrinsic, inner and outer drivers of the physical state of space

Fig. 5 details the typical impacts of space climate and Space Weather with special attention to the physics of the living matter. In particular, the technological and environmental effects of Space Weather are categorized in Fig. 6, which shows the relevant entities of Fig. 5 at a higher level of detail.

6 Conclusions

We described the preliminary work carried out to build a foundation ontology for Space Weather based on a careful analysis of the domain terminology and of the physical framework. The use of IHMC Cmaps proved to be an appropriate choice both for organizing the relevant knowledge in graphical form

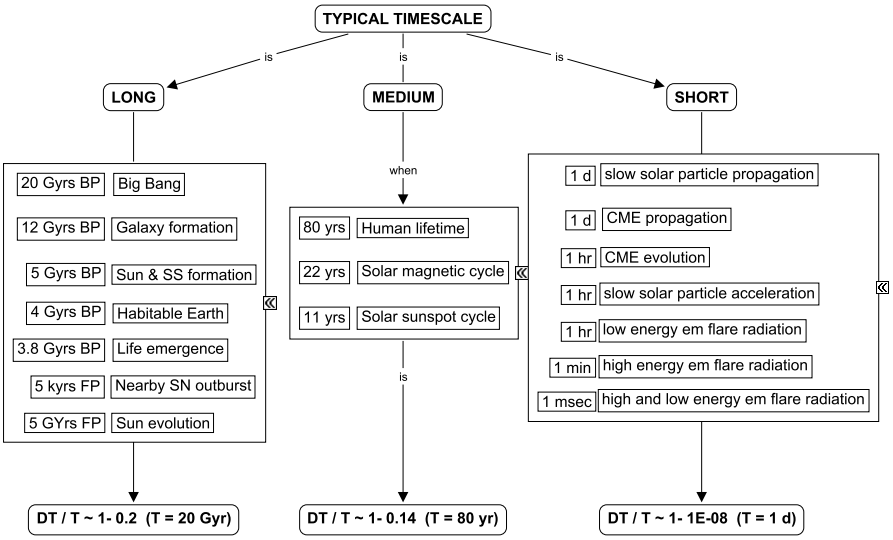

Fig. 4. Cmap which describe the typical timescales

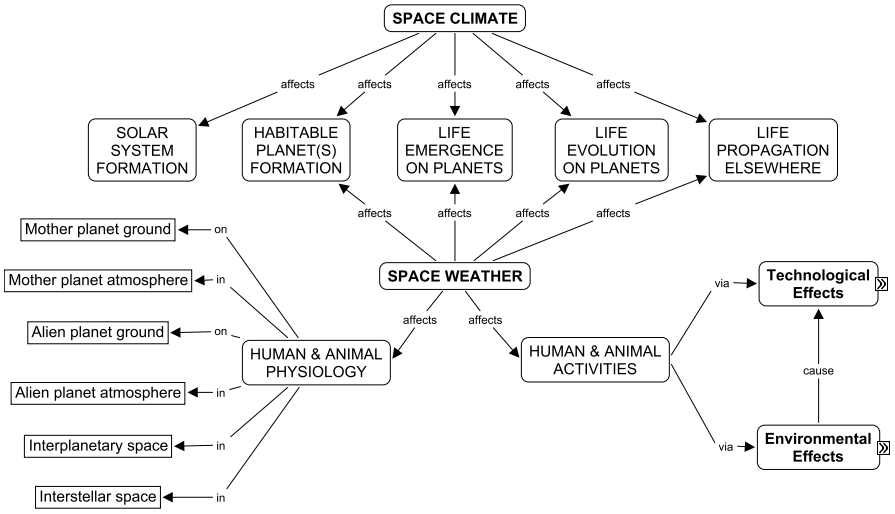

Fig. 5. Cmap of space climate and Space Weather impacts

via a multi-platform, flexible software tool and for making coding this knowledge in a machine-readable format suitable to be processed in a VO environment. The main aim was to clearly set the definitions and the operational and physical domains as a first step towards a Space Weather ontology and to the building of a Space Weather knowledge model. The first set of Cmaps has been publishing on a dedicated Cmap server in order to share them and to stimulate their fine tuning and their extension by the Space Weather community. A significant amount of work has anyway to be performed as a joint, multi-disciplinary

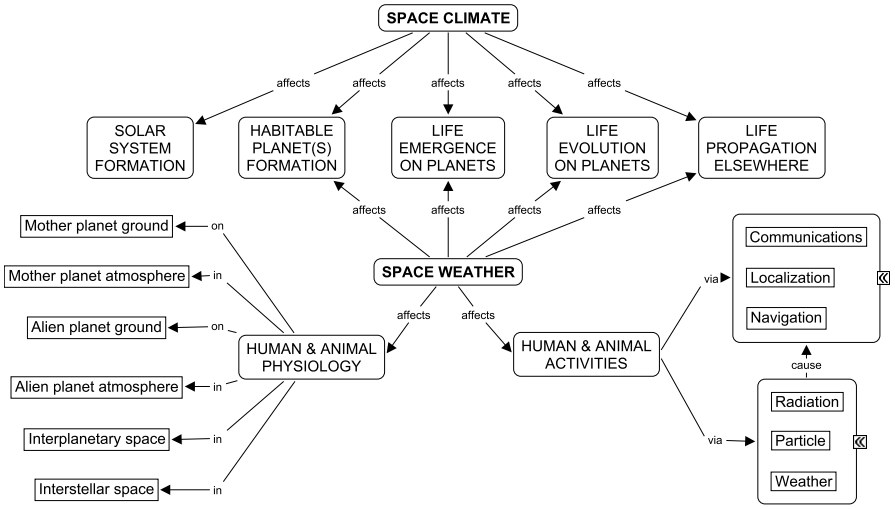

Fig. 6. Cmaps of space climate and Space Weather with a higher level of details

effort to consolidate the ontology to an operational level, which is a must for the incorporation in new generation semantic applications.

Acknowledgements: This work has been carried out in the framework of COST Action 724 and it has been partially supported by the Italian Space Agency (ASI) under contract "Analisi dati sole e plasma", WP 2700 - SOHO/Ground based joint analysis.

References

Messerotti, M.: Embedding knowledge in scientific databases via concept maps as metadata. In: Sawaya-Lacoste, H. (ed) Proc. of the Second Solar Cycle and Space Weather Euroconference, 24–29 September 2001, Vico Equense, Italy. ESA SP-477, Noordwijk: ESA Publications Division, ISBN 92-9092-749-6, 607–610 (2002)

Messerotti, M.: Virtual Observatories and Virtual Grids: The Interplay in Fully Exploiting Solar-Terrestrial Data, CODATA 2006, Beijing, China, October 2006, http://www.codata.org/06conf/presentations/F1/F1_Messerotti/VirtualObservatories.pdf

Messerotti, M.: Building a Foundation Ontology for Solar Space Weather. In: Lundstedt, H. (ed) Proc. of Workshop on Solar Activity: Exploration, Understanding and Prediction, 19–21 September 2005, Lund, Sweden. ESA CDROM, Noordwijk: ESA Publications Division (2007)

Messerotti, M.: Advancing Virtual Observatories via Knowledge Management, IUGG Meeting 2007, Perugia, Italy, 2-13 July 2007. http://www.iugg2007perugia.it/

Part VI

Conclusion

COST724: Conclusions and way ahead

A. Belehaki[1] and J. Lilensten[2]

[1] Ionospheric Group, Institute for Space Applications and Remote Sensing, National Observatory of Athens, Metaxa and Vas. Pavlou, 15236 Palaia Penteli, Greece belehaki@space.noa.gr
[2] Laboratoire de Planetologie de Grenoble, OSUG-CNRS, France
jean.lilensten@obs.ujf-grenoble.fr

1 Conclusion

European institutes active on space physics have a long tradition on monitoring and modeling space phenomena leading to space weather effects. The contribution of these institutes to advance our knowledge in space research was often pioneering. Nevertheless until recently there was a total lack of coordination of research activities in the field of space weather phenomena monitoring, model and prediction in Europe causing several barriers in the transformation of the European know-how to space weather products, required by the users' community, including the European industry. On the other hand related activities in the US have been systematically coordinated and supported by national funding agents. COST Action 724 "Developing the scientific basis for monitoring, modeling and predicting Space Weather" achieved to coordinate, for the first time, the existing national activities in Europe with the involvement of 28 countries. Over the last four years, COST Action 724 established a strong European community around space weather, through the organization of working meetings, management committee meetings, regular workshops and international conferences (European Space Weather Week), international schools and important publications in books, special issues and peer review journals. In addition, COST Action 724 developed the first prototype of the operational pan-European Space Weather Portal that offers access to the most important space weather servers operated by European research institutes and Regional Warning Centers and hosts multi-lingual public outreach pages.

Within the Action's life time significant progress has been achieved on fundamental topics related to the deeper understanding of physical processes underpinning space weather and to their modeling and prediction, through the activities performed by the three working groups of the Action.

Working Group 1 was active on monitoring and prediction of solar activity. Important contributions have been made on the identification, analysis and development of models relevant to solar activity as driver of Space Weather effects. The available information is organized in concept maps for deeper understanding of the interrelationships. Finally an extensive work has been carrying out for the definition of a foundation ontology of Space Meteorology to properly define the concepts of Space Weather, Space Climate and their drivers in the broadest scientific context.

Working Group 2 was focused on the studies related to the Earth's radiation environment and its effects on the magnetosphere, ionosphere, atmosphere, technological systems and human health. Important contributions have been made, including: the development of a comprehensive model of the interaction of cosmic rays (CR) of solar and galactic origin with the Earth's magnetosphere; studies of interactions of the CR particles with the Earth atmosphere and validation of CR induced ionization models, applicable to different heights in the atmosphere; development of a Real Time Database of Neutron Monitor Obser-

vations; development of probabilistic models of Solar Energetic Particle fluxes and fluences as well as SEP event forecasting models; development of techniques and instrumentation for using CR intensities and anisotropies for forecasting large space weather events; satellite measurements of plasma waves and neutral and charged-particle radiation in the ionosphere, magnetosphere and solar wind; development of models for trapped particle radiation and its interaction with the magnetospheric plasma waves were developed; investigation of the effects of space radiation on human health by carrying out an extensive campaign of dose measurements at spacecraft and aircraft altitudes; review of radiation effects on technology on-board spacecraft and compilation of a list of reported spacecraft anomalies due to space weather events.

Working Group 3 has focused on analyzing, modeling and predicting the physical response of geospace (comprising the Earth's magnetosphere, the ionized and neutral atmosphere and the ground) to certain types of solar disturbances, primarily CME. This involved modeling the evolution of transient events (ICME and SEP) through interplanetary space and their interaction with the Earth environment. Plasma-physical models of the propagation of CMEs on various background solar wind categories have been developed using an MHD concept. The dynamics of the magnetosphere-ionosphere system in response to the arrival of bursty solar events has been modeled, the variable state of the magnetosphere during geomagnetic storms has been modeled physically and empirically, and physical models describing the dynamics of the thermosphere (neutral and ionized) have been developed, including the impact of geomagnetic storms on the thermosphere. Semi-empirical models of solar wind-geospace interaction (mostly based on a neural network approach) have been developed with the objective to facilitate the construction of operational space weather forecast schemes (concentrating on geomagnetic activity forecast).

In order to fulfill the objectives of this COST Action for the coordination of the European effort in the development of space weather services, several activities were carried out in the frames of Working Group 4 leading to the development of the first prototype version of the European Space Weather Web Portal (ESWWP) reached in the address http://www.spaceweather.eu. This Portal provides access to the following facilities: a) an archiving facility that has been set up, for the interactive storage, search and retrieval of the available models with a full description and references and of data information via a united web interface, b) a catalogue devoted to the European web sites related to space weather, c) a model interface web portal, which provides access to a prototype implementation of remote model and data base access tools.

The Action's results had strong impact in the European scientific scene. The Action achieved to demonstrate to the decision makers in Europe that space weather phenomena and their effects have scientific and societal impact that needs to be taken into account in order to have reliable technological systems operated in space and to secure the modern society from potential problems due to space weather (i.e electric power failures, health problems due to radiation effects, communication and broadcast problems). This is a requirement not only because European researches deserves systematic support to achieve scientific advances in this field that will lead to reliable space weather services but also because Europe has to meet the challenge of the US space research and industrial development.

2 The way ahead

The heightened sensitivity of increasingly sophisticated technology to fluctuations in the solar-terrestrial environment and the effects of the radiation environment in humans' health makes it increasingly important to be able to forecast adverse conditions, or analyze the features of the disturbed system that cause operational problems. In the next future, the European space weather community ought to concentrate on the following issues:

- Systematic studies for the definition of space weather products that meet the needs of the industry
- Development of models for reliable space weather products and their on line implementation
- Development of strong links with the industry including the European Space Agency
- Coordination of existing national efforts for space weather prediction and development of strong links with the Regional Warning Centers
- Development of coordinating activities with related US organizations and laboratories through joint research activities, joint special observational campaigns, organization of joint international schools and workshops.

COST Action 724 created the space weather European community, bringing together more than 60 experts on space weather. It is now our aim to develop further stronger links between the European researchers, the industry and the US laboratories in order to transfer our knowledge to space weather products and services useful for our society.